Author:
Li, Shu-Xin

Title:
High temperature creep-fatigue and crack growth behaviour of a single crystal nickel base superalloy.

HIGH TEMPERATURE CREEP-FATIGUE AND CRACK GROWTH BEHAVIOUR OF A SINGLE CRYSTAL NICKEL BASE SUPERALLOY

BY

Shu-Xin Li (M.Sc.)

A thesis submitted to the University of Bristol
in accordance with the requirements of
the degree of Doctor of Philosophy
in the Department of Mechanical Engineering
in the Faculty of Engineering

August 1993

Advanced Engineering Materials Research Laboratory
Department of Mechanical Engineering
University of Bristol
Bristol BS8 1TR

TO MY PARENTS, WIFE AND DAUGHTER

ABSTRACT

This thesis presents an experimental and theoretical investigation on the high temperature creep-fatigue and crack growth behaviour of SRR99 single crystal nickel base superalloy. The aim of the research is to examine the effects of temperature, strain dwells and crystal orientation on the high strain endurance and crack growth characteristics of single crystal SRR99 under creep-fatigue conditions, and to establish a high temperature predictive life assessment method for single crystals. Low cycle fatigue (LCF) tests, using smooth bar specimens with different crystal orientations, have been conducted at 750°C, 950°C and 1050°C under different types of loading with or without strain dwells. Short crack growth tests, using corner crack specimens, have also been performed at the same temperature and loading conditions.

The smooth bar specimen results exhibit a significant orientation dependence, with the [001] orientation showing the longest life and the [111] orientation the shortest. The effects of strain dwells are found to be dependent on both temperature and cycle type. In general, a compressive dwell is more damaging than a tensile dwell at 750°C, but the reverse is true at 1050°C. Subsequent analysis has revealed that the influence of strain dwells on the creep-fatigue and crack growth behaviour of single crystal SRR99 is via the simultaneous effects of mean stress, additional inelastic strain and time dependent damage. An anisotropic viscoplastic constitutive model has been developed and successfully used to simulate the orientation and cycle type dependent mechanical response under creep-fatigue conditions.

The high temperature crack growth behaviour of single crystal SRR99 is different from similar polycrystalline materials. For short cracks, the crack growth rate is found to be nearly independent of crack length. A traditional fracture mechanics approach does not provides an adequate description for correlating crack growth rate. Crack growth in single crystal SRR99, under high temperature LCF conditions, is influenced more by the global deformation of the specimen.

Several conventional life prediction methods have been evaluated for application to single crystal SRR99, but the results are unsatisfactory. A mean stress modified strain range partitioning method has been proposed, which gives reasonable life prediction results for single crystal SRR99 under creep-fatigue conditions. Furthermore, a new life prediction methodology, using a combination of the constitutive model and a life prediction technique, has been developed and applied successfully to predict the fatigue and creep-fatigue life of single crystal SRR99 at 950°C.

DECLARATION

The accompanying dissertation entitled "High Temperature Creep-Fatigue and Crack Growth Behaviour of a Single Crystal Nickel Base Superalloy" is submitted in support of an application for the degree of Doctor of Philosophy in Engineering at the University of Bristol. The dissertation is based on independent work by the candidate - all contributions from others have been acknowledged fully in the text. This work has not been submitted for any other degree or diploma at this University or any other institution.

I declare that the above statements are true.

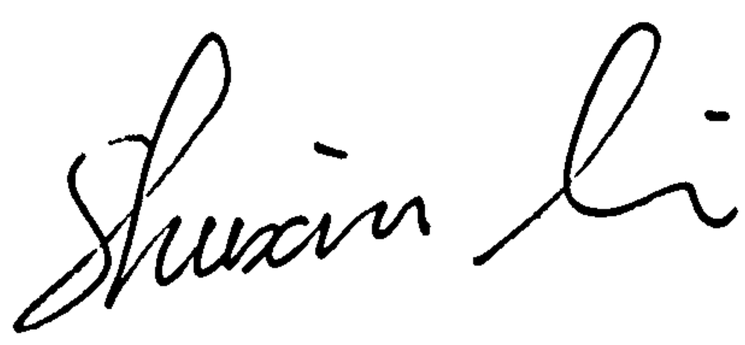

Shu-Xin Li (M.Sc.)

August 1993

ACKNOWLEDGEMENTS

I wish to express my sincere thanks to my supervisor, Dr. D. J. Smith, for his continuous guidance, advice and encouragement during the time of this research. I am also grateful to Professor E. G. Ellison, who suggested this research project, for many stimulating discussions and valuable advice. My gratitude is extended to Dr. Steve Kimmins for his time and effort to read this dissertation and provide many perceptive comments and valuable suggestions.

I would also like to thank the members of the Advanced Engineering Materials Research Group for providing a warm and productive environment in which to work, and for their friendship, encouragement and good cheer.

My thanks are also extended to the staff of the mechanical engineering workshop, and in particular to Troy Swankie and Mr. David Ogden for their technical assistant in the experiments.

Financial support provided by Rolls Royce Plc is gratefully acknowledged.

I would like to thank Drs. A. Chambers and S. Williams in Rolls Royce for providing test specimens and technical support throughout the project. Thanks are also due to Dr. G. Harrison in DRA Pyestock for providing the creep data of single crystal SRR99.

Finally, I would like to thank my family, and all of my friends, for their continuous support and help in many different ways.

CONTENTS

LIST OF TABLES

LIST OF FIGURES

CHAPTER 1
INTRODUCTION

Nickel base superalloys are being used in the form of single crystals due to superior creep, fracture and fatigue properties over conventionally cast alloys (Kear et al [1967], Walter et al [1987], Chan et al [1987]). The design of advanced jet engines with improved performance has led to the increasing development of single crystal nickel base superalloys in recent years, since the efficiency of gas turbine for jet engines relies in part on the temperature capability of turbine blade and vane materials. Most of these components are usually made of conventionally cast nickel base superalloys. For high temperature applications, these are several disadvantages associated with the grain boundaries in a material. First, alloy strength is lowered because the grain boundaries are a source of weakness at high temperature particular those which lie perpendicular to the applied stress. Creep life and thermal fatigue life are both badly affected by these transverse boundaries. Second, alloying additions are required to strengthen grain boundaries and many of these additions lower the incipient melting temperature of the alloy. This limits the maximum allowable heat treatment temperature and prevents the realisation of the full strength potential of the alloy.

In order to eliminate the transverse boundaries, directionally solidified casting was introduced. In this way the grains can be made to grow in one preferred orientation (along the length of the blade) and have no transverse boundaries. The mechanical properties obtained from directionally solidified (DS) material show significant improvements in thermal fatigue resistance, creep life and ductility in the longitudinal direction, i.e. parallel to grain orientation. The Young's modulus along the major axis of DS material is reduced by 30%. The principal reasons for the improvement in creep and ductility properties lie in the absence of transverse grain boundaries and in the preferred crystallographic orientation of the grains. The combination of no transverse grain boundaries and this preferred orientation often results in doubling the creep life and gives a six times increase in thermal fatigue life compared with conventionally cast nickel base superalloys (Kounitzky et al [1991]). However, the transverse properties tend to be unaffected.

A further development of directional solidification is the production of single crystals to eliminate all the grain boundaries in the turbine blades. The absence of other grain boundaries further enhances creep properties. Single crystal nickel base superalloys have three times the creep life of DS superalloys. Furthermore, since the blade

contains no grain boundaries there is no need to add in the alloy elements which are traditionally used to strengthen these boundaries. When these elements (C,B,Zr,Hf) are excluded from nickel base alloys the melting point is raised appreciably. This allows high temperature heat treatments to be applied to single crystal alloys that cannot be used with conventionally cast (CC) or DS superalloys. The heat treatments optimise the microstructure of the alloy and allow the full strength potential to be achieved. The combination of these factors gives creep life improvements of about 6 times, thermal fatigue life improvement of about ten times and significant improvements in impact resistance and tensile performance over conventionally cast material (Kounitzky et al [1991]).

The properties of single crystal nickel base superalloys vary considerably depending on how the crystal structure is aligned relative to the applied stress. In conventionally cast superalloys this is unimportant as there is a large number of randomly oriented grains so 'average' properties are given. However, the lack of grain boundaries in single crystal alloys leads to material anisotropy which produces orientation dependent material response. All the mechanical properties, including elastic response, yielding and flow behaviour, creep, fatigue and fracture properties are highly dependent on crystal orientation and temperature. The properties of a single crystal superalloy can change rapidly if the direction of the applied stress differs greatly from the preferred growth direction. Therefore, a fundamental requirement for the successful application of single crystal material is a clear understanding of the influence of orientation on mechanical behaviour.

Turbine blades are subjected to elevated temperature up to 1100°C during turbine operation, thus the design of turbine blades for resistance to combined creep-fatigue failure has received considerable attention for conventionally cast nickel base superalloys. Numerous attempts (Manson [1973], Ostergren [1976], Bernstein [1982], Ellison et al [1984], Saltsman and Halford [1988]) have been made to develop methods of predicting creep-fatigue life in order that generalised design rules based on representative test conditions can be applied to the wide variety of stress-time-temperature conditions occurring in a turbine blade during service. Since single crystal nickel base superalloys have not been used extensively for turbine blades, there has been no systematic study on the high temperature mechanical properties and creep-fatigue life behaviour of single crystal nickel base superalloys. Taking into account the anisotropic material response, it is expected that the creep-fatigue response and crack growth behaviour of a single crystal will be significantly different in comparison with conventionally cast polycrystalline nickel base superalloys.

The principal objective of this work is to establish a high temperature predictive life assessment method for single crystal nickel base superalloy SRR99 under complex loading and temperature conditions representative of service. The investigation will examine the effects of tensile, compressive and balanced dwell periods on the high strain endurance of the alloy for temperatures in the range 750°C to 1050°C. The short crack growth characteristics of the single crystal will also be determined at the same temperature and loading conditions.

In response to the need for a comprehensive understanding of the creep-fatigue life behaviour of single crystal nickel base superalloys, the test programme consisted of not only creep-fatigue tests but also simple mechanical tests to define basic material properties. This allowed the development of models to describe the influence of crystal orientation on mechanical response and creep-fatigue life behaviour. Consequently an anisotropic viscoplastic constitutive model is developed to simulate the cyclic mechanical response under creep-fatigue conditions and combined with life assessment approaches for life prediction.

Chapter 2 is a brief review of the previous work on single crystal nickel base superalloys with particular reference to the influence of orientation and temperature on the mechanical properties, on creep and fatigue behaviour, as well as on crack growth characteristics. Chapter 3 reviews the various life prediction methods developed for polycrystalline materials under high temperature low cycle fatigue (HT-LCF) conditions. The special characteristics of fatigue life behaviour , and the additional consideration of establishing a life assessment method for single crystal nickel base superalloys is examined

The experimental programme is described in Chapter 4, and Chapter 5 gives the experimental results for various tests. The analyses of the influence of crystal orientation on the deformation behaviour obtained from the tests is described in Chapter 6. Chapter 7 presents an anisotropic viscoplastic constitutive model for single crystal superalloy and gives the numerical simulation results on the cyclic mechanical behaviour of single crystal SRR99 at 950°C.

In Chapter 8, the various conventional life assessment approaches are directly used for the fatigue and creep-fatigue life prediction of single crystal SRR99, with some modification to take into account the special characteristics of single crystals. Then the constitutive model is combined with life assessment approaches to predict the

creep-fatigue life of single crystal SRR99 under various loading conditions. The predicted results are then compared with experimental results.

Chapter 9 presents the characteristics of creep-fatigue crack growth from short initial cracks in single crystal SRR99 under fatigue-creep conditions. Both global strain methods and fracture mechanics approaches are used to correlate crack growth rates under various loading conditions. A general discussion is given in Chapter 10. Chapter 11 summarizes the conclusions and suggests potential future work.

CHAPTER 2
REVIEW OF PREVIOUS WORK

2.1 Introduction

A typical nickel base single crystal superalloy consists of an face centred cubic (fcc) solid solution strengthened γ matrix with precipitated γ' particles. The precipitates have an ordered fcc structure and are coherent with the surrounding matrix. Fig.2.1 shows a unit cell of the base structure of a nickel base superalloy single crystal, and the three main cubic symmetry orientations [001]-[010]-[100]. Due to the anisotropic structure of the single crystals, the mechanical response of a single crystal superalloy is very complex. All the mechanical properties, including elastic response, yielding and flow behaviour, creep, fatigue as well as fracture properties are related to crystal orientation and temperature. Consequently, an anisotropic constitutive model is required to describe the orientation dependent deformation behaviour of a single crystal nickel base superalloy at high temperature.

In this Chapter, a review of the mechanical properties, creep behaviour, low cycle fatigue behaviour and crack propagation characteristics of single crystal nickel base superalloys will be presented in sections 2.2 to 2.5 respectively. Section 2.6 gives a review on the development of plasticity and viscoplasticity constitutive models and their applications for single crystals.

2.2. Mechanical Properties

2.2.1 . Elastic Behaviour

A nickel base single crystal superalloy , as a cubic single crystal, though possessing the highest possible crystal symmetry, still requires three elastic constants to define its elastic response. The elastic stress strain relationship for single crystal nickel base superalloy in the single crystal main symmetry axis, i.e. [001]-[010]-[100], can be written as;

$$\begin{vmatrix}\varepsilon_{11}\\ \varepsilon_{22}\\ \varepsilon_{33}\\ \varepsilon_{23}\\ \varepsilon_{31}\\ \varepsilon_{12}\end{vmatrix} = \begin{vmatrix} \frac{1}{E} & \frac{-\nu}{E} & \frac{-\nu}{E} & 0 & 0 & 0\\ \frac{-\nu}{E} & \frac{1}{E} & \frac{-\nu}{E} & 0 & 0 & 0\\ \frac{-\nu}{E} & \frac{-\nu}{E} & \frac{1}{E} & 0 & 0 & 0\\ 0 & 0 & 0 & \frac{1}{2G} & 0 & 0\\ 0 & 0 & 0 & 0 & \frac{1}{2G} & 0\\ 0 & 0 & 0 & 0 & 0 & \frac{1}{2G}\end{vmatrix} \begin{vmatrix}\sigma_{11}\\ \sigma_{22}\\ \sigma_{33}\\ \sigma_{23}\\ \sigma_{31}\\ \sigma_{12}\end{vmatrix} \qquad (2.1)$$

There are three independent material constants, Young's modulus E, Poisson's ratio ν, shear modulus G. Using this stress-strain relationship, the orientation dependence in the elastic stress and strain can be modelled by transforming equation (2.1) into any given orientation. The stress and strain transformation matrixes for a cubic single crystal are given in Appendix V, it can be seen that the elastic response will be different for specimen tested with different crystal orientation.

The test data (Miner et al [1986]) on the longitudinal elastic modulus for single crystal nickel base superalloy Rene N4 at 760°C and 980°C showed strong dependence on crystal orientation. At 760°C, Young's modulus varies from 104 GPa in the most compliant [001] direction to 253 GPa in the stiffest [111] direction. At 980°C the trend is the same, but the elastic modulus decreases with increasing test temperature.

The transverse elastic anisotropy under a uniaxial loading for different crystal orientations has been studied by Yang [1985]). The transverse strain induced by longitudinal stress, in general, varies sinusoidally around the longitudinal axis. Only for loading in the [111] and [001] directions, the transverse response is isotropic. For all other loading directions, the transverse response shows various degrees of anisotropy. For the case of a nickel base single crystal, the highest degree of anisotropy is seen when loaded in [011] crystallographic direction.

2.2.2. Yielding and Flow Behaviour

The yield strength of single crystal alloys is a function of the material orientation relative to the direction of the applied stress . Very complicated yielding behaviour is exhibited by nickel base superalloys containing a high volume fraction of the γ' phase.

Nearly constant or increasing yielding strength is observed with increasing temperature up to some peak temperature. Significant tension/compression asymmetry in yield strength was observed by many researchers (Copley, Kear and Rowe [1972], Takeuchi and Kuramoto [1973], Sheh [1984], Umakoshi et al [1984], Miner et al [1986], Milligan and Antolovich [1987], Poubanne [1990]). Slip on the cubic rather than octahedral planes is frequently observed at high temperature for loading along orientations near the [111] direction. Finally, even when normal octahedral slip does operate, yielding stresses frequently do not follow Schmid's law (see following section) as a function of tensile axis orientation. Above a critical temperature, approximately 700-760°C, there is a sharp drop in the yield strength, cubic slip become more predominant, and the tension/compression asymmetry is less significant. Single crystal superalloys also exhibit strain rate sensitivity and cyclic hardening. In general, the main factors which influence the flow behaviour of nickel base single crystal alloys, besides the composition of the materials, are temperature, crystal orientation and strain rate.

Critical Resolved Shear Stress and Schmid's Law. The basic yielding (plastic deformation) mechanism in a single crystal will be slip. Plastic flow occurs by slip on certain planes in particular directions. The extent of slip in a single crystal depends on the magnitude of the shear stress produced by external loads, the geometry of the crystal structure and the orientation of the active slip planes with respect to the shearing stresses. Slip begins when the shearing stress on the slip plane in a slip direction reaches a threshold value. This value is called the ***Critical Resolved Shear Stress (CRSS)***. The fact that the different tension loads to produce slip in single crystals of different orientations can be rationalised by the CRSS was first recognised by Schmid [1931]. ***Schmid's Law*** expresses the CRSS, τ_S, for slip in a specified slip direction $[l_2,m_2,n_2]$ on the slip plane $[l_3,m_3,n_3]$ in terms of angles made by the direction $[l_1,m_1,n_1]$ of the applied tensile stress to the surface normal of the slip plane, φ, and the slip direction, θ, Fig.2.2, in the form

$$\tau_s = \sigma_y \cos\theta\cos\varphi \qquad (2.2)$$

or

$$\sigma_y = \tau_s / \cos\theta\cos\varphi = \tau_s / S_{[l_2,m_2,n_2]\{l_3,m_3,n_3\}} \qquad (2.3)$$

where σ_y is the yield stress, $S_{[l_2,m_2,n_2]\{l_3,m_3,n_3\}} = \cos\theta\cos\varphi$ is called *Schmid Factor.* The details on the derivation of the Schmid's law and the calculation of Schmid factor are given in Appendix I.

The active slip systems in nickel base single crystal alloys, as a fcc crystal, depend upon crystal orientation with respect to the applied loads, temperature and strain rate, and could involve one or more types of slip. Three primary slip systems are illustrated in Fig.2.3. These are;

(a). Slip on the four {111} octahedral planes in the three directions similar to the [110] direction.

(b). Slip on the four {111} octahedral planes in the three directions similar to the [112] direction.

(c). Slip on the three {100} cube planes in the directions similar to the [110] directions.

There are 30 possible slip components in a fcc single crystal alloy. The flow behaviour of the alloy is determined by which of the slip systems becoming active.

Effects of temperature and crystal orientation. The effects of temperature and the orientation of the tensile axis on the flow stress of a single crystal nickel base superalloy Mar-M200 were studied by Kear and Piearcey [1967] and Copley et al [1972]. They obtained several important results, which were also later confirmed by Giamei [1979] from the measurement of flow stress in compression. these are:

(i) The flow stress of single crystal (SC) alloy remains almost constant up to about 800°C and then drops sharply. However, there is a small increase between 400 and 800°C.

(ii) The CRSS for [110]{111} slip tends to increase as the loading orientation moves away from [001].

(iii). Cubic slip occurs at low temperature in samples oriented near [111] and results in the apparently low CRSS for [110]{111} slip observed in [111] oriented sample.

(iv). At temperatures above about 800°C, cube slip occurs in samples of all orientations, except for the cubic -oriented samples.

A number of investigations have been carried out on various nickel base single crystal alloys, such as PWA1480 (Milligan and Antolovich [1987], [1990]), AM1 (Guedou and Honnorat [1990], Poubanne [1990]), Rene N4 (Miner et al [1986a 1986b]), SRR99 [Ghosh et al [1991], Sun and Hazzledine [1988]). Some of studies have confirmed the above results, and also some new results have been revealed.

By slip trace analysis, transmission electron microscopy (TEM) analysis of dislocation burgers vectors and the measurement of tensile axis rotation, the temperature dependence of CRSS for cubic slip and octahedral slip in Rene N4 assuming Schmid's Law has been studied by Miner et al [1986a, 1986b]. The results indicated that primary cubic slip occurred for orientations near [111] at all temperatures, including room temperature. The range of orientations exhibiting cubic slip increased with increasing temperature until at 870°C, where only orientations very near the [001] or [011] exhibited octahedral slip.

The CRSS for cubic slip in Rene N4 exhibited a peak near 760°C, similar to that observed for octahedral slip. Above 760°C, the strength began to drop rapidly. Such behaviour is typical of high γ' volume fraction nickel base superalloys and has been documented for several similar systems [Beardmore et al [1969], Copley et al [1972], Tensen et al [1980], Nathal et al [1982], Shah and Duhl [1984], Milligan and Antolovich [1987], Guedou and Honnorat [1990]).

Tension -compression anisotropy exists for both octahedral and cubic slip. The CRSS for cubic slip is higher in compression than in tension at 760°C. The opposite occurs at 980°C. The same behaviour has been observed in the single crystal PWA1480 studied by Shah and Duhl [1984]. The CRSS for octahedral slip generally is higher in compression than in tension over the whole temperature range, except at 760°C, i.e. the peak of yield strength, where the CRSS for octahedral slip for the [001] orientation is higher in tension than in compression.

Test results for Rene N4 also show deviations from Schmid's law for orientations exhibiting octahedral slip. This phenomenon was described by a model developed by Lall, Chin and Pope [1979] (LCP model), which is an extension of the model of Takenchi and Kuramoto [1973].

Strain Rate Effects. Leverant et al [1971] have investigated the strain-rate dependence of the CRSS of single crystal MAR-M200 with a [001] tensile axis. The results indicated that samples deformed at 760°C (near the peak in the flow stress

versus temperature response) showed a very small positive strain-rate dependent flow stress. However, samples tested at higher temperatures exhibited a strong, positive strain - rate dependence. Similar trends have been reported in the studies of PAW1480 (Milligan et al [1987]), and UDIMET 115 (Russell et al [1985]).

Leverant et al [1971] suggest that a change in the dependence of flow stress on strain rate accompanied a change in the mode of deformation. By TEM analysis they correlated the dislocation arrangement with the dependence of flow stress on strain rate. A strain-rate-independent flow stress is found when shear of the γ-γ' structure occurs by the diffusionless shearing of a/2[110] dislocation pairs in coarse, heterogeneously distributed planar slip bands. A strain-rate-dependent flow stress occurs when diffusion is rapid relative to the imposed strain rate. Shear of the γ' particles then occurs by the viscous glide of a/2[110] or a/3[112] dislocations. Subsequent dislocation cross slip and climb results in a homogenous distribution of dislocations.

2.3. Creep Behaviour

The majority of the creep studies of single crystal nickel base superalloys have been concentrated within the temperature range where the major anisotropic effect is exhibited, i.e. in the range 750°C to 850°C. Kear and Piearcey [1967] were the first to study the creep behaviour of superalloy single crystals of various orientations. Their results reveal that the substantial improvement in creep life of single crystal over conventionally cast or directionally solidified alloys occurs between 750°C and 850°C for crystals with orientations near [001] and [111]. Conversely very short lives were exhibited by crystals orientated near [011]. At 980°C crystallographic orientation was found to have much less influence on the creep life.

Effect of γ' Volume Fraction. The creep strength of nickel base superalloys depends strongly on the volume fraction of γ'. The studies (Fleischer [1963]) on the creep- rupture life of a series of nickel base alloys (in which the γ' volume fraction varies from 0 to 100%) indicated that a maximum creep life occurred at γ' volume fraction of approximately 60 vol.%. The reasons for the existence of a peak at 60 vol.% rather than some other volume fraction are not known clearly. However, most of the nickel base superalloys have γ' volume fraction near 60%, for example, Rene N4 65.vol.%; PWA1480, 55-60 vol.%; SRR99, 60 vol%; Mar-M200, 60 vol%.

Orientation, Temperature, and Stress Dependence. The anisotropy in creep behaviour has been extensively studied for single crystals of MAR-M20 (Kear and Piearcey [1967, Leverant et al [1971], 1973] Oblak and Rand [1974]) and MAR-M247 (Mackay and Maier [1982], Leverant et al [1970]). In general, the functional dependence of the creep behaviour in the two alloys was found to be same.

At a temperature of about 760°C, the degree of anisotropy in stress rupture lives is often large. Single crystals Mar-M20 orientated near [011] have much shorter rupture lives than crystals oriented near [001]. MAR-M247 single crystal showed similar behaviour, and also very long rupture lives were observed for samples orientated near [111]. Ghosh et al [1990] pointed out that several experimental studies (Winstone [1989], Sun and Hazzledine [1988]) on the anisotropic creep behaviour of single crystal superalloys have given apparently contradictory results regarding whether [001] or [111] crystal orientations are strongest in uniaxial tensile creep. Thus, further work is needed to determine the facts.

Large differences in creep lives were found for differently orientated samples. In order to understand the orientation dependence of the extent and rate of creep, Leverant and Kear [1970] considered the Schmid factors and multiplicity of slip for the {111}[112] slip system. In general, crystals having orientations with high Schmid factors are more favourably orientated for slip than crystals with low Schmid factors. Thus, a crystal with an orientation near [111] should exhibit the highest stress rupture life. This in part is because the [111] orientation provides the lowest Schmid factor for [112] slip of 0.31 and strong work hardening may occur due to interactions between mobile dislocations gliding within several intersecting systems. Although the results has been confirmed by a number of workers (Kear and Piearcey [1967], Paidar et al [1982], Mackay and Maier [1982], Pearson et al [1981]), there are still some arguments about whether [111] or [001] orientations exhibit the longest creep rupture lives (Ghosh et al [1990], Winstone [1989], Sun and Hazzledine [1988]).

The effect of crystal orientation on the creep properties of nickel base alloys in the temperature regime over 1000°C is much less pronounced. In fact the material behaviour appears to be isotropic in terms of creep life. The explanation for this is the thermal activation of the other slip systems at this temperature. For instance slip on the {100} planes becomes energetically favourable. However, the increased mobility of dislocations due to thermally activated climb and cross slip processes enhances creep rates overall.

2.4. Low Cycle Fatigue (LCF) Behaviour

The LCF behaviour of a nickel base single crystal superalloy will be much more complex than tensile or creep behaviour, because at elevated temperatures, plastic flow, creep, and relaxation may occur simultaneously under cyclic loading. The deformation behaviour and the fatigue crack initiation and growth mechanisms of single crystal alloys may vary markedly with both temperature and crystal orientation as well as cyclic loading conditions.

The orientation and temperature dependence of the cyclic yield strength, tension - compression anisotropy and flow behaviour in LCF tests are generally similar to those observed in tensile tests . Experimental results on PWA1480 (Milligan [1990]), Rene N4 (Gabb. et al [1989]) and AM1 (Poubanne [1990]) nickel base single crystal superalloys show that the magnitude and orientation dependence of tension-compression anisotropy is quite significant at lower temperatures (below 760°C-800°C), but generally not so at higher temperatures. A similar tension -compression anisotropy has been observed in single crystal Ni_3Al by Ezz et al [1982] and in another single crystal PWA1480 nickel base superalloy by Shah and Duhl [1984].

In contrast, the temperature and orientation dependence of cyclic work-hardening behaviour is opposite to the trends described above. At lower temperatures (below 760°C), only slight work-hardening was observed for several nickel base single crystal superalloys. For example, in Rene N4 (Gabb et al [1986]) and AM1 (Poubanne [1990]), the orientation dependence of work-hardening is also very small at lower temperatures, the calculated hardening exponents for all orientations, including the [001], [011], [111], [236], [027] and [145], for Rene N4 is about 0.20. At higher temperatures, work hardening becomes large and strong work hardening anisotropy for different orientations is observed. Both Rene N4 and AM1 show the highest hardening in the [001] orientation compared with other orientations. It is quite surprising to note the markedly low hardening level of the [111] orientation.

It is well known that the LCF lives of single crystal superalloys are typically better than the polycrystalline alloys. This improved fatigue behaviour has been attributed to a change in the mode of crack propagation from intergranular in conventionally cast materials to transgranular in single crystals. LCF tests on nickel base single crystal superalloys Mar-M200 (Chan et al [1987a,1987b])], Rene N4 (Poubanne [1990]) and PWA1480 (Millian [1990]) all show similar fatigue fracture modes. Fatigue crack initiation occurred at carbides or micropores, and subsequent crack

growth takes place by either a stage I or stage II mode. Fracture behaviour is also strongly dependent on temperature, crystal orientation and cyclic frequency (i.e., strain rate)

At high frequency and low temperature there is planar heterogeneous slip and crystallographic cracking along {111} slip planes. This is termed stage I cracking. On the other hand, at low frequency and high temperature there is very homogeneous slip and cleavage fracture, perpendicular to the stress axis direction. This type of crack is termed stage II cracking. Thus, there are two classes of crack observed in single crystal nickel base superalloys. The first, stage I or mode II crack is shear induced and may lead to a pure shear failure. The second, stage II or mode I crack is cleavage in nature and may lead to brittle or cleavage failure.

2.5. Fatigue Crack Propagation Characteristics

The fatigue crack propagation behaviour of single crystal nickel base superalloys, which are naturally anisotropic, has been characterised as a function of temperature, frequency, stress state and crystallographic orientation (Crompton & Martin [1984a,b], Chan et al [1987], Lerch & Antolovich [1990], Diboine et al [1990]). At elevated temperature under creep-fatigue conditions, crack growth can be cycle dependent, time dependent, or a combination of these two, depending on temperature and test conditions (Yang [1991]).

Temperature Effects. Several studies (Chan et al [1987], Lerch & Antolovich [1990], Diboine et al [1990]) have recognised that test temperature has a strong effect on the fatigue fracture surface morphology for single crystals. At low and intermediate temperature, a fatigue crack propagates predominately along the {111} crystallographic planes. Consequently, the fatigue cracks in such uniaxial fatigue tests may be under mixed loading modes I, II and III. At high temperature, the fatigue crack propagation path is flatter, and macroscopically perpendicular to the applied tensile stress. The fracture surface appears to be non-crystallographic, although detailed fracture features may be obscured by oxidation (Bouse [1984], Crompton & Martin [1984a], Yang [1991]). The temperature at which the fracture behaviour changes is not very well defined. Non-crystallographic propagation is generally reported at temperatures above 760°C, but it has also been observed at 600°C (Crompton & Martin [1984a). It is generally agreed that crystallographic growth at high temperature is inhibited as a result of the more homogeneous deformation ahead of the crack tip. Thermally activated cross-slip allows the dislocations to move

between slip planes, resulting in less severe strain concentrations on individual slip plane and a more homogeneous distribution of plastic deformation.

The cyclic crack growth rates in single crystal Rene N4, as a function of temperature from room temperature up to 1093°C, have been studied by Lerch and Antolovich [1990]. In terms of stress intensity factor ΔK, the crack growth rates were found to similar for all specimens tested at or below 927°C. At higher temperatures (1038°C and 1093°C), the crack growth rate is about one order of magnitude higher and appears to increase with increasing temperature. Lerch and Antolovich [1990] claimed that at high temperatures, there is a significant degradation of the material due to oxygen embrittlement, which may substantially reduce the ΔK required to propagate a crack. Test results of fatigue crack propagation in single crystal Mar-M200, obtained by Chan et al [1987], indicated however that there is no significant different in the crack growth rates of specimens orientated in the [010] and [111] orientations at 25°C and 980°C in terms of ΔK_{eff} (which is a combination of ΔK_I, ΔK_{II} and ΔK_{III} to take into account the effect of the mixed mode loading feature of the crack propagating in a crystallographic manner). The lack of a temperature effect on crack growth rates for the Mar-M200 single crystal, may be attributed to the high test frequency (10 to 20 Hz) compared with the frequency (0.5 Hz) used by Lerch and Antolovich [1990] for Rene N4.

Orientation Effects. There are, however, some conflicting results regarding the influence of crystal orientation on fatigue crack propagation behaviour. Chan et al [1987] reported that the effect of crystal orientation on crack growth rate in single crystal Mar-M200 depends on test temperature. At room temperature, it is found that the crack growth rate in Mar-M200 exhibits a significant orientation dependence. For a given effective stress intensity factor, ΔK_{eff}, and at R=0.1 (R is the fatigue test stress ratio), the highest crack growth rate is observed in the [023] orientation, while the lowest growth rates are in the [111] and [150] orientations. The growth rates of the [010] and [110] specimens are comparable to but slightly lower than for the [230] specimen at an equivalent ΔK_{eff}. However at 980°C, the crack growth rates obtained from specimens with crystal orientations [010], [011], [111] and [211] show that the effects of crystallographic orientation and stress state do not significantly affect the crack growth rates of Mar-M200 under load-controlled conditions with either uniaxial cyclic loading or combined cyclic loads and torque (Chan et al [1987]). Crompton and Martin [1984a] also reported no crystal orientation effect on crack growth rate in Mar-M002 single crystals neither at 600°C and 850°C, nor even at room temperature.

The test results obtained by Lerch and Antolovich [1990] for single crystal Rene N4 at 704°C indicated that there does appear to be an orientation effect on fatigue crack growth rate for Rene N4. The investigation of the influence of crack growth direction in [001] single crystal CMSX-2 at 650°C (Deferesne and Remy [1990]) has also shown a strong influence of secondary crystallographic orientation on crack growth rate. The fatigue crack growth rate along the [110] direction is almost 10 times that along the [010] direction. However, Diboine et al [1990] reported that the fatigue crack growth rates in single crystal PWA 1480 at 870°C are only weakly dependent on the secondary orientation. In summary, it is clear that the crystallographic orientation effect on fatigue crack growth rate is complicated. It depends on temperature, the geometry of test specimen and the test loading conditions.

Influence of Loading Parameters. The influence of frequency on the fatigue crack growth rate of single crystal Mar-M002 at different temperatures has been studied by Crompton and Martin [1984] in conjunction with a detailed investigation of the crack tip plastic zone. At room temperature, the loading frequency was observed to have little influence on the plastic zone size and crack growth rate. However, at a high temperature, a decrease in the frequency gave rise to an increase in the plastic zone size at a constant stress intensity. Consequently, crack growth rates are observed to increase with decreasing frequency. The measurement of the distribution of the strain within the plastic zone has indicated that the crack growth mechanism is associated with crack tip plasticity.

Yang [1991] has studied the crack growth behaviour of single crystal SRR99 under fatigue, creep and fatigue-creep condition at 750°C, 950°C and 1050°C. It is found that the factors, such as temperature, frequency and cyclic load ratio R, may influence the feature of crack growth mechanisms at elevated temperature. Crack growth in a test may be dominated by a cycle dependent fatigue mechanism, time dependent creep mechanism and both fatigue and creep mechanisms. At 750°C, it has been found that frequency does not significantly affect the crack growth rate and that crack growth is controlled by a cycle dependent fatigue mechanism. Similar frequency insensitive fatigue crack growth behaviour has also been observed in single crystal Mar-M002 at 600°C by Crompton and Martin [1984a]. At 950°C, crack propagation is observed to be strongly dependent on frequency. Crack growth rate increases with decreasing frequency, and a change of the mechanism controlling crack growth from a cycle dependent fatigue mechanism to a time dependent creep mechanism with decreasing frequency, has been observed. At 1050°C, frequency has

little effect on the crack growth rate as crack growth mechanism is dominated by time dependent creep. The effect of R ratio on crack growth rate is found to be similar over the temperature range 750°C to 1050°C. An increase in the R ratio causes an increase in crack growth at a given ΔK value.

Yang [1991] has identified a number of parameters with which to correlate crack growth rate for single crystal SRR99 at elevated temperature. It is found that when crack growth is dominated by a cycle dependent fatigue mechanism, crack growth rate is best correlated with stress intensity factor ΔK. When crack growth is dominated by time dependent creep, crack growth rate is better correlated with the C* rather than stress intensity factor. This is similar to the results obtained for polycrystalline materials (Nikbin & Webster [1984], [1987], Winstone et al [1985], Webster [1987]).

A feature of earlier work on fatigue crack growth in single crystal nickel base superalloys at high temperature has been the lack of results under test conditions common to low cycle fatigue (LCF) testing. Invariably, crack propagation tests have been performed under load (or stress) control with R≥0, whilst LCF tests are generally conducted under fully reversed strain control with R= -1 initially. Also the effect of dwell time on the crack growth behaviour of single crystals has not yet been studied. It is well known that loading conditions have a strong influence on crack growth, especially at high temperature where creep and environmental effects can be expected to be important. Therefore, the fatigue crack growth behaviour of single crystal nickel base superalloys subjected to typical LCF loading conditions needs to be further investigated.

2.6. Cyclic Constitutive Model Development

2.6.1. Overview

Inelastic responses, such as creep-plastic interaction, cyclic hardening and softening, ratcheting, and interaction of rate and history dependence in metals have been examined in recent years by the use of sophisticated servo-controlled testing equipment. At the same time, to describe these responses, constitutive modelling of cyclic plasticity and cyclic viscoplasticity has developed markedly. Various models based on different concepts have been proposed and improved by many investigators, for example, two-surface plasticity models based on the concept of the bounding surface in stress space (Dafalias and Popov. [1975], [1976], Krieg, [1975]) and the

nonlinear kinematic hardening rule which has been used extensively by Chaboche and co-workers(Chaboche [1977], [1986], Chaboche and Nouailhas, [1989a], [1989b]). Introducing an intrinsic time measure, Valanis [1971] derived the first version of the endochronic theory which has been improved and used by Valanis and others extensively (Valanis [1980], [1984], Watanabe and Atluri [1986a, 1986b]. The Bodner and Partom viscoplasticity model was constructed in 1972 (Bodner and Partom [1972]) and applied to describe high temperature inelastic deformation under various loading conditions (Chan and Lindhom [1990]; Chan et al [1989], [1990]).

At elevated temperature, inelastic deformation is very complicated. Because creep-plasticity interaction, recovery of hardening, and so on, may take place simultaneously, it is difficult to separate time-independent (plasticity) and time-dependent (creep) deformation. In this case, to take into account creep-plasticity interaction, it is usual to assume unified constitutive models, in which creep strain and plastic strain are regarded as inelastic strain identically. A number of "unified" constitutive models have been proposed for describing inelastic behaviour such as creep, relaxation, plasticity, and viscoplasticity. The unified constitutive models seem to be successful in describing inelastic deformation at elevated temperature, as seen from many recent applications (Blnachrad and Lemione [1988], Chaboche and Nouailhas [1989], Chan and Lindholm [1990], Chan et al [1989, 1990], Eftis et al [1989], Hire and Igari [1985], Inoue et al [1985,1989], Nouailhas [1987,1989], Taguchi et al [1989], Yao and Krempl [1985], Lee and Krempl [1991]).

Modelling of the time-dependent behaviour of single crystal superalloys started with the crystallographic approach. It is assumed that the overall behaviour of a single crystal under given loading condition is controlled by the deformation characteristics of a certain number of active slip systems. The contributions of each slip system are summed up using established procedures of time-independent crystal plasticity theory (Walker & Jordan [1985]; Cailletand [1988]; Dame [1985]). Early developments in the crystallographic approach are attributed to Taylor [1937], Bishop and Hill [1951], and Bishop [1952]. The application of the crystallographic approach to single crystal nickel base superalloys began with the work of Paslay ae al [1970, 1971], and more recently by Dame and Stouffer [1988], Stouffer et al [1990], Walker and Jordan [1985], Cailletaud [1987, 1988]. In general, the constitutive equations which describe the viscoplasticity behaviour of each slip system are similar to the form of other unified constitutive equations in the phenomenological constitutive models.

Since there are a large number of different constitutive models, it is not intended to review the individual models in the following sections. Instead, the fundamental

characteristics of the viscoplasticity constitutive models with particular reference to the unified models will be described in Section 2.6.2, followed by a summary of the applications of constitutive models for single crystal nickel base superalloys.

2.6.2. The Characteristics of the Viscoplasticity Constitutive Models

Inelastic cyclic straining of metals and alloys induce many complex phenomena which have to be described separately or simultaneously by constitutive models. In general, the constitutive equations for the mechanical behaviour of materials are based on either one of the two following thermodynamical concepts:

(a) The present state of the material depends upon the present values and the past history of the observable variables only (total strain, temperature ,etc...)

(b) The present state of the material depends upon the present values of both observable and a set of internal state variables.

The first concept was used for example by Valanis [1971-1980] in the development of the endochronic theory, by Krempl [1975] in viscoplasticity, by Guelin et al [1977] in the hereditary theory with direct memory events.

The second approach has been developed in various ways, using the concept of yield surface in the case of time-independent plasticity and multiplayer (Besseling [1958]) or multiyield surface models (Mroz [1967], Dafallas & Popov [1976], Krieg [1975]). The time-dependency was introduced either by separating plastic and creep strains (Robinson et al [1976]) , taking into account the coupling effects through the hardening rules (Kawai-Ohashi [1987], Contest and Cailletaud [1987]) or in the framework of unified constitutive equations .

During recent years, the development of elastic-plasticity constitutive equations which are suitable for arbitrary loading histories over a broad temperature range is mainly based on the second approach, because it is felt that changes and evolution of microstructure (with deformation) are better described by using a set of internal variables and proper evolution laws for these variables. This is particularly important in the case of non-proportional loading. Since in the unified theory framework plastic strain and creep strain are not separated, the term 'plastic' is often used to represent plastic in time-independent case, and inelastic (plastic and creep) in the time-dependent case. The essential features of these theories are: (1) a flow law

relating the inelastic strain rate and the other observable and internal state variables, (2) an evolution equation for the internal state variables which represent the material's resistance to further plastic flow.

The flow law, or strain rate equation, gives the inelastic strain rate $\dot{\varepsilon}_{ij}^{in}$ in terms of the deviatoric stress $\sigma_{ij}^{'}$ (where $\sigma_{ij}^{'} = \sigma_{ij} - \delta_{ij}\sigma_{kk}$), the internal variables (e.g., K and X_{ij}), and the temperature T, i.e.

$$\dot{\varepsilon}_{ij}^{in} = \dot{\varepsilon}_{ij}^{in} (\sigma_{ij}^{'}, \mathrm{K}, X_{ij}, \mathrm{T}) \tag{2.4}$$

On the other hand, the evolutionary equations describe the rate of change of the internal variables due to stress, current structure and temperature, i.e.

$$\dot{K} = \dot{K}(\sigma_{ij}^{'}, X_{ij}, K, T) \tag{2.5}$$

and

$$\dot{X}_{ij} = \dot{X}_{ij}(\sigma_{ij}^{'}, X_{ij}, K, T) \tag{2.6}$$

Typically, two internal variables are chosen as the minimum set. One internal variable which is associated with kinematic hardening or deformation-induced anisotropy, is often termed as "backstress" and is given by a second-order tensor X_{ij}. Mechanically, back stress X_{ij} defines the centre of the loading or yield locus. This back stress X_{ij} affects the magnitude of the superimposed applied stress needed to produce additional plastic flow and thus produces the Bauschinger effect i.e. the type of anisotropy associated with kinematic hardening. The other internal variable is associated with isotropic hardening effects to describe cyclic hardening or softening. In rate-dependent plastic theories, it is included, most often, as a viscous drag stress, K, implying that the inherent resistance to dislocation glide is dependent upon the deformation history. Hence, these two internal variables are associated with microstructurally local stresses produced by dislocation rearrangements. To describe other experimental phenomena which may be associated with other micromechanisms, additional internal variables can be introduced (Chaboche [1989]).

Formulation of Plastic Flow Laws. The wide number of formulations of flow and evolutionary equations for rate- and history- dependent plastic flow present some

similarities. Basically the unified constitutive models assume that the total strain rate can be divided into elastic and inelastic components

$$\dot{\varepsilon}_{ij} = \dot{\varepsilon}^{e}_{ij} + \dot{\varepsilon}^{in}_{ij} \tag{2.7}$$

The inelastic strain rate $\dot{\varepsilon}^{in}_{ij}$ represents all aspects of inelastic behaviour in both monotonic and cyclic regimes, such as, plastic flow, creep and stress relaxation, etc. Constitutive equations have been formulated either with or without the use of a yield criterion.

All theories developed within the classical framework of thermodynamics with internal variables explicitly assume the existence of a thermodynamic potential (e.g. free energy), from which the relations between state variables and associated thermodynamic forces are defined. Based on this concept, four basic forms of flow law have been identified by Marchand et al [1991], all satisfying plastic incompressibility ($\dot{\varepsilon}^{in}_{kk}$ =0) and the generalised form can be written as:

$$\dot{\varepsilon}^{in}_{ij} = \frac{\partial f(\sigma'_{ij}, X'_{ij}, K, T)}{\partial \sigma'_{ij}} = \lambda(\sigma'_{ij}, X'_{ij}, K, T)(\sigma'_{ij} - X'_{ij}) \tag{2.8}$$

where σ'_{ij} and X'_{ij} are the deviatoric components of stress and back stress respectively, K and T are the drag stress and temperature respectively. The function f(σ'_{ij}, X'_{ij},K, T,) is the flow potential which can be derived from the resolved shear stress rule for slip on every system within the polycrystalline material. $\lambda(\sigma'_{ij}, X'_{ij}, K, T)$ is the plastic multiplier which is intended to represent the resistance of the inelastic state to plastic flow, e.g. hardening and damage.

For example, in the time-independent plastic theory, the Von-Mises flow potential (yield function) is defined as:

$$f = J(\sigma'_{ij}, -X'_{ij},) - R - k \qquad = 0 \tag{2.9}$$

where k is the initial size of the yielding surface, R its evolution (increase or decrease). J denotes the Von-Mises distance between the deviatoric stress σ'_{ij} and back stress tensor X_{ij}

$$J(\sigma'_{ij}, -X'_{ij},) = \sqrt{\tfrac{3}{2}(\sigma'_{ij} - X'_{ij})(\sigma'_{ij} - X'_{ij})} \tag{2.10}$$

The well known Prandtl-Reuss flow rule

$$\dot{\varepsilon}_{ij}^{p} = \lambda \sigma_{ij}^{'} \tag{2.11}$$

can be considered as the particular form when the back stress X_{ij} is zero and the mulitiplier λ is a constant. Equation (2.8) is independent of the yield condition and can only be applied for proportional loading (with no unloading), it states that the material response (plastic strain $\dot{\varepsilon}_{ij}^{p}$) to stress is isotropic and independent of stress-history.

Therefore the difference in the various forms of flow laws rely on the different construction of the flow potential, f, and the plastic multiplier λ.

Evolutionary Equations for Internal Variables. The general framework of the evolutionary equations for the internal variables is usually based on the Bailey-Orowan theory (Poirier [1976]), in which the inelastic deformation occurs under a hardening process evolving with deformation and a thermal recovery process evolving with time. The evolution rate of an internal variable is then the difference between the hardening rate and the thermal recovery rate. Saturation of the drag stress or back stress variables is reached when the effects of hardening and recovery cancel each other in the state variable evolutionary equations. Hence, the general forms of the evolutionary equations for the drag stress K (isotropic hardening variable) and back stress X_{ij} (kinematic hardening variable) are as follows

$$\dot{K} = h_1(K)\dot{\bar{\varepsilon}}^{in} - h_2(X_{ij}, K, T)\dot{\bar{\varepsilon}}^{in} - r_1(K, T) \tag{2.12}$$

$$\dot{X}_{ij} = h_3(X_{ij})H_{ij} - d(X_{ij}, T)D_{ij} - r_2(X_{ij}, T)R_{ij} + w(X_{ij}, T)TW_{ij} \tag{2.13}$$

where $\dot{K}$ and $\dot{X}_{ij}$ are the evolution rates of drag stress and back stress. $h_1(\,)$, $h_2(\,)$ and $r_1(\,)$ in Eq.(2.12) are the hardening function, dynamic recovery function and static thermal recovery functions respectively for K, $\dot{\bar{\varepsilon}}^{in}$ is the equivalent inelastic strain rate, where $\dot{\bar{\varepsilon}}^{in} = \sqrt{\frac{3}{2}\dot{\varepsilon}_{ij}^{in}\dot{\varepsilon}_{ij}^{in}}$. $h_3(\,)$, $d(\,)$ and $r_2(\,)$ are the hardening, dynamic recovery and static thermal recovery function for X_{ij} respectively. The function $w(X_{ij},T)$ represents the hardening or recovery associated with the rate of temperature change. The terms of H_{ij}, D_{ij}, R_{ij} and W_{ij} are the directional indices of $h_3(\,)$, $d(\,)$ and $r_2(\,)$ and $w(\,)$, respectively. The choices of the directional indices and the hardening and recovery functions vary substantially between theories. For example, some models utilise $\dot{\varepsilon}_{ij}^{in}$ (the directional rule) while others employ the

stress deviator σ'_{ij} or the overstress stress deviator $(\sigma'_{ij} - X_{ij})$ as the indices of H_{ij} or D_{ij}.

Similarities between various models proposed on the basis of completely different concepts have been discussed by a number of investigators (Marquis [1979] Chaboche and Rousseleis [1983], Watanabe and Atulri [1986a,b], Ohno & Wang [1990], Ohno [1990]). The fundamental features are the choice of at least two internal variables in the model, one second order tensor variable (back stress) to describe kinematic hardening and one scalar variable (drag stress) to describe isotropic hardening. Additional internal variables may be added only in special cases, depending on the particular material and loading conditions. The significant difference between various models is the difference in the construction of the evolutionary equations of the internal variables. It is important to acknowledge these similarities and differences to be able to understand and develop further the models. This is particularly the case when the anisotropic yield and creep behaviours of single crystal materials have to considered.

2.6.3. Applications of Constitutive Models for Single Crystal Superalloys

A significant feature of the development and application of constitutive models for single crystals is that most investigations have concentrated on the crystallographic approaches. A comprehensive review of the crystallographic constitutive models for nickel base single crystal superalloys has been carried out by the author (Li, [1991]). It is shown that the general procedure in the development of a crystallographic model includes three distinct steps over two operating levels, i.e. macroscopic and microscopic levels, as shown in Fig.2.4.

At the macroscopic level, the constitutive model is also based on a unified viscoplasticity theory, the macroscopic strain is partitioned into an elastic and a inelastic strain as described in Eq.(2.6). The elastic constitutive relations are written directly at the macroscopic level using classical elasticity theory. For cubic symmetry single crystals, the orthotropic elastic constitutive equations are the same as those given in Eq.(2.1). The macroscopic relations between stress and inelastic strains are obtained through the localisation and homogenisation steps linked with the microscopic constitutive equation step, in which the constitutive law is written in the form of relation between the resolved shear stress τ^s on each slip system and the inelastic shear strain rate $\dot{\gamma}^s$ on the same system.

The fundamental requirement for the application of the crystallographic model is the identification of the active slip systems in the single crystal under a given loading condition. Consequently, the advantage of this kind of model is that it is directly based on the physical deformation mechanisms of the single crystal. The different microstructural changes and the deformation characteristics of the various slip systems can be taken into account in the model. It is therefore relatively easy, in principle, to model the influence of crystal orientation, temperature and strain rate on the deformation behaviour of the single crystals, because these effects are related to the number and type of active slip systems during deformation. Hence, the behaviour can be described by involving the corresponding slip systems in the crystallographic model.

However, in practice, there are several disadvantages related to crystallographic models. First, the most general crystallographic model incorporates all the possible slip systems irrespective of their relative importance. For example, there are 30 different slip systems in a cubic nickel base single crystal, but these slip systems are not usually active at same time. The number and type (octahedral or cubic) of active slip systems are dependent on crystal orientation, temperature and loading conditions. Therefore, it is difficult to accurately determine the accurate number and type of active slip systems in the crystallographic model under a given loading condition, especially under a complex loading condition since the slip systems may change with deformation. Second, the constitutive equations in the crystallographic model are written at the microscopic level for each slip system. Consequently, it is not easy to determine the material parameters in the model, and to evaluate the capability of the constitutive equations by experimental tests, since the deformation of each slip system can not be separated in laboratory tests. Third, the interaction of each slip system, for example the cross slip as discussed in section 2.1.2. is difficult to include in the crystallographic models. Finally, an obvious disadvantage is the large number of equations to be solved in the crystallographic model.

The phenomenological constitutive models, especially the unified models as discussed in section 2.6.1 and 2.6.2, have been well developed and applied, with some success, to describe the cyclic plasticity and viscoplasticity behaviour of polycrystalline materials. However, the study of the applicability of these models to the single crystal superalloys is very limited. This may be because the mechanical behaviour of single crystals has mainly attracted the interest of physicists and material scientists in the

past, as single crystals were not widely used as structural materials until the last decade.

An attempt was made recently by Choi and Krempl [1989] to adopt the orthotropic unified theory of viscoplasticity based on overstress (VBO) (developed by Lee and Krempl [1988] for polycrystalline materials) for a cubic single crystal, and to describe the tension/compression tests in the [001], [110] and [111] directions. However, this was only a theoretical study with no experimental investigation. Therefore, the ability of the constitutive theory to model the real deformation behaviour of a single crystal has not been evaluated. Furthermore, the large number of material constants in the VBO model. are not easily to be determined by simple laboratory tests

More recently, the Chaboche viscoplasticity model [1989] was modified by Nouailhas [1990] for modelling the cyclic mechanical behaviour of single crystal CMSX-2 at elevated temperature. Although the model was only used for simple unaxial cases under continuous cycling conditions, it is felt by the author that this would be a promising approach, because the Chaboche model has been widely used for various polycrystalline materials (Chaboche [1986,1989], Chaboche and Nouailhas [1989a, 1989b]). A comparison carried out by the author (Li [1991]) on several cyclic plasticity and viscoplasticity models indicated that the Chaboche model is relatively well, if not better, developed than other several models currently widely used. The Chaboche model is capable of modeling both cyclic plasticity and viscoplasticity phenomena, including the important rate effects and other time dependent processes such as creep, relaxation and recovery (Chaboche [1989]), and it has comparatively few material constants all of which can be determined by simple experimental tests.

Based on above review of the cyclic plasticity and viscoplasticity constitutive models, the Chaboche model was chosen to be used in the present work. The further development of the Chaboche model to model the general cyclic mechanical behaviour of single crystal SRR99 under fatigue-creep conditions will be presented in Chapter 7.

CHAPTER 3

HIGH TEMPERATURE LOW CYCLE FATIGUE LIFE ASSESSMENT

3.1. Introduction

The considerable interest in creep-fatigue life prediction during the last several decades has resulted in a large number of attempts to develop life prediction methods (Manson [1965], Coffin [1973], Ostergren [1976], Halford et al [1977]). Although some methods are commonly applied, no one model has yet gained widespread acceptance for high temperature low cycle fatigue (HT-LCF) life prediction. The primary difficulty in predicting HT-LCF behaviour is the degree of interaction of creep and/or environmental attack, with the fatigue process.

This part of the background review is divided into three sections. First, a number of high temperature low cycle fatigue life prediction methods, which will be used to assess the fatigue-creep life behaviour of single crystal SRR99 in Chapter 8, are briefly described. Then an evaluation of some prominent time dependent models used to predict the HT-LCF behaviour of polycrystalline materials, especially nickel base superalloys, will be reviewed and compared. Finally, taking into account the specific deformation characteristics of single crystals, the application and development of the life prediction models for single crystal superalloys under high temperature low cycle fatigue conditions is discussed.

3.2. Life Prediction Models

3.2.1. Coffin- Manson Law

Most low cycle fatigue prediction techniques at elevated temperature have been extensions of the well-known Coffin-Manson equation (Coffin [1954], Manson [1953]),

$$\Delta\varepsilon_p N_f^{\beta_1} = C_1 \qquad (3.1)$$

where $\Delta\varepsilon_p$ is the plastic strain range, N_f is the cycles to specimen failure, β_1 and C_1 are material constants.

Equation (3.1) has been shown to provide a good method for correlating room temperature fatigue test results for a wide range of materials. Plastic strain range is the only material deformation parameter required, as a measure of damage, for purely time-independent deformation.

At elevated temperature both time-independent and time-dependent inelastic strains may occur. Common engineering practice is to refer to the time-independent inelastic strain as plastic strain, and the time-dependent inelastic strain as creep strain. Therefore, at elevated temperatures, the total inelastic strain, $\Delta\varepsilon_{in}$, is

$$\Delta\varepsilon_{in} = \Delta\varepsilon_p + \Delta\varepsilon_c \tag{3.2}$$

where $\Delta\varepsilon_p$ and $\Delta\varepsilon_c$ are the plastic and creep components respectively.

The extended Coffin-Manson Law (Coffin [1973, 1974]) to elevated temperature low cycle fatigue conditions may be written as

$$\Delta\varepsilon_{in} N_f^{\beta_1} = C_1 \tag{3.3}$$

where β_1 and C_1 are isothermal material constants relevant to the temperature being investigated. When inelastic strain is low in relation to the elastic limit, cyclic life is better described by a combination of the Coffin-Manson (Coffin [1954], Manson [1953]) and Basquin [1910] relations in the form

$$\Delta\varepsilon_T = \Delta\varepsilon_e + \Delta\varepsilon_{in} = \frac{B'}{E} N_f^{-\beta'} + A' N_f^{-\alpha'} \tag{3.4}$$

where B', β', A' and α' are material constants, $\Delta\varepsilon_T$ is the total strain range and E is Young's modulus.

Manson [1965] has further proposed the Universal Slopes Methods for predicting LCF life as

$$\Delta\varepsilon_T = \frac{3.5\sigma_u}{E} N_f^{-0.12} + D^{0.6} N_f^{-0.6} \tag{3.5}$$

where σ_u and E are ultimate strength and Young's modulus respectively, and D=ln[100/(100-RA)] is a measure of the fracture ductility, where RA is a reduction

in area (in %). The implication of this equation is that in the elastic region the fatigue strength is governed by the tensile strength whereas at large inelastic strains it is governed by ductility. This equation defines adequately the LCF behaviour of most materials at room temperature (Manson [1965], Muralidharan and Manson [1988]). At elevated temperature where creep and/or stress relaxation become significant, modification of equation (3.5) is required.

3.2.2. Damage Function Approach

This method was first proposed by Ostergren [1976a] for predicting hold time and frequency effects in LCF at elevated temperature . It follows from the consideration that low cycle fatigue is essentially a problem of crack propagation Therefore only the deformation occurring in the portion of the cycle when the crack faces are open contributes to the state of damage through crack propagation. During the crack closure part of the cycle no localised damaging effects should occur. Hence, the basic assumption of the method is that the net tensile hysteresis energy is a measure of damage and can be approximated by $\sigma_t \Delta\varepsilon_{in}$, where σ_t is the peak tensile stress. The life is predicted by using a power-law relationship between the damage and the life N_f :

$$N_f = C_2 (\sigma_t \Delta\varepsilon_{in})^{\beta_2} \tag{3.6}$$

where C_2 and β_2 are isothermal material constant. Equation (3.6) was shown (Ostergren [1976a]) to include the influence of mean stress in view of the identity

$$\sigma_t = \sigma_m + \frac{\Delta\sigma}{2} \tag{3.7}$$

where σ_m and $\Delta\sigma$ are mean stress and stress range of the fatigue cycle respectively, When the mean stress is zero, Equation (3.6) reduces to the well known Coffin -Manson equation.

3.2.3. Frequency Modified Damage Function (FMDF)

It is well known that the hold times in strain controlled fatigue tests at elevated temperature may have a pronounced effect on cycle life. The effect appears to result from such factors as increased inelastic strain range, change of mean stress, and time dependent damage introduced by hold time. The time dependent damage appears to consist largely of intergranular cracking due to both creep and environmental

reactions (Manson [1973], Coffin [1970], Wells et al [1971]). From the above analysis it is known that equation (3.6) is capable of including the effects of increased inelastic strain range and the change of mean stress caused by the hold time. However, when time dependent damage mechanisms become significant, an additional modification is found to be necessary. This led to the development of the Frequency Modified Damage Function (FMDF) model by Ostergren [1976b].

$$N_f = C_3 (\sigma_t \, \Delta\varepsilon_{in})^{\beta_3} \, \nu^m \tag{3.8}$$

where C_3, β_3 and m are temperature dependent material constants and ν is the frequency. The frequency term selected for use in Eq (3.8) is dependent upon the sensitivity of the material to different waveshapes. If a material is waveshape insensitive, i.e., time dependent damage is independent of waveshape, then, ν is defined as the frequency of total cycling (Ostergren [1976b]).

$$\nu = \frac{1}{T} = \frac{1}{T_o + T_t + T_c} \tag{3.9}$$

where T is cycle period, T_o , T_t and T_c are the continuous cycling, tensile hold and compressive hold times, respectively.

If material is waveshape sensitive, i.e., time dependent damage is dependent on waveshape, then ν is defined as

$$\begin{cases} \nu = \dfrac{1}{T_o + T_t + T_c} & T_t \geq T_c \\ \nu = \dfrac{1}{T_o} & T_t < T_c \end{cases} \tag{3.10}$$

3.2.4. Mean Stress Models

The influence of mean stress in low cycle fatigue has been handled in numerous ways, Nihel et al [1986] has reviewed the capability and accuracy of several models to predict the mean stress effects on fatigue life of unnotched specimens using strain-controlled fatigue tests. The most commonly used methods have been proposed by Morrow [1965] and Smith, Watson and Topper (SWT model) [1970].

For low cycle fatigue with zero mean stress, the fatigue behaviour consists of total, elastic and plastic strain amplitudes versus reversals to failure and is mathematically modelled by the well known Coffin-Manson equation

$$\frac{\Delta\varepsilon_T}{2}=\frac{\Delta\varepsilon_e}{2}+\frac{\Delta\varepsilon_p}{2}=\frac{\sigma_f'}{E}(2N_f)^b+\varepsilon_f'(2N_f)^c \qquad (3.11)$$

where σ_f' is the fatigue strength coefficient, b is the fatigue strength exponent, ε_f' is the fatigue ductility coefficient, c is fatigue ductility exponent and E is Young's modulus.

To account for the mean stress in low cycle fatigue, Morrow (1965) suggested that the mean stress could be taken into account by modifying the elastic term in equation (3.11) by the mean stress, σ_m, such that

$$\frac{\Delta\varepsilon_T}{2}=\frac{\Delta\varepsilon_e}{2}+\frac{\Delta\varepsilon_p}{2}=\frac{\sigma_f'-\sigma_m}{E}(2N_f)^b+\varepsilon_f'(2N_f)^c \qquad (3.12)$$

Morrow's equation (3.12) implies that the mean stress has influence only on the elastic strain-life relationship. According to Morrow, a tensile mean stress can thus be considered to reduce the fatigue strength coefficient, and a compressive mean stress to increase the coefficient.

The Smith, Watson & Topper (SWT) Model has a general strain function form

$$\sqrt{\sigma_{max}(\varepsilon_T/2)E}=f(2N_f) \qquad (3.13)$$

where σ_{max} is the maximum stress at the half-life of each test. This strain function can be derived by manipulation of the low cycle fatigue equation (3.11) as

$$\sigma_{max}\frac{\Delta\varepsilon_T}{2}=\frac{(\sigma_f')^2}{E}(2N_f)^{2b}+\sigma_f'\varepsilon_f'(2N_f)^{b+c}$$

$$=\frac{A}{E}(2N_f)^{\alpha}+B(2N_f)^{\beta} \qquad (3.14)$$

A satisfactory correlation of mean stress data from strain controlled tests has been obtained using the SWT model by several researchers such as Nihei et al [1986], Fatemi et al [1987] and Cordes et al [1988].

However, it should be pointed out that the above mean stress models are used for taking into account the mean stress caused by non-fully reversed strain control or stress control tests under continuous cycling conditions, i.e. mean stress and mean strain both exist. For the mean stress induced by strain dwell during fully reversed strain control (no mean strain) tests, the application of these mean stress models has not been well studied.

3.2.5 Strain Range Partitioning (SRP)

This approach have been used extensively by many investigators (Manson et al [1971], [1975], Manson [1973], Halford et al [1978], Nazmy [1983]). The concept of the strain range partitioning method is that in any hysteresis loop there are combinations of just two directions of straining: tension and compression, and two types of inelastic strains, i.e., time dependent strain (creep) and time independent strain (plasticity). By combining the two directions with the two types of strains, four strain ranges, as shown in Fig.3.1, are obtained.

(i) $\Delta\varepsilon_{pp}$ -- Completely reversed plasticity
(ii) $\Delta\varepsilon_{cc}$ -- Completely reversed creep.
(iii) $\Delta\varepsilon_{cp}$ -- Tensile creep reversed by compressive plasticity.
(iv) $\Delta\varepsilon_{pc}$ -- Tensile plasticity reversed by compressive creep.

These four component strain ranges, $\Delta\varepsilon_{pp}$, $\Delta\varepsilon_{cc}$, $\Delta\varepsilon_{cp}$ and $\Delta\varepsilon_{pc}$ are related, respectively, to N_{pp}, N_{cc}, N_{cp} and N_{pc}, where N_{ij} is the fatigue life when the total inelastic strain is purely one of the strain range $\Delta\varepsilon_{ij}$. These relationships have the normal form of the Coffin-Manson equation,

$$N_{ij} = C_{ij} \quad \Delta\varepsilon_{in}^{\beta_{ij}} \tag{3.15}$$

where C_{ij}, β_{ij} are isothermal material constants for each strain range.

The fatigue life N_f in the complex cyclic condition which includes fatigue- creep interaction at elevated temperature is predicted by the Interactive Damage Rule (IDR):

$$\frac{1}{N_f} = \frac{F_{pp}}{N_{pp}} + \frac{F_{pc}}{N_{pc}} + \frac{F_{cp}}{N_{cp}} + \frac{F_{cc}}{N_{cc}} \qquad (3.16)$$

where $F_{ij} = \frac{\Delta\varepsilon_{ij}}{\Delta\varepsilon_{in}} \qquad (ij \Rightarrow pp, cc, cp, pc)$

Accurate use of strain range partitioning (SRP) method is dependent on a detailed knowledge and analysis of the cyclic stress-strain hysteresis loop for that part of the component which is under consideration, together with a comprehensive description of all the basic component strain range equations for the material and temperature of interest. In principle, determination of the basic lifetime relationships is done by carrying out a series of tests in which the inelastic strain range consists of only the strain combination of interest, but in practice, the "ideal" cycle can only be obtained for the pp strain combination. Therefore, one of the major problems associated with the SRP approach is the requirement for baseline data from complex hold-time tests.

Implicit in the SRP approach is the assumption that stress and temperature alone do not affect the life time relation and that the influence of these parameters is due only to their effect on the inelastic strain range. While it is recognised that environmental effects may also be significant the model does not as yet encompass these, nor is it clear at present how cycles involving strain ratcheting can be processed.

3.2.6. Linear Damage Summation Rule

The usual engineering definition of damage, which ignores the detail of the damage process, corresponds to the life ratios and leads to the use of the linear life fraction assumption for combined fatigue and creep loading

$$\sum \frac{N}{N_{fp}} + \sum \frac{t}{T_c} = 1 \qquad (3.17)$$

where N / N_{fp} is the cyclic fraction of the life fraction and t / T_c the time dependent fraction, N_{fp} and T_c are the life endurances under pure fatigue and creep rupture respectively, with similar loading conditions to the combined fatigue-creep loading.

Equation (3.17) implies that there is no interactive effect of one form of damage on the rate of development of the other. In this case, fatigue damage and creep damage can be defined as

$$\begin{cases} D_f = \dfrac{N}{N_{fp}} \\ D_c = \dfrac{t}{T_c} \end{cases}$$

The linear life fraction rule , in terms of damage cumulative, can be expressed as

$$D = \sum D_f + \sum D_c \leq 1 \qquad (3.18)$$

The Linear Life Fraction Rule which links the Robinson's [1952] rule for creep damage and Miner's [1945] rule for fatigue damage in terms of linear damage summation is purely phenomenological, and has no mechanistic basis. Justification for its applicability is, therefore, limited to conditions where for example the cycle is heavily dominated by one or other fraction. In the case of strain controlled tests with hold times, when creep and fatigue interaction occurs, its application is more difficult to justify. The assumption that tensile and compressive hold periods are equally damaging is contrary to experience, and rupture data for compressive creep are not easy to obtain. Three problems also arise with determination of creep life fraction in this tests. Firstly, the stress continuously relaxes during a strain controlled dwell period; secondly, the stress relaxation is different in successive cycle due to cyclic hardening and / or softening; and finally, the creep rupture properties determined in monotonic tests may not be appropriate to the cyclically hardening or softening materials.

3.3. Application of Life Prediction Methods

The relative merits of one or more of the life prediction methods in predicting the lives of specific materials have been assessed by a number of investigators (Leven [1973], Priest and Ellison [1982], Bernstein [1982], Batte [1983]). To illustrate the type of problem to which life prediction methods are applied in practice and where comparisons can be made between the different methods, four types of laboratory test have been considered:

(1) strain controlled tests with or without hold periods at constant stress or strain,

(2) creep tests under cyclic stress or strain,
(3) creep and fatigue tests performed alternately,
(4) strain-controlled tests under athermal conditions,

Tests of type (4), generally known as thermo-mechanical fatigue tests, will not be included in this review because they are not directly relevant to the isothermal tests considered in this study. Results from tests of types (2) and (3) are too few to allow analysis to be performed which would make life prediction methods to be assessed. The strain controlled fatigue test is the most common test in studying creep- fatigue interactions. Therefore, a review of the application of several life prediction methods will be based on type (1) tests only in the following section .

One of the most comprehensive examinations of the applicability of life prediction methods was presented by Leven [1973]. A series of 20 tests on a 1% Cr-Mo-V rotor forging steel at 538°C, with hold times of up to 1.0 h at constant (tensile) stress or constant (tensile and/or compressive) strain formed the basic data. Analyses were carried out using the linear damage summation method , the frequency-modified Coffin-Manson equation and the strain range partitioning approach. The conclusion was that all of the methods could predict life (cycle to failure) with a factor of 2. With respect to Cr-Mo-V rotor steel, similar conclusions were reached by Kuwabara and Nitta [1977] and by Batte [1983]. Batte has claimed, however, that at low strain ranges the linear damage summation approach gave non-conservative predictions (Batte [1983]). Melton [1982] compared the frequency modified Coffin-Manson method, the strain range partitioning approach and Ostergren's damage function methods, and found the data to be best described by the frequency modified Cofffin-Manson method. Bisego, Fossati and Ragazzoni [1982] claimed better fit of the data with the strain range partitioning approach than with the linear damage summation approach . Based on the comparison of seven different life prediction methods, including the linear damage summation rule, the frequency modified damage function and the strain range partitioning approaches, applied to 1 Cr-Mo-V steel at 565°C, Priest and Ellison [1982] claimed that strain based approaches are generally more accurate than their stress based counterparts. This infers that strain, and not stress, is a more correct parameter with which to describe creep-fatigue damage. For 1Cr-Mo-V steel used in their studies, they found that the damage modified strain range partitioning approach yielded the best prediction.

For nickel based superalloys, Nazmy and Wuthrich [1984] compared the applicability of the strain range partitioning approach, the frequency modified Coffin-Manson

method and the Ostergren damage function approach to life prediction of IN 738 and concluded that the strain range partitioning approach gave the best results. For the same alloy, the ability to predict fatigue lives to within a factor of 2 has been claimed for SRP by Marchionni et al [1986]. However there are also documented instances of the unsuccessful application of strain range partitioning approach to IN 738 and to Rene 95 nickel base superalloys have also been documented (Hyzack [1985]). For a cobalt-based Vane alloy MAR-M 509, the SRP method was found only to predict life within a factor of 3 (Remy et al [1986]). For IN 738 LC, Persson et al [1986] claim better correlation with the Ostergren damage function approach than with the Coffin-Manson relationship. Bernsten [1982] compared the frequency modified damage function and strain range partitioning approaches and reported that the frequency modified damage function method was more successful in life prediction for Rene 95 at 650°C than the strain range partitioning method.

Results from most studies show that even the best of the available methods can predict life only to within a factor of 2 to 3. Some of the cited reasons for these inaccuracies include the failure of the methods to model changing stress-relaxation and creep characteristics caused by strain softening or hardening, the use of monotonic creep data instead of cyclic creep data, and lack of sufficiently extended-duration test data.

It is clear from the above review that there are divergent opinions regarding which damage approach provides the best basis for life prediction. It is also clear that a number of variables, such as test temperature, strain range, frequency, time and cycle type, as well as the length of hold, waveform, ductility of material, and damage characteristics, affect the fatigue life. The conclusions made in any investigation may therefore apply only to the envelope of material and service conditions relevant to a specific application.

3.4. Life Prediction for Single Crystal Alloys

3.4.1. Life Correlation

There has been very little work on the life prediction of single crystal alloys under high temperature low cycle fatigue conditions. Few life correlation studies have been reported in the literature.

The orientation and temperature dependence of low cycle fatigue behaviour of nickel base single crystal Rene N4 was studied by Gabb et al [1986]. Specimens loaded along six crystallographic orientations, [001], [011], [111], [145], [231] and [023] were studied at temperatures of 760°C and 980°C using strain controlled continuous cycling tests. Life correlation with total strain range, inelastic strain range and modulus-normalised-elastic stress range were attempted. The analysis showed that a large amount of scatter is evident in a plot of fatigue life against both total and inelastic strain range at 760°C and 980°C. However the elastic modulus normalisation of the elastic strain range gave a satisfactory life prediction for both temperatures. When correlation with the inelastic strain range, the fatigue life at 760°C appears to be relatively insensitive to crystal orientation. However, when correlated with total strain range, there is a strong orientation dependence due to the effect of elastic modulus on stress response. At 980°C, fatigue life was slightly lower than in 760°C, but remained highly orientation dependent when assessed on a total strain range basis, whereas fatigue life correlated with inelastic strain range showed a modest orientation dependence.

The influence of orientation on the low cycle fatigue of single crystal Mar-M200 at 650°C was studied by Chieragatti and Remy [1991]. Specimens with crystallographic orientations near [001], [111], [213] and [101] were tested under fully reversed strain conditions. Fatigue life was correlated with total strain range, total stress range and plastic strain range respectively. In terms of the total strain range, the orientation dependence of fatigue life was very large. Longer lives were observed for the [001] orientation, while shorter lives were exhibited by the [111] orientation. These results are similar with those obtained by Gabb et al [1989] for single crystal Rene N4 at 760°C and 980°C, as well as the results for single crystal AM1 at 950°C reported by Remy [1993]. Chieragatti and Remy [1991] and Remy [1993] claimed that the orientation dependence was mostly due to the variation of the elastic modulus with orientation. The fatigue life was almost insensitive to specimen orientation using the stress range or the plastic strain range for the range of fatigue lives they investigated.

The marked effect of elastic modulus on the low cycle fatigue life of nickel base single crystal superalloys has also been reported by Anton [1984]. A number of randomly oriented single crystals were tested at 870°C and it was found that the specimens having greater elastic modulus failed at considerably shorter lives.

The creep-fatigue behaviour of Ni-Co-Al-Y coated PWA 1408 nickel base superalloy single crystals was investigated by Miner et al [1982] using specimens with crystal orientations within 7° with the [001]. Both fatigue and creep-fatigue tests were

conducted at 1015°C and 1050°C under total strain range control. Creep-fatigue cycles employed constant stress dwells at the maximum and/or minimum load. The fatigue and creep-fatigue life results were correlated with a model of the form $N_f = \alpha\Delta\sigma^{\gamma}$, where $\Delta\sigma$ is the total stress range and α and γ are temperature dependent material constants. This provided a better correlation than similar single variable models containing the total strain range, $\Delta\varepsilon_T$, maximum stress, σ_t, or the average cycle time t_{avg}. Although the Coffin-Manson model $N_f = C\,\Delta\varepsilon_{in}^{\beta}$ could correlate with most of the test data, a model including both $\Delta\varepsilon_{in}$ and $\Delta\sigma$ provided considerably better correlation than those based on any single parameter, such as $\Delta\varepsilon_{in}$ alone, or two parameter model containing $\Delta\varepsilon_{in}$ and σ_t, or $\Delta\varepsilon_{in}$ and t_{avg}. For both tests at 1015°C and 1050°C, the model $N_f = \alpha\Delta\varepsilon_{in}^{\beta}\Delta\sigma^{\gamma}$ provided the best fit of all.

In terms of hold time effects, it was found that creep did not have great effect on the cycle life of the coated single crystal PWA1480 , except in that it permitted inelastic strain,. The creep-fatigue lives were not much different from those for the continuous cycling tests. Though the fatigue life for tests with tensile dwells was found to be shorter than that produced by other loading cycles, it was only shorter by about 30% on average for other cycle tests. Therefore it was concluded that neither creep nor environmental degradation significantly affected the fatigue and creep-fatigue life of the coated single crystal PWA1480. Miner et al [1982] claimed that this is because the mechanisms of creep degradation in polycrystalline alloys such as grain boundaries cavitation or sliding obviously cannot occur, and also because the environment could not affect the internal crack propagation mode of failure because of the coating.

3.4.2. Overview on Model Development

Orientation Dependence. Due to the highly anisotropic mechanical behaviour, it is expected that the LCF endurance of single crystal nickel base superalloys will be strongly dependent on orientation. This has been shown by previous studies (Gabb et al [1986], Chieragatti and Remy [1991]). Furthermore, the orientation dependent creep fatigue properties may show a quite different correlation with other mechanical properties than seen in polycrystalline alloys. For instance, it is well recognised (Halford et al [1977], Miller et al [1984], Gabb et al [1986]) that for polycrystalline alloys, fatigue life assessed on an inelastic strain basis can often be related to tensile ductility. The lower the ductility, the lower the creep-fatigue endurance. However a contrasting result has been reported by Gabb et al [1986] for nickel base single crystal Rene N4. Although the tensile ductility of a specimen in a [011] orientation

was higher than that of the [001] orientation (0.73 and 0.19 for [011] and [001] respectively at 750°C), the [001] specimen displayed a superior fatigue life compared with that of the [011] specimen. Miner et al [1986] claimed that this may have resulted from different inelastic deformation mechanisms (active slip systems) acting during fatigue. Hence, further research work is required to assess the influence of orientation in the low cycle fatigue life prediction methods for single crystal nickel base superalloys.

Time-Dependent Damage Mechanisms. As documented by extensive testing reported in the literature for polycrystalline alloys (Coffin [1973], Manson [1973], Ostergren [1976], Priest et al [1983], Miller et al [1984], Reuchet and Remy [1983], Viswanathan [1989], Plumbridge and Ellison [1987]), the time-dependent damage that develops in high temperature low cycle fatigue consists, for the most part, of intergranular damage resulting from a number of processes such as grain boundary sliding and the stress-controlled diffusion of vacancies to grain boundaries, and crack development due to environmental interactions. Environmental effects such as oxidation are frequently more prevalent along grain boundaries since diffusion along the boundaries is faster and particles prone to oxidation may also be located on these boundaries. The resultant effect of such time-dependent damage is often a transition in the manner of crack propagation through a specimen from one of purely transgranular propagation to one with an increased proportion of intergranular cracking. For polycrystalline alloys, the time-dependent damage mechanisms may generally be related to grain boundaries. However, for a single crystal superalloy, there is not any grain boundary for the development of above kind of time-dependent damage, and, as a result, intergranular cracking mode will be absent. Therefore, further study of the time-dependent damage mechanisms and creep-fatigue interactions under low cycle fatigue conditions for single crystal nickel base superalloys is needed to clarify their role in the life prediction models.

CHAPTER 4
EXPERIMENTAL PROGRAMME

4.1. Material and Specimens

The material used in this work is the single crystal SRR99, a high γ' volume fraction nickel base superalloy. Its composition is given in Table 4.1. The material was provided by Rolls Royce in the form of specimens. The material was fully heat treated, i.e. solution treated, plus 1 hour at 1100°C as a dummy aluminising treatment and then ageing for 16 hours at 870°C. The microstructure of SRR99 after the above heat treatment consisted of regularly packed cube-shaped coherent γ' particles in a face-centred cubic (f.c.c.) matrix γ. The volume fraction of γ' is about 60%. The crystal orientation of each specimen was measured by Rolls Royce using the Laue back reflection X-ray technique.

Two specimen geometries, a smooth bar specimen (Fig.4.1) and a corner crack specimen (Fig.4.2), were used. Both geometries were button ended specimen with alignment and loading faces perpendicular to the specimen axis. The smooth bar specimen had a parallel gauge length with a circular cross section of diameter about 8.5 mm, and was used to examine the deformation properties and low cycle fatigue (LCF) behaviour. The corner crack specimen had a gauge length of square cross section (7x7 mm) and a notch of 0.3mm surface length at one of the corners (Fig.4.2), and was designed to investigate crack growth characteristics of SRR99 under similar fatigue-creep conditions experienced in LCF tests.

4.2. Experimental Equipments and Measurements

4.2.1. Test Machine

The tension-compression rig used was a Mand Servohydraulic test machine (type 302-100). The machine has a capacity of ±100 KN and can be controlled in load, position or extension modes. A 'BBC B' microcomputer was used to generate a triangular waveform command signal, with the option of introducing hold periods at tensile or compressive peaks. Loads were measured by an AC conditioning signal to eliminate the interference caused by the radio frequency (RF) generator and associated heating coil. The machine load cell was calibrated against a standard load cell and was found to be accurate to within 0.1% of range. Alignment of the loading column was checked using a strain-gauged specimen. Bending stresses on the

specimen were less than 2% of the applied stresses. Electrical insulation of the specimen from the load frame was achived by fitting 'Tufnel' plates and bushes in flanges at the top and bottom of the loading rods, thus allowing potential drop (PD) crack growth measurement to be used.

4.2.2. Extensometry

Since strain was the control parameter in all tests, an accurate and reliable strain measurement was essential. The extensometer used in this work was a MTS High Temperature Axial Extensometer (Fig.4.3). This is a side contacting extensometer with two ceramic quartz rods being located by spring pressure onto the side of the gauge length of the specimen. Specimen deflections are transmitted to the extensometer body by the movement of the rods. The extensometer body contains a strain gauged beam bent by the rod deflection. Beam bending unbalances the strain gauge bridge and produces an output proportional to specimen deflection. The extensometer body was mounted within a heat shield, and both body and shield were cooled by a compressed air blast or by cooling water. The 'hold down' force for the extensometer is provided by a pair of flat springs which act directly onto the ends of the quartz rods; these springs also provide an upward force to compensate for the extensometer's weight. Calibration of the extensometer is performed using a split specimen and clip gauges. The extensometry was calibrated so that an output of 1 volt is obtained from a displacement of 30μm, Fig.4.4.

4.2.3. Temperature Control and Heating

Specimen heating was by an ideal induction 10KW RF induction heater. The water cooled heating coil consisted of five turns of 1/8" copper tube all wound in the same direction: two turns at each end of the specimen provide most of the heat input while a single turn of larger diameter maintained the temperature in the centre of the gauge length. The coil diameter and spacing were found by experiment to give temperature gradients within ± 3°C over the specimen gauge. Temperature control was achieved by using a Pt/Pt 13% Rh thermocouple, attached to the specimen in the centre of the gauge length coupled to an Eurotherm 3 term controller. Two further thermocouples were mounted at the ends of the gauge length to monitor temperature. Since temperature distribution within the specimen was very sensitive to coil position, great care was needed to ensure that the coil was placed in exactly the same position each time the specimen was set up.

In the tests performed by Ellison et al [1984] the thermocouple were attached to the specimen by pulling the thermocouple junction onto the surface of the specimen with a length of nichrome wire wrapped around the specimen. At high temperature (900°C and 1000°C), creep occurs in these wires and consequently during long tests they may fail causing the test to be stopped. A system was developed which used spring loaded ceramic probes to hold the thermocouples onto the specimens (Fig.4.5). This allowed testing at temperatures up to 1100°C.

4.2.4. Crack Growth Measurement

On corner crack specimens, fatigue crack growth was monitored using the direct current potential drop (DCPD) technique and using a MAYES PD system. Two large strips of nimonic sheets were spot-welded on the top and bottom parts of the specimen, Fig.4.6, outside the gauge length, to provide a constant 15 A direct current through the specimen. To measure the PD in the vicinity of the crack, 50μm diameter pure nickel wires were carefully spot-welded on either side of the notch. Two nickel wires were also spot-welded on the specimen away from the notch to act as the PD reference leads, Fig.4.6. To protect the monitoring leads, the wires were insulated with a heat resistant sleeving. Additionally to ensure that the spot welds were not subjected to undue damage the sleeved leads were secured with a small trip of nimonic sheet at a position outside the gauge length of the specimen.

According to Rolls Royce [1989], the positioning of the monitoring wires on the both sides of the notch is critical particularly for the purpose of calibration of voltage as a function of crack length during crack growth. Since it was anticipated that accurate positioning (within ±0.3mm) could not be achieved for each specimen it was decided that the most practical approach was to position the wires as accurately as possible and then to carry out post test measurement to subsequently provide a calibration curve for each test. The detailed calibration method will be given in Chapter 5.

4.3. Test Procedures

Prior to setting up each test the aligment of the loading and specimen was checked by looking for specimen bending with a clip gauge. At each stage in the setting-up procedure checks were performed to examine the elastic response of each specimen and to check the response of the extensometer and load cell. Any major deviation from an expected value indicated a problem with equipment calibration, extensometer set-up or the crystallographic orientation in the specimen.

Except for the additional basic mechanical properties tests, which were performed under strain control at a strain rate of $2\times10^{-5}\ s^{-1}$, all the high temperature fatigue-creep tests, including low cycle fatigue tests and corner crack tests, were conducted under fully reversed total strain control at a strain rate of $4\times10^{-3}\ s^{-1}$. Four types of different loading, i.e. continuous cycling (denoted 0/0), cycling with tensile (t/0) or compression (0/t) and balanced dwell (t/t) were used for the fatigue tests. A schematic of the cycle types is shown in Fig.4.7. In all the tests with dwells at peak tensile or compressive strain, the dwell time was 2 minutes. This time was defined in the project specification by Rolls Royce. It was an adequate period for a significant degree of stress relaxation at high temperatures.

Throughout the tests, a continuous record was made of the load-time and strain-time history in both low cycle fatigue and corner crack tests, as well as the PD output-time history in the corner crack tests. Hysteresis loops were also recorded regularly throughout the tests using a X-Y recorder. Specimen failure of the smooth bar tests was defined as fracture of the specimen or as a 30% drop off in load range from the load saturation plateau, depending on which occurred first.

Each corner crack specimen was first precracked at room temperature to create a sharp tipped crack approximately 1mm long on the surface under stress control at a frequency of 0.5 Hz with a stress ratio, R, of 0.1. Then, high temperature tests were performed under the same temperature and loading conditions as in the smooth bar tests. The extension of crack growth at high temperature was limited to about 1mm for two reasons: firstly, to obtain detailed information about consequences of a small amount of crack growth, and secondly to prevent complete failure of the specimen so that a post test measurement of crack length could be made for PD calibration purposes.

4.4 Test Matrix

Tests to determine the basic mechanical properties of single crystal SRR99 were performed to investigate the influence of orientation and temperature. Of particular interest was the elastic modulus and yield stress. The elastic modulus was measured for all the low cycle fatigue and corner crack specimens at both room temperature and at either 750°C, 950°C or 1050°C. In addition, six special tests using specimens with substantially different orientations were performed at 20°C, 300°C, 600°C,

750°C, 850°C, 950°C and 1050°C to systematically study the orientation and temperature dependence of the elastic behaviour of SRR99. The orientations of these specimens, using a unit stereographic triangle, are shown in Fig.4.8a.

Three specimens with significantly different orientations (Fig.4.8b) were used to conduct yield stress measurement tests at temperature of 20°C, 300°C, 600°C, 750°C, 850°C, 950°C and 1050°C. The same specimen was used repeatedly in tension/compression tests at different temperatures to eliminate errors due to variation in orientation between specimens.

The test matrix for low cycle fatigue tests using smooth bar specimens is given in Table 4.2. A total of 33 tests; 11 at 750°C, 15 at 950°C and 7 at 1050°C, were carried out. Among them 13 tests were subjected to continuous cycling (0/0), 9 tests and 8 tests with compressive (0/t) and tensile (t/0) dwells respectively, and 3 tests with balanced (t/t) dwells. The crystal orientation of the specimens used for tests at 750°C, 950°C and 1050°C are shown in Fig.4.9a, Fig.4.9b and Fig.4.9c respectively.

Table 4.3 shows the test matrix for corner crack tests. The total number of specimen tested was 24, with 7 tests at 750°C, 10 tests at 950°C and 7 tests at 1050°C. The crystal orientations of corner crack specimens are given in Fig.4.10a, Fig.4.10b and Fig.4.10c for tests at 750°C, 950°C and 1050°C respectively. It can be seen that variations in the crystal orientation for corner crack specimens was much smaller than that for smooth bar specimens. Most of the orientations for corner crack specimens were within 10 degrees of the [001] orientation.

CHAPTER 5
EXPERIMENTAL RESULTS

5.1. Introduction

This chapter presents the overall test results, including the tests on fundamental mechanical properties, low cycle fatigue behaviour and crack growth characteristics of single crystal SRR99. A summary of the additional tests on the high temperature elastic properties (labelled as HTE tests), and on the yielding strength (labelled as STP tests), of single crystal SRR99 are given in Tables 5.1a and 5.1b respectively. The test results for the smooth bar specimens under fatigue-creep conditions are given in Tables 5.2a, 5.2b and 5.2c for tests at 750°C , 950°C and 1050°C respectively. The corner crack tests at 750°C, 950°C and 1050°C are summarised in Tables 5.3a, 5.3b and 5.3c respectively.

The presentation of the results in this Chapter is divided into three parts; (i) deformation properties, (ii) fatigue and fatigue-creep life behaviour and (iii) crack growth behaviour.

5.2. Deformation Properties

5.2.1. Elastic Properties

As shown in Tables 5.1 and 5.2, significant variations of elastic modulus in smooth bar specimens were observed at both room temperature and high temperatures, whilst the changes of elastic modulus for corner crack specimen are relatively very smaller in comparison with smooth bar specimens. This is a result of the large differences in the crystal orientation of the smooth bar specimens as demonstrated in Fig.4.8 and Fig.4.9. The variation of elastic moduli at 20°C and 950°C for different orientations is shown in Fig.5.1. It can be seen that the elastic moduli vary considerably with the crystal orientation, the trends being similar at both temperatures. The elastic modulus was higher for specimens with an orientation close to the [111] and lower for specimens near the [001] orientation, with a smooth variation between these two extremes.

Figure 5.2 presents the elastic modulus as a function of temperature, obtained from the additional elastic modulus measurement tests. The elastic modulus generally decreases with increasing temperature for all specimen orientations, with near [001] specimens showing the lowest value for E and near [111] specimens exhibiting the highest value for E over the temperature range from 20°C to 1050°C. Another interesting feature is the change in the slope dE/dT, where T is temperature, at temperature about 650°C, this temperature appears to be independent of crystal orientation.

5.2.2. Yielding Behaviour

The yield stress of SRR99 as a function of temperature was obtained from the additional tests for the three orientations subjected to unidirectional tension and compression and is presented in Fig.5.3. The results provide an overview of the temperature and orientation dependence of the yield strength of single crystal SRR99. All specimen orientations show a yield strength plateau between room temperature and 600°C, followed by an increase in yield strength with temperature between 600 to 750°C. A significant drop in strength occurs beyond 750°C, although the rate of decrease is less for temperatures beyond about 900°C. Such behaviour is typical of high γ' volume fraction nickel base superalloy single crystals and has been documented for several similar nickel base single crystal systems. (Nathal et al [1982], Shah and Duhl [1984], Walter et al [1987].

At elevated temperatures, it is well known that yielding can be associated with a thermally activated processes, therefore the temperature dependence yield strength data can be presented in the form of an Arrhenius-type relationship. Fig.5.4 is a plot of the modulus-normalised yield strength σ_y / E as a function of the inverse of temperature (1/T) and represents a relationship of the form;

$$\frac{\sigma_y}{E} = A[\exp(\frac{Q'}{RT})] \qquad (5.1)$$

where σ_y — Yield strength

E — elastic modulus at temperature T

Q' — apparent activation energy

A — material constant

R — gas constants

Fig.5.4 illustrates three distinct temperature regions which can be distinguished for the orientations examined for at both tension and compression. In each temperature region, the orientation dependence of yield strength is well represented by parallel lines on the diagram. At low temperatures (below 600°C), the apparent activation energy Q' was equal to zero, and thermal activation is not a important factor in this temperature region. At high temperatures (above 750°C), Q' is approximately constant, equal to 50KJ/mol, which is similar to the value for PWA1480 (Walter et al [1987]). It is apparent that the activation energy is nearly independent of temperature and orientation as well as the applied stress direction, i.e. tension or compression. At intermediate temperatures, a transition from the low temperature to the high temperature behaviour occurred. The unusual negative activation energy for Q' observed in this temperature region, which have also found for several similar nickel base single crystal superalloys (Shah and Duhl [1984], Miner et al [1986]), is not well understood in terms of its physical aspects. Since yield strength results were obtained only at 600°C and 750°C, it is not clear whether the boundary of the temperature transition region depends on crystal orientation and applied uniaxial stress senses as reported for other nickel base single crystals (Heredi and Pope [1986]).

From Fig.5.3, it can be seen that the orientation dependence of yield strength was not significant above 750°C. Below 750°C, specimen STP1 (near [111] orientation) has largest compressive yield strength, but it only has the largest tensile yield strength below 300°C. Above 300°C, the largest tensile yielding strength is found in the specimen STP2 with orientation near the [001]. The tension-compression asymmetry can be seen more clearly in Fig.5.5, where the tensile and compressive yield stresses are compared for each specimen as a function of test temperature. The yield stress of specimen STP1, (near [111] orientation), was lower in tension than in compression (Fig.5.5a), and the reverse is true for specimen STP2, (near [001] orientation) (Fig.5.5b). Specimen STP3, which was in the middle of the standard stereotriangle, exhibited no significant tension-compression yielding strength asymmetry (Fig.5.5c)

5.2.3. Cyclic Hardening/Softening Characteristics

Figure 5.6 shows the variation of the total stress range, $\Delta\sigma$, versus the number of applied cycle, N, normalised with respect to the fatigue life, N_f, obtained at different strain ranges for the four cycle types at 950°C. It can be seen that SRR99 exhibits cyclic stability when subjected to continuous cycling . However when 2 minute dwells at tensile or compressive peak strains were introduced, cyclic softening was

observed in both unbalanced (dwell in tension or compression) and balanced (dwell both in tension and compression) cycles. In the unbalanced cycle , cyclic softening occurs rapidly at the first 10% of life. At higher stress ranges, the extent of cyclic softening is greater. After this early softening stage, the stress ranges are essentially constant during the remaining life. For balanced dwell cycles , continuous cyclic softening was apparent, with the stress range reducing rapidly during the first 5-10% of life, and then dropping continuously at a lower rate until about 75% of life, when final unstable behaviour occurred.

At 1050°C, SRR99 exhibited cyclic softening, as shown in Fig.5.7, for all cycle types. However, higher softening rates were observed for tests with tensile or compressive dwells in comparison with continuous cycling tests.

At 750°C, SRR99 showed cyclic stability, Fig.5.8, regardless of the cycle type. This can be partly attributed, as will be discussed in Chapter 6, to the tests at 750°C being dominated by elastic behaviour.

In order to compare the hardening/softening behaviour at different temperatures, a hardening/softening parameter, HF, is defined as:

$$HF = \frac{\Delta\sigma_N - \Delta\sigma_1}{\Delta\sigma_1} \qquad (5.2)$$

where $\Delta\sigma_1$ and $\Delta\sigma_N$ are the stress ranges at the initial and cycle N respectively. Positive HF values indicates cyclic hardening whilst negative HF values describes softening.

A systematic comparison between the cyclic softening behaviour of SRR99 for tests at 750°C, 950°C and 1050°C, in terms of HF, at 20 percent and 80 percent life, is given in Table 5.4. It is seen that the cyclic stability of SRR99 depends on both cycle type and temperature. At 750°C, SRR99 showed cyclic stablility regardless of cycle type. At 950°C, a stable response was only observed in the continuous tests (0/0), while cyclic softening was found in tests with both unbalanced (0/t, t/0) and balanced (t/t) dwells. However, at 1050°C, all the tests with or without dwells exhibit cyclic softening response. The level of cyclic softening for tests with tensile dwell is generally larger than that for tests with compressive dwell, and the balanced dwell exhibits the largest cyclic softening at both 950°C and 1050°C. By comparing results from tests at 950°C and 1050°C, it is evident that

temperature enhanced the cyclic softening, with cyclic softening rates higher at 1050°C than that at 950°C under same loading conditions.

5.2.4. Cyclic Stress-Strain Response

The cyclic stress-strain response, in terms of total strain range for the tests under various cyclic loading conditions, are shown in Figs 5.9a, b and c for tests at 750, 950 and 1050°C respectively. The values of the orientation parameter A_{hkl} for some of the specimens, are also shown in Fig.5.9. This orientation parameter is defined in Chapter 6 (see Section 6.1) as $A_{hkl} = \left(h^2k^2 + k^2l^2 + h^2l^2\right) \Big/ \left(h^2 + k^2 + l^2\right)^2$, A_{hkl} varies from zero for the [001] orientation to 1/3 for the [111] orientation and is intermediate between these values for other orientations. From Fig.5.9, it is evident that the cyclic stress-strain behaviour is highly orientation dependent for the three temperatures. At the same total strain range, specimens with orientations close to [111] exhibited the largest stress range, whilst specimens near the [001] orientation displayed a lower stress range.

Figures 5.10a and Fig.5.10b show the relationships between total stress range and the cyclic inelastic strain range for tests at 950°C and 1050°C respectively. For the tests at 750°C, it was found that the inelastic deformation was very small in comparison with elastic strain. Consequently, it is difficult to quantify the inelastic strain range in each test. From Fig.5.10, it can be seen that the cyclic stress-strain response in terms of inelastic strain range exhibited a cycle type dependent feature. The introduction of strain dwells either in tension or in compression increased the inelastic deformation. The influence of crystal orientation may also have some effect on the inelastic deformation response, but based on the limited test data, no consistent orientation effect can be identified. The test results shown in Fig.5.11, obtained from continuous cycling tests at 950°C, do not appear to be sensitive to orientation.

5.2.5. Stress Relaxation Behaviour

The amount of stress relaxation occurring during each hold, at maximum (tensile) and minimum (compressive) strains, obtained from the tests at 950°C is shown in Fig.5.12a and Fig5.12b . The stress relaxation behaviour for tensile or compressive dwell tests is similar, that is, stress relaxation occurrs rapidly during the first 5% of life after which the degree of stress relaxation is considerably reduced. For the

balanced dwell tests (shown in Fig.5.12c) stress relaxation behaviour is found to be different from the results obtained from the unbalanced dwell tests. At the start of the test, for about 5% of life, the amount of stress relaxation in a tensile dwell (denoted by $|\partial\sigma^+|$) increases with increasing cycle number, whilst the amount of stress relaxation in the compressive dwell (denoted by $|\partial\sigma^-|$) decreases. Thereafter, for most of the remaining life, the amount of stress relaxation in both tensile and compressive dwells increases steadily and the magnitude of stress relaxation in tension and in compression is approximately equal although $|\partial\sigma^+|$ is slightly larger than $|\partial\sigma^-|$. The total amount of stress relaxation $|\partial\sigma| = |\partial\sigma^+| + |\partial\sigma^-|$ increases steadily with increasing numbers of cycle. The influence of crystal orientation on stress relaxation behaviour is shown in Fig.5.13 by the comparison of two specimens with orientations close to [001] and [111] respectively. Since the initial stress level preceeding stress relaxation strongly depended on crystal orientation, the total amount of stress relaxation for different orientations is different. However, the stress relaxation behaviour as a function of cycle number was observed to be similar.

Figures 5.14 illustrates the stress relaxation response at 1050°C as a function of cyclic life fraction for tests with tensile, compressive and balanced dwells. In the early stages of each test the stress relaxation response at 1050°C is similar to that at 950°C, i.e., a large amount of stress relaxation occurred during the first 5% of life. However, after this initial stage, the stress relaxation response at 1050°C is different to that at 950°C. The total amount of stress relaxation remains almost constant up to 50% of life and then increases again with cycle number thereafter, rather than being constant until failure as in the 950°C tests.

At 750°C, the total amount of stress relaxation for all the tests is very small, since the tests are dominated by elastic behaviour as indicated by the cyclic stress-strain response.

The total amount of stress relaxation, $|\partial\sigma|$, obtained at half life cycle ($(N/N_f = 50\%)$) as a function of total strain range, $\Delta\varepsilon_T$, for tests at 950°C and 1050°C are given in Fig.5.15 and Fig.5.16 respectively. The values of the orientation parameter, A_{hkl}, for some specimens are also included in Fig.5.15 and Fig.5.16 to illustrate the influence of crystal orientation on the stress relaxation behaviour. The results indicate significant orientation dependent characteristics. At the same total strain range, specimens near [111] exhibit the largest degree of stress relaxation whilst specimens near [001] reveal the lowest amount of stress relaxation. The degree of stress relaxation increases as the crystal orientation moves away from [001].

5.2.6. Mean Stress Response

The strain dwell at peak strain during creep-fatigue loading resulted in stress relaxation. As a result significant mean stress effects were observed in tests with tensile or compressive dwells at 750°C, 950°C and 1050°C. At 750°C, even though the total amount of stress relaxation is very small, the mean stresses induced by the strain dwells was significant. Therefore, although all the tests were conducted under completely reversed strain control with a strain ratio $\varepsilon_{min}/\varepsilon_{max}=-1$, the stress ratio R($\sigma_{min}/\sigma_{max}$) changes according to the cycle type. Since mean stress $\sigma_m=\sigma_{max}$ (1+R)/2, the mean stress response can be alternatively represented by the stress ratio. Stress ratios larger than -1, less than -1 or equal to -1 represent negative, positive and zero mean stress respectively. A comparison of stress ratio as a function of cyclic life fraction at 950°C is given in Fig.5.17 for continuous cycling (0/0), compressive dwell (0/t) and tensile dwell (t/0) tests as well as balanced dwells (t/t) tests. It can be seen that compressive dwells induced significant positive mean stress (R>-1) and tensile dwells lead to large negative mean stress(R<-1). Some positive mean stress and negative mean stress values are also observed for the continuous tests and balanced dwells tests.

Similar mean stress behaviour have been observed in tests at 750°C, Fig.5.18, and 1050°C, Fig.5.19. In general, the stress ratio increases or decreases very quickly during the first 10 percent of life and then remains essentially constant or changes slowly with increasing numbers of cycle. It is also observed that the magnitude of the stress ratio decreases for tests with tensile dwell (t/0) and is larger than the increase for tests with compressive dwell, i.e. the absolute values of mean stress in tensile dwell tests are generally larger than those for compressive dwell tests.

The effect of orientation on mean stress response is presented in Fig.5.20. It is found that the influence of orientation is associated with the difference in inelastic deformation between tests with same total strain ranges. The lower the inelastic strain, the larger the mean stress. The specimens with orientations close to [111] exhibit larger inelastic deformation compared with the near [001] orientation specimens. As a result the mean stress level for near [111] specimen is observed to be lower than that for near [001] specimen.

5.2.7. Corner Crack Tests

The global deformation responses, including cyclic softening behaviour, the mean stress response and stress relaxation during strain dwells etc., of corner crack tests for the small crack extensions studied in this work were found generally to be similar to the mechanical behaviour of the smooth bar tests presented in the previous sections.

As an example, Fig.5.21 shows the mean stress response for some of the corner crack tests at 950°C. The mean stress behaviour observed in corner crack tests and smooth bar tests is very similar. A compressive dwell induces a significant positive mean stress (R<-1), and a tensile dwell leads to a large negative mean stress (R>-1), while the continuous cycling tests and tests with balanced dwell generally exhibits a minimal mean stress response.

Other test results on the cyclic mechanical behaviour obtained from corner crack tests will be given in Chapter 6, and compared with orientation modified cyclic mechanical response of smooth bar tests.

5.3. Fatigue Life Behaviour

5.3.1. Correlation with Total Strain Range

Fatigue lives of single crystal SRR99 smooth bar specimens in terms of total strain range are shown in Figs.5.22a, b and c for tests at 750°C, 950°C and 1050°C respectively. The values of the orientation parameter A_{hkl} for some of the specimens are also shown in Fig.5.22 to illustrate the influence of crystal orientation. It is evident that the fatigue life is highly orientation dependent for all the tests with or without strain dwells at the three temperature studied. The [001] orientation, for a given total strain range and cycle type, exhibits the longest fatigue life. The fatigue life decreases as the orientation moves away from [001]. It is also observed that cycle type has a large influence on the fatigue life behaviour.

At 750°C, for the tests using specimens with similar orientations (i.e. specimens sb7502, sb7506, sb7503 and sb7510), unbalanced dwell tests exhibited significantly different fatigue lives compared with continuous cycling tests. At the same strain

amplitude, a test with compressive dwell (sb7506) showed remarkably shorter life than that of a continuous tests (sb7502). In contrast, a test with a tensile dwell (sb7510) revealed a significantly longer life than that of a continuous cycling test (sb7503).

The fatigue lives at 1050°C, in terms of total strain, exhibit a totally different cycle dependence compared with those at 750°C. Introduction of a dwell, either in tension (sb1506) or in compression (sb1504) reduced fatigue life compared with a continous cycling test (sb1502) at 1050°C, and a tensile dwell exhibited a more damaging effect than a compressive dwell.

5.3.2. Correlation with Inelastic Strain Range.

Fatigue life at 950°C as a function of the inelastic strain range at half life is plotted in Fig.5.23. It can be seen that no significant and consistent orientation dependence, such as in Fig.5.22 b is evident. However, a significant cycle type dependent life behaviour is observed in terms of inelastic strain range. Continuous cycling (0/0) and fatigue-creep tests with compressive dwells (0/t) exhibited the same life behaviour, while fatigue-creep tests with tensile dwells (t/0 and t/t) have the longer lives in comparison with continuous cycling and compressive dwell tests.

The fatigue life behaviour of SRR99 at 1050°C, in terms of inelastic strain range, is plotted in Fig.5.24, there is no significant and consistent cycle type dependent characteristics, such as seen in Fig.5.23 for tests at 950°C. All the test results obtained from the limited tests, including continuous cycling tests and tests with tensile or/and compressive dwells appear to fall within the same scatter band.

5.4 Crack Growth Behaviour

5.4.1 PD Calibration

A theoretical PD calibration for a corner crack specimen was obtained by Pickard [1981] by finite element analysis. Fig 5.25 shows the corner crack specimen with definitions of the PD parameters. The potential across the crack V_c is normalised with respect to the remote potential gradient $V_{grad}=V_{rem}/X$, where X is the distance between the remote potential PD leads. The variation of normalised PD with crack length is given by

$$\frac{V_c}{V_{grad}} = \frac{4a}{\pi} - z - \frac{2z}{\pi}\sin^{-1}\left[\frac{a^2 - z^2}{a^2 + z^2}\right] \qquad (5.3)$$

where 2z is the distance between the potential leads spot welded across the notch. As $z \to 0$, V_c corresponds to the measured PD across the crack alone. However when $z > 0$, V_c corresponds to the perturbed potential drop. The measured PD , V_m, is given by

$$V_m = V_c + 2zV_{grad} \qquad (5.4)$$

The above PD calibration implies that for the same crack length a, the PD output voltage V_m should same for different tests if z is a constant , because V_{grad} should be a material constant. However, as the experimental work progressed in this study , it was found that the PD output for tests with similar crack length were significantly different. Therefore the theoretical PD calibration, Eq.(5.4), obtained by Pickard [1981] for corner crack specimen appeared unreliable for the high temperature tests, probably because of the use of an induction heating system. In order to obtain a suitable PD calibration method, the interaction of the induction heating system and the PD measurement system was studied and the details of the analysis are given in Appendix II.

Based on the analysis, a calibration precedure was performed based upon matching experimental values of the change in crack length, Δa , and PD voltage change, ΔV_m. Figs 5.26a, b, c and d show the experimental results for ΔV_m and Δa from the fatigue and fatigue-creep tests at 750°C, 950°C 1050°C respectively together with the results at room temperature obtained during fatigue pre-cracking and after high temperature tests. It can be seen that there is an almost linear relationship between ΔV_m and Δa for all the case where

$$\Delta V_m = \eta\, \Delta a \qquad (5.5)$$

where η is a temperature dependent material constant. The values of η obtained from the experimental data for tests at different temperature are given in Table 5.5. It can be seen that η increases with temperature, which corresponds to the increase of the electrical resistivity of the material with temperature.

Therefore, in the crack growth tests, each test was interrupted prior to specimen failure and the crack length is measured by microscope. This value, together with the final PD value, could be used to calibrate the test PD data using Eq.(5.5).

5.4.2 Crack Growth Characteristics

The morphology of crack growth in single crystal SRR99 was found to be significantly different at room temperature (fatigue pre-cracking) to that under fully reversed cyclic loading at high temperature. The crack growth direction at room temperature was observed to be associated with crystallographic features, occurring on the {111} planes. However, at high temperature, crack growth directions were generally normal to the applied stress axis, i.e. mode I crack growth in the [001] directions, although a few irregular crack growth directions were also observed in some tests, which can be attributed to the influence of secondary orientation as pointed out by Defresene and Remy [1990].

Figures 5.27a, b and c illustrate typical results for the amount of crack growth as a function of the number of test cycles for tests at 750°C, 950°C and 1050°C respectively. In general, it is observed that crack extension at high temperatures increases almost linearly with the number of cycles for tests with dwells in tension and/or in compression. Although some evidence of non-linear crack extension was observed for continuous cycling tests at the last stages of crack propagation, the crack extension up to about 1mm was found to be take place approximately at a constant rate.

The influence of strain dwells on the crack growth behaviour of single crystal SRR99 was found to be temperature dependent. The results in Fig.5.27a and b for the tests at 750°C and 950°C show that with the introduction of a compressive and/or tensile dwell crack extension was accelerated compared with continuous cycling tests, with compressive dwells being more damaging than tensile dwells. However, at 1050°C, the tensile dwells exhibited more damaging effects on crack propagation than the compressive dwells. This temperature dependent influence of strain dwell on crack growth behaviour of single crystal SRR99 can be attributed to a combination of mean stress and time dependent damage (creep damage and environmental degradation) induced by strain dwells, which will be discussed in detail in Chapter 6.

In the field of creep-fatigue testing, there is often some consideration of whether significant crack growth occurs during dwells (particularly tensile dwells).

Unfortunately with the small degree of total crack growth in each cycle in these tests, it is not possible to see this aspect. A measurable increment of crack growth is only obtained after a number of cycles.

CHAPTER 6

INTERPRETATION OF THE INFLUENCE OF ORIENTATION ON DEFORMATION BEHAVIOUR

6.1. Anisotropic Elasticity Analysis

The single crystal nickel base superalloy SRR99 is a crystal of cubic symmetry and its elastic properties can be determined using anisotropic elasticity theory (Lekhnitskii [1963]). The strain response, ε, in a direction characterised by the direction cosines (l',m',n') of the crystal when subjected to a uniaxial stress, σ, applied in a direction (t_1,t_2,t_3), Fig.6.1, can be given by (see Appendix.III).

$$\varepsilon(l',m',n') = \sigma [S_{11}\cos^2 Q + S_{12}\sin^2 Q + 2(S_{11} - S_{12} - S_{44}/2) \times (l'm't_1t_2 + m'n't_2t_3 + n'l't_1t_3)] \quad (6.1)$$

where Q is the angle between the direction of the strain measurement and that of the uniaxial applied stress. The elastic compliance constants S_{11}, S_{12} and S_{44} are considered further below. When the strain measurement direction is in the same direction as the stress, i.e. when (l',m',n') = (t_1,t_2,t_3) and Q=0 , then

$$\varepsilon_{11} = \sigma[S_{11} - 2(S_{11} - S_{12}) - \frac{S_{44}}{2})(l'^2m'^2 + m'^2n'^2 + n'^2l'^2)] \quad (6.2)$$

The direction (l',m',n') is usually given by the direction ratios (h,k,l) of the plane normal. Replacing (l',m',n') by (h,k,l) in equation (6.2), Young's modulus $E_{[hkl]}$ for a given crystal orientation (h,k,l) is expressed as

$$E_{[hkl]} = \frac{\sigma}{\varepsilon_{11}} = (S_{11} - 2SA_{hkl})^{-1} \quad (6.3)$$

where

$$S = (S_{11} - S_{12}) - \frac{S_{44}}{2} \quad (6.4)$$

and

$$A_{hkl} = \frac{h^2k^2 + k^2l^2 + l^2h^2}{(h^2 + k^2 + l^2)^2} \quad (6.5)$$

with $S_{11} = \frac{1}{E_{[001]}}$, $S_{12} = -\frac{\nu_{[001]}}{E_{[001]}}$, $S_{44} = \frac{1}{G_{[001]}}$

The elastic constants $E_{[001]}$, $\nu_{[001]}$ and $G_{[001]}$ are usually determined using experimental techniques for the [001] direction. A_{hkl} is an orientation parameter which varies from zero for the [100] direction to 1/3 for the [111] direction, and is intermediate between these values for other (h,k,l) directions.

There are no results available in the open literature for the three elastic constants $E_{[001]}$, $\nu_{[001]}$ and $G_{[001]}$ for SRR99 or other similar single crystal nickel base superalloys. In the following the elastic constants at room temperature (20°C) for pure nickel are used, with $S_{11} = 7.99 \times 10^{-6}$ MPa^{-1}, $S_{12} = 8.44 \times 10^{-6}$ MPa^{-1} and $S_{44} = 3.12 \times 10^{-6}$ MPa^{-1} (Cottrell [1975]). Together with the crystal orientations (h,k,l) given in Table.5.2b, Young's moduli were calculated using Eq.6.3. Figure 6.2 compares the calculated values with experimental results obtained in this study at 20°C, a good agreement is clear. In contrast, there are no elastic constants available for pure nickel at 950°C, and therefore it was not possible to compare experimental results with theoretical calculations.

From the earlier analysis, it can be seen that the single crystal superalloy SRR99, though possessing the highest possible cubic crystal symmetry, still requires three independent material constants, Young's modulus $E_{[001]}$, Poisson's ratio $\nu_{[001]}$ and shear modulus $G_{[001]}$ in the principal crystal orientation [001] to define its elastic responses in other directions [h,k,l]. For an anisotropic material, the Young's modulus $E_{[001]}$ in the [001] orientation is relatively easy to measure. However it is much more difficult to obtain $\nu_{[001]}$ and $G_{[001]}$ as a function of orientation. For engineering applications, it would be useful to use an orientation parameter which can be used directly to correlate the elastic modulus in a given direction with the elastic constant $E_{[001]}$.

Equation (6.3) can be rewritten as:

$$\frac{1}{E_{[hkl]}} = (S_{11} - 2SA_{hkl}) \tag{6.6}$$

substituting for S_{11} and S and rearranging yields

$$E_{[hkl]} = \frac{E_{[001]}}{f(A_{khl})} \tag{6.7}$$

where $f(A_{hkl})$ is called the orientation function proposed in this work in the form

$$f(A_{hkl}) = 1 - D\,A_{hkl} \tag{6.8}$$

with

$$D = 2 + 2\,\nu_{[001]} - \frac{E_{[001]}}{G_{[001]}} \tag{6.9}$$

The material constant D can either be determined if the elastic constants $E_{[001]}$, $\nu_{[001]}$ and $G_{[001]}$ are known, or can be obtained directly from experiments by plotting the results in the form $E_{[001]}/E_{[hkl]}$ versus the orientation parameter A_{hkl}. The experimental results for SRR99 are shown in this form in Fig.6.3 for tests at 20°C and 950°C.

There appears to be no significant difference between results shown in this form for tests at 20°C and 950°C. A linear relationship between $E_{[001]}/E_{[hkl]}$ and A_{hkl} is evident for both temperatures with a linear least squares regression fit yielding D=1.8. The regression was based on 12 observations each at 20°C and 950°C. The correlation coefficients are 0.97 and 0.95 for tests at 20°C and 950°C respectively, with standard deviation of estimate for the ratio $E_{[001]}/E_{[hkl]}$ is 0.020 and 0.011 respectively. The results show that the material constant D appears to be relatively insensitive to temperature for single crystal SRR99 .

A further verification of effectiveness of the proposed orientation function $f(A_{hkl})$ in estimating the influence of orientation on elastic modulus was obtained by using the test results from the additional HET tests. Since the crystal orientations of the specimens used in tests HET05 and HET06 are very near [001], the average values of the elastic moduli of HET05 and HET06 were taken to define the elastic moduli $E_{[001]}$ at various temperatures. The orientation dependence of elastic moduli of other specimens were calculated by using Eq.(6.3) together with the orientation parameter given in Table.5.1a. Fig.6.4 compares the calculated and experimental results. The correlation coefficient based on 36 observations over a range of temperatures and orientations between the calculated and experimental results is 0.96 illustrating a good agreement between the calculated and experimental results.

The orientation modified elastic modulus $E_{hkl}f(A_{hkl})$ of single crystal SRR99 as a function of temperature is given in Fig.6.5. It can be seen that an orientation

independent correlation for modified modulus with temperature can be established. A least squares regression fit to the modified elastic modulus data with temperature yields the following equations for Young's Modulus of single crystal SRR99 in the low temperature range (below 650°C) and high temperature range (above 650°C) respectively as:

$$E_{[hkl]} f(A_{hkl}) = \begin{cases} 113.32 - 0.031T & (0 < T < 650^{\circ}C) \\ 138.82 - 0.0695T & (650^{\circ}C \le T < 1050^{\circ}C) \end{cases} \quad (6.10)$$

These equations are based on 18 observations each. The standard error of estimates of E(T) and the correlation coefficients for Eq.(6.10) are 8 GPa and 0.9 and 6 GPa and 0.96 for T<650°C and T≥650°C respectively. The estimate of the temperature at which the slope of E(T) changes is 650°C. The standard error of estimates of E(T) from Eq.(6.10) show that the temperature at which the slope of E(T) changes abruptly can vary statistically by ±25°C from its mean estimate of 650°C.

In conclusion , the orientation and temperature dependent elastic modulus of single crystal nickel base superalloy SRR99 can be expressed as

$$E_{[hkl]}(T) = \begin{cases} E_{[001]} \dfrac{113.32 - 0.31T}{1 - 1.80 A_{hkl}} & (0 < T < 650^{\circ}C) \\ E_{[001]} \dfrac{138.82 - 0.695T}{1 - 1.80 A_{hkl}} & (650^{\circ}C \le T < 1050^{\circ}C) \end{cases} \quad (6.11)$$

6.2. Orientation and Temperature Dependent Yielding Behaviour

For single crystal superalloys, yielding is dominated by slip within the crystal. Different yield strengths can be rationalised to the different active slip systems. Since no slip traces were observed on the specimen during tests , identification of the slip system was made primarily by using Schmid's law. For specimen axes defined to be in the standard sterographical triangle, the primary octahedral slip system for SRR99, a cubic single crystal, is $(111)[\bar{1}01]$ and the primary cubic slip system is $(001)[\bar{1}01]$ Comparing the Schmid's factors listed in Table 6.1, it can be seen that specimens STP2 and STP3 both have largest value of Schmid's factor for $(111)[\bar{1}01]$, and

STP1 shows largest Schmid's factor for (001)[$\bar{1}$10]. Therefore, it was concluded that STP2 and STP3 exhibited primary octahedral slip and STP1 showed primary cube slip.

The temperature and orientation dependence of the critical resulting shear stress (CRSS) for (111)[$\bar{1}$01] slip, including the effect of the loading direction (tension or compression), is shown in Fig.6.6. The significantly lower CRSS for (111)[$\bar{1}$01] for specimen STP1 further indicates that this specimen might undergo cube slip over the entire range of temperatures tested. The plot also indicates the failure a simple interpretation of of Schmid's law. Based on Schmid's Law, the CRSS of STP2 and STP3 specimens should be equivalent since both specimens were expected to deform by octahedral slip. Figure 6.6 shows that this was not the case and the deviation occurs in tension and compression in a different way. The CRSS for (111)[$\bar{1}$01] slip measured in compression generally increases at a fixed temperature as the orientation moved away from [001]. The compressive CRSS for (111)[$\bar{1}$01] for STP3 was higher than that of STP2 over the temperature range. However, the tensile CRSS for (111)[$\bar{1}$01] for STP3 was only higher at temperature below 600°C and became slightly lower than STP2 at 750°C. This indicates that the deviation from Schmid's law depends both on orientation and loading direction.

The temperature and orientation dependence of the CRSS for (111)[$\bar{1}$01] and the tension compression flow asymmetry in high volume fraction γ' nickel base superalloys have been studied by several investigators (Copley and Kear [1967], Takeuchi and Kuramuto [1973], Lall et al [1979], Paidar et al [1984]). One of the most successful theories suggested is that of the cross-slip model (Lall et al [1979]). A summary of the tension/compression asymmetry of yield stress predicted by the cross-slip model for γ' alloy is plotted in Fig.6.7, where the orientations of the specimens studied in this work are also indicated. The tension/compression asymmetry of CRSS for (111)[$\bar{1}$01] measured in SRR99 single crystal as a function of orientation is found to be in fair agreement with the prediction of the cross slip model. For the specimen oriented near [001], STP2, the CRSS for (111)[101] slip measured in tension is larger than that in compression, Fig.6.8b. The asymmetry in reversed as the specimen orientation is moved to the opposite side of the stereotriangle near [111] and [011] (STP1, Fig.6.8a). The main difference between the present work and the predictions of the cross-slip model is in the orientation for which the asymmetry disappears. The result of the present study (STP3 Fig.6.8c) indicates that the asymmetry should vanish on the right side of the line C=T in Fig.6.7 and perhaps close to that line, but definitely not on the left side as predicted by Paidar

et al [1984]. The results in this study are in agreement with that reported by Heredia and Pope [1986] for PWA 1480 nickel base single crystal.

In terms of cross-slip model, the yield stress of SRR99 single crystal, including the asymmetry effect, can be modelled effectively using the equation proposed by Lall et al (Lall, Chin and Pope [1979]). The LPT model which is, in fact, a modification of Schmid's law with additional terms to take into account of the cross-slip effect can be written as

$$\sigma_y\, S_1 = T_n + A_0 \exp[(-H_0 + A_2 S_2 + \delta\, A_3 S_3)/RT] \qquad (6.12)$$

where the Schmid's factors S_1, S_2 and S_3 are defined in Table 6.1; T_n is analogous to the normal CRSS for octahedral slip at a given temperature; σ_y is the yield stress; H_o is the activation energy; A_0, A_2 and A_3 are constants; and δ is +1 for loading in tension and -1 for loading in compression.

In order that the present data can be precisely evaluated in terms of above model, Eq.(6.12) has been approximated in a linear form , so that linear regression analysis may be applied. The exponent of $\exp[(A_2S_2 + \delta A_3S_3)/RT]$, which is always small in practice, may be approximated as $(1+(A_2S_2 + \delta A_3S_3)/RT)$. After rearrangement of terms the variables are separated in the form

$$1/\sigma_y = b_1S_1 + b_2S_2 + b_3S_3 \qquad (6.13)$$

where
$$b_1 = 1/[T_n + A_0 \exp(-H_0/RT)$$
$$b_2 = (-b_1A_0A_2/RT)\exp(-H_0/RT)$$
$$b_3 = (-b_1A_0\delta\, A_3/RT)\exp(-H_0/RT)$$

In this form, the orientation dependence of yield stress at a given temperature can be numerically evaluated by linear regression analysis.

Fig.6.9 and Fig.6.10 compares the observed yield stress of SRR99 single crystal and those predicted in turn, by Schmid's Law, and the cross-slip model as described in Eq.(6.13) for temperatures from 20°C to 750°C. It is apparent that the cross slip model predicts a better fit to the data than that due to Schmid's law. However, the cross-slip model does has two extra free parameters, which would be expected to provide the better curve fit. The fact that it does partly explain the yield asymmetry

provides the best grounds for accepting it has a physical basis. The values of the coefficients in the cross slip model as determined by regression analysis are presented in Table.6.2.

6.3. Orientation Modified Cyclic Mechanical Responses

6.3.1. Modified Cyclic Stress-Strain Relationship

The influence of crystal orientation on the cyclic stress-strain response of single crystal SRR99 is taken into account primarily by using the orientation function $f(A_{hkl})$ proposed in Section 6.1. Fig.6.11a, 6.11b and 6.11c illustrate the results for smooth bar tests at 750°C, 950°C and 1050°C respectively where the total strain ranges $\Delta\varepsilon_T$ are modified by the orientation function $f(A_{hkl})$. The results obtained from corner crack tests are also shown in these Figures. It can be seen that the modified cyclic stress-strain relationships exhibit neither significant orientation nor cycle type dependent characteristics. All the test data at each temperature can be approximately placed on a single curve.. The curve for tests at 950°C and 1050°C, Figs 6.11b and 6.11c respectively, shows both a elastic and a inelastic region. However, at 750°C, it appears that elastic strains dominate, Fig.6.11a. The slope of the line from a log-log fit obtained by linear regression is 97.5 GPa which is nearly the same as experimentally determined average Young's Modulus of 98.3 GPa at 750°C. Therefore, it is concluded that all the fatigue tests at 750°C were dominated by elastic deformation.

The good agreement between the modified smooth bar test results and the corner crack test results which are obtained from the specimens with orientations near the [001] indicated that the modified stress -strain curves are representative to the [001] behaviour of SRR99 single crystal.

6.3.2. Effects of Orientation on Stress Relaxation

Correlation on Total Stress Relaxation. The total magnitude of stress relaxation as a function of total strain range exhibits a significant orientation dependence for tests at 950°C and 1050°C (as shown in Chapter 5). Stress relaxation during a dwell at constant strain is a consequence of the conversion of elastic strain to inelastic (creep) strain. Therefore, the extent of stress relaxation is plotted in Fig.5.15 and Fig.5.16 against a modified strain range, using the orientation function $f(A_{hkl})$ to take

into account the influence of crystal orientation. The modified results are given in Fig.6.12 and Fig.6.13 for tests at 950°C and 1050°C respectively. The relationship between the total amount of stress relaxation and the modified half strain range can be expressed as

$$|\delta\sigma| = Q\{\frac{\Delta\varepsilon_T}{2} f(A_{hkl})^{-1}\}^q \qquad (6.14)$$

where Q and q are temperature dependent material constants. The results obtained from corner crack tests are also presented in Fig.6.12 and Fig.6.13. The values of Q and q obtained from the correlation were 6.41×10^6 and 2.15, and 1.62×10^4 and 0.985 for tests at 950°C and 1050°C respectively. It can be seen that Eq.(6.14) appears to be applicable to stress relaxation during either tensile or compressive strain dwells, as well as to both smooth bar tests and corner crack tests.

Description of Relaxation Curves. In order to study the stress relaxation behaviour during each strain hold period and to compare the stress relaxation response with creep response, creep tests results in the [001] orientation provided by DRA Pyestock [1992] have been analysed using the exponential model in the CRISPEN (Dyson and Mclean [1989]) programme. The secondary creep rates as a function of the applied stress level for creep tests from 750°C to 1050°C are plotted in Fig.6.14. The secondary creep data at each temperature can be approximately presented in a power law form as

$$\dot{\varepsilon} = A_1\sigma^{n_1} \qquad (6.15)$$

The temperature dependent material constants A_1 and n_1 for each temperature obtained by regression analysis are listed in Table 6.3. It can be seen that the exponent n_1 generally decreases as temperature increases, except at 1050°C where only two test data are available and the exponent n is larger than at 950°C and 900°C.

In analysing stress relaxation data during a hold time, the total strain (ε_T) was partitioned into elastic strain ($\varepsilon_e = \sigma/E$), plastic strain (ε_{pp}) and creep strain (ε_c) components as

$$\varepsilon_T = \frac{\sigma}{E} + \varepsilon_{pp} + \varepsilon_c \qquad (6.16)$$

where E is the elastic modulus. For single crystal SRR99, the orientation dependent elastic modulus E can be expressed as $E_{[001]} f(A_{hkl})^{-1}$. Therefore, during a constant strain dwell, $\dot{\varepsilon}_T$=0 and $\dot{\varepsilon}_{pp}$ =0, and differentiating Eq.(6.16), leads to ;

$$\dot{\varepsilon}_c = -\frac{\dot{\sigma}}{E_{[001]} f(A_{hkl})^{-1}} \tag{6.17}$$

From the creep data provided by DRA Pyestock [1992], it is found that the creep strain accumulated during 2 minutes dwells is far less than the primary creep strain observed in the creep tests. In this case, the creep strain during dwell is often modelled (Plumbridge and Ellison [1991], Zamrik and Davis [1991]) by a time-hardening primary creep law of the form ;

$$\varepsilon_c = C_c \sigma^{n_c} t^{m_c} \tag{6.18}$$

Differentiating gives the creep strain rate;

$$\dot{\varepsilon}_c = m_c C_c \sigma^{n_c} t^{m_c - 1} \tag{6.19}$$

The stress relaxation behaviour based on this creep law is obtained by substituting equation (6.19) into equation (6.17) and integrating

$$\sigma(t) = \left[(n_c - 1) E_{[001]} f(A_{hkl})^{-1} C_c t^{m_c} + \sigma_0^{(1-n_c)} \right]^{\frac{1}{(1-n_c)}} \tag{6.20}$$

where σ_0 is the initial stress at the onset of stress relaxation. Eq.(6.20) has three unknown material constants m_c, n_c and C_c. To determine the value of each from a single stress relaxation curve, the value of one constant must be assumed in order to evaluate the other two by least squares analysis. It is often assumed (Plumbridge and Ellison [1991], Zamrik and Davis [1991]) that the stress exponent n_c equals to the stress exponent n_1 for secondary creep (Eq.(6.15)).

Stress relaxation data from the tensile dwell tests at $\Delta\varepsilon_T$=1.0% are shown in Figs.6.15 and 6.16 for tests at 950°C (sb9512) and 1050°C (sb1506) respectively, together with curves representing Eq.(6.20) using the creep stress exponents n_c=n_1=6.2 and n_c=n_1=6.9 for tests at 950°C and 1050°C respectively. It can be seen that good fits are obtained at both temperatures. The material constants m_c and C_c onbtained are 0.4602 and 0.146, and 0.361 and 148.96 respectively for tests at 950°C and 1050°C.

Using these material constants to predict the stress relaxation behaviour during compressive dwell, different results have been obtained from tests at 950°C and 1050°C. Fig.6.17 shows the experimental data from test sb1504 at 1050°C with strain range $\Delta\varepsilon_T$=1.0% and the predicted curve using Eq.(6.20) with the material constants obtained from the tensile dwell test at same strain range. A good agreement is apparent. However, a similar comparison between experimental data for a compressive dwell test (sb9510) at 950°C and the predicted stress relaxation curve, Fig.6.18, shows a large difference. The predicted change in stress is much less than actually measured stress. The reason for the difference may be attributed to the influence of the orientation of the specimens used in tensile and compressive dwells. The tensile dwell specimen (sb9512) is near the [111] orientation and the compressive dwell specimen (sb9510) is near the [001] orientation. A comparison of the material constants relevant to creep behaviour, m_c and C_c, obtained by direct fitting of the relaxation curves at half life of tests at 950°C and 1050°C are given in Table 6.4. It can be seen that values of m_c and C_c exhibit large variation as a results of the different orientation of the specimens used in the tests. Therefore the stress relaxation equation (6.20) based on the time hardening rule, which has been extensively used for polycrystalline materials (Plumbridge and Ellison [1991], Zamrik and Davis [1991]) is only of limited use for single crystal SRR99. A anisotropic constitutive model will be developed in Chapter 7, which can describes, among other mechanical properties, the general orientation dependent stress relaxation behaviour of single crystal SRR99.

6.4. Orientation Modified Creep-Fatigue Life Behaviour

It has been pointed out in Chapter 5 (Section 5.3), that the fatigue life of single crystal SRR99 is highly orientation dependent, with the [001] orientation for a given total strain range and cycle type providing the longest fatigue life. The fatigue life decreases as the orientation moves away from [001]. The effect of orientation on the fatigue life has been taken into account primarily by modifying the total strain range using the orientation function $f(A_{hkl})$. Figs.6.19a, 6.19b and 6.19c. illustrate the fatigue life behaviour in terms of the modified total strain range. It is clear that the influence of orientation on fatigue and fatigue-creep life can be rationalised. The effects of tensile or compressive dwells on the fatigue life of single crystal SRR99 are clearly revealed as explained in the following paragraphs.

At 750°C, unbalanced dwell tests exhibit significantly different fatigue lives compared with continuous cycling tests. At the same strain amplitude, tests with a compressive dwell show remarkably shorter lives than those of continuous tests. In contrast, tests with tensile dwell result in significant longer lives than those of continuous tests, whilst a fatigue test with balanced dwells has a similar fatigue life to a continuous cycling test.

At 950°C, the correlation of fatigue life with orientation modified total strain range, Fig.6.19b, generally shows no significant cycle dependent characteristics when compared with the correlation at 750°C. Nevertheless, some slight cycle dependent trends may just be discovered. At the same strain range, the ratio of the lives of tests with a tensile dwell to the lives of continuous tests is usually, but not always, greater than unity. On the other hand, the ratio of the fatigue lives of the tests with compressive dwells to the fatigue lives of continuous tests is often less than unity. This indicates that the influence of cycle type on fatigue life at 950°C has a similar trend as that for 750°C, but the strength of the influence at 950°C is much weaker than that at 750°C.

The fatigue lives at 1050°C, Fig.6.19c, as a function of total strain exhibit a quite different cycle dependence compared with those at 750°C and 950°C. From Fig.6.19c, it is clear that the introduction of a dwell, either in tension or in compression will reduce fatigue life at 1050°C, with a tensile dwell more damaging than compressive dwell, and a balanced dwell further damaging still.

The different effects of cycle type on the fatigue life behaviour, for various temperatures, may be attributed to the combination of mean stress effect and time dependent damage (creep damage and environmental degradation) .

At 750°C, as pointed out in section 6.3.1, the fatigue tests are dominated by elastic deformation, only with little inelastic strain, and it is expected that the creep damage should not be important. The influence of cycle type on fatigue life can be mainly attributed to the mean stress induced in the unbalanced dwell tests. A compressive dwell causes a positive mean stress and is found to be detrimental to fatigue life, whilst tensile dwell results in negative mean stress and is beneficial.

At 950°C and 1050°C, where significant stress relaxation occurs, creep damage should also be important. Tensile dwells introduce a negative mean stress which is beneficial to fatigue endurance compared with a zero mean stress in the continuous

tests. At the same time, creep occurring during a tensile stress relaxation will cause some creep damage and consequently reduce fatigue life. The fatigue life at these temperatures will depend on the combination of these two opposing effects induced by a strain dwell. In addition, since the high temperature fatigue and creep-fatigue tests were all performed in the air, the environmental attack, such as oxidation, will also influence the fatigue life. It is to be expected that creep damage and environmental degradation will be more important at 1050°C than that at 950°C. As a result, the fatigue life for the tests with a tensile dwell at 950°C is of the same order as that for continuous tests, whilst the tests with a tensile dwell at 1050°C exhibit significant shorter lives than for continuous tests.

CHAPTER 7

DEVELOPMENT OF AN ANISOTROPIC VISCOPLASTIC CONSTITUTIVE MODEL AND SIMULATIONS

7.1. Introduction

The experimental results presented in the previous Chapters indicate that the mechanical response of single crystal SRR99, with intrinsic orientation dependent anisotropic characteristics, is significantly different from polycrystalline materials. A simple approach has been proposed in Chapter 6 to take into account the influence of orientation on cyclic mechanical response in terms of total strain and stress ranges, so that the total stress and strain response can be calculated and used for life prediction under simple loading conditions. However, in the design and structural integrity assessment of a component under complex loading conditions, such as a multiaxial stress state, it is necessary to know precisely the changes of stress and strain during a cycle, not only the total stress and strain ranges. In this case a realistic material model, i.e. a constitutive model describing the anisotropic mechanical characteristics related to a single crystal, is indispensable. It should be available in a multiaxial form for use in conjunction with a finite element method, or a similar analysis, so that a component can be assessed for structural stability and integrity under the complex conditions representative of service.

The anisotropic viscoplastic constitutive model presented in this Chapter is a modification of the Chaboche model which was proposed initially for isotropic materials. The details of the Chaboche model can be found in the literature (Chaboche [1989]). The development of the Chaboche model required to take into account the anisotropic characteristics of single crystal is presented in section 7.2. The procedure for the determination of the material parameters in the model is described in section 7.3. The computer calculation methods for the simulation of the cyclic mechanical response of single crystal SRR99 at 950°C are described in section 7.4. Finally, the simulation results are compared with the experimental results in section 7.5.

7.2. Constitutive Equations

The constitutive model is based on a unified theory that separates the total strain in the principal axes (i.e. crystallographic axes [001]-[010]-[100] in the case of a cubic

single crystal) of a material into elastic and inelastic components, such that;

$$\varepsilon_{ij}^{T} = \varepsilon_{ij}^{e} + \varepsilon_{ij}^{in} \tag{7.1}$$

where ε_{ij}^{T} is the total strain, ε_{ij}^{e} are the elastic strain components, and ε_{ij}^{in} are the inelastic strain components (no distinction is made between plastic and creep strain) in the principal axes system. The thermal strain is not included in equation (7.1) because the proposed model at this stage is developed for isothermal conditions.

The elastic constitutive equation for general anisotropic material is well known. In the principal coordinate system, the constitutive equations, as shown in Chapter 6 (AIII.4), can be generally expressed as

$$\varepsilon_{ij}^{e} = S_{ijkl}\,\sigma_{kl} \tag{7.2}$$

where S_{ijkl} represents the elastic compliance matrix. The number of independent coefficients for this matrix is related to the anisotropy of the material. For single crystal SRR99 with cubic symmetry, only three independent coefficients in the matrix S_{ijkl} are required.

The viscoplastic flow law is obtained from the normality hypothesis with a viscoplastic potential Ω in the form

$$\dot{\varepsilon}_{ij}^{in} = \frac{\partial \Omega}{\partial \sigma_{ij}} \tag{7.3}$$

The visoplastic potential Ω is expressed in the similar form as in the Chaboche model [1989]

$$\Omega = \frac{K^{*}}{n+1}\left\langle \frac{f}{K^{*}} \right\rangle^{n+1} \tag{7.4}$$

where f is the anisotropic yielding function which represents a yield surface of plasticity inside which the deformation behaviour remains elastic, K* and n are two constants characterising the viscosity state of the material and strongly depend on the temperature. The bracket $\langle\rangle$ is defined as

$$\langle u \rangle = \begin{cases} u & if \quad u > 0 \\ 0 & if \quad u \le 0 \end{cases} \tag{7.5}$$

The anisotropic yield behaviour of single crystals is conventionally described by Schmid's law in the crystallographic level. However, as discussed in Chapter 6, for single crystal SRR99, and other single crystal nickel base superalloys extensively studied by other researchers (Copley and Kear [1967], Lall et al [1979], Paidar et al [1984]), Schmid's Law can not describe the yielding behaviour properly. The cross-slip model described in Chapter 6 shows some improvement on Schmid's law, but it is still at the crystallographic level and can only be used in crystallographic models. Since the anisotropic constitutive model proposed in the present work is a phenomenological macroscopic model, a phenomenological yielding function which modifies the Von Mises criterion with a fourth-order tensor M_{ijkl} is adopted. It can be expressed as a generalised Hill's criterion in the form

$$f = [\tfrac{3}{2} M_{ijkl} (\sigma'_{ij} - X'_{ij})(\sigma'_{kl} - X'_{kl})]^{\frac{1}{2}} - R - k \tag{7.6}$$

where σ'_{ij} and X'_{ij} represent the components of the deviation of stress tensor σ_{ij} and back stress tensor X_{ij} respectively. The yielding function, f, represents the elastic limit surface, i.e. the yield surface equation, k is the initial size of the yield surface, and R is the isotropic hardening parameter which describes the change (expansion or compression) of the yield surface.

The fourth order tensor, M_{ijkl} , can describe the initial anisotropy of the material and possibly an induced anisotropy, depending on whether the components are constants or variables. At this stage, various possibilities can be considered for the induced anisotropy, such as the formulation of Lee and Zavert [1979], in which M_{ijkl} is introduced as a new internal variable with an associate growth law, or a Baltov and Sawczuk [1961] type model where the components of the tensor are defined as a function of the plastic strain. In this work, the components of M_{ijkl} are taken as constants for mainly describing the initial anisotropy of single crystal SRR99.

Using the proposed viscoplastic potential Ω and the yielding function f given in Eqs.(7.4) and (7.6) respectively, the inelastic strain rate can be derived as

$$\dot{\varepsilon}_{ij}^{in} = \frac{\partial \Omega}{\partial \sigma_{ij}} = \dot{p} \frac{\partial f}{\partial \sigma_{ij}} \tag{7.7}$$

where $\dot{p}$ is the total accumulated inelastic strain rate, given by

$$\dot{p} = \left[\frac{2}{3} M^{-1}_{ijkl}\, \dot{\varepsilon}^{in}_{ij}\, \dot{\varepsilon}^{in}_{kl}\right]^{\frac{1}{2}} = \left\langle \frac{f}{K^*} \right\rangle^n \tag{7.8}$$

The inelastic deformation induced anisotropy is described mainly by introducing two fourth-order tensors N_{ijkl} and Q_{ijkl} into the evolution equation for the back stress X_{ij} in the form;

$$\dot{X}_{ij} = \frac{2}{3} N_{ijkl}\ \dot{\varepsilon}^{in}_{kl} - Q_{ijkl}\ X_{kl}\ \dot{p} \tag{7.9}$$

Although all the components of the tensors N_{ijkl} and Q_{ijkl} are taken as constants in this work, it is also possible, as for the tensor M_{ijkl}, to consider N_{ijkl} and Q_{ijkl} as new internal variables with associated growth laws if it is necessary. This obviously leads to a more complex model.

Cyclic softening or hardening, which corresponds to a decrease or increase in the size of the elastic domain, is described by introducing the isotropic hardening variable R. The variation law of R is described in a conventional form (Goodall et al [1980]) given by

$$\dot{R} = \mathrm{b}\,(\mathrm{Q} - \mathrm{R})\,\mathrm{p} \tag{7.10}$$

where p is the total accumulated inelastic strain ($p = \int \dot{p} dt$), b and Q are the material constants which vary with temperature.

The generalised form of the anisotropic viscoplasticity constitutive equations in a general coordanite system is given in Appendix.IV, where the following notations are used

$$[\sigma]^t \equiv [\sigma_1 = \sigma_{11}, \sigma_2 = \sigma_{22}, \sigma_3 = \sigma_{33}, \sigma_4 = \sigma_{13}, \sigma_5 = \sigma_{23}, \sigma_{16} = \sigma_{12}]$$

$$[\varepsilon]^t \equiv [\varepsilon_1 = \varepsilon_{11}, \varepsilon_2 = \varepsilon_{22}, \varepsilon_3 = \varepsilon_{33}, \varepsilon_4 = 2\gamma_{13}, \varepsilon_5 = 2\gamma_{23}, \varepsilon_{16} = 2\gamma_{12}]$$

For single crystal SRR99, taking into account the cubic symmetry properties of the material, the matrices S_{ij} M_{ij}, N_{ij} *and* Q_{ij} in Appendix.IV can be reduced to the

simple forms as described in the following

The elastic compliance matrix for a cubic symmetry single crystal with only three independent coefficients can be written in the form;

$$S_{ij} = \begin{bmatrix} S_{11} & S_{12} & S_{12} & 0 & 0 & 0 \\ S_{12} & S_{11} & S_{12} & 0 & 0 & 0 \\ S_{12} & S_{12} & S_{11} & 0 & 0 & 0 \\ 0 & 0 & 0 & S_{44} & 0 & 0 \\ 0 & 0 & 0 & 0 & S_{44} & 0 \\ 0 & 0 & 0 & 0 & 0 & S_{44} \end{bmatrix} = \begin{bmatrix} \frac{1}{E} & \frac{-\nu}{E} & \frac{-\nu}{E} & 0 & 0 & 0 \\ \frac{-\nu}{E} & \frac{1}{E} & \frac{-\nu}{E} & 0 & 0 & 0 \\ \frac{-\nu}{E} & \frac{-\nu}{E} & \frac{1}{E} & 0 & 0 & 0 \\ 0 & 0 & 0 & \frac{1}{2G} & 0 & 0 \\ 0 & 0 & 0 & 0 & \frac{1}{2G} & 0 \\ 0 & 0 & 0 & 0 & 0 & \frac{1}{2G} \end{bmatrix} \quad (7.11)$$

Similar reduction can be also made for the anisotropic matrices of M_{ij}, N_{ij} and Q_{ij} in a general form as

$$[]_{ij} = \begin{bmatrix} []_{11} & []_{12} & []_{12} & 0 & 0 & 0 \\ []_{12} & []_{11} & []_{12} & 0 & 0 & 0 \\ []_{12} & []_{12} & []_{11} & 0 & 0 & 0 \\ 0 & 0 & 0 & []_{44} & 0 & 0 \\ 0 & 0 & 0 & 0 & []_{44} & 0 \\ 0 & 0 & 0 & 0 & 0 & []_{44} \end{bmatrix} \quad (7.12)$$

where [] can be replaced by M, N or Q respectively. Furthermore, using the assumption that plastic strain occurs at constant volume, the number of independent coefficients of the anisotropic matrices M_{ij}, N_{ij} and Q_{ij} can be further reduced to two for each matrix in the form

$$[]_{ij} = \begin{bmatrix} []_{11} - []_{12} & 0 & 0 & 0 & 0 & 0 \\ 0 & []_{11} - []_{12} & 0 & 0 & 0 & 0 \\ 0 & 0 & []_{11} - []_{12} & 0 & 0 & 0 \\ 0 & 0 & 0 & []_{44} & 0 & 0 \\ 0 & 0 & 0 & 0 & []_{44} & 0 \\ 0 & 0 & 0 & 0 & 0 & []_{44} \end{bmatrix} \quad (7.13)$$

where [] can be replaced by M, N or Q respectively.

7.3. Determination of Material Parameters

Though a general procedure for the determination of material parameters in the proposed constitutive model is given in this section, the application of the procedure to single crystal SRR99 was performed only for the tests at 950°C, because the tests at 750°C exhibited very little inelastic deformation and there was no enough data obtained from tests at 1050°C.

7.3.1. Constitutive Equations for the Uniaxial Cases

In order to determine the material parameters involved in the constitutive model, the general constitutive equations given in Appendix IV are used for the special cases when unaxial loading is applied along the crystal orientations [001] and [111].

Uniaxial Loading Along [001]. In this case, since the only non-zero component of the stress tensor is $\sigma_1 = \sigma$, the constitutive equations are reduced to

$$\dot{\varepsilon}_1^{jn} = \left\langle \frac{\left|\sigma - \frac{3}{2} X_1\right| \sqrt{M_{11} - M_{12}} - k - R}{K^*} \right\rangle^n \sqrt{M_{11} - M_{12}}\ sign(\sigma - \tfrac{3}{2} X_1) \quad (7.14a)$$

$$\dot{\varepsilon}_2^{jn} = \dot{\varepsilon}_3^{jn} = -\frac{1}{2}\ \dot{\varepsilon}_1^{jn} \quad (7.14b)$$

$$\dot{\varepsilon}_4^{jn} = \dot{\varepsilon}_5^{jn} = \dot{\varepsilon}_6^{jn} = 0 \quad (7.14c)$$

$$\dot{X}_1 = \frac{2}{3}(N_{11} - N_{12})\,\dot{\varepsilon}_1^{jn} - (Q_{11} - Q_{12})\ X_1\ \dot{p} \quad (7.14d)$$

$$\dot{X}_2 = \dot{X}_3 = -\frac{1}{2}\ \dot{X}_1 \quad (7.14e)$$

$$\dot{X}_4 = \dot{X}_5 = \dot{X}_6 = 0 \quad (7.14f)$$

where:

$$\dot{p} = \frac{\left|\dot{\varepsilon}_1^{jn}\right|}{\sqrt{M_{11} - M_{12}}} \quad (7.14g)$$

Uniaxial Loading Along [111]. Direction [111] represents the cube diagonal of single crystal SRR99. In this case the constitutive equations are reduced to

$$\dot{\varepsilon}_1^{jn} = \left\langle \frac{|\sigma - \frac{3}{2} X_1| \sqrt{M_{44}/2} \quad - k - R}{K^{\bullet}} \right\rangle^{n} \sqrt{M_{44}/2} \quad sign(\sigma - \tfrac{3}{2} X_1) \quad (7.15a)$$

$$\dot{\varepsilon}_2^{jn} = \dot{\varepsilon}_3^{jn} = -\frac{1}{2}\, \dot{\varepsilon}_1^{jn} \quad (7.15b)$$

$$\dot{\varepsilon}_4^{jn} = \dot{\varepsilon}_5^{jn} = \dot{\varepsilon}_6^{jn} = 0 \quad (7.15c)$$

$$\dot{X}_1 = \frac{2}{3} N_{44}\, \dot{\varepsilon}_1^{jn} - Q_{44}\, X_1\, \dot{p} \quad (7.15d)$$

$$\dot{X}_2 = \dot{X}_3 = -\frac{1}{2}\, \dot{X}_1 \quad (7.15e)$$

$$\dot{X}_4 = \dot{X}_5 = \dot{X}_6 = 0 \quad (7.15f)$$

where:

$$\dot{p} = \frac{\left|\dot{\varepsilon}_1^{jn}\right|}{\sqrt{M_{44}/2}} \quad (7.15g)$$

It is observed that for these two special orientations, i.e. [001] and [111], the transverse strains ($\dot{\varepsilon}_2^{jn}$ *and* $\dot{\varepsilon}_3^{jn}$) are equal and the loading does not produce any shear deformation ($\dot{\varepsilon}_4^{jn} = \dot{\varepsilon}_5^{jn} = \dot{\varepsilon}_6^{jn} = 0$). This is not the case for other directions where all components of the strain tensor may be non-zero.

From the preceeding pair of constitutive equations, it is seen that the coefficients of $(M_{11} - M_{12})$, $(N_{11} - N_{12})$ and $(Q_{11} - Q_{12})$ are completely uncoupled from M_{44}, N_{44} and Q_{44} for these two crystal orientations. Therefore, tests in the [001] and [111] directions are sufficient to fully determine all the coefficients of the anisotropic matrices M_{ij}, N_{ij} and Q_{ij}. This is one of the advantages of this model compared with crystallographic models (Li [1991]).

The general form of the stress response for uniaxial tensile loading along the [001]

and [111] crystal orientations can be expressed as;

$$\sigma = X + k' + K'^{*}(\dot{\varepsilon}^{in})^{1/n} = X + k' + \sigma_v \tag{7.16}$$

The viscous stress, or overstress, $\sigma_v = f(\dot{\varepsilon}^{in})$ is the time dependent part in this model. It describes the strain rate effects and other viscoplastic characteristics of single crystal superalloys. The difference in the stress response for the two directions is then given by

$$\sigma_{[001]} = \frac{3}{2}X_{[001]} \pm \frac{k+R}{\sqrt{M_{11}-M_{12}}} \pm \frac{K^{*}}{(M_{11}-M_{12})^{(n+1)/n}}(\dot{\varepsilon}_1^{in})^{1/n} \tag{7.17a}$$

$$\sigma_{[111]} = \frac{3}{2}X_{[111]} \pm \frac{k+R}{\sqrt{M_{44}/2}} \pm \frac{K^{*}}{\left(M_{44}/2\right)^{(n+1)/n}}(\dot{\varepsilon}_1^{in})^{1/n} \tag{7.17b}$$

It can be seen that for a given strain rate, the ratio between the viscouse stress for the two directions depends on the ratio between the values of $(M_{11}-M_{12})$ and M_{44}. This implies that the orientation dependent viscosity effect is also taken into account in the model.

7.3.2. Identification of Material Parameters

Yield Parameters k and M_{ij}. Under monotonic loading or in the first half cycle of fatigue tests, the initial tensile yielding stress for different crystal orientations can be expressed as

$$\sigma^{y}_{[001]} = \frac{k}{\sqrt{M_{11}-M_{12}}} \tag{7.18a}$$

$$\sigma^{y}_{[111]} = \frac{k}{\sqrt{M_{44}/2}} \tag{7.18b}$$

$$\sigma^{y}_{[lmn]} = g(k, M_{11}-M_{12}, M_{44}, l, m, n) \tag{7.18c}$$

In the general case, three groups of tests using specimens with different orientations can determine the three material parameters k, $(M_{11}\text{-}M_{12})$ and M_{44}. Since it is the ratio between $(M_{11}\text{-}M_{12})$ and M_{44}, rather than their absolute values, that determines

the anisotropy of a cubic single crystal, $(M_{11}-M_{12})$ is taken as unity in this work. Therefore, only two groups of tests using specimens with [001] and [111] orientations are required to determine the yield parameters in principle.

Back Stress Parameters N_{ij} and Q_{ij} . The back stress, **X**, for uniaxial tension along [001] and [111], given in Eqs.(7.13d) and (7.14d), can be expressed in a general form as;

$$\dot{X} = N\dot{\varepsilon}^{in} - Q X\left|\dot{\varepsilon}^{in}\right| = (N - QX)\dot{\varepsilon}^{in} \tag{7.19}$$

Integration of this equation leads to;

$$X = \frac{N}{Q}(1 - e^{-Q\varepsilon^{in}}) \tag{7.20}$$

From the curve $X=f(\varepsilon^{in})$, which can be obtained by using the unloading of cyclic tests at various strain ranges (see Fig.7.1), the parameters N and Q can be determined, i.e. N_{11}-N_{12} and Q_{11}-Q_{12} from the [001] tests, N_{44} and Q_{44} from the [111] tests. For single crystal SRR99, the experimental results at 950°C are given in Figs.7.2a and 7.2b for tests using specimens near [001] and [111] respectively.

Viscosity Parameter K* and n. These two parameters describe the time dependent characteristics in the model. They can be determined by creep or relaxation tests under monotonic or cyclic conditions. In this work these two parameters are identified from the relaxation data obtained from the strain dwell periods. Since the parameters k, N_{ij} and Q_{ij} have been determined in the previous stages, then from the expression for viscous stress;

$$\sigma_v = \sigma - X - k' = K^*(\dot{\varepsilon}^{in})^{\frac{1}{n}} = f(\dot{\varepsilon}^{in}) \tag{7.21}$$

The parameter K* and n can be determined from the σ_v *vs* $\dot{\varepsilon}^{in}$ curve and from the relation

$$Log(\sigma_v) = \frac{1}{n'} Log(\dot{\varepsilon}^{in}) + Log(K^*) \tag{7.22}$$

The inelastic strain rate can be calculated directly using the relaxation curves in the simplified form;

$$\dot{\varepsilon}^{in} = -\frac{\dot{\sigma}}{E} \approx \frac{\Delta\sigma}{E\,\Delta t} \tag{7.23}$$

In this work, since a curve fit to the stress relaxation curves has been performed in Chapter 6, (section 6.3.2), by using the time hardening equation, where;

$$\sigma(t) = \left[(n_c - 1)\, E_{[001]}\, f(A_{hkl})^{-1} C_c\, t^{m_c} + \sigma_0^{(1-n_c)}\right]^{1/(1-n_c)} \tag{7.24}$$

then the inelastic strain rate during stress relaxation can be easily calculated by

$$\dot{\varepsilon}^{in}(t) = -\frac{\dot{\sigma}(t)}{E}$$

$$= C_c m_c \left[(n_c - 1) E_{[001]} f(A_{hkl})^{-1} C_c\, t^{m_c} + \sigma_0^{(1-n_c)}\right]^{n_c/(1-n_c)} t^{(m_c-1)} \tag{7.25}$$

Fig.7.3 shows a plot of the relationship between viscous stress, σ_v , and inelastic strain rate, $\dot{\varepsilon}^{in}$, during stress relaxation tests with specimen directions close to the [001] and [111] orientations for single crystal SRR99 at 950°C.

Isotropic hardening parameters Q and b. The relationship between the isotropic hardening parameter, R, and the accumulated inelastic strain, p, can be obtained from an integration of Eq.(7.10);

$$R = Q\,(1 - e^{-bp}) \tag{7.26}$$

With the assumption that the stress increase/decrease at each cycle is due only to isotropic hardening/softening, the parameter, b, is approximately determined using a relationship suggested by Goodall et al [1980];

$$\frac{\sigma_M - \sigma_{M0}}{\sigma_{Ms} - \sigma_{M0}} \cong \frac{R}{Q} = 1 - e^{-bp} \tag{7.27}$$

where σ_{M0} and σ_{Ms} are the maximum stress for the first and stabilised cycles respectively. The experimental results obtained for single crystal SRR99 at 950°C are presented in Fig.7.4. In the calculation of Fig.7.4, the maximum stresses are replaced by the total stress ranges to eliminate the mean stress influence.

Practical Method for Determination of the Materials Parameters. It is important

to note that the above procedures form the basis for the determination of material parameters in the proposed constitutive model in principle. In practice, especially when there are not enough experimental data available, as is the case for this work, an iterative scheme is necessary. The initial values of the material parameters were first determined using the limited experimental data , then these material constants were used to integrate the viscoplastic equations to predict stress-strain response at specific points, such yielding point and maximum stress point, on the hypothesis loop. Adjustments of the material parameters was then made to improve the predicted response at these specific points. This procedure was repeated for several important points around the hypothesis loop under different loading conditions. In this way, the material parameters were optimised to achieve the best predicted response. This method has been successfully used to determine the material constants in the viscoplastic models of Bodnor & Parton [1975], Krieg et al [1978], Schmidt & Miller [1981] and Walker [1981]. The application of this method in this work, as shown by the simulation results presented in the next section, also appears fairly satisfactory. The final material parameters for single crystal SRR99 at 950°C was given in Table 7.1. In addition, these values allow the fits to data to be plotted in Figs. 7.2, 7.3 and 7.4.

7.4. Computer Simulations.

The simulation using the proposed anisotropic constitutive model for the cyclic mechanical responses of single crystal SRR99 at 950°C was performed using two methods; the software program SIMNON (Elmquist et al [1986]) and a group of FORTRAN programmes written for this work. SIMNON is a commercial package for the simulation and calculation of non-linear differential equations, and has been successfully used for many applications. However, SIMNON can only be used for simple one dimensional differential equations. Therefore, SIMNON was used in this work as a benchmark to verify the accuracy of the FORTRAN programmes written for this work. Most of the simulations were conducted using FORTRAN programmes.

The constitutive equations given in Appendix IV have the property of stiffness due to their rate dependent nature. As a consequence, special care was exercised in the numerical time integration in the FORTRAN programmes. The selection of a stable time-marching scheme was important to provide a solution to the set of stiff differential equations. The use of the explicit Euler method was precluded because of

its severe stability restriction on time-step size (Argyris et al [1978]). One alternative is to employ an implicit scheme, such as the trapezoidal method, which has substantially wider stability limits than does the Euler method, but which requires iterations to converge to the correct solution. Another alternative is to use an implicit time operator which is made explicit through the use of gradients to approximate the functions at the end of the time step. This is termed the forward gradient method and has been used successfully for various stiff viscoplastic equations (Zirin et al [1982], Peirce et al [1983], Han and Kremple [1986]), and has been used here.

The constitutive equations, given in Appendix IV, as a set of nonlinear differential equations, can be written in a general form as

$$\begin{cases} \dot{\sigma} = \sigma(\sigma, \varepsilon^e, \varepsilon^{in} X) \\ \dot{\varepsilon}^e = \varepsilon^e(\sigma, \varepsilon^e, \varepsilon^{in} X) \\ \dot{\varepsilon}^{in} = \varepsilon^{in}(\sigma, \varepsilon^e, \varepsilon^{in} X) \\ \dot{X} = X(\sigma, \varepsilon^e, \varepsilon^{in} X) \end{cases} \tag{7.28}$$

The forward gradient approach with a general implicit operator θ assumes that over a time interval Δt;

$$\Delta y = [(1-\theta)\dot{y}_t + \theta \dot{y}_{t+\Delta t}]\Delta t \tag{7.29}$$

with

$$y \equiv \begin{Bmatrix} \sigma \\ \varepsilon^e \\ \varepsilon^{in} \\ X \end{Bmatrix} \quad \text{and} \quad 0 \le \theta \le 1 \tag{7.30}$$

Here, a subscript is used to denote the time at which arguments of y are evaluated, e.g. $\dot{\sigma}_t = \sigma[\sigma(t), \varepsilon^e(t), \varepsilon^{in}(t), X(t)]$. The parameter θ can range from 0 to 1, with θ =0 corresponding to a simple Euler time integration scheme, and θ=1 equivalent to a one-step scheme of the multistep method (Han and Krempl [1986]). A comparison of the simulation errors (defined as difference betwen experimental strain input and simulation strain output) using different θ values is given in Fig.7.5. It is evident that the simulation with θ=0.5 gives the minimum error compared with other θ values. Therefore θ=0.5 was used for the simulations in the present study. Further saving of computing time has been achieved by using variable time-step size, especially during

the stress relaxation period, with a very small time step size in the first several seconds of relaxation, i.e. 1% of the normal time step used in other parts of the simulation.

A reasonable time-step size has been determined by comparing the FORTRAN simulation results with those from the SIMNON simulations in the simple [001] and [111] cases, and by comparing the input strain, $(\Delta\varepsilon_T)_{input} = \dot{\varepsilon}_T \Delta t$, with the output strain, $(\Delta\varepsilon_T)_{output} = \varepsilon_T(t+\Delta t) - \varepsilon_T(t)$, at each time step to keep the relative error to less than 2%. Figure7.6 gives an example of the relative errors for a simulation of the hypothesis loops of tests sb9501, sb9502 and sb9506.

The details of the group of FORTRAN programmes together with those written in SIMNON are given in Appendix VI.

7.5.Simulation Results

The simulation results of continuous cycling stress-strain behaviour for two specimens (sb9501 and sb9506) with very different crystal orientations and a total strain range, $\Delta\varepsilon_T = 1.0\%$, are presented in Fig.7.7a and 7.7b. Figure 7.7c compares the simulated and experimental stress-strain hysteresis loop for a specimen (sb9502) with a crystal orientation intermediate to the two specimens shown in Figs.7.7a and 7.7b. The experimental results indicate the influence of orientation on the cyclic stress-strain response. For the same total strain range, the [001] orientation exhibits lower maximum and minimum stresses and low plastic deformation, whilst the [111] orientation shows higher peak stresses and larger plastic strain. The calculated responses reflect this cyclic mechanical behaviour with the simulation results in good agreement with the experimental results.

Simulations has also been performed to model the influence of orientation on the material response in the fatigue-creep tests with tensile or compressive dwells. Experimental and simulated results are compared for three different test specimens, sb9510, sb9512 and sb9515, with various crystal orientations. Steady-state results are shown in Figures 7.8a through 7.8c for tests with tensile, compressive and balanced dwells respectively. The predicted stresses over the whole cycle for the three tests are all very close to the experimental data showing that the effect of crystal orientation on stress relaxation is also well described. In particular, the total stress relaxation during the 2 minute strain dwell in the near [111] specimen (sb9512) is much larger than that in the near [001] specimen (sb9510).

Figures 7.9a, 7.9b and 7.9c show that the stress relaxation response varies with crystal orientation during the 2 minute strain dwells in tension or in compression. It is observed that the simulation predicts fairly well the relaxation curves with stresses dropping quickly during the first 5 to 10 seconds and then changing relatively slowly in the remaining time. The stress relaxation responses within the 2 minute dwell, either in tension or in compression, were found to be similar in the balanced dwell test.

A feature of the cyclic mechanical behaviour of single crystal SRR99 in the tests with unbalanced strain dwells (a dwell in tension or in compression) is the mean stress behaviour. This is also well simulated by the constitutive model. Figure 7.10a illustrates the simulation result for a test (sb9513) with a tensile dwell. It should be noted that the mean stress changes rapidly in the first several cycles and then remains constant in the following cycles. This observation is in good agreement with the experimental results described in Chapter 5 (section 5.2.6). For the purpose of comparison, Figures 7.10b shows simulation results with a compressive dwell for a hypothetical specimen with the same orientation as sb9513. The effect of tensile or compressive strain dwells is clearly demonstrated in Fig.7.10, with tensile dwell inducing negative mean stress, whilst compressive dwell causing positive mean stress.

Simulated and experimental results which include the cyclic hardening/ softening behaviour of single crystal SRR99, and also provide an overview of the ability of the constitutive model to simulate the mechanical behaviour, are shown in Figs.7.11 and 7.12 for tests without or with strain dwells respectively. The simulated total stress response agrees well with the experimental data for most of the cyclic life. Both calculated and experimental results indicate that single crystal SRR99 exhibits cyclic stability during continuous cycling tests. The tests show initial cyclic softening in the first 5 to 10 percent of cyclic life and then remain stable until about 80 percent cyclic life when tensile (Fig.7.12a) or compressive (Fig.7.12b) dwells are introduced. The model also provides good predictions of the initial softening behaviour observed in the balanced test, but fails to simulate the continuous softening response. However, the relative error in total stress range between the simulated and experimental results is less than 10% until 70-80 percent of cyclic life. The main difference between the simulated and experimental results for all the tests occurs at the final stage of cyclic life. The experimental results show a rapid decrease in stresses leading to final rupture of the specimen. This is attributed to the effect of the

accumulated material damage. The model does not include damage evolution and cannot predict the final stress response caused by accumulated material damage during fatigue-creep tests. The continuous softening behaviour observed in the balanced dwell test at 950°C may be also attributable to the influence of accumulated material damage including its long test duration at high temperature. However, the balanced dwell test does soften more severely than both the unbalanced dwell tests and this is not fully understood.

In addition, it is observed that the stress level obtained by simulation of specimen sb9502 (Fig.7.11c) is generally higher than that found experimentally, although the relative error is less than 7% in the most parts of the cyclic life. This difference may be related to a possible error in the specimen orientation measurement. There is strong evidence for this in Fig.7.7c as the simulated elastic response is also different from that observed experimentally. The elastic modulus calculated from the simulation was larger than that obtained from experiment. Since the larger the elastic modulus, the further the crystal orientation from the [001], and the higher the total stress level, it is likely that the real orientation of specimen sb9502 (Fig.7.11c) is further from the [001] orientation than measured.

CHAPTER 8
CREEP-FATIGUE LIFE PREDICTION

8.1. Introduction

Two types of life prediction approaches have been studied and used in this work for the life assessment of single crystal SRR99 under fatigue and creep-fatigue conditions. In Section 8.2, the conventional life prediction methods mentioned earlier in Chapter 3 are directly applied to predict the lives of SRR99 single crystal. Some modifications have been proposed to take into account the particular deformation characteristics of single crystal SRR99. For this approach, the deformation behaviour observed at half life cycle has been chosen as the representative behaviour of single crystal SRR99 under various loading conditions. The stress and strain data obtained from the experimental loops at half life cycle have been used in the various life prediction models to predict life and show the correlation between experiment and theory. In Section 8.3, an attempt is made to combine life prediction under low cycle fatigue with the constitutive model developed for single crystal SRR99. In this approach, the quantities of interest, such as stress and strain, for various life prediction methods have been determined from the calculated hysteresis loops by using the constitutive model instead of from the experimental data, and the life prediction is based on the deformation behaviour of each cycle during the fatigue life instead of only on the half life cycle.

8.2. Conventional Life Prediction Approaches

8.2.1. Coffin-Manson Law

The Coffin-Manson equation applied to the high temperature LCF conditions discussed in Section 3.2.1. can be written as;

$$\Delta\varepsilon_{in} N_f^{\beta_1} = C_1 \tag{8.1}$$

where β_1 and C_1 are temperature dependent material constants. Eq.(8.1) is used for the life prediction of single crystal SRR99 data obtained at 950°C and 1050°C, but not for the tests at 750°C, since the inelastic strain is very small (see Section 6.3.1).

Two approaches have been used to determine the temperature dependent material constants β_1 and C_1. In the life correlation, β_1 and C_1 are determined by all the experimental data relating to the temperature being investigated. For life prediction, β_1 and C_1 are determined from certain number of experimental data, and are then used to predict other test results.

The values of the constants β_1 and C_1 obtained by the first approach, i.e. by correlating all the experimental data at 950°C and 1050°C respectively with Eq.(8.1), are given in Table 8.1. Figs.8.1a and 8.1b present the life correlation results for tests at 950°C and 1050°C respectively. It can be seen that the test data at 1050°C are well correlated within a factor of two. However, the life correlation plot for tests at 950°C separates data according to whether they experienced tensile strain dwells or not. All the tests without tensile dwells, i.e. continuous cycling (0/0) and tests with compressive dwells (0/t), correlate to form the overpredicted bounding line, whilst the tests with tensile dwells (t/0 and t/t) correlate to give the underpredicted bounding line. This can be attributed to the combined effects of mean stress and time dependent damage induced in the fatigue-creep tests as discussed in section 6.4.

Using the material constants β_1 and C_1 determined by analysis of only the continuous cycling data, also given in Table 8.1, the creep-fatigue life of the tests with strain dwells have been predicted. The comparison between the predicted and observed lives for tests at 950°C and 1050°C is shown in Figs.8.2a and 8.2b respectively. The creep-fatigue lives of single crystal SRR99 at 1050°C, based on the limited test data, are well predicted within a factor of two using the material constants obtained from the continuous cycling tests. At 950°C, the tests with compressive dwells are also well predicted. However, the tests with tensile dwells (t/0 and t/t) are underpredicted, the ratios between the observed and predicted lives for all the tests with tensile dwells are greater than a factor of two. These results indicate that the fatigue life behaviour of the continuous cycling tests and the tests with compressive dwells is similar, based upon total inelastic strain.

8.2.2. Damage Function Approach.

The damage function approach proposed by Ostergren [1978] has been widely used to predict high temperature low cycle fatigue life where strain dwells are introduced in the fatigue tests. The power law relationship between the damage function $\sigma_t \Delta\varepsilon_{in}$ and the fatigue life N_f is written as;

$$N_f = C_2 \, (\sigma_t \, \Delta\varepsilon_{in})^{\beta_2} \qquad (8.2)$$

where C_2 and β_2 are temperature dependent material constants, σ_t and $\Delta\varepsilon_{in}$ are the tensile stress and the inelastic strain range respectively. The damage function approach in this form is in fact a modification of the Coffin-Manson law, where the additional tensile stress indirectly represents the effect of mean stress. As in the use of the Coffin-Manson law, uncertainties arise in selecting the most appropriate data from which to determine the values of constants C_2 and β_2.

The material constants C_2 and β_2 , determined by the continuous cycling test data and by the best-fit of all the test data obtained at 950°C or 1050°C, are given in Table 8.2. The correlation results based on the best-fit material constants are shown in Figs.8.3a and 8.3b for tests at 950°C and 1050°C respectively. The predicted fatigue/ creep-fatigue life, and the experimental life correlate within a factor of two for all the tests at 950°C or 1050°C. However, the correlation still exhibits differences in terms of cycle types. The predicted lives for tests with tensile dwells (t/0 and t/t) are found to be shorter than experimental lives for tests at 950°C, and longer for tests at 1050°C. If the material constants obtained from analysis of the continuous cycling test data only were used for life prediction, Figs.8.4a and 8.4b, the results also show the cycle type dependent characteristics and the scatter band for the tests at 1050°C is even larger than in Fig.8.3b. The ratio of predicted and observed lives at 1050°C for all the tests with tensile dwells (t/0 and t/t) is greater than two.

Overall, the damage function approach shows an improvement in the life prediction for single crystal SRR99 in comparison with Coffin-Manson method, but still segregates the test data based on the cycle types.

8.2.3. Frequency Modified Damage Function Approach

As indicted earlier in Section 3.2.5, the damage function approach, which modifies the Coffin-Manson law to include the mean stress induced by strain dwells is a time-independent life prediction method. When time dependent mechanisms are present, such as creep-fatigue interaction, a frequency modified damage function approach is used. This approach modifies Eq.(8.2) by including a frequency term which takes into account the time dependency;

$$N_f = C_3 \, (\sigma_t \, \Delta\varepsilon_{in})^{\beta_3} \; \nu^m \qquad (8.3)$$

where m, C_3 *and* β_3 are temperature dependent material constants and ν is the frequency. The frequency selected for use in Eq.(8.3), as discussed in Section 3.2.5, is dependent upon the sensitivity of the material to different waveshapes.

Since it was not possible to determine in advance which frequency term would be appropriate for single crystal SRR99, different terms were fitted to the test data. The term which provides the best fit to the data, follows from some studies on polycrystalline materials (Ostergren [1976b]), is the frequency defined as;

$$\begin{cases} \nu = \dfrac{1}{T_o + T_t + T_c} & T_t \geq T_c \\ \nu = \dfrac{1}{T_o} & T_t < T_c \end{cases} \tag{8.4}$$

where T_o , T_t and T_c are times for the continuous cycling portion, the tension hold time and the compression hold time, respectively. Obviously, the frequency used for the tests with tensile dwells (t/0 and t/t) is different from that used in the tests without tensile dwells (0/0 and 0/t), i.e. single crystal SRR99 is sensitive to waveshape. This frequency selection seems reasonable because it reflects the different life behaviour observed in the tests with or without tensile dwells and the segregation of data according to cycle type obtained by the damage function approach.

The best-fit equations for the tests at 950°C and 1050°C are found to be

$$950°C \qquad N_f = 316.96(\sigma_t \Delta\varepsilon_{in})^{-1.094}\ \nu^{-0.1675} \tag{8.5}$$

$$1050°C \qquad N_f = 1294.195\,(\sigma_t \Delta\varepsilon_{in})^{-1188}\ \nu^{0.2715} \tag{8.6}$$

The life prediction results based on Eqs.(8.5) and (8.6) are shown in Figs.8.5a and 8.5b respectively. The scatter band for data in both figures are less than a factor of two. No segregation according to cycle type isobserved, for example, as in Figs.8.3a and 8.3b.

The sensitivity to the selection of the test data in determining the material constants for the frequency modified damage approach was examined. If the continuous cycling (0/0) test data only were used to determine the material constants m, C_3 and β_3, which are given in Table 8.3, for use in Eq.(8.3) to predict creep-fatigue lives of the tests with strain dwells, then significant segregation of the results in terms of cycle type is observed, Fig.8.6a and 8.6b. The tests with compressive dwells are well

predicted at both 950°C and 1050°C. However, the predicted life of tests with tensile dwells (t/0, t/t) is more than 10 times longer than that of experimental life observed at 950°C, and 6 times shorter observed at 1050°C. It is evident that the frequency modified damage function approach is more sensitive to the selection of data in determining the material constants than is found in other methods, e.g. the Coffin-Manson law or the damage function approach.

8.2.4. Mean Stress Models

Pure Fatigue Behaviour. The low cycle fatigue behaviour under the completely reversed condition, i.e. both mean stress and mean strain equal zero, of single crystal SRR99 can be described using the continuous cycling (0/0) test data via the conventional Coffin-Manson equation, as discussed in Section 3.2.4., in the form;

$$\frac{\Delta\varepsilon_T}{2}=\frac{\Delta\varepsilon_e}{2}+\frac{\Delta\varepsilon_p}{2}=\frac{\sigma_f^{'}}{E_{[001]}f(A_{hkl})^{-1}}(2N_f)^b+\varepsilon_f^{'}(2N_f)^c \quad (8.7)$$

where $\sigma_f^{'}$ is the fatigue strength coefficient, b is the fatigue strength exponent, $\varepsilon_f^{'}$ is the fatigue ductility coefficient, c is fatigue ductility exponent and $E_{[001]}$ is Young's modulus of the [001] orientation of single crystal SRR99. Here the elastic term is modified by using the orientation function $f(A_{hkl})$. Correlating the elastic and plastic strain ranges for the tests at 950°C and 1050°C, and using a log-log linear regression method, the conventional low cycle fatigue behaviour of single crystal SRR99 at 950° C and 1050°C can be expressed as

at 950°C

$$\frac{\Delta\varepsilon_T}{2}=\frac{1573.6}{E_{[001]}f(A_{hkl})^{-1}}(2N_f)^{-0.1653}+0.1191\,(2N_f)^{-0.7423} \quad (8.8)$$

at 1050°C

$$\frac{\Delta\varepsilon_T}{2}=\frac{996.7}{E_{[001]}f(A_{hkl})^{-1}}(2N_f)^{-0.1569}+0.903\,(2N_f)^{-0.9201} \quad (8.9)$$

The tests at 750°C, as discussed in Section 6.3.1, are dominated by elastic deformation, the plastic strain range for all the tests being very much smaller than the

elastic strain range. The total strain range is approximately equal to the elastic strain and the continuous cycling fatigue behaviour can be described as;

$$\frac{\Delta\varepsilon_T}{2} = \frac{2480.8}{E_{[001]} f(A_{hkl})^{-1}} (2N_f)^{-0.1628} \tag{8.10}$$

Morrow's Mean Stress Model. The fatigue life prediction by Morrow's mean stress model for a given strain amplitude is obtained by solving the following equation (see Section 3.2.4.)

$$\frac{\Delta\varepsilon_T}{2} = \frac{\sigma_f' - \sigma_m}{E_{[001]} f(A_{hkl})^{-1}} (2N_f)^b + \varepsilon_f' (2N_f)^c \tag{8.11}$$

using the measured mean stress at approximately half-life and the known low cycle fatigue properties σ_f' ,b, ε_f' and c determined from the continuous cycling tests. The nonlinear equation (8.11) was solved by using a Newton-Raphson numerical method using a FORTRAN program.

A comparison of the fatigue lives predicted by Morrow's model with experimental fatigue lives is shown in Figs.8.7a, 8.7b and 8.7c for tests at 750°C, 950°C and 1050°C respectively. At 750°C a fairly good correlation between observed life and predicted life can be obtained, Fig8.7a, even though Morrow's model seems to overestimate the creep-fatigue lives for the tests with compressive dwells and underestimates the creep-fatigue lives for the tests with tensile dwells. For tests at 950°C and 1050°C, the predicted and experimental lives for 0/0 and 0/t tests, excepting for one test with a small total strain range and long life, can be correlated within less than a factor of two. However, the observed lives for t/0, especially in the longer life region, and for the t/t tests are significantly shorter than those predicted by Morrow's model.

Smith, Watson & Topper (SWT) Model. The SWT model discussed in Section 3.2.4 in the form

$$\sigma_{max} \frac{\Delta\varepsilon_T}{2} = \frac{(\sigma_f')^2}{E_{[001]} f(A_{hkl})^{-1}} (2N_f)^{2b} + \sigma_f' \varepsilon_f' (2N_f)^{b+c}$$

$$= \frac{A}{E_{[001]} f(A_{hkl})^{-1}} (2N_f)^{\alpha} + B (2N_f)^{\beta} \qquad (8.12)$$

has also been used for the life prediction of single crystal SRR99. The temperature dependent material constants A, B, α and β obtained from the continuous cycling tests alone, at 750°C, 950°C and 1050°C, are given in Table 8.4.

The nonlinear equation (8.12) has been solved by using the maximum stress at approximately half life and the Newton-Raphson numerical method. The fatigue lives predicted by the SWT model are compared with the experimental results in Figs.8.8a, 8.8b and 8.8c. for tests at 750°C, 950°C and 1050°C respectively.

The correlation between the actual life and the predicted life using the SWT model for all the tests at 750°C is fairly good. All the data obtained for tests with or without strain dwells can be collapsed into a single scatter band. The scatter in life in Fig.8.8a is less than a factor of two. The significant cycle type dependent characteristics found by using Morrow's model are not observed. A comparison between the lives obtained experimentally and the lives predicted by the SWT model for tests at 950°C and 1050°C shows a similar trend. That is, the actual lives for tests with tensile dwells (t/0, t/t) are much shorter than the predicted lives. Since time dependent damage can be expected to be important in the tensile strain dwell at 950°C and 1050°C, it appears that the SWT model is likely provide a more realistic representation for the mean stress effect on the fatigue behaviour of single crystal SRR99.

8.2.5. Modified Strain Range Partitioning (SRP) Method.

The Strain Range Partitioning (SRP) model extends the Coffin-Manson law by considering the interaction of time-dependent inelastic (or creep) strains and time-independent inelastic (or plastic) strains. The equations of the conventional SRP model with an Interaction Damage Rule discussed in Section 3.2.5 can be written as

$$\begin{cases} N_{ij} = C_{ij} (\Delta \varepsilon_{in})^{\beta_{ij}} \\ (N_f)^{-1} = \sum \dfrac{F_{ij}}{N_{ij}} \end{cases} \qquad (8.13)$$

with

$$F_{ij} = \frac{\Delta\varepsilon_{ij}}{\Delta\varepsilon_{in}} \tag{8.14}$$

In the above equations, the subscripts ij represent the four inelastic strain ranges pp, pc, cp and cc, see Fig.3.1, N_{ij} is the cycles to failure if $\Delta\varepsilon_{in}$ equals each ij strain component respectively; C_{ij} and β_{ij} are temperature dependent material constants.

The above SRP model has been used to correlate the test data of single crystal SRR99 obtained at 950°C and 1050°C. It is found that the SRP model in the conventional form is not applicable to these data.. All the tests with tensile dwells at 950°C and some of them at 1050°C yielded negative values for N_{cp} and N_{cc}, and the partitioned $\Delta\varepsilon_{pc}$ and N_{pc} relationships for the tests with compressive dwells also have a large scatter. This results are attributed to the mean stress effect induced by strain dwells.

In order to use SRP model in the life prediction, eight parameters must be determined, by laboratory testing, to define the basic strain range versus life relationships (Eq.(8.13)) under simple strain loading, i.e. pp, pc, cp or cc conditions. In practice, only pure pp tests can be performed, and pure pc, cp and cc experiments cannot be conducted directly. Therefore, in the commonly used evaluation procedures the data have to be reduced to 'pure' data using the already known pp parameters. For example;

$$\left(N_{cp}\right)^{-1} = F_{cp}\left(\frac{1}{N_f} - \frac{F_{pp}}{N_{pp}}\right) \tag{8.15}$$

If there is no mean stress in the strain dwell tests, the pp strain seperated out from the total inelastic strain, can be regarded as the equivalent pure pp strain in the continuous cycling tests. However, if there is a significant mean stress induced by strain dwells, the partitioned pp strain will not be equivalent to the pure pp strain in terms of the effect on fatigue life. As a result, the partitioned pp strain must be modified by the mean stress to be equivalent to pure pp strain.

In the present work, a simple method is proposed to take into account the mean stress effect on pp fatigue life. The partitioned pp strain for the tests with a mean stress are modified to an equivalent pure pp strain with zero mean stress in the form;

$$\left(\Delta\varepsilon_{pp}\right)_{\sigma_m=0} = \left[\frac{\sigma_{max}}{\Delta\sigma/2}\right]^{\gamma} \left(\Delta\varepsilon_{pp}\right)_{\sigma_m} \tag{8.16}$$

Using the modified SRP model, and the material constants given in Table 8.5, the test data obtained in the tests with and without strain dwells at 950°C, Fig.8.9a, correlate well within a scatter band, defined by the ratio of predicted to observed life, less than 2. For the 1050°C tests, based on more limited data, the modified SRP model also correlates the predicted life and the test results to within a factor of two, Fig.8.9b.

8.2.6. Linear Damage Summation Rule

The only internationally accepted method for predicting creep-fatigue endurance is described in ASME Code N-47 [1974] and is known as the Linear Damage Summation Rule. Assuming that the fatigue damage and creep damage in each cycle are given by;

$$\begin{cases} D_f = \dfrac{1}{N_{fp}} \\ \\ D_c = \displaystyle\int_0^{t_h} \frac{dt}{T_c(t)} \end{cases} \tag{8.17}$$

where N_{fp} is the fatigue life in the pure fatigue test, and $T_c(t)$ is the creep rupture time corresponding to the loading condition at the time of interest, t_h is the total strain dwell time. The summation of the fatigue damage and creep damage leads to the determination of the number of cycles to failure for the combined fatigue and creep test

$$D = N_f(D_f + D_c) = N_f\left[\frac{1}{N_{fp}} + \int_0^{t_h} \frac{dt}{T_c(t)}\right] \leq 1 \tag{8.18}$$

Normally, D at failure is chosen to be one. Therefore the creep-fatigue life for a test with strain dwells can be written as;

$$N_f = \frac{1}{\left[\dfrac{1}{N_{fp}} + \displaystyle\int_0^{t_h} \frac{dt}{T_c(t)}\right]} \tag{8.19}$$

This method, as mentioned earlier in Section 3.2.6 has been found to be inaccurate when applied to different materials and various fatigue-creep loading conditions. In the present work certain modifications and assumptions have been made to extend the applicability of this method for single crystal SRR99 data. First, the evaluation of fatigue damage has been modified to include the mean stress effect observed in the fatigue-creep tests. This is done by using the SWT Mean Stress Model to calculate the pure fatigue life of the tests with strain dwells. Second, the compressive dwell was assumed not to induce time-dependent creep damage. Only the tensile dwells in the t/0 and t/t tests are considered to cause creep damage. This assumption is supported by the data for single crystal SRR99, where the 0/0 and 0/t endurances pair well, as do the t/0 and t/t results. Third, since there is a lack of creep data on single crystal SRR99, the virgin creep data obtained by monotonic tensile creep tests using the [001] specimens has been used to calculate the creep rupture $T_c(t)$. The creep damage in each cycle, induced by the tensile strain dwell, where stress relaxation has occurred, has been assessed numerically using the stress relaxation data at the half-life cycle. This has been modelled by using the time hardening rule (see Section 6.3.1) in the form;

$$\sigma(t) = \left[(n'-1)E_{[001]} f(A_{hkl})^{-1} C t^{m} + \sigma_0^{(1-n')}\right]^{\frac{1}{(1-n')}} \tag{8.20}$$

The creep rupture time $T_c(\sigma)$ as a function of applied stress and based on the data obtained by DRA Pyestock [1992] can be well represented by a Dorn type function;

$$T_c(\sigma) = \log^{-1}\left[A_c + B_c\sigma + C_c \log(\sigma) + G_c / T\right] \tag{8.21}$$

where T is the creep test temperature (K), A_c, B_c, C_c and G_c are material constants. For single crystal SRR99 at temperature between 950°C and 1050°C, the values of A_c, B_c, C_c and G_c are -9.24, -5.02×10^{-3}, -1.167 and 19240 respectively, when the units of the rupture time, T_c, and applied stress, σ, are hours and MPa respectively. The correlation is shown in Fig.8.10.

The predictions obtained using the above method for single crystal SRR99 at 950°C and 1050°C are given in Fig.8.11a and Fig.8.11b respectively. It can be seen that the predicted lives for the tests with tensile dwells (t/0 and t/t) are larger than the experimental lives. The ratio of creep damage to fatigue damage is found to be very small ($D_c/D_f \leq 10\%$). One reason for the poor correlation could be the use of the virgin creep data obtained from the DRA uniaxial creep tests using the [001]

specimens only, since the creep damage mechanism in the repeated short term relaxation may be different from that in the long term monotonic creep test, and also the crystal orientation probably has a significant influence on the creep rupture behaviour (Kear [1974], Mackay and Maier [1982], Pope and Ezz [1984]). Another possible reason is the creep-fatigue interaction which is not considered in the linear damage summation rule. If there is interaction between fatigue damage and creep damage, the value of D might be less than 1 as discussed in the ASME Code N-47 [1974]. The results also indicate that the difference between predicted and experimental life for the tests with a long life, and for the tests with balanced dwells, is larger than for the short life tests. This may be attributed to another type of time dependent damage, such as oxidation during the long duration creep-fatigue tests in air, or thermal degradation of the microstructure.

8.3. Life Prediction Combined with the Constitutive Model

8.3.1. General Comments

As mentioned in Section 3.2., most life prediction methods which emanate from the original Coffin-Manson Law require a typical cycle, normally the half-life cycle, from which the relevant quantities must be determined. This kind of method has the advantage that only one cycle has to be considered in the analysis. However, uncertainties arise in the application of these methods. The typical cycle chosen must be able to represent the deformation behaviour of the material during the fatigue and fatigue-creep tests. If the material exhibits cyclic hardening or softening, the deformation behaviour changes during cycling, it is not possible to take into account of these changes in the life prediction. Furthermore, when these methods are used for complex loading conditions, such as including a dwell period with creep and stress relaxation, it then becomes necessary to know precisely the shapes of the hysteresis loops so that relevant quantities for the various life prediction methods can be deduced. Experimentatally, the hysteresis loops are determined during a test, and the relevant quantities can be read directly from the test record. However, when using developed life prediction methods for the design of a component operating under a given loading condition, the deformation behaviour must be obtained by calculation. In this case the combination of a life prediction method with a realistic material model, i.e. constitutive model, is indispensable. The appropriate hysteresis loops can be computed using the constitutive equations under a given loading condition. These quantities are then used as input to the life prediction method.

In this Section, the anisotropic viscoplastic constitutive model developed in Chapter 7 is used in combination with the life prediction methods for the life assessment of single crystal SRR99 under fatigue-creep conditions at 950°C. Of course, the quantities necessary to predict the life are different for different life prediction methods and loading conditions, and the constitutive model should be capable of determining these quantities. This will further demonstrate the applicability of the proposed constitutive model for single crystal SRR99.

8.3.2. Life Assessment Techniques

The life prediction methods which can be used to evaluate the life spent under variable loading must be formulated in incremental form. The integration of the constitutive equation for each cycle provide the quantities of interest for the life prediction method and allows evaluation of the material damage induced by each cycle. The accumulated damage during each cycle is then added, and failure is defined when the accumulated damage reaching a critical value. In this work, two approaches will be illustrated, use of the Linear Damage Summation Rule and use of the modified SRP method proposed in this work.

Life prediction combined with a constitutive model has been achieved by writing a group of subroutines in the FORTRAN programs described in Chapter 7, in connection with the simulation of the cyclic mechanical deformation behaviour of single crystal SRR99. This approach has been only applied to the tests at 950°C in this section, since there is not enough test data for the simulations at 750°C and 1050°C for the reasons mentioned in Chapter 7. The details of the subroutines and the connections with the simulation programs are given in Appendix VI.

In the conventional life prediction methods, only one cycle is chosen to represent the cyclic mechanical deformation characteristics of the material at a given loading condition. Consequently, the life prediction equations are in a form which only includes the stress and strain variables of that typical cycle. Also, the material damage induced in each cycle is assumed to be same. However, the combined life prediction technique which takes into account the change of the stress and strain during fatigue life due to the material softening or hardening, is based on the cyclic deformation characteristics of each cycle. Therefore, the life prediction equations need to be modified into an incremental form to calculate the accumulated material damage induced in each cycle.

Linear Damage Summation Rule. This method can be easily written in the incremental form as;

$$D=\sum_{1}^{N_f}D_f(N)+\sum_{1}^{N_f}D_c(N) \tag{8.22}$$

with

$$\begin{cases} D_f(N)=\dfrac{1}{N_{fp}(N)} \\ \\ D_c(N)=\displaystyle\int_0^{t_h}\frac{dt}{T_c(N,t)} \end{cases} \tag{8.23}$$

where $N_{fp}(N)$ is the number of cycles to failure under the loading condition similar to the condition in cycle N but not including creep, and is determined by the SWT mean stress model;

$$\sigma_{max}(N)\frac{\varepsilon_T}{2}=\frac{A}{E_{[001]}f(A_{hkl})^{-1}}[2N_{fp}(N)]^{\alpha}+B[2N_{fp}(N)]^{\beta} \tag{8.24}$$

$T_c(N,t)$ is the creep rupture time under stress $\sigma(N,t)$ and is determined by the DORN type function;

$$T_c(N,t)=Log^{-1}[A_c+B_c\sigma(N,t)+C_cLog[\sigma(N,t)]+G_c/T] \tag{8.25}$$

where $\sigma_{max}(N)$ is the maximum stress at cycle N, $\sigma(N,t)$ is the stress, as a function of time, during the strain dwell period at cycle N. A, B, α, β and $A_c, B_c, C_c\ G_c$ are the temperature dependent constants defined in Eq.(8.12) and Eq.(8.21) respectively. The values of $\sigma_{max}(N)$ and $\sigma(N,t)$ are then calculated by the constitutive equations, and the same material constants A, B, α, β and $A_c, B_c, C_c\ G_c$ as in Section 8.2.6 are used in the life prediction.

A comparison of the predicted fatigue and creep-fatigue lives, using the Linear Damage Summation Rule combined with constitutive model, with the experimental lives is given in Fig.8.12. In the calculations, similar assumptions to those used in Section 8.2.6 for the conventional method have been employed. It can be seen that the predicted and experimental lives can only be correlated to within a factor of three

for all tests, although one compression dwell test showed an even larger disagreement, as it did for the conventional life prediction approach. The large scatter bands observed both in conventional and combined methods indicates that the application of the Linear Damage Summation Rule to single crystal SRR99 at 950°C under the loading conditions examined in this work is unsuccessful. The possible reasons may be due to the limited creep rupture data, the small inelastic deformation in the tests and the difference in the time dependent damage mechanisms under creep-fatigue conditions for single crystal in comparison with the polycrystalline materials.

Strain Range Partitioning (SRP) Method. The SRP method can be converted to an incremental form as;

$$\begin{cases} N_{ij}(N) = C_{ij}\left[\Delta\varepsilon_{in}(N)\right]^{\beta_{ij}} \\ D_f(N) = \left[N_f(N)\right]^{-1} = \sum\left[\dfrac{F_{ij}(N)}{N_{ij}(N)}\right] \end{cases} \tag{8.26}$$

with

$$F_{ij}(N) = \frac{\Delta\varepsilon_{ij}(N)}{\Delta\varepsilon_{in}(N)} \tag{8.27}$$

The accumulated damage is the summation of the damage induced in each cycle $D_f(N)$ in the simple form;

$$D = \sum_{1}^{N_f} D_f(N) = \sum_{1}^{N_f}\left(\sum \frac{F_{ij}(N)}{N_{ij}(N)}\right) = 1 \tag{8.28}$$

The modification of the mean stress effect is described by;

$$\left[\Delta\varepsilon_{pp}(N)\right]_{\sigma_m=0} = \left[\frac{\sigma_{\max}(N)}{\Delta\sigma(N)/2}\right]^{\gamma}\left[\Delta\varepsilon_{pp}(N)\right]_{\sigma_m(N)} \tag{8.29}$$

The definitions of N_{ij}, $\Delta\varepsilon_{in}$, F_{ij}, $\Delta\varepsilon_{ij}$ etc. are similar as those given in Section 8.2.5, except that they are now a function of cycle number. The same material constants determined in Section 8.2 have been used in the above life prediction techniques. All the stress and strain components have been directly computed by the simulation of creep-fatigue tests using the constitutive model.

The results of the calculations using the mean stress modified strain range partitioning (SRP) method with constitutive model simulations are shown in Fig.8.13, where the observed life is plotted versus the calculated life of single crystal SRR99 under various loading conditions at 950°C. Almost all the test lives are well predicted to within factor of two, although two data points show a slightly greater discrepancy. These two under-predicted tests (Sb9505 and Sb9609), with the smallest total strain range of 0.5% of all the tests, exhibit very little inelastic deformation. Therefore they are very sensitive to the various measurement errors in the experiments and errors in the input parameters from the computer simulations. For example, with a variation of the crystal parameter θ from 4.5 degrees to 9 degrees, which is within the error of the crystal orientation measurements, the predicted life for the continuous cycling test (Sb9505) is reduced by 30%. Therefore, taking into account the fact that the material constants have all been determined by the test data at the half life cycle, and the various possible errors in the measurements, the predicted results from the mean stress modified SRP method appear to be acceptable. The good results obtained by both conventional and combined methods indicate that the proposed mean stress modified SRP method is a suitable life prediction method for the high temperature performance of single crystal SRR99.

Although only two approaches have been demonstrated in this Section, since the constitutive model and the life prediction method are uncoupled at the present stage, any other suitable life prediction approach can be used in principle in combination with the constitutive model.

CHAPTER 9
CHARACTERISING CRACK GROWTH RATES

9.1. Introduction

As shown in Chapter 5 (section 5.4.2), the crack growth behaviour of single crystal SRR99 exhibits different characteristics compared with polycrystalline materials. The crack length of single crystal SRR99 in corner crack tests with tensile or compressive dwells at high temperature increases almost linearly with the number of cycles. For continuous cycling tests, although some evidence of non-linear crack growth is observed during the last stage of crack propagation, the crack extension up to about 1mm is found to take place approximately at a constant rate. Therefore, the crack growth rate of single crystal SRR99 at high temperatures for crack extensions not larger than 1mm shows no clear dependence upon crack length as is commonly noted for polycrystalline materials (Skeleton [1978], [1982]). A nearly constant crack growth rate over a certain crack extension range has also been observed by Chieragattir and Remy [1991] in single crystal MAR-M200 nickel base superalloy at elevated temperature. Since the main objective of this aspect of the work is to investigate the influence of temperature and cyclic type (with or without strain dwells) on the fatigue crack growth behaviour of single crystal SRR99, the average crack growth rate over the initial crack extension of 1mm is used to define the crack growth in the following analysis.

Two approaches, global strain and fracture mechanics, have been employed in the analysis of crack growth characteristics observed in the corner crack tests. In Section 9.2., the fatigue crack growth rate (FCGR) data have been correlated with the global strain parameters. The results have been analysed in terms of the various factors that would be expected to influence the crack propagation of single crystal SRR99 at elevated temperature. The crack propagation behaviour has also been compared with the low cycle fatigue behaviour observed in the smooth bar tests. In Section 9.3, a fracture mechanics approach has been used, and the crack growth rate has been analysed in terms of the cyclic J integral. The possible crack propagation mechanisms, which depend on both temperature and cycle type (with or without strain dwells), have been studied.

9.2. Crack Growth Analysis: Global Strain Methods

9.2.1 Total Strain

The crack growth rate of single crystal SRR99 for high temperature corner crack tests up to a crack extension of about 1 mm is found to be approximately constant for any given temperature under fully reversed cyclic loading. The average crack growth rate (extension per cycle) for each test can be plotted as a function of total strain range. Fig.9.1a, b and c illustrate the relationships between average crack growth rate da/dN and applied total strain range $\Delta\varepsilon_T$ for tests at 750°C, 950°C and 1050°C respectively. Although based on a limited number of tests, the general trends of the crack growth characteristics in single crystal SRR99 and its dependence on temperature and cyclic type with or without strain dwells can be clearly observed.

It can be seen that the crack propagation of single crystal SRR99 is accelerated by the introduction of a strain dwell either in tension (t/0) or in compression (0/t), as well as under both tension and compression (t/t) for tests performed at all the temperatures. However, the difference in crack growth rate between continuous cycling tests and tests with strain dwells is strongly dependent on temperature. At 750°C and 950°C, the crack growth rates in compressive dwell tests are higher than those in tensile dwell tests, but at 1050°C, a reversed situation is observed. The crack growth rate in the balanced dwell tests is higher than that in tensile dwell tests and lower than that of compressive dwell tests at 750°C and 950°C. However, it has the highest crack growth rate, among all the tests, at 1050°C. These results indicate that a tensile dwell is detrimental in its effect on crack growth of single crystal SRR99 as temperature increased. The temperature and cycle type dependence of crack growth behaviour in single crystal SRR99 tests can be attributed to a combination of the factors listed and discussed below.

Mean Stress Effect. The experimental results of cyclic mechanical response given in Chapter 5 indicate that the introduction of a strain dwell in a corner crack test induces a significant mean stress for single crystal SRR99. An unbalanced compressive dwell induces a large positive mean stress and a tensile dwell, a negative mean stress. Consequently, although all the tests are conducted under fully reversed total strain control, the actual stress ratio R ($\sigma_{min}/\sigma max$) for different cycle types is different. The stress ratio R increases in the compressive dwell tests (0/t) and decreases in the tensile dwell tests (t/0), and is almost constant ($R=-1$) in the

continuous cycling and balanced dwell tests. The influence of stress ratio on fatigue crack growth rate at elevated temperature has been widely studied for both polycrystalline materials (Mall et al [1990], Dimopulos et al [1988]) and single crystal nickel base superalloys (Crompton and Martin [1984], Diboine et al [1990]). In both cases, the fatigue crack growth rates (FCGRs) have been found to increase with increase of stress ratio, which is in agreement with the high fatigue crack growth rates in single crystal SRR99 observed in the tests with compressive strain dwells in this study.

The Role of Plastic (or Creep) Zone Ahead of the Crack Tip. It is well known that fatigue crack growth behaviour is controlled by the stress and strain distribution ahead of crack tip (Kujawsk and Ellyin [1984], Crompton and Martin [1984]). Introduction of a hold time (dwell), decreasing frequency or increasing temperature in the elevated temperature fatigue crack propagation tests will change the plastic or creep zone size and the stress and strain distribution ahead of crack tip, and consequently influence the fatigue crack growth rates. The effects of temperature and frequency on fatigue crack propagation of single crystal MAR-M002 at elevated temperature has been explored by Crompton and Martin [1984] in conjunction with a detailed investigation of crack tip plastic zone. It is reasonable that the fatigue crack growth rate should increase with decreasing frequency if failure is considered to take place when a critical strain is achieved over a critical distance within the crack tip plastic zone. Therefore, the accelerated crack propagation in SRR99 observed in the tests with strain dwells may partly attributed to the creep zone and possibly increased plasticity ahead of crack tip in these tests compared with continuous cycling tests.

Creep Damage. Fatigue crack propagation has been widely reported to be sensitive to creep damage and creep-fatigue interaction at elevated temperature (Liu and Oshida [1986], Shahinian et al [1989], Mall et al [1990]). In polycrystalline materials, transgranular crack propagation may occur at high frequency and low temperature, but a decrease in the frequency or introduction of a hold time and increasing temperature may give rise to intergranular crack growth and an associated increase in the crack propagation rate. It has been considered that this behaviour may arise from creep deformation localised to grain boundaries, leading to sliding and cavitation. For single crystal materials, although crack propagation can only occur in a transgranular manner, the effect of creep damage on fatigue crack propagation may still exist. Under creep deformation, damage cavities can be formed from the expansion and cracking of casting pores and crack growth occurs by linking of these pores in front of the main crack (Yang [1991]). The high fatigue crack growth rate in single crystal

SRR99, observed in tensile dwell tests at 1050°C, may be a result of such creep damage at high temperature.

Environmental (Oxidation) Attack. The importance of environmental attack (oxidation) on low cycle fatigue and crack growth behaviour at elevated temperature has been recognised for some time in polycrystalline materials and various mechanisms and models have been proposed to describe the oxidation assisted grain boundary cracking process (Solomon [1973], Antolovich et al [1981], Liu and Oshida [1986]) . For single crystal superalloys, although the grain boundary failure modes are eliminated, the effect of oxidation on the crack initiation and crack propagation has been found to exist still. Wright [1988] has studied the interaction of oxidation and low cycle fatigue in single crystal Rene N4 at 1093°C, and reported that both crack initiation and crack propagation processes of single crystal Rene N4 were influenced by oxidation. The low cycle fatigue life of single crystal Rene N4 was significantly decreased under conditions which are environmentally more severe. Hence it would be expected that oxidation may also influence the crack growth behaviour of single crystal SRR99 in the present study, especially at 1050°C, since the tests were performed at air.

Crack Closure. It has been noted that crack closure has a significant influence on fatigue crack propagation for both polycrystalline materials (Dowling and Iyyer [1987], Huseyin and Sun [1989]) and single crystal superalloys (Crompton and Martin [1984], Diboine et al [1990]). The effect arises because only the cyclic loading when the crack is open can cause crack growth. The crack opening stress depends on loading conditions, such as the stress ratio R, and closure can be microstructally sensitive. Closure may influenced by surface roughness, the restraint of the elastic material surrounding the crack tip plastic zone, and oxidation products. Therefore, the above four factors discussed above (mean stress, creep damage etc.), could all influence fatigue crack closure in the corner crack tests. Since the tests performed for single crystal SRR99 were conducted under fully reversed total strain control conditions, the crack closure point may be expected to vary with cycle type and hence result in different fatigue crack growth rates

In summary, all the above factors could influence the crack propagation characteristics of single crystal SRR99 observed in this study, however the contribution of each factor varies with different temperature and cycling conditions. The high crack growth rate observed at 750°C for compressive dwell tests could mainly be a result of the mean stress effect, since creep damage and oxidation would

be expected to be relatively small at this temperature. On the other hand, the observed high crack growth rate at 1050°C in the tensile dwell tests may be a combination of the effects of creep damage and oxidation.

9.2.2. Inelastic Strain

The fatigue crack growth rates can be plotted as a function of inelastic strain range. The correlation results are presented in Fig.9.2a and b for tests at 950°C and 1050°C respectively. Test results at 750°C are not given in this form since the inelastic strain in the tests at 750°C is very small, as indicated in Chapter 5. Consequently, it is difficult to separate out the inelastic strain range in these tests. The correlation results in terms of inelastic strain range exhibit different features compared with those based on the total strain range. At 950°C, the fatigue crack growth data obtained from continuous cycling tests and compressive dwell tests fall on a line with a crack growth rate nearly 10 times higher than the line due to tests with tensile dwells (t/0 and t/t). At 1050°C, despite limited data, the crack growth rates in the tests with or without strain dwells can all be correlated together about a single line. Comparing the above corner crack tests data, Fig.9.2a and b, with the low cycle fatigue data obtained from the smmoth bar tests, Fig.5.23 and 5.24, which including crack initiation and crack propagation, the similarity of the cycle type and temperature dependent characteristics is evident. Both results indicate that with the introduction of a tensile dwell the fatigue life reduces as temperature increases.

9.3. Crack Growth Analysis: Fracture Mechanics Methods

9.3.1 Calculation of the Cyclic J Integral

The cyclic J integral, ΔJ, has been widely recognised (Dowling [1987], Kiramura and Halford [1989], Plumtree and O'Conner [1989]) as a useful nonlinear fracture mechanics parameter for crack growth analysis in low cycle fatigue where large plastic deformation is present. The cyclic J integral for a infinite body with a short surface crack (Dowling [1976], Plumtree and O'Connor [1989]) is expressed as the sum of elastic and plastic terms where;

$$\Delta J = \Delta J_e + \Delta J_p = M_J [\pi \Delta \varepsilon_e + f(n') \Delta \varepsilon_p] \Delta \sigma a \qquad (9.1)$$

where $\Delta\sigma$, $\Delta\varepsilon_e$ and $\Delta\varepsilon_p$ are stress range, elastic strain range and plastic strain range respectively. M_J is a boundary crack-shape correlation factor, and f(n') is a function of the work hardening exponent , n' , in the cyclic stress-strain relation, where

$$\Delta\varepsilon_p = A\Delta\sigma^{n'} \tag{9.2}$$

For a semicircular surface crack M_J and f(n') are given by Dowling [1976] as

$$M_J = 0.506 \tag{9.3}$$

$$f(n') = 3.85\sqrt{n'}\,(1-\frac{1}{n'})+\frac{\pi}{n'} \tag{9.4}$$

For corner crack specimen used in this study, the crack is assumed to be one half of a semi-circular surface crack, and Eqs(9.1) to (9.4) can be readily applied. From the stress-strain relationship given in Chapter 5, the work hardening exponent n' for tests at 950°C and 1050°C was determined as 2.51 and 4.2 respectively, from which the function f(n') was calculated as 4.59 and 6.76 for tests at 950°C and 1050°C respectively. Since the 750°C tests are dominated by elastic deformation, only the elastic part of the J integral is used in the following analysis.

It should be noted that Eq.(9.1) to (9.4) are only strictly applicable to the continuous cycling tests. For the tests with strain dwells, based on the concept that the cyclic J integral is representative of the strain energy dissipated during fatigue cycles, the J integral is approximately calculated by using the total inelastic strain range $\Delta\varepsilon_{in}$ to replace the plastic strain range $\Delta\varepsilon_p$ in Eq.(9.1). The fatigue crack growth rate da/dN, as a function of cyclic J integral ΔJ, has been usually expressed in a power law form as

$$\frac{da}{dN} = C_J\,\Delta J^{\beta_J} \tag{9.5}$$

where C_J and β_J are temperature dependent material constants. From Eq.(9.1), it is clear that the cyclic J integral increases with crack length, therefore Eq.(9.5) implies that fatigue crack growth rate da/dN should also be a function of crack length. However, the experimental results obtained from the corner crack tests indicate that the fatigue crack growth rate da/dN in single crystal SRR99 at elevated temperature is approximately constant over a range where crack extension is less than 1mm. Therefore, strictly, the fracture mechanics approach appears not to be applicable to

short crack growth behaviour of single crystal SRR99 in the corner crack tests. Nevertheless, in order to illustrate the fundamental crack growth characteristics of single crystal SRR99 observed in the present study, the average values of J integral over the crack extension of interest will be used to correlate the corresponding average crack growth rate da/dN.

9.3.2. Correlation between da/dN and ΔJ

The total cyclic J integral ΔJ has been used to correlate the fatigue crack growth rate of single crystal SRR99 under various temperature and loading conditions. The results are presented in Fig.9.3a, b and c for tests at 750°C, 950°C and 1050°C respectively. It can be seen that the fatigue crack growth behaviour based on total cyclic J integral ΔJ, averaged over a test, exhibits similar temperature and cycle type dependent features as noted when total strain range as a correlation parameter (Fig.9.1a, b and c). The fatigue crack growth rates are higher in the tests with strain dwells than these in continuous cycling tests. Compressive dwell tests exhibit higher crack growth rates than tensile tests at 750°C and 950°C, but show lower crack growth rates at 1050°C. The difference in the fatigue crack growth rates between tests with and without strain dwells observed in Fig.9.3a, b and c is also found to be similar to that shown in Fig.9.1a, b and c.

Further similarities between the global strain and the fracture mechanics approach in describing fatigue crack growth behaviour of single crystal SRR99 can be seen in the correlation of da/dN with the inelastic J integral ΔJ_{in}. Fig.9.4a and b show the relationship between da/dN and ΔJ_{in} for tests at 950°C and 1050°C respectively. If compared with Fig.9.2a and b, where da/dN is correlated with inelastic strain range $\Delta \varepsilon_{in}$, then similar temperature and cycle type dependent crack growth characteristics in terms ΔJ_{in} and $\Delta \varepsilon_{in}$ are apparent.

9.3.3. Correlation between da/dN with J_{max}

As discussed in Section 9.2, crack closure may have a significant influence on fatigue crack propagation in the present corner crack tests, since all the tests were performed under fully reversed total strain control conditions. It was anticipated that a measure of the extent of crack closure could be obtained by using the PD monitoring technique. However, the test results were ambiguous. Although some changes in PD, which may be caused by crack closure, have been observed during some tests, a systematic correlation between PD change and the expected crack closure could not

be obtained. Therefore, to approximately estimate the crack closure in the low cycle fatigue crack propagation tests, the stress range from zero to maximum stress σ_{max} has been taken to be crack opening stress range. This approximation has been usually used by other workers as an estimate of the crack opening stress in low cycle fatigue crack growth tests when accurate crack closure measurements are not available (Diboine at al [1990])

Using σ_{max} to replace $\Delta\sigma$ in Eq.(9.1), the maximum (or effective) cyclic J integral J_{max} was calculated and used to correlate the fatigue crack growth rate. The results showing da/dN versus J_{max} for tests at 750°C, 950°C and 1050°C are given in Fig.9.5a, b and c respectively. The fatigue crack propagation characteristics in single crystal SRR99, in terms of J_{max}, is different from that based on ΔJ, since the crack closure effect is almost eliminated.

At 750°C, the crack growth data of tests with strain dwells, either in tension (t/0) or in compression (0/t), as well as in both tension and compression (t/t) can be approximately correlated together within a scatter band. However, the one balanced dwell test (t/t) exhibits a slightly higher crack growth rate compared with the unbalanced dwell tests (0/t and t/0). The crack growth rate data of the continuous cycling tests (0/0) forms another line in the plot. At a given J_{max}, the crack growth rate in the tests with strain dwells is nearly 6 times higher than that in continuous cycling tests. This accelerated crack propagation observed in the tests with strain dwells may be attributed largely to the plastic zone induced by the strain dwells. Since creep damage and the oxidation effect are small at 750°C, fatigue crack propagation at this temperature may be associated predominately with crack tip plasticity. Crompton and Martin [1984] have studied the crack tip plasticity and fatigue crack growth in single crystal MAR-M002 at 600 and 850°C and suggested that a similar process as proposed by McClinton and Irwin [1964] may occur and control crack propagation. As discussed earlier in this chapter, they consider that fracture may arise when a critical fracture strain is exceeded within a part of the plastic zone. Their detailed examination of the fracture surface confirmed the existence of plastic controlled failure of material at the crack tip. For single crystal MAR-M002 at temperature between 600 and 850°C, Crompton and Martin [1984] found that fatigue crack growth rates increase with decreasing frequency. In the present study, the introduction of a strain dwell also decreases the cyclic frequency. Therefore, the high crack growth rates observed in the tests with strain dwells at 750°C may be attributed to the plastic zone induced by the strain dwells, the size of this zone being larger than in continuous cycling tests.

When the test temperature increases to 950°C and 1050°C, creep damage and environment attack are expected to be more important in dominating fatigue crack propagation. As a result, Fig.9.5b and 9.5c show that the tensile strain dwell is more damaging. Indeed, the crack growth rates of tensile dwell tests are higher than those of both continuous cycling and compressive dwell tests. The difference in crack growth rates between tensile dwell and compressive dwell tests increases as temperature increases from 950°C to 1050°C. This behaviour could be attributed to creep damage and oxidation assisted fatigue crack propagation. It is well known that creep damage may accelerate fatigue crack propagation at high temperature via cavities forming in the creep zone ahead of the crack tip that may then link to form the main crack (Antolovich et al [1981], Liu and Oshida [1986]). Creep damage has been found to be different in tensile and compressive loading conditions and usually occurs faster under tensile stresses than compressive stresses. Therefore, it is to be expected that a tensile dwell will induce more creep damage than a compressive dwell, and, consequently, fatigue crack growth rates in the tensile dwell tests should be higher than in compressive dwell tests. This is in agreement with the experimental results given in Fig.9.5b and 9.5c. Oxidation-assisted fatigue crack growth can be viewed as the repeated formation and rupture of an oxide layer at the crack tip, thus exposing fresh metallic material to the environment (Antolovich et al [1981], Liu and Oshida [1986]). A tensile mechanical loading in the oxide above some critical fracture strain will cause the brittle oxide to fracture (Coffin [1972], Neu and Huseyin [1989]), and a large compressive loading can cause buckling of the oxide or complete spallation (Tien and Davidson [1974], Skelton [1974], Challenger et al [1981]). It has been found that tensile oxide fracture is especially detrimental for crack initiation and crack growth, because the repeated oxide fracture can accelerate crack growth into fresh material (Challenger et al [1981], Reuchet and Remy [1983]). The above oxidation-assisted fatigue crack growth mechanism indicates that the oxidation effect should be more important in the tensile than compressive dwell tests. Therefore, the accelerated fatigue crack propagation observed in the tensile dwell tests for single crystal SRR99 at 950°C and 1050°C may be a combination of creep damage and oxidation damage.

In order to illustrate the effect of temperature on fatigue crack growth behaviour in single crystal SRR99 under different loading conditions, fatigue crack growth rate, da/dN, is plotted as a function of J_{max} for continuous cycling tests, tests with tensile dwells and tests with compressive dwells in Fig.9.6a, b and c respectively. The same temperature dependent feature for different cycle type tests is observed, with the

highest fatigue crack growth rate at 1050°C and lowest at 750°C. Increasing test temperature leads to increased crack growth rate regardless of test cycle type.

Finally, based on the correlation results analysed in this chapter, the fatigue crack growth behaviour in single crystal SRR99, at various temperatures, can be summarised. At 750°C, fatigue crack propagation is dominated by the local plastic zone ahead of the crack tip, the accelerated fatigue crack growth in the tests with strain dwells being attributed to the plastic zone which is larger than for continuous cycling tests. At 950°C and 1050°C, creep damage and oxidation may also have a large influence on fatigue crack propagation. An interaction between fatigue damage, creep damage and oxidation may occur at these temperatures, especially at 1050°C. The large fatigue crack growth rates observed in the tests with strain dwells, particularly in the tensile dwell tests may be a result of both creep and oxidation damage. A detailed metallurgical examination of the fatigue crack propagation mechanisms at different temperatures and loading conditions, in a programme of future work, is needed to confirm these conclusions.

CHAPTER 10
DISCUSSIONS

10.1 Effect of Dwell Time on Low Cycle Fatigue Life

As documented by extensive testing reported in the literature (Lord and Coffin [1973], Manson [1973], Ostergren [1976], Miller et al [1984]), hold (dwell) times in total strain controlled low cycle fatigue testing often have a pronounced effect on the cyclic life for polycrystalline materials. For various materials, at different temperatures, there are conflicting arguments as to whether tension or compression hold times are the more damaging. Test results on AISI 304 steel at 707°C (Berling [1969] showed that tension hold times are more damaging than equivalent hold times in compression, or in tension and compression combined. However, test results on a CrMoV steel and cast nickel base superalloy, Rene 80, at 871°C (Lord and Coffin [1973], Leven [1973]) indicated that compression hold times are more damaging. A summary concerning on the relative severity of tension versus compression hold times for polycrystalline materials at various temperatures has been given by Plumbridge and Ellison [1987].

There are few investigations on the effect of hold times on the low cycle fatigue behaviour of single crystal superalloys. The results on single crystal SRR99, in this study, indicate that the influence of hold (dwell) times on fatigue life is strongly dependent on temperature. In the lower temperature range studied, i.e. 750°C, a compressive dwell is found to reduce fatigue life, whilst a tensile dwell increases fatigue life, in comparison with continuous cycling tests. This is associated with the development and maintenance of a high level of mean stress during asymmetric cycling. Compressive dwells produce a large tensile mean stress which enhances fatigue crack initiation and propagation by virtue of an increased stress ratio (see Chapter 5), whilst tensile dwells generate compressive mean stress which can prolong life over that for continuous cycling. With increasing temperature, i.e. 950°C , a compressive dwell becomes less damaging and the fatigue life shows an insignificant cycle type dependence. At high temperatures, i.e. 1050°C, tensile dwells become the most detrimental as the influence of time dependent damage, that is, creep damage and environmental degradation processes, predominates. Therefore, the change of the fatigue life of single crystal SRR99 when strain dwells are introduced is a combined result of mean stress, increased inelastic strain and time dependent creep damage and oxidation, caused by the dwell (hold) time. A logical explanation for the

effect of dwell (hold) times on the low cycle fatigue life of a single crystal superalloy lies in the relative contributions of above various factors.

10.2 Crack Initiation in Single Crystal SRR99

A low cycle fatigue test in a plain (i.e. unnotched) specimen can be split into two parts, crack initiation and crack propagation to failure. A deeper understanding of the influence of temperature and cycle type (with or without dwell times) on the low cycle fatigue life of single crystal SRR99 may be achieved by investigating their effects on crack initiation and crack propagation. The crack propagation behaviour of single crystal SRR99 has been obtained from corner crack tests. The results presented in Chapter 9 can be used to estimate the crack propagation stage in the smooth round bar tests, so that the crack initiation behaviour of single crystal SRR99 can be approximately estimated.

From Chapter 9, the crack propagation rate da/dN in single crystal SRR99 in terms of total strain range $\Delta\varepsilon_T$ can be expressed as

$$\frac{da}{dN}=C_a(\Delta\varepsilon_T)^{\beta_a} \tag{10.1}$$

where C_a and β_a are temperature and cycle type dependent material constants. Based on the limited number of test data, it appears that the slopes of da/dN versus $\Delta\varepsilon_T$, for a given temperature in the tests with strain dwells, is the same, i.e., β_a has the same value for tests with tensile, compressive and balanced dwells at a given temperature. From the test results given in Chapter 9, the values of C_a and β_a have been calculated and are presented in Table 10.1.

Therefore, if crack propagation is assumed to occur from the initiated crack length, a_0, to the final crack length, a_f, the crack propagation life, N_c, can be calculated by the integration of Eq.(10.1) and expressed as;

$$N_c=\frac{a_f-a_0}{C_a}(\Delta\varepsilon_T)^{-\beta_a} \tag{10.2}$$

Hence, crack initiation life N_i can be readily obtained from;

$$N_i=N_f-N_c \tag{10.3}$$

where N_f is the fatigue life obtained in the smooth bar low cycle fatigue tests.

The definition of an initiation crack length and a final crack length for calculation of the crack initiation life and crack propagation life in the low cycle fatigue tests is always a matter of controversy. In the present work, an initiation crack length is arbitrarily defined as 30μm, and the final crack length is defined as 1.5mm, based on the observation of the final surface crack length and the calculation of the stress drop in the final stage of smooth round bar tests.

Based on the above assumptions, using Eqs.10.2 and 10.3, the crack initiation life and crack propagation live for the smooth bar tests have been calculated. Fig.10.1 to Fig.10.3 present the results of N_i and N_c as a function of total strain range (orientation modified) for tests at 750°C, 950°C and 1050°C respectively. It should pointed that these results are only approximate for crack initiation and propagation in the smooth bar tests, since the extrapolation of the limited crack propagation data obtained from the corner crack tests to smooth bar tests is questionable. Nevertheless, from this simple analysis an overview of the influence of strain dwells and temperature on the crack initiation and propagation in single crystal SRR99 can be obtained.

From Fig.10.1, it can be seen that a compressive dwell is more detrimental than other cycle type tests to crack initiation and crack propagation at 750°C. The tensile dwell tests exhibit longer initiation lives but show shorter propagation lives compared with continuous cycling tests. At 1050°C, Fig10.3, introduction of dwells, either in tension or in compression, causes a reduction in both crack initiation and propagation lives, with tensile dwells being more detrimental. As indicated earlier, this is attributable to creep damage and oxidation during tensile dwells. At 950°C, Fig.10.2, the effect of strain dwells on the crack initiation life is not significant, although most compressive dwell tests show slightly shorter lives and tensile dwell tests exhibit somewhat longer lives compared with continuous cycling tests. The influence of strain dwells on crack propagation at 950°C is similar to that at 750°C. Both tensile and compressive dwells reduce the crack propagation life, with compressive dwells being more damaging.

As indicated in Section 10.1, the influence of dwell times on low cycle fatigue life, which consists of a crack initiation and crack propagation stage is a combination of mean stress, increased inelastic strain and time dependent damage (creep and

oxidation). The observed crack initiation and crack propagation behaviour, as shown in Fig.10.1 to Fig10.3, clearly indicates the competitive effect of these factors. At 750°C, the influence of a strain dwell can mainly be attributed to the mean stress, since creep damage and oxidation effects can be expected to be small at this temperature. The large reduction both in crack initiation and crack propagation life observed in the compressive dwell tests is the result of the large tensile mean stress induced by compressive dwells. In contrast, at 1050°C, although the negative mean stress induced by tensile dwells may be beneficial for crack initiation and propagation, tensile dwell tests still exhibit the shortest lives in both crack initiation and crack propagation. These results indicate that creep damage and environment effects are more important than mean stress at 1050°C.

The influence of temperature on the crack initiation behaviour of single crystal SRR99 can be related to the crack initiation mechanism. The investigations (Anton [1984], Wright [1988]) on fatigue crack initiation of several single crystal nickel base superalloys has found that crack initiation in a single crystal, at different temperatures, is a competitive process between initiation from pores and oxidation-induced initiation. Defresne and Remy [1990] reported that cracks in CMSX-2 and MAR-M200 single crystals always initiated at a casting micropore, both internal or located at surface, in the low cycle fatigue tests at 650°C. In contrast, Wright [1988] has found that crack initiation in Rene N4 single crystal at 1093°C mainly occurred by oxidation-induced initiation. Fatigue assisted cracking and spalling of oxide products produce a roughened and pitted surface. With further cycling, these pits developed into oxide spikes and then sharp fatigue cracks. The low cycle fatigue tests performed by Anton [1984] on the [001] and randomly aligned nickel base superalloy single crystals at temperature ranging from 650°C and 1000°C has revealed the general characteristics of temperature dependent crack initiation in single crystals. At temperatures below 980°C, corrosion cracking at a surface occurs slowly, while cracks initiating at pores grow at a quicker rate and dominate the crack initiation process. At 980°C and above, however, surface oxidation crack growth is favoured and the crack initiation process is dominated by oxidation. The actual temperature at which this transition occurs is dependent on alloy chemistry, pore size and distribution, as well as the surface conditions. For example, the test results on PWA1480 single crystal coated by Ni-Co-Cr-Y indicated that internal crack initiation at pores was the predominant failure mode even at 1050°C (Miner et al [1986]).

For single crystal SRR99, although detailed fractographic and metallographic examinations of the fracture surface have not been made, the temperature dependent fatigue crack initiation processes can be expected to be similar to that in other nickel base single crystal superalloys, because their overall fatigue life behaviour, as a function of temperature , which will be compared in Section 10.4, is very similar. Indeed, direct observation of the specimen surface and the failure modes in the tests could partially confirm that similar crack initiation processes occurred in single crystal SRR99. At 750°C, the specimen surface revealed little oxidation and few cracks were observed. Most tests were terminated when the maximum stable stress dropped to about 20%. At 1050°C, the specimen surface was found to be heavily oxidised and a number of cracks were observed on the specimen surface, most tests were ended by the observation of a long crack appearing on the surface. At 950°C, some tests were terminated by stress drop, while others were stopped upon the appearance of a long crack on the specimen surface. The above observations indicate that crack initiation in single crystal SRR99 is dominated by initiation from pores at 750°C and by oxidation-induced initiation at 1050°C, and with a combination of both at 950°C. A further detailed metallographic examination of the fracture surfaces is required to confirm these conclusions.

The crack initiation mechanisms discussed above are in agreement with the observed crack initiation behaviour of single crystal SRR99, as shown in Fig.10.1 to Fig.10.3. At 750°C, crack initiation at pores is usually associated with high stresses opening the pores. The tensile stress applied to the specimen may be the main driving force for crack initiation from pores. As a result, a compressive dwell test with a high cyclic tensile stress (positive mean stress) exhibit a shorter crack initiation life, whilst a tensile dwell test with a low cyclic tensile stress (negative mean stress) shows a longer crack initiation life. At 1050°C, since oxidation-induced crack initiation is a time dependent process, and both tensile and compressive dwell tests have a longer during time in each cycle compared with continuous cycling tests, the crack initiation lives in both tensile and compressive tests are shorter than those in the continuous cycling tests. The larger reduction in crack initiation life in the tensile dwell test compared with the compressive test indicates that oxidation associated with a tensile stress is more damaging than under a compressive stress (Challenger et al [1981], Reuchet and Remy [1983]).

10.3. Evaluation of Life Prediction Techniques

In chapter 8, six different conventional life prediction approaches, namely the Coffin-Manson law, the damage function approach, the frequency modified damage function method, the mean stress models, the modified strain range partitioning method and the linear damage summation rule, plus two life prediction approaches combined with the constitutive model have been used for the life assessment of single crystal SRR99 under fatigue and creep-fatigue conditions. In general, those methods which take into account the cycle type, or waveshape, as well as allowing for the difference between tensile and compressive dwells, have given relatively good life predictions. These methods are the mean stress modified SRP and frequency modified damage function methods. On the other hand, those methods which use the same strain and/or stress parameter for the various types of tests give poor life predictions, for example, the Coffin-Manson law and mean stress models. These life prediction results can be rationally analysed in terms of the low cycle fatigue damage mechanisms, i.e. crack initiation and crack propagation mechanisms as discussed previously, in single crystal SRR99.

It has been pointed out in Section 10.2 that low cycle fatigue is a process of crack initiation and crack propagation. The results presented in Chapter 9 and Section 10.2 have indicated that both the crack initiation and crack propagation life periods in single crystal SRR99 under fatigue and creep-fatigue conditions are strongly dependent on cycle types and temperatures. The variation of low cycle fatigue life, i.e. crack initiation and crack propagation life periods, for different cycle type tests at a given temperature is a combination of the effects of mean stress, inelastic deformation and the time dependent aspects, creep damage and environmental interaction. Therefore, the life prediction models must include and appropriately represent these effects. Since the contribution of each effect depends on temperature, the applicability of the life prediction models can be also expected to be temperature dependent. At 750°C, an analysis on crack initiation and crack propagation indicates that mean stress is the predominant factor and the influence of time dependent damage is negligible. In agreement with the above analysis, the mean stress models which modify the conventional Coffin-Manson equation by including the mean stress effect give fairly good predictions. At 950°C and 1050°C, both crack initiation and crack propagation analysis indicates that there are simultaneous effects of mean stress, additional inelastic deformation and time dependent creep damage and environment, induced during the tensile and compressive dwells, which need to be taken into account in the life prediction models. The emphasis of conventional

models is on individual effect either on mean stress, such as in the mean stress models, or take into account only the additional inelastic strain, such as in the Coffin-Manson law and the conventional strain range partitioning (SRP) method without mean stress modification. Consequently, these models gave poor life predictions for single crystal SRR99. The damage function approach, which includes both mean stress and inelastic strain effects, still failed to identify the different effects of inelastic strains induced by tensile and compressive dwells. As a result this method still segregates test data into different groups which depend on cycle type. In these life prediction models, the time dependent damage effects have not been taken into account, although in some cases consideration of the additional inelastic strain induced by strain dwells may indirectly reflect the effect of time dependent damage. This is because both of them are dependent on the dwell types and the dwell times, and the material deterioration caused by time dependent damage usually increases the inelastic strain. The reasons for the unsuccessful application of the linear damage summation rule to single crystal SRR99 have been discussed in Chapter 8 and primarily attributed to the use of virgin static creep data to calculate the cyclic creep damage during stress relaxation, and also to the creep-fatigue interaction in the low cycle fatigue tests. Based on the analysis of crack initiation and propagation mechanisms, another reason for the inaccuracy of the linear damage summation rule, is that environmental effects, such as oxidation, are not taken into account in the method.

The frequency modified damage function method and the mean stress modified strain range partitioning method proposed in the present work provided the best correlations among the life prediction methods evaluated. This is to be expected since these two methods take into account, in different ways, the simultaneous effects of various factors which influence the low cycle fatigue life of single crystal SRR99. The frequency modified damage function method includes an additional frequency term to describe the cycle type (or waveshape) dependent characteristics. It has been claimed that the frequency term can take into account environmental and other time dependent effects in fatigue at high temperature (Coffin [1973], Ostergren [1976]). The concept of SRP is based on the recognition of differences in the cyclic stress-strain history (hysteresis loop) which develop from two directions of straining, i.e. tension and compression, and in the two types of inelastic strain, either time independent (plastic) or time dependent (creep). The characteristics, capabilities and the applications of SRP to high temperature low cycle fatigue prediction has been the subject of extensive investigations (Manson [1973], Batte [1983], Bernstein [1982], Namy [1983]). The applicability of SRP to a variety of structural steels and alloys

(Manson et al [1971], Stentz et al [1978], Priest and Ellison [1982], Miller et al [1984]) as well as high temperature nickel base alloys (Nazmy [1983], Day and Thomas [1984], Remy et al [1986]), and even to thermal-mechanical fatigue (Halford and Manson [1976]) indicates that this method can take into account both time independent and time dependent damage developed during low cycle fatigue. The application of conventional SRP to single crystal SRR99 failed because of the mean stress effects. The proposed mean stress modified SRP method, which overcomes this shortcoming in the conventional SRP method, provides a good life predictions for tests at both 950°C and 1050°C .

The sensitivity of the life prediction methods to the material constants and how they are determined has also been examined in Chapter 8. A significant feature of the life prediction correlations is that the fatigue life of the tests with compressive dwells can usually be well predicted by using the material constants determined from continuous cycling test data, as long as the additional inelastic strain and/or mean stress induced by the compressive dwell has been taken into account in the prediction. The fatigue life of the tests with tensile dwells can not be predicted accurately in this simple way. These results further indicates the different effects caused by tensile dwells and compressive dwells in single crystal SRR99. For polycrystalline materials, the different effects of tensile and compressive dwells on high temperature fatigue life have been recognised by many investigators (Ostergren [1976], Day and Thomas [1984], Kitamura and Halford [1989]), and have been attributed to the different damage processes caused by tensile and compressive dwells. Metallographic examination of the failed strain controlled fatigue specimens showed dwell (hold) times in tension tend to cause intergranular failures and compressive dwell (hold) times tend to cause transgranular failures in polycrystalline materials (Ostergren [1976], Kitamura and Halford [1989]). Therefore, the failure mechanisms in continuous cycling and compressive dwell tests tend to be similar in the polycrystalline materials. For single crystal superalloys, the failure mechanisms under all test conditions is the same, i.e. a transgranular failure mode. The difference between tensile and compressive dwells can not be usually explained by using the failure mechanisms observed in polycrystalline materials. Further investigation is needed to clarify the different damage mechanisms caused by tensile and compressive dwells in single crystal superalloys.

Most conventional low cycle fatigue life predictive techniques for high temperature have emanated from the original Coffin-Manson law. A common feature of these methods is to postulate a typical cycle, normally the half life cycle, from which the

relevant quantities, which are assumed to control the fatigue life, in the models must be determined. Clearly, uncertainties may arise in whether this typical cycle represents the cyclic deformation and damage evolution behaviour of the fatigue tests, especially in the case when complex cyclic stress responses, such as hardening or softening, cycle dependent mean stress and stress relaxation, are observed in the fatigue tests. The influence of cyclic hardening and softening on life predictions has already been studied in many investigations (Leven [1973], Curran and Wundt [1976], Marphy et al [1979], Ellison and Paterson [1976], Batte [1983]). The results indicate that if a material cyclically hardens or softens, life prediction will be inaccurate if these changes during test life are not taken into account. Also the degree to which a material may harden or soften may be dependent on the strain range, hold period and temperature, in which case accurate life prediction may be extremely difficult. These problems are common to all conventional types of life prediction methods, and cannot be overcome by choice of a particular method.

A new life prediction method should include as much cyclic deformation information as possible. In this case, the combination of life prediction and a realistic material model, i.e. constitutive model, is indispensable. In Chapter 8, a first attempt has been made to combine the viscoplastic constitutive model proposed for single crystal SRR99 with life prediction methods. Due to the limited test data, the applicability of the combined life prediction methods has only been demonstrated on single crystal SRR99 at 950°C. The life prediction results have been found to be comparable to those obtained by conventional methods. This can be attributed to two factors. First, single crystal SRR99 at 950°C exhibits stable cyclic behaviour in continuous cycling tests and becomes cyclically stable after an initial period of softening, up to 10% of life, in the tests with strain dwells. Therefore, the overall influence of cyclic softening on fatigue life is not significant. Second, the effect of mean stress can already be taken into account in the conventional methods modified in this work. However, four potential advantages of the combined life prediction technique should be noted. First, this technique can be used to predict fatigue life under complex loading conditions, such as under interspersed creep and fatigue, and step loading conditions, since the changes in the stress and strain under different loadings can be computed by constitutive model. Second, the combined life prediction technique not only predicts the final fatigue life, but it can also evaluate material deterioration, i.e. damage accumulation, at different loading stages and henec predict residual life. Third, this technique may be expected to be particularly useful in thermomechanical fatigue life prediction, because in thermomechanical fatigue the cyclic mechanical responses are extremely complex, resulting in an irregular hysteresis loop. Quantities, such as

inelastic strain, are very difficult to determine even directly using the experimental loops. These difficulties can be solved by using a constitutive model to simulate the cyclic mechanical responses. Finally, it is anticipated that this technique, with some further development, and in conjunction with a finite element code, or similar stress analysis method, could be used in the design of a structural component, such as turbine blades, operating under complex conditions representative of service.

10.4 Comparison of SRR99 With Other Nickel Base Superalloys

The most striking feature of the results obtained from the low cycle fatigue tests of single crystal SRR99 is the influence of orientation. Anisotropic elastic theory provides a fundamental basis for predicting the influence of crystal orientation on the elastic behaviour of a single crystal alloy. In Chapter 6, a simple correlation of the elastic moduli using the orientation function $f(A_{hkl})$ has been proposed and used to take account of the effects of crystal orientation on the cyclic mechanical response and the fatigue life of single crystal SRR99. This analysis should also be applicable to other single crystal nickel base superalloys.

Gabb and co-workers [1986] presented results for the elastic moduli of the single crystal nickel base superalloys PWA1480 and Rene N4. For PWA1480, tested at 650°C, the elastic modulus was measured for specimen orientations [001], [2520], [3610], [011], [236] and [111]. For Rene N4, crystal orientations [001], [011], [111], [145], [236] and [023] were studied at 760°C and 980°C. These data are re-analysed here using the correlation method proposed in the present work. Fig.10.4 shows the measured elastic moduli $E_{[hkl]}$ normalised with respect to $E_{[001]}$ as a function of orientation parameter A_{hkl} for PWA1480 and Rene N4 at various temperatures. The results from this study on SRR99 at both room temperature and 950°C are also presented in Fig.10.4. It can be seen that there appears to be a simple linear relationship between $E_{[001]} / E_{[hkl]}$ and the orientation parameter, A_{hkl}, for all the single crystals over a wide range of temperatures. The results indicate that the material constant D in the orientation function, $f(A_{hkl}) = 1 - D A_{hkl}$, is not only insensitive to temperature but also insensitive to the composition difference of nickel base single crystal superalloys. Therefore, the proposed orientation function $f(A_{hkl})$ could be used to correlate the orientation influence on the elastic behaviour of other single crystal superalloys.

Results similar to those given in Chapter 5 for single crystal SRR99 have reported by Gabb et al [1986] in that the low fatigue life of single crystal Rene N4 at both 760°C

and 980°C is strongly dependent on crystal orientation. Fig.10.5a and Fig.10.6a show results plotted against total strain range. The longest fatigue life is observed in tests on the [001] orientation, while the [111] orientation yielded the shortest lives. This orientation dependent fatigue behaviour has also been reported by Remy [1993] for single crystal AM1 at 950°C, Fig.10.7a. However, both Gabb et al [1986] and Remy [1993] did not discuss quantitatively the correlation between crystal orientation and fatigue life.

In chapter 6, the orientation function $f(A_{hkl})$ has been used to modify the total strain range to take account the orientation influence on fatigue life of single crystal SRR99. A re-analysis has been performed on the test data obtained by Gabb et al [1986] and Remy [1993], so that an orientation modified strain range is obtained. The fatigue life as a function of the orientation modified total strain range for single crystal Rene N4 is plotted in Fig.10.5b and Fig.10.6b for tests at 760°C and 980°C respectively. The correlation results for single crystal AM1 at 950°C are given in Fig.10.7b. It can be seen that the scatter shown in Fig10.5b, 10.6b and 10.7b is much less than that in Fig.10.5a, 10.6a and 10.7a. The significant improvement in the correlation between the orientation modified total strain range and low cycle fatigue life for single crystal SRR99, Rene N4 and AM1 at various temperatures indicates that a low cycle fatigue master curve, irrespective of orientation , can be obtained for a given single crystal at a given temperature and loading condition. There remains some evidence of scatter in the correlation results, as shown in Fig.10.5b, 10.6b and 10.7b, but this is probably due to inherent material scatter and/or the different influence of orientation on the plastic behaviour compared with the elastic properties. Nevertheless, it is shown in this study that the role of orientation via the elastic response is the dominant feature of these tests. The proposed orientation function $f(A_{hkl})$ can be used to correlate the influence of orientation on the cyclic mechanical response and fatigue life behaviour of single crystal nickel base superalloy, particularly at small strain ranges with little inelastic deformation, the conditions where most applications exist, when design work is consequently performed..

The similarity of the mechanical properties and fatigue life behaviour of various single crystal nickel base superalloys has been recognised by recent investigations (Gabb et al [1986], Remy [1993]). However, direct comparison has not yet been performed. In terms of the orientation modified total strain range, the low cycle fatigue lives of single crystal SRR99, Rene N4 and AM1 at different temperatures are compared in Fig.10.8 and Fig.10.9. From Fig.10.8 it can be seen that the fatigue life behaviour of single crystal SRR99 at 750°C is very similar to that of Rene N4 at

760°C. In Fig.10.9, a extremely good correlation between the fatigue life data of single crystal SRR99 and AM1 at 950°C is apparent. The fatigue life data for single crystal Rene N4 at 980°C also fall within the same scatter band of SRR99 and AM1 data. However it appears that most of the Rene N4 data fall slightly below the correlation curve. This indicates that most tests on Rene N4 at 980°C exhibit slightly shorter lives than SRR99 and AM1 at 950°C. Overall, these comparisons clearly indicate the similarity of the fatigue life behaviour of these single crystal nickel base superalloys

Finally, to demonstrate the superior high temperature fatigue behaviour of nickel base single crystals over conventional polycrystalline nickle base superalloys, a comparison is made between single crystal SRR99 and polycrystalline nickel base superalloy Mar-M002. Both Mar-M002 and SRR99 superalloys were provided by Rolls Royce plc, and the latter is a derivative of the former material. The test results on Mar-M002 were also produced in the same laboratory as used for this study by Ellison et al [1984]. Fig.10.10 compares the fatigue life of SRR99 with Mar-M002 at 750°C, and Mar-M002 at 1000°C with SRR99 at 950°C and 1050°C (no test at 1000°C for SRR99 was performed). A significant improvement on high temperature fatigue life is obvious for single crystal SRR99. At a given total strain range, the fatigue life of SRR99 single crystal is nearly ten times longer than that of the polycrystalline nickel base superalloy Mar-M002.

CHAPTER 11
CONCLUSIONS AND FUTURE WORK

11.1 Concluding Comments

In this study, two test geometries, using a smooth round bar and a corner crack specimen, have been tested under four different loading conditions, namely, continuous cycling, cycling with tensile dwell, compressive dwell and balanced dwell, at three temperatures, 750°C, 950°C and 1050°C. This has been done to investigate the low cycle fatigue behaviour and crack growth characteristics of single crystal SRR99. Additional tests on the elastic properties and yielding behaviour have also been conducted over a temperature range from room temperature to 1050°C. The experimental results and the analysis performed in the previous Chapters lead to the following conclusions.

1. The most striking feature of the results obtained from the smooth round bar tests is the influence of crystal orientation. Based on the analyses of these results, a simple approach which describes the anisotropic elastic behaviour of single crystal nickel base superalloys has been developed. This approach has been used successfully to correlate the influence of crystal orientation on cyclic mechanical response and fatigue life behaviour for single crystal SRR99, particularly at small strain ranges, . It has also been successfully utilised in a re-analysis of other single crystal nickel base superalloys.

2. The temperature dependent yield behaviour of single crystal SRR99 has been found to be similar to other single crystal nickel base superalloys, with an unusual increase in yield strength over the temperature range 600°C to 750°C. A significant orientation dependent anisotropy in yielding stress has been observed for single crystal SRR99, with [001] exhibiting a larger tensile yield stress than compressive yield stress and [111] showing the opposite yield behaviour. The observed yielding behaviour has been found not to obey Schmid's Law. A cross-slip model has been successfully used to describe the orientation dependent yielding behaviour.

3. The cyclic mechanical responses of smooth bar tests and corner crack tests have been found to be similar. The cyclic stability of SRR99 depends on both temperature and cycle type. At 750 °C, SRR99 exhibits cyclic stability under all the cyclic testing conditions. At 950°C, cyclic stability is only found in continuous cycling tests. Rapid cyclic softening is observed during the first 10% of life in tests with both unbalanced

and balanced dwells. At 1050°C SRR99 showed continuous cyclic softening during fatigue regardless of the cycle type employed in tests.

4. Significant mean stress effects have been observed at the three temperatures studied. The stress ratio, R, in the completely reversed strain controlled tests with strain dwells changed rapidly during the first 10 percent of life. Decreases in the tests with tensile dwells which produce a compressive mean stress, and increases in compressive dwell tests, which induce a tensile mean stress.

5. The cyclic stress-strain relationship, in terms of total strain range, is found to be strongly dependent on orientation. For the same total strain range, the [001] orientation shows the lowest stress response, whilst the [111] orientation exhibits the greatest stress response. However, in terms of the cyclic plastic strain range, the cyclic stress response is relatively insensitive to orientation.

6. The introduction of two minute strain dwells produces significant stress relaxation at 950°C and 1050°C, but not at 750°C. The early stage of stress relaxation at 950°C and 1050°C is similar, with the total amount of stress relaxation during each cycle decreasing rapidly during the first 5% of life, the stress then remaining constant thereafter. Differences occurred during the last 50% of life where the total amount of stress relaxation increased at 1050°C but remained fairly constant at 950°C. The total amount of stress relaxation for tests with the same total strain range exhibits a significant orientation dependence. The amount of stress relaxation increases as the orientation moves away from [001].

7. The fatigue life of single crystal SRR99 is strongly dependent on crystal orientation. Under the same loading conditions, the longest fatigue life is observed for tests in the [001] orientation, while the [111] orientation yields the shortest fatigue life. Temperature and strain dwells also have a significant influence on the fatigue and creep-fatigue life of SRR99. In terms of the orientation modified total strain range, the shortest fatigue life is observed in the tests with a compressive dwell at 750°C, but at 1050°C the tests with a tensile dwell exhibit the shortest life. Compared with continuous cycling tests, tests with tensile dwells show remarkably longer lives at 750°C, significantly shorter lives at 1050°C, and almost identical lives at 950°C; tests with compressive dwells always exhibit shorter lives than continuous cycling tests at all temperatures. Subsequent analysis revealed that the influence of strain dwells on the fatigue and creep-fatigue life of SRR99 was via the simultaneous effects of mean stress, additional inelastic strain, and time dependent damage during strain dwells.

8. An anisotropic viscoplastic constitutive model has been developed and successfully used to simulate the cyclic mechanical response of single crystal SRR99 under creep-fatigue conditions at 950°C. The simulations give good results, particularly in terms of the overall stress response, the shape of the hysteresis loops, the development of mean stress as well as the stress relaxation response during strain dwells for various orientations and cycle types.

9. Several conventional life prediction methods, which have been widely used for high temperature life prediction for polycrystalline materials, have been evaluated in this work. Only the frequency modified damage function method has been found to be applicable for single crystal SRR99. A modification to the conventional strain range partitioning (SRP) method has been proposed which takes into account the effect of mean stress. This modified SRP method provides a fairly good method for predicting the creep-fatigue life of single crystal SRR99.

10. A new life prediction methodology using the combination of a constitutive model and a life prediction technique has been developed and has been applied to predict the fatigue and creep-fatigue life of SRR99 at 950°C. This methodology, which is based on the accumulation of material damage at each cycle and takes into account the variations in the cyclic mechanical response, such as material softening, could provide a realistic life assessment approach for single crystal superalloys. It is anticipated that this approach can be used in conjunction with finite element analysis to provide a method by which a component can be assessed for structureal stability and integrity under the complex temperature and loading conditions representative of service.

11. The crack growth behaviour of single crystal SRR99 is found to be different to similar polycrystalline superalloys. For short cracks, the crack growth rates observed in the corner crack specimens are found to be nearly independent of crack length. A traditional fracture mechanics approach does not provide an adequate or unambiguous description for correlating crack growth rates. It is suggested that shorter crack growth behaviour of a single crystal may be controlled by the local material structural and deformation characteristics, such as slip systems and local stress strain concentrations. Correlation of short crack growth rates with a global strain parameter may be a more suitable approach. Secondary crystal orientations also appear to have an influence.

12. A significant influence of temperature and strain dwells on fatigue crack growth in

single crystal SRR99 is observed. Crack growth rates increase with increasing temperature. Introduction of strain dwells, either in tension or in compression, are found to accelerate crack propagation in SRR99. A compressive dwell is found to be more damaging than a tensile dwell at 750°C, but the reverse is true at 1050°C. Subsequent analyses indicated that there are a combination of effects due to mean stress, plastic deformation ahead of the crack tip, creep damage, environmental attack and crack closure at different temperature and strain cycling conditions. At 750°C, fatigue crack propagation may be dominated by local plastic deformation ahead of a crack tip, whilst creep damage and oxidation may have a larger influence on fatigue crack growth at 1050°C.

13. Based on the crack growth behaviour obtained from corner crack tests, crack initiation in the smooth bar tests has been estimated. The results reveal the influence of temperature and strain dwells on crack initiation in single crystal SRR99. A similar crack initiation mechanism to that observed in other single crystal nickel base superalloys is expected to occur in single crystal SRR99. If this is so then crack initiation will be dominated by pore initiation at 750°C and by oxidation-assisted initiation at 1050°C, with a mixture of these at 950°C.

14. The analyses in this work have also shown that the mechanical response and fatigue life behaviour of single crystal SRR99 is representative of a general class of single crystal nickel base superalloys being used and under investigation for gas turbine blade applications. The comparison of the fatigue life of SRR99 with its equivalent polycrystalline superalloy indicates a significant improvement on high temperature fatigue behaviour in single crystals.

11.2 Recommendations for Future Work

1. The present project has put the emphasis on the mechanical analyses of the creep-fatigue life behaviour and crack growth characteristics of single crystal SRR99. Detailed metallographic investigations of the crack initiation and propagation mechanisms, as well as the creep damage and oxidation mechanisms in single crystals are needed.

2. More smooth bar tests at 1050°C and corner crack tests are required to complete the test data base for further systematic analyses of the creep-fatigue life behaviour and

the crack growth behaviour of single crystal SRR99.

3. Investigation of the effects of crystal orientation, including secondary orientations, on crack propagation in single crystal SRR99 is recommended.

4. Further development of the constitutive model for single crystals to include fatigue damage and creep damage evolution equations is needed to describe the interaction between cyclic mechanical deformation and creep-fatigue damage evolution. The combination of a constitutive model with damage analyses is expected to be able to accurately predict the overall deformation history, including the final stage, and also the lifetime of single crystals under creep-fatigue cyclic loading.

5. The viscoplasticity constitutive model can be used for the detailed study of the local deformation and damage behaviour at the crack tip of the corner crack specimens by applying FEM analysis. It is anticipated that this approach could provide a better interpretation of the crack growth behaviour of single crystal superalloys.

REFERENCES

Ai S.H., Lupinc V. and Maldini M. [1990], "Creep fracture mechanics in single crystal superalloys", in High Temperature Materials for Power Engineering, (Eds. Bachelet et al), PartII, p1027.

Antolovich S.D., Liu S., and Hancock P., [1981], "Low cycle fatigue behaviour of Rene 80 at elevated temperature", Metall. Trans., Vol.12A, pp.473-481.

Anton D.L., [1983], "Fracture of nickel-base superalloy single crystals", Mater. Sci. and Engng, Vol.57, pp97-105.

Anton D.L., [1984], "Fatigue crack growth in anisotropic superalloy single crystals", in Fatigue '84, pp1361-1369.

Anton D.L., [1984], "Low cycle fatigue characteristics of <001> and randomly aligned superalloy single crystals" Acta Metall., Vol.32, No.10 pp1669-1679.

Argyris J.H., Vaz L.E. and Willam K.J., [1978], "Improved solution methods for inelastic rate processes", Computer Methods in Appl. Mech. & Engng., Vol.16, pp231-277.

Batte A.D., [1983], "Creep-fatigue life prediction", in Fatigue at High Temperature, (Ed. Sketlton R P), Applied Sci. Publishers Ltd, pp365-401.

Basquin O.H., [1910], "The experimental law of endurance tests" Proc. ASTM, 10, 625-630.

Baltov P. and Sawczuck A., [1965], "A rule of anisotropic work-hardening", Acta Mechanica, Vol.1, pp.1-81.

Beardmore P., Davis R.G. and Johnston T.L., [1969], "On the temperature dependence of the flow stress of nickel-base alloys" Trans. Metall., Vol.245, pp.1537-45.

Bernstein H.L., [1982], " An evaluation of four creep-fatigue models for a nickel - based superalloy in low cycle fatigue and life prediction", ASTM STP 770, (Eds. Amzallage C. et al), ASTM, pp.105-134.

Berling J.T. and Conway J.B., [1970], " A new approach to the prediction of low-cycle fatigue data", Metal. Trans, Vol.1, pp805-809.

Besseling J.F., [1958], " A theory of elastic, plastic and creep deformation of an initially isotropic material showing anisotropic strain-hardening creep recovery and secondary creep". ASTM J. Appl. Mech., Vol.80, P.529.

Blnachrad P. and Lemione P., [1988], " Constitutive modeling of 17-12 Mo SPH stainless steel behavior at high temperature", J. Pressure Vessel Tech., Vol.110, pp.51-58.

Bisego V., Fossati C. and Ragazzoni S., [1982], " An energy based criterion for low cycle fatigue damage evaluation", in Material Behaviour at Elevated Temperatures and Component Analysis, (Eds. Yamada Y., et al), ASME, New York, PVP vol.60.

Bishop J., [1952], "A theoretical examination of the plastic deformation of crystals by glide", Phil. Mag., p.51.

Bishop J. and Hill R., [1951], "A theoretical derivation of the plastic properties of a polycrystalline face-centered metal", phil. Mag., vol.42, p.1298.

Bodner S.R. and Partom Y., [1972]," A large deformation elastic-viscoplatic analysis of a thick-walled spherical shell". ASME J. Appl. Mech., vol.39, pp.751-757.

Bodner S.R. and Partom Y., [1975], "Constitutive equation for elastic-viscoplastic strain-hardening materials", ASTM J. Appl. Mech., Vol.42, pp.385-389.

Bodner S.R., Partom I. and Partom Y., [1979], "Uniaxial cyclic loadung of elastic-viscoplastic materials", ASME J. Appl. Mech., Vol.46, pp.805-810.

Boismier D.A. and Sehitoglu Huseyin, [1990], "Thermo-mechanical fatigue of Mar-M247: Part I: Experiments, Part II: Life prediction" ASTM J. of Engng. Mater. Technol., Vol.112, pp.68-79-89.

Bricknell R.H., and Woodford D.A., [1981], "The embrittlement of nickel following high temperature air exposure", Metall. Trans. A, Vol.12A, pp.425-433.

Cailletaud G., Kaczmarek H., and Policella H., [1984], "Some elements on the multiaxial behaviour of 316 stainless steel at room temperature", Mater.& Mech., Vol.3, pp.333-347.

Cailletaud G., [1987], "Une approche micromecanique phenomenoloique du comportement inelastique des metaux" (in Franch), Thesis de Doctoral d'etat, Universite Paris 6.

Cailletaud G., [1988], "Une approach micromecanique du comportement plastique des polycristaux", Rev. Phys. Appl., Vol.23, pp.353-365.

Caron P. and Khan T., [1983], "Improvement of creep strength in a nickel-base single- crystal superalloy by heat treatment", Mater. Sci. Engng., Vol.61, pp.173-184.

Chaboche J.L., [1977], " Viscoplastic equation for the description of cyclic and anisotropic behavior of metals", Bull. Acad. Sci. Ser. Sci. Tech., Vol.25,pp.33-42.

Chaboche J.L. and Rousselier G., [1983], "On the plastic and viscoplastic constitutive equations", J. Pressure. Vessel. Technol., Vol.105, pp.153-164.

Chaboche J.L., [1986], " Time-independent constitutive theories for cyclic plasticity", Int. J. Plast., Vol.2, pp.149-188.

Chaboche J.L., [1989], " Constitutive equations for cyclic plasticity and viscoplasticity", Int. J. Plast., Vol.5, pp.247-302.

Chaboche J.L. and Nouailhas D., [1989a], "Constitutive modeling of ratchetting effects", ASME J. Engng. Mater. Technol., vol.111, pp.384-392.

Chaboche J.L. and Nouailhas D., [1989b], "A unified constitutive model for cyclic viscoplasticity and its application to varius stainless steels", ASTM J. Engng,. Meter. Technol., Vol.111, pp.424-430.

Challenger K.D., Miller A.K. and Brinkman C.R. [1981], "An explanation for the effects of hold periods on the elevated temperature fatigue behaviour of $2\frac{1}{2}C_r - 1M_0$ steel", ASTM J. Engng. Mater. Technol. Vol103, pp7-14.

Chan K.S. and Lindholm U.S., [1990a], "Inelastic deformation under nonisothermal loading", ASME J. Engng. Meter. Technol., Vol.112, pp.15-25.

Chan K.S., Lindholm U.S., Bodner S.R. and Walker K.P., [1989], "High temperature inelastic deformation under uniaxial loading; theory and experiment", ASME J. Engng. Meter. Technol., Vol.111, pp.345-353.

Chan K.S., Lindholm U.S., Bodner, R.S. and Nagy, A., [1990], "High temperature inelastic deformation of the B1900+Hf alloy under multiaxial loading; theory and experiment", ASME J. Engng. Meter. Technol., Vol.112, pp.7-14.

Chan K.S. and Leverant G.R., [1987], " Elevated-temperature fatigue crack growth behaviour of Mar-M200 single crystals" , Metall. Trans. A, Vol.18A, pp.593-602.

Chan K.S., Hack J.E. and Leverant G.R., [1987], " Fatigue crack growth in Mar-M200 single crystals" , Metall. Trans. A, Vol.18A, pp.581-591.

Chen H. and Krempl E., [1986], "An adaptive time-stepping scheme for the viscoplasticity theory based on overstress", Computer Struc., Vol.22, pp-573-578.

Chen H. and Krempl E., [1986], "A two-step finite element time-intergration schem for the viscoplasticity theory based on overstress", Computer Struc., Vol.22, pp625-628.

Chieragatti R. and Remy L., [1991], "Influence of orientation on the low cycle fatigue of MAR-M200 single crystals at 650°C I. Fatigue life behaviour; II. Cyclic stress-strain behaviour", Mater. Sci. and Engng., A141, pp1-22.

Choi S.H. and Krempl E., [1989], "Viscoplasticity theory based on overstress applied to the modeling of cubic single crystals", Eur. J. Mech. A/Solids, Vol.8, pp.219-233.

CODE CASE N-47, ASME boiler and pressure vessel code, ASME, New York, 1974.

Coffin L.F. Jr, [1954], "A study of effects of cyclic thermal stresses on a ductile meyal", Transaction of ASME, Vol.76, pp.923-949

Coffin L.F., Jr., [1970], " The effect of frequency on high temperature , low-cycle fatigue", in Proc. of the Air Force Conf. on Fatigue of Aircraft Structures & Materials, AFFDL-TR-70-144 , Wright-Patterson AFB, Ohio, pp.301-311.

Coffin L.F., [1972], "The effect of high vacuum on the low cycle fatigue law", Metall. Trans., Vol.3, pp1777-1788.

Coffin L.F., [1973], "Fatigue at high temperature", in Fatigue at Elevated Temperature, ASME STP520, pp.5-36.

Coffin L.F., [1974], "Fatigue at high temperature-predict and interpretation", Proc. Inst. Mech. Eng., Vol.188, pp.9-74.

Coffin L.F., [1976a], " The prediction of wave shape effects in time-dependent fatigue " in Proc. 2nd Int. Conf. Mechanical Behaviour of Materials, Boston, Mass., Fedreation of Materials Science, pp.866-870.

Coffin L.F., [1976b], " Instablity effects in thermal fatigue " in Thermal Fatigue of Materials and Components, ASTM STP 612, pp.227-238

Coffin L.F., [1977], "Fatigue at high temperature", in Advances in Research on Strength and Fracture of Materials, ICF4, (Ed., Taplin D.M.R.), Pregamon Press, Vol.1, pp.263-281.

Cottrell A., [1975], *An Introduction to Metallurgy*, Edward Arnold Publishers Ltd

Contesti E. and Cailletaud G. [1987], "Description of creep-plasticity interaction with non-unified constitutive equations: application to an austenitic stainless steel" in 6th Int Seminar on Inelastic Analysis and Life Prediction in High Temperature Environment. Paris.

Copley S.M., Kear B.H. and Rowe G.M., [1972], " The temperature and orientation dependence of yielding in Mar-M200 single crystal", Mater. Sci. Engng., Vol.10, pp.87-91.

Cordes T.S., Berns H.D., Lingenfelser D.J., Mahoney B.J. and Testin R.A., [1988], "A SWT fatigue mean stress model for A356-T6 cast aluminum alloy", in Fatigue and Fracture Toughness of A356-T6 Cast Aluminum Alloy, (Ed. Stephens R I) SAE SP-760, pp39-47.

Crompton J.S. and Martin J.W., [1984], "Crack growth in a single crystal superalloy at elevated temperature", Metall. Trans. A, Vol.15a, pp1711-1719.

Crompton J.S. and Martin J.W., [1984], "Crack tip plasticity and crack growth in a single crystal superalloy at elevated temperature" Mater. Sci. and Engng., Vol.64, pp37-43.

Curran R.M. and Wundt B.M., [1976], "Continuation of a study of low-cycle fatigue interaction in steels at elevated temperatures", ASME-MPc Symp.Creep-Fatiguie Interaction, MPC-3, pp203-283.

Dafailas Y.F. and Popov E.P., [1975], "A model of nonlinearly hardening materials for complex loading", Acta Mech., Vol.21, pp.173-192.

Dafailas Y.F.and Popov E.P, [1976], "Plastic internal variables formalism of cyclic plasticity", ASTM J. Appl. Mech., Vol.98, pp.645-651.

Dafailas Y.F., [1986], " Bounding surface plasticity, I: Mathematical foundation and hypoplasticity", ASCE J. Eng. Mech., Vol.112, pp.966-987.

Dame L.T., [1985], "Anisotropic constitutive model for nickel based single crystal alloys; Development and finite element implementation", PhD Dissertation, University of Cincinnati.

Dame L.T., and Stouffer D.C.,[1988], "A crystallogrphic model for nickel base single crystal alloys", ASME J. Appl. Mech., Vol.55, pp.325-331.

Day M.F. and Thomas G.B., [1985], "Analysis of the low-cycle fatigue behaviour of two Ni-Cr-base alloys", Fatigue Frac. Eng. Mater. Struc., Vol.8 Vol.1, pp33-48.

Defresne A. and Rem L., [1990], "Fatigue behaviour of CMSX-2 superalloy [001] single crystals at high temperature, I: Low cycle fatigue of notched specimens, II: Fatigue crack growth", Mater. Sci. & Engng. A129, pp45-64.

Diboine A., Peltier J.M. and Pellox R.M., [1990], "Fatigue crack propagation in a single crystal nickel base superalloy", in High Temperature Fracture and Mechanics, EGF6 (Ed. by Bensussan P.), Mech. Engineering Publication, London, pp412-446.

Dimopulos V., Nikbin K.M. and Webster G.A., [1988], "Influence of cyclic to mean load ratio on creep/fatigue crack growth", Metall. Trans. Vol.19A, P.873

Dowing N.E., [1976], "Geometry effects of the J-integral approach to elastic-plastic fatigue crack growth", in Cracks and Fracture: Ninth Conference, ASTM 601, Philadelphia, pp19-32.

Dowling N.E. and Iyyer N.S., [1987], "Fatigue crack growth and closure at high cyclic strain", Mater. Sci. & Eng., Vol.96, pp99-107.

DRA Pyestock, [1992], private Communication.

Dyson B. and Mclean M., [1989], "CRISPEN Software Guide" NPL Report DMM[C]1.

Eftis J., Abder-Kader M.S. and Jones D.L., [1989], "Comparisons betwwen the modified Chaboche and Bodner-Partom viscoplastic constitutive theories at high temperature", Int. J. Plast., Vol.5, pp.1-27.

Elmquist H., Astrom K.J. and Schonthal T., [1986], *SIMNON User's Guide for MS-DOS Computer*, Studentlitteratur AB, Lund.

Ellis J.R., Jakub M.T., Jaske C.E., and Utah D.A., [1975], " Elevated temperature fatigue and creep-fatigue properties of annealed 2 1/2 Cr-1Mo steel", in Structural Steels for Sevice at Elevated Temperature in Nuclear Power Generation, (Ed. Schaeffer A.O.), ASME New York, pp.213-246.

Ellison E.G., and Plumbridge W.J., and Dean, M.S., [1984], "Turbine blade material behaviour and life prediction" Report No. 84/12, Dept. of Mech. Engng., University of Bristol.

Ellison E.G. and Paterson A.J.F., [1976], "Creep fatigue interactions in a 1CrMoV steel", Proc. Inst Mech. Engng. Vol.190, pp311-350.

Ezz, S., Pope D. and Paidar, V., [1982], "The tension/ compression flow stress asymmetry in Ni3[Al,Nb] single crystals", Acta Metall., Vol.30, p.921-926.

Fatemi A. and Stephens R.I., [1987], "Tensile mean stress effects on uniaxial fatigue behaviour of 1045 HR steel" in Fatigue '87, (Eds. Ritchie R O and Starke E A Jr), Vol.1, pp5 37-546.

Feller M., and Thomas L., [1989], "Correlation of microstructure and creep stages in the <100> oriented superalloy SRR99 at 1253 K ", Metal. Trans. A, Vol.20A, pp.1233-1238.

Fleischer R.L., [1963], "Substitutional solution hardening", Acta Metall., Vol.11, pp.203-209.

Floreen S. and Kane R.H., [1980], "An investigation of the creep-fatigue-environment interaction in a nickel base superally", Fatigue Frac. Engng. Mat. & Struc., Vol.2, pp.401-412.

Gabb T.P., Welsch G., Miner R.V. and Gayda J., [1989], "The low cycle fatigue deformation response of a single-crystal superalloy at 650C", Mater. Sci. & Engng. A108, pp189-202.

Gabb T.P., Gayda J., and Miner R.V., [1986], "Orientation and temperature dependent of some mechanical properties of the single crystal nickel base

superalloy Rene 4 Part II: low cycle fatigue behaviour", Metall. Trans. A, Vol.17A, pp.497-505.

Gell M., and Leverant G.R., [1973], "Mechanisms of high temperature fatigue, in Fatigue at Elevated Temperature, ASTM STP 520, Philadelphia, p.37.

Ghosh R.N., Curtis R.V. and Mclean M., [1992] " High temperature defgormation in engineering alloys - modelling for strain or load control", Acta. Metall.,. Vol.40, pp.3075-3083.

Goodall I.W., Hales R. and Walters D.J., [1980], "On constitutive relation and failure criteria of an austenitic steel under cyclic loading under high temperature", IUTAM Symp., Leicester, Springer-Verlag.

Guedou J.Y. and Honnorat Y., [1990], " Mechanical behaviour modeling of a nickel base single crystal superalloy" in Constitutive Laws of Plastic Deformation and Fracture, (Eds. Krausz A.S. et al), Kluwer Academic Publishers, pp.35-41.

Guelin H.S. and Stutz P. [1977], "Une nouvelle classe de lois de comportement decrivant les grande deformation visco-plastiques", Arch. Mech. Stosow, Vol.29, p.1.

Halford G.R., Saltsman J.F. and Hirschberg M.H., [1977], " Ductility normallized SRP life relations for creep-fatigue life prediction " in Proc. Conf. Environmental Degradation of Engineering Materials, Blackburg, Viginia, USA, pp.599-612.

Halford G.R. and Nachtigall A.J., [1978], in Proc. AGARD Conf. " The charaterization of low cycle high temperature fatigue by the strain range partitioning method," Conf. Proc. 234, 1978, p.2.

Halford G.R. and Manson S.S., [1976] "Life prediction of thermal mechanical fatigue using strain range partitioning" in Thermal Fatigue of Material and Components, ASMT STP612, Philadephia, ASMT, pp239-254.

Han C. and Krempl E., [1986], "A two-step finite-element time-integration scheme for the viscoplaticity theory based on overstress", Computer & Stru. Vol.22, No,4, pp625-628.

Hertzberg R.W., [1974] "Discussin of fatigue crack propagation in martensitic and austenitic steels", Metal. Trans. Vol.5, pp306-307.

Heredia F.E. and Pope D.P., [1986], "The tension/compression flow asymmetry in a high r' volume fraction nickel base alloy", Acta Metall. vol.34, No.2, pp1323-1332.

Hiroe T. and Igari T., [1985], "The viscoplasticity theory applied to the strain rate effect of 2 1/4Cr--1Mo steel at 600 C", in Trans of the 8th Int. Conf. on Structural Mechanics in Reactor Technology, Vol.L, Brussels, Elsevier, Amsterdam, pp.29-36.

Howland C. and Brown C.W., [1984], "The effect of orientation on fatigue crack growth in a nickel-base single crystal superalloy", in Fatigue '84, pp1349-1355.

Huseyin Sehitoglu and Wei Sun, [1989], "The significance of crack closure under high temperature fatigue crack growth with hold time", Engng. Frac. Mech., Vol.33, No.3 pp371-388.

Hyzack J.M. and Bernstein H.L., [1978], "An analysis of the low cycle fatigue behaviour of superalloy Rene 95 by strain range patitioning", AGARD Conf. Adborg, Demark, CP-243.

Inoue T., Igati T., Yoshida F., Suzuki. A. and Murakami S., [1985], "Inelastic behavior of 2 1/4Cr-1Mo steel under plasticity-creep interaction condition", Nucl. Engng. Des., Vol.90, pp.287-297.

Inoue T., Ohno N., Suzuki A. and Igari, T., [1989], "Evaluation of inelastic constitutive models under plasticity-creep interaction for 2 1/4Cr-Mo steel at 600 C", Nucl. Engng. Des., Vol.114, pp.295-309.

Kawai M. and Ohashi, [1987], "Coupling effect between creep and plasticity of type 316 stainless steel at elevated temperature" in 2nd Int Conf. on Constitutive Laws for Engng. Materials : Theory and Application, Tuson, (Eds. Arizona et al), Elsevier.

Kear B.H.and Piearcey B.J, [1967], " Tensile and creep properties of single crystals of the nickel -base superalloy Mar-M200", Trans. AIME, Vol.239, p.1209.

KearB.H., [1974], in ' Order-disorder transformations in alloys', (ed. H. Warlinmont) New York, Springer-Verlag, pp.440-474.

Kitamura T. and Halford G.R., [1989], "A nonlinear high temperature fracture mechanics basis for strainrange partitioning", NASA Technical Memorandum 4133.

Koterazawa R. and Takayoshi N., [1991], "Creep-fatigue crack growth and fractography of a type 304 stainless steel at elevated temperature", Fatigue Frac. Mater. Struc. Vol.14, pp1-9.

Kounitzky A., Wortmann J. and Agarwal P.N., [1991], "A single crystal casting processs for high-temperature components", Mater. Design, Vol.12, pp323-330.

Krempl E., [1975], "On the interaction of rate-and history dependence in structural metals", Acta Mech., Vol.22, p.53.

Krempl E., McMahon J.J. and Yao D.,[1986], "Visco-plasticity based on overstress with a differential growth law for the equilibrum stress", Mech. of Mater., Vol.5, pp.35-48.

Krempl E. and Yao D., [1987], " The viscoplasticity theory based on overstress applied to ratchetting and cyclic hardening", in Low-cycle Fatigue and Elasto-plastic Behaviour of Materials, (Ed. Rie K.T.), Elsevier Applied Science, pp.137-148.

Krempl E. [1987], "Isotropic and orthotropic formulation of the the viscoplasticity theory based on overstress" in Constitutive Laws for Engng Materials: Theory and Application, (Ed. Desai C.S. et al), Elsevier, Vol.1, pp.137-148.

Krieg R.D., [1975], "A practical two surface plasticity theory", ASME J. Appl. Mech., Vol.42, pp.641-646.

Krieg R.D., Swearengen J.C. and Rohde, R.W., [1978], "A physical based internal variable model for rate-dependent plasticity", in Inelastic Behavior of Pressure Vessel and Piping Components. PVP-PB-028, (Eds. Chang T.Y and Kremple E.) ASME, New York, pp.15-28.

Kujawski D. and Ellyin F., [1984], "A fatigue crack propagation model", Eng. Frac. Mech., Vol.20, pp695-704.

Kumar V., Morjaria M. and Mukherjee, [1980] "Numerical integration of some stiff constitutive models of inelastic deformation", Trans. ASME, J. Engrg. Mater. Tech., vol.102, pp92-96.

Kuwabara K., and Nitta A., [1977], " Estimation of thermal fatigue damge in steam turbine rotors", Report 277001, Central Research Institute for the Electric Power Industry [Japan].

Lall C., Chin S. and Pope D., [1979], "The orientation and temperature dependence of the yield stress of Ni3[Al,Nb] single crystals", Metall. Trans A, Vol.10A, P.1323-1332.

Lee D. and Zaverl F., [1978], "A generalized strain rate dependent constitutive equation for anisotropic metals", Acta. Mechanica, Vol.29, pp.1771-1780.

Lee K.D., and Krempl E., [1991], "An orthotropic theory of viscoplasticity based on overstress for thermomechanical deformations", Int. J. Solids Struct., Vol.27, pp.1445-1459.

Lerch B.A. and Antolovich S.D., [1990], "Fatigue crack propagation behavior of a single crystalline superalloy" Metall. Trans. A, Vol.21A, pp.2169-2177.

Lekhnitskii S.G., [1963], *Theory of Elasticity of an Anisotropic Body*, Holden-Day, Inc., San Francisco.

Leverant G.R. and Kear B.H., [1970], "The mechanism of creep in gamma prime precipitation-hardened nickel base alloys at intermediate temperature", Metall. Trans., Vol.1A[i], pp.491-518

Leverant G.R., Gell W. and Hopkins S.W., [1971], "The effect of strain rate on the flow stress and dislocation behavior of precipitation-hardened nickel base alloy ", Mater. Sci. Engng., Vol.8, p.125-133.

Leven M.M., [1973], "The interaction of creep and fatigue for a rotor steel", ASME J. Exp. Mech., Vol.13, pp353-372.

Leverant R., Kear B.H. and Oblak J.M, [1973], "Creep of precipitation-hardened nickel-base alloy single crystals at high temperature", Metall. Trans., V.4, 355-362.

Li S.X. , [1991], "Life assessment of turbine blade materials under creep-fatigue conditions: Literature review", Dept. of Mech. Engng., University of Bristol.

Liu M.C.M., and Krempl E., [1979], "A uniaxial viscoplasticity based on total strain and overstress", J. Mech. Phys. Solids, Vol.27, p.377.

Liu H.W. and Oshida Y., [1986], "Grain boundary oxidation and fatigue crack growth at elevated temperature", Theor. and appl. Frac. Mech., Vol.6, pp85-94.

Lord D.C. and Coffin L.F., [1973], " Low cycle fatigue hold time behaviour of cast Rene 80", Metal. Trans., Vol.4, pp.1647-1653.

Mackay R.A. and Maier R.D., [1982], "Influence of orientation on the stress rupture properties of nickel-base superalloy single crystals", Metall. Trans., Vol.13A, pp.1747-1754.

Mall S., Staubs E.A. and Nicholas T., [1990], "Investigation of creep/fatigue interaction on crack growth in a Titanium Aluminide alloy", J. Eng. Mat. Tech. Vol.112, pp435-441.

Manson S.S., [1953], " Behavior of materials under conditions of thermal stress" NACA-TN-2933,NASA- Lewis Research Certre, Cleveland, Ohio.

Manson S.S., [1965], "Fatigue - A complex subject - some simple approximations", Exper. Mech., Vol.5, No.7, pp.193-226.

Manson S.S., Halford G.R., and Hirschberg M.H., [1971], "Creep-fatigue analysis by strain-range partitioning", in Proc.Symposium on Design for Elevated Temperature Environment, ASME, New York, pp.12-28.

Manson S.S., [1973], "The challenge to unify treatment of high temperature fatigue - a partisan proposal based on strainrange partitioning", in Fatigue at Elevated Temperature, ASTM STP 520, Philadelphia, pp.744-774

Manson S.S., Halford G.R., and Hirschberg M.H., [1975], "Strainrange partitioning- - A tool for characterizing high-temperature, low-cycle fatigue," NASA TMX-71691, NASA-Lewis Research Centre, Cleveland, Ohio.

Majumdar S. and Maiya P.S., [1976], "A damage equation for creep-fatigue interaction", in ASME-MPC Symp. on Creep-fatigue Interaction, MPC-3, ASME, New York, pp.323-336.

Majumdar S. and Maiya P.S., [1978], " Wave shape effects in elevated temperature low-cycle fatigue of type 304 stainless steel", in Inelastic Behavior of Pressure Vessel and Piping Components, PVP-PB-028, ASME, New York, pp.43-54.

Majumdar S., and Maiya P.S., [1979], "An interactive damage equation for creep-fatigue interaction", in Proc. of 3rd Int. Conf. on Mechanical Behaviour of Materials, ICM3, Vol.12, pp. 101-109.

Marchand N.J. and Moosbrugger J.C., [1991], "Non-linear structural modeling for life predictions: Physical mechanisms and continuum theories" Int. J. Pres. Ves. & Piping Vol.47, pp79-112.

Marchionni M., Ranucci D., and Picco E., [1986], "High temperature fatigue life prediction of a Nickel base superalloy by the strain range partitioning method", in Proc. of High Temperature Alloys for Gas Turbines and other Applications, (Eds.Betz W. et al) Riedel Publishing Co., Boston, pp.1629-1638.

Marquis, D., [1979], " Modelisation et identification de l'ecrousissage anisotrope des metaux", These Universite Paris 6.

Melton K.N., [1982], "Strain wave shape and frequency effects on the high temperature low cycle fatigue behaviour of 1CrMoV Ferritic Steel", Mater. Science Engng., pp.21-28.

Meric L., Poubanne P. and Cailletaud G., [1991a], "Single crystal modeling for structural calculations: Part 1 -- model presentation" , ASME J. of Eng. Mater. Tech., Vol.113, pp.162-170.

Meric L., and Cailletaud, G., [1991b], "Single crystal modeling for structural calculations: Part 2 -- finite element implementation" , ASME J. of Eng. Mater. Tech., Vol.113, pp.171--182..

Miller A., [1976], "An inelastic constitutive model for monotonic, cyclic and creep deformation", ASME J. Eng. Mat. Tech., Vol.98, pp.97-113.

Miller D.A., Priest R.H. and Ellison E.G., [1984], "A review of material response and life prediction technique under creep-fatigue loading conditions " High Temp. Mater., Proc., Vol.16, pp.115-194.

Milligan W.W. and Antolovich S.D., [1987], "Yielding and deformation behavior of the single crystal superalloy PWA1408", Metall. Trans. A, Vol.18A, pp.85-95.

Milligan W.W. and Antolovich S.D., [1990], "The cyclic deformation of PWA1408 single crystal as a function of temperature, strain rate and orientation", in

Constitutive Laws of Plastic Deformation and Fracture, (Eds. Krausz A.S. et al), Kluwer Academic Publishers, pp.43-48.

McClintock F.A. and Irwin G.R., [1964], ASTM STP381, P.84.

Mall S., Staubs E.A. and Nicholas T., [1990], Investigation of creep/fatigue interaction on crack growth in a titanium aluminide alloy", J. Engng. Mater. Sci. Vol.112, pp435-441.

Miner M.A., [1945], "Cumulative damage in fatigue", J appl. Mech. Vol.12, A159-A164.

Miner R.V., Gayda J. and Hebsar G., [1982], "Creep-fatigue behaviour of Ni-Co-Cr-Al-Y coated PWA1480 superalloy single crystals" in Low Cycle Fatigue and Life Prediction, ASTM STP 770, (Eds. Amzallag C., Leis B.N. and Rabbe P.), ASTM, pp.105-134.

Miner R.V., Gabb T.P, Gayda J. and Hemker K.J., [1986a], "Orientation and temperature dependence of some mechanical properties of the single crystal nickel base superalloy Rene N4: part III. Tension-Compression Anisotropy", Metall. Trans. A, 17A, pp.507-512.

Miner R.V., Voigt R.C., Gayda J. and Gabb T.P.,, [1986b], "Orientation and temperature dependence of some mechanical properties of the sinle - crystal nickel - base superalloy Rene N4: part I. Tensile behaviour", Metall. Trans. A, Vol.17A, pp.491-496.

Morrow, J.D., [1968], "Fatigue properties of metals' in Fatigue Design Hamdbook, Society of Automotive Engrs, Warrendale, PA, USA, section 3.2.

Mroz Z., [1967], "On the description of anisotropic work-hardening", J. Mech. Phys. Solids, Vol.15, p.163.

Murphy M.C., Stringer M.B. and Batte A.D., [1979], "The elastic-plastic behaviour of a 1/2%CrMoV steam turbine casting steel during high strain thermal fatigue", Proc. DVM Int. Symp. on Low-Cycle Fatigue Strength and Elasto-Plastic Bebehaviour of Materials, Stuugart, pp53-62.

Muradlidharan U. and Manson S.S., [1988], "A modified universal slopes equation for estimation of fatigue characteristics of metals", ASME J. Eng. Mater. Tech., Vol.110, pp55-58.

Nathal M.V., Maier R.D. and Ebert E.J., [1982], "The influence of coblat on the tensile and stress-temperature properties of the nickel-base superalloy", Metall. Trans. A, Vol.13A, pp.1767-1774.

Nathal M.V., and Ebert E.J., [1985], "Elevated temperature creep-rupture behaviour of the single crystal nickel -base superalloy NASAIR 100", Metal. Trans. A, Vol.16A, pp.427-439.

Nazmy M.Y., [1981], "The applicability of strain range partitioning to high temperature low cycle fatigue life prediction of IN 738 alloy", Fatigue Engng. Mater. Struct., Vol.4, pp.253-256.

Nazmy M.Y., [1983], "High temperature low cycle fatigue of IN 738 and application of strain range partitioning" Metall. Trans A, Vol.14A, pp.449-461.

Nazmy M.Y., and Wuthrich C., [1984], "The predictive capability of three high temperature low cycle fatigue models in alloy In738", in Mechanical Behaviour of Materials IV, (Eds. Carlsson J. and N.G. Ohlson), Pergamon Press, New York.

Neu R.W. and Huseyin Sehitoglu [1989], "Thermomechanical fatigue, oxidation, and creep: Part I. damage mechanisms, Part II. life prediction", Metall. Trans. A, Vol.20A, pp.1755-1769-1783

Nihei M., Heuler P., Boller C. and Seeger T.,[1986], "Evaluation of mean stress effect on fatigue life by use of damage parameters", Int. J. Fatigue, Vol.8, No.3, pp119-126

Nikbin K.M. and Webster G.A., [1984], in "Creep and fracture of engineering materials and Structure", PartII, (Eds. Wilshire B. and Owen D.R.J.,) Pineridge Press, Swansea, p1091.

Nikbin K.M. and Wwbster G.A., [1987], "Prediction f crack growth under cree-fatigue lading cnditins", ASTM STP942, pp281-292.

Nouailhas D., [1987], "A viscoplastic modeling applied to stainless steel behaviour", in Proc. of 2nd Int. Conf. on Constituitive Laws for Engineering Materials; Theory and Application, (Eds. Tucson A.Z., et al), Elsevier, New York, pp.717-724.

Nouailhas D., [1989], "Unified modeling of cyclic visco-plasticity; application to austenitic stainless steels", Int. J. Plast., Vol.5, pp.501-520.

Nouailhas D. [1990] "Anisotropic constitutive equations for cyclic viscoplasticity: Application to the case of materials with cubic symmetry" Rech. Aerosp., No.3, pp11-28.

O'connor B.P.D. and Plumtre A.C. [1988], "Fatigue crack propagation behaviour and damage accumulation relationship in an aluminium alloy", in Fracture Mechanics, Nineteenth Symp. ASTM STP969, ASTM, Philadelphia, pp787-799.

Oblak J.M. and W.H. Rand, [1974], in 'Proc. 32nd Annual Meeting of Electron Microscopy Society of America' [ed C.J. Arceneauk], 502-503.

Ohasin Y., Kawai Y., [1985], "Inelastic behaviour of type 316 stainless steel under multiaxial non-proportional cyclic stressing at elevated temperature", J. Engng. Mater. and Technol., Vol.107, pp.101-

Ohno N., [1990], "Recent topics in constitutive modeling of cyclic plasticity and viscoplasticity", Appl. Mech. Rev., Vol.43, pp.283-295.

Ohno N., and Wang J., [1991], "Tansformation of a nonlinear kinematic hardening rule to a multisurface form under isothermal and nonisothermal conditions", Int. J. Plast., Vol.7, pp.879-891.

Ohno N., and Wang J., [1992], "Nonisothermal constutitve modelling of inelastic based on bounding syrface", Nuclear Engng. & Design, Vol.133, pp369-381.

Ostergren W.J., [1976a], "A damage function and associated failure equations for predicting hold time and frequency effects in elevated temperature low cycle fatigue", J. of Testing and Evaluation, Vol.4, pp.327-39.

Ostergren W.J., [1976b], "Correlation of hold time effects in elevated temperature low cycle fatigue using a frequency modified damage function", in ASME-MPC Symp. on Creep-Fatigue Interactions, pp.179-202.

Paidar V., Yamagnchi M., Pope D.P. and Vitek V., [1982], "Dissociation and core structure of <110> screw dislocation in Li2 ordered alloys- II effectd of an applied shear stress", Philos. Mag. A., V.45, 883.

Paider V., Pope D.P., and Vitek V., [1984], "A theory of the anomalous yield behaviour of LI order alloys", Act Metall., Vol.32, pp.435-449.

Paslay P., Wells C., and Leverant G., [1970], "An analysis of primary creep of nickel based superalloy single crystals", J. Appl. Mech., Vol.37, p.759.

Paslay P., Wells C., Leverant G. and Burck L., [1971], "Creep of single crystal nickel-based superalloy tubes under biaxial tension", J. Appl. Mech, Vol.38, p.623.

Peirce D., Shih C.F. and Needleman A., [1984] "A tangent modulus method for rate dependent solids", Computer struc., Vol.18, pp875-887.

Persson P.O., Persson C., Burman G., and Lindblom Y., [1986], "The behaviour of Nimonic 105 and Inco 738 LC under creep and LCF testing", in Proc. of High Temperature Alloys for Gas Turbines and Other Applications, W. Betz et al Ed., D. Riedel Publishing Co., Boston, pp.1501-1516.

Pearson D.D. et al, [1981], "Factors controlling the creep behaviour of nickel-base superalloy", in Creep and fracture of Engineering Materials and Structures, (Eds. Wilshire B and Owen D.R.J.), Proc. Int. Conf. Held at University College, Swansea, pp.213-233.

Pickard A.C., [1981], "An analysis of the electrical potential distribution in the corner cracked and fin cracked testpieces" Rolls-Rolyce Report, private communication.

Plumbridge W.J., and Ellison E.G., [1987], "Low-cycle fatigue behaviour of superalloy blade materials at elevated temperature", Mater. Sci. Tech., Vol.3, pp.706-715.

Plumtree A. and O'Connor B.P.D., [1989], "Damage accumulation and fatigue crack propagation in a squeeze-formed aluminium alloy", Int. J. Fatigue, Vol.11, pp249-254.

Plumbridge W.J. and Ellison E.G., [1991], "Stress response behaviour of a cast nickel base superalloy subjected to combined creep-fatigue", Fatigue Frac. Engng. Mater. Struc., Vol.14 No.4, pp373-389.

Pollck T.M. and Argn Ali S., [1987], "Creep resistance f nickel base superalloy single crystals", in Creep and Fracture of Engineering Materials and Structures, (Eds. Wilshire B. and Evan R.W.), The IMETALS, London, p.287.

Poirier J.P., [1976], *Plasticite a Haute Temperature des Solide Cristalline*, Eyrolles Press Ch.9.

Pope D.P. and Ezz S.S, [1984], "Mechanical properties of Ni_3Al and nickel-base alloys with high volume fraction of γ' ", Int. Metals Reviews, Vol.29, no.3, pp.136-167.

Pope D., and Heredia F., [1984], "The tension/ compression asymmetry in high volume fraction nickel base single crystals" in: 5th Int. Symp. on Superalloys, ASM, Metals Park, OH.

Poubanne P., [1990], "Anisotropic mechanical behaviour modeling of a nickel base single crystal superalloy" in Constitutive Laws of Plastic Deformation and Fracture, (Eds. Krausz A.S. et al), Kluwer Academic Publishers. pp.49-55.

Priest R.H. and Ellison E.G., [1982], "An assessment of life analysis techniques for fatigue-creep situations", Res Mechanica, Vol.4, pp.151-157.

Priest R.H., Beauchmap D.J., and Ellison E.G., [1983], "Damage during creep-fatigue damage" in Advances in Life Prediction Methods, ASME Conf., Albany, ASME, pp.115-122.

Remy L. [1993] High temperature fatigue of superalloys" in Fatigue '93, (Eds. Bailon J P and Dickson J I) EMAS U.K vol.II, pp825-834.

Remy L., Rezai Aria F., Danzer R. and Hoffelner W., [1986], " Comparison of life prediction methods in Mar M509 Under high temperature fatigue", in High temperature Alloys for Gas Turbine and Other Applications, (Eds. Betz W. et al) D.Riedel Publishing Co., Boston, Part II, pp.1617-1628.

Reuchet J. and Remy L., [1983], "Fatigue Oxidation interaction in a superalloy -- application to life prediction in high temperature low cycle fatigue", Metall. Trans. A, Vol.14A, pp.141-149.

Robinson E.L., [1952], "Effect of temperature variation on long time rupture strength of steels", Trans. ASME, Vol.74, pp777-781.

Robinson D.N., Pugh C.E. and Corum J.M., [1976], "Constitutive equations for describing high-temperature inelastic behavior of structural alloys" in Specialists meeting on high-temperature structural design technology of LMFBRs,IAEA report IWEGFR/11, Int. Atomic Energy Agency, pp.44-57.

Rolls Royce, private Communication, July 1989.

Russell R., Jenson and John, K. Tien, [1985], "Temperature and strain rate dependence of stress-strain behaviour in a nickel-base superalloy", Metall. Trans. A, Vol.16A, pp.1049-1068.

Saltsman J.E. and Halford G.R., [1989], "Procedures for characteristizing an alloy and predicting cyclic life with the total strain version of strainrange partitioning " NASA Technical Memo. 4102.

Shahinian P. and Sadananda K. [1979] "Effect of stress ratio and hold-time on fatigue crack growth in alloy 718", J. Eng. Mater. Technol., Vol.101, pp152-163.

Shahinian P. and Sadananda K., [1989], "Creep and fatigue crack growth behaviour of some cast nickel-base alloys", Mater. Sci. and Engng., Vol108A, pp131-140.

Shah D., [1983], "Orientation dependence of creep behaviour of single crystal (Ni_3Al)", Scripta Metall., Vol.17, p.997-1002.

Shah D.M. and Duhl D.N.,, [1984], "The effect of orientation, temperature and gamma prime size on the yield strength of a single crystal nickel base superalloy", in Superalloys 1984, Proc. 5th Int. Symposium on Superalloys, (Eds. Gell M. et al), AIME Warrendale PA. pp.105-14.

Schmid E. and Siebel G., [1931], I Electrachew, Vol.37, P.447.

Schmidt C.G. and Miller A.K., [1981], "A unified phenomenological model for non-elastic deformation of type 316 stainless steel, Parts I and II", Res. Mechanica, Vol3, pp109-129, PP175-193.

Sheh, M.Y. and Stouffer, D.C., [1990], " A crystallographic model for the tensile and fatigue response for Rene N4 at 982 C", J. Appl. Mech, Vol.57, pp.52-31.

Sherry A.H., [1984], "The deformation and fracture of single crystal superalloy" M.S. Thesis, University of Manchester.

Sherry A.H. and Pilkington R., [1987], "Pore morphlogy changes in a single crystal alloy during creep at high temperature", in Creep and Fracture for Engineering Materials and Structures, (Eds. Wilshire B and Evan R W), The IMETALS, London, p.333

Skelton R.P. [1978], "Crack growth during high strain fatigue of 0.5 $C_r - M_o - V$ steel at 825 K", Mater. Sci. Engng., Vol.32, pp.211-219.

Skelton R.P. and Haigh J.R., [1978], "Fatigue crack growth rates and thresholds in steels under oxidising conditions" Mater. Sci. & Engng. Vol36, pp17-25.

Skelton R.P., [1981], "Growth of short cracks during high strain fatigue and thermal cycling", in Low-Cycle Fatigue and Life Prediction, (Eds.Amzallag C et al) ASTM STP770, pp337-381.

Smith K.N, Watson P. and Topper T.H., [1970], " A stress-strain function for the fatigue of metals", J. of Mater. JMLSA ,Vol.5, No.4, pp767-778.

Solomon H.D. and Coffin L.F., [1973], "Effects of frequency and environment on fatigue crack growth in A286 at 1100F" in Fatigue at Elevated Temperature, ASTM STP520, . pp112-122.

Stentz R.H., Berling J.T. and Conway J.B., [1978], "An application of strain range partitioning to copper base alloys at 538C", AGARD-cp-243.

Stouffer D.C., Sheh M.Y. and Dam L.T., [1990], "Anisotropic constitutive model of a single crystal superalloy at elevated temperasture" , Appl. Mech Rev., Vol.43, no.5, pp.s345-s352.

Sun Y.Q. and Hazzledine P.M., [1988],"A TEM weak-beam study of dislocation in r' in a deformed Ni-based superalloy", Phil. Mag., A58, p.603-618.

Suzuki A., [1986], "A modified fraction model for the viscoplastic behavior of metals", in Proc. of Int. Conf. on Creep, Tokyo, pp.471-476.

Taguchi K. and Uno T., [1989], "Application of unified constitutive equation to inelastic deformation behavior of modified 9Cr-1Mo steel at 550°C", Trans JSME Ser A Vol.55, pp.1560-1565.

Takeuchi S. and Kuramoto E., [1973], "Temperature and orientation dependence of the yield stress in Ni_3Ga single crystals", Acta Metall., Vol.21, pp.415-425.

Taylor G., [1937], "Plastic strains in metals", J. Inst. Metals, Vol.62, p.307.

Tensen R.R., Hopson T.E. and Tien J.K., [1980], in Superalloy 1980, Proc. 4th Int. Symposium on Superalloys, (Eds. Tien J.K. et al), ASM Metals Park OH, pp.679-688.

Thomas G.B., [1982], "Low cycle fatigue and life prediction methods", in Proc. High Temperature Alloys for Gas Turbines 1982, (Eds. Brumetand B. et al), Reidel Publishing Co., pp.291-317.

Tien J.K. and Davidson J.M., [1974], in Stress Effects and the Oxidation of Metals (ed. Cathcart J V), TMS-AIME, pp200-219

Umakoshi Y., Pope D. and Vitek V., [1984], "The asymmetry of the flow stress in $Ni_3(Al,Ta)$ single crystals", Acta Metall., Vol.32, No.3, p.449-456.

Valanis K.C., [1971], "A theory of viscoplasticity without a yield surface", Arch. Mech., Vol.23, pp.517-551.

Valanis K.C., [1980], "Fundamental consequences of a new intrinsic time mearsure; plasticity as a limit of the endochronic theory", Arch. Mech., Vol.32, p.171-191.

Valanis K.S., [1984], "Continuum foundations of endochronic plasticity", ASME J. Eng. Mat. Tech., Vol.106, pp.367-375.

Walker K.P., [1981], "Research and development program for nonlinear structural modeling with advanced time-temperature dependent constitutive relationships" NASA CR-165533, NASA.

Walker K.P. and Jordan E.H., [1985], "Biaxial constitutive modeling and testing of a single crystal superalloy at elevated temperatures", in Biaxial and Muliaxial Fatigue, EGF3, (Eds. M W. Brown and K.J. Miller), Mechanical Engineering Publications, London, pp.145-147.

Walter W, Milligan and Antolovich D.A., [1987], "Yieldind and deformation behaviour of the single crystal superalloy PWA 1480", Metall. Trans. A, Vol.18A, pp85-95.

Wang G., Yao D., and Krempl E., [1983], "Viscoplasticity based on overstress with an integral growth law for the equilibrium stress", RPI report MMl-83-2.

Watanabe O., and Atluri S N , [1986a], "Internal time, general internal variable, and multi-yield-surface theories of plasticity and creep ; a unified of concepts", Int. J. Plas., Vol.2, pp.37-57..

Watanabe, O., and Atulri, S N, [1986b], "Constitutive modeling of cyclic plasticity and creep, using internal time concepts", Int. J. Plast., Vol.2, pp.107-134.

Webster G.A., [1987], "High temperature fatigue crack growth in superalloy blade materials", Mat. Sci. & Tech., Vol.3, p.716.

Wells C.H., Sullivan C.P. and Gell M., [1971], "Mechanisms of fatigue in the creep range", in Metal Fatigue Damage-Mechanisms, Detection, Avoidance, and Repair, ASTM STP 495, Philadelphia, p.61.

Wilson D.A., Deluca D.P., Cowles B.A. and Stucke M.A., [1987], "Fatigue crack growth resistance of advanced blade materials", J. of Engng. for Gas Turbine and Power, Vol.109, pp176-181.

Winstone M.R., Nikbin K.M. and Webster G.A., [1985], "Modes of failure under creep/fatigue loading of a Nickle-based superally", J. of Materials, Vol.20, pp2471-2476.

Winstone M., [1989], in Proc. of MTU Seminar on Single Crystals, Munich.

Viswanathan R., Beck C.G., and Johnson R.L., [1979], "Low cycle fatigue behaviour of Udimet 710 at elevated temperatures", Research Report 79-1D 4 STABL-R3, Westinghouse Research Laboratories, Pittsbugh.

Viswanathan R., [1989], *Damage Mechanisms and Life Assessment of High Temperature Components*, ASM Int. Publisher, U.S.A..

Woodford D.A., [1981], "Environmental damage of a cast nickel base superalloy", Metall. Trans. A, Vol.12A, pp.299-308.

Wright P.K., [1988], "Oxidation-fatigue interaction in a single crystal superalloy", in Low Cycle Fatigue (Eds. Solomon et al), ASTM STP942, pp558-575.

Yang S.W., [1985], "Elastic constants of a monocrystalline nickel base superalloy", Metall. Trans. A, Vol.16A, pp.661-665.

Yang R., [1991], "Creep-fatigue crack growth in a nickel base superalloy" Ph.D thesis,University of London.

Yao D., and Krempl E., [1986], "Viscoplasticity theory based on overstress , the prediction of monotonic and cyclic proportional and nonproportional loading paths of an aluminum alloy", Int. J. Plast., Vol.1, pp.259-274.

Zamrik S.Y. and Davis D.C., [1991], "A ductility exhaustion approach for axial fatigue-creep damage assessment using Type 316 stainless steel", J. Pressure Vessel Tech. Vol.113, pp180-186.

Zirin R.M. and Krempl E., [1982], "A finite element time integration method for the theory of viscoplasticity based on infinitesimal total strain", J. Pressure Vessel Tech., Vol.104, pp130-136.

APPENDIX I
SCHMID'S LAW AND SCHIMID'S FACTORS

Consider a cylindrical single crystal with cross-section A and a crystal orientation $[l_1,m_1,n_1]$ loaded by a uniaxial load P (Fig.2.2). The direction of the normal to the slip plane is $[l_2,m_2,n_2]$ and the slip direction is $[l_3,m_3,n_3]$. The angle between the tensile axis and the normal to the slip plane is φ, and the angle which the slip direction makes with the tensile axis is θ. Hence, the area of the slip plane inclined at the angle φ will be $A/\cos\varphi$, and the component of the axial load acting in the slip plane in the slip direction is $P\cos\theta$. Therefore, the resolved shear stress, τ, is given by

$$\tau=\frac{P\cos\theta}{A/\cos\varphi}=\frac{P}{A}\cos\varphi\cos\theta \qquad \text{(AI.1)}$$

Schmid's Law states that yielding occurs when the resolved shear stress reaches the value of the **Critical Resolved Shear Stress (CRSS), τ_s ;**

$$\tau_s=\frac{P_y\cos\theta}{A/\cos\varphi}=\frac{P_y}{A}\cos\varphi\cos\theta=\sigma_y\cos\varphi\cos\theta \qquad \text{(AI.2)}$$

or

$$\sigma_y=\tau_s/\cos\varphi\cos\theta=\tau_s/S_{[l_2,m_2,n_2]\{l_3,m_3,n_3\}} \qquad \text{(AI.3)}$$

where σ_y is the uniaxial yield stress, $S_{[l_2,m_2,n_2]\{l_3,m_3,n_3\}}=\cos\varphi\cos\theta$ is called **Schmid's Factor**. For a given slip system and loading direction, **Schmid's Factor** can be calculated by the following equations.

$$\cos\theta=\frac{l_1l_3+m_1m_3+n_1n_3}{\sqrt{l_1^2+m_1^2+n_1^2}\sqrt{l_3^2+m_3^2+n_3^2}} \qquad \text{(AI.4)}$$

$$\cos\varphi=\frac{l_1l_2+m_1m_2+n_1n_2}{\sqrt{l_1^2+m_1^2+n_1^2}\sqrt{l_2^2+m_2^2+n_2^2}} \qquad \text{(AI.5)}$$

APPENDIX II

ANALYSIS OF THE INFLUENCE OF HEATING SYSTEM ON PD CALIBRATION

As the experimental work progressed, it was found that the PD voltage outputs for the tests with similar crack lengths were significantly different. Fig.AII.1 shows the PD voltage as a function of temperature during heating, In this figure, V_c is the PD across the notch, and V_r is the reference PD; 1st V_c (or V_r) and 2nd V_c (or V_r) correspond to the first and second time measurement. It can be seen that V_c does not vary smoothly with temperature, and V_r decreases almost continuously with temperature. This measurements have been repeated several times and the results obtained were found to be essentially the same in each case, the absolute values of the PD voltage changed when the position of the heating coil was adjusted, but the overall trend of PD with temperature remained similar.

Several factors have been considered to explain these observations. First, it is likely that the temperature field may influence the PD measurement because the electrical resistivity of material will vary with temperature. However, since nickel superalloys increase their resistivity with temperature, this should lead to increase of PD with temperature. In contrast a sharp reduction in V_r with temperature was observed and V_c did not vary significantly.

A second factor considered was the influence of induction heating. The main principles of induction heating, including electromagnetic induction, 'skin effect' and heat transfer , have been given in detail by Davies and Simpson [1979]. Based on these principles, if the heating coil is long enough, the distribution of the magnetic field can be assumed to be homogenous along the axial direction of the specimen. Therefore, from the theory of electromagnetic induction, the induced current in the specimen is orthogonal to the magnetic field. That is to say, the current direction is orthogonal to the direction of the direct current supply of PD system. Consequently, it is to be expected that there is no interaction. However, since the heating coil in this study has a limited length, the distribution of the magnetic field is no longer homogenous and the direction of magnetic lines are not entirely parallel with the longitudinal axis of the specimen. The result is that the induced current is no longer orthogonal to the direction of the PD direct current supply. Consequently an interaction causes the PD to vary with temperature, since the temperature increase is accompanied by an increase in the induced current density. It was therefore predicted

that in the upper half of the specimen the PD voltage will be increased and in the lower half of the specimen the PD will be reduced.

To verify above analysis, a simple test was carried out, whereby 7 wires were spot-welded along the gauge length of a specimen as shown in Fig.AII.2. During heating, the voltages across different wires were measured. Some of the results are shown in Fig.AII.3. It can be seen that in the upper half of the specimen the voltages, for example V_{13}, increased with temperature. From a comparison between voltages V_{12} and V_{23}, it was clear that the further the two wires were from the middle of the specimen, the more the voltage increased with temperature. In contrast, in the lower half of the specimen, the PD voltages, for example V_{37}, decreased with temperature.

From above it was clear that the RF induction heating system had a significant influence on the measurement of PD. The measured PD voltage from the experiments therefore includes two parts

$$V_m = V_{pd} + V_{\inf} \qquad \text{(AII.1)}$$

where V_m is the PD measured directly from test, V_{pd} is the real PD generated by Mayes PD system, V_{inf} is the additional PD caused by induction heating system.

For a test at constant temperature, V_{inf} is a constant, but between different tests V_{inf} may not be the same, since the shape and the position of the heating coil may not be the same from test to test regardless of the care taken in the setting-up procedure. Therefore it is not possible to extract the useful PD information V_{pd} directly from the measured V_m, Since

$$V_m^1(a) = V_{pd}(a) + V_{\inf}^1 \qquad (for\ test\ 1) \qquad \text{(AII.2)}$$

$$V_m^2(a) = V_{pd}(a) + V_{\inf}^2 \qquad (for\ test\ 2) \qquad \text{(AII.3)}$$

and $$V_{\inf}^1 \neq V_{\inf}^2$$

However, let us consider PD measurements at two crack lengths a_1 and a_2, where for test 1

$$\begin{cases} V_m^1[a_1] = V_{pd}^1[a_1] + V_{\inf}^1 \\ V_m^1[a_2] = V_{pd}^1[a_2] + V_{\inf}^1 \end{cases} \quad \text{(AII.4)}$$

for test 2

$$\begin{cases} V_m^2[a_1] = V_{pd}^2[a_1] + V_{\inf}^2 \\ V_m^2[a_2] = V_{pd}^2[a_2] + V_{\inf}^2 \end{cases} \quad \text{(AII.5)}$$

Then

$$V_m^1[a_2] - V_m^1[a_1] = V_{pd}^1[a_2] - V_{pd}^1[a_1] \quad \text{(AII.6a)}$$

$$V_m^2[a_2] - V_m^2[a_1] = V_{pd}^2[a_2] - V_{pd}^2[a_1] \quad \text{(AII.7b)}$$

i.e. $$\Delta V_m^1[\Delta a] = \Delta V_{pd}^1[\Delta a] \quad \text{(AII.6b)}$$

$$\Delta V_m^2[\Delta a] = \Delta V_{pd}^2[\Delta a] \quad \text{(AII.7b)}$$

If the probe spacing, z, of the two tests is assumed to be same, then $V_{pd}^1[\Delta a] = V_{pd}^2[\Delta a]$, and we then have

$$\Delta V_m^1[\Delta a] = \Delta V_m^2[\Delta a] = \Delta V_{pd}[\Delta a] \quad \text{(AII.8)}$$

Therefore if we correlate the PD difference $\Delta V_m[\Delta a]$ to the corresponding change in crack length Δa, instead of correlating PD measurement $V_m[a]$ to the corresponding crack length a , the influence of the induction heating system on PD measurement can be eliminated, i.e. the PD calibration will in the form as

$$\Delta V_m[\Delta a] = f([\Delta a]) \quad \text{(AII.9)}$$

or $$\Delta a = f^{-1}(\Delta V_m[\Delta a]) \quad \text{(AII.10)}$$

This PD calibration method was adopted in this study and further details can be found in the main body of text in Chapter 5.

APPENDIX III
ANISOTROPIC ELASTIC STRAIN ANALYSIS FOR SINGLE CRYSTALS

Taking the crystal symmetry axis O'X'Y'Z' as a reference axis system, Fig.6.1, the strain response in a direction characterised by the direction cosines (l',m',n') of a single crystal under uniaxial loading with the stress applied in the direction (t_1,t_2,t_3), can be determined using anisotropic elasticity theory. The general stress and strain transformations are

$$\sigma_{(t_1,t_2,t_3)} = t_1^2\sigma_{11} + t_2^2\sigma_{22} + t_3^2\sigma_{33} + 2t_1t_2\sigma_{12} + 2t_2t_3\sigma_{23} + 2t_1t_3\sigma_{13} \qquad \text{(AIII.1)}$$

$$\varepsilon_{(l'm'n')} = l'^2\,\varepsilon_{11}\; m'^2\,\varepsilon_{22} + n'^2\,\varepsilon_{33} + 2l'm'\,\varepsilon_{12} + 2m'n'\,\varepsilon_{23} + 2l'n'\,\varepsilon_{13} \qquad \text{(AIII.2)}$$

For a cubic single crystal, the stress-strain relationships can be expressed as;

$$\left.\begin{aligned}
\sigma_{11} &= C_{11}\varepsilon_{11} + C_{12}\varepsilon_{22} + C_{12}\varepsilon_{33} = \sigma t_1^2 \\
\sigma_{22} &= C_{12}\varepsilon_{11} + C_{11}\varepsilon_{22} + C_{12}\varepsilon_{33} = \sigma t_2^2 \\
\sigma_{33} &= C_{11}\varepsilon_{12} + C_{12}\varepsilon_{22} + C_{11}\varepsilon_{33} = \sigma t_3^2 \\
\sigma_{23} &= 2C_{44}\,\varepsilon_{23} = \sigma t_2\,t_3 \\
\sigma_{13} &= 2C_{44}\,\varepsilon_{13} = \sigma t_1\,t_3 \\
\sigma_{12} &= 2C_{44}\,\varepsilon_{12} = \sigma t_1\,t_2
\end{aligned}\right\} \qquad \text{(AIII.3)}$$

$$\left.\begin{aligned}
\varepsilon_{11} &= S_{11}\sigma_{11} + S_{12}\sigma_{22} + S_{12}\sigma_{33} = \sigma(S_{11}t_1^2 + S_{12}t_2^2 + S_{12}t_3^2) \\
\varepsilon_{22} &= S_{12}\sigma_{11} + S_{11}\sigma_{22} + S_{12}\sigma_{33} = \sigma(S_{12}t_1^2 + S_{11}t_2^2 + S_{12}t_3^2) \\
\varepsilon_{33} &= S_{12}\sigma_{11} + S_{12}\sigma_{22} + S_{11}\sigma_{33} = \sigma(S_{12}t_1^2 + S_{12}t_2^2 + S_{11}t_3^2) \\
\varepsilon_{23} &= S_{44}\,\sigma_{23}/2 \\
\varepsilon_{13} &= S_{44}\,\sigma_{13}/2 \\
\varepsilon_{12} &= S_{44}\,\sigma_{12}/2
\end{aligned}\right\} \qquad \text{(AIII.4)}$$

where C_{11}, C_{12} and C_{44} are the elastic stiffness constants and S_{11}, S_{12} and S_{44} are the elastic compliance constants. The relationship between them is given by;

$$\left.\begin{aligned}
(S_{11} - S_{12}) &= 1/(C_{11} - C_{12}) \\
(S_{11} + 2S_{12}) &= 1/(C_{11} + 2C_{12}) \\
S_{44} &= 1/C_{44}
\end{aligned}\right\} \qquad \text{(AIII.5)}$$

with $S_{11} = \dfrac{1}{E_{[001]}}$, $S_{12} = \dfrac{-\nu_{[001]}}{E_{[001]}}$, $S_{44} = \dfrac{1}{G_{[001]}}$,

where $E_{[001]}$, $G_{[001]}$, and $\nu_{[001]}$ are the elastic modulus, shear modulus and Poisson's ratio respectively. From these equations, the elastic strain in the direction (l',m',n') is given directly in terms of the uniaxial stress applied to single a crystal by

$$\begin{aligned}
\varepsilon_{(l'm'n')} = \sigma\Big[& S_{11}\cos^2 Q + S_{12}\sin^2 Q + 2(S_{11} - S_{12} - S_{44}/2) \\
& \times (l'm't_1t_2 + m'n't_2t_3 + n'l't_1t_3) \;\Big] \qquad \text{(AIII.6)}
\end{aligned}$$

where Q is the angle between the direction of strain measurement and that of the uniaxial applied stress.

APPENDIX IV

AN ANISOTROPIC VISCOPLASTICITY CONSTITUTIVE MODEL

Total strain rate can be decomposed into elastic and inelastic strain tensors;

$$\dot{\varepsilon}_{ij} = \dot{\varepsilon}^{e}_{ij} + \dot{\varepsilon}^{in}_{ij} \qquad \text{(AIV.1)}$$

The stress and strain tensors can be reduced to vectors, with the following notation;

$$[\sigma]^{t} \equiv [\sigma_1 = \sigma_{11,}\ \sigma_2 = \sigma_{22,}\ \sigma_3 = \sigma_{33,}\ \sigma_4 = \sigma_{13,}\ \sigma_5 = \sigma_{23,}\ \sigma_{16} = \sigma_{12,}]$$

$$[\varepsilon]^{t} \equiv [\varepsilon_1 = \varepsilon_{11,}\ \varepsilon_2 = \varepsilon_{22,}\ \varepsilon_3 = \varepsilon_{33,}\ \varepsilon_4 = 2\gamma_{13,}\ \varepsilon_5 = 2\gamma_{23,}\ \varepsilon_{16} = 2\gamma_{12,}]$$

Along the loading axis, the anisotropic viscoplasticity model for single crystals used in this study can be summarised as follows.

The elastic strain rate is given by;

$$\dot{\varepsilon}_{e} = B^{-1}_{ij}\, S_{jk}\, A_{kl}\, \sigma_l = B^{-1}_{ij}\, C^{-1}_{jk}\, A_{kl}\, \sigma_l \qquad \text{(AIV.2)}$$

where S_{ij} and C_{ij} represent the elastic compliance matrix and stiffness matrix respectively, and A_{ij} and B_{ij} are the stress and strain transformation matrices, defined as;

$$[\sigma_i]_{crystal} = A_{ij}[\sigma_j]_{loading} \qquad \text{(AIV.3a)}$$

$$[\varepsilon_i]_{crystal} = B_{ij}[\varepsilon_j]_{loading} \qquad \text{(AIV.3b)}$$

The components of A_{ij} and B_{ij} for a cubic single crystal are derived in Appendix V. A^{-1}_{ij}, B^{-1}_{ij} and A^{t}_{ij}, B^{t}_{ij} represent the inverse and transposed matrices of A_{ij} and B_{ij} respectively.

The anisotropic yielding surface is defined as;

$$f = \sqrt{\tfrac{3}{2}(\sigma^{'}_i - X^{'}_i)^{t}\, A^{t}_{ij} M_{jk} A_{kl} (\sigma^{'}_l - X^{'}_l)} \quad - R - k \qquad \text{(AIV.4)}$$

A viscoplastic potential has the form;

$$\Omega=\frac{K^{\bullet}}{n+1}\left[\frac{f}{K^{\bullet}}\right]^{(n+1)} \qquad \text{(AIV.5)}$$

The inelastic strain rate is then described by

$$\dot{\varepsilon}_i^{jn}=\frac{\partial\Omega}{\partial\sigma_i}=\frac{3}{2}\left(\frac{f}{K^{\bullet}}\right)^{n}\frac{B_{ij}^{-1}M_{jl}A_{lk}(\sigma_k^{'}-X_k^{'})}{\sqrt{\frac{3}{2}(\sigma_i^{'}-X_i^{'})^{t}A_{ij}^{t}M_{jk}A_{kl}(\sigma_l^{'}-X_l^{'})}} \qquad \text{(AIV.6)}$$

A kinematic hardening rule is used to describe the evolution of the internal (or back stress) variable **X**

$$\dot{X}_i=\left(\tfrac{3}{2}A_{ij}^{-1}N_{jk}B_{kl}\,\dot{\varepsilon}_l^{jn}\right)-\left(A_{ij}^{-1}Q_{jk}A_{kl}\,X_l\,\dot{p}\right) \qquad \text{(AIV.7)}$$

with

$$\dot{p}=\sqrt{\tfrac{2}{3}\left(\dot{\varepsilon}_i^{jn}\right)^{t}B_{ij}^{t}M_{jk}^{-1}B_{kl}\left(\dot{\varepsilon}_l^{jn}\right)} \qquad \text{(AIV.8)}$$

The isotropic hardening variable R is described as;

$$\dot{R}=b\,(Q-R)\,p \qquad \text{(AIV.9)}$$

In the above equations, $\sigma_i^{'}$ *and* $X_i^{'}$ represent the deviatoric components of stress and back stress respectively. p and $\dot{p}$ are the total accumulated inelastic strain and strain rate respectively. k, K*, n, Q and b are temperature dependent material constants. The anisotropic behaviour of single crystal is described by the introduction of the three tensors M_{ij}, N_{ij} and Q_{ij}. The components of the three tensors are defined as temperature dependent material constants

APPENDIX V

STRESS AND STRAIN TRANSFORMATION MATRICES FOR SINGLE CRYSTAL

The direction cosines are to be determined between the crystallographic directions [100]-[010]-[001] and the loading direction X_1, and the directions X_2 and X_3, which are orthogonal to X_1, as shown in Fig.AV.1. The loading direction X_1, which is described by the direction ratios (l,m,n) can be written in a vector form as;

$$\vec{X}_1 = \frac{l}{\sqrt{l^2+m^2+n^2}}\vec{i} + \frac{m}{\sqrt{l^2+m^2+n^2}}\vec{j} + \frac{n}{\sqrt{l^2+m^2+n^2}}\vec{k} \qquad \text{(AV.1)}$$

The direction X_2, which is at 90° to X_1, can be assigned arbitrarily by $\vec{X}_2 = a\vec{i} + b\vec{j} + 0\vec{k}$, and the third direction X_3 which is at 90° to both X_1 and X_2 can be described as $\vec{X}_3 = c\vec{i} + d\vec{j} + e\vec{k}$. The values of *a*, *b*, *c*, *d* and *e* can be determined by the vector dot products;

$$\begin{cases} la + mb = 0 \\ lc + md + ne = 0 \\ \dfrac{ml}{(l^2+m^2+n^2)} + ab + cd = 0 \\ \dfrac{nl}{(l^2+m^2+n^2)} + de = 0 \\ \dfrac{mn}{(l^2+m^2+n^2)} + de = 0 \end{cases} \qquad \text{(AV.2)}$$

The solution of Eq.(AV.2) gives the direction cosines between the crystallographic directions, [100]-[010]-[001], and the loading directions, X_1-X_2-X_3, as

	[100]	[010]	[001]
X_1	$\dfrac{l}{\sqrt{l^2+m^2+n^2}}$	$\dfrac{m}{\sqrt{l^2+m^2+n^2}}$	$\dfrac{n}{\sqrt{l^2+m^2+n^2}}$
X_2	$\dfrac{-m}{\sqrt{l^2+m^2}}$	$\dfrac{l}{\sqrt{l^2+m^2}}$	0
X_3	$\dfrac{-nl}{\sqrt{(l^2+m^2+n^2)(m^2+l^2)}}$	$\dfrac{-mn}{\sqrt{(l^2+m^2+n^2)(m^2+l^2)}}$	$\dfrac{l^2+m^2}{\sqrt{(l^2+m^2+n^2)(m^2+l^2)}}$

From the stress and strain transformation principles (Lekhnitskii [1963]), the rotation from the loading axes to the crystallographic axes are;

$$[\sigma_i]_{crystal} = A_{ij}[\sigma_j]_{loading}$$

$$[\varepsilon_i]_{crystal} = B_{ij}[\varepsilon_j]_{loading}$$

and the transformation matrices A_{ij} and B_{ij} are obtained for a cubic single crystal in the forms;

$$A_{ij} = \frac{1}{\Delta_1 \Delta_2}\begin{bmatrix} l^2\Delta_2 & m^2\Delta_1 & l^2n^2 & 2lmn\sqrt{\Delta_1} & -2l^2n\sqrt{\Delta_2} & -2lm\sqrt{\Delta_1\Delta_2} \\ m^2\Delta_2 & l^2\Delta_1 & m^2n^2 & -2lmn\sqrt{\Delta_1} & -2m^2n\sqrt{\Delta_2} & 2lm\sqrt{\Delta_1\Delta_2} \\ n^2\Delta_2 & 0 & (\Delta_2)^2 & 0 & 2n\Delta_2^{3/2} & 0 \\ mn\Delta_2 & 0 & -mn\Delta_2 & l\Delta_2\sqrt{\Delta_1} & (\Delta_2 - n^2)m\sqrt{\Delta_2} & nl\sqrt{\Delta_1\Delta_2} \\ \ln\Delta_2 & 0 & -nl\Delta_2 & -m\Delta_2\sqrt{\Delta_1} & (\Delta_2 - n^2)l\sqrt{\Delta_2} & -mn\sqrt{\Delta_1\Delta_2} \\ lm\Delta_2 & -ml\Delta_1 & lmn^2 & (m^2 - l^2)n\sqrt{\Delta_1} & -2l\ mn\sqrt{\Delta_2} & (l^2 - m^2)\sqrt{\Delta_1\Delta_2} \end{bmatrix}$$

$$B_{ij} = \frac{1}{\Delta_1 \Delta_2}\begin{bmatrix} l^2\Delta_2 & m^2\Delta_1 & l^2n^2 & lmn\sqrt{\Delta_1} & -l^2n\sqrt{\Delta_2} & -lm\sqrt{\Delta_1\Delta_2} \\ m^2\Delta_2 & l^2\Delta_1 & m^2n^2 & -lmn\sqrt{\Delta_1} & -m^2n\sqrt{\Delta_2} & lm\sqrt{\Delta_1\Delta_2} \\ n^2\Delta_2 & 0 & (\Delta_2)^2 & 0 & n\Delta_2^{3/2} & 0 \\ 2mn\Delta_2 & 0 & -2mn\Delta_2 & l\Delta_2\sqrt{\Delta_1} & (\Delta_2 - n^2)m\sqrt{\Delta_2} & nl\sqrt{\Delta_1\Delta_2} \\ 2nl\Delta_2 & 0 & -2nl\Delta_2 & -m\Delta_2\sqrt{\Delta_1} & (\Delta_2 - n^2)l\sqrt{\Delta_2} & -mn\sqrt{\Delta_1\Delta_2} \\ 2lm\Delta_2 & -2ml\Delta_1 & 2lmn^2 & (m^2 - l^2)n\sqrt{\Delta_1} & -2l\ mn\sqrt{\Delta_2} & (l^2 - m^2)\sqrt{\Delta_1\Delta_2} \end{bmatrix}$$

with

$$\Delta_1 = (l^2 + m^2 + n^2)$$

$$\Delta_2 = (l^2 + m^2)$$

APPENDIX VI
NUMERICAL SIMULATION PROGRAMMES

A.VI.1. Introduction

This appendix presents the computer programmes for the simulation of the stress and strain response of single crystal SRR99 under fatigue and creep-fatigue loading conditions using the anisotropic constitutive model developed in Chapter 7. Life predictions using the Linear Damage Summation Rule and the Mean Stress Modified Strain Range Partitioning Method combined with the constitutive model, discussed in Chapter 8, are also included in the FORTRAN programme.

The general flow chart for the FORTRAN programme is given in Fig.A.VI.1.

In the FORTRAN Programme, the cycle type (0/0, 0/t, t/0, t/t) , the crystal orientation parameters (l,m,n), the total strain range and the strain rate in the strain controlled fatigue tests, as well as the cycle number to be simulated, are all directly inputted from the keyboard at the beginning of the simulations. The material constants given in Table 7.1. are inputted by a input file named MNQC.dat.

A list of the FORTRAN programme is given in section A.VI.2.

In addition, the commercial package SIMNON was also used in this work for the comparison with above FORTRAN programme in the simple case, since SIMNON can only be used for the simulation of one dimensional differential equations without tensor calculations. The programme written for SIMNON to simulate the continuous cycling test, using a specimen with the [001] orientation, is given in section A.VI.3.

A.VI.2. List of FORTRAN Programme

```
C ***************************************************************
C *       SIMULATION PROGRAMME OF THE VISCOPLASTICITY  MODEL FOR                *
C *            SINGLE CRYSTAL NICKEL BASE SUPERALLOYS                           *
C *                                                                             *
C *  This Program is for Simulating Stress-Strain Response of Single Crystal SRR99 Under  *
C *   Creep-Fatigue  Conditions, and Combining Life Prediction Using LINEAR DAMAGE  *
C *   SUMMATION and MEAN STRESS MODIFIED STRAIN RANGE PARTITIONING Methods       *
C ***************************************************************
```

```
C.....MAIN PROGRAM.....

                    PROGRAM SIMUCYC

c ..... cycle type: O/O--continuous cycling test, O/T--compressive dwell
c ..... test, T/O--tensile dwell test,  T/T-- balanced dwell test

          REAL TWT, MMMM, L,M,N
          INTEGER NN, NNNN,ICYC

          PRINT *, '"INPUT CYCLE TYPE, O/O = 1, O/T = 2, T/O = 3, T/T = 4"'
                PRINT *, 'CYCLE TYPE ='
                 READ *, ICYC
          PRINT *, '"INPUT ORIENTATION PARAMTERS L,M,N (F4.2)"'
                PRINT *, 'L ='
                READ *,  L
                PRINT *, 'M ='
                READ *, M
                PRINT *, 'N ='
                READ *, N
          PRINT *, '"INPUT STRAIN RATE  (F10.5)"'
                PRINT *, 'STRAIN RATE ='
                READ *,  MMMM
          PRINT *, '"INPUT TOTAL STRAIN RANGE"'
                PRINT *, 'TOTAL STRAIN RANGE ='
                READ *,   TWT
                  TWT = TWT/2.0
          PRINT *, '"INPUT SIMULATION CYCLE NUMBERS NC"'
                PRINT *, 'CYCLE NUMBER ='
                READ *,  NN
          IF (ICYC.EQ.1) THEN
                NNNN = NN*2.1
          ELSE  IF (ICYC.EQ.4) THEN
                NNNN = NN*4.1
          ELSE  IF (ICYC.EQ.3) THEN
                NNNN = NN*3.2
          ELSE
                  NNNN = NN*3.1
           END IF

                  IF (ICYC.EQ.1)  THEN
                   CALL CYC00 (L,M,N,MMMM,TWT,NNNN)
                  ELSE
                   CALL CYCTT (L,M,N,MMMM,TWT,NNNN,ICYC)

10              END IF
                   END


c-----%%%%%%%%%%%%%%%%%%%%%%%%%%%%%%%%%%%%%%%%%%%%%%%%%%%%%%%%%%%%%%%%%%%%%%%
c--------- Subroutine for Continuous Cycling  Tests

          SUBROUTINE CYC00 (LI,MI,NI,MMMM,TWT,NNNN)
```

```
      REAL S(6),X(6),W(6),WP(6),WE(6),WR(6)
      REAL WPR(6),WER(6),XR(6),TT,SR(6),MMMM,TWT,MWW,WMM,QQQ
      REAL BBB,AAR,AAK,LI,MI,NI,DMMM,W11,NPP,PW1,PW2
      REAL ATMA(6,6), BIMA(6,6), BTMIB(6,6), AINB(6,6)
      REAL AIQA(6,6), AICB(6,6),BISA(6,6),RK, RKK,EN
      INTEGER NNNN,IWNN,IWKK,NJ1
      EXTERNAL  MATCA

      CALL MATCA (ATMA,BIMA,BTMIB,AINB,AIQA,AICB,BISA,RK,RKK,EN)

c---- input time step ifor output data
      OPEN (UNIT=5, FILE='LMN.DAT')
       READ (5,50)  TT,IWNN
50    FORMAT (F10.2,I10)
      CLOSE (UNIT=5, STATUS='KEEP')
          NJ1=INT((TWT*2)/(MMMM*TT).0.5)
      WRITE (*,52) LI, MI, NI, MMMM, NNNN,TT,TWT,IWNN,NJ1
52    FORMAT  (3F10.2, F10.6,I10,F10.4,F10.6,2I10)

51    FORMAT  (6E16.5)
      DMMM=MMMM

c------loops for calculation (LOOP-10)
      DO 10,  III=1, NNNN

      IF (III.EQ.1) THEN
       NJ=NJ1/2
      ELSE
          NJ=NJ
      END IF


      DO 20, JJJ=1, NJ
       WRITE (*,501) JJJ, NJ
501   FORMAT (2I10)
       W11=W11.DMMM*TT

      IF (ABS(W11) .GE. TWT) THEN
        DMMM=-DMMM
      END IF
        WR(1)=DMMM

C.....
      CALL SIMU (S,W,WP,WE,X,SR,WR,WPR,WER,XR,TT,QQQ,BBB,
     x  BIMA,AINB,AIQA,BISA,AICB,ATMA,BTMIB,EN,RK,RKK,AAR,AAK)
C.....

c ********** Using SRP Method **********
       OPEN (UNIT=19, FILE='SRP0.OUT')
      IF (ABS(S(1)).LT.5.0 .AND. WP(1).GT.0.0)  THEN
        PW1=WP(1)
      ELSE IF (ABS(S(1)).LT.5.0 .AND. WP(1).LT.0.0) THEN
        PW2=-WP(1)
      END IF

      IF (W11.GE.TWT .AND. PW1.GT.0.00000001)  THEN
        NPP=0.543*(PW1.PW2)**(-1.1085)
        WRITE (19,1001) S(1),PW1,PW2,NPP
1001   FORMAT (3X,5E16.6)
       END IF
C **************************************************
c---- output data to files
        IWKK=INT(JJJ/IWNN)
        MWW=((JJJ.0.0)/(IWNN.0.0))
        WMM=IWKK-MWW
      OPEN (UNIT=10, FILE='SMC1.OUT')
      IF (WMM.EQ.0.0) THEN
        WRITE (10,1000) S(1),W(1), W11,WP(1),X(1),X(2),X(5)
      END IF
1000  FORMAT (2X, 8E15.6,3X)
20    CONTINUE
```

```
10    CONTINUE
                END

C ***********************************************************************
c---------Subroutine for  Tests with Strain Dwells

      SUBROUTINE CYCTT (LI,MI,NI,MMMM,TWT,NNNN,ICYC)

       REAL ATMA(6,6), BIMA(6,6), BTMIB(6,6), AINB(6,6)
       REAL AIQA(6,6), AICB(6,6),BISA(6,6),RK, RKK
       REAL S(6),X(6),W(6),WP(6),WE(6),WR(6)
       REAL WPR(6), WER(6), XR(6),TT,TT1,TT2,SR(6),MMMM,TWT,QQQ
       REAL BBB,AAK,AAR,EN, LI,MI,NI,DMMM, MWW,WMM ,ATT,W11,SUMT
       REAL TEMP, QC, WP11, SMAX,SMEN, SMIN,WP10,PW1,PW2,PPW
       REAL WPP11, WPP22,WPP33,CYCI
       INTEGER NJ,NJ1,NJ2,JJJ,IIN,NNNN,IWNN,IWKK,IIWNN,ICYC,IICYC
       EXTERNAL  MATCA,LDAMA,FDAMA1, SRP

      CALL MATCA (ATMA,BIMA,BTMIB,AINB,AIQA,AICB,BISA,RK,RKK,EN)


c---- input time step for out put data
          OPEN (UNIT=5, FILE='LMNTT.DAT')
          READ (5,50) TT1,TT2,IWNN, QQQ,BBB,AAK,AAR,TEMP,IIN
50      FORMAT (2F10.2, I10, 5F10.2,I10)
          CLOSE (UNIT=5, STATUS='KEEP')
       NJ1=INT((TWT*2.0)/(MMMM*TT1).0.5)
       NJ2=INT((60/(60*TT1)).(30/(30*TT1)).(20/(20*TT1))
   x    .(9/(TT1*2)).(1.0/TT2).0.5)
          WRITE (*,52) LI,MI,NI,MMMM,NNNN,TT1,TT2,TWT,IWNN,NJ1,NJ2,
   x   QQQ,BBB,AAK,AAR,TEMP,IIN

52      FORMAT (3F10.2, F10.6,I10,3F10.6,3I10,5F10.2,I10)
51       FORMAT  (6E16.5)
            DMMM=MMMM
c------loops for calculation (LOOP-10)
          IF (ICYC.EQ.4 ) THEN
                  IIN=1
                  IICYC=2
                  CYCI=2.0
           ELSE IF (ICYC.EQ.2) THEN
                  IIN=1
                  IICYC=3
                  CYCI=3.0
            ELSE
                  IIN=2
                  IICYC=3
                  CYCI=3.0
           END IF
         DO 10,  III=IIN, NNNN
          IF (III.EQ.IIN) THEN
           DMMM=MMMM
           NJ=NJ1/2
           TT=TT1
          ELSE IF ((INT(III/IICYC))-((III.0.0)/CYCI).EQ.0.0)  THEN
           DMMM=0.0
           WP10=WP(1)
           WP11=0.0
           NJ=NJ2
           TT=TT2
         ELSE IF (W11.GE.(TWT-0.000001))   THEN
           DMMM=-MMMM
           NJ=NJ1
           TT=TT1
         ELSE
           DMMM=MMMM
           NJ=NJ1
           TT=TT1
         END IF
           ATT=0.0
```

```
          DO  20,  JJJ=1, NJ
             WR(1)=DMMM
             WRITE (*,21) JJJ
21        FORMAT (3I10,6E13.4)
c------(NJ:step in each half cycle and dwell)
             ATT=ATT.TT
            IF (ATT.GE.60)  THEN
             TT=TT1*60
            ELSE IF (ATT.GE.30) THEN
             TT=TT1*30
            ELSE IF (ATT.GE.10) THEN
             TT=TT1*20
            ELSE IF (NJ.GE.(NJ2-1)  .AND. ATT.GE.1)  THEN
             TT=TT1*2
            ELSE
             TT=TT
            END IF

C.....
          CALL  SIMU (S,W,WP,WE,X,SR,WR,WPR,WER,XR,TT,QQQ,BBB,
     x  BIMA,AINB,AIQA,BISA,AICB,ATMA,BTMIB,EN,RK,RKK,AAR,AAK)
C .....
C ..... Cal. Wpp for SRP.....
            IF (WPR(1).EQ.0.0 .AND. SR(1).LT.0.0) THEN
            IF (S(1).LT.10.0 .AND. WP(1).GT.0.0) THEN
                  PW1=WP(1)
            END IF
            END IF
            IF (WPR(1).EQ.0.0 .AND. SR(1).GT.0.0) THEN
            IF (S(1).LT.10.0 .AND. WP(1).LT.0.0) THEN
                  PW2=WP(1)
            END IF
            END IF
             PPW=PW1-PW2
C **************************************************
C.....call LDAMA for Creep Damage cal. (LDR Method)
             IF (DMMM.EQ.0.0)  THEN
            CALL LDAMA (S(1),TT,TEMP,QC,WP(1),WP11,WP10)
             IF (W11.GT.0.0)   THEN
              WPP11=WP11
             ELSE
              WPP22=-WP11
             END IF
             END IF
              W11=W11.DMMM*TT
              SUMT=SUMT.TT
c----- output data to files
            IF (TT.GE.(TT1*20))  THEN
             IIWNN=IWNN*2
            ELSE IF (TT.LE.TT2)  THEN
             IIWNN=IWNN*20
            ELSE IF (TT.GE.(TT1*2))  THEN
             IIWNN=IWNN*4
            ELSE
                  IIWNN=IWNN
            END IF
             IWKK=INT(JJJ/IIWNN)
             MWW=((JJJ.0.0)/(IIWNN.0.0))
             WMM=IWKK-MWW
             OPEN (UNIT=10, FILE='SMC1.OUT')
            IF (WMM.EQ.0.0 .AND. (III.LE.13 .OR. III.GE.90))  THEN
                  WRITE (10,1000) S(1),W11,W(1),X(1),X(3),X(5)
            END IF
                  OPEN (UNIT=20, FILE='SMC2.OUT')
                  OPEN (UNIT=21, FILE='SMC3.OUT')
            IF (JJJ.EQ.NJ .AND. NJ.NE.NJ2)  THEN
            IF (S(1).GT.0.0) THEN
C **************************************************

c..... Cal. Fatigu Damage
          CALL FDAMA1 (S(1), TWT, WE(1), DF)
                  SMAX=S(1)
```

```
                    SMEN=(SMAX.SMIN)/2.0
                    WPP33=WPP11.WPP22
c ..... Cal. SRP  Per Cycle
              IF (WPP33.LT.0.0 .OR. PPW.LT.0.0)   THEN
              GOTO  1111
              END IF

              IF (WPP33.GT.0.0 .AND. PPW.GT.0.0)  THEN
               IF (ICYC.EQ.3 .AND. ICYC.EQ.4) THEN
             CALL SRP (SMAX, SMEN, WPP33, PPW,ICYC)
              END IF
              END IF
C ***************************************************

              ELSE
                    SMIN=-1.0*S(1)
              IF (ICYC.EQ.2) THEN
                    CALL SRP(SMAX,SMEN,WP11,WP(1), ICYC)
              END IF
                    WRITE (21,1000) S(1),QC,DF
             END IF
             END IF
1000      FORMAT (2X, 9E15.6)
1001      FORMAT (2X, 1E15.6, 3I10)
20     CONTINUE
10     CONTINUE
1111      END


c----%%%
```

```
              K11=RKK-AAK*R11
             END IF
             IF (FC.LE.0.0)   THEN
              WP0=0.0
             ELSE
              WP0=(1.5*((FC/K11)**EN))/(FF.RK)
             END IF
            DO  200,  I=1,6
              WPR(I)=0.0
            DO 300,  J=1,6
              WPR(I)=WPR(I).WP0*BIMA(I,J)*DSX(J)
300    CONTINUE
200    CONTINUE
210     FORMAT (6E13.6)
C---- calculates p rate PR and x rate XR(6)
            CALL SIMU01 (WPR, BTMIB, PP)
             IF (PP .LE. 1E-18)  THEN
                    PR=0.0
             ELSE
                    PR=SQRT((2.0/3.0)*PP)
             END IF
            DO  400,  I=1,6
                    XR(I)=0.0
            DO 500,  J=1,6
              XR(I)=XR(I).(2.0/3.0)*AINB(I,J)*WPR(J)-AIQA(I,J)*X(J)*PR
500    CONTINUE
400    CONTINUE
2000    FORMAT (3X, 6E13.3)
C------calculates elastic and total strain rate WER(6) and WR(6)
            DO  800,  I=1,6
                    WER(I)=0.0
                    WR(I)=0.0
            DO 900,  J=1,6
                    WER(I)=WER(I).BISA(I,J)*SR(J)
900    CONTINUE
                    WR(I)=WER(I).WPR(I)
800    CONTINUE
                    P111=P111.PR*TT
c------calculates all the total variables
              DO 888, I=1,6
                S(I)=S(I).(SRT(I).SR(I))*0.5*TT
                X(I)=X(I).(XRT(I).XR(I))*0.5*TT
                WP(I)=WP(I).(WPRT(I).WPR(I))*0.5*TT
                WE(I)=WE(I).(WERT(I).WER(I))*0.5*TT
                W(I)=W(I).(WRT(I).WR(I))*0.5*TT
888       CONTINUE
              DO 881, I=1,6
               SRT(I)=SR(I)
               XRT(I)=XR(I)
               WPRT(I)=WPR(I)
               WERT(I)=WER(I)
               WRT(I)=WR(I)
881         CONTINUE
                    END

c ..........................................................................................
            SUBROUTINE SIMU01 ( SW,A, FP)
c------ this subroutine calculates f and p'
               REAL  SW(6), A(6,6), FP, M(6)
            DO 10 I=1, 6
               M(I)=0
            DO 20 J=1,6
              M(I)=M(I).SW(J)*A(J,I)
20     CONTINUE
10     CONTINUE

              FP=0.0
            DO 30 I=1,6
              FP=FP.M(I)*SW(I)
30     CONTINUE
```

```
      END

c ..........
      SUBROUTINE  MATCA (ATMA,BIMA,BTMIB,AINB,AIQA,AICB,BISA,RK,RKK,EN)
C     this is main PROGRAM FOR matrix CALCULATION
       REAL  LI, MI, NI, RMI(6,6), RS(6,6)
      REAL A(6,6), B(6,6), BT(6,6), AT(6,6), AI(6,6),BI(6,6)
      REAL RM(6,6), RN(6,6), RQ(6,6), RC(6,6), RK, RKK, EN
      REAL ATMA(6,6), BIMA(6,6), BTMIB(6,6), AINB(6,6)
      REAL AIQA(6,6), AICB(6,6), BISA(6,6)
      EXTERNAL  MATAB, MATRA, INVERS, MULMAT

c------this part input materials parameters from data file MNQC.DAT
       OPEN (UNIT=3, FILE='MNQC.DAT')
       READ (3,10) (RM(I,I), I=1,6)
       READ (3,10) (RN(I,I), I=1,6)
       READ (3,10) (RQ(I,I), I=1,6)
       READ (3,10) (RC(I,I), I=1,6)
       READ (3,10) RC(1,2),RC(2,1),RC(1,3),RC(2,3),RC(3,1),RC(3,2)
       READ (3,10) RK, RKK, EN
       WRITE (*,10) RK, RKK, EN
10    FORMAT (6E13.3)

      OPEN (UNIT=13, FILE='MNQC.OUT', STATUS='UNKNOWN')
      WRITE (13,10) (RM(I,I), I=1,6)
      WRITE (13,10) (RN(I,I), I=1,6)
      WRITE (13,10) (RQ(I,I), I=1,6)
      WRITE (13,10) (RC(I,I), I=1,6)
      WRITE (13,10) RC(1,2),RC(2,1),RC(1,3),RC(2,3),RC(3,1),RC(3,2)
      WRITE (13,10) RK, RKK, EN
      CLOSE (UNIT=13, STATUS='KEEP')
C---- input orientation parameter l, m, n from data file LMN.DAT

      OPEN (UNIT=5, FILE='LMN.DAT')
      READ (5,50)  LI, MI, NI
       WRITE (*,50) LI,MI,NI
50      FORMAT (3F10.5)
        CLOSE (UNIT=5, STATUS='KEEP')
C----calculats  matrix A and B
        CALL MATAB (LI, MI, NI, A, B)
c------computes transpose matrix AT, BT,
       CALL MATRA  (A,AT)
       CALL MATRA  (B,BT)
c----- computes inverse matrix AI, BI, RMI, RS(=RCI)
       CALL INVERS (A, AI)
       CALL INVERS (B, BI)
       CALL INVERS (RM, RMI)
       CALL INVERS (RC, RS)
c------- computes material matrix
       CALL MULMAT (AT,RM, A, ATMA)
       CALL MULMAT (BI,RM,A, BIMA)
       CALL MULMAT (BT,RMI,B, BTMIB)
       CALL MULMAT (AI, RN, B, AINB)
       CALL MULMAT (AI,RQ,A, AIQA)
       CALL MULMAT (AI,RC,B, AICB)
       CALL MULMAT (BI, RS, A, BISA)
      END

c ..........
      SUBROUTINE  MATAB (LI, MI, NI, A, B)
C------This subroutine calculates MATRIX Aij and Bij
        REAL LI, MI, NI, IA, IB, IAA, IBB
        REAL A(6,6), B(6,6)

          IA=(LI*LI.MI*MI.NI*NI)
          IB=(LI*LI.MI*MI)
          IAA=(IA)**0.5
          IBB=(IB)**0.5
          WRITE (*, 2000) IA, IB, IAA, IBB
2000    FORMAT (10X,F16.4, 10X, F6.2, 10X, F6.2, 10X, F6.2)
```

```
A11 = LI*LI/IA
A12 = MI*MI/IB
A13 = LI*LI*NI*NI/(IA*IB)
A14 = 2.0*LI*MI*NI/(IB*IAA)
A15 = -2.0*LI*LI*NI/(IBB*IA)
A16 = -2.0*LI*MI/(IBB*IAA)
A21 = MI*MI/IA
A22 = LI*LI/IB
A23 = MI*MI*NI*NI/(IA*IB)
A24 = -2.0*MI*LI*NI/(IB*IAA)
A25 = -2.0*MI*MI*NI/(IBB*IA)
A26 = 2.0*LI*MI/(IBB*IAA)
A31 = NI*NI/IA
A32 = 0.0
A33 = IB/IA
A34 = 0.0
A35 = 2.0*NI*IBB/IA
A36 = 0.0
A41 = MI*NI/IA
A42 = 0.0
A43 = -MI*NI/IA
A44 = LI/IAA
A45 = (IB-NI*NI)*MI/(IA*IBB)
A46 = LI*NI/(IAA*IBB)
A51 = LI*NI/IA
A52 = 0.0
A53 = -LI*NI/IA
A54 = -MI/IAA
A55 = (IB-NI*NI)*LI/(IA*IBB)
A56 = -MI*NI/(IAA*IBB)
A61 = LI*MI/IA
A62 = -LI*MI/IB
A63 = LI*MI*NI*NI/(IA*IB)
A64 = (MI*MI-LI*LI)*NI/(IB*IAA)
A65 = -2.0*LI*MI*NI/(IA*IBB)
A66 = (LI*LI-MI*MI)/(IAA*IBB)

B11 = LI*LI/IA
B12 = MI*MI/IB
B13 = LI*LI*NI*NI/(IA*IB)
B14 = LI*MI*NI/(IB*IAA)
B15 = -LI*LI*NI/(IBB*IA)
B16 = -LI*MI/(IBB*IAA)
B21 = MI*MI/IA
B22 = LI*LI/IB
B23 = MI*MI*NI*NI/(IA*IB)
B24 = -MI*LI*NI/(IB*IAA)
B25 = -MI*MI*NI/(IBB*IA)
B26 = LI*MI/(IBB*IAA)
B31 = NI*NI/IA
B32 = 0.0
B33 = IB/IA
B34 = 0.0
B35 = NI*IBB/(IA)
B36 = 0.0
B41 = 2.0*MI*NI/IA
B42 = 0.0
B43 = -2.0*MI*NI/IA
B44 = LI/(IAA)
B45 = (IB-NI*NI)*MI/(IA*IBB)
B46 = LI*NI/(IAA*IBB)
B51 = 2.0*LI*NI/IA
B52 = 0.0
B53 = -2.0*LI*NI/IA
B54 = -MI/(IAA)
B55 = (IB-NI*NI)*LI/(IA*IBB)
B56 = -MI*NI/(IAA*IBB)
B61 = 2.0*LI*MI/IA
B62 = -2.0*LI*MI/IB
B63 = 2.0*LI*MI*NI*NI/(IA*IB)
B64 = (MI*MI-LI*LI)*NI/(IB*IAA)
B65 = -2.0*LI*MI*NI/(IA*IBB)
```

```
                B66 = (LI*LI-MI*MI)/(IAA*IBB)

c   OPEN FILE STORE MATRIX AIJ AND BIJ
                OPEN (UNIT = 1, FILE = 'AAA.OUT', STATUS = 'UNKNOWN')
                OPEN (UNIT = 2, FILE = 'BBB.OUT', STATUS = 'UNKNOWN')
                WRITE (1, 1000) A11, A12, A13, A14, A15, A16
                WRITE (1, 1000) A21, A22, A23, A24, A25, A26
                WRITE (1, 1000) A31, A32, A33, A34, A35, A36
                WRITE (1, 1000) A41, A42, A43, A44, A45, A46
                WRITE (1, 1000) A51, A52, A53, A54, A55, A56
                WRITE (1, 1000) A61, A62, A63, A64, A65, A66
                WRITE (2, 1000) B11, B12, B13, B14, B15, B16
                WRITE (2, 1000) B21, B22, B23, B24, B25, B26
                WRITE (2, 1000) B31, B32, B33, B34, B35, B36
                WRITE (2, 1000) B41, B42, B43, B44, B45, B46
                WRITE (2, 1000) B51, B52, B53, B54, B55, B56
                WRITE (2, 1000) B61, B62, B63, B64, B65, B66
1000        FORMAT (2X, 6E13.6)
                CLOSE (UNIT = 1, STATUS = 'KEEP')
                CLOSE (UNIT = 2, STATUS = 'KEEP')

                OPEN (UNIT = 1, FILE = 'AAA.OUT', STATUS = 'OLD')
                OPEN (UNIT = 2, FILE = 'BBB.OUT', STATUS = 'OLD')
              DO 10, I = 1,6
                READ (1,1000) (A(I,J), J = 1,6)
10      CONTINUE
            DO 20, I = 1,6
              READ (2,1000) (B(I,J), J = 1,6)
20      CONTINUE
              CLOSE (UNIT = 1, STATUS = 'KEEP')
              CLOSE (UNIT = 2, STATUS = 'KEEP')
                    END

c ..........
              SUBROUTINE MATRA ( AA, AAT)
C------ this is for matrix transpose i.e AATij = AAji
                REAL AA(6,6), AAT(6,6)
              DO 10, I = 1,6
              DO 20, J = 1,6
                AAT(I,J) = AA(J,I)
20      CONTINUE
10      CONTINUE
                    END


c ..........
              SUBROUTINE MULMAT (A,B, C, D)
C------this subroutine is for three matrix multplication A.B.C = D
                REAL A(6,6), B(6,6), C(6,6), D(6,6), AB(6,6)
              DO 10, I = 1, 6
              DO 20, J = 1,6
                AB(I,J) = 0.0
              DO 30, K = 1,6
                AB(I,J) = AB(I,J).A(I,K) * B(K,J)
30      CONTINUE
20      CONTINUE
10      CONTINUE

              DO 40,  I = 1, 6
              DO 50,  J = 1,6
                D(I,J) = 0.0
              DO 60,  K = 1,6
                D(I,J) = D(I,J).AB(I,K) * C(K,J)
60      CONTINUE
50      CONTINUE
40      CONTINUE
                END

c ..........
              SUBROUTINE  INVERS (A, AI)
c = = = = = this subroutine computes the INVERSE of a Matrix AI = A-1
                REAL A(6,6),AI(6,6), AB(6, 12)
```

```
C----- form  AB = ( A II )
          DO  101, I=1, 6
          DO 102, J=1,12
           IF ((I.6).EQ.J) THEN
                  AB(I,J) = 1.0
           ELSE
                  AB(I,J) = 0.0
           END IF
102    CONTINUE
101    CONTINUE

          DO 911, I=1,6
          DO 912,  J=1,6
            AB(I,J) = A(I,J)
912    CONTINUE
911    CONTINUE
              M = 6
              N = 12
          DO 30, K = 1, M
          DO 40, Q = K, M
           IF (ABS(AB(Q,K)).GT.0.1)  GO TO 110
40     CONTINUE
              WRITE(*,45)
45       FORMAT(' NO SOLUTION')
           GOTO 290
110    DO 50, P = 1, N
                  S = AB(K, P)
                  AB(K, P) = AB(Q, P)
                  AB(Q, P) = S
50     CONTINUE
                   T = 1 / AB(K, K)
          DO 60, R = 1, N
                  AB(K, R) = T * AB(K, R)
60     CONTINUE
          DO 70,  I = 1,M
                  Y = -AB(I, K)
            IF (I.EQ.K)  GO TO 70
          DO 80, J = 1, N
                   AB(I, J) = AB(I, J) . Y * AB(K, J)
80       CONTINUE
70       CONTINUE
30       CONTINUE

C-----seperate solution AI from AB
          DO 901, I=1,6
          DO 902, J=7,12
                 JJ=J-6
                 AI(I,JJ)=AB(I,J)
902    CONTINUE
901    CONTINUE
290     END


c ***********************************************************************
        Subroutins for Life Prediction
c.......................................................................

SUBROUTINE SRP (SMAX, ST, WCPP, WPPP,ICYC)
 REAL SMAX, ST, WCP, WPP, MWPP, WIN, FPP,FCP
 REAL  NPP, NCP, NF, DD, DSRP,ACP,BCP,AAA,WCPP,WPPP
 INTEGER ICYC

   OPEN (UNIT=7, FILE='SRP.OUT')
   WRITE (7,20) SMAX,ST,WCPP,WPPP

 IF (ICYC.EQ.2) THEN
   WPP=-WPPP
   WCP=-WCPP
   ACP=0.5616
   BCP=1.11
 ELSE  IF (ICYC.EQ.3) THEN
   WCP=WCPP
```

```
          WPP=WPPP
          ACP=0.892
          BCP=1.2
        ELSE IF (ICYC.EQ.4) THEN
          WCP=WCPP
          WPP=WPPP
          ACP=2.2047
          BCP=1.1
        END IF

C       OPEN (UNIT=7, FILE='SRP.OUT')
          WRITE (7,20) SMAX,ST,WCP,WPP,NPP,NCP,DSRP,NF

          AAA=2.6
          MWPP=(SMAX/ST)**AAA*WPP
            WIN=MWPP.WCP
            FPP=MWPP/WIN
            FCP=WCP/WIN
            NPP=0.543*WIN**(-1.1085)
            NCP=ACP*WIN**(-1.0*BCP)
        DD=(FPP/NPP.FCP/NCP)
            NF=1.0/DD
            DSRP=DSRP.DD
C       OPEN (UNIT=7, FILE='SRP.OUT')
          WRITE (7,20) SMAX,ST,WCP,WPP,NPP,NCP,DSRP,NF
20      FORMAT (4X, 10E16.6)
        END

c ..........
        SUBROUTINE LDAMA (SS,TT,TEMP,QC,WP1,WP11,WP10)
        REAL SS,TT,LTR,TR,DQC,QC, SUMT,TEMP,WP1,WP11,WP10,S

          S=ABS(SS)
          WP11=WP11.(WP1-WP10)
          LTR=-9.235-0.00502*S-1.167*LOG10(S).19240.0/TEMP
          TR=3600*10**LTR
          DQC=TT/TR
          QC=QC.DQC
          SUMT=SUMT.TT
C       OPEN (UNIT=2, FILE='DAT.OUT')
C       WRITE (2,20) WP1,WP11,WP10
C 20     FORMAT (2X, 5E12.5)
          WP10=WP1
        END

c ..........
        SUBROUTINE FDAMA1 (S,TWT,WE,DF)
          REAL S,TWT,WE,DF,A0,A,B,C,D,Y,FF1,F2,N0,N1,E
          A0=2476342.85
          B=187.42
          C=0.3306
          D=0.90756
          E=S/WE
          A=A0/E
          Y=TWT*S
          N0=100.0
          J=10000
          OPEN (UNIT=4, FILE='FDAMA.OUT')
        DO 100 I=1, J
          FF1=A/(N0**C).B/(N0**D) -Y
          F2=A*(-C)/(N0**(C.1)).B*(-D)/(N0**(D.1))
          N1=N0-FF1/F2
        IF (ABS(N1-N0).LE.0.01) THEN
          DF=DF.1.0/N1
          WRITE (4,20) S,TWT,E,DF,N1,N0
20      FORMAT (5X, 6E13.6)
          GOTO 200
          END IF
          N0=N1
100   CONTINUE
200   END
```

A.VI.3. List of SIMNON Programme

```
"Simulation of 0/0 test using the [001] specimen
continuous system cycl001
state s w wp x p
time t
der ds dw dwp dx dp
aa=abs(s-1.5*x)*SQRT(m11m22)-k
a=if aa<0 then 0 else aa
dwp=((a/kk)^n)*SQRT(m11m22)*sign(s-1.5*x)
dw=z
ds=(E*dw)-(E*dwp)
dp=abs(dwp)
dx=((2/3)*(n11n22)*dwp)-((q11q22)*x*dp)
kk:1700
k=110
E=89.29e3
n11n22=310.0e3
q11q22=600
n=3.6
m11m22=1.0
z:4e-3
end


macro cycl001m
"simulation of 0/0 test with the [001] specimen
syst cycl001
init s:0.0
init w:0.0
store s w x wp
simu 0 1.25 0.01/cyc101  0.05
par z:-4e-3
simu 1.25 3.75  0.01 -cont/cyc102 0.05
par z:4e-3
simu 3.75 6.25 0.01 -cont/cyc103  0.05
par z:-4e-3
simu 6.25  8.75 0.01 -cont/cyc104  0.05
par z:4e-3
simu 8.25  10.75 0.01 -cont/cyc105  0.05
" plot stress-strain curve
axes h -0.006 0.006 v -600 600
show s(w)/cycl01
show s(w)/cycl02
show s(w)/cycl03
show s(w)/cycl04
show s(w)/cycl05
end
```

Table 4.1. Alloy Compositions of Single Crystal SRR99

Elements	Ni	C	Cr	W	Al	Co	Ta	Ti
Wt %	Bal.	0.015	8.5	9.5	5.5	5.0	2.8	2.2

Table 4.2. Test Matrix for Smooth Bar Specimen

Temperature (°C)	Continuous Cycling (0/0)	Compressive Dwell (0/t)	Tensile Dwell (t/0)	Balanced Dwell (t/t)
750	5	3	2	1
950	6	4	4	1
1050	2	2	2	1

Table 4.3. Test Matrix for Corner Crack Specimen

Temperature (°C)	Continuous Cycling (0/0)	Compressive Dwell (0/t)	Tensile Dwell (t/0)	Balanced Dwell (t/t)
750	2	2	2	1
950	3	2	4	1
1050	2	2	2	1

Table 5.1a. The Results of the Additional High Temperature Elastic Modulus Measurements Tests

Specimen No.	Temperature Dependent Young's Modulus (GPa)						Crystal Orientation Parameters					
	$E_{20^\circ C}$	$E_{300^\circ C}$	$E_{600^\circ C}$	$E_{750^\circ C}$	$E_{950^\circ C}$	$E_{1050^\circ C}$	θ deg.	ρ deg.	h	k	l	A_{hkl}
HTE1	278.0	256.7	241.9	225.7	192.6	172.0	51.4	42.7	-0.85	0.92	1.0	0.33
HTE2	256.0	238.0	214.0	200.0	169.0	151.0	48.5	31.8	-0.59	0.96	1.0	0.31
HTE3	156.0	144.0	131.0	120.0	101.0	89.0	25.5	25.4	-0.20	0.43	1.0	0.156
HTE4	124.3	115.0	105.0	95.0	79.0	70.0	7.4	1.8	-0.004	0.13	1.0	0.016
HTE5	119.0	109.0	98.0	89.2	72.0	65.0	5.1	44.2	-0.06	0.06	1.0	0.008
HTE6	121.0	112.0	102.0	90.0	74.0	67.0	5.4	27.5	-0.04	0.08	1.0	0.009

Table 5.1b. The Results of the Additional Yield Stress Measurement Tests

Specimen No.	STP1		STP2		STP3	
	Yield Stress (MPa)		Yield Stress (MPa)		Yield Stress (MPa)	
Temperature	σ_y^+	σ_y^-	σ_y^+	σ_y^-	σ_y^+	σ_y^-
20°C	1049	1042	864.7	850.2	843.5	856.4
300°C	835.7	921	864.8	850.2	834.9	839.2
600°C	825.7	835.7	889.9	823.8	796.2	783.2
750°C	844.3	895.4	1000	850.2	860.7	847.3
850°C	533	496.6	563.8	444.8	542.3	430.4
950°C	380	375.2	365.6	325.5	321.3	271.1
1050°C	201.1	192.3	185	182.3	185	219.5

Specimen No.	Crystal Orientation Parameters					
	θ deg.	ρ deg.	h	k	l	A_{hkl}
STP1	51.4	42.7	-0.85	0.92	1.0	0.33
STP2	5.1	44.2	-0.06	0.06	1.0	0.007
STP3	27.9	26.2	-0.23	0.48	1.0	0.18

Table 5.2a. The Results of Smooth Bar Tests at 750°C

Specimen No.	Cycle Type	Strain Range	Young's Modulus (GPa)		Cycles to Failure	Crystal Orientation Parameters					
		$\Delta\varepsilon_T$ %	$E_{20°C}$	$E_{750°C}$	N_f	θ	ρ	h	k	l	A_{hkl}
sb7501	0/0	1.00	149.1	98.8	10956	6.0	7.7	-0.014	0.104	1.0	0.01
sb7502	0/0	1.00	133.3	101.1	12016	11.0	15.9	-0.053	0.187	1.0	0.035
sb7503	0/0	1.20	163.0	104.1	2440	12.0	20.5	-0.074	0.199	1.0	0.041
sb7504	0/0	0.88	131.4	97.0	18405	2.9	24.3	-0.021	0.046	1.0	0.002
sb7505	0/0	1.10	137.3	106.1	3188	11.0	32.2	-0.103	0.164	1.0	0.035
sb7506	0/t	1.00	128.2	102.8	2350	9.6	21.5	-0.062	0.157	1.0	0.027
sb7507	0/t	1.00	135.0	107.9	1867	20.0	11.0	-0.069	0.357	1.0	0.103
sb7508	0/t	0.88	232.3	194.0	143	46.7	23.3	-0.420	0.975	1.0	0.286
sb7509	t/0	1.20	124.6	100.7	7346	4.3	18.50.	-0.024	0.071	1.0	0.005
sb7510	t/0	1.36	130.2	103.4	4183	5.9	9.8	-0.018	0.102	1.0	0.010
sb7511	t/t	1.00	147.8	119.8	3190	18.2	10.0	-0.057	0.324	1.0	0.088

Note: 0/0→ Continuous Cycling Tests; 0/t→ Compressive Dwell Tests; t/0→Tensile Dwell Tests; t/t→Balanced Dwell Tests.

Table 5.2b The Results of Smooth Bar Tests at 950°C

Specimen No.	Cycle Type	Strain Range	Young's Modulus (GPa)		Cycles to Failure	Crystal Orientation Parameters					
		$\Delta\varepsilon_T$ %	$E_{20°C}$	$E_{750°C}$	N_f	θ	ρ	h	k	l	A_{hkl}
sb9501	0/0	1.00	287.9	205.1	139	49.8	44	-0.822	0.851	1.0	0.328
sb9502	0/0	0.88	212.1	150.8	351	34.0	40.3	-0.436	0.514	1.0	0.238
sb9503	0/0	0.70	158.7	109.5	620	25.6	33.1	-0.262	0.401	1.0	0.159
sb9504	0/0	0.60	167.3	118.7	5214	23.0	24.5	-0.176	0.386	1.0	0.132
sb9505	0/0	0.50	*	85.3	70853	9.7	7.0	-0.021	0.170	1.0	0.028
sb9506	0/0	1.00	124.5	89.6	2271	5.1	44.2	-0.062	0.064	1.0	0.008
sb9507	0/t	0.70	297.3	219.3	199	47.6	43.4	-0.752	0.796	1.0	0.322
sb9508	0/t	0.60	241.8	167.1	462	41.7	27.1	-0.250	0.855	1.0	0.261
sb9509	0/t	0.50	*	90.8	1477	7.4	1.8	-0.004	0.130	1.0	0.016
sb9510	0/t	1.00	133.7	89.80	770	18.7	34.8	-0.193	0.278	1.0	0.095
sb9511	t/0	1.00	*	119.0	468	18.8	38.3	-0.211	0.267	1.0	0.095
sb9512	t/0	1.00	224.3	183.3	244	43.6	27.1	-0.434	0.848	1.0	0.287
sb9513	t/0	0.70	133.2	89.6	2700	12.8	7.3	-0.029	0.225	1.0	0.048
sb9514	t/0	1.20	117.6	79.0	1230	3.4	5.6	-0.006	0.059	1.0	0.004
sb9515	t/t	0.70	173.0	124.6	686	27.9	26.2	-0.234	0.475	1.0	0.179

Note: 0/0→ Continuous Cycling Tests; 0/t→ ompressive Dwell Tests; t/0→Tensile Dwell Tests; t/t→Balanced Dwell Tests.
* Not measured

Table 5.2c. The Results of Smooth Bar Tests at 1050°C

Specimen No.	Cycle Type	Strain Range	Young's Modulus (GPa)		Cycles to Failure	Crystal Orientation Parameters					
		$\Delta\varepsilon_T$ %	$E_{20^\circ C}$	$E_{750^\circ C}$	N_f	θ	ρ	h	k	l	A_{hkl}
sb1501	0/0	0.70	118.2	66.70	6655	4.4	23.7	-0.031	0.07	1.0	0.005
sb1502	0/0	1.00	118.8	69.20	1140	2.5	11.7	-0.009	0.043	1.0	0.001
sb1503	0/t	0.70	121.2	74.20	1254	5.4	27.5	-0.044	0.084	1.0	0.008
sb1504	0/t	1.00	106.0	71.50	866	9.9	43.2	-0.119	0.127	1.0	0.028
sb1505	t/0	0.70	238.8	155.3	306	41.7	27.4	-0.410	0.791	1.0	0.279
sb1506	t/0	1.00	121.1	71.50	557	7.2	4.3	-0.009	0.126	1.0	0.015
sb1507	t/t	0.70	115.2	66.10	555	3.8	32	-0.035	0.056	1.0	0.004

Note: 0/0→ Continuous Cycling Tests; 0/t→ Compressive Dwell Tests; t/0→Tensile Dwell Tests; t/t→Balanced Dwell Tests.

Table 5.3a. The Results of Corner Crack Tests at 750°C

Specimen No.	Cycle Type	Strain Range	Young's Modulus (GPa)		Cycles to Δa = 1mm	Crystal Orientation Parameters					
		$\Delta\varepsilon_T$ %	$E_{20^\circ C}$	$E_{750^\circ C}$	N_C	θ	ρ	h	k	l	A_{hkl}
c7501	0/0	1.00	121.1	94.05	3570	5.5	24.8	-0.040	0.087	1.0	0.009
c7502	0/0	1.20	115.9	90.91	1560	3.0	28.3	-0.025	0.046	1.0	0.003
c7503	0/t	1.00	123.3	96.80	420	10.5	11.2	-0.036	0.182	1.0	0.032
c7504	0/t	1.20.	116.2	90.25	170	4.3	20.6	-0.026	0.070	1.0	0.006
c7505	t/0	1.00	123.2	89.90	1850	1.3	36.7	-0.013	0.018	1.0	0.001
c7506	t/0	1.20	129.8	99.10	930	4.4	29.8	-0.038	0.067	1.0	0.006
c7507	t/t	1.00	115.6	94.44	700	3.4	38.7	-0.037	0.046	1.0	0.004

Note: 0/0→ Continuous Cycling Tests; 0/t→ Compressive Dwell Tests; t/0→Tensile Dwell Tests; t/t→Balanced Dwell Tests.

Table 5.3b. The Results of Corner Crack Tests at 950°C

Specimen No.	Cycle Type	Strain Range	Young's Modulus (GPa)		Cycles to Δa = 1mm	Crystal Orientation Parameters					
		$\Delta\varepsilon_T$ %	$E_{20^\circ C}$	$E_{750^\circ C}$	N_C	θ	ρ	h	k	l	A_{hkl}
c9501	0/0	0.60	127.6	81.6	6250	2.4	14.9	-0.011	0.041	1.0	0.001
c9502	0/0	0.70	131.1	77.7	4350	2.3	20.7	-0.014	0.038	1.0	0.002
c9503	0/0	0.80	130.5	80.4	1280	2.4	20.8	-0.015	0.039	1.0	0.002
c9504	0/t	0.60	131.1	78.4	420	4.9	22.7	-0.011	0.041	1.0	0.002
c9505	0/t	0.70	132.1	83.3	200	10.1	28.0	-0.033	0.079	1.0	0.007
c9506	t/0	0.70	129.6	86.8	1176	7.8	35.8	-0.080	0.111	1.0	0.018
c9607	t/0	0.76	129.1	82.3	790	9.4	42.3	-0.111	0.122	1.0	0.026
c9508	t/0	0.80	128.2	86.1	550	4.8	2.8	-0.004	0.084	1.0	0.007
c9509	t/0	1.00	123.9	80.0	196	4.6	8.5	-0.012	0.079	1.0	0.006
c9510	t/t	0.70	124.1	82.2	320	3.3	14.4	-0.014	0.056	1.0	0.003

Note: 0/0→ Continuous Cycling Tests; 0/t→ Compressive Dwell Tests; t/0→Tensile Dwell Tests; t/t→Balanced Dwell Tests.

Table 5.3c. The Results of Corner Crack Tests at 1050°C

Specimen No.	Cycle Type	Strain Range	Young's Modulus (GPa)		Cycles to $\Delta a = 1mm$	Crystal Orientation Parameters					
		$\Delta\varepsilon_T$ %	$E_{20^\circ C}$	$E_{750^\circ C}$	N_C	θ	ρ	h	k	l	A_{hkl}
c1501	0/0	0.60	118.1	67.1	1230	2.8	9.7	-0.008	0.048	1.0	0.002
c1502	0/0	0.70	122.3	70.5	910	5.6	27.0	-0.045	0.087	1.0	0.009
c1503	0/t	0.60	119.3	69.1	625	3.4	23.9	-0.024	0.054	1.0	0.004
c1504	0/t	0.70	117.3	67.3	350	4.0	20.5	-0.024	0.065	1.0	0.005
c1505	t/0	0.60	121.1	69.3	370	8.2	35.9	-0.084	0.117	1.0	0.020
c1506	t/0	0.70	117.2	67.8	225	4.5	30.1	-0.039	0.068	1.0	0.006
c1507	t/t	0.60	125.6	73.5	250	4.2	9.6	-0.012	0.072	1.0	0.005

Note: 0/0→ Continuous Cycling Tests; 0/t→ Compressive Dwell Tests; t/0→Tensile Dwell Tests; t/t→Balanced Dwell Tests.

Table 5.4. Comparison of Cycle Softening Behaviour at Different Temperatures

Temperature °C	Cycle Type	Total Strain Range $\Delta\varepsilon_T$ %	$HF_{20\%}$	$HF_{50\%}$	$HF_{80\%}$
750	0/0	1.20	-0.5	-1.2	-1.3
950	0/0	0.70	0.0	0.0	-2.0
1050	0/0	0.70	-11.7	-16.2	-20.7
750	0/t	1.00	-0.7	0.0	0.08
950	0/t	0.70	-6.5	-6.50	-6.5
1050	0/t	0.70	-11.4	-14.5	-18.4
750	t/0	1.20	-0.5	-0.08	-0.65
950	t/0	0.70	-7.5	-9.10	-11.7
1050	t/0	0.70	-17.7	-27.0	-42.5
				-	
750	t/t	1.00	0.0	0.0	-0.17
950	t/t	0.70	-4.3	-14.6	-23.80
1050	t/t	0.70	-11.9	-21.1	-25.0

Table 5.5. Coefficient η for PD Calibration at Different Temperatures

Temperature	20°C	750°C	950°C	1050°C
η	0.57	0.66	0.72	0.77

Table 6.1. Schmid's Factors of the Additional Yield Stress Measurement Tests

Spec. No.	h	k	l	S_1	S_2	S_3	S_4
STP1	-0.85	0.92	1.0	0.314	0.469	-0.165	0.487
STP2	-0.06	0.06	1.0	0.430	0.045	0.192	0.085
STP3	-0.23	0.48	1.0	0.489	0.325	-0.044	0.390

Note: $S_1 = S_{(111)[\bar{1}01]}$, $S_2 = S_{(010)[\bar{1}01]}$

$S_3 = S_{(111)[1\bar{2}1]}$, $S_4 = S_{(001)[\bar{1}10]}$

Table. 6.2. The Coefficients of the LCP Model Used for Single Crystal SRR99

Temperature	b_1 (10^{-3}) MPa^{-1}	b_2 (10^{-3}) MPa^{-1}	b_3 (10^{-3}) MPa^{-1}
20°C	2.77	-0.590	-0.0052
300°C	2.76	-0.503	-0.0052
600°C	2.74	-0.256	-0.238
750°C	2.55	-0.269	-0.466

Table 6.3. Stress Exponent in Power Law Creep Equation

Temperature	750°C	850°C	900°C	950°C	1050°C
Exponent n	13.16	9.73	6.76	6.19	6.9

Table. 6.4. The Coefficents in Time Hardening Stress Relaxation Rule

Spec. No.	E (GPa)	C_c	m_c	n_c
sb9512	183.3	0.1468	0.4602	6.19
sb9513	89.6	90.169	0.245	6.19
sb9514	80.0	4.553	0.2527	6.19
sb9515	124.6	0.5335	0.3636	6.19
sb1505	155.3	40.66	0.745	6.90
sb1506	71.50	166.74	0.351	6.90
sb1507	66.10	176.06	0.3302	6.90

Table 7.1. Material Constants Used in the Constitutive Model for Single Crystal SRR99 at 950°C

Parameter	Numerical Value	Unit
S_{11}	1.162×10^{-5}	MPa^{-1}
S_{12}	-4.512×10^{-6}	MPa^{-1}
S_{44}	1.135×10^{-5}	MPa^{-1}
M_{11}-M_{12}	1.0	
M_{44}	3.9	
k	110	MPa
n	3.6	
K*	1700	$MPa.s^{-1}$
Q	60.0	MPa
b	50.0	
N_{11}-N_{12}	310000	MPa
N_{44}	50464	MPa
Q_{11}-Q_{12}	600	
Q_{44}	700	

Table 8.1. Material Constants in Coffin-Manson Law

	950°C		1050°C	
	Based on best-fit	Based on 0/0 data	Based on best-fit	Based on 0/0 data
β_1	0.947	0.902	0.547	0.480
C_1	0.887	0.577	0.127	0.0824

Note: 0/0 → Continuous cycling tests

Table 8.2. Material Constants in Damage Function Approach

	950°C		1050°C	
	Based on best-fit	Based on 0/0 data	Based on best-fit	Based on 0/0 data
β_2	-0.946	-0.989	-1.478	-1.438
C_2	500.08	407.84	529.23	746.28

Note: 0/0 → Continuous cycling tests

Table 8.3. Material Constants in Frequency Modified Damage Function Approach

	950°C		1050°C	
	Based on best-fit	Based on 0/0 data	Based on best-fit	Based on 0/0 data
β_3	-1.1001	-1.094	-1.188	-1.2061
C_3	316.96	101.16	1294.20	2897.34
m	-0.1675	-0.9257	0.2715	0.7998

Note: 0/0 → Continuous cycling tests

Table 8.4. Material Constants for SWT Model

Constants	A(GPa)	α	B	β
750°C	6150.40	-0.3260		
950°C	2476.34	-0.3306	187.43	-0.9076
1050°C	985.414	-0.3137	896.40	-1.0768

Note: 0/0 → Continuous cycling tests

Table 8.5. Material Constants for Modified SRP Method

	C_{pp}	β_{pp}	C_{pc}	β_{pc}	C_{cp}	β_{cp}	C_{cc}	β_{cc}	γ
950°C	0.543	-1.108	0.562	-1.11	0.892	-0.120	2.205	-1.108	2.60
1050°C	0.255	-1.530	0.104	-1.530	0.0272	-1.530	0.0721	-1.530	0.50

Table 10.1 The Values of C_a and β_a in the Relationship $da/dN = C_a(\Delta\varepsilon_T)^{\beta_a}$

Temperature	750°C		950°C		1050°C	
Cycle types	C_a (mm/cycle)	β_a	C_a (mm/cycle)	β_a	C_a (mm/cycle)	β_a
0/0	0.00028	4.53	0.0015	4.0	0.0022	2.0
0/t	0.0024	5.01	0.0126	3.0	0.0040	1.43
t/0	0.0054	5.01	0.0035	3.0	0.0065	1.43
t/t	0.0014	5.01	0.0089	3.0	0.0083	1.43

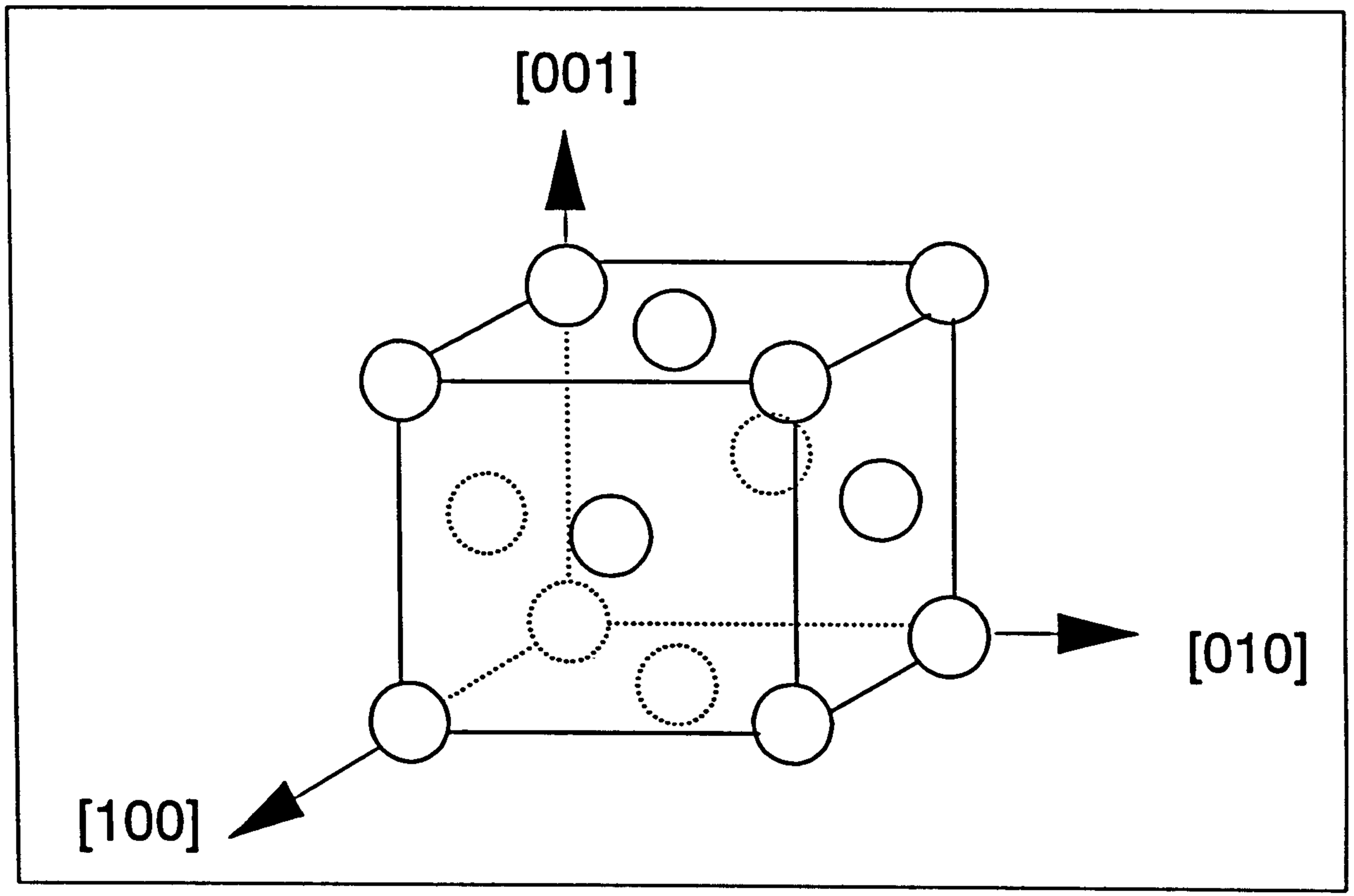

Fig.2.1. The Unit Cell of the Basic Structure of a Single Crystal Nickel Base Superalloy

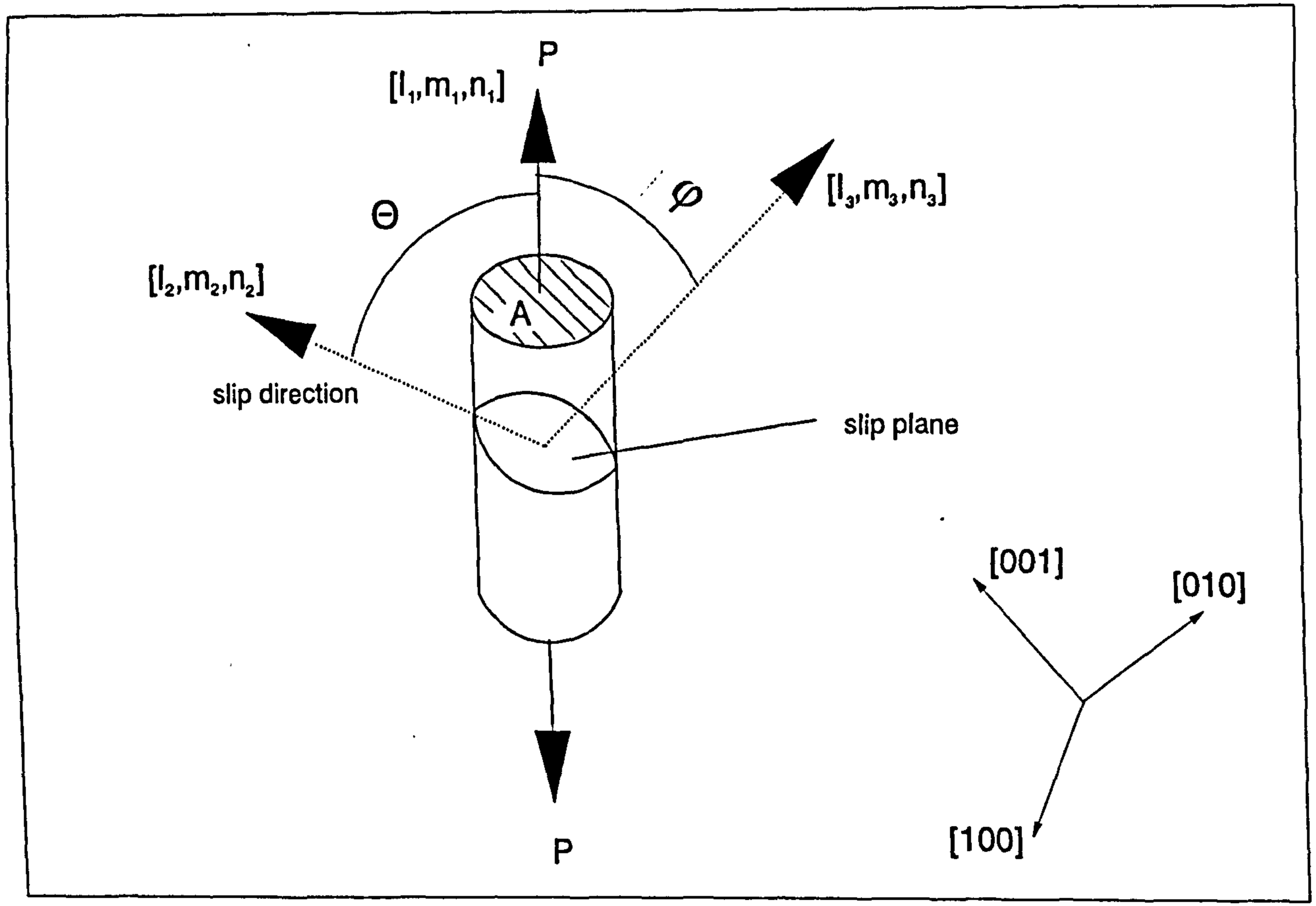

Fig.2.2. Diagram for Calculating Critical Resolved Shear Stress

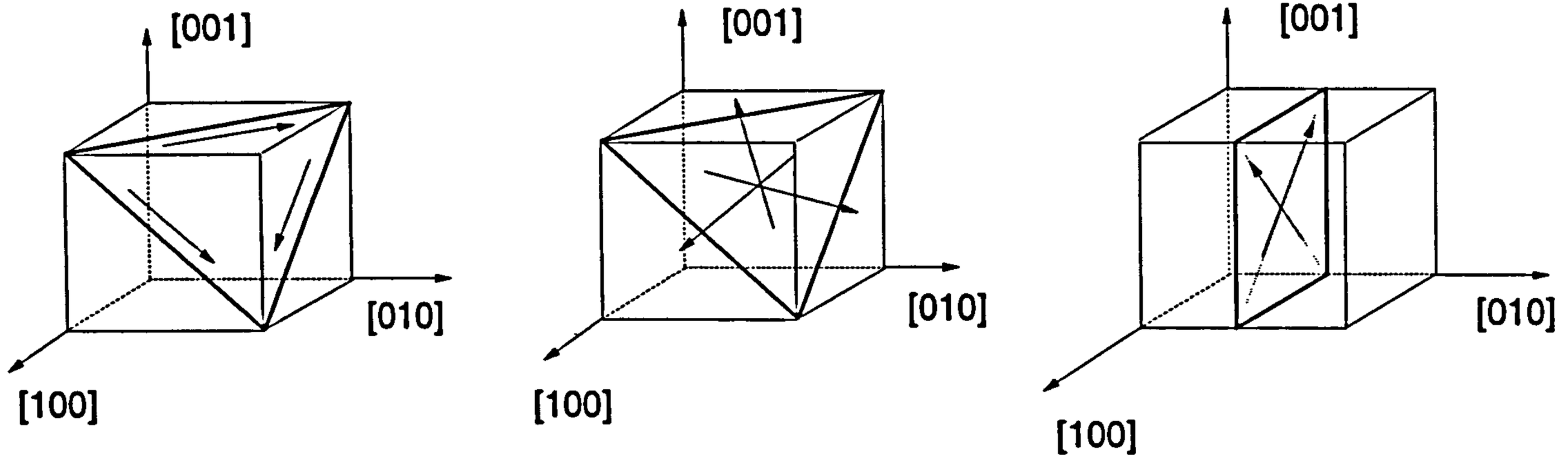

(a). Slip system [110]{111}
4 planes {111}
3 directions [110] by plane
Total 12 systems

(b). Slip system [112]{111}
4 planes {111}
3 directions [112] by plane
Total 12 systems

(c). Slip system [110]{100}
3 planes {100}
2 directions [110] by plane
Total 6 systems

Fig.2.3. Schematic of the Slip Systems in Single Crystal Nickel Base Superalloys

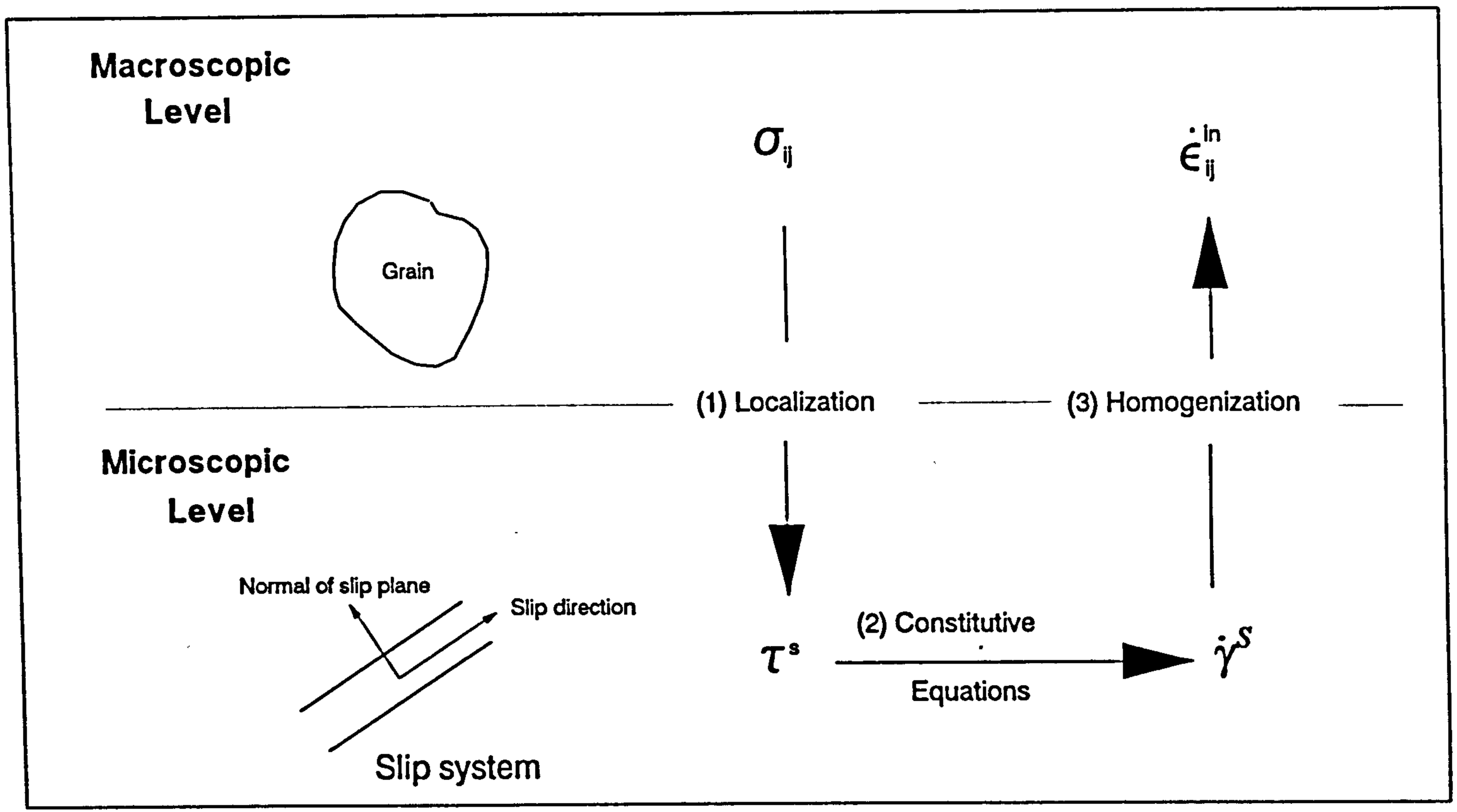

Fig.2.4. The General Procedure in Developing a Crystallographic Model

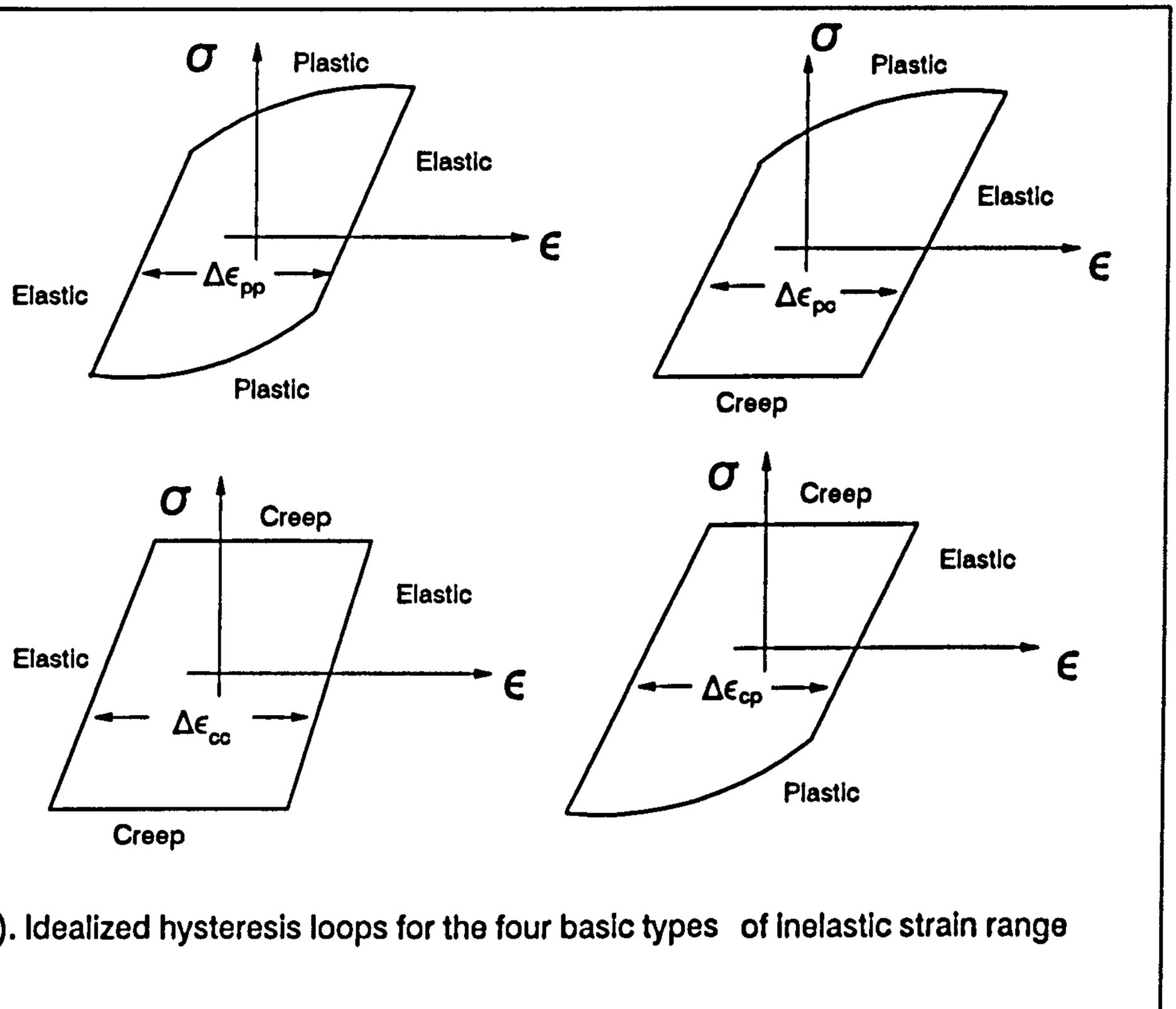

Fig.3.1. Strainrange Partitioned Hysteresis Loops

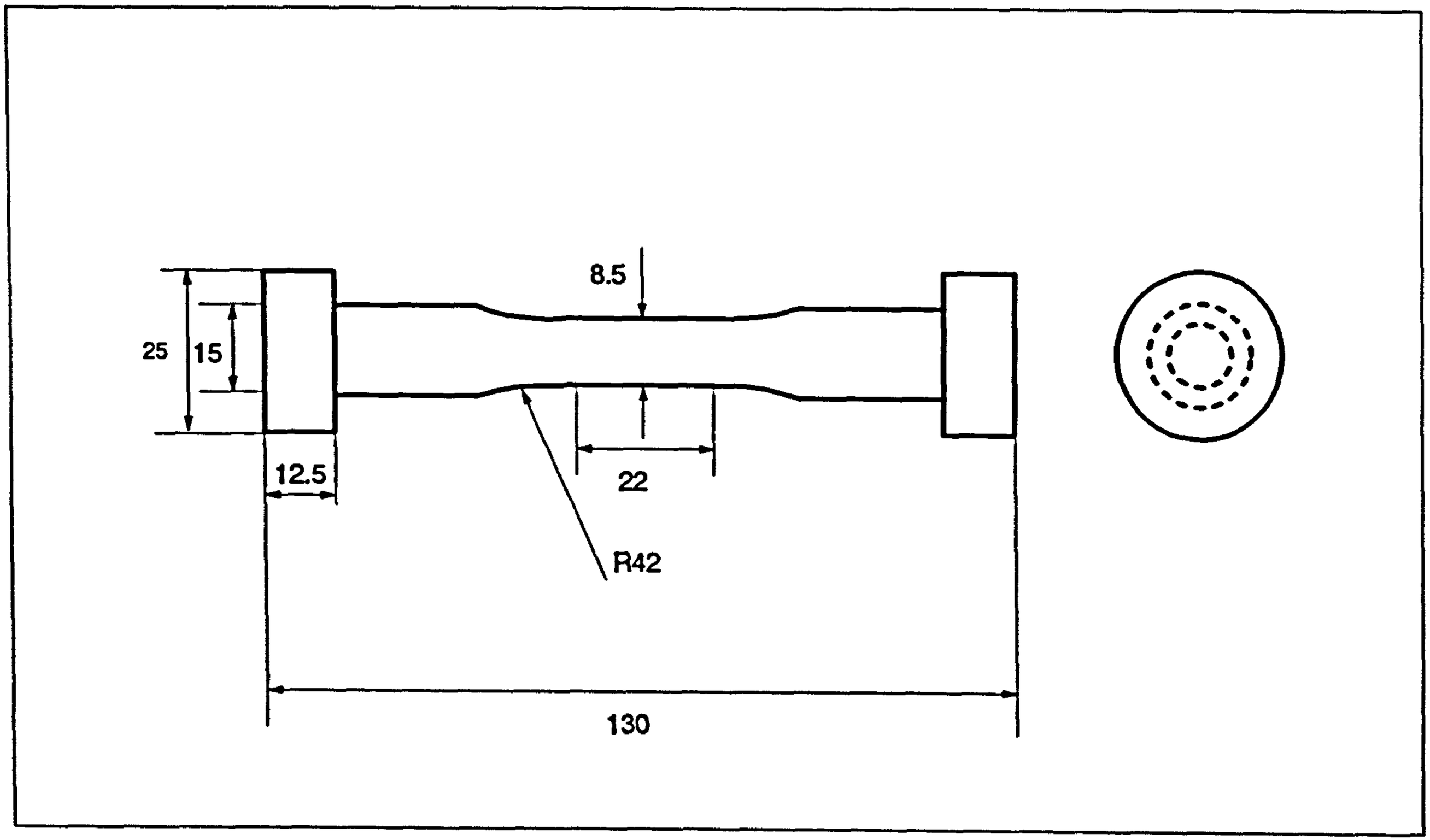

Fig.4.1. Smooth Bar Specimen Geometry (dimensions in mm)

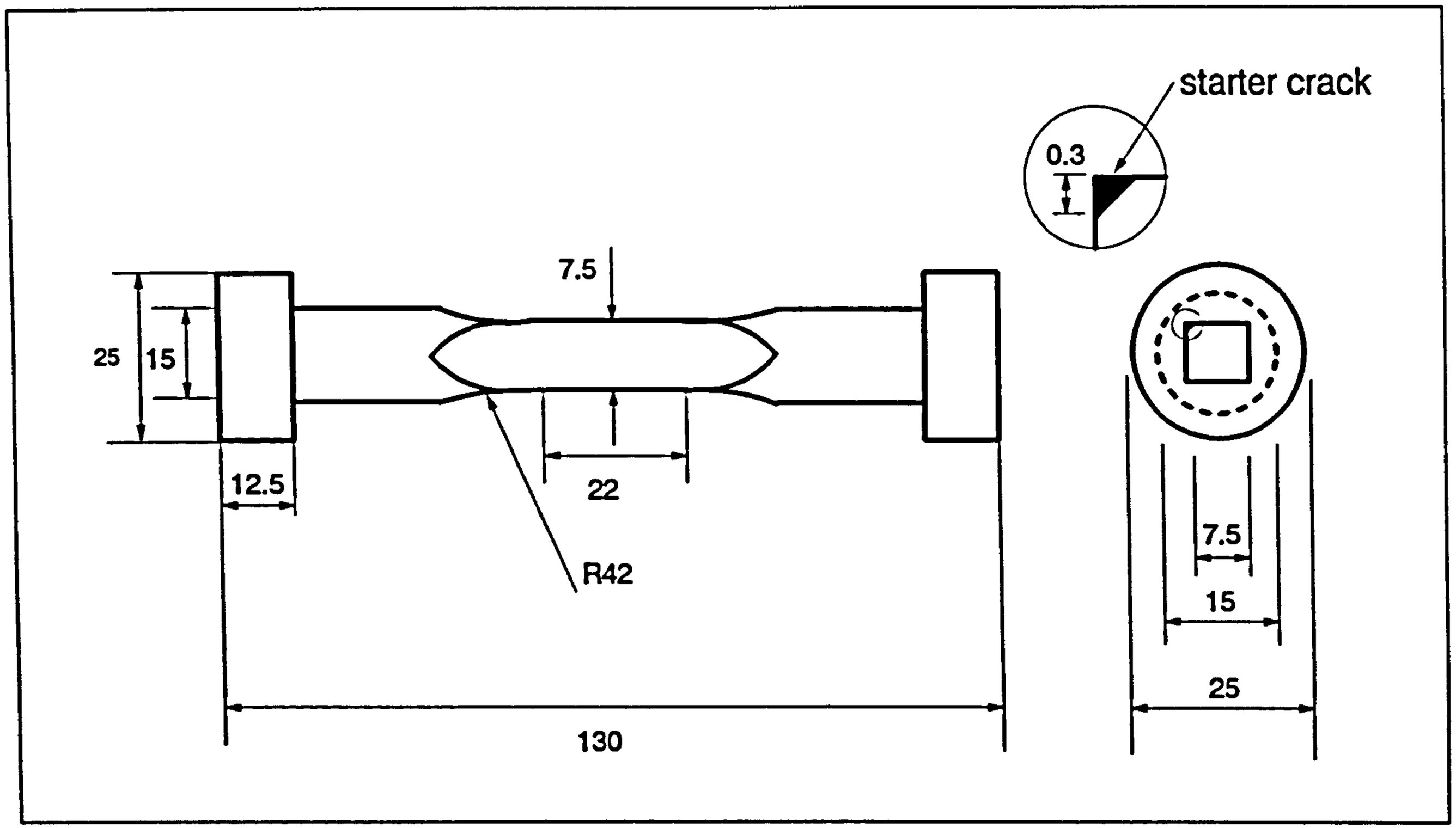

Fig.4.2. Corner Crack Specimen Geometry (dimensions in mm)

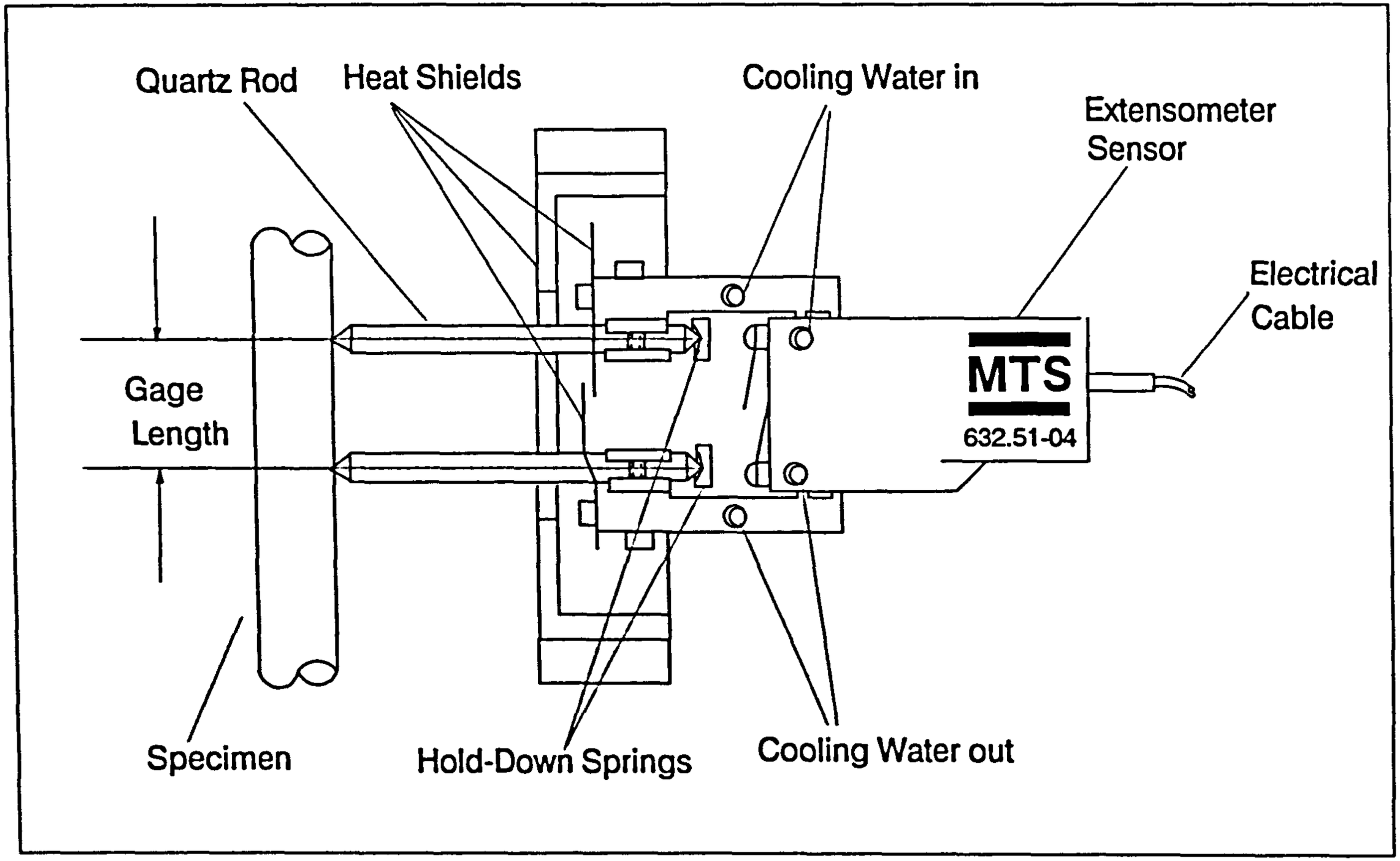

Fig.4.3. The MTS High-Temperature Axial Extensometer

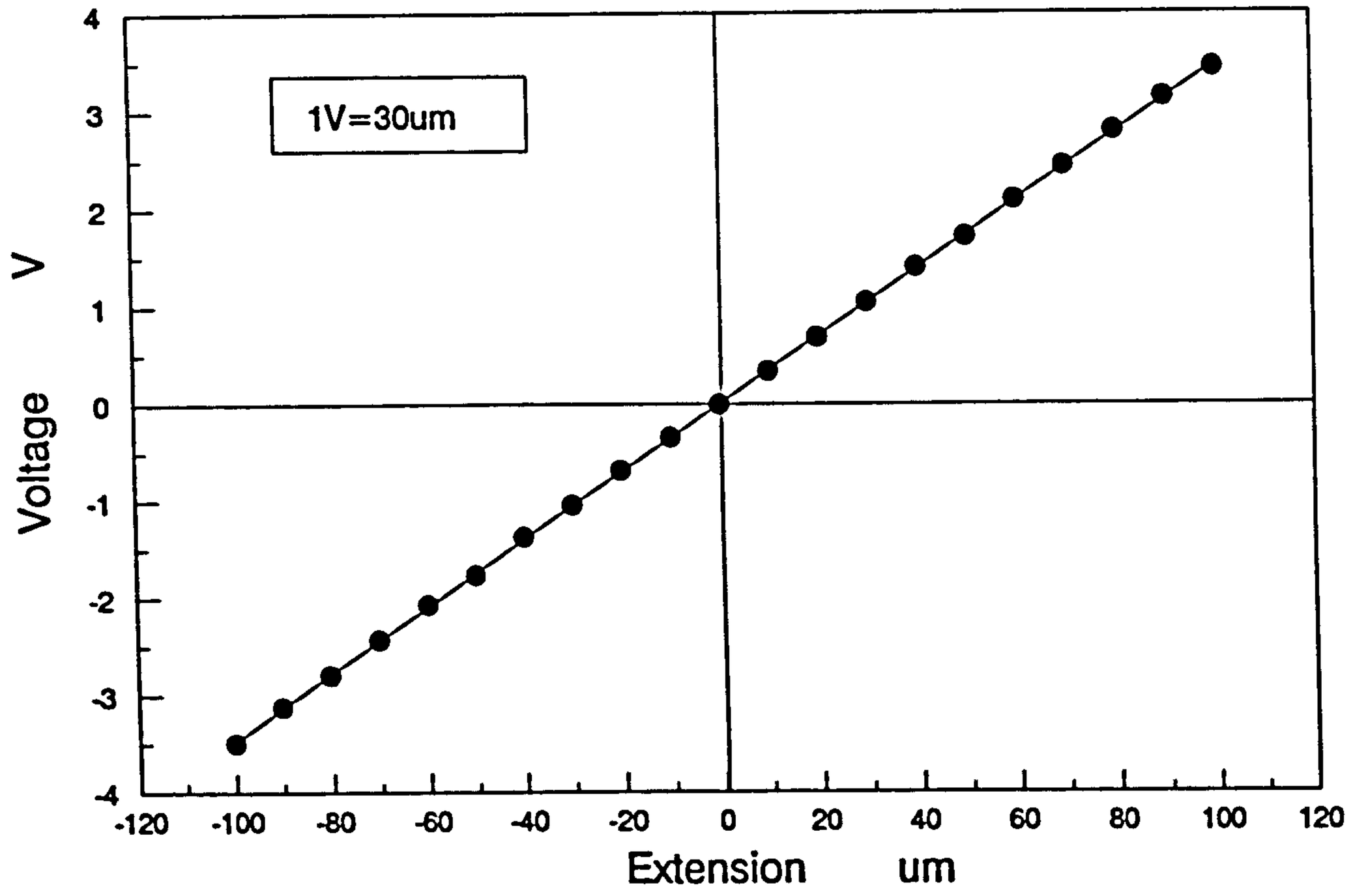

Fig.4.4 MTS Extensometer Calibration Curve

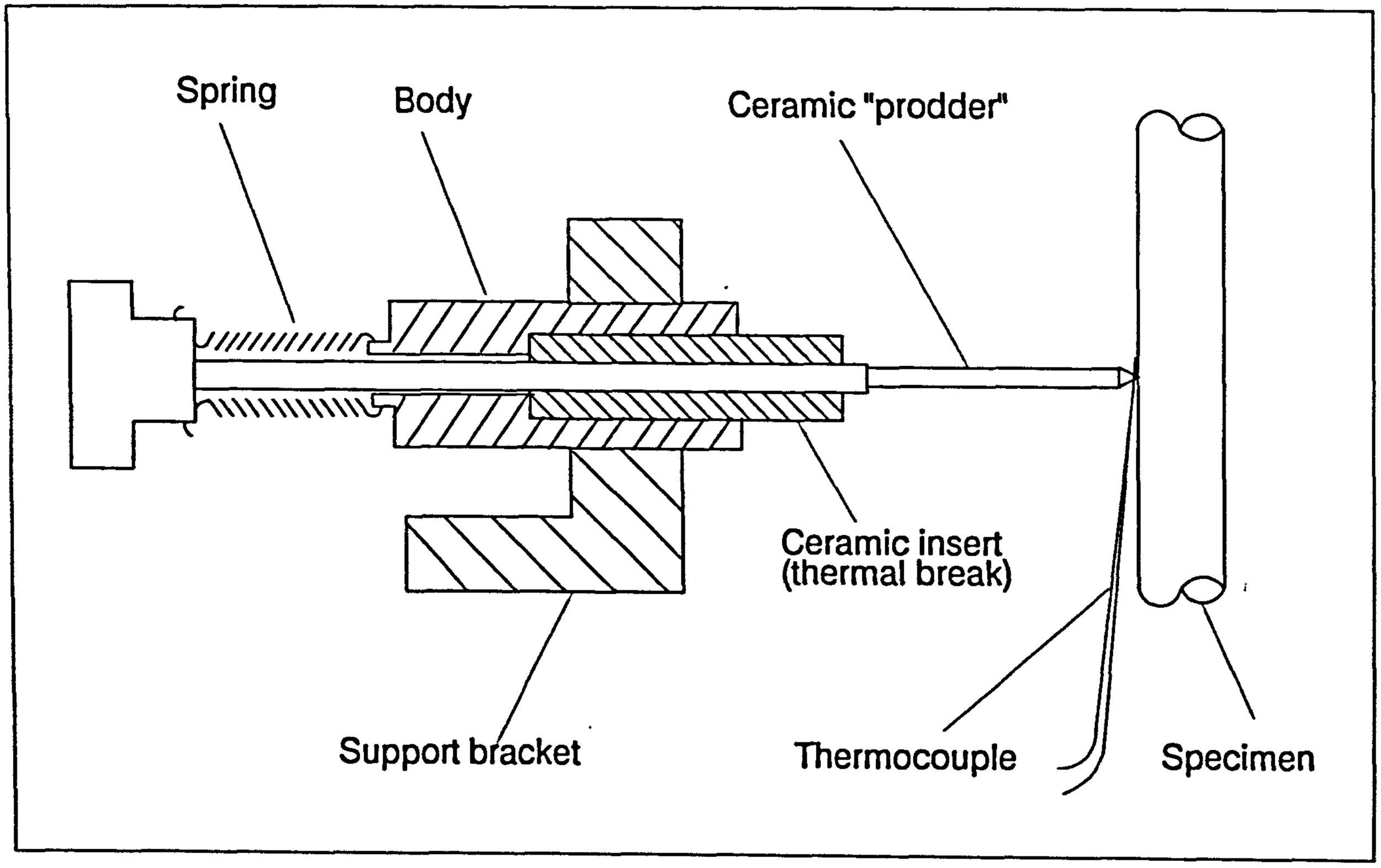

Fig.4.5. Thermocouple Attachment Probe

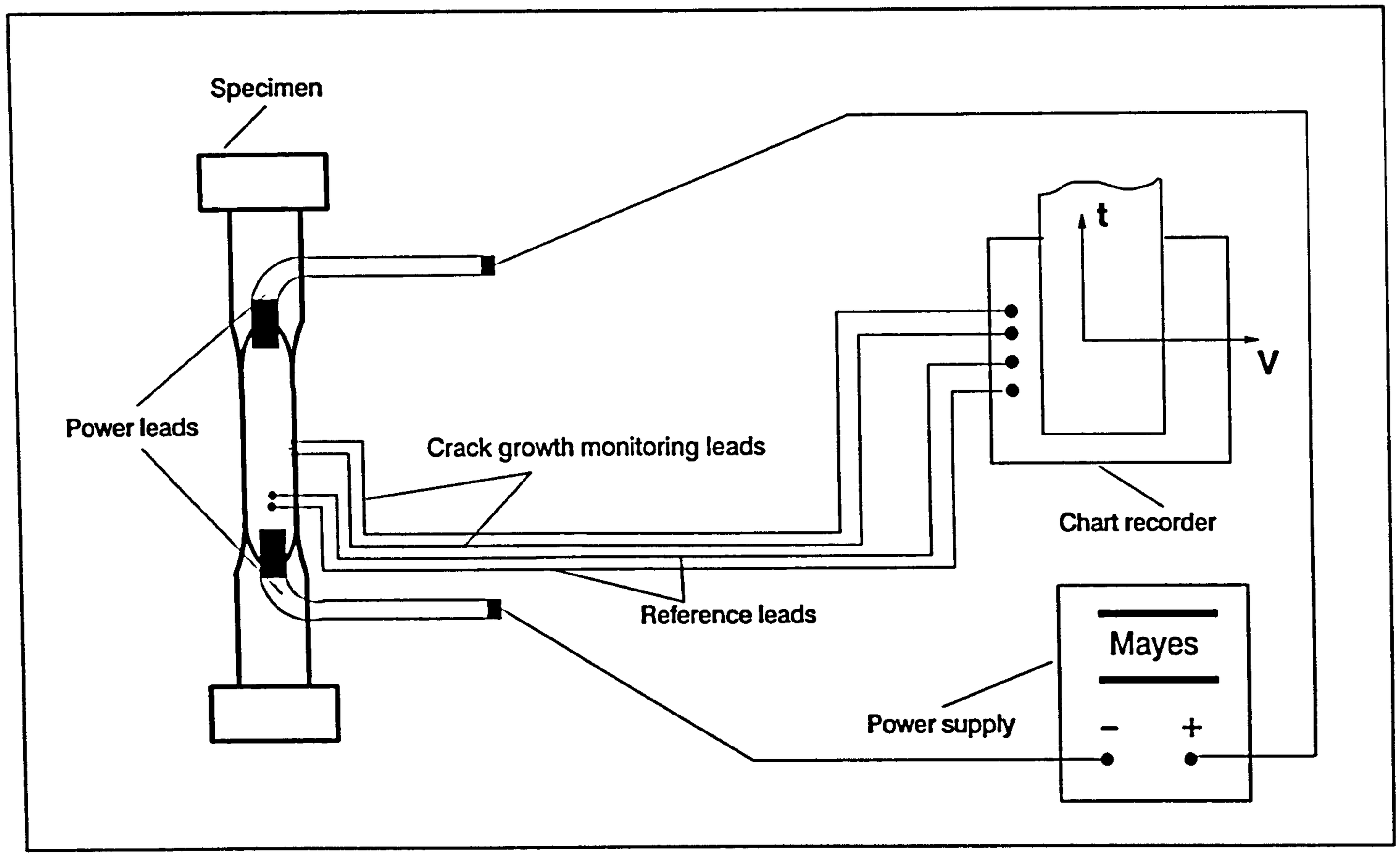

Fig.4.6. Crack Growth Measurement PD System

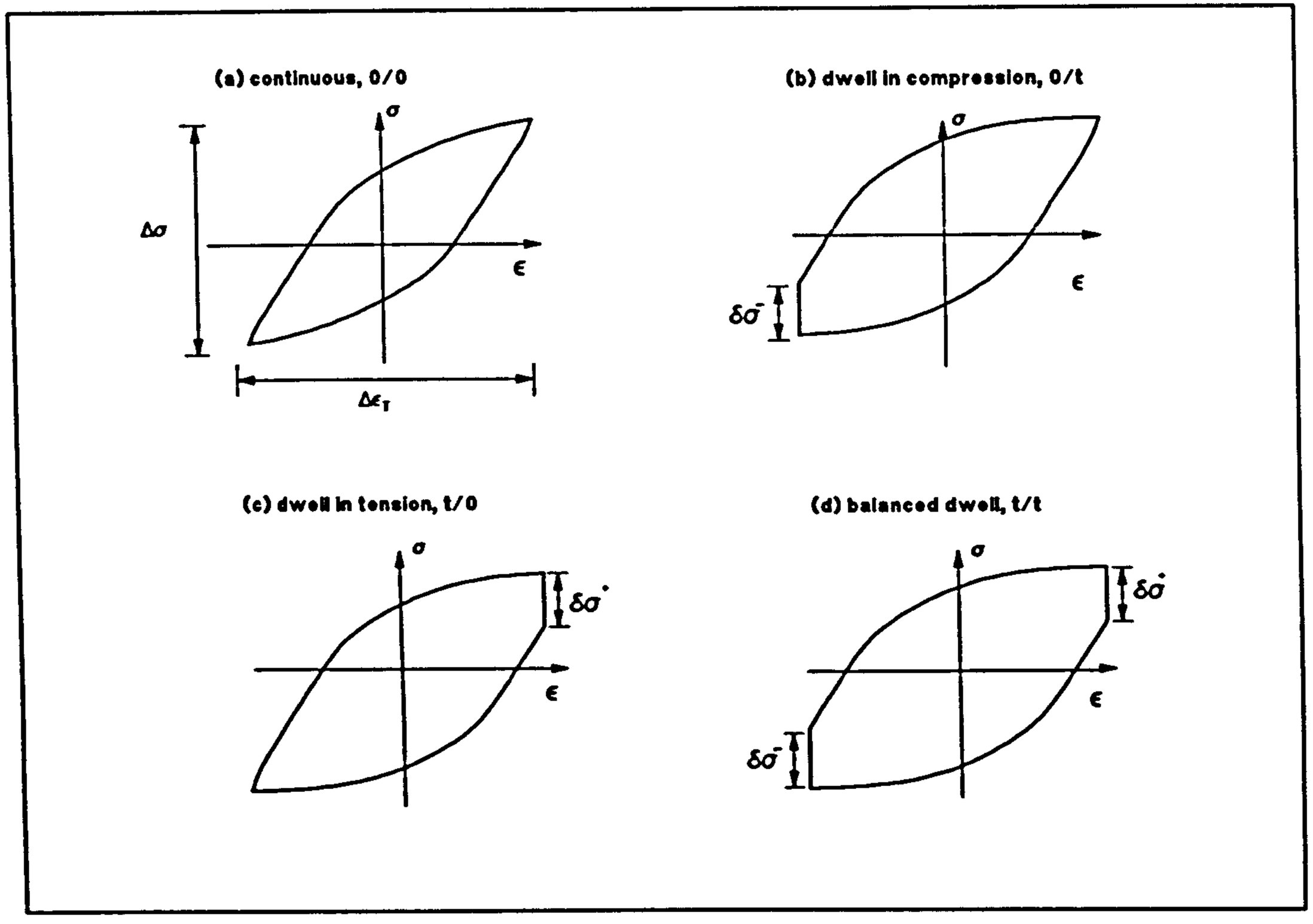

Fig.4.7. Types of Hysteresis Loops Used for Test Programme

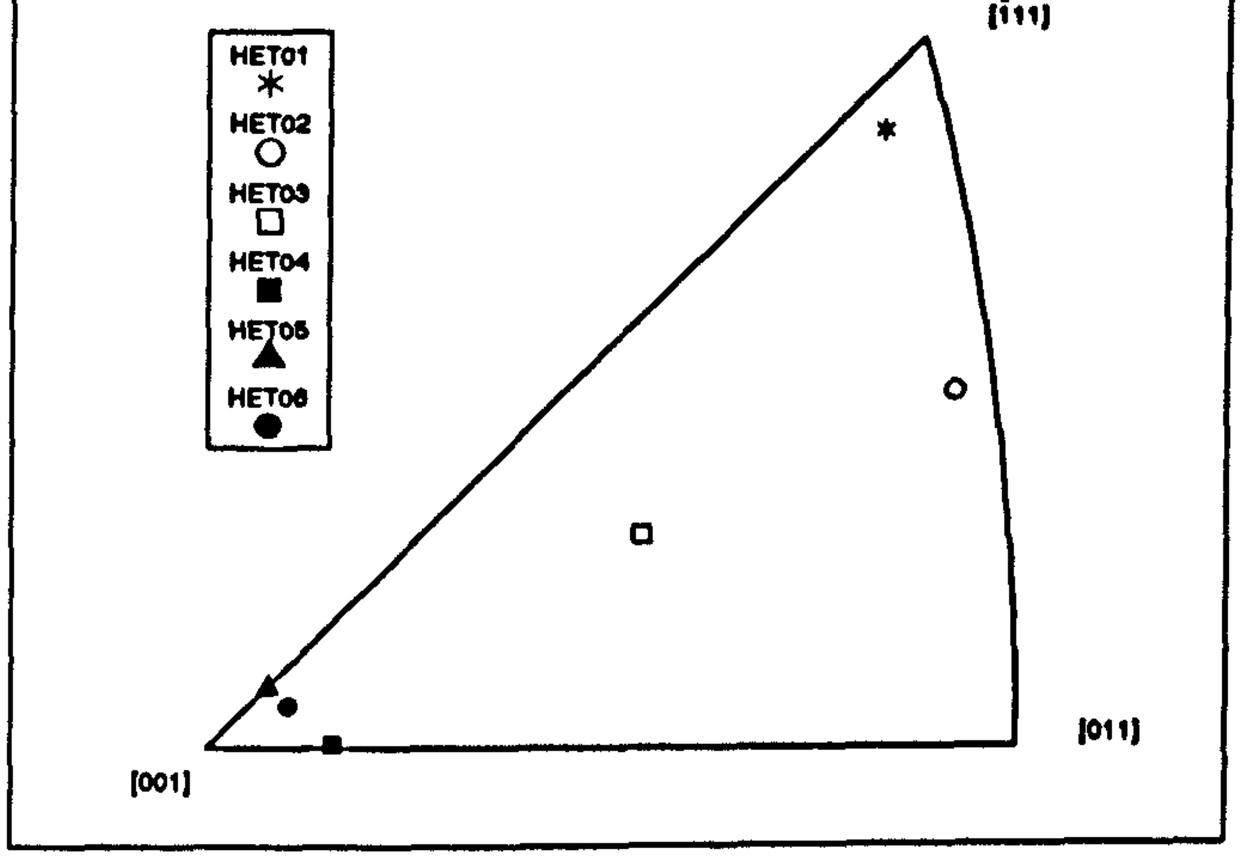

(a). High temperature elastic modulus tests

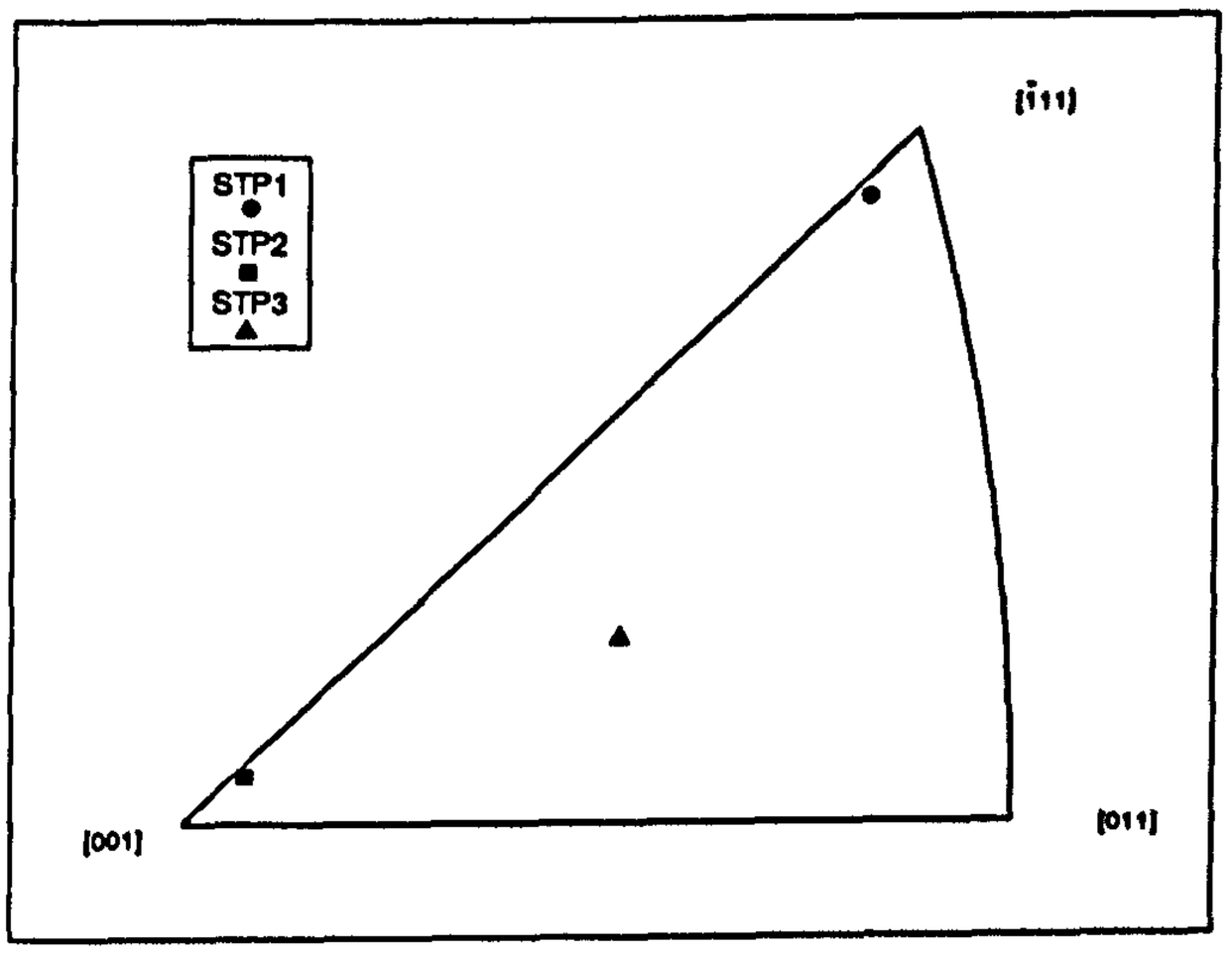

(b). Yield stress measurement tests

Fig.4.8. Crystal Orientation for the Specimens for the Additional Mechanical Tests

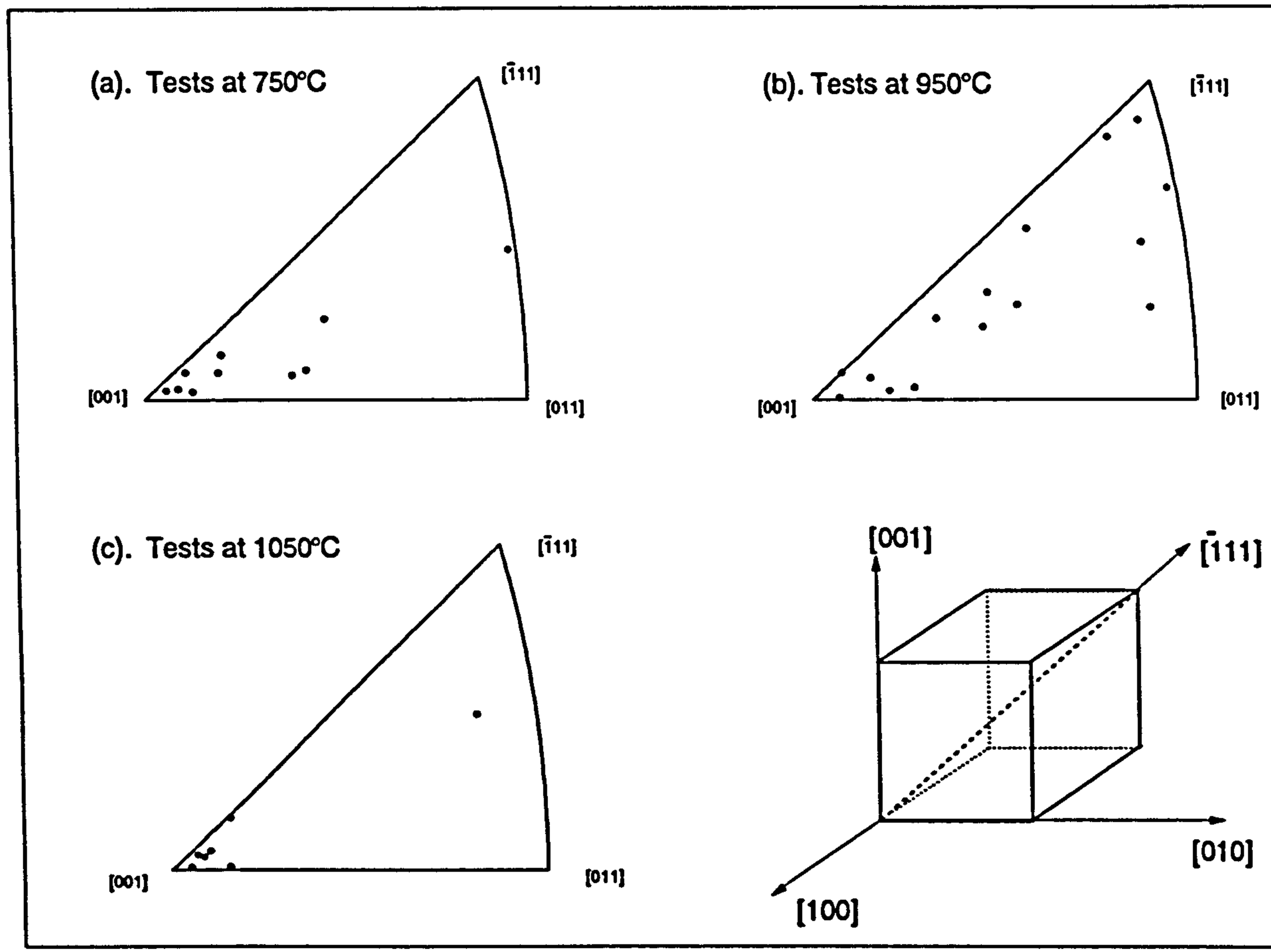

Fig.4.9. Crystal Orientations for Smooth Bar Specimens

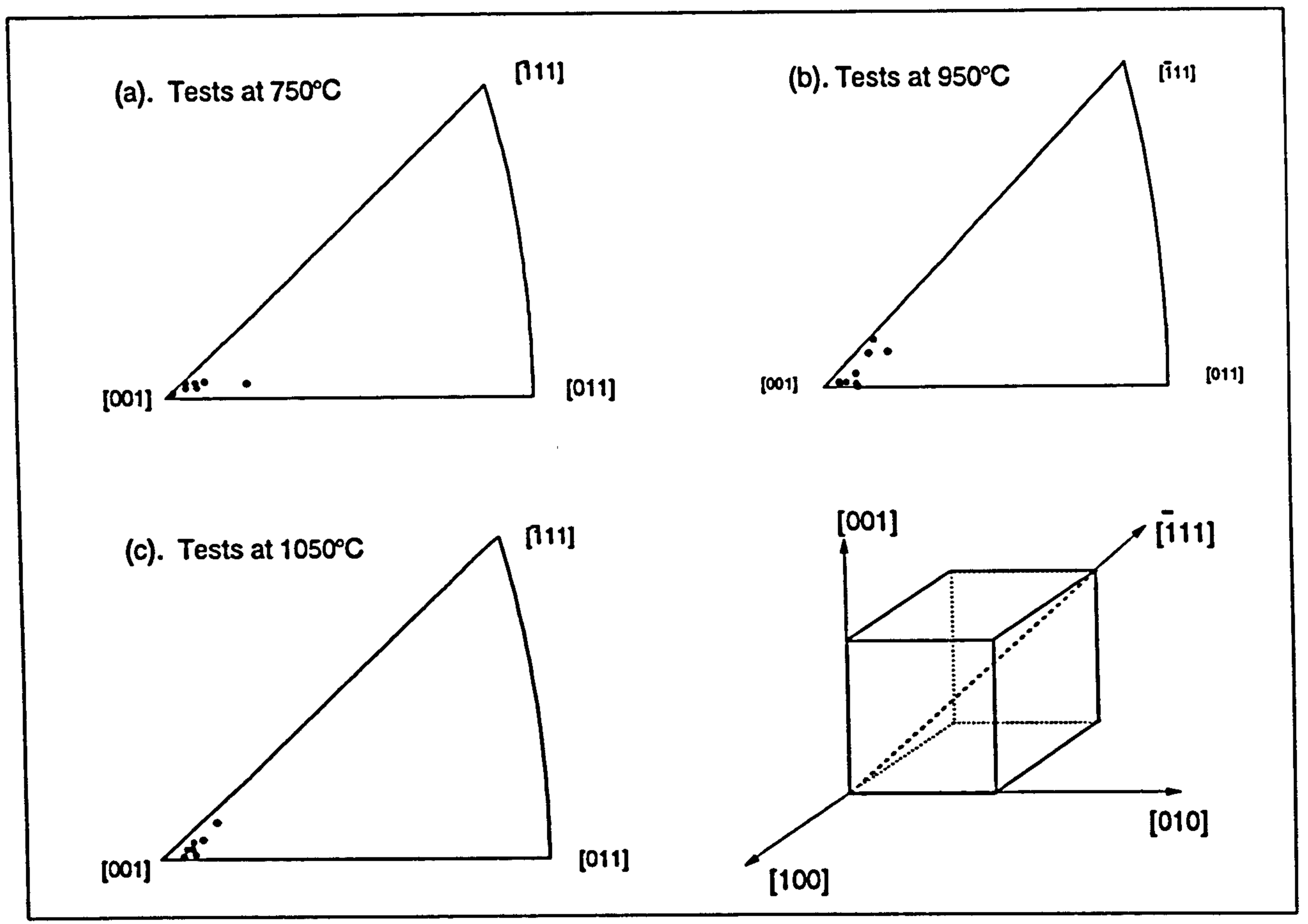

Fig.4.10. Crystal Orientations of Corner Crack Specimens

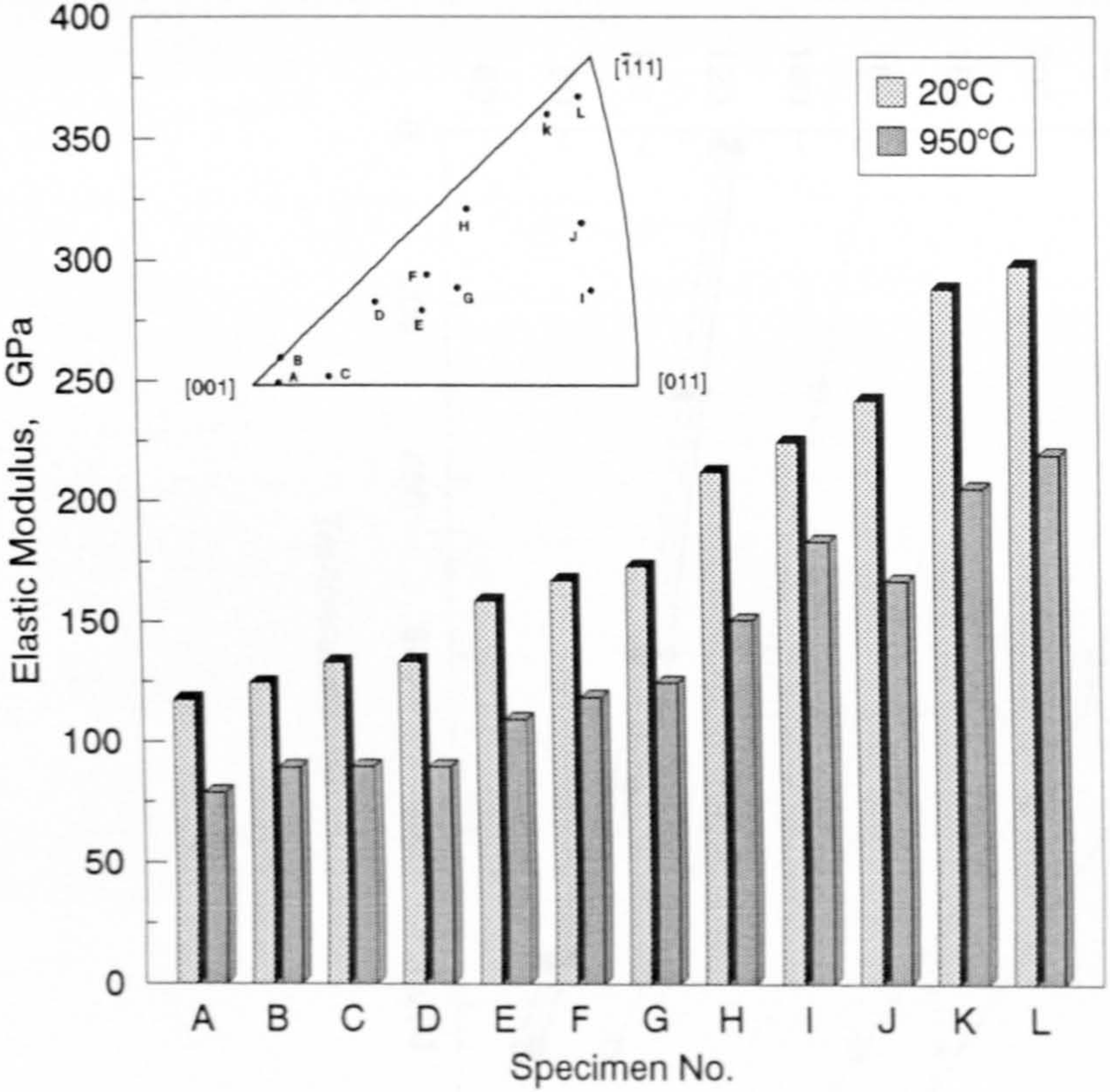

Spec. No.	Label
sb9514	A
sb9506	B
sb9513	C
sb9510	D
sb9503	E
sb9504	F
sb9515	G
sb9502	H
sb9512	I
sb9508	J
sb9501	K
sb9507	L

Fig.5.1. Variation of Elastic Modulus with Specimen Orientations

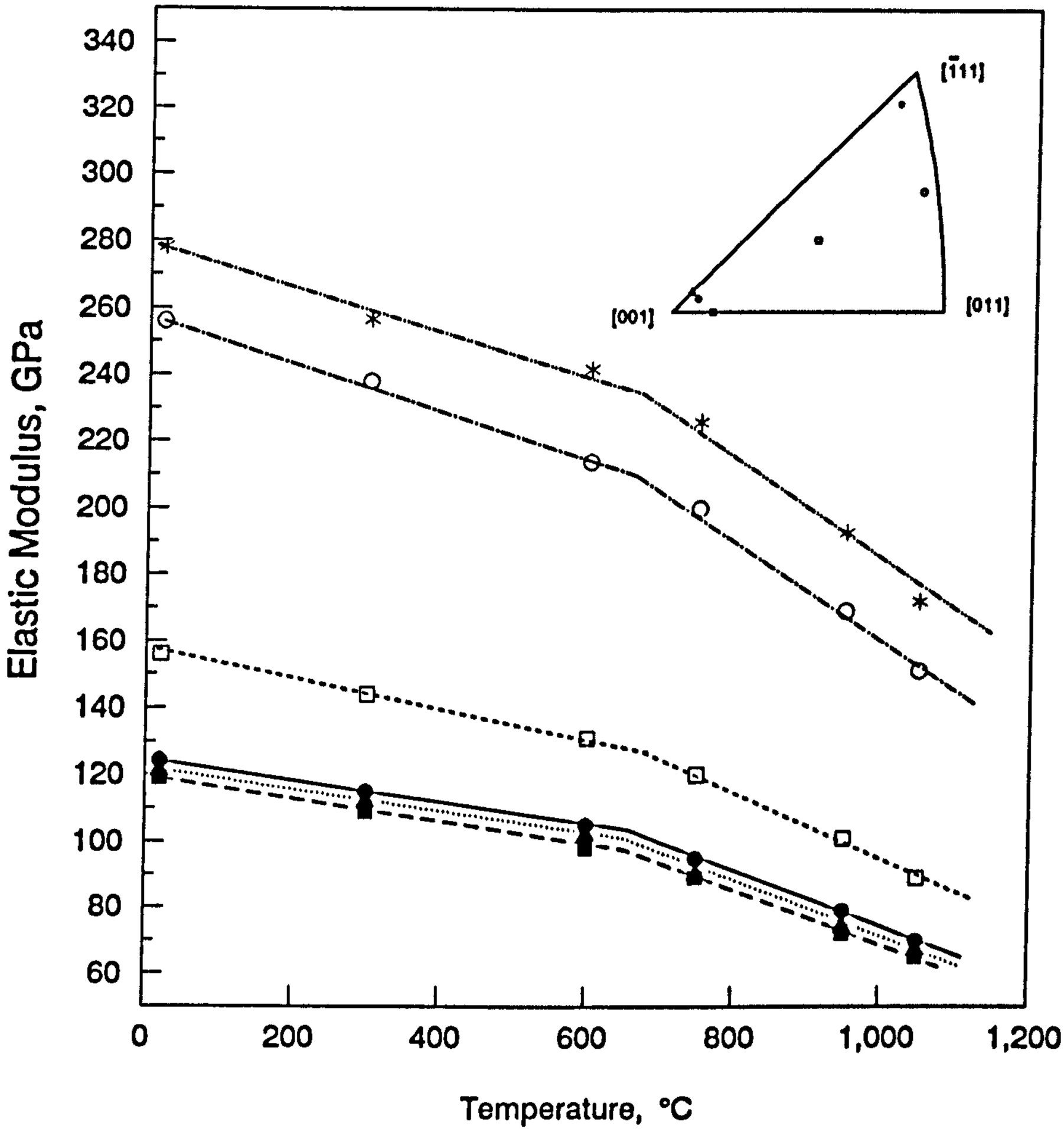

Fig.5.2. Elastic Moduli for Different Orientations over a Range of Temperatures

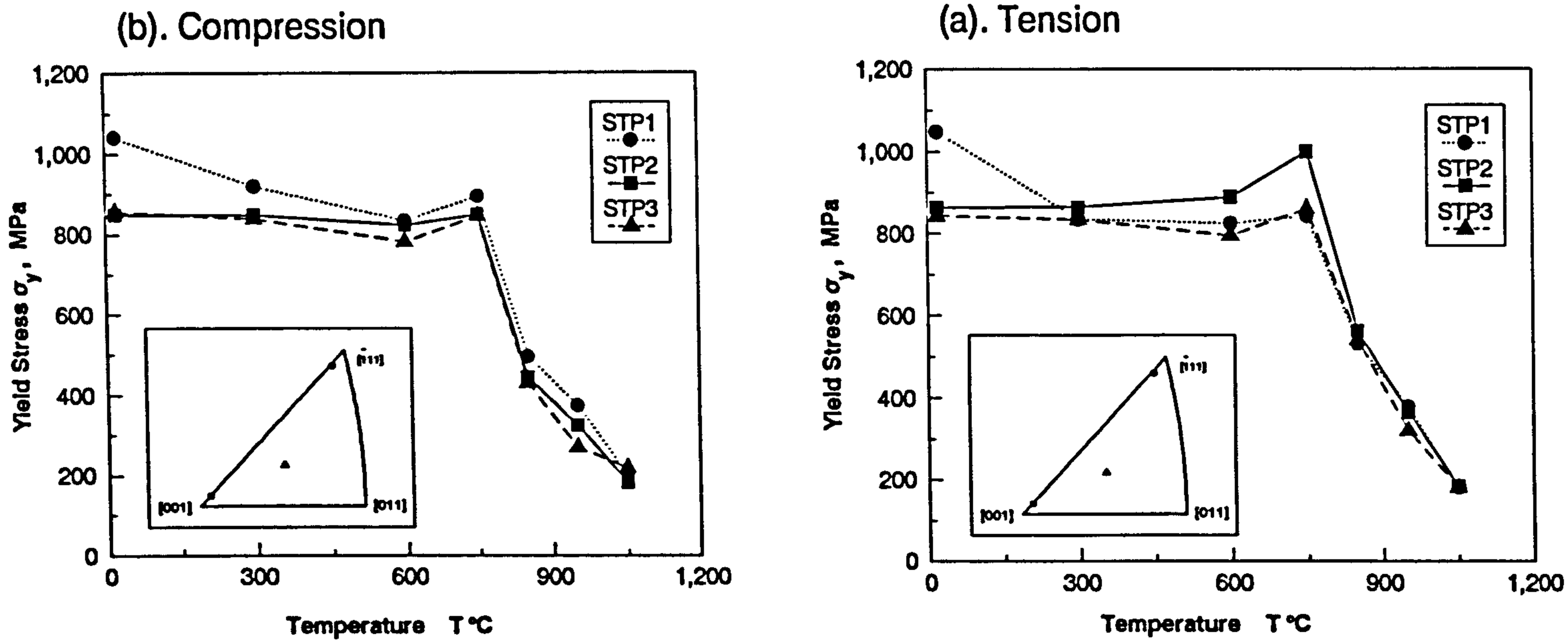

Fig.5.3. Variation of Yield Stress with Temperature

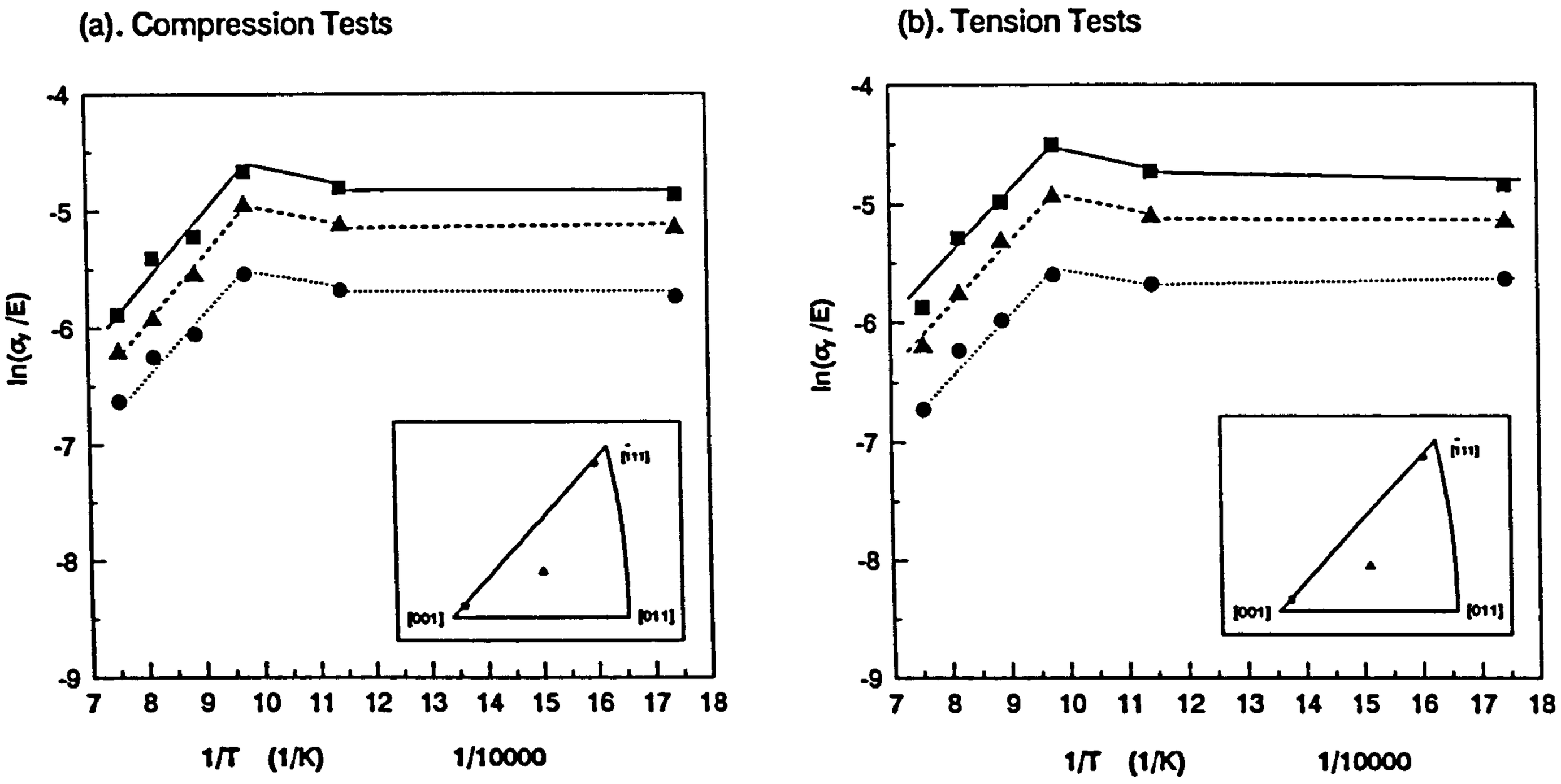

Fig.5.4. Arrhenius Representation of Yield Stress

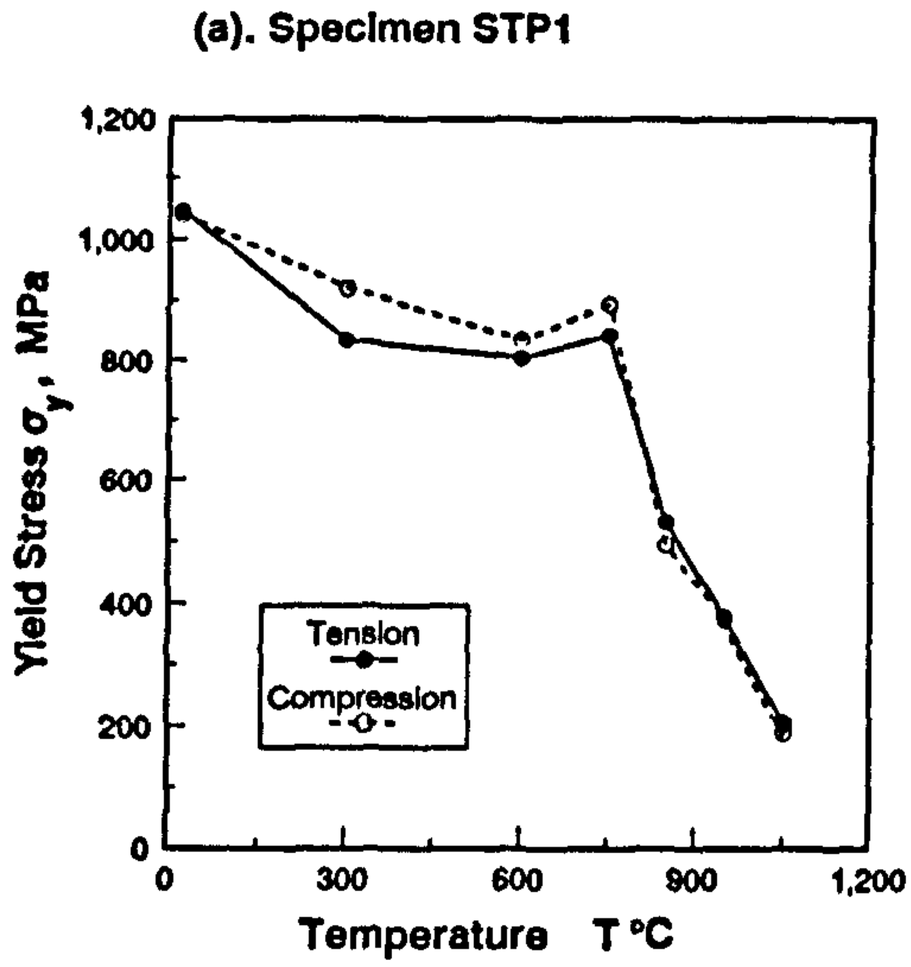

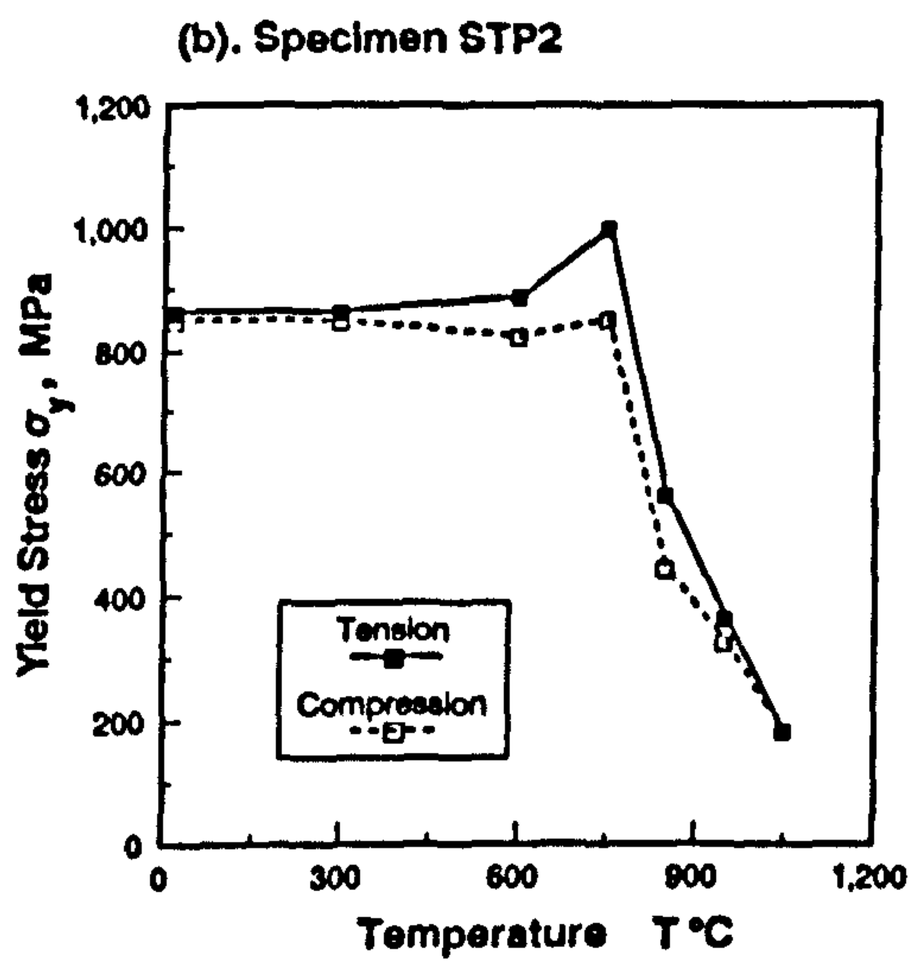

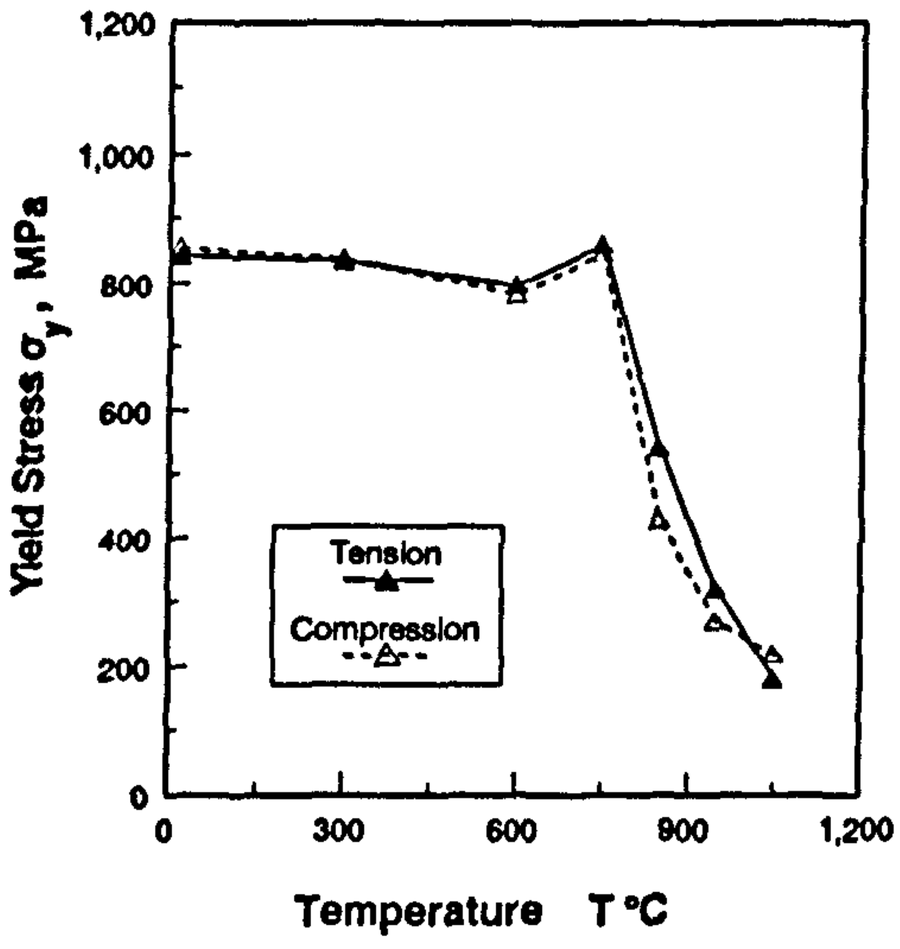

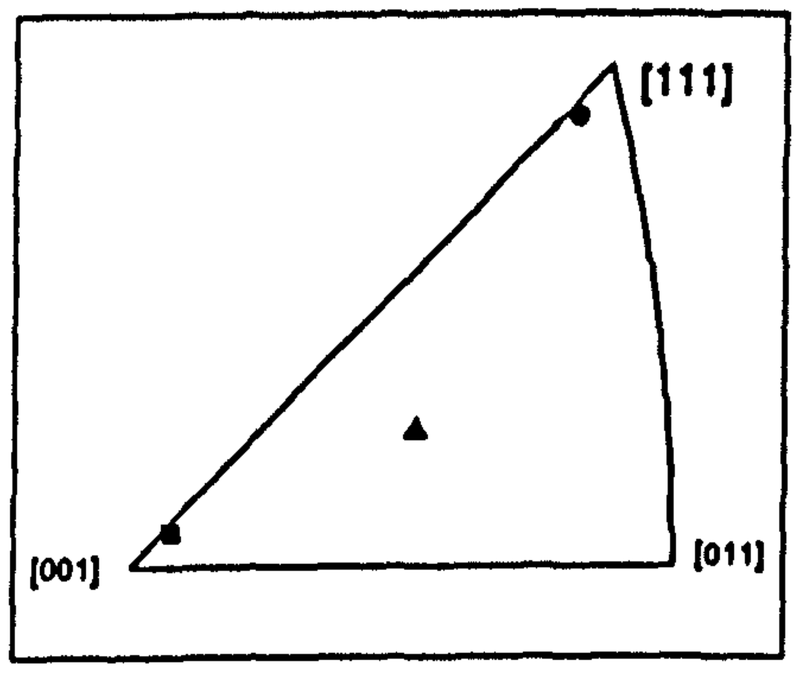

Fig.5.5. Comparison Between Tensile and Compressive Yield Stress

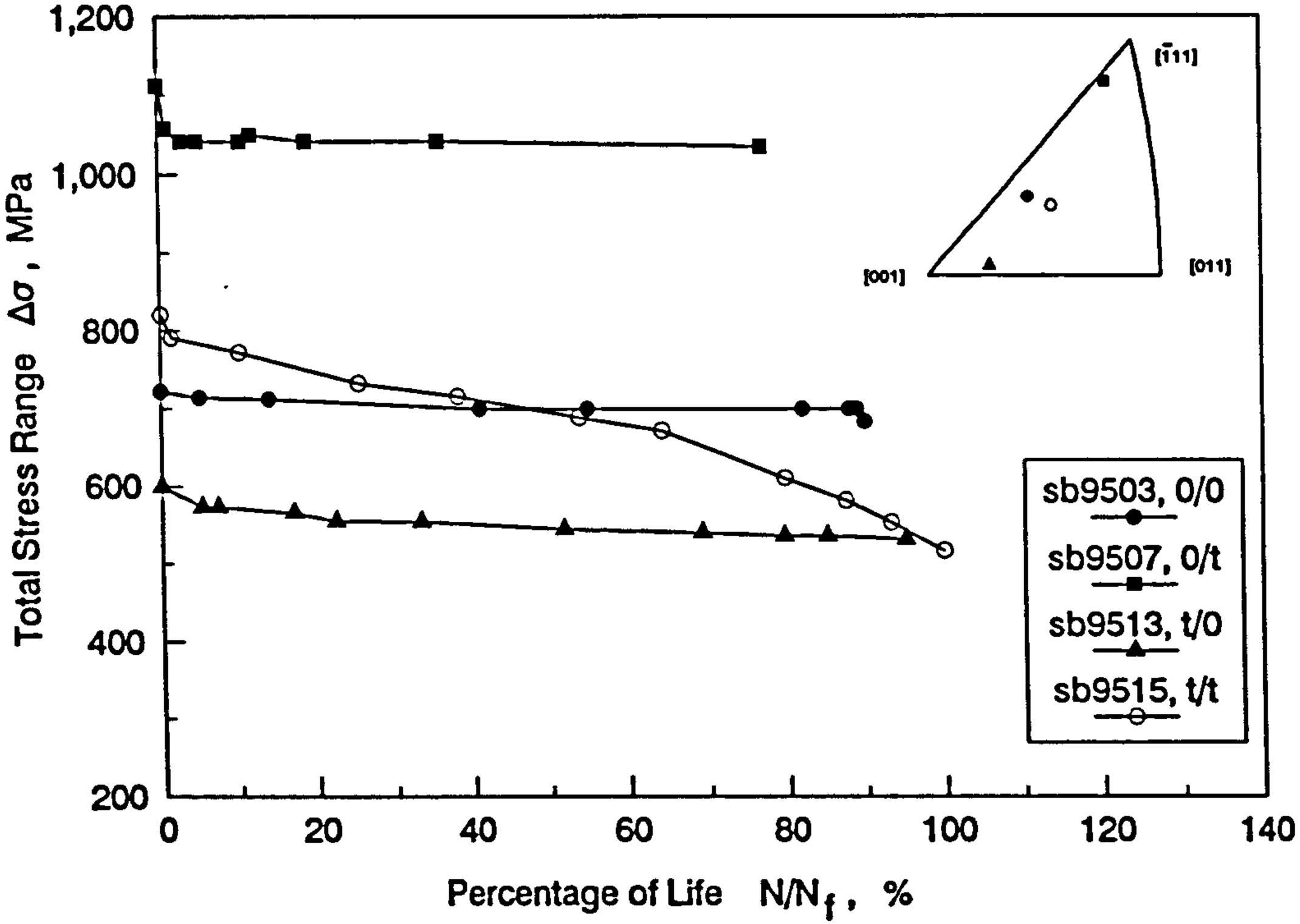

Fig.5.6. Variation of Total Stress Range with Cycle Number (T=950°C)

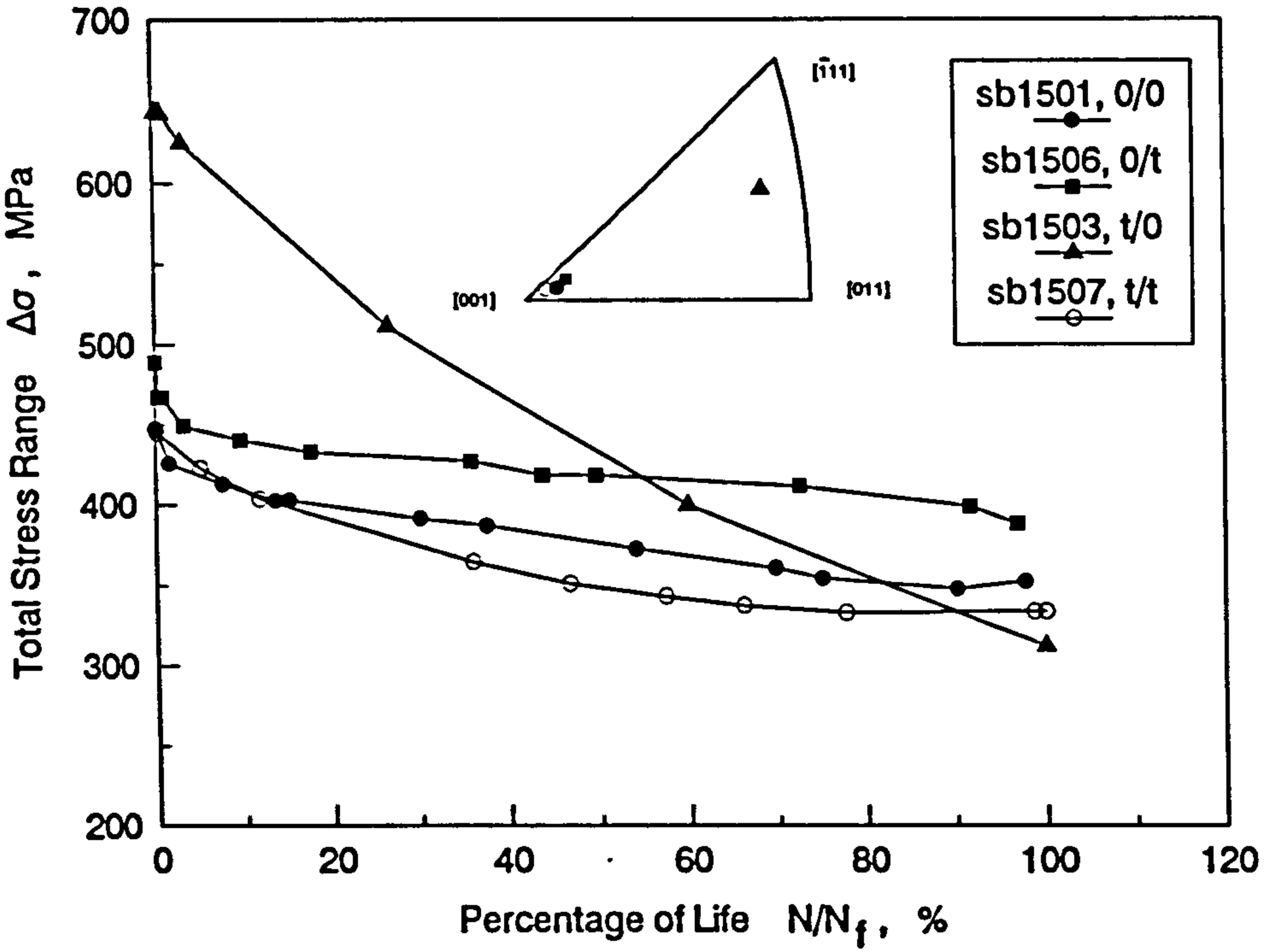

Fig.5.7. Variation of Total Stress Range with Cycle Number (T=1050°C)

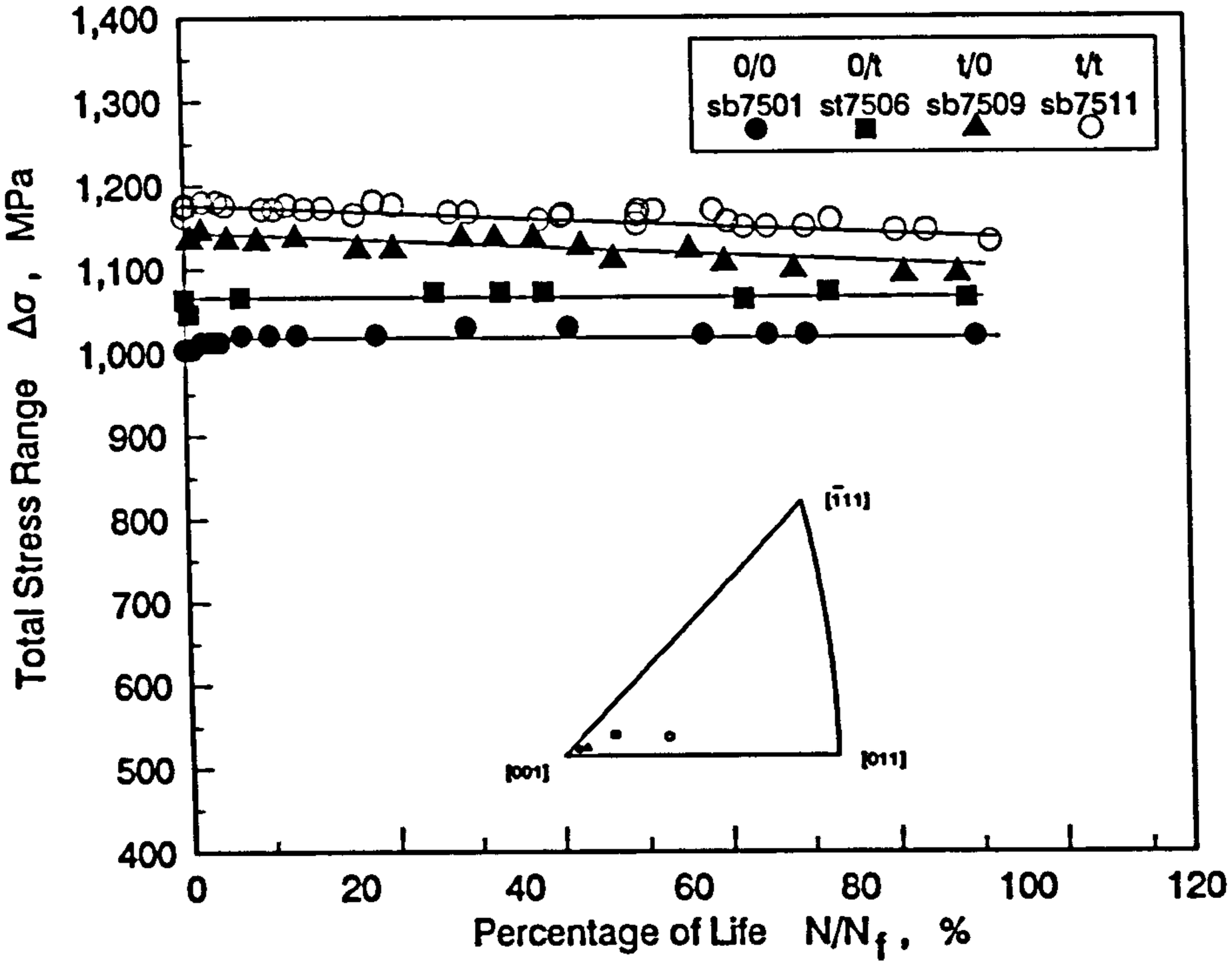

Fig.5.8. Variation of Total Stress Range with Cycle Number (T=750°C)

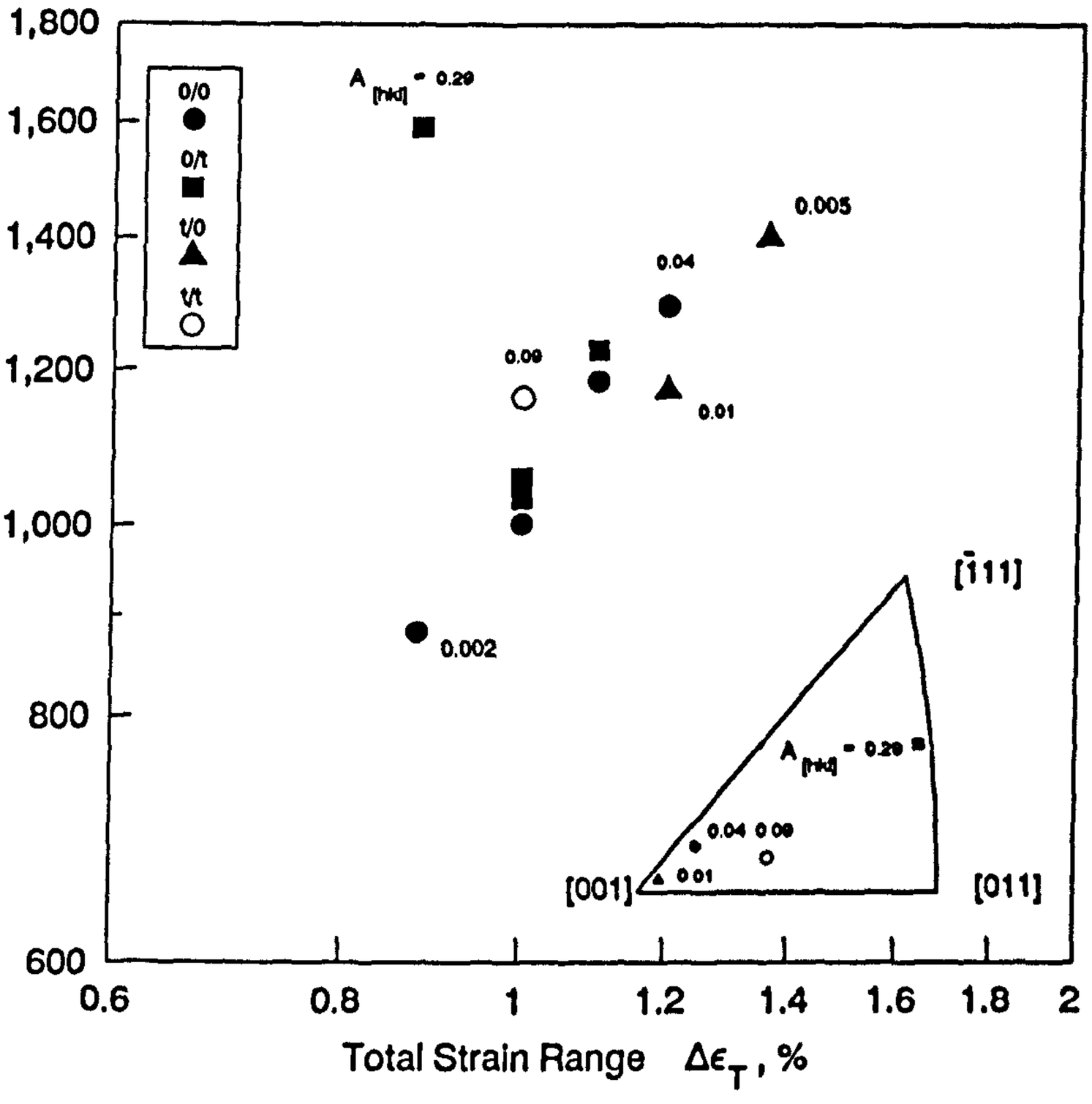

Fig.5.9a. Cyclic Stress - Strain Relationship

(T=750°C)

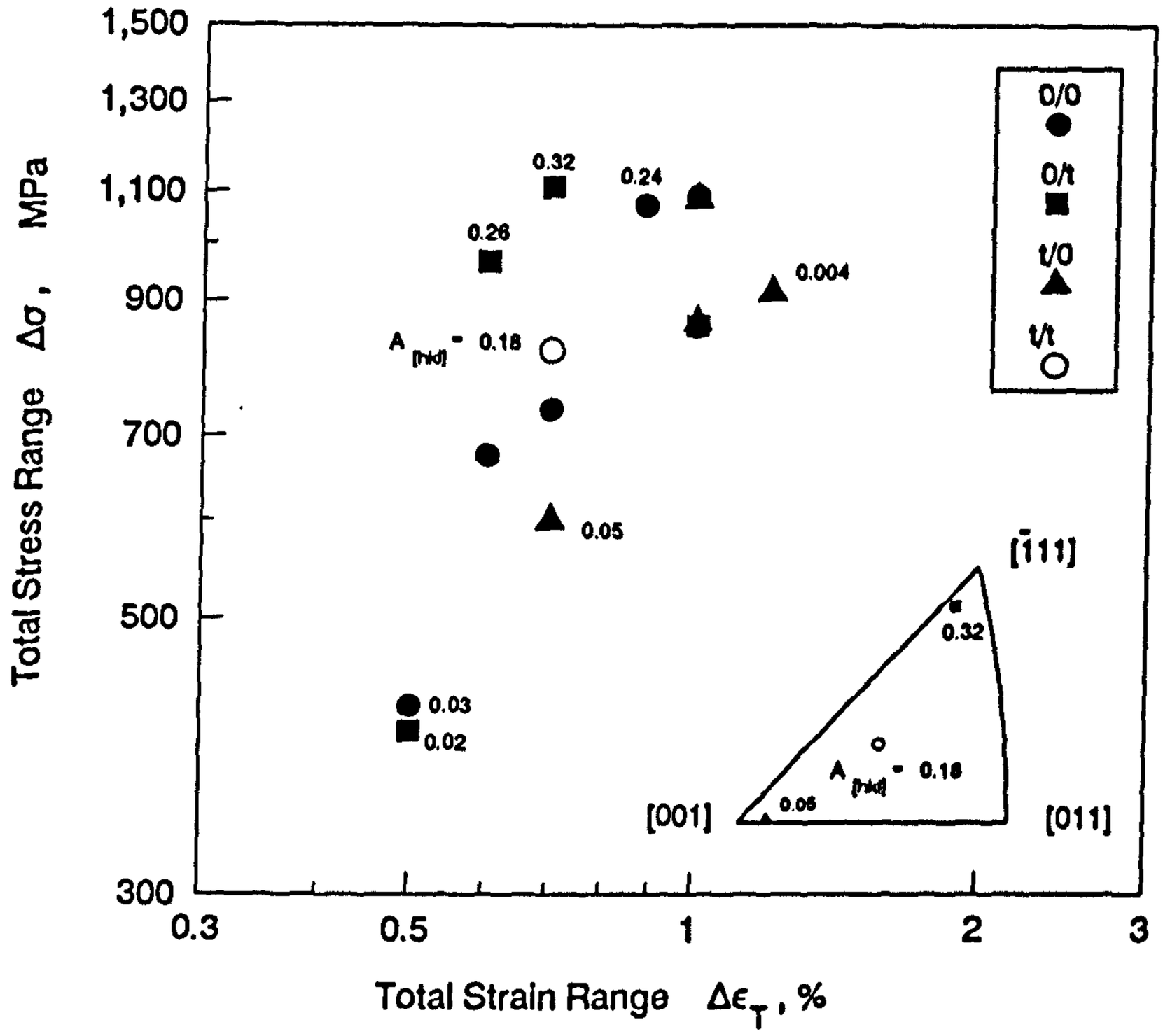

Fig.5.9b. Cyclic Stress-Strain Relationship
(T=950°C)

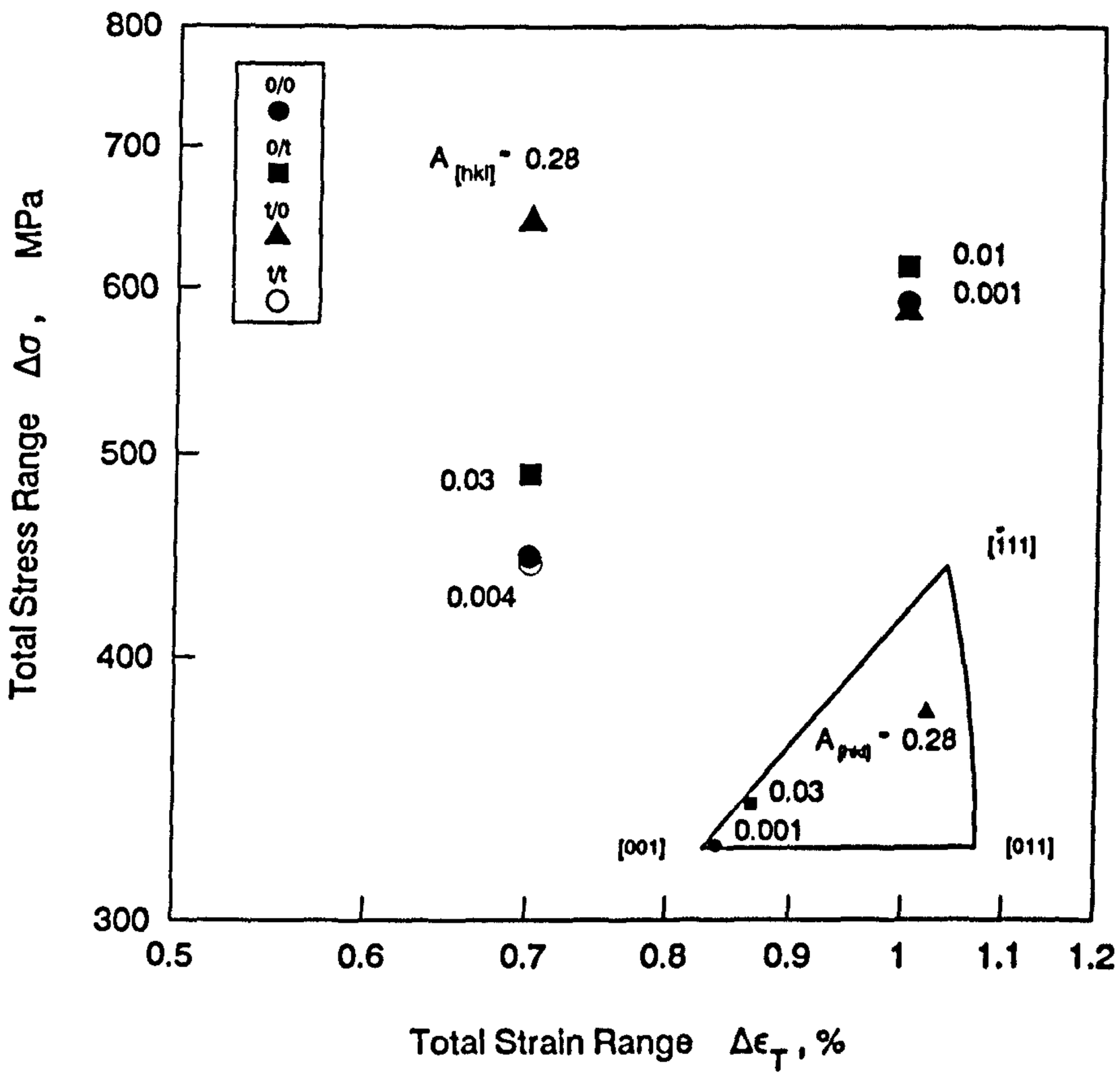

Fig.5.9c. Cyclic Stress - Strain Relationship (T=1050°C)

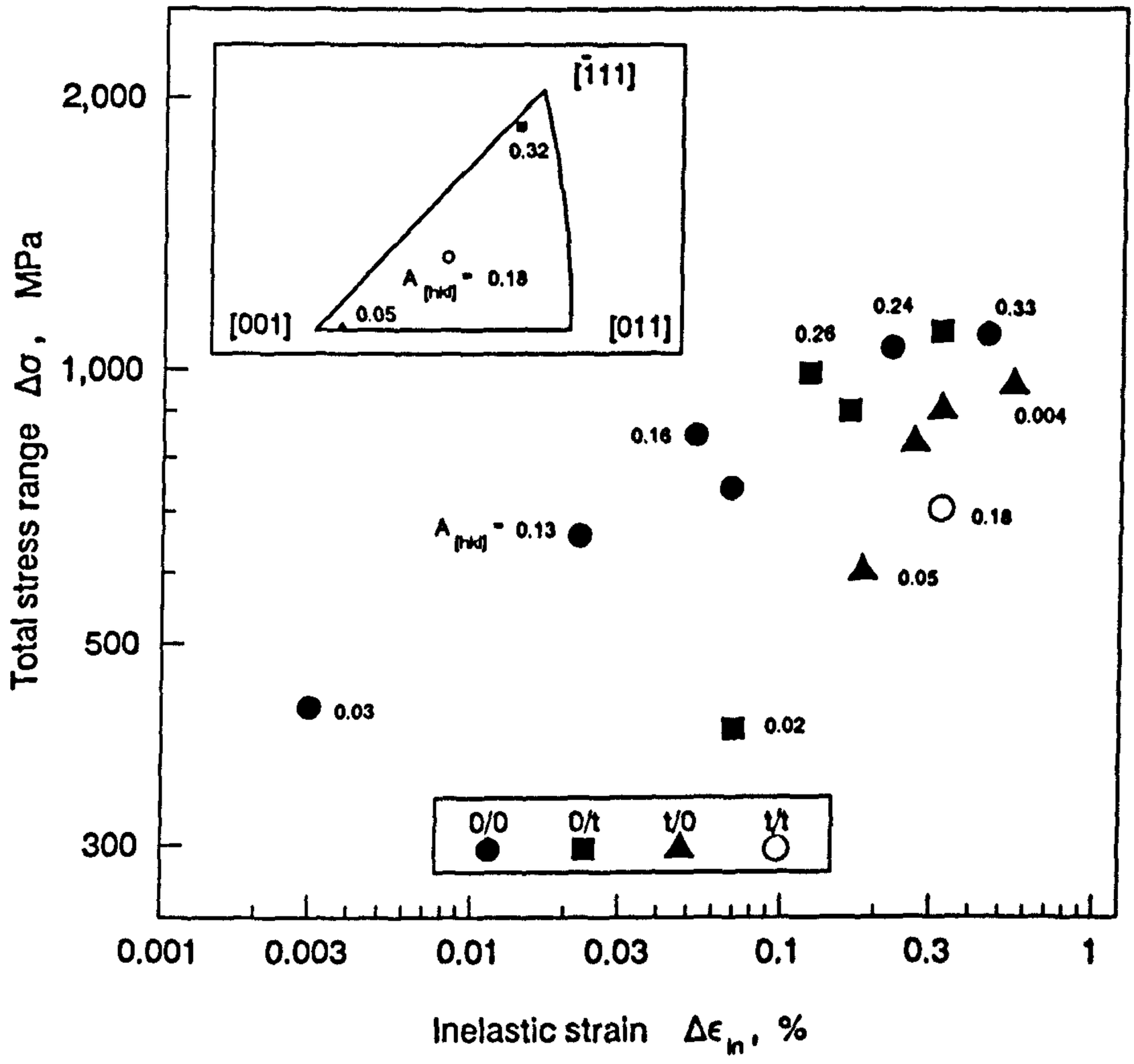

Fig.5.10a. Cyclic Stress-Inelastic Strain Response (T=950°C)

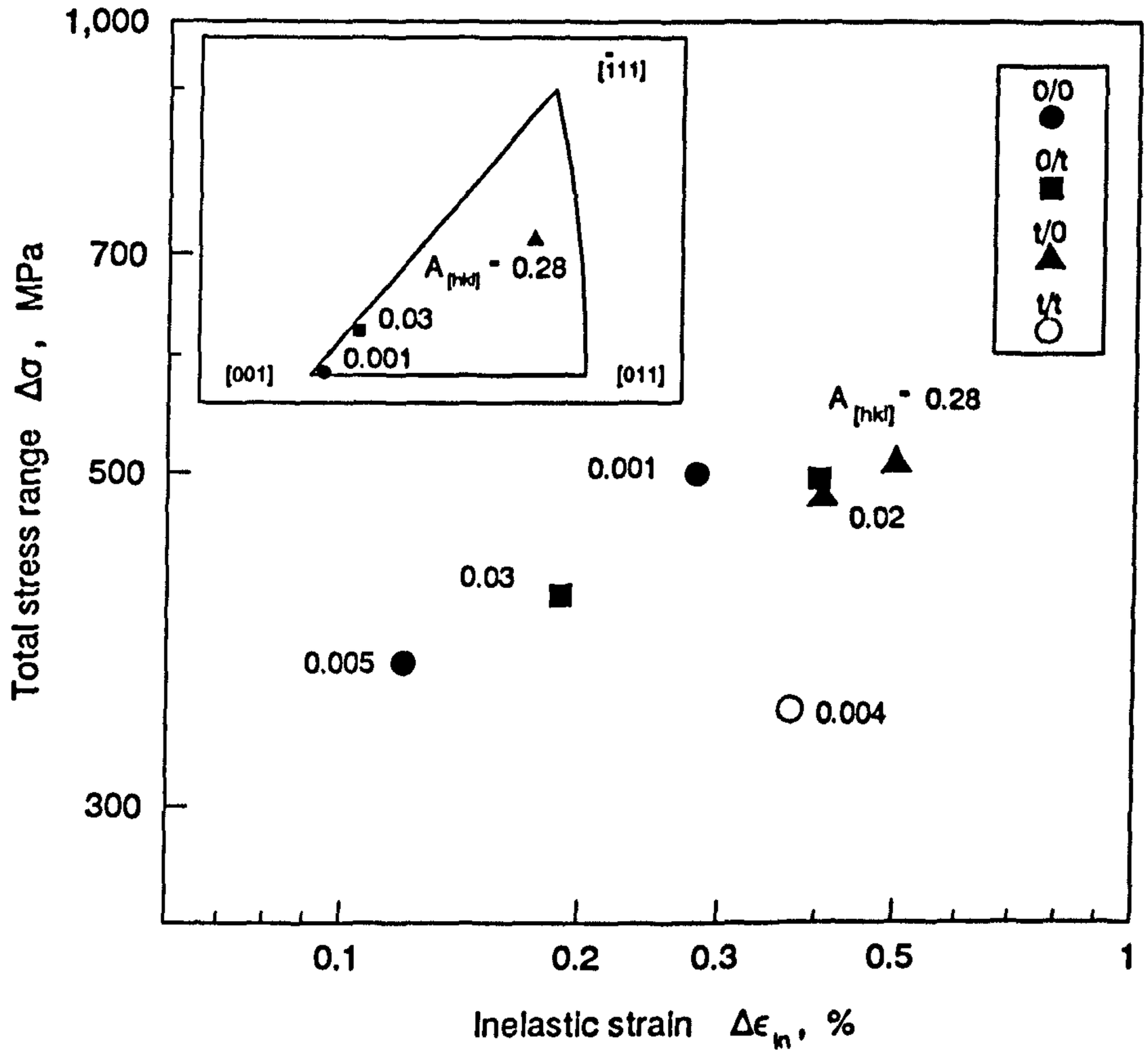

Fig.5.10b. Cyclic Stress-Inelastic Strain Response (T=1050°C)

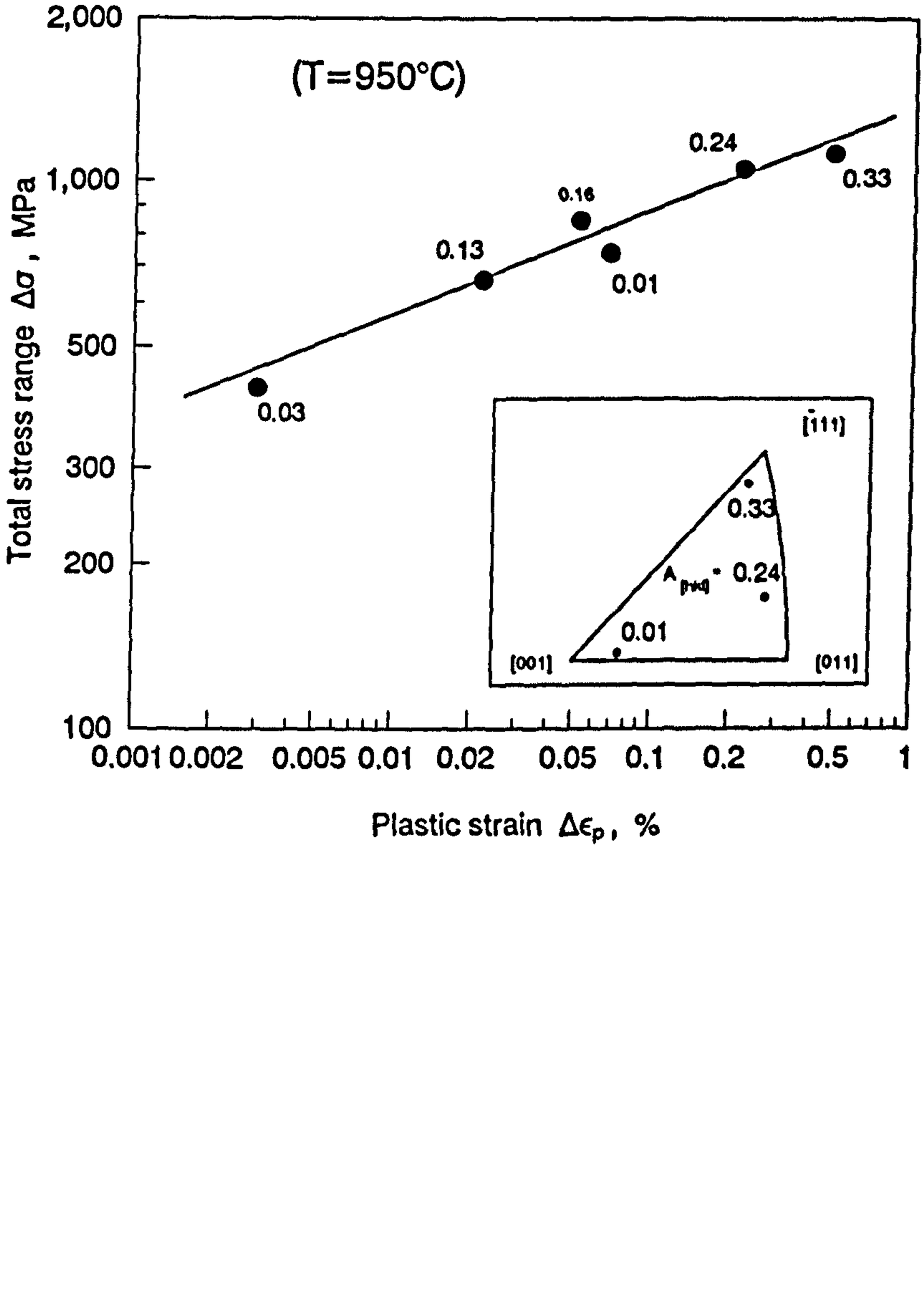

Fig.5.11. Cyclic Stress-Plastic Strain Response of Continuous Cycling Tests at 950°C

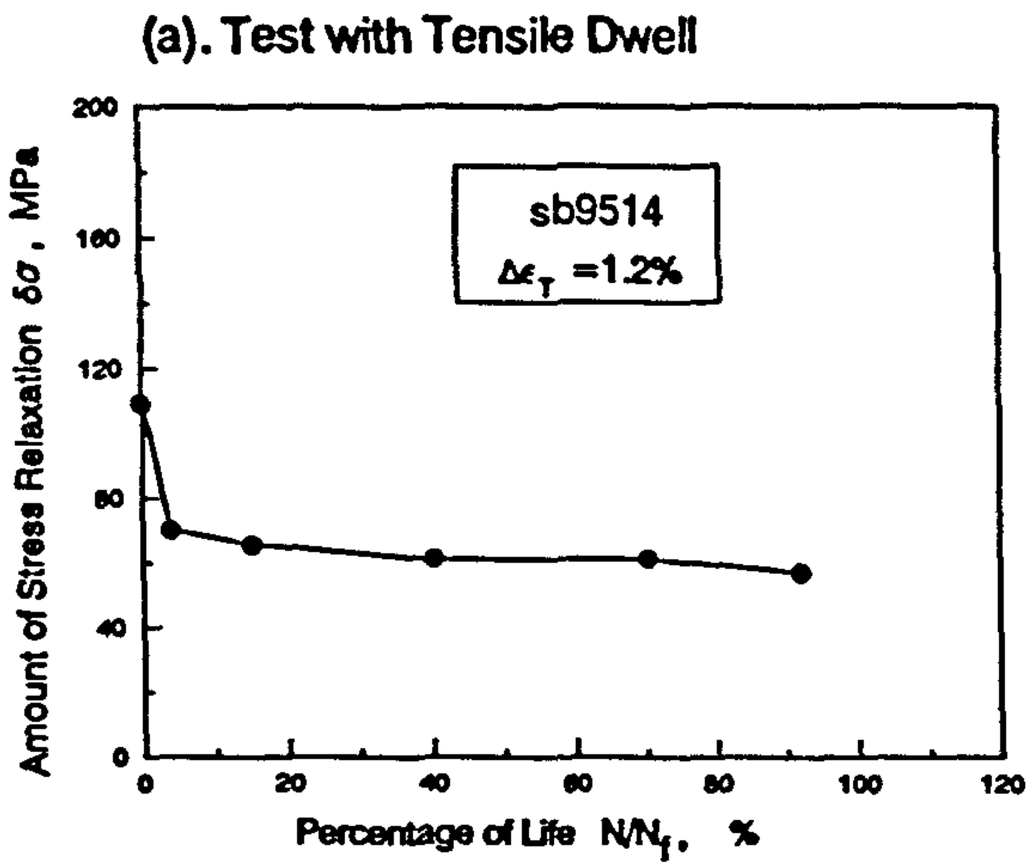

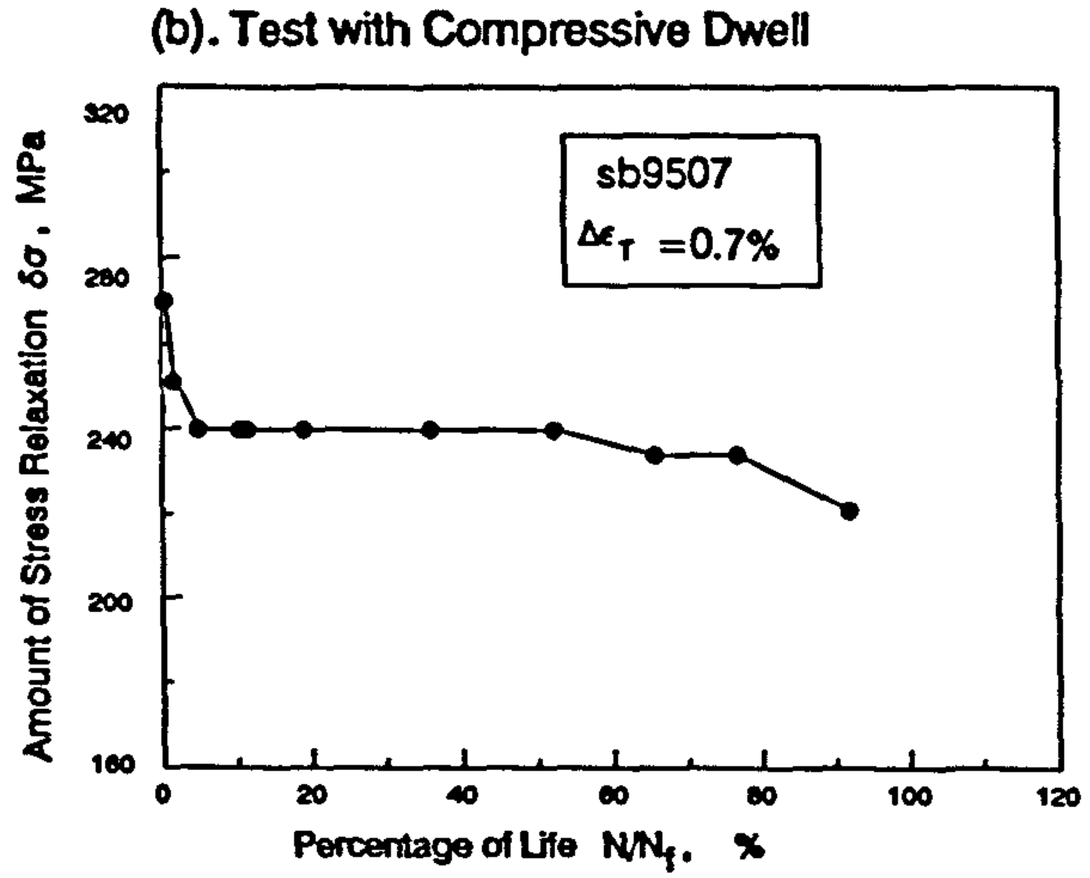

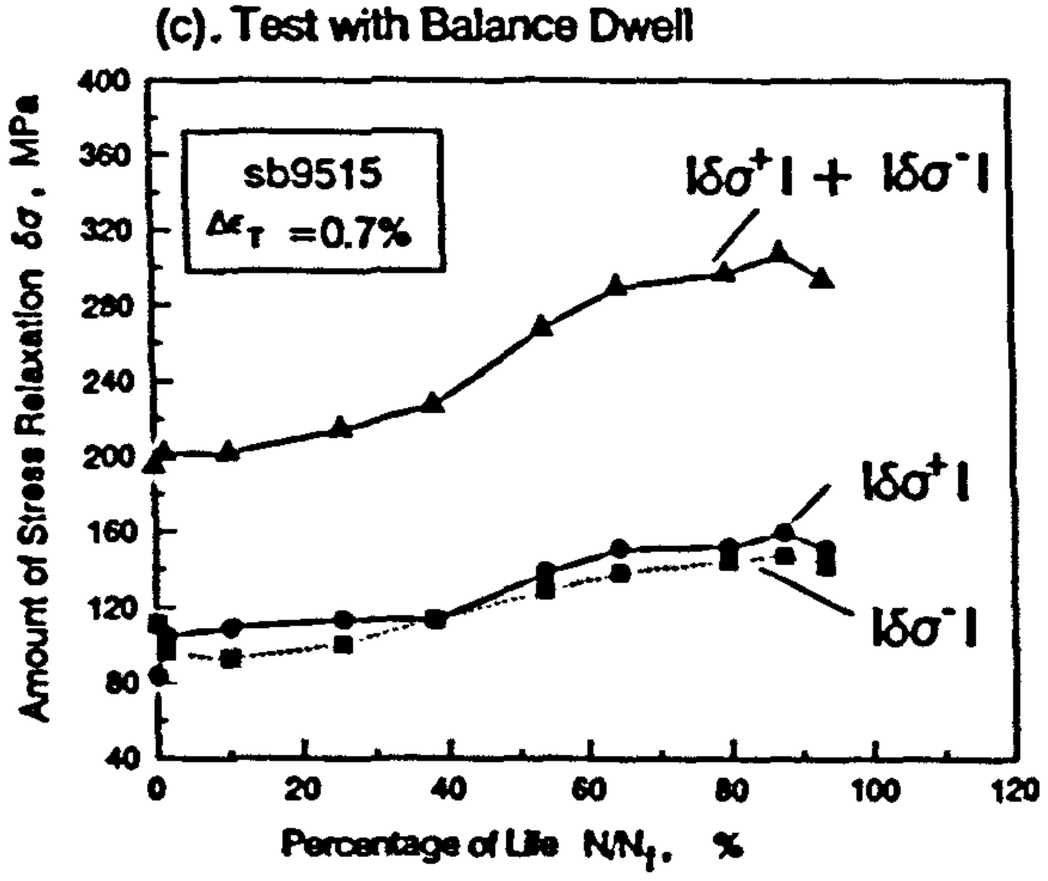

Fig.5.12. Amount of Stress Relaxation as a Function of Cycle Number in the Tests at 950°C

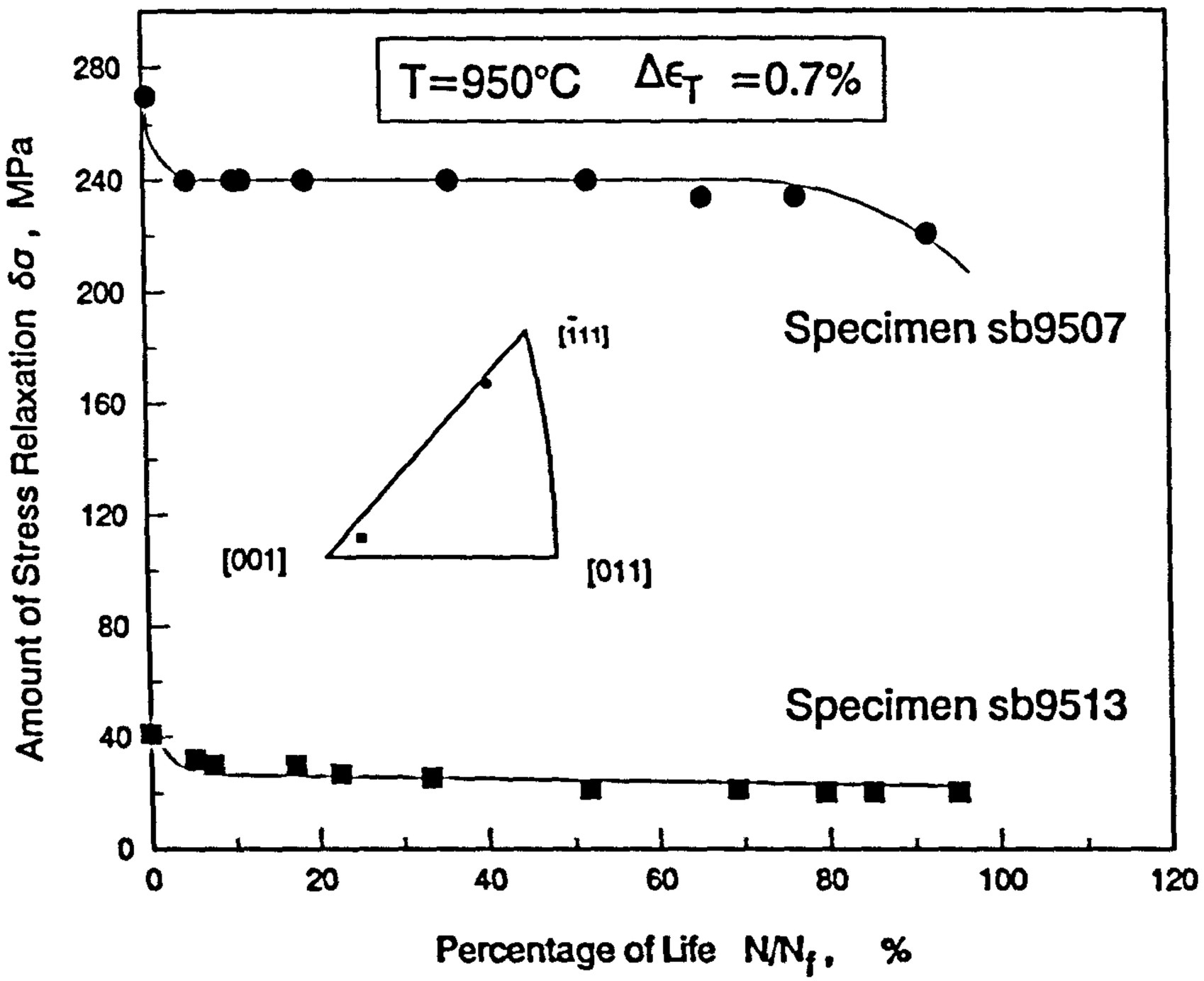

Fig.5.13. Comparison of Stress Relaxation Response of Tests with Different Orientations

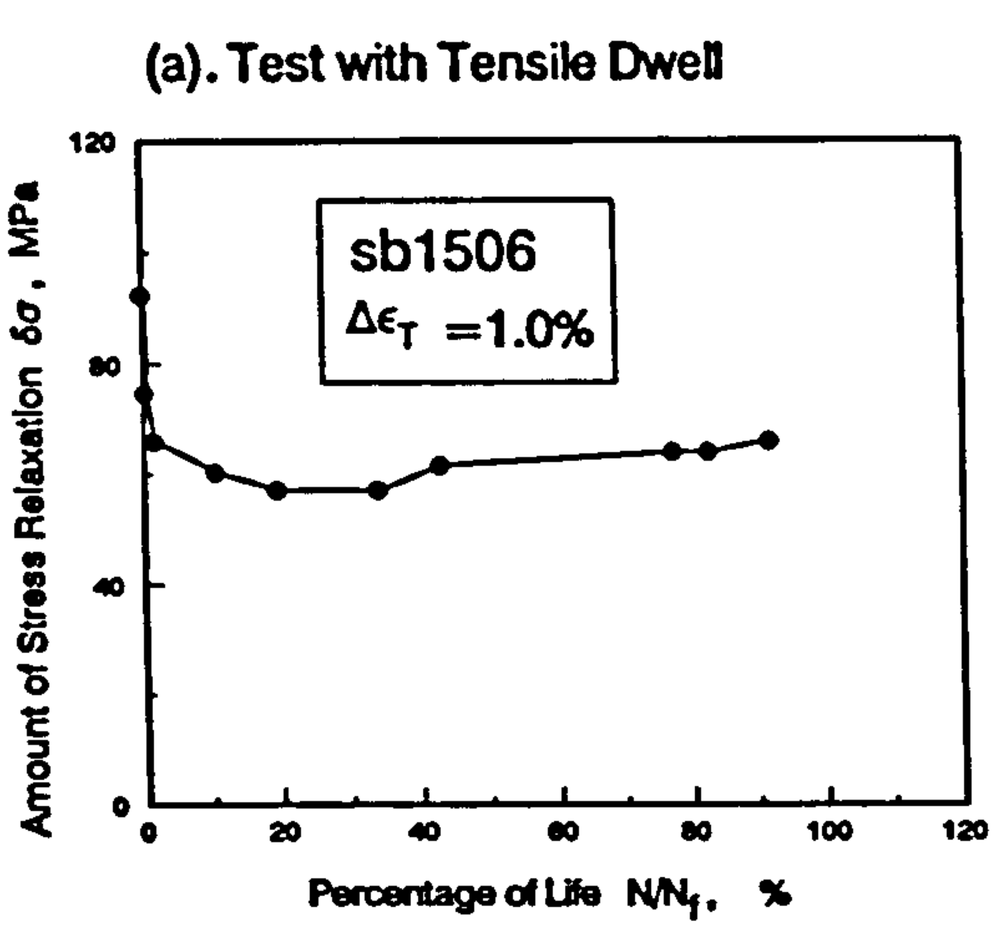

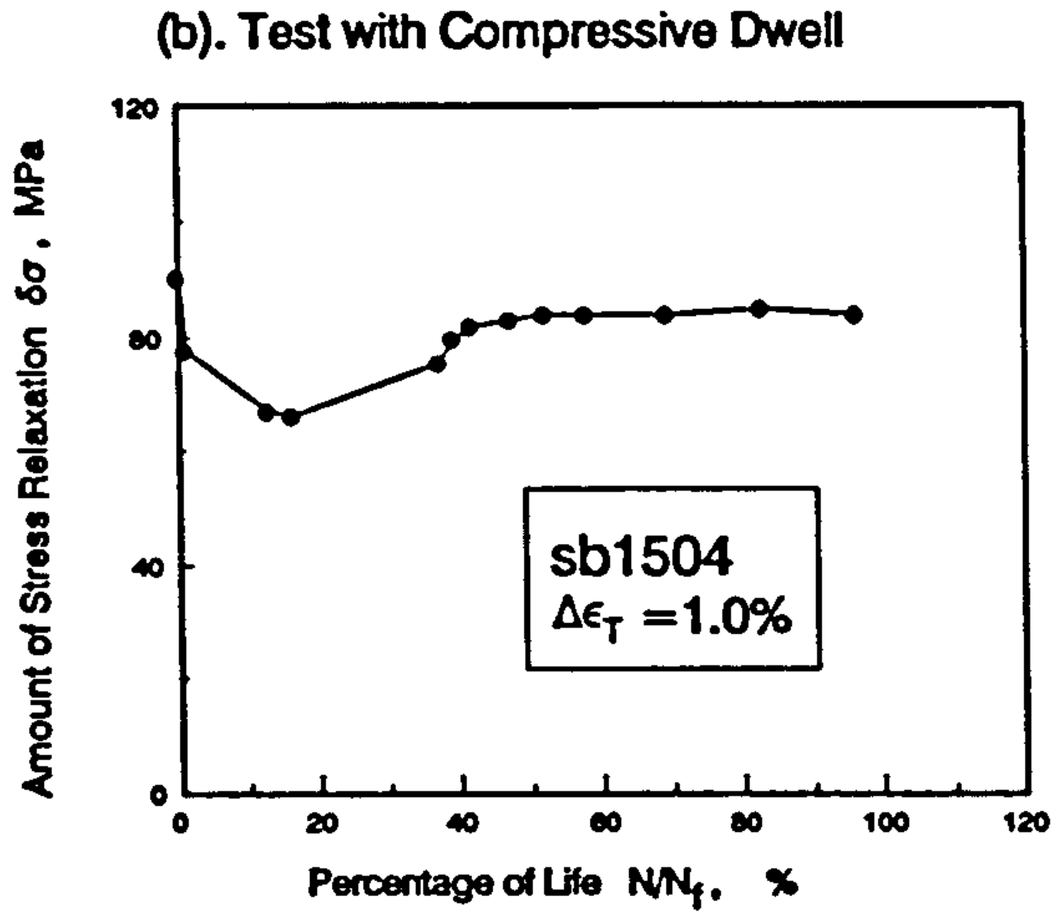

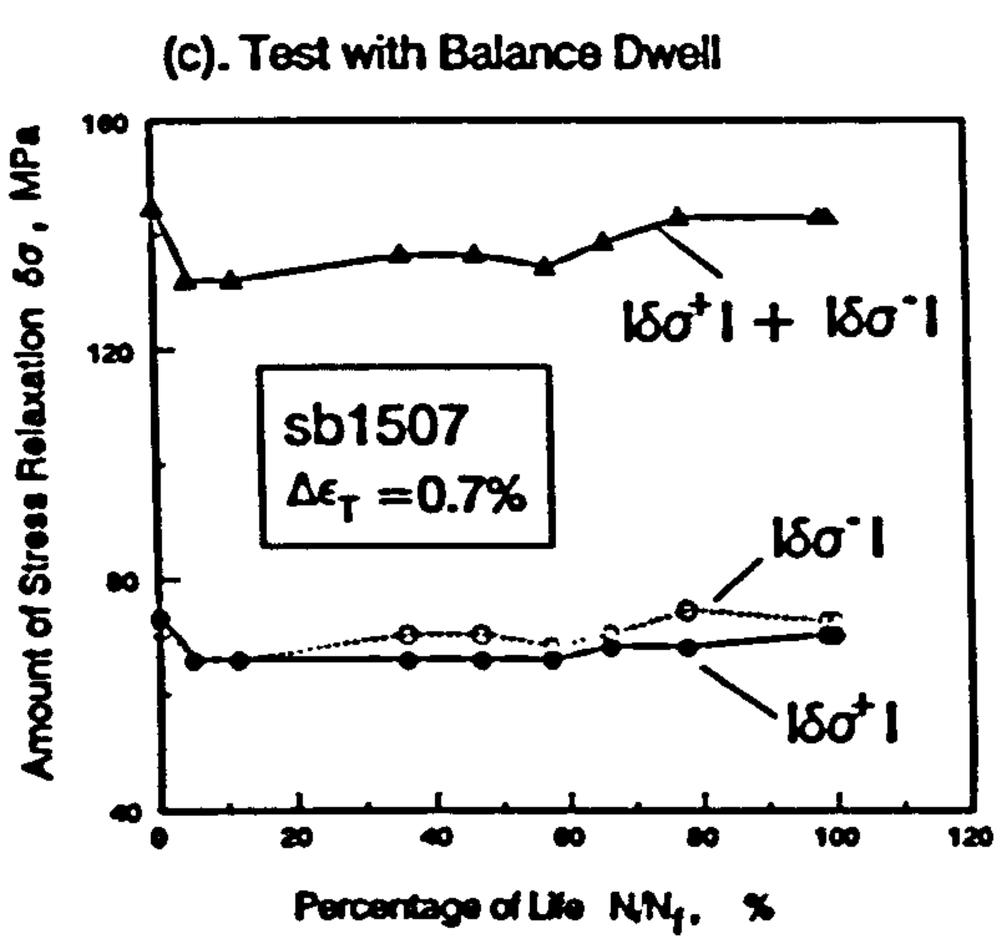

Fig.5.14. Amount of Stress Relaxation as a Function of Cycle Number in the Tests at 1050°C

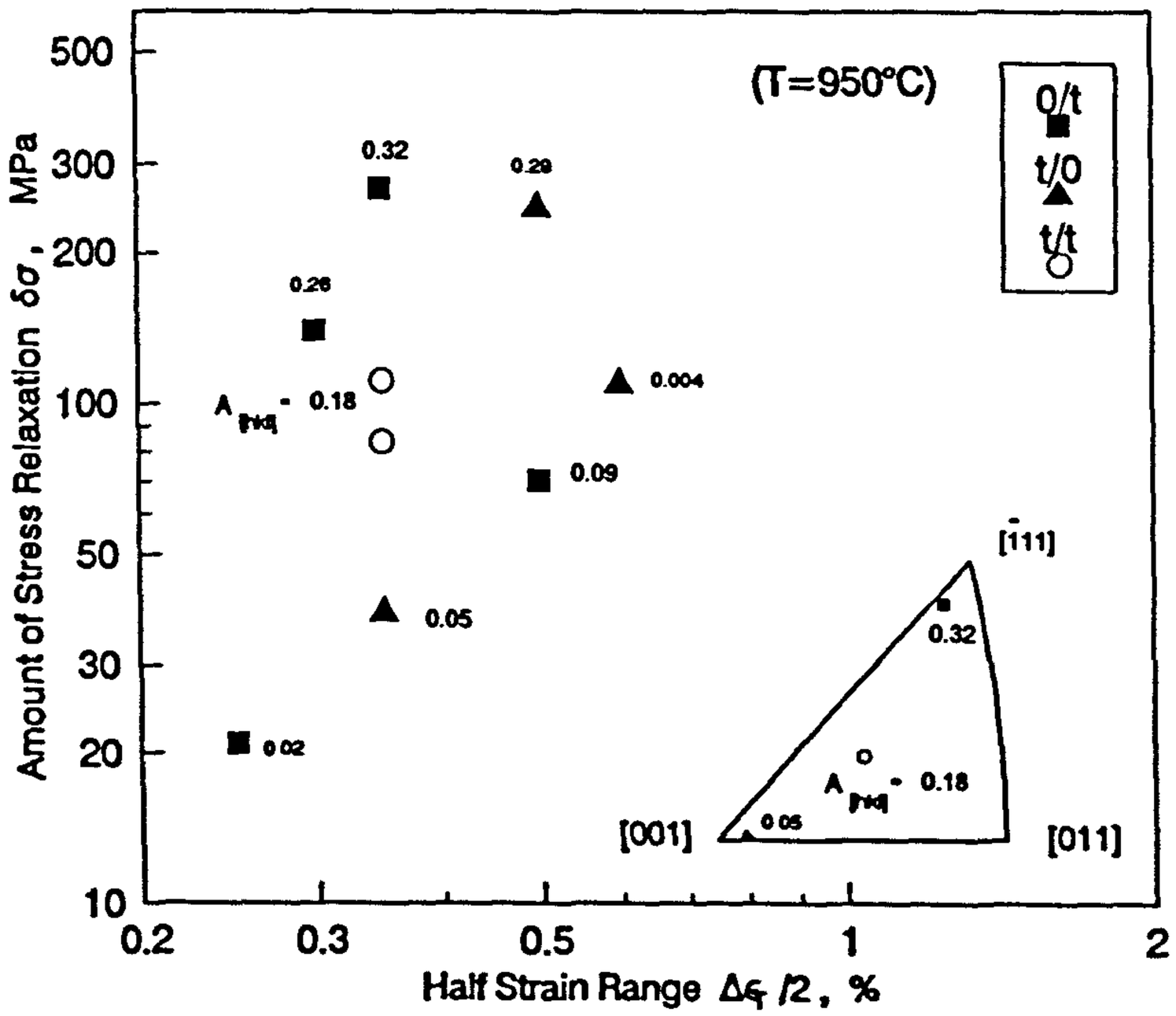

Fig.5.15. Amount of Stress Relaxation as a Function of Strain Range (T=950°C)

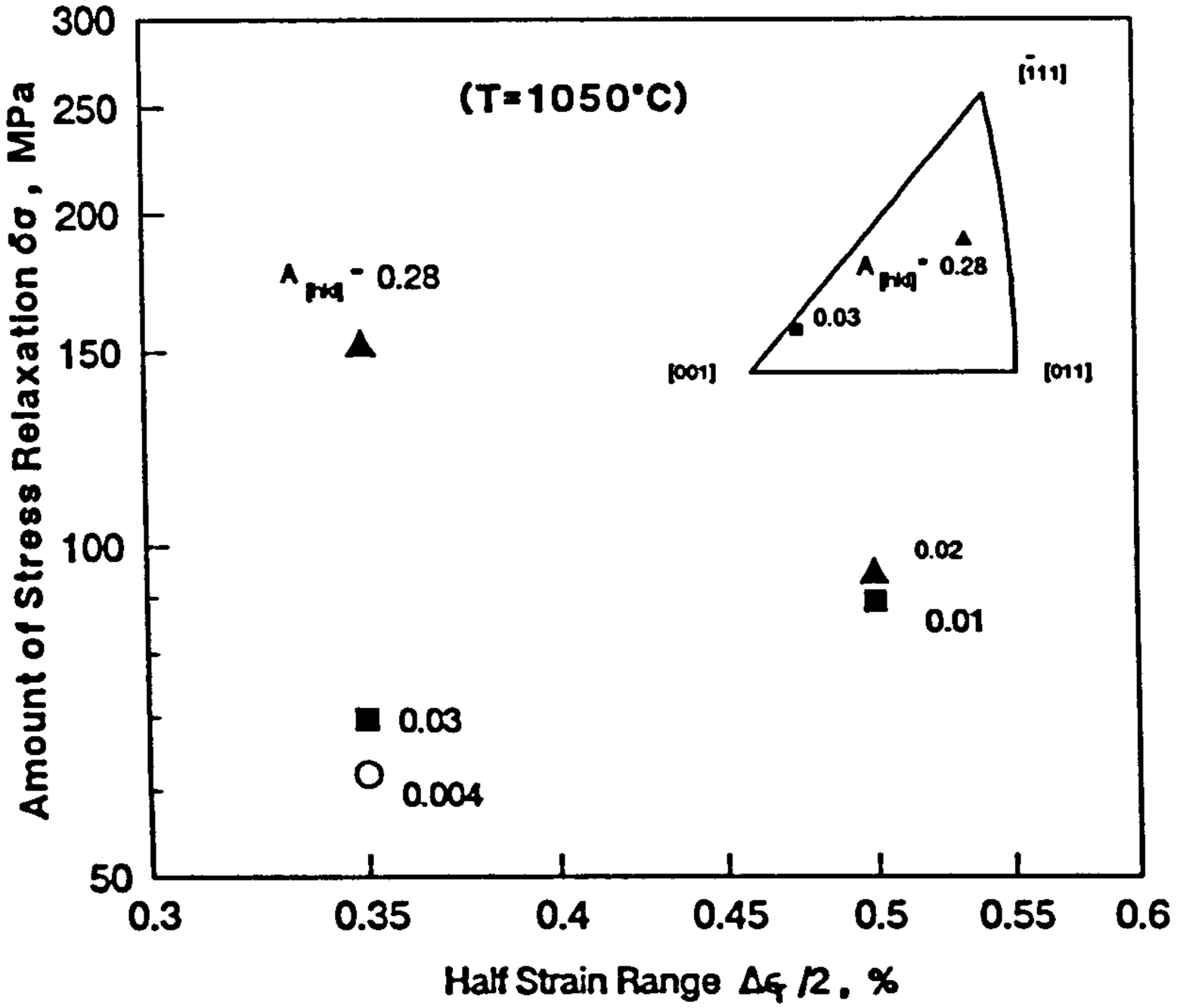

Fig.5.16. Amount of Stress Relaxation as a Function of Strain Range (T=1050°C)

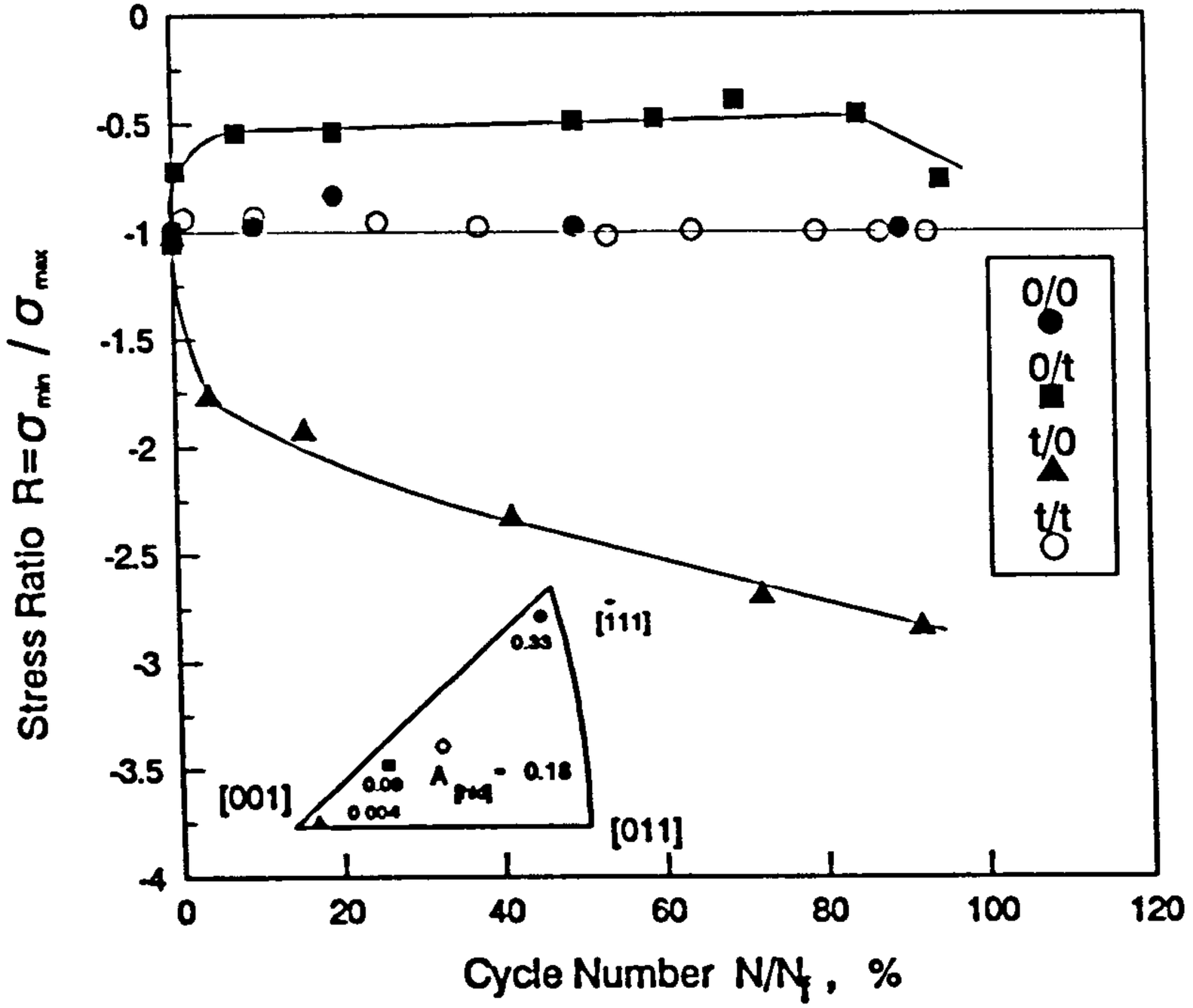

Fig.5.17. Variation of Stress Ratio R with Cycle Number (T=950°C)

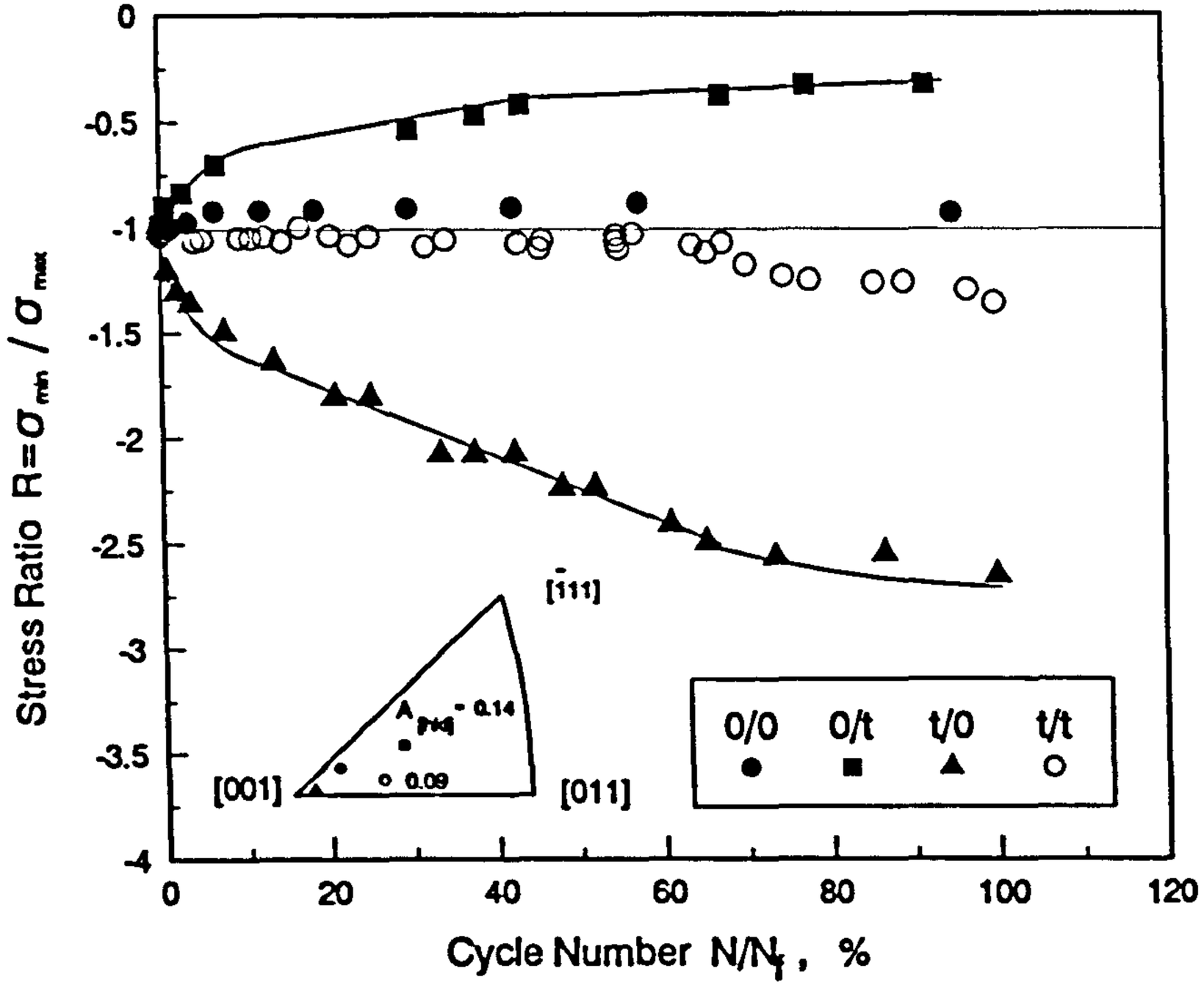

Fig.5.18. Variation of Stress Ratio R with Cycle Number (T=750°C)

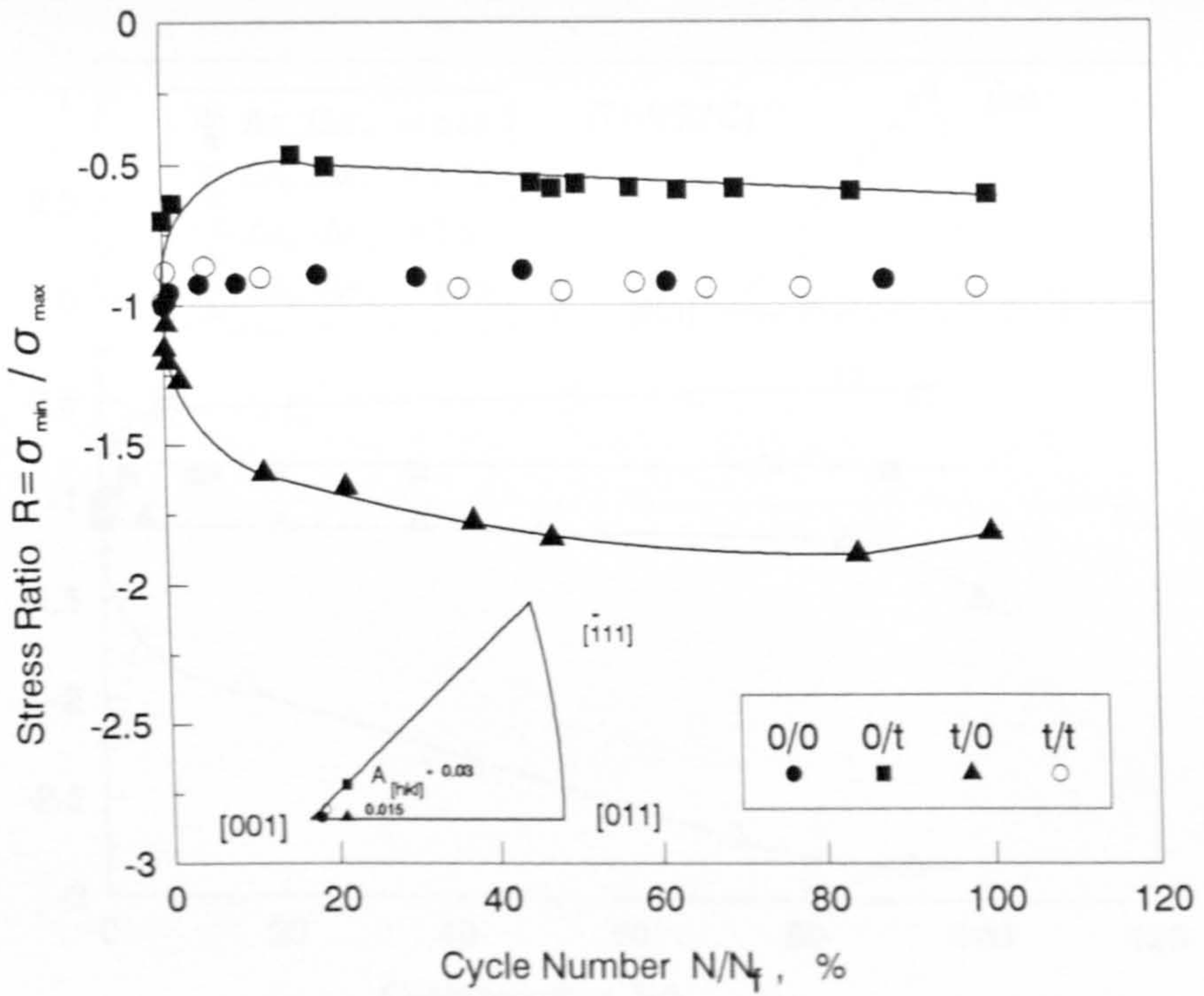

Fig.5.19. Variation of Stress Ratio with Cycle Number (T=1050°C)

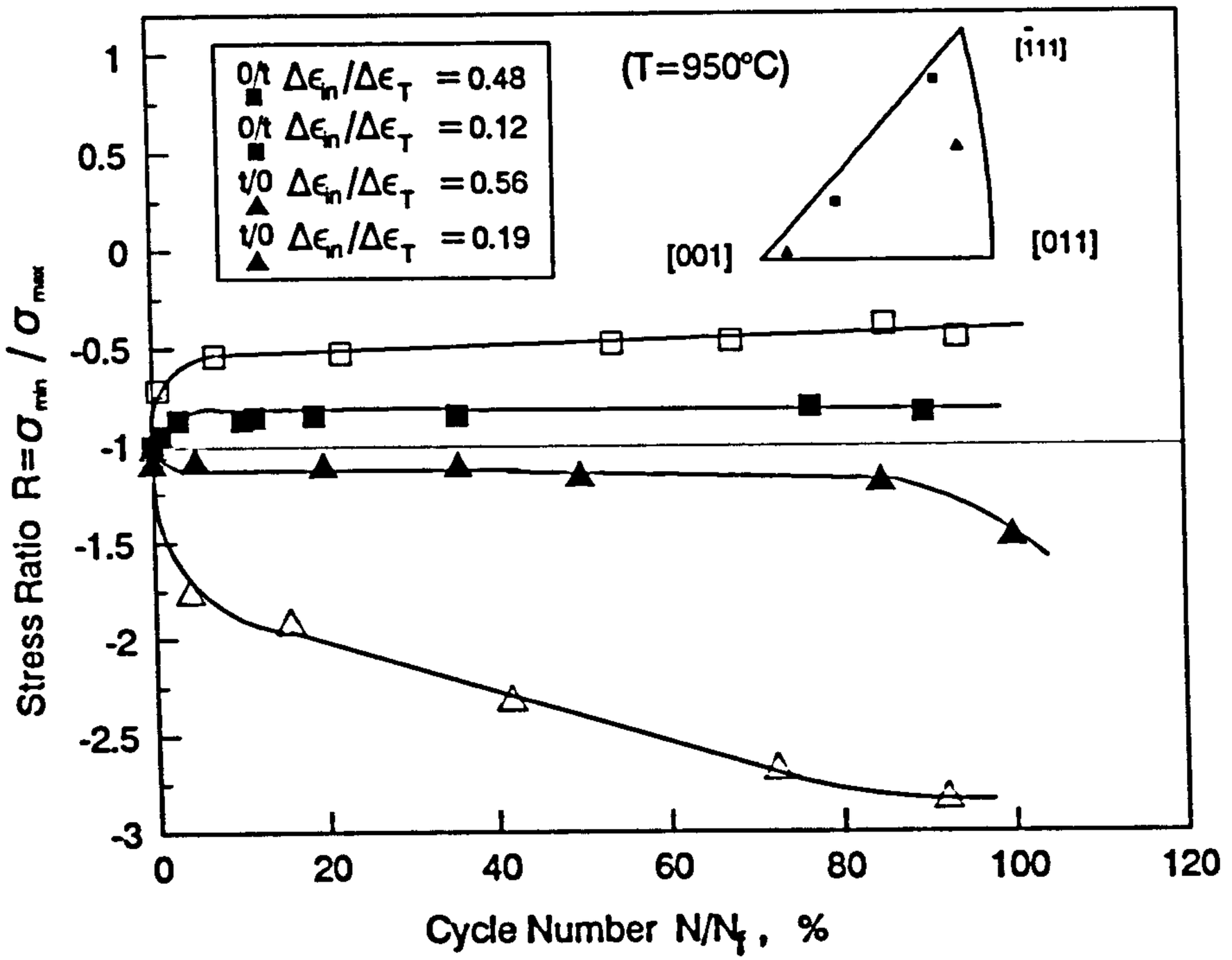

Fig.5.20. Influence of Orientation and Inelastic Strain on Mean Stress Response

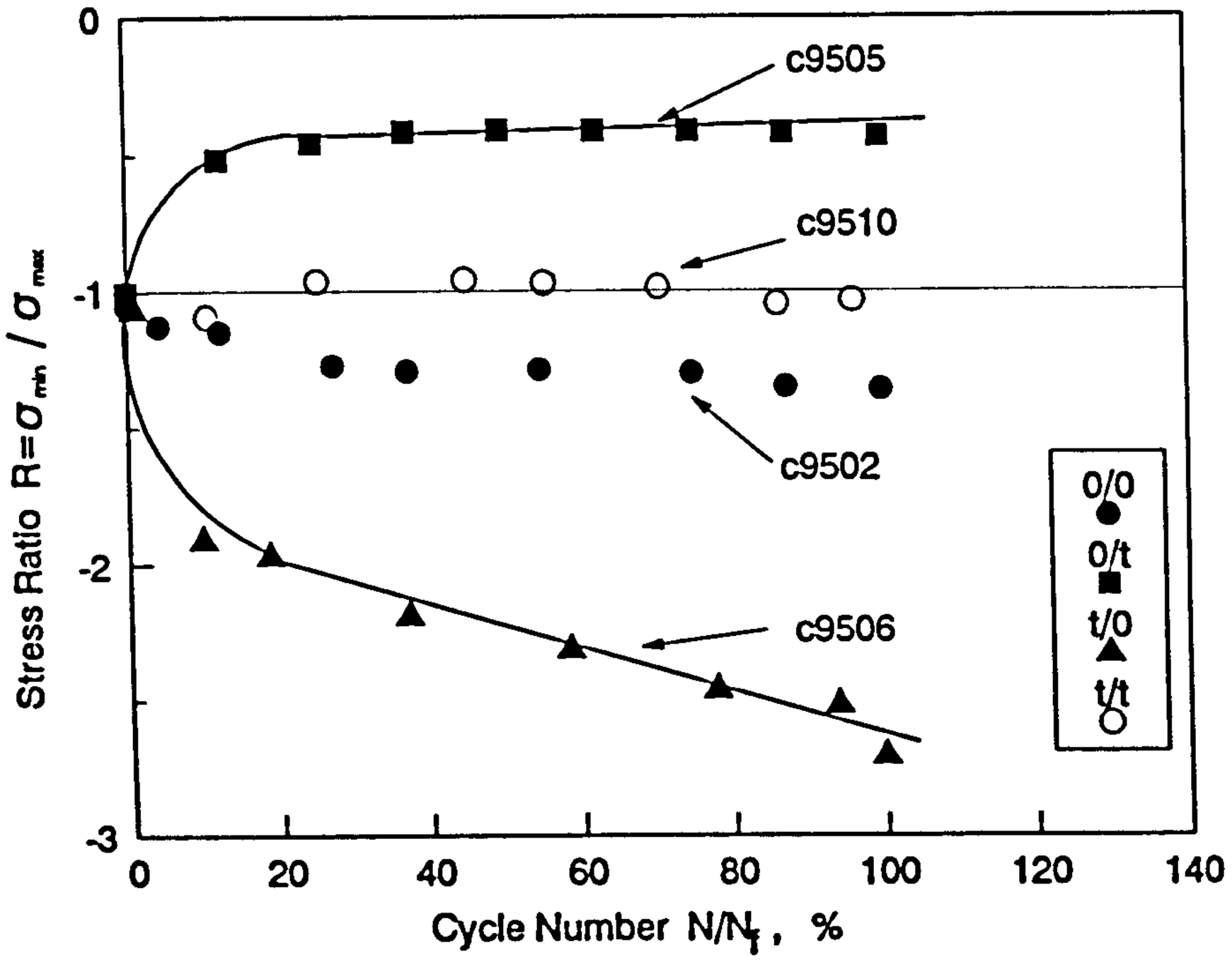

Fig.5.21. Variation of Stress Ratio with Cycle Number in the Corner Crack Tests at 950°C

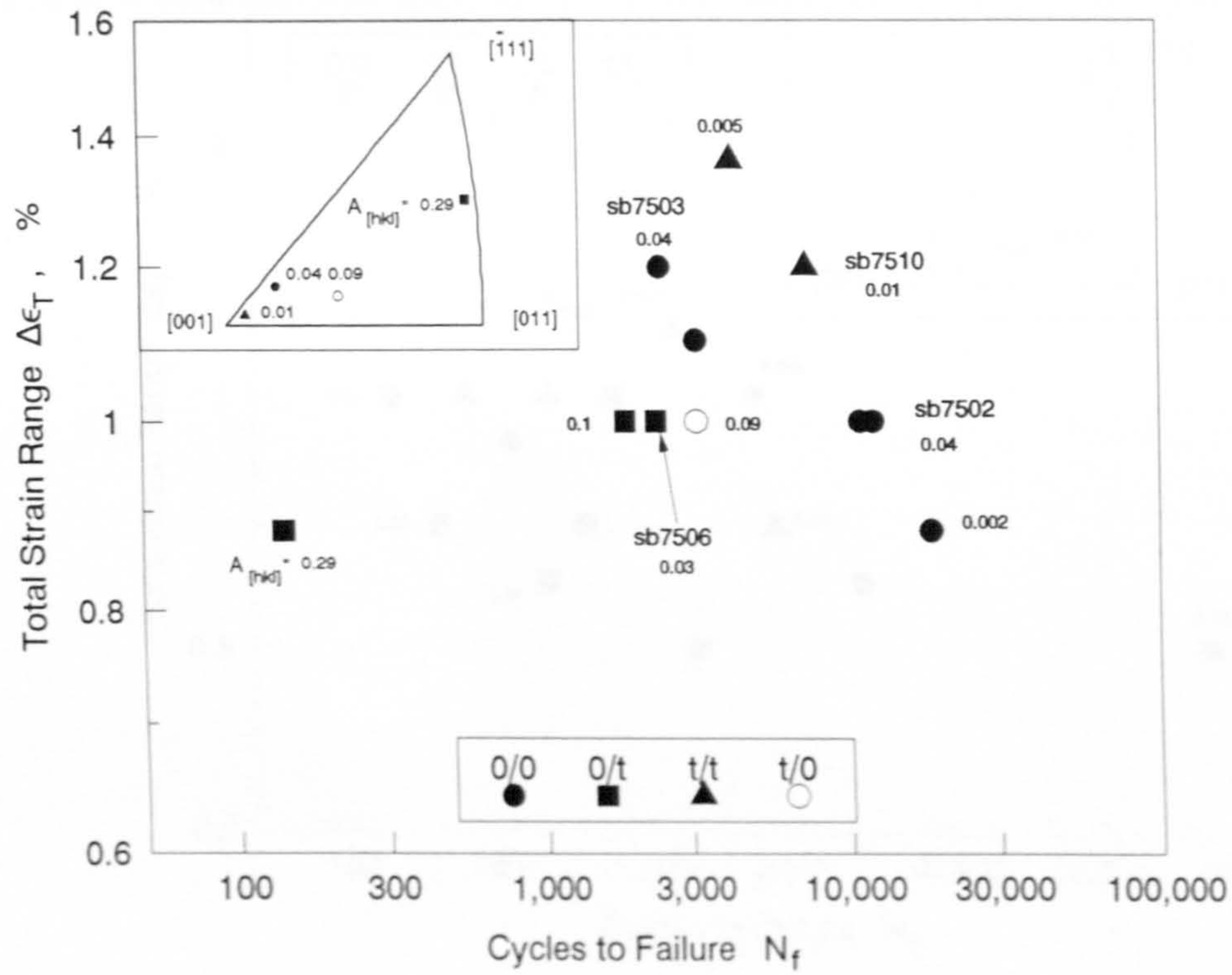

Fig.5.22a. Fatigue-Creep Life on a Total Strain Range Basis at 750°C

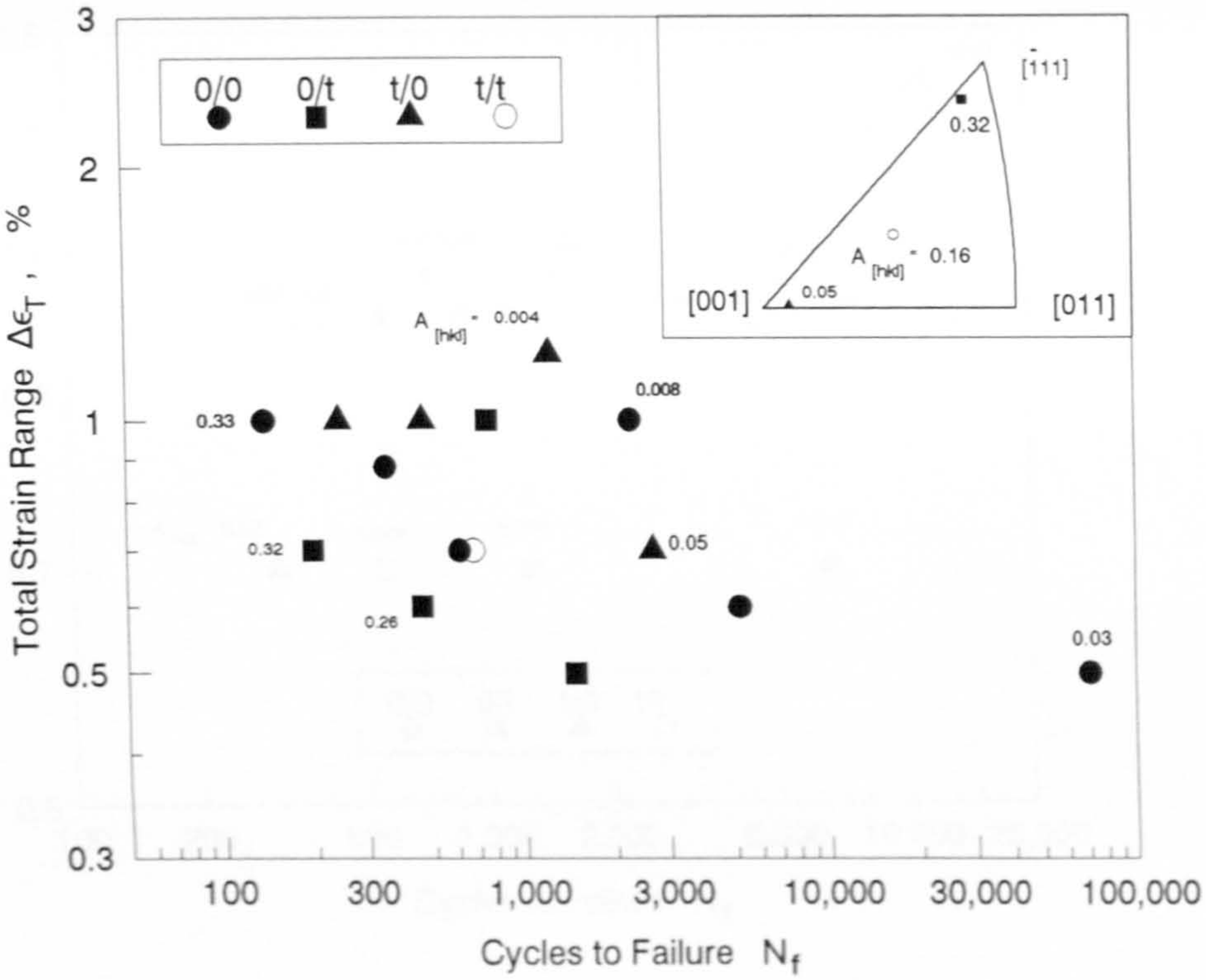

Fig.5.22b. Fatigue-Creep Life on a Total Strain Range at 950°C

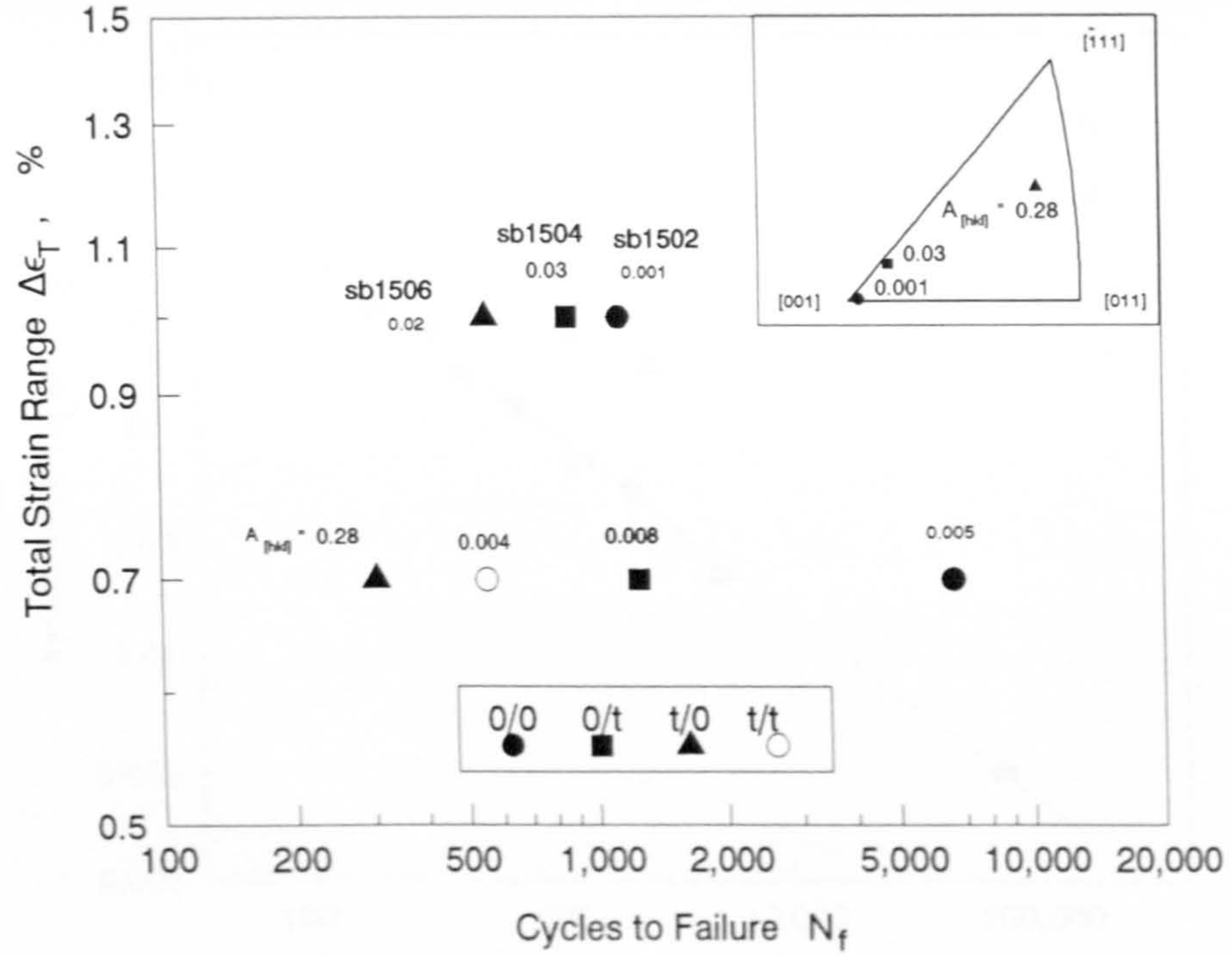

Fig.5.22c. Fatigue-Creep Life on a Total Strain Range Basis at 1050°C

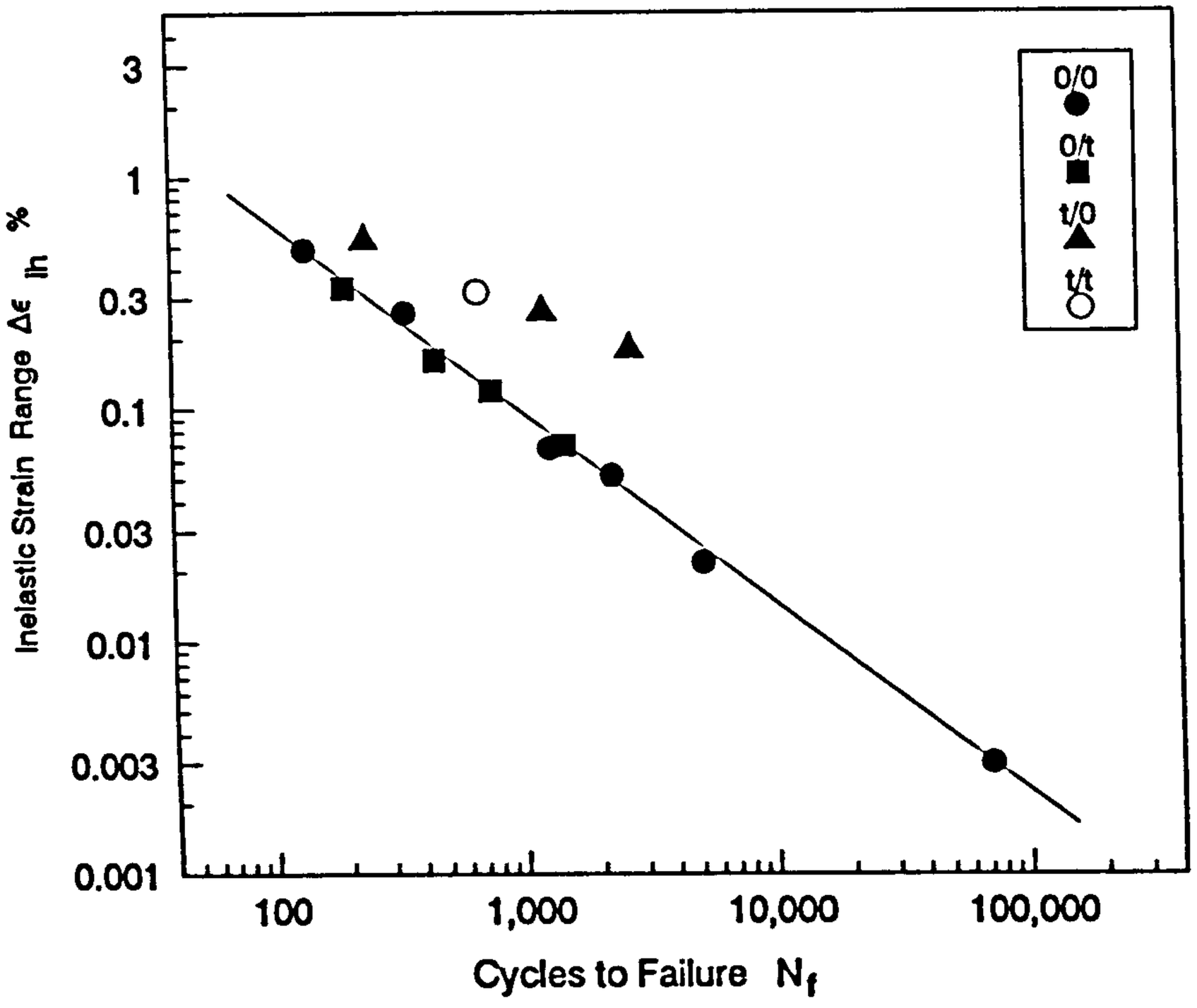

Fig.5.23. Fatigue-Creep Life as a Function of Inelastic Strain Range (T=950°C)

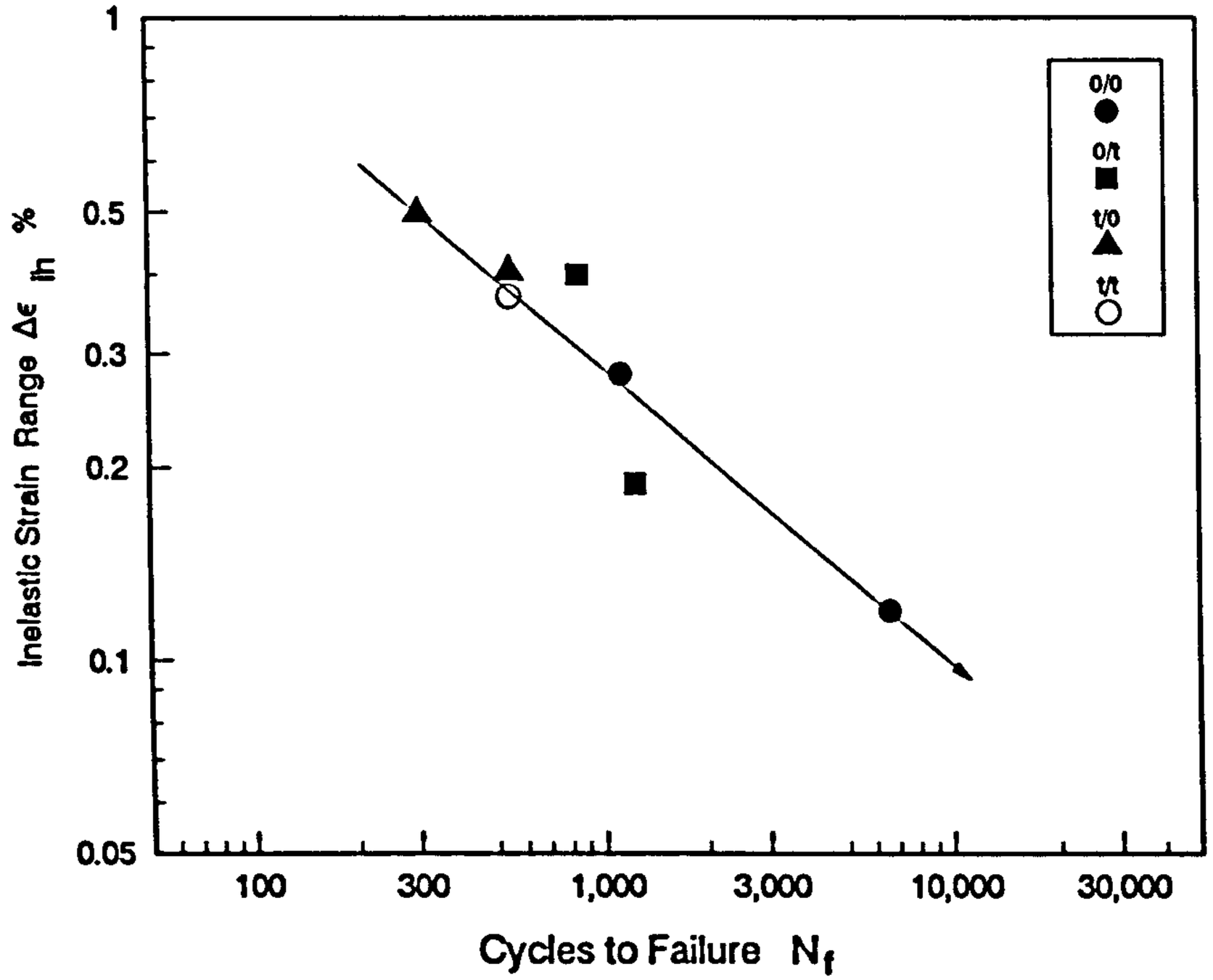

Fig.5.24. Fatigue-Creep Life as a Function of Inelastic Strain Range (T=1050°C)

R: Reference pd Probes
N: Notch pd Probes
T: Thermocouple

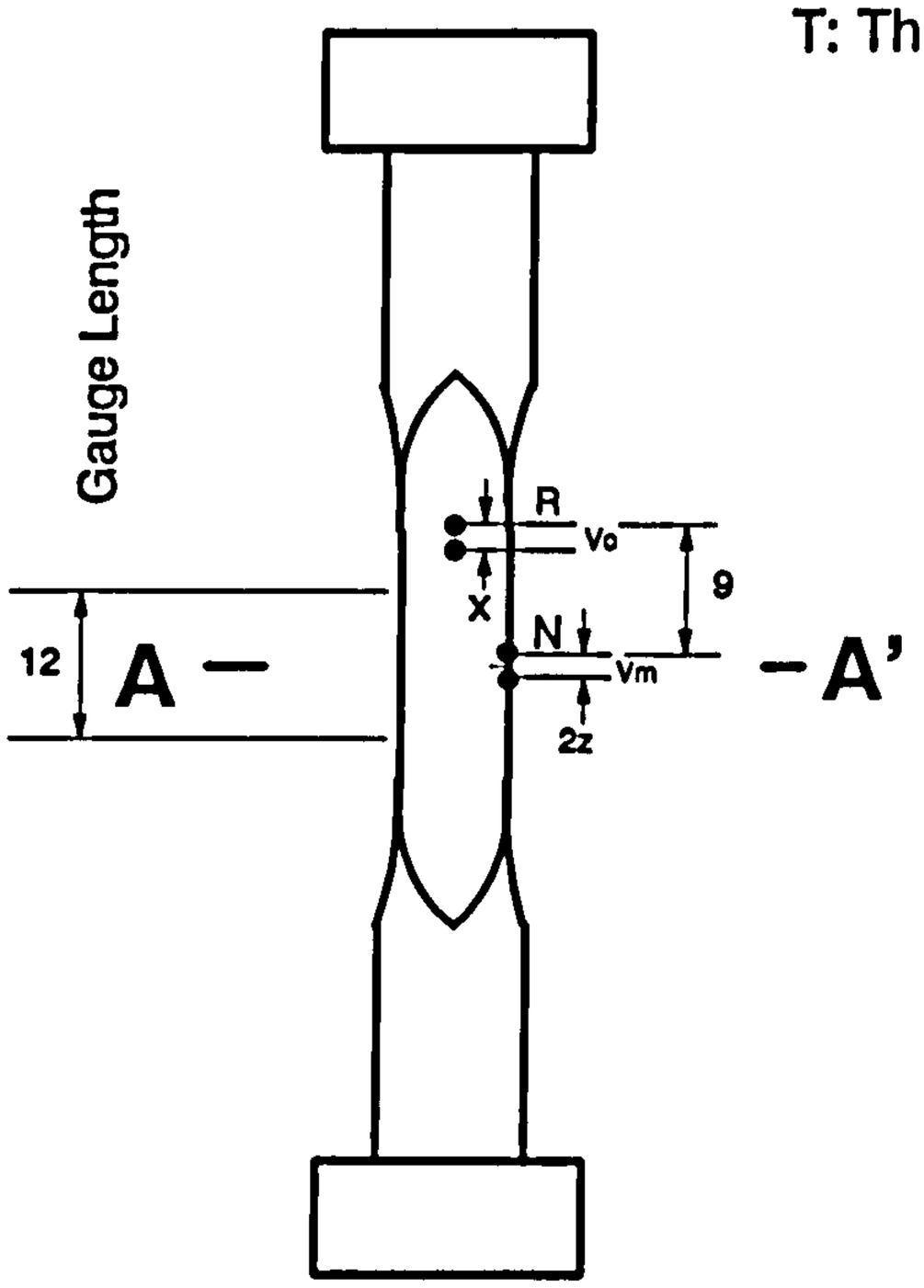

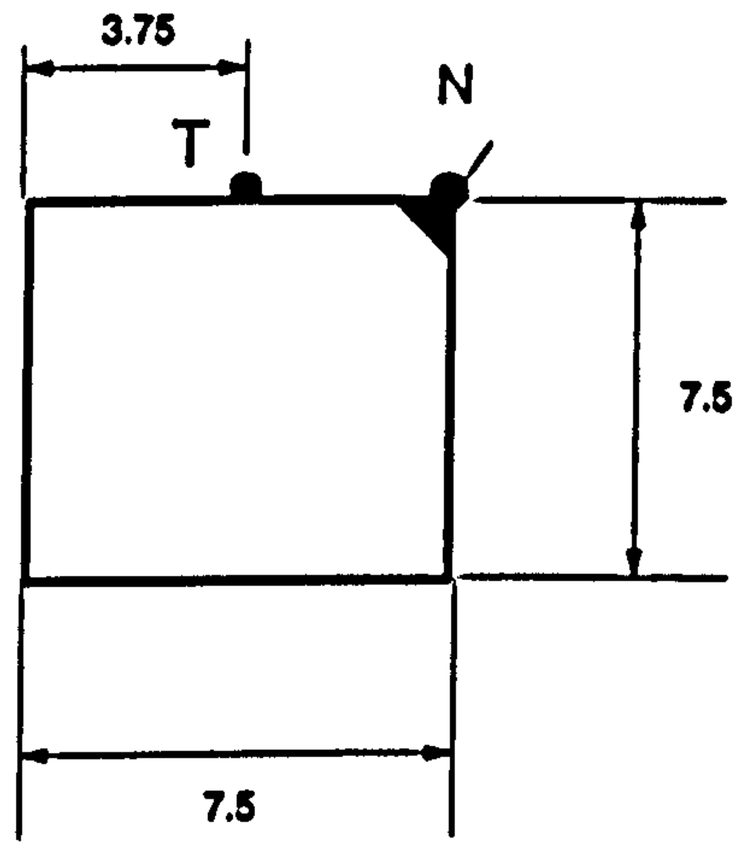

Enlarged Section A-A'

Fig.5.25. PD Lead Locations on the Corner Crack Specimen (dimensions in mm)

(a). PD Calibration at 750°C

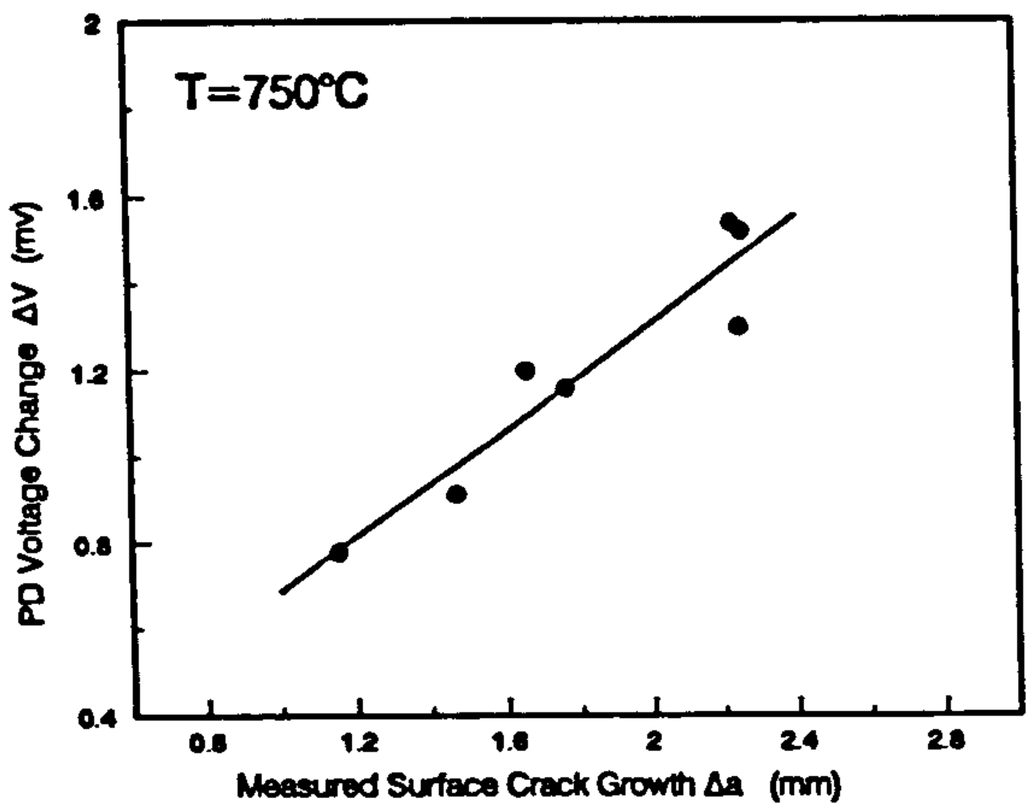

(b). PD Calibration at 950°C

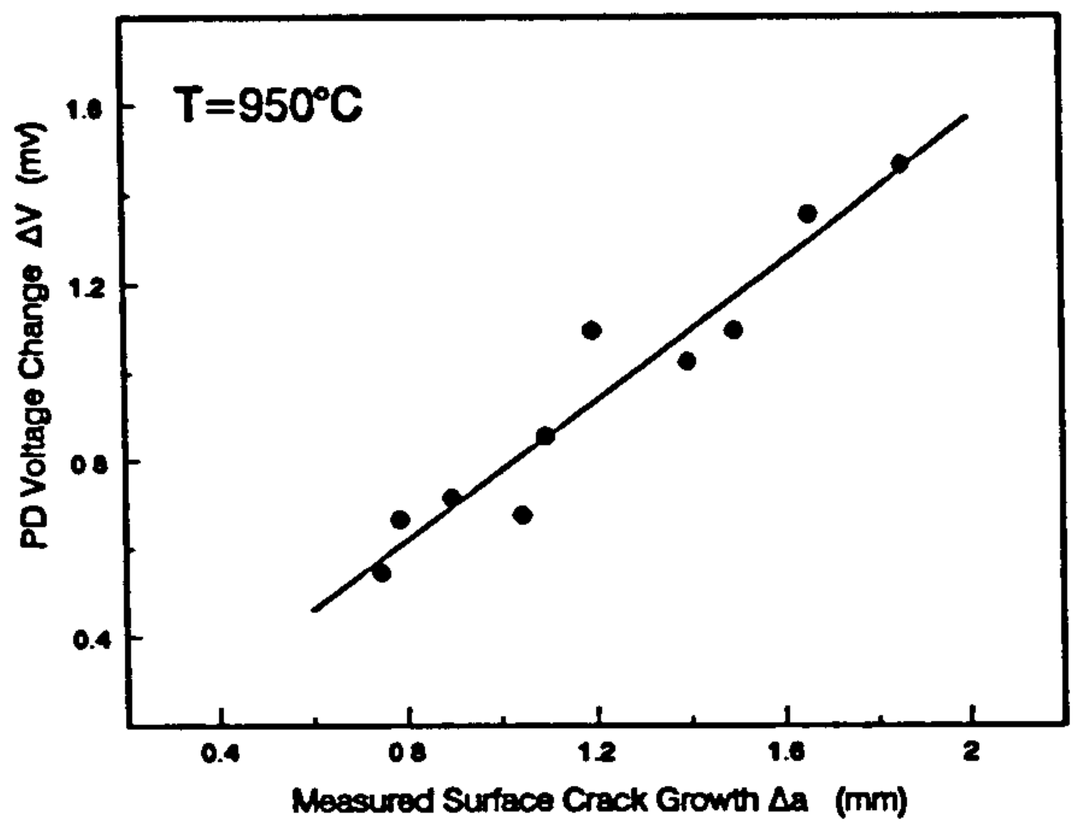

(c). PD Calibration at 1050°C

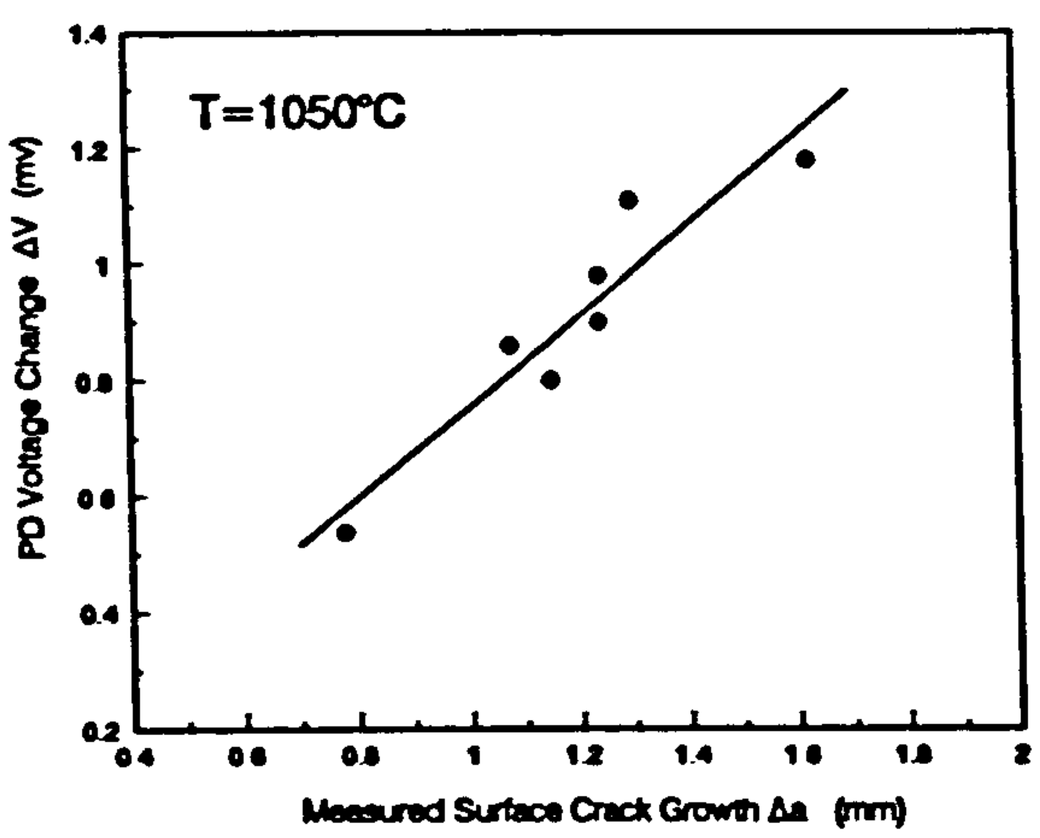

(d). PD Calibration at 20°C

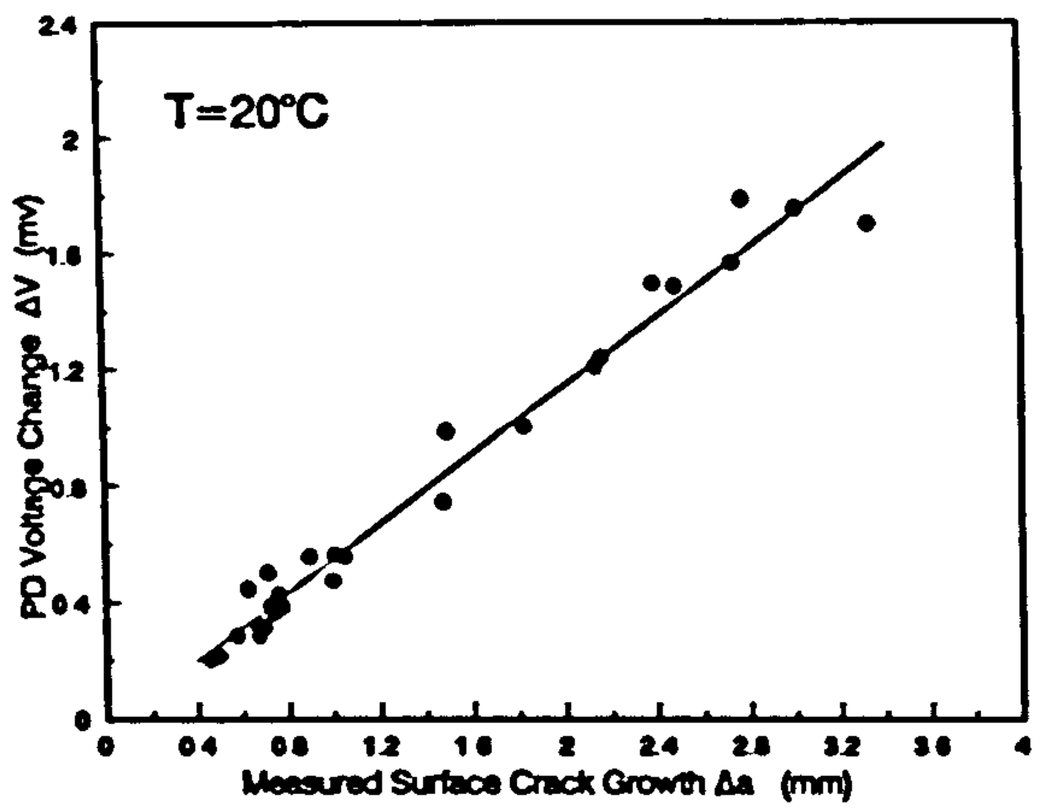

Fig.5.26. PD Calibrations at Different Temperatures

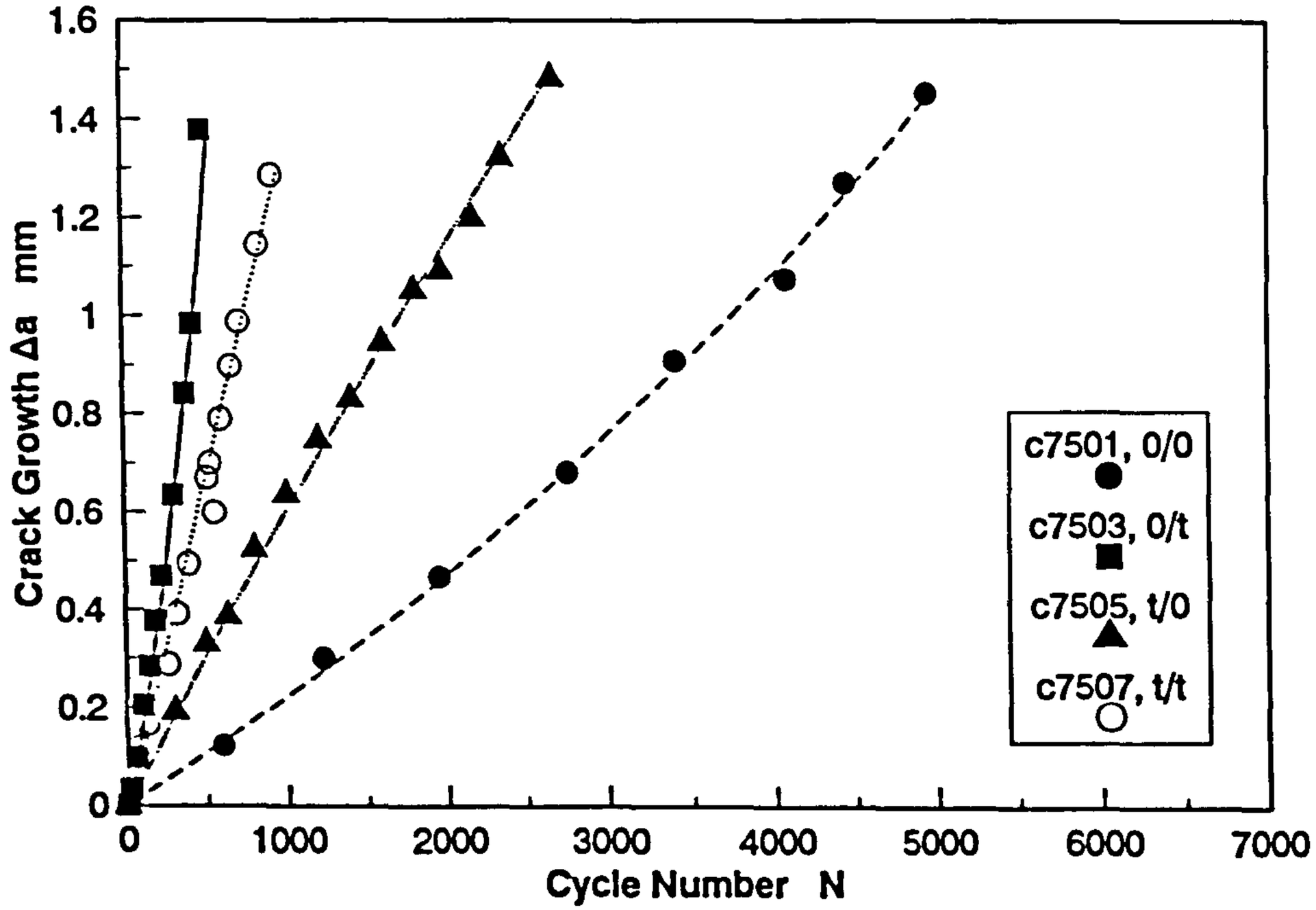

Fig.5.27a. Crack Extension with Cycle Number During Different Tests (T=750°C)

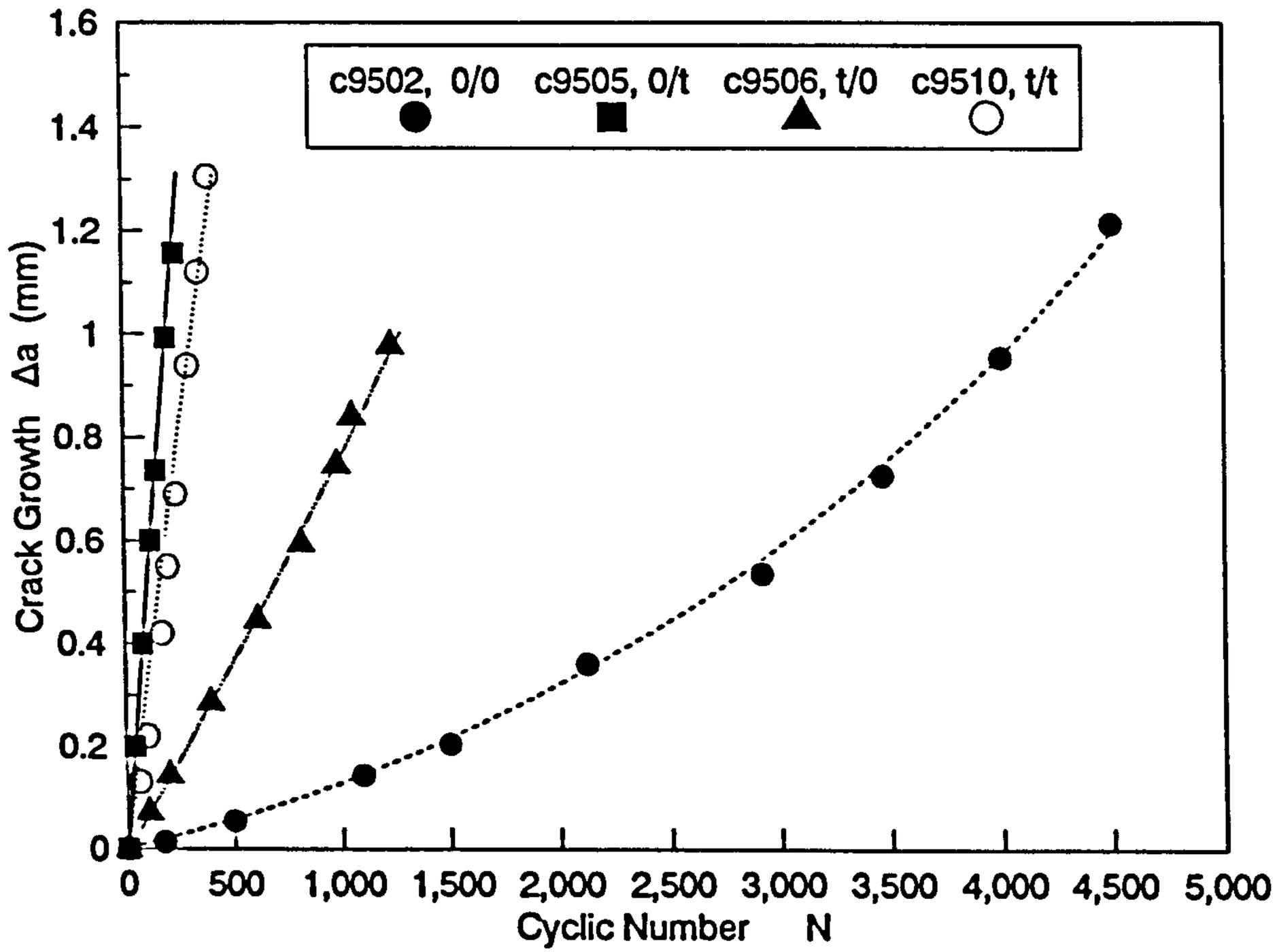

Fig.5.27b. Crack Extension with Cycle Number During Different Tests at 950°C

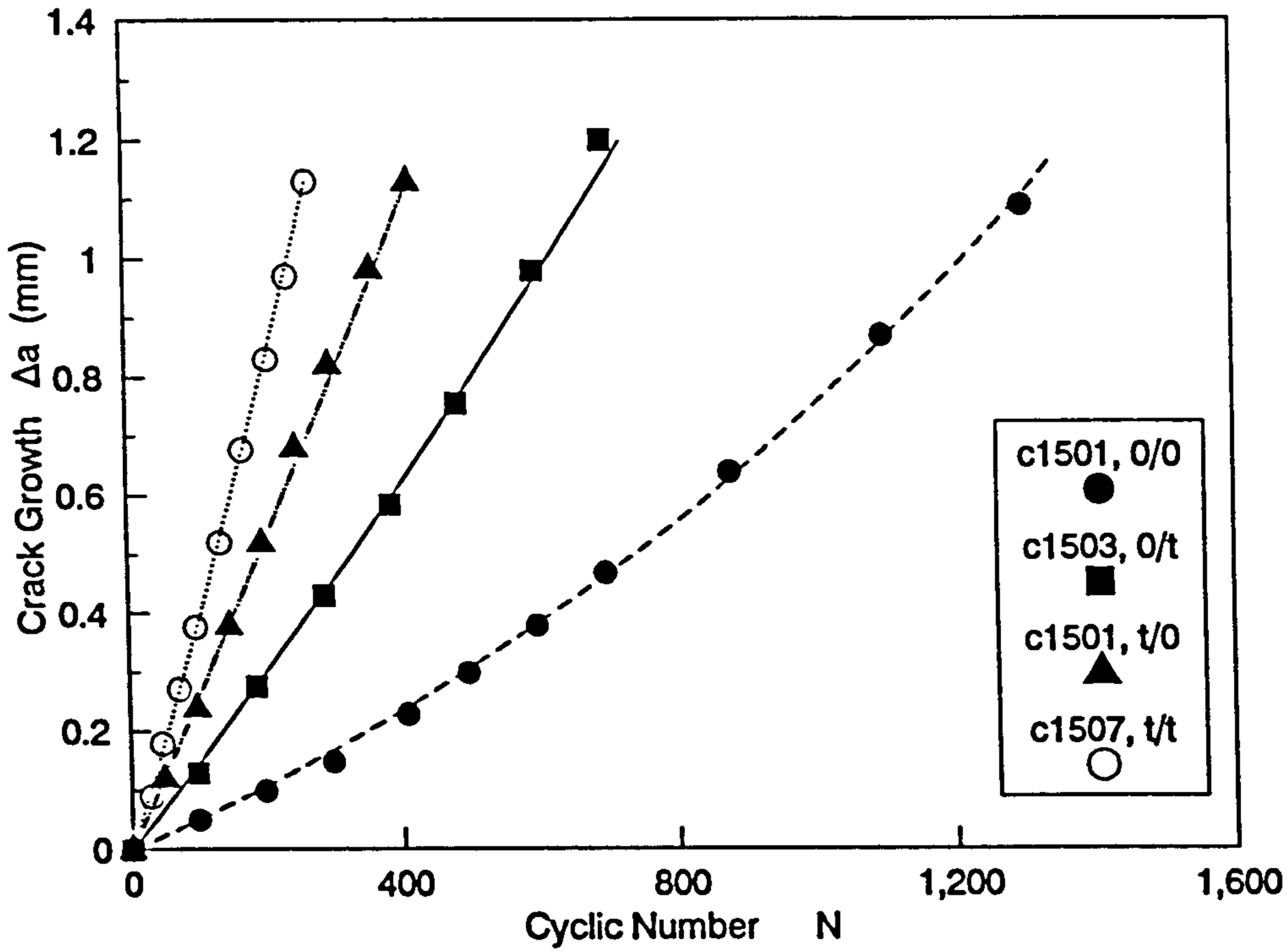

Fig.5.27c. Crack Extension with Cycle Number During Different Tests at 1050°C

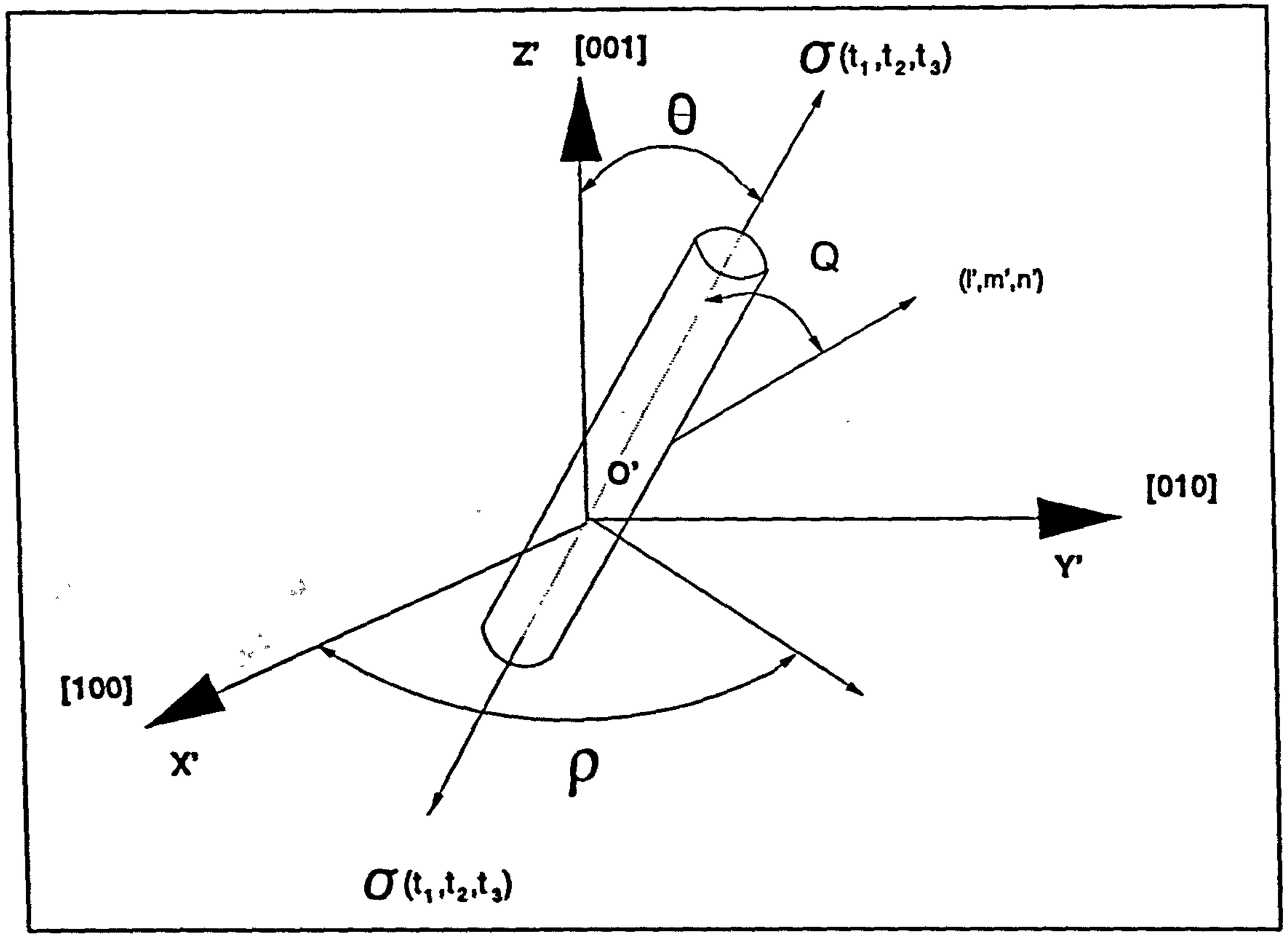

Fig.6.1. Crystal Orientation Axis System

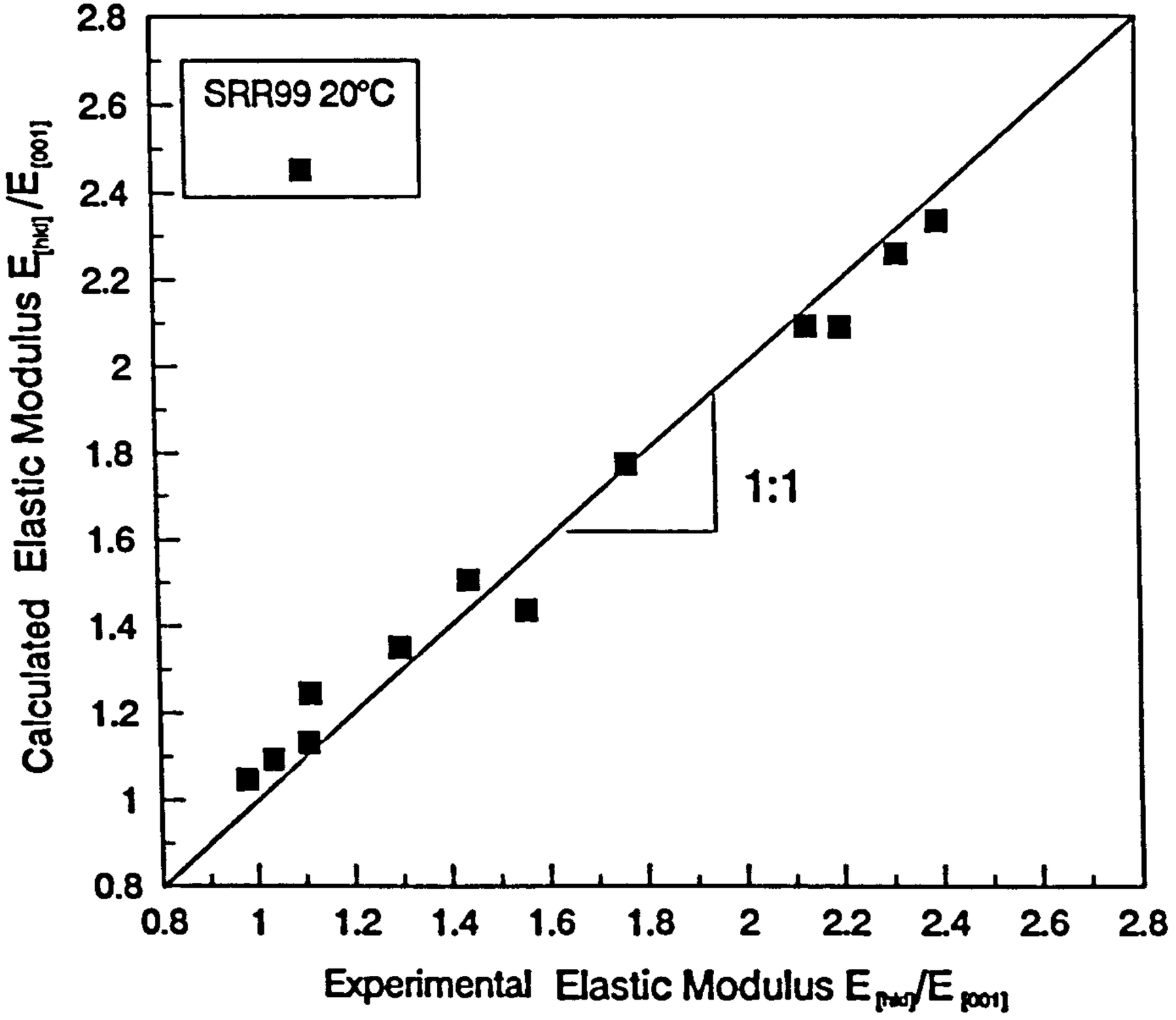

Fig.6.2. Comparison Between the Calculated and Experimental Elastic Modulus at 20°C

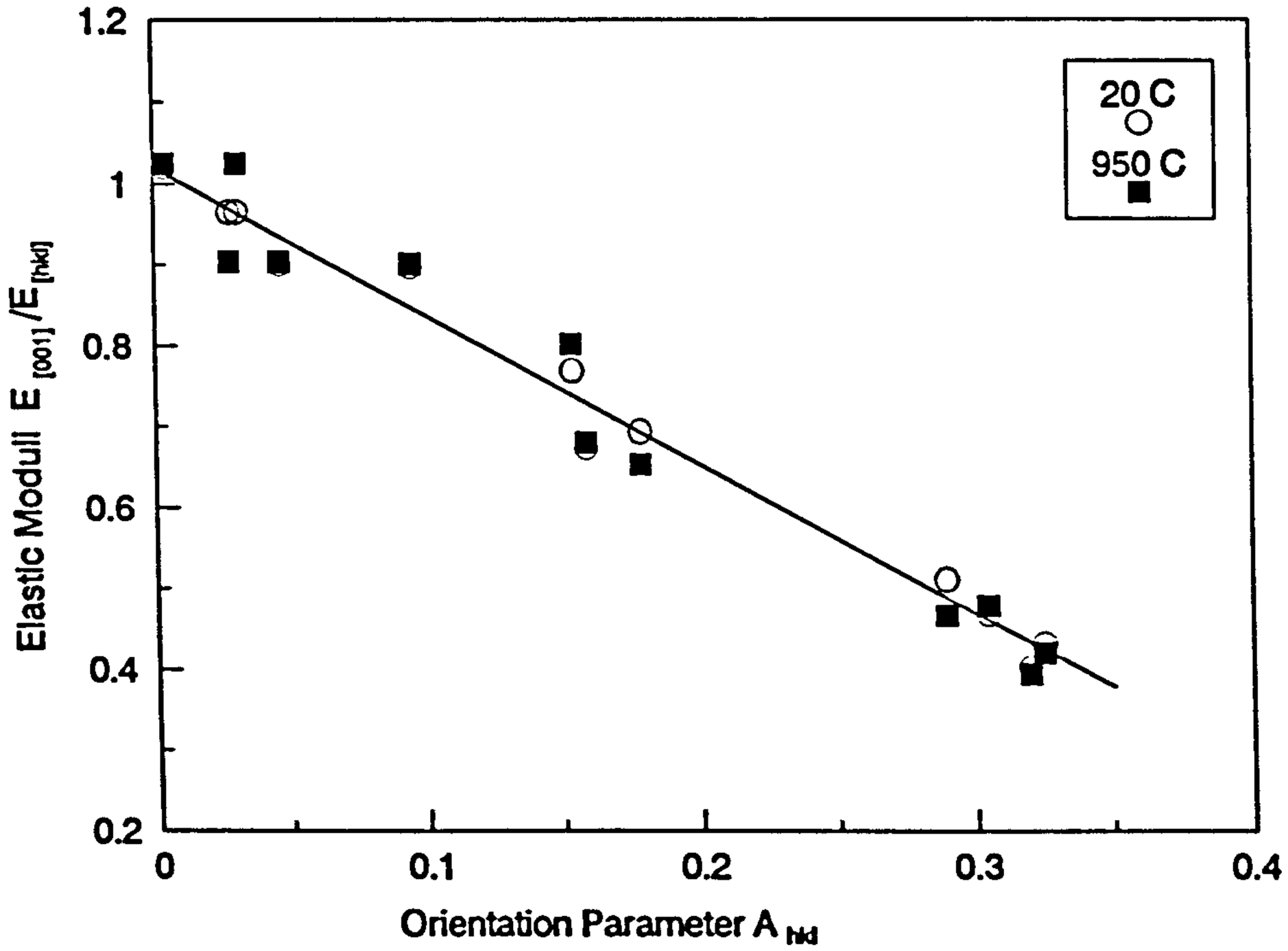

Fig.6.3. Elastic Modulus for Single Crystal SRR99 as Function of Orientation Parameter A_{hkl}

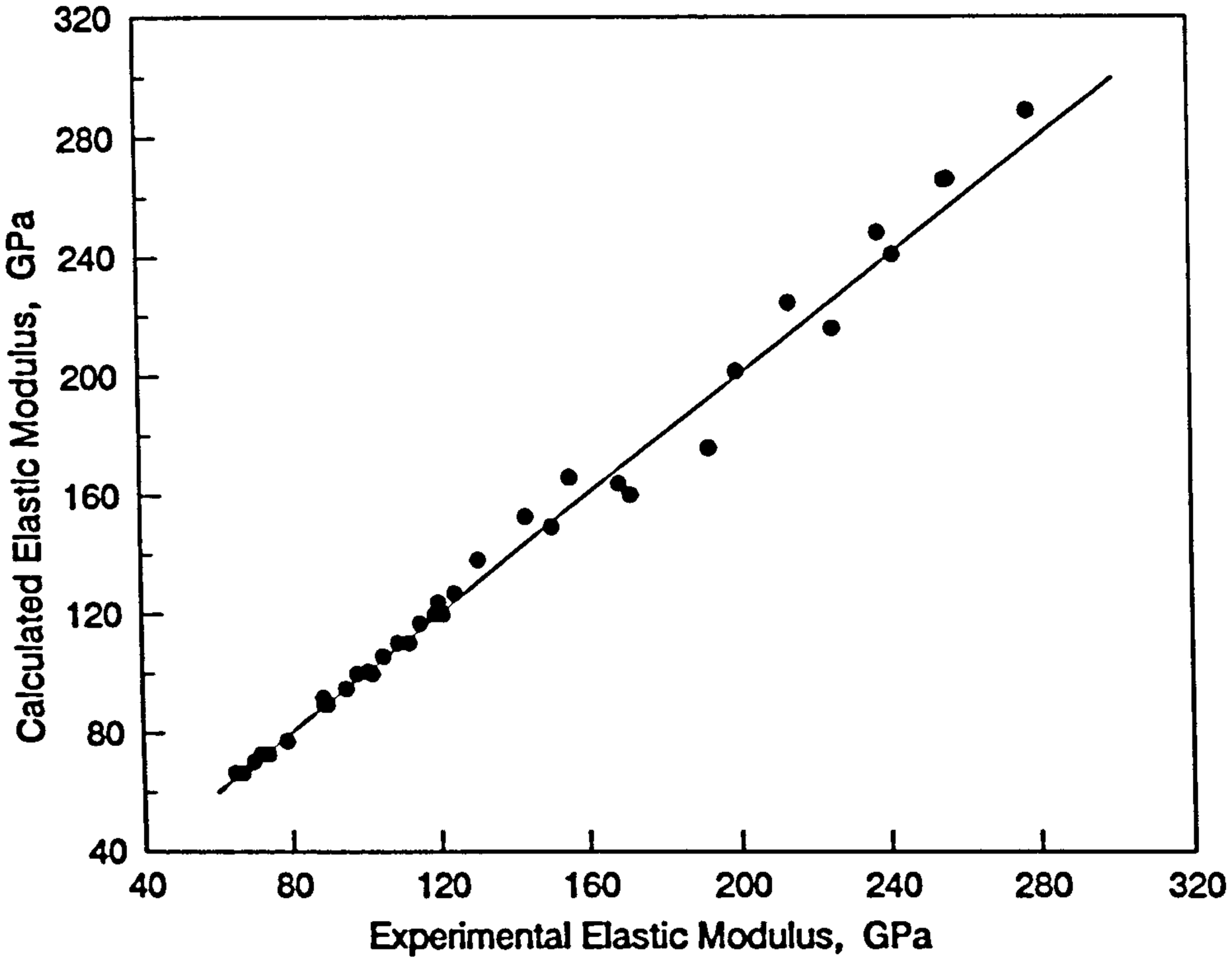

Fig.6.4. Comparison of the Calculated and Experimental Elastic Modulus of the Additional HTE Tests

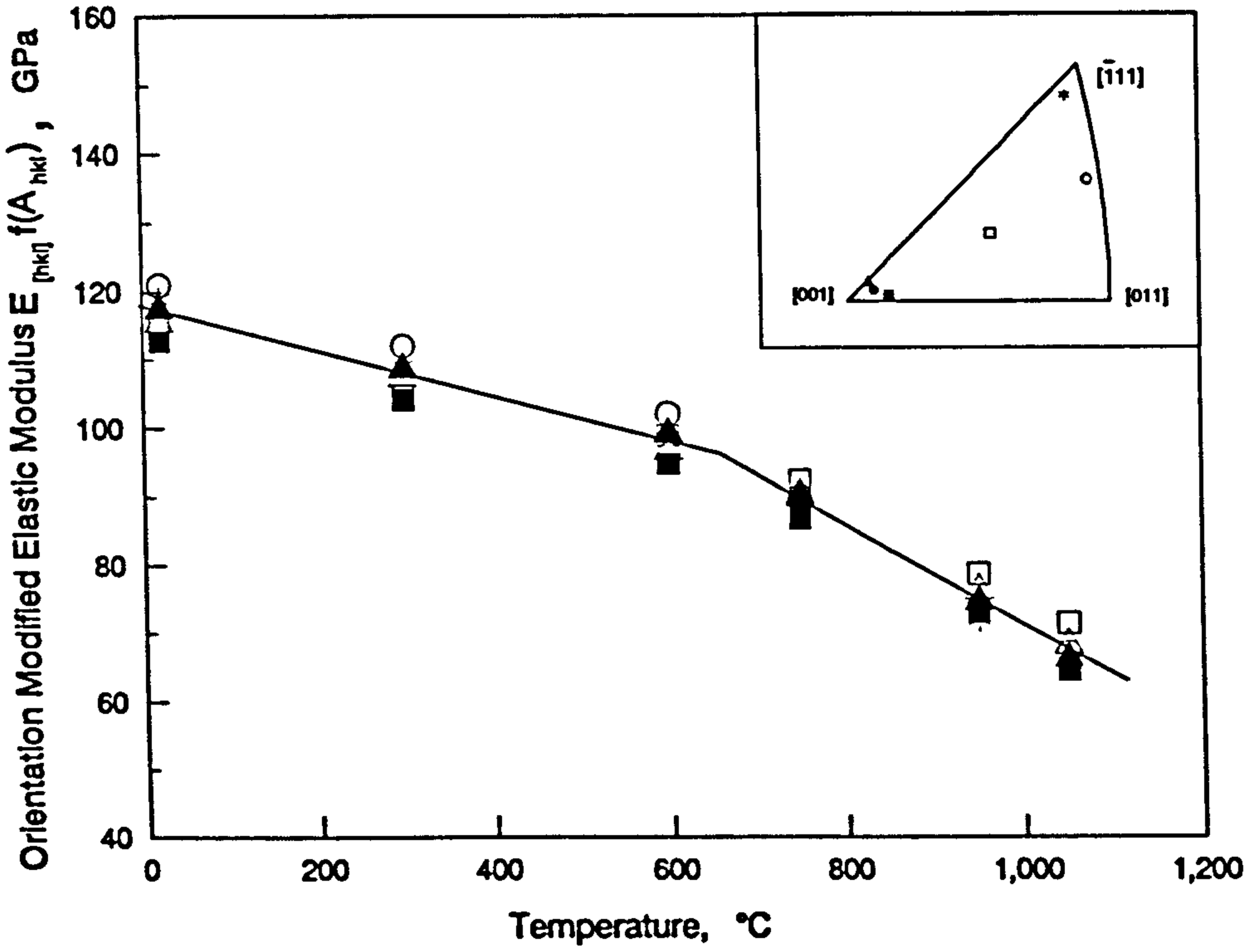

Fig.6.5. Orientation Modified Elastic Modulus as a Function of Temperature

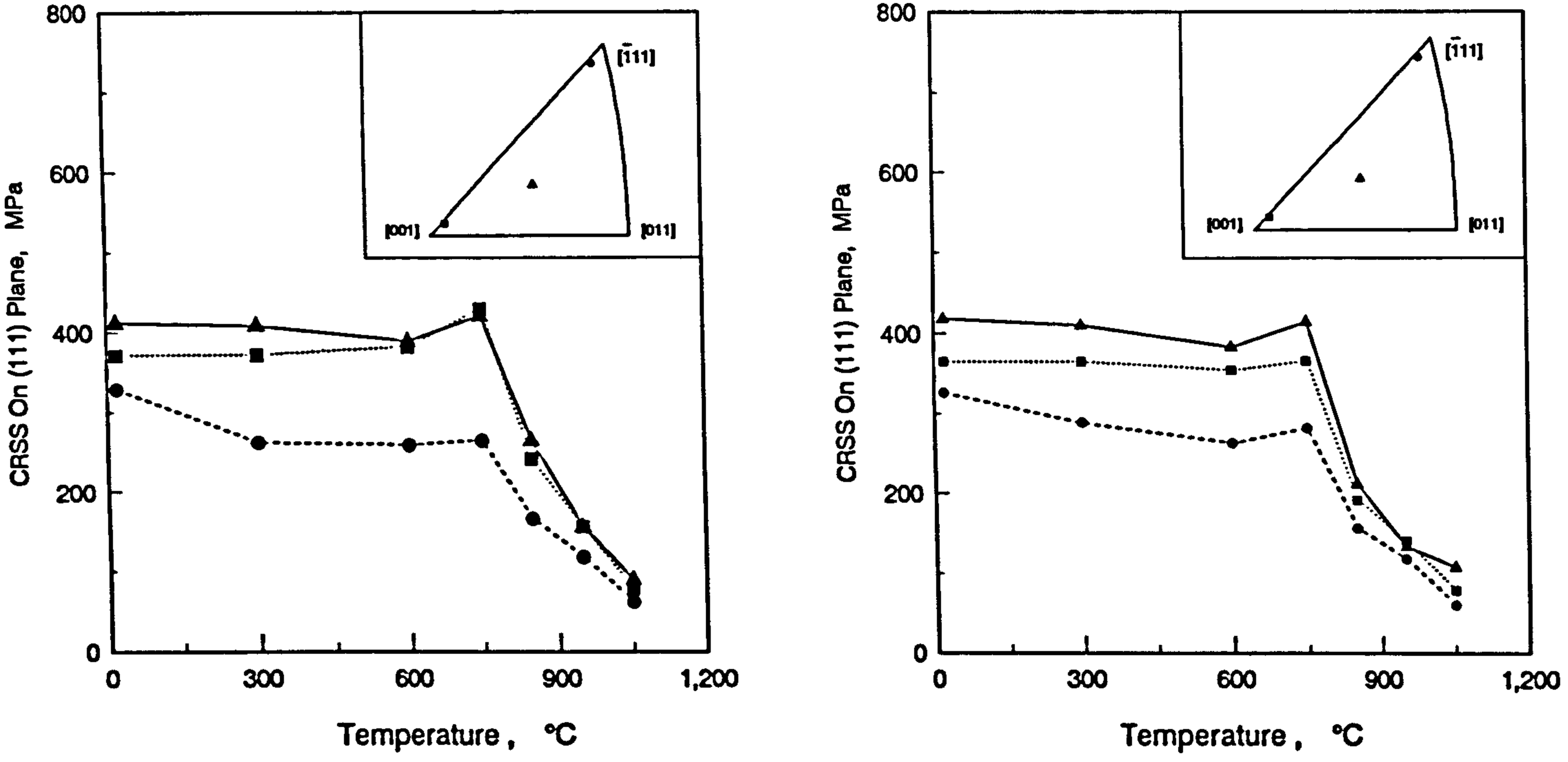

Fig.6.6. Comparison of CRSS on (111) for Different Orientations

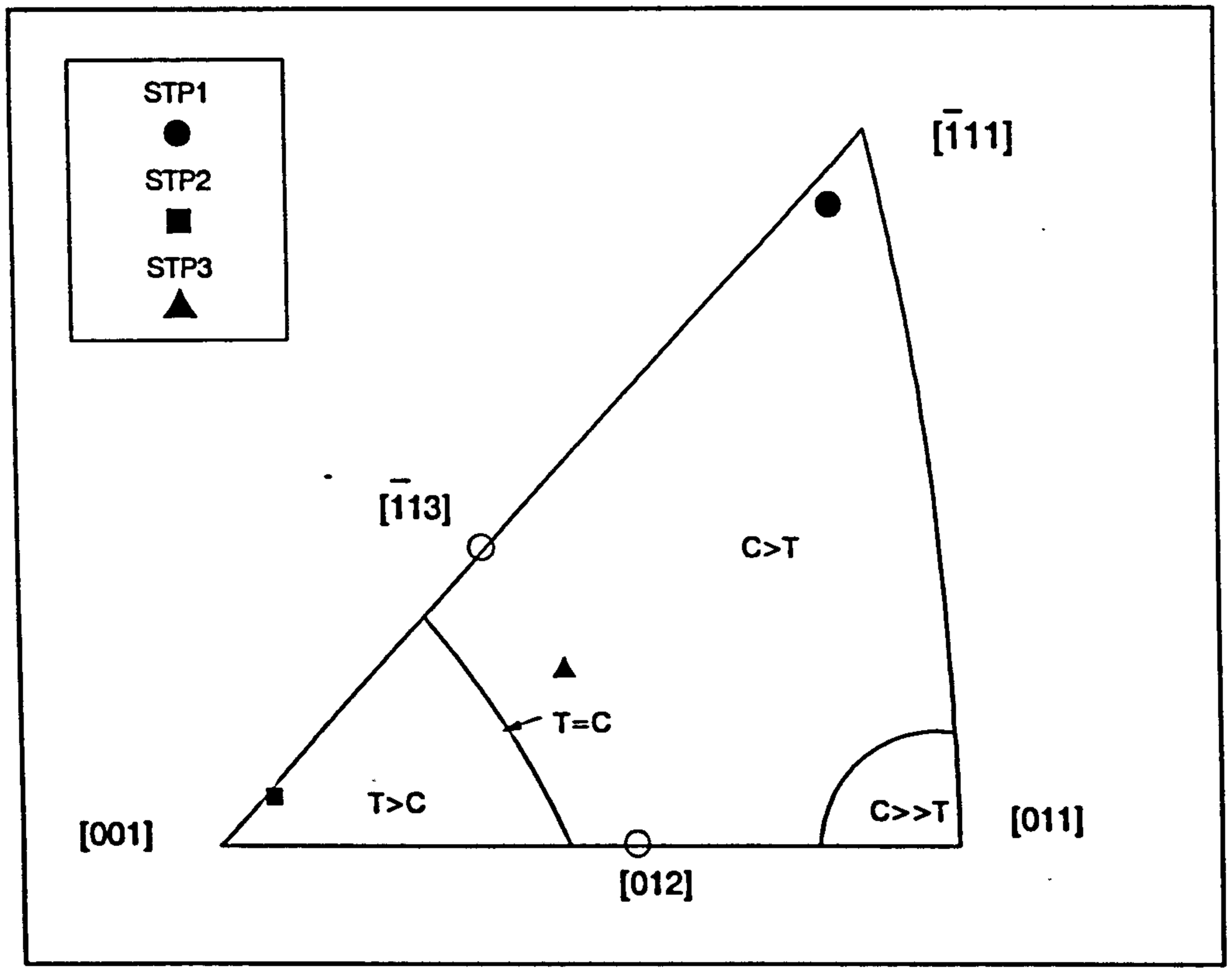

Fig.6.7. Summary of Tension/Compression Asymmetry Predicted from the Cross-Slip Model for Yield Stress of γ' Alloy

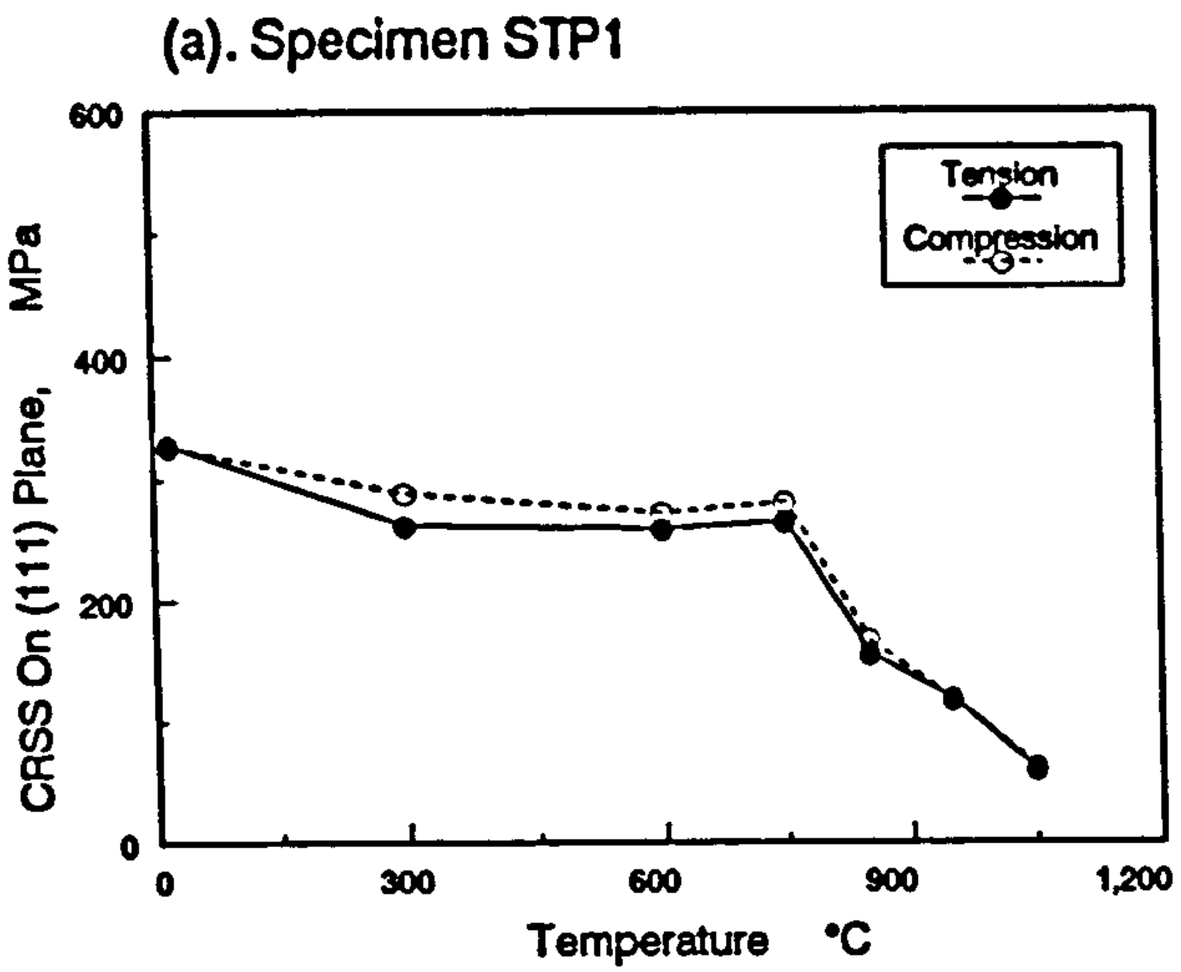

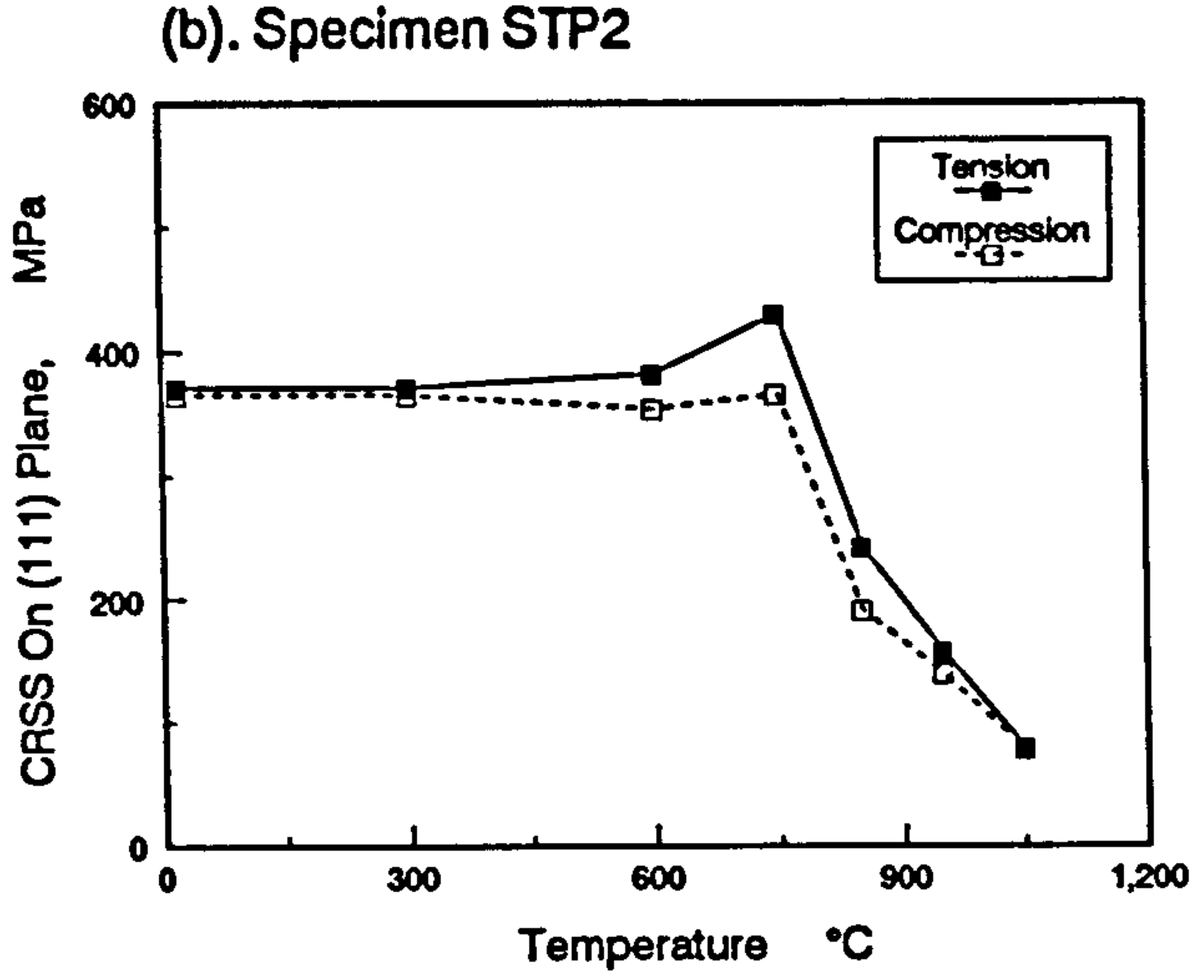

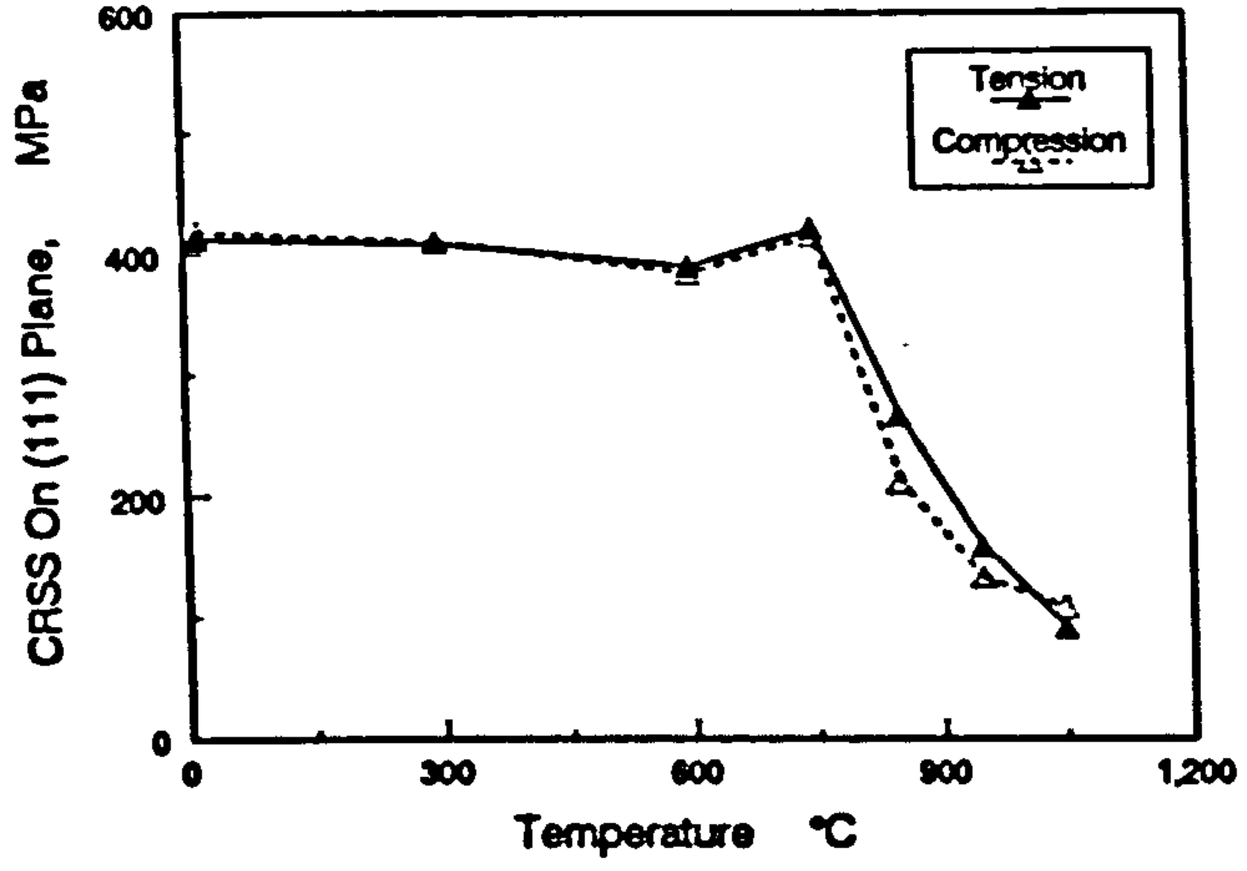

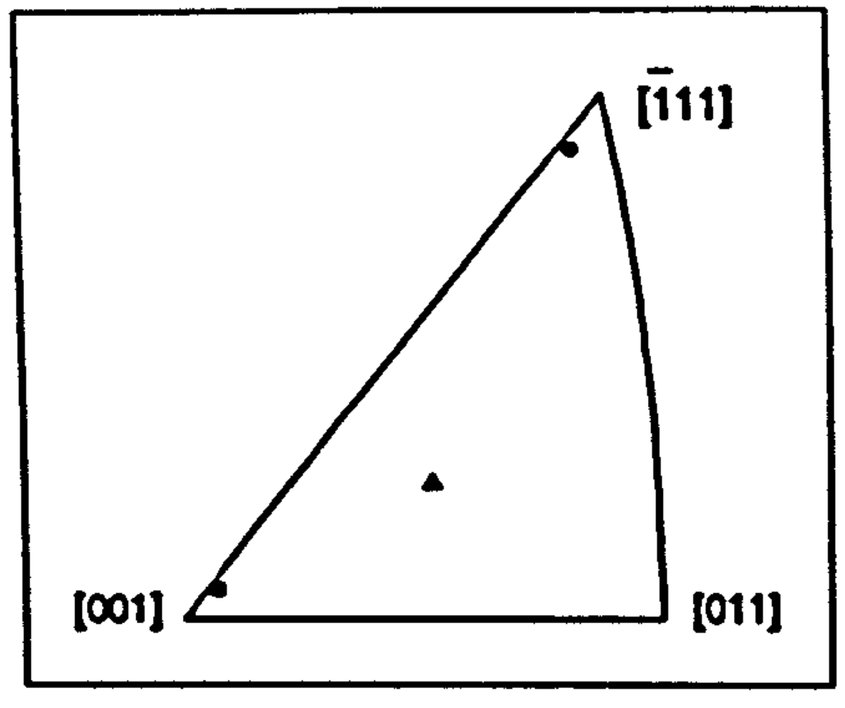

Fig.6.8. Comparison of Tensile and Compressive CRSS on (111) for Different Orientations

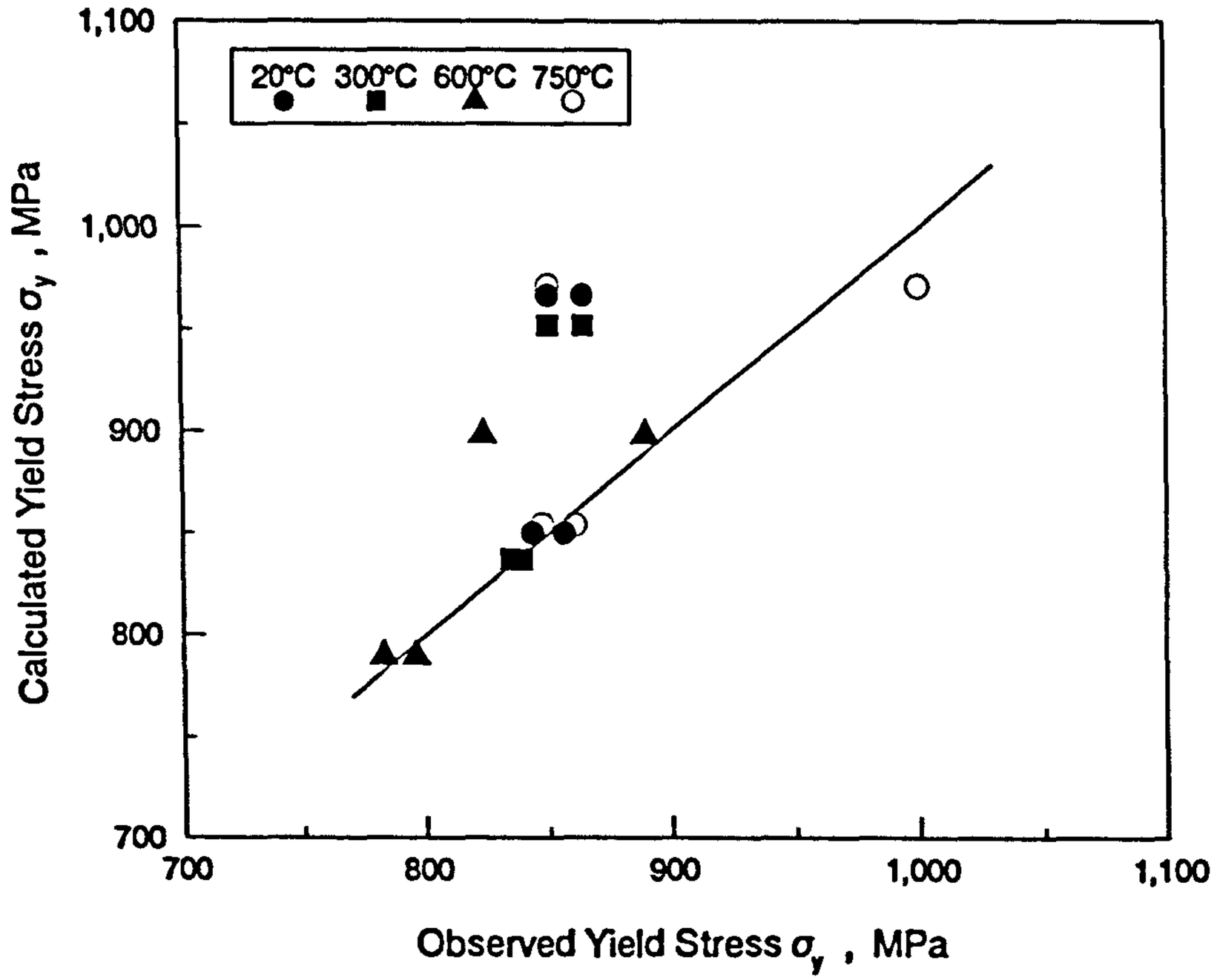

Fig.6.9. Comparison Between Observed and Calculated Yield Stress Using Schmid's Law

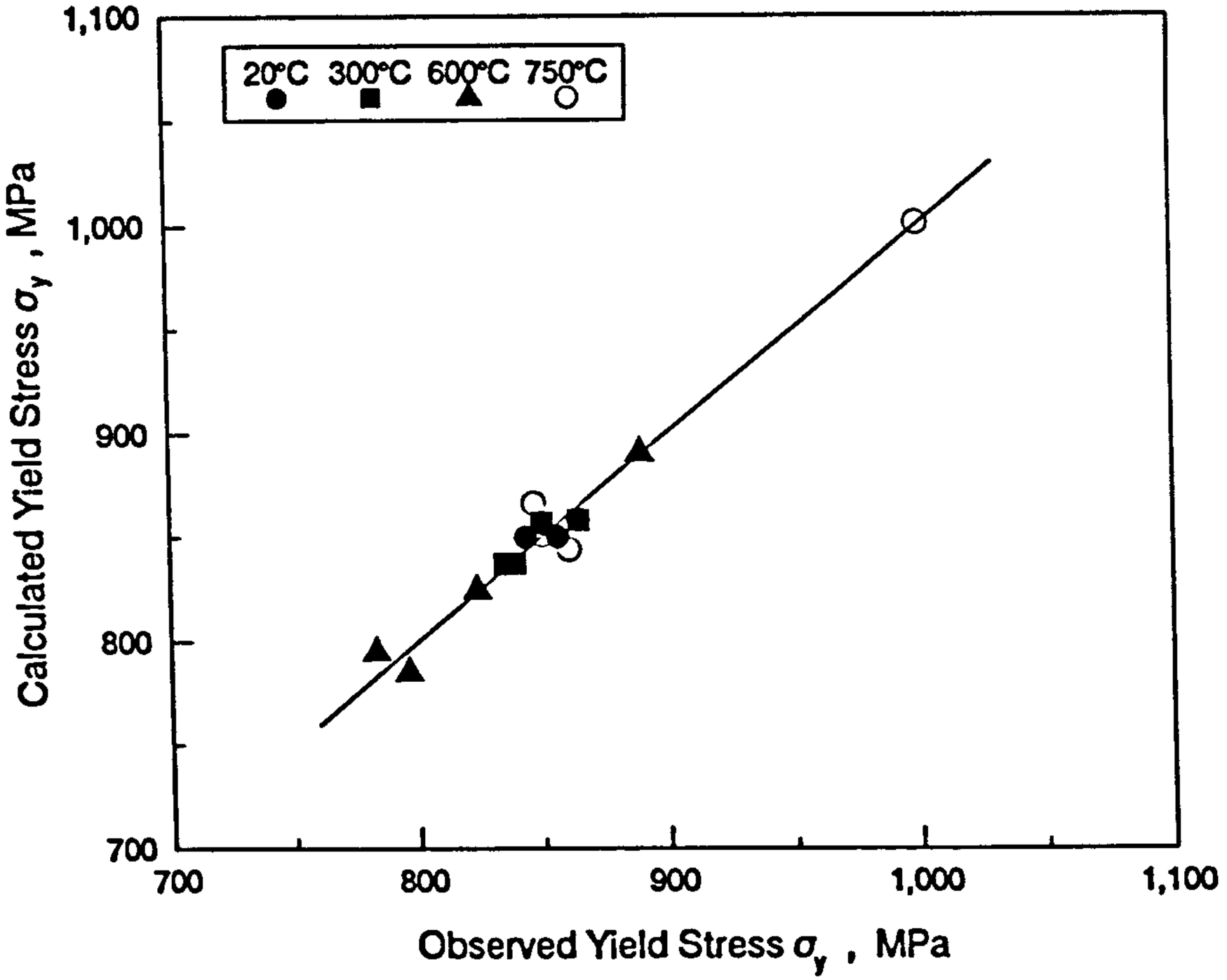

Fig.6.10. Comparison Between Observed and Calculated Yield Stress Using Cross-Slip Model

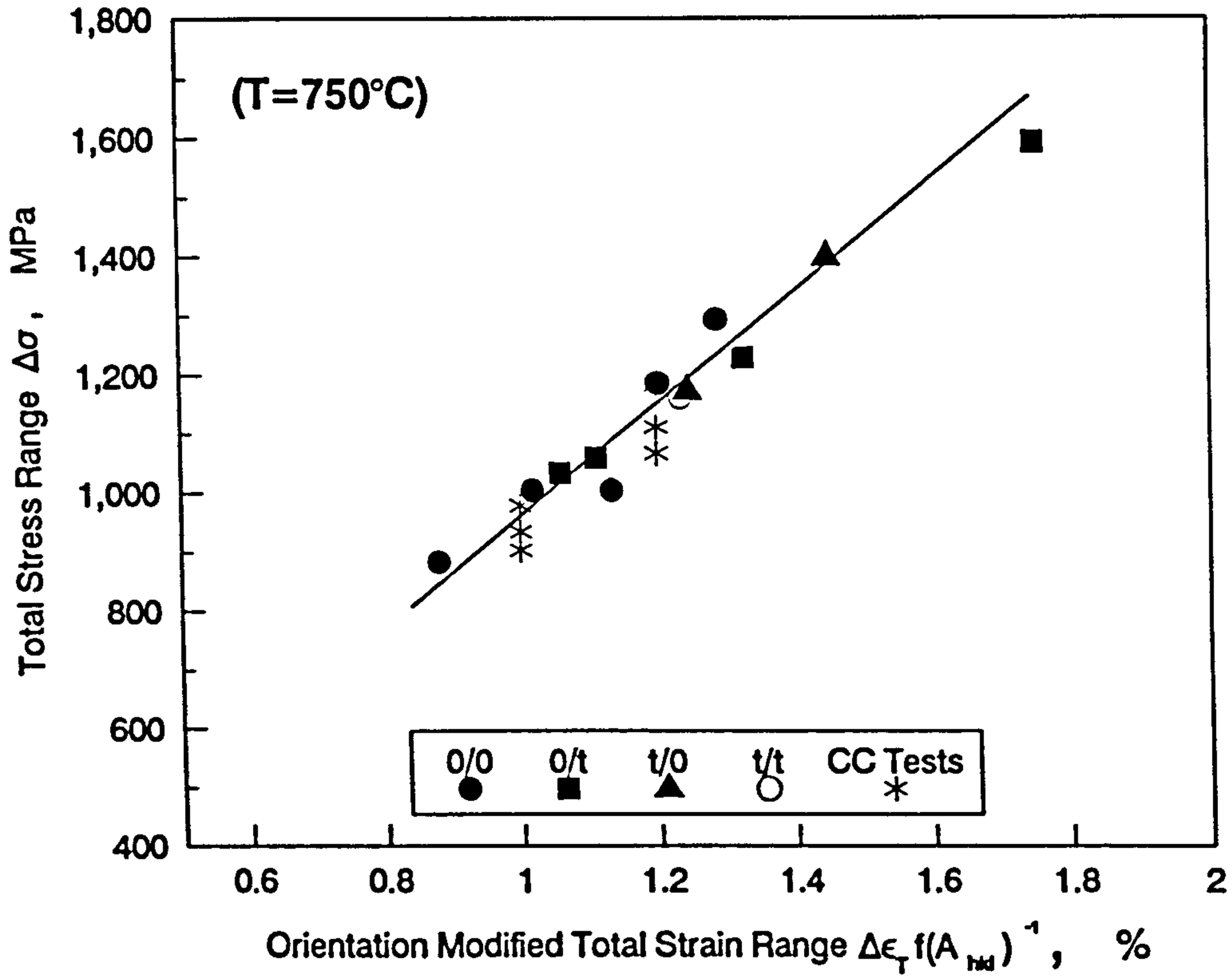

Fig.6.11a. Orientation Modified Cyclic Stress-Strain Curve at 750°C

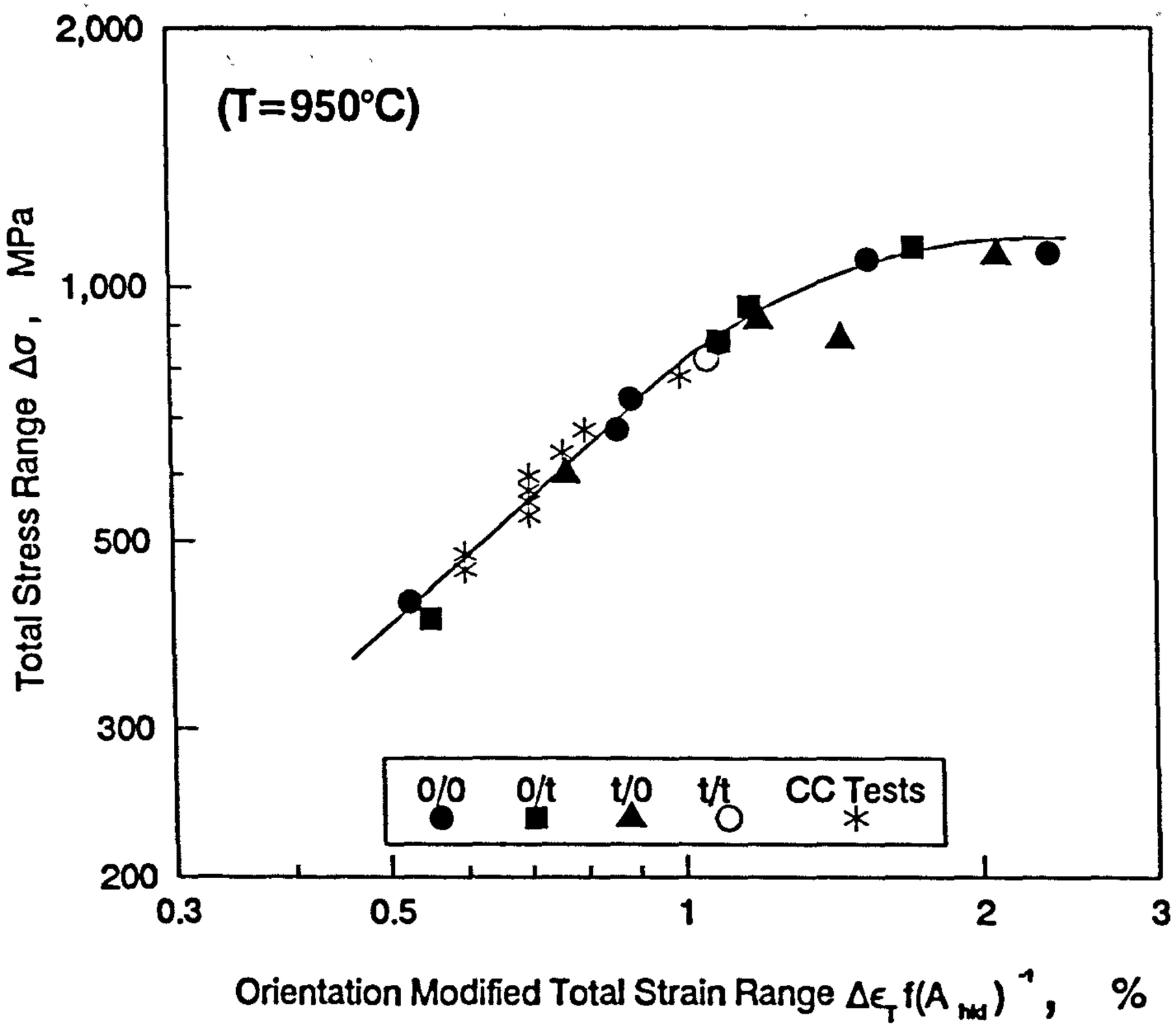

Fig.6.11b. Orientation Modified Cyclic Stress-Strain Curve at 950°C

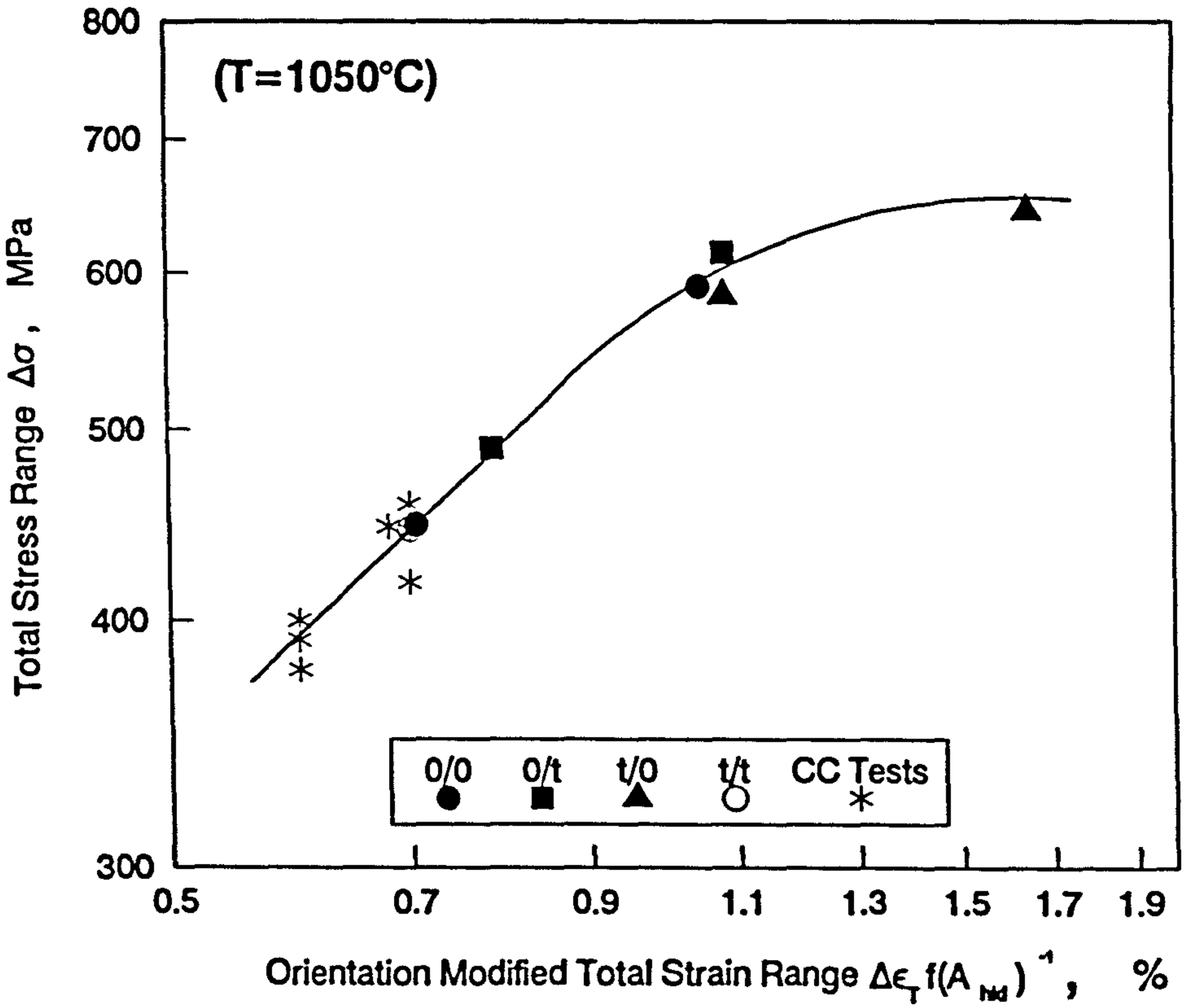

Fig.6.11c. Orientation Modified Cyclic Stress-Strain Curve at 1050°C

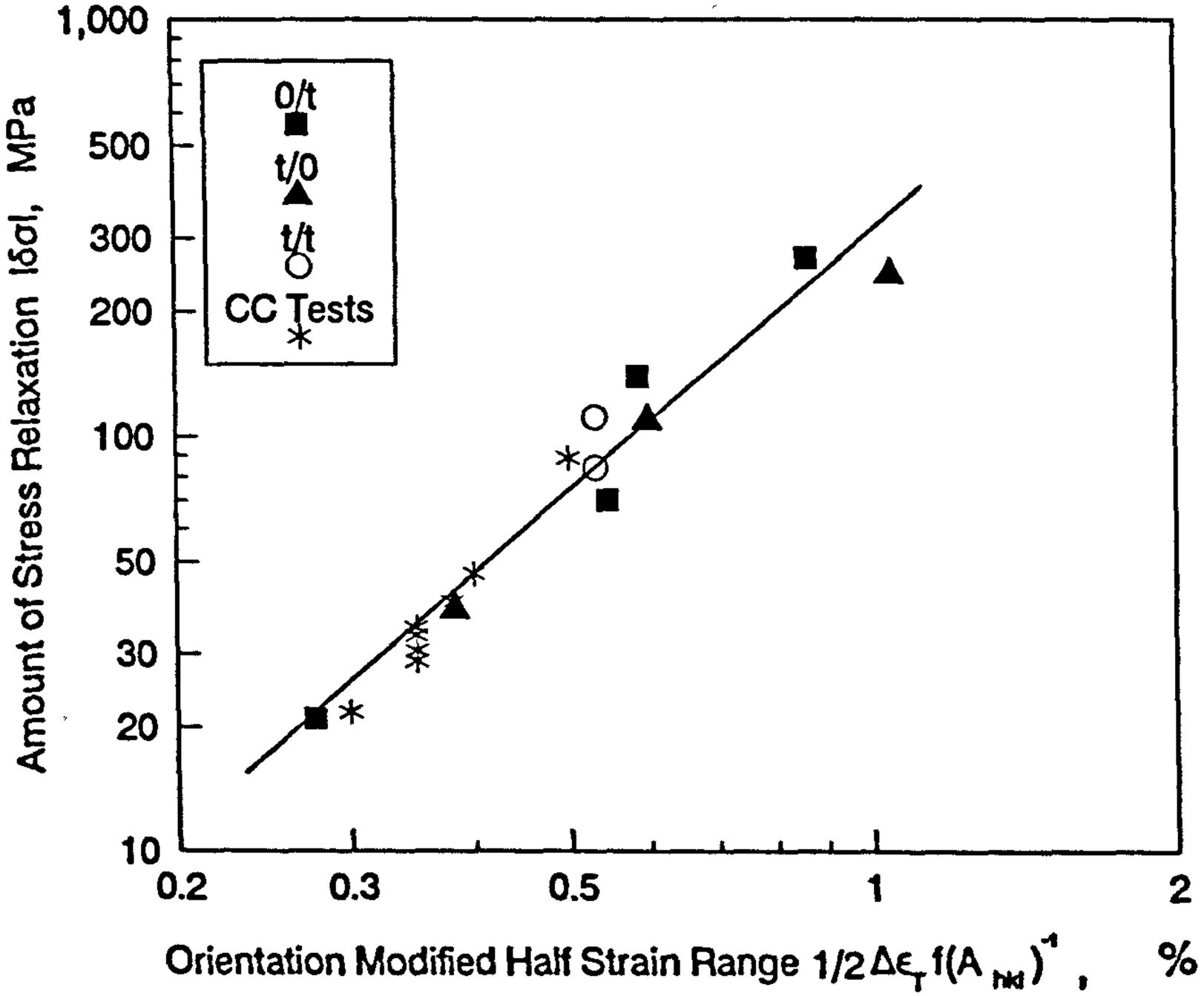

Fig.6.12. Orientation Modified Total Stress Relaxation at 950°C

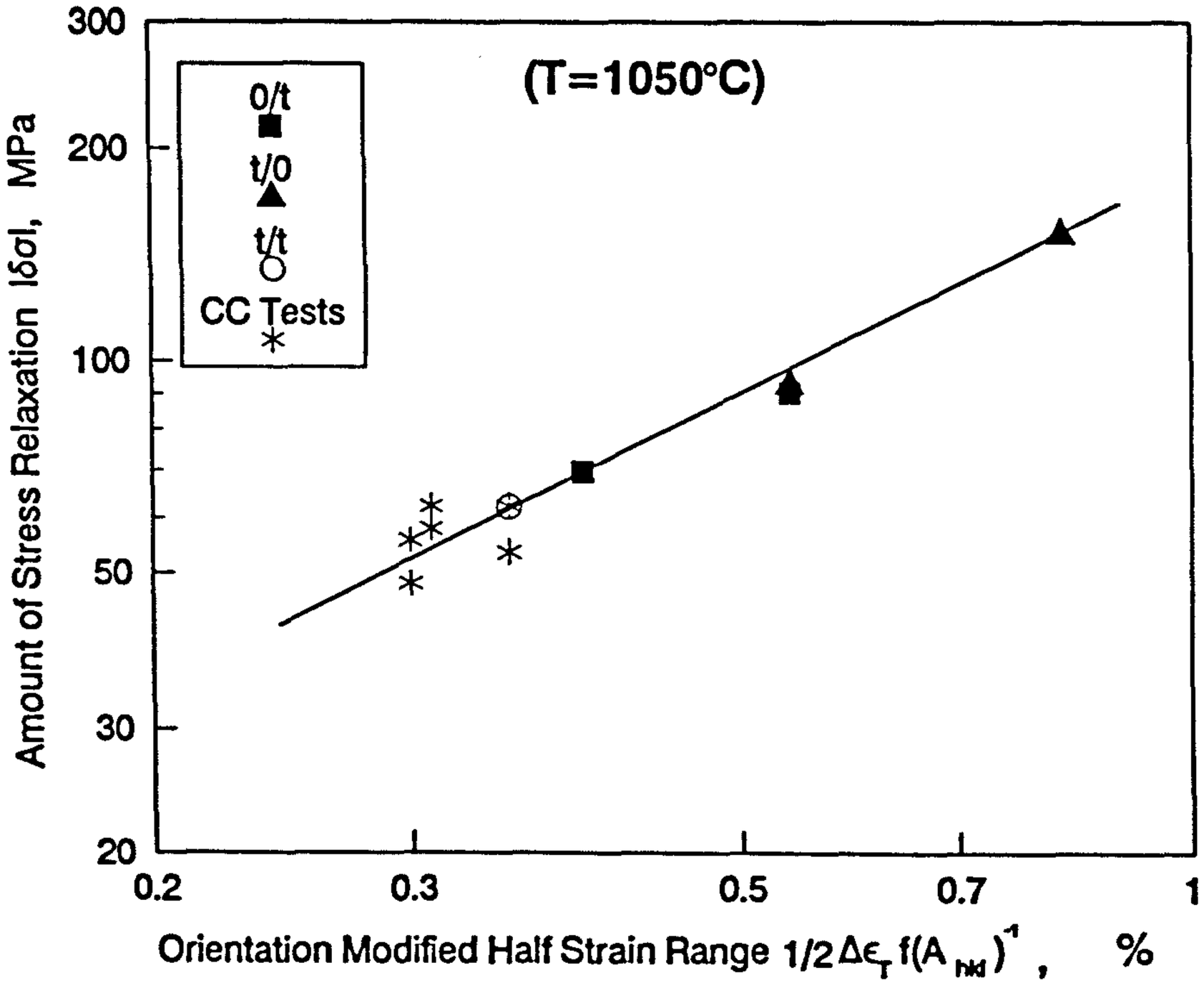

Fig.6.13. Orientation Modified Total Stress Relaxation at 1050°C

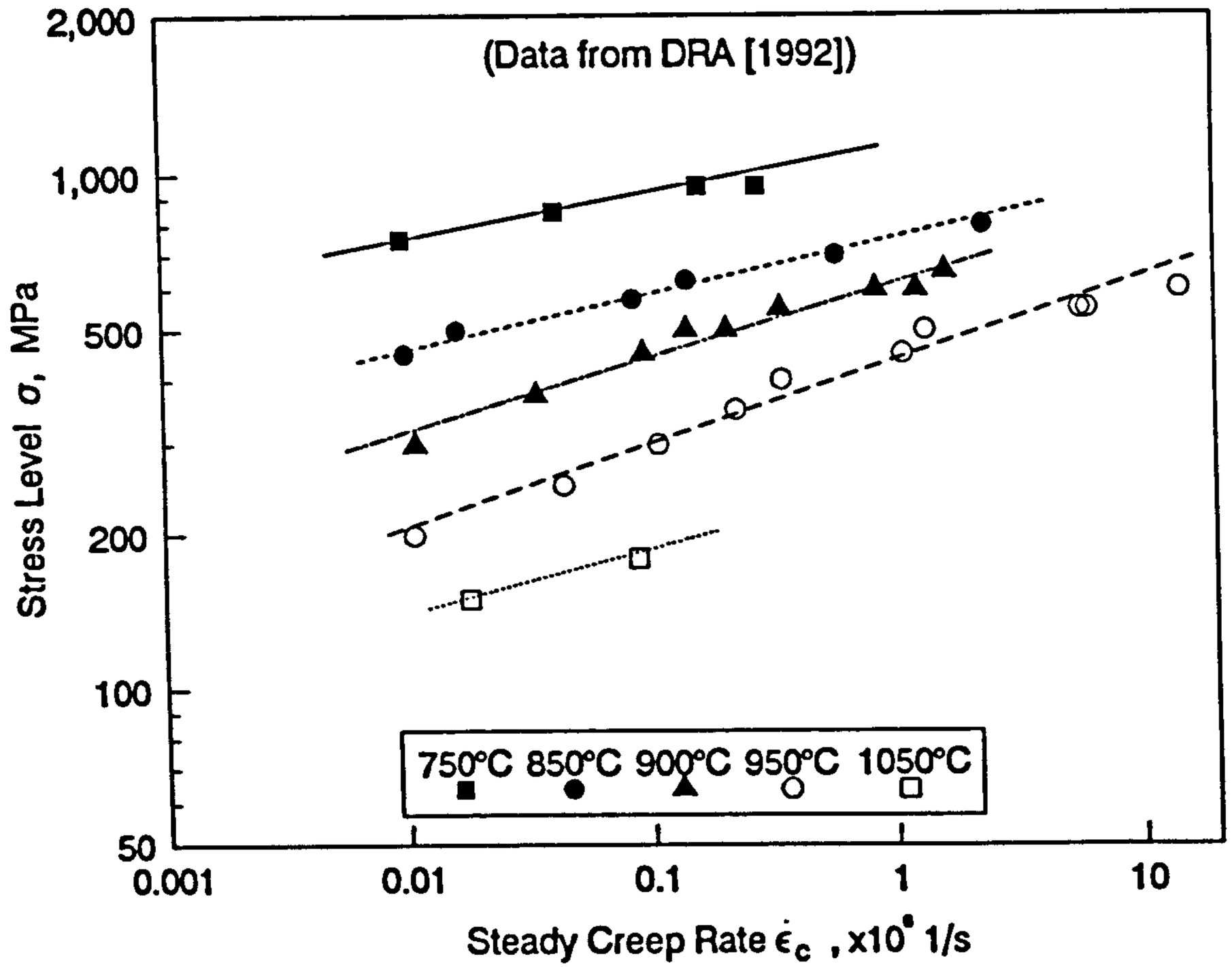

Fig.6.14. Steady State Creep Rate as a Function of Stress Level

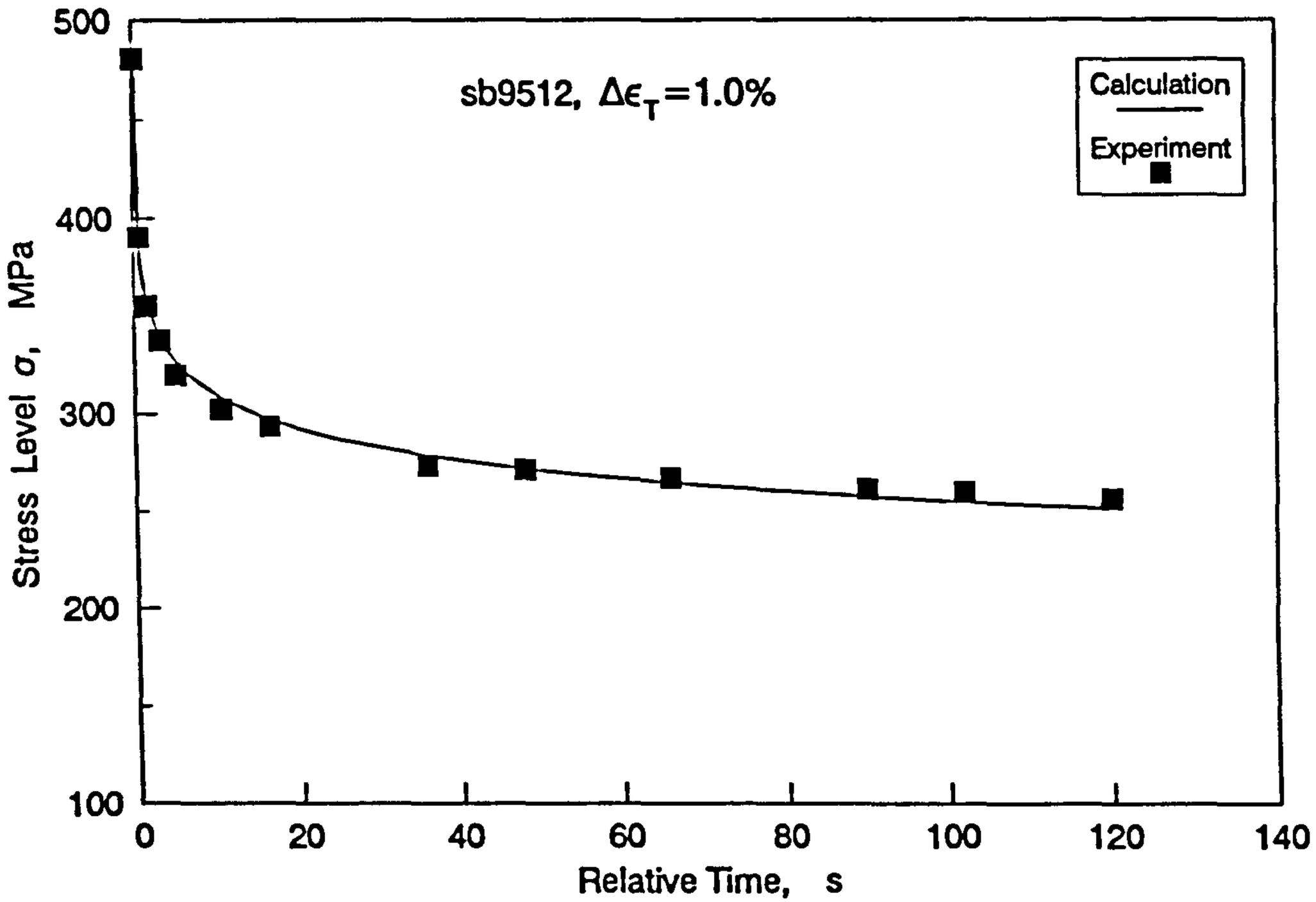

Fig.6.15. Tensile Stress Relaxation Curve at 950°C

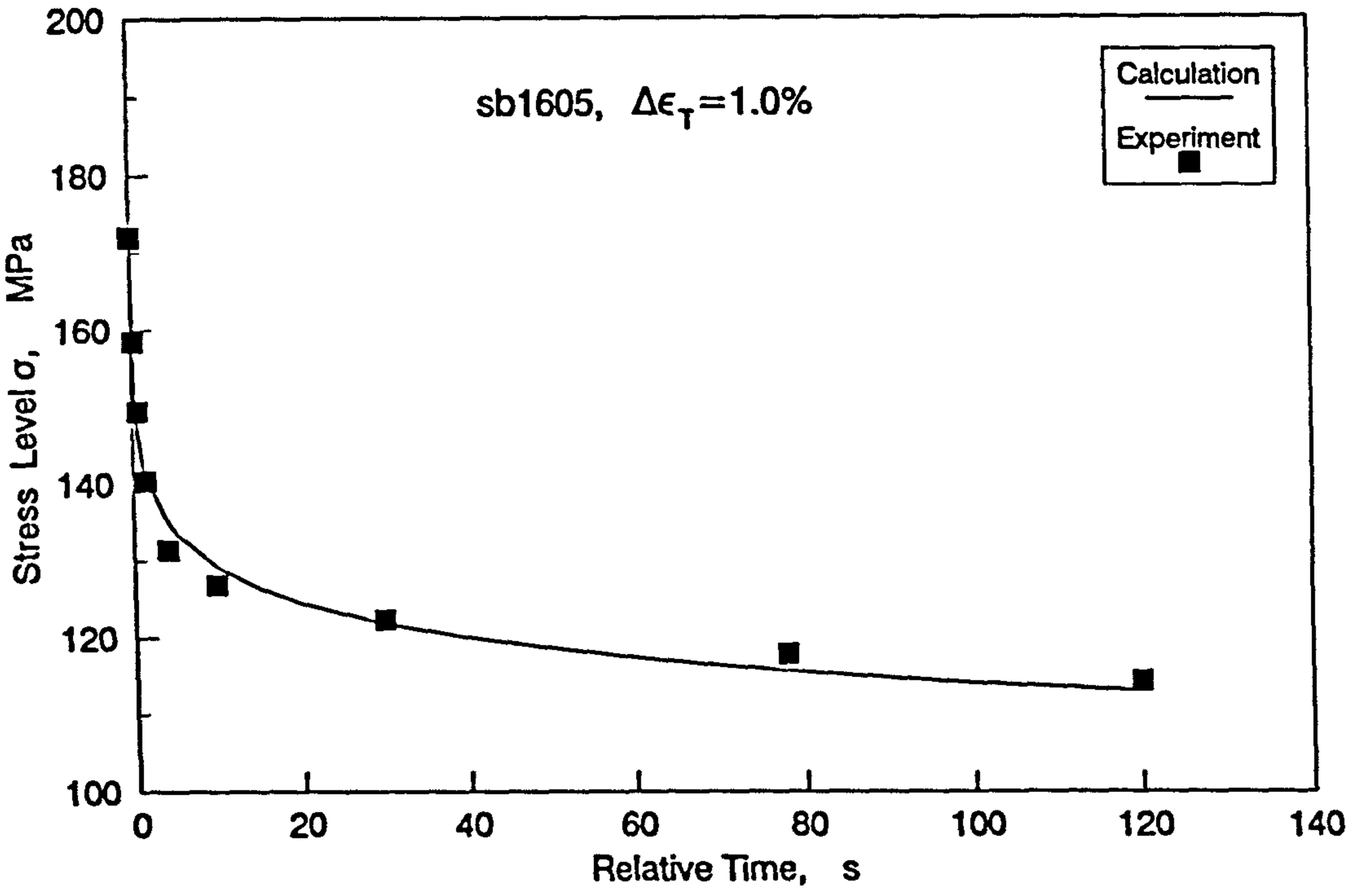

Fig.6.16. Tensile Stress Relaxation Curve at 1050°C

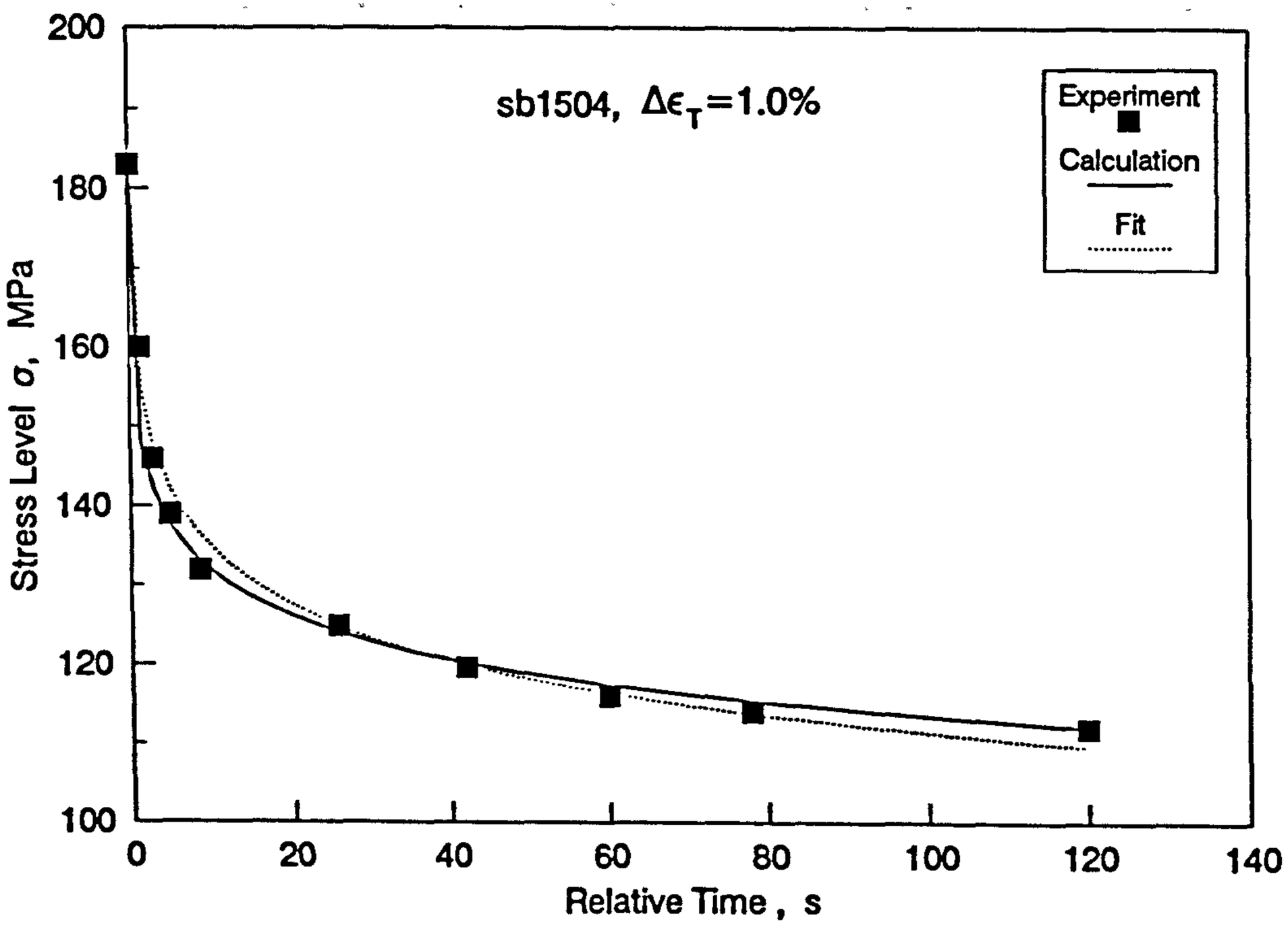

Fig.6.17. Compressive Stress Relaxation Curve at 1050°C

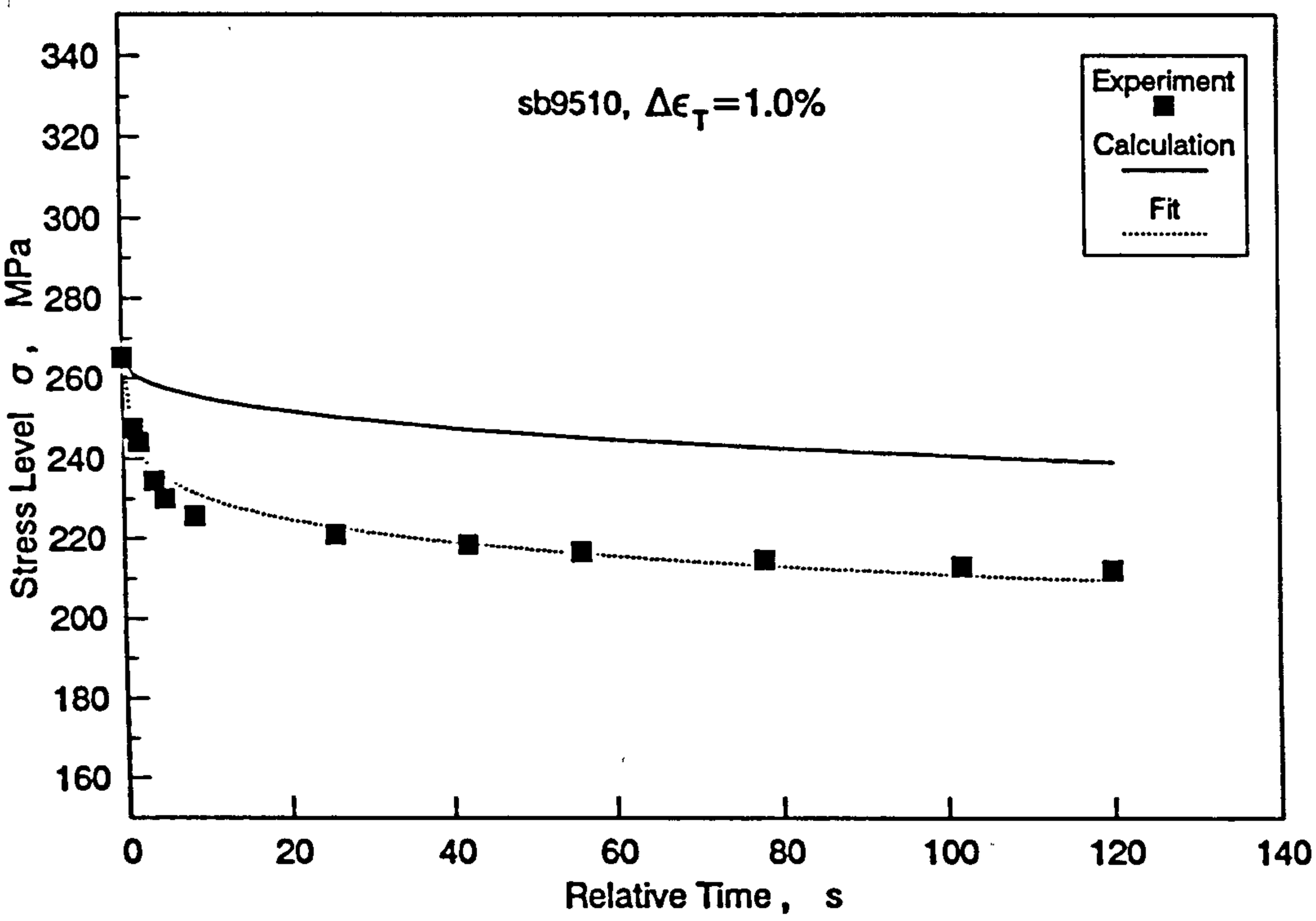

Fig.6.18. Compressive Stress Relaxation Curve at 950°C

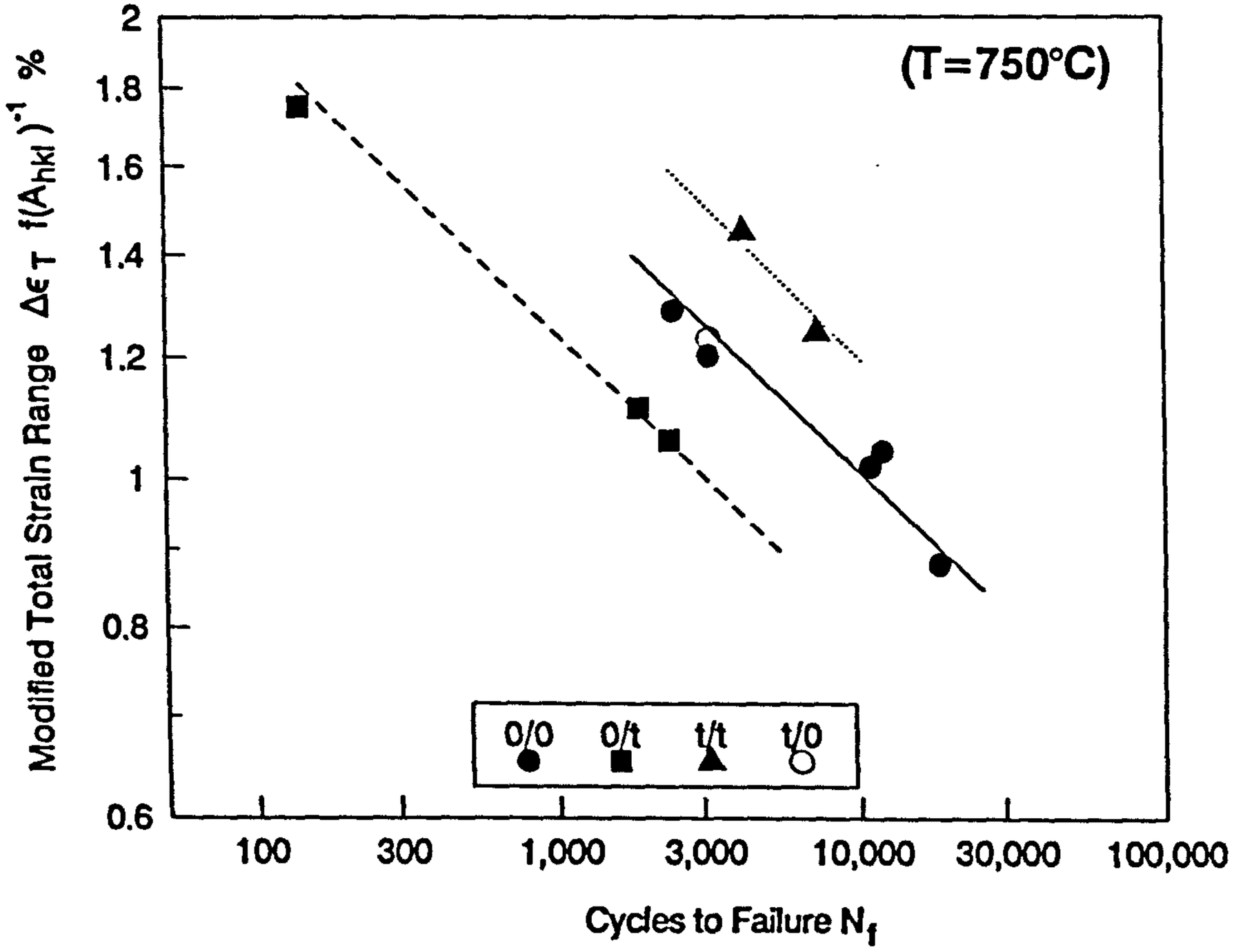

Fig.6.19a. Orientation Modified Fatigue Life at 750°C

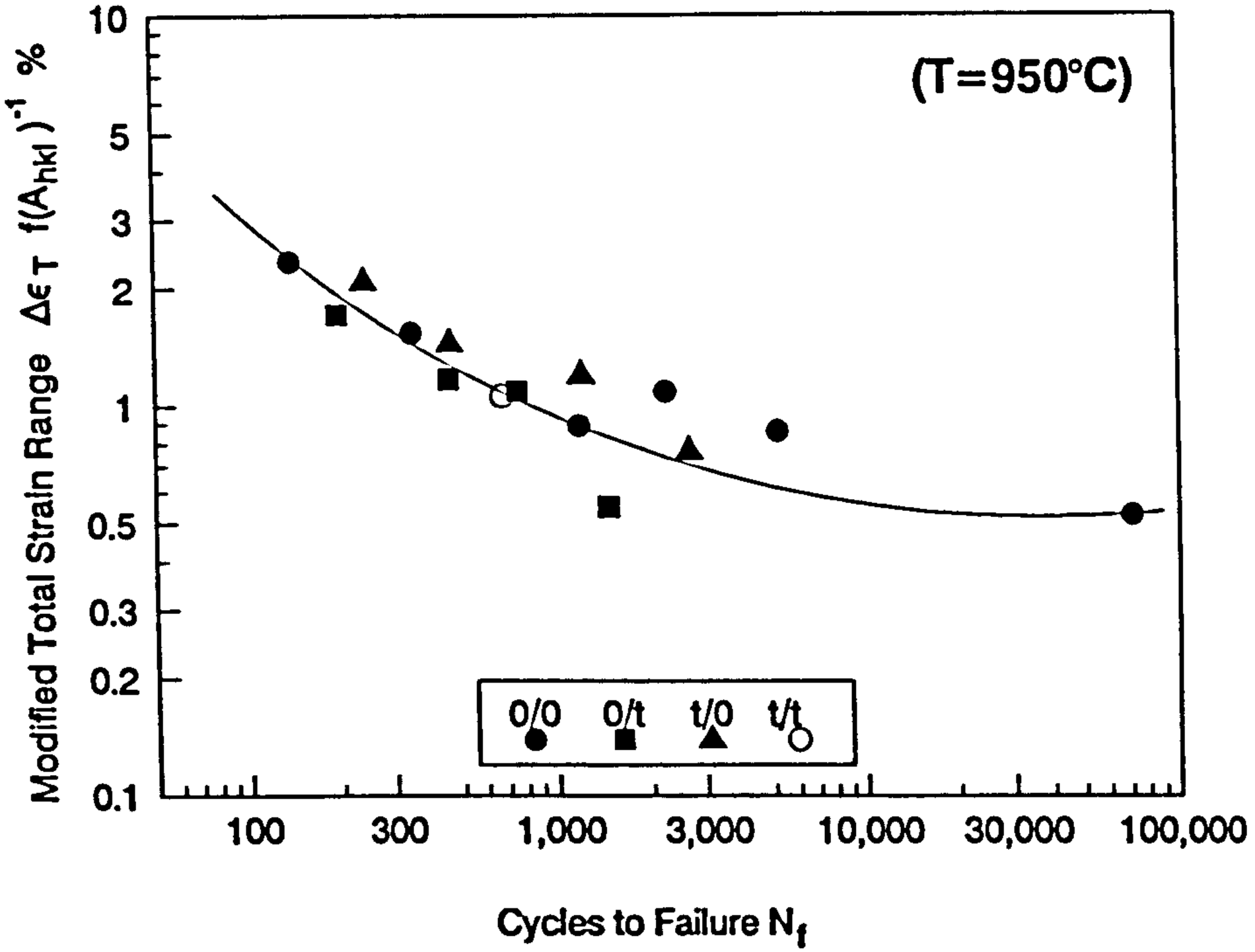

Fig.6.19b. Orientation Modified Fatigue-Creep Life at 950°C

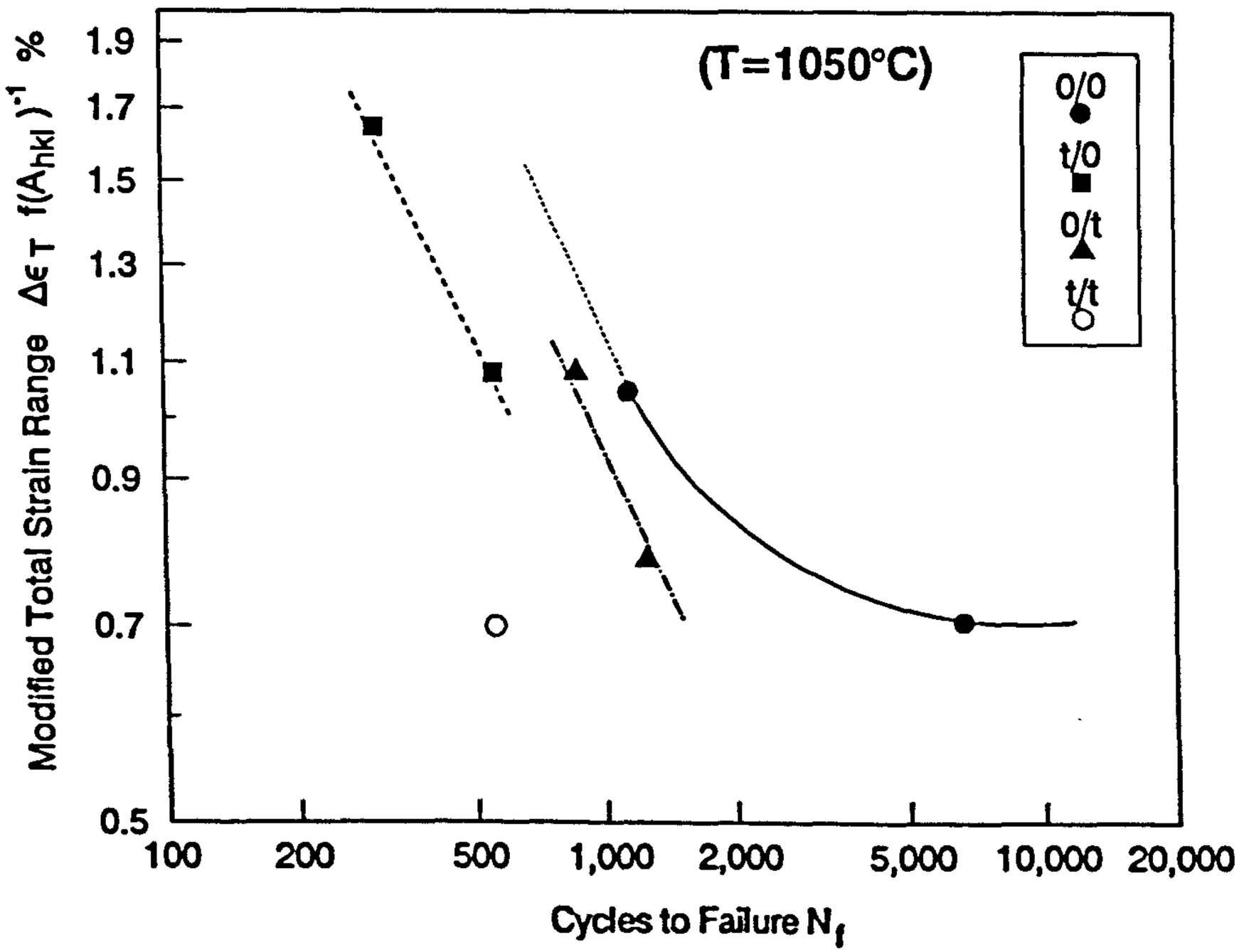

Fig.6.19c. Orientation Modified Fatigue-Creep Life at 1050°C

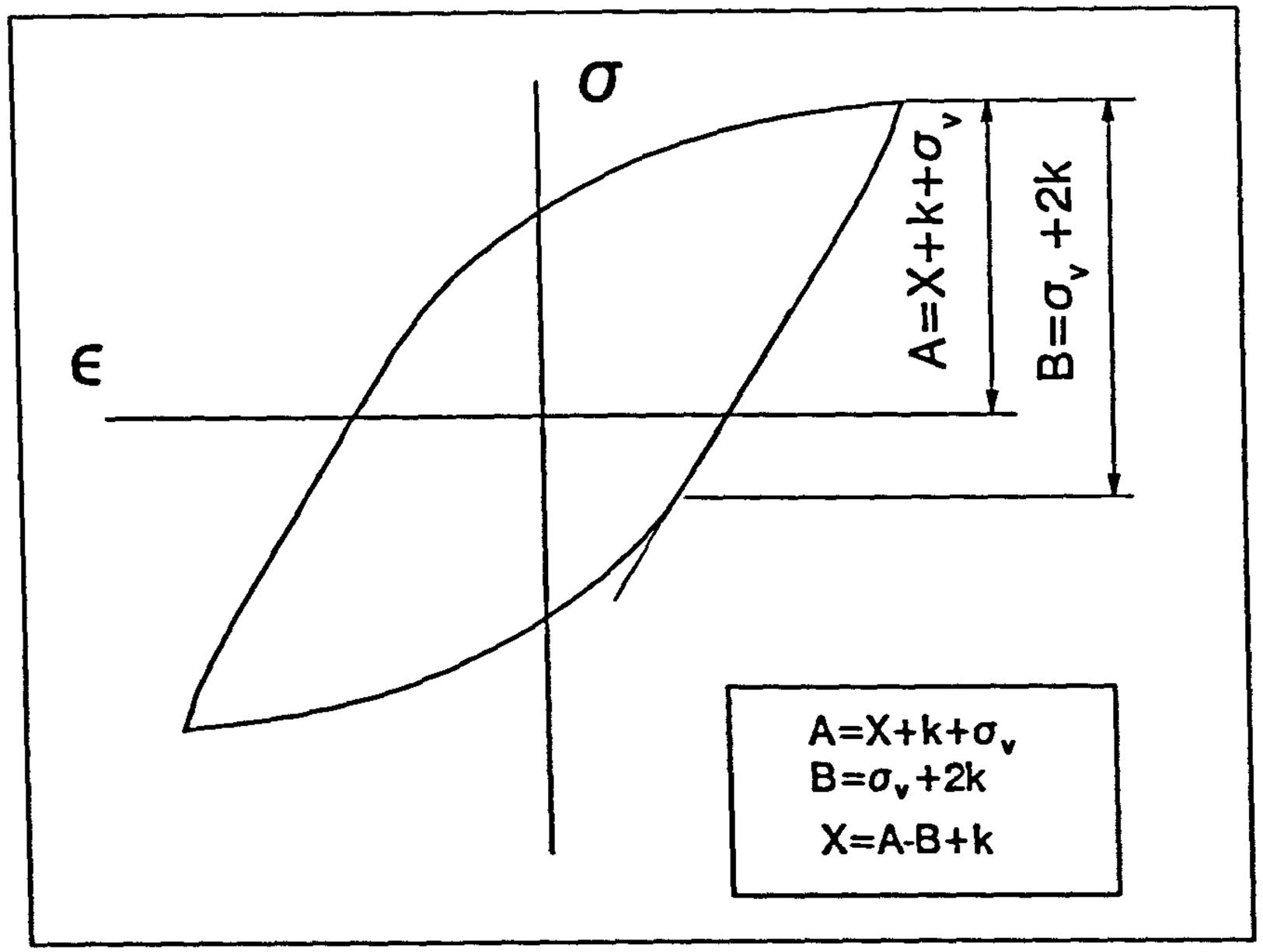

Fig.7.1. Illustration for the Determination of the Back Stress

(a). [001] Orientation

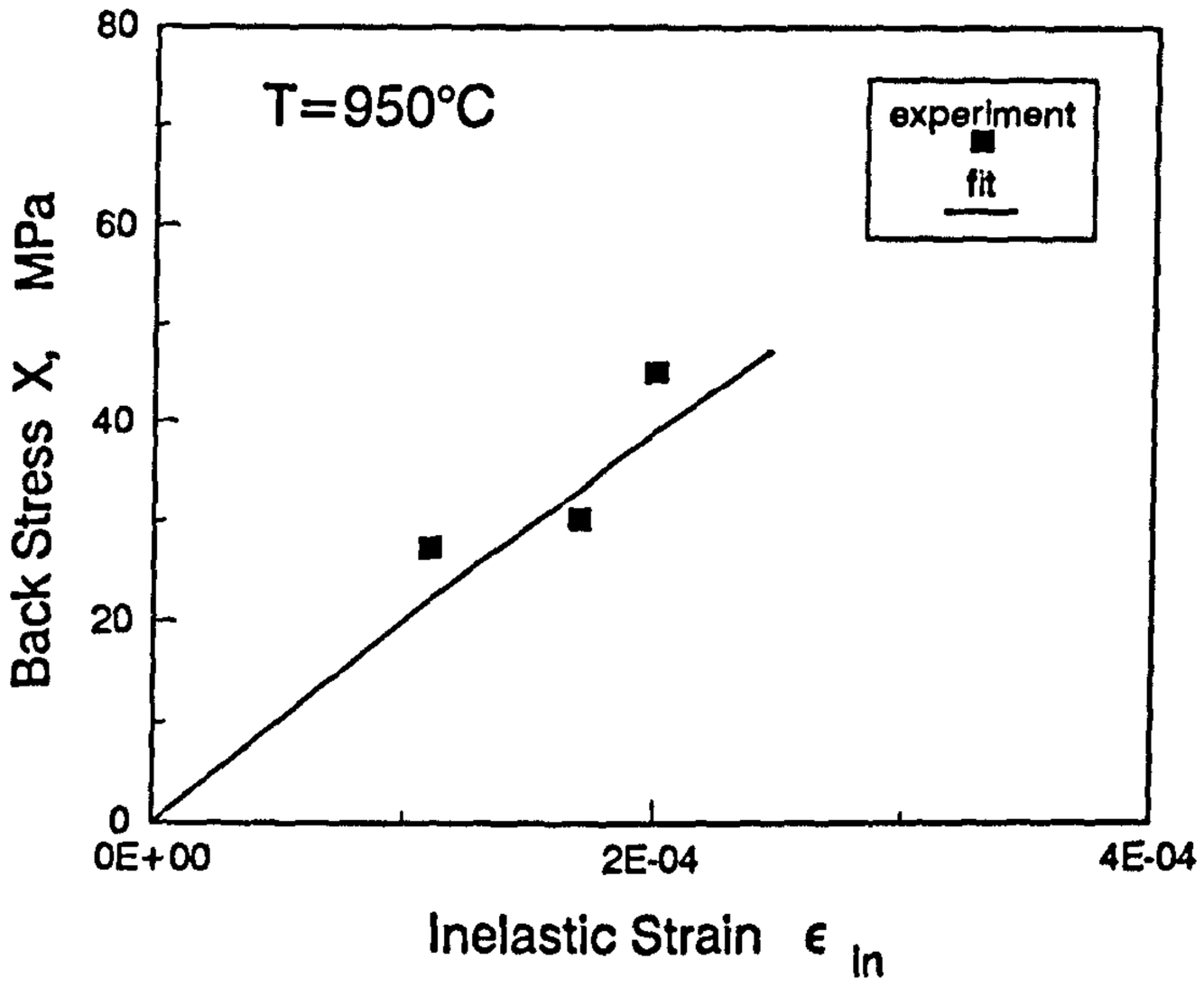

(b). [111] Orientation

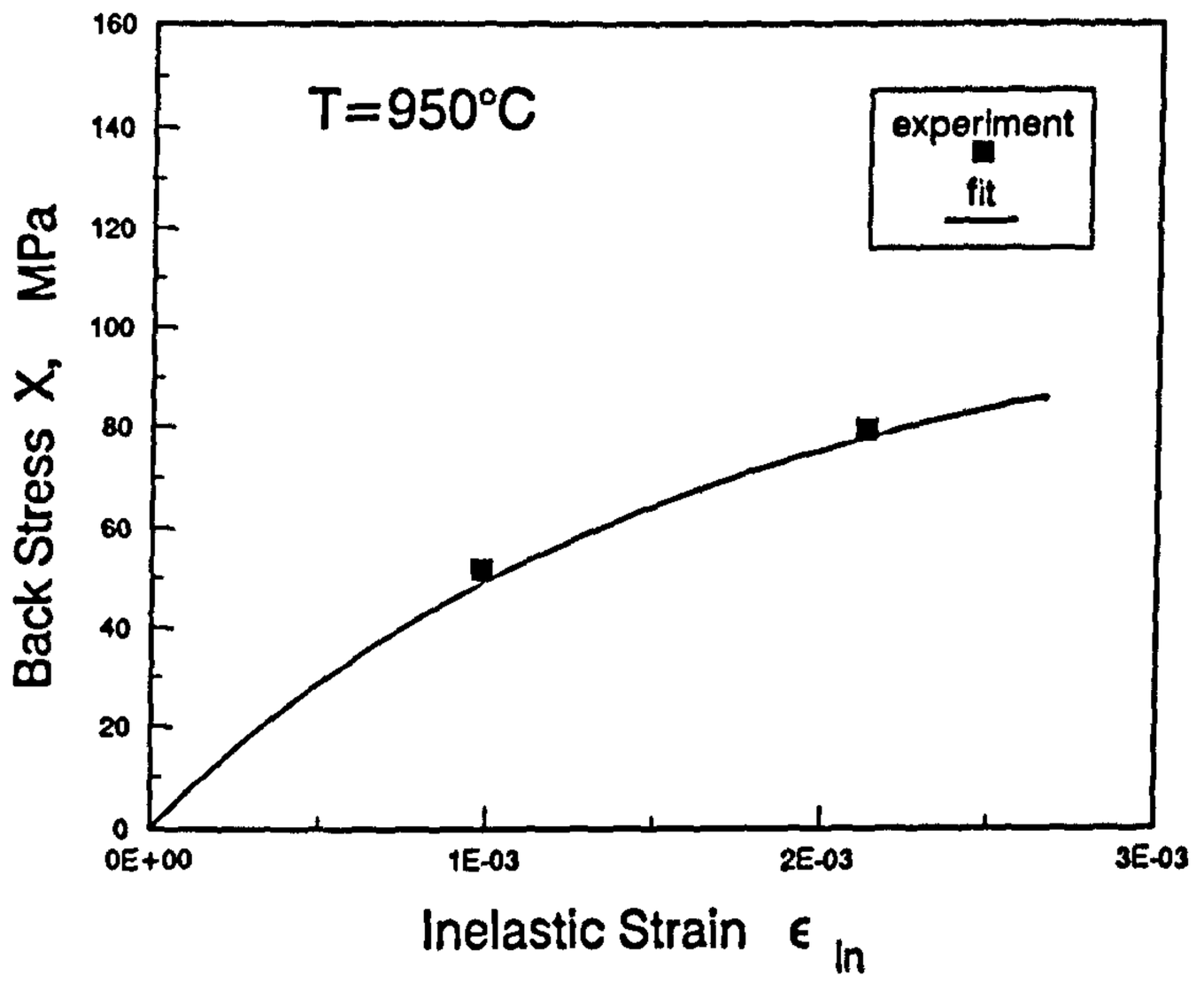

Fig.7.2. Back Stress as a Function of Inelastic Strain

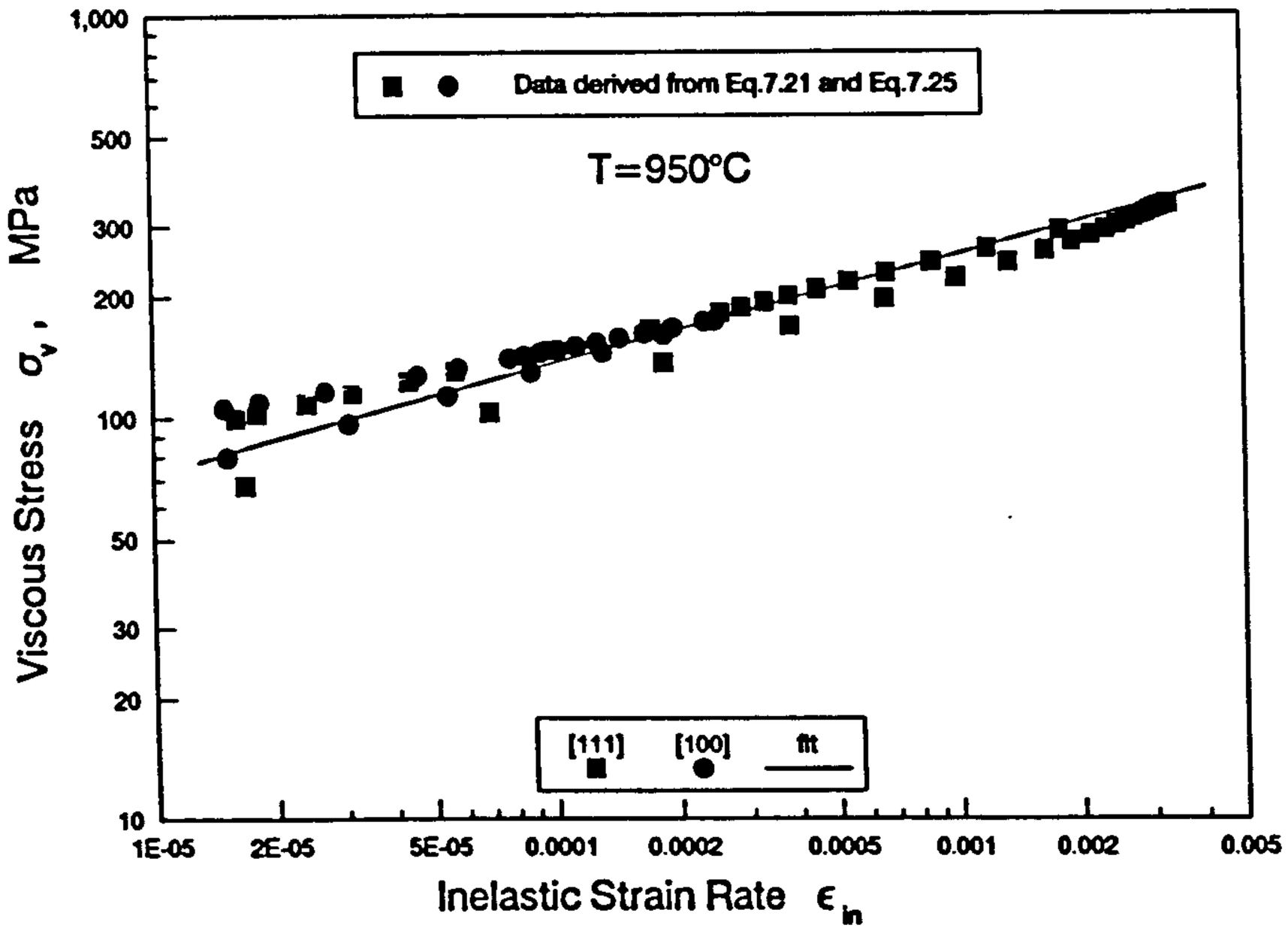

Fig.7.3. Determination of Viscosity Parameters

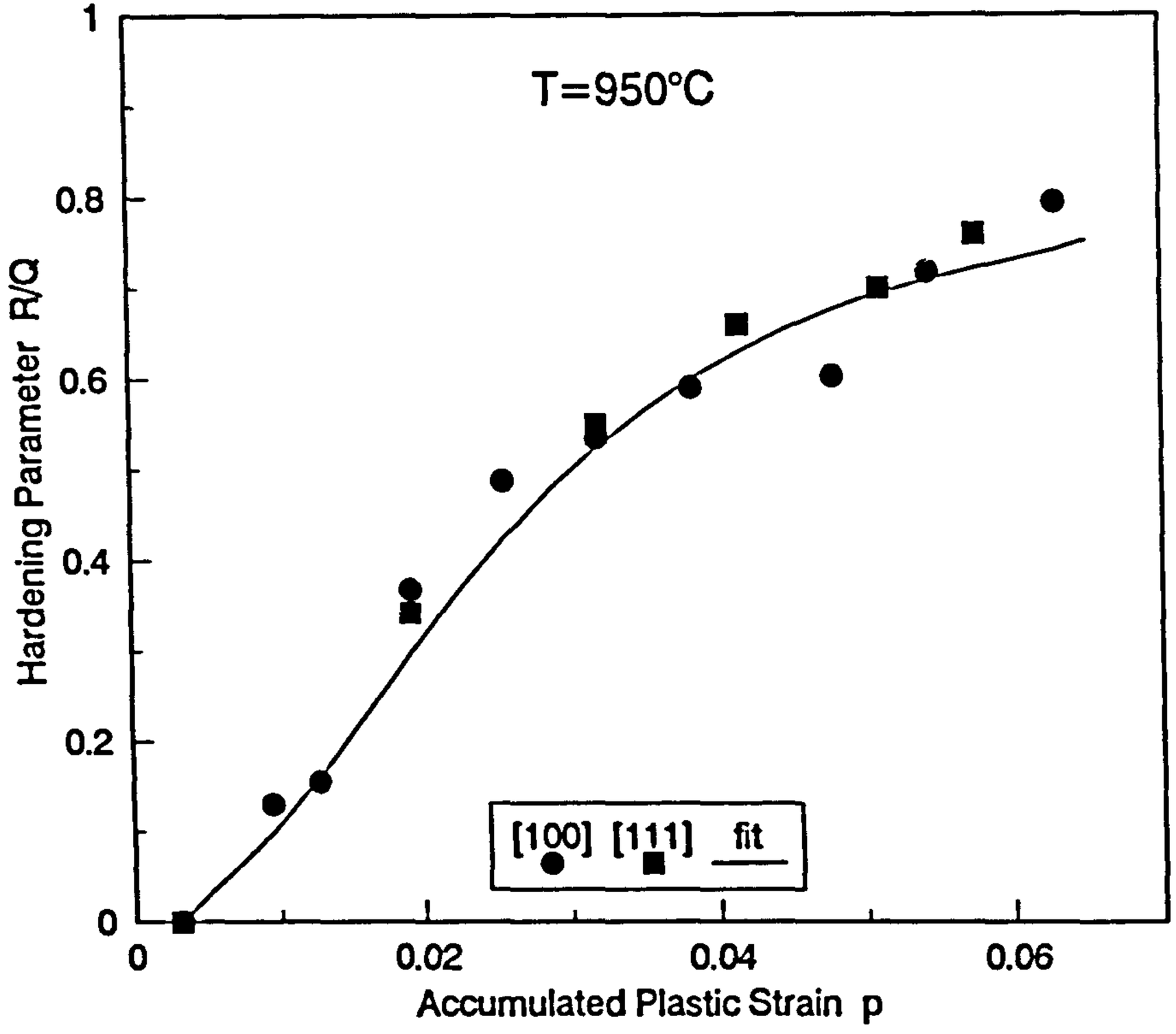

Fig.7.4. Determination of Parameter b

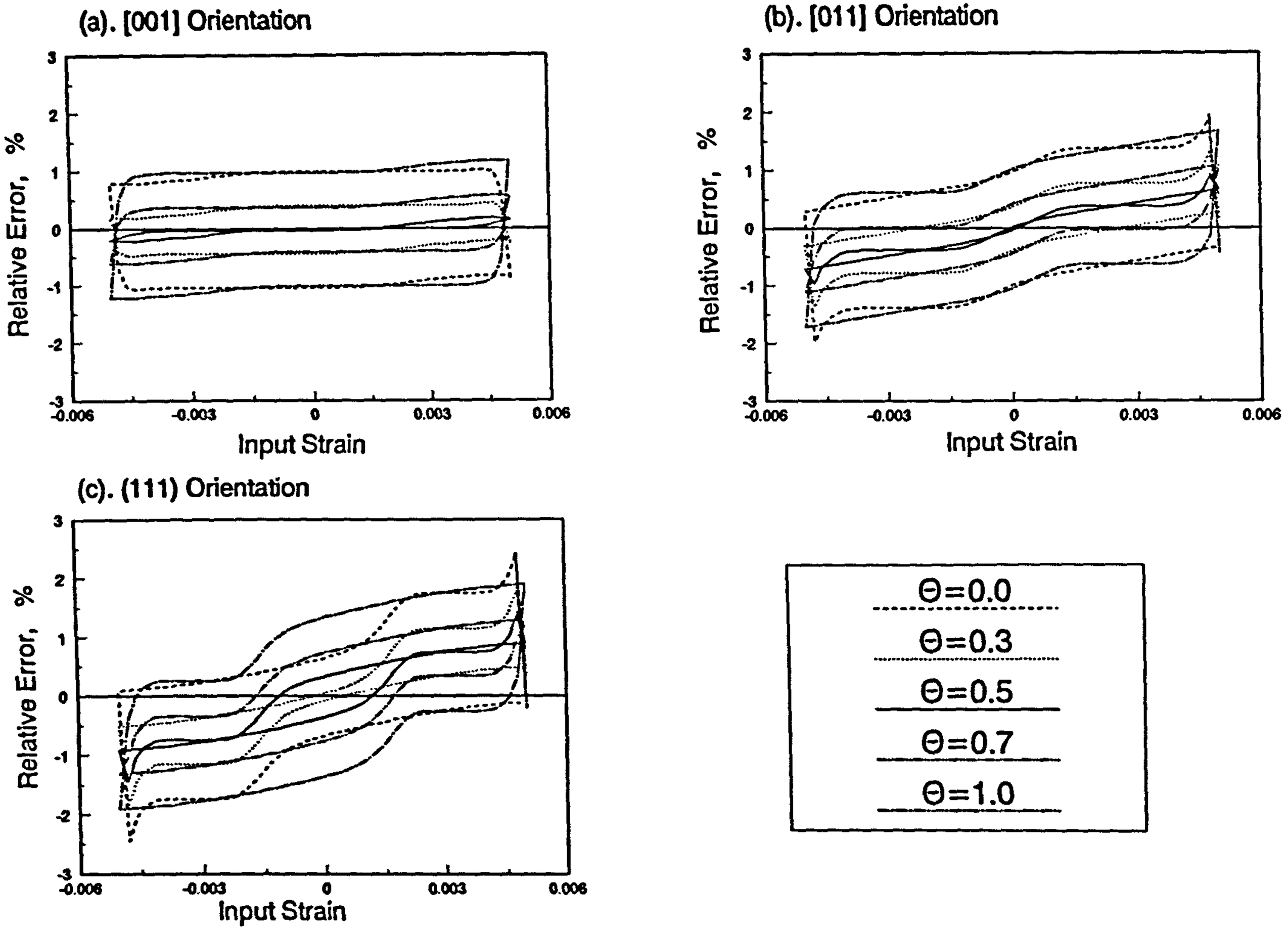

Fig.7.5. Comparison of the Simulation Errors Using Different Θ Values

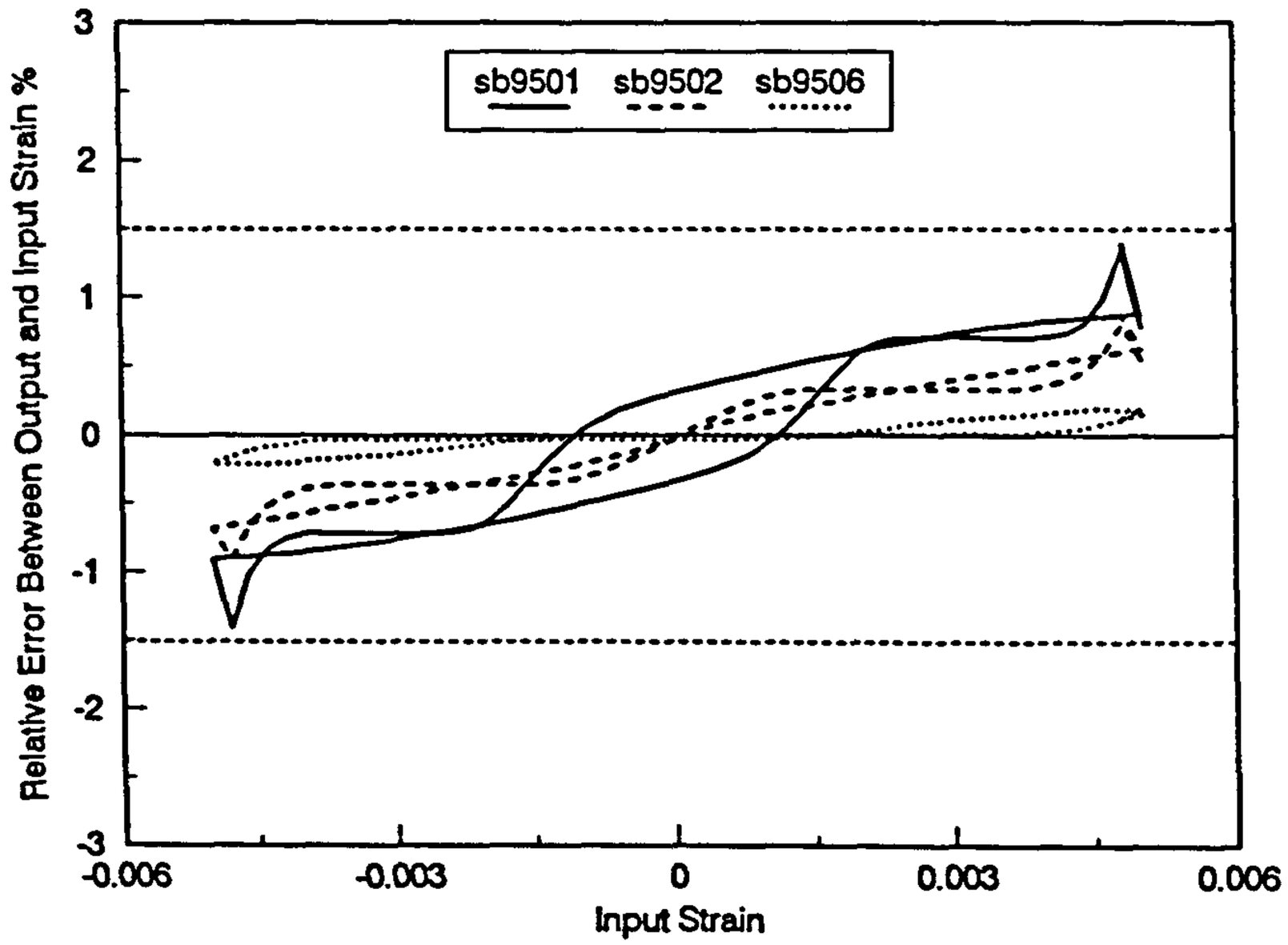

Fig.7.6. Simulation Errors for Different Tests

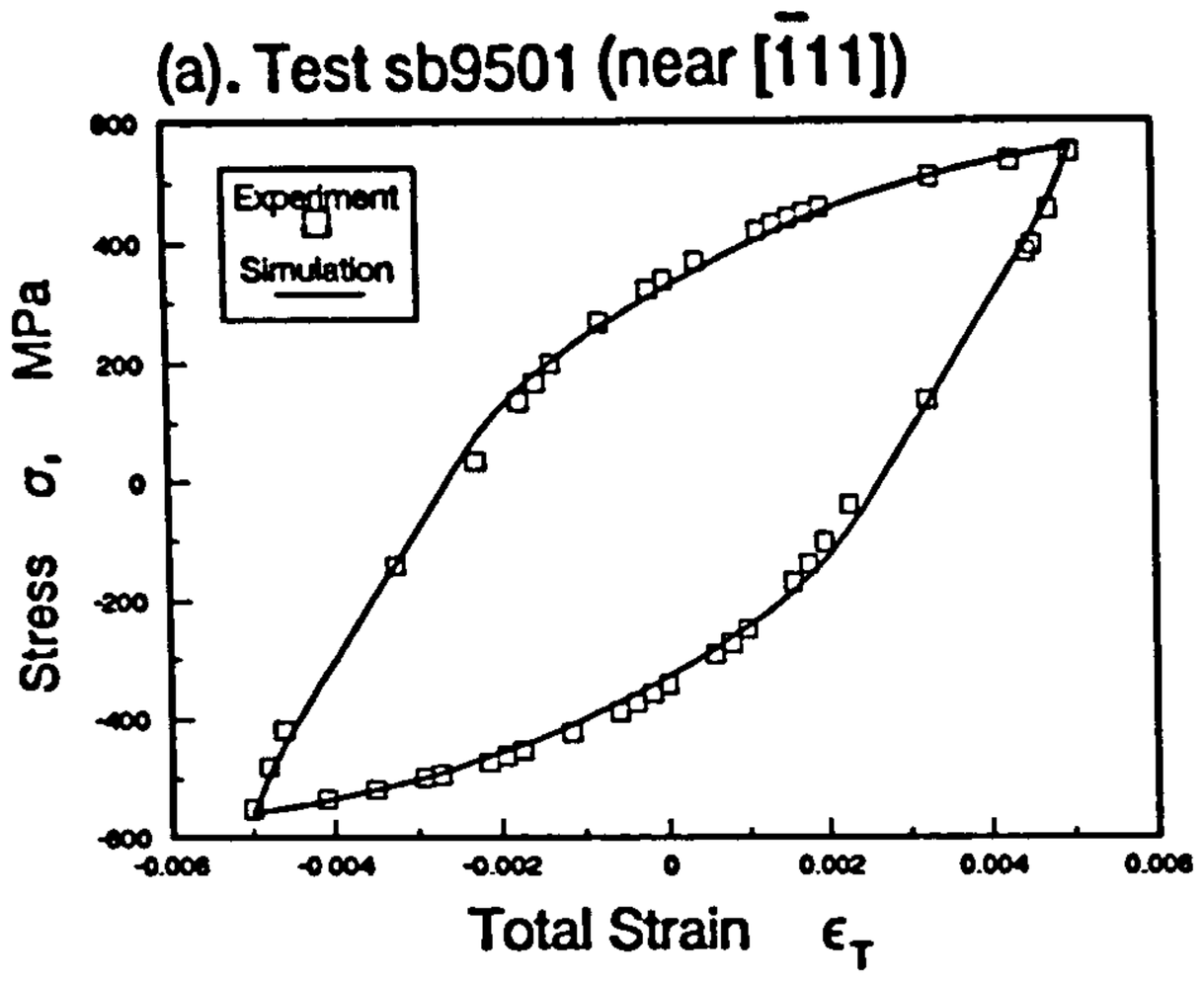

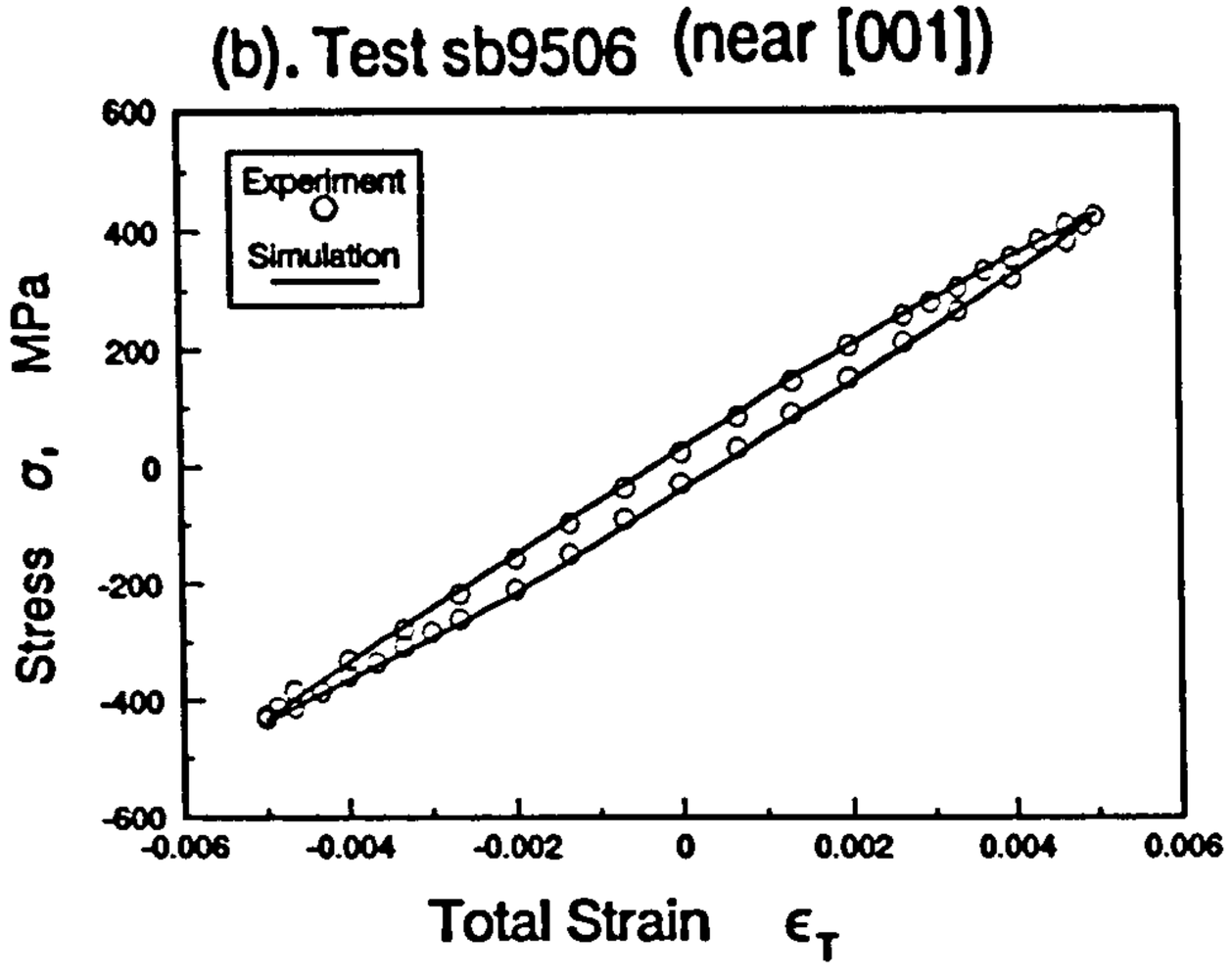

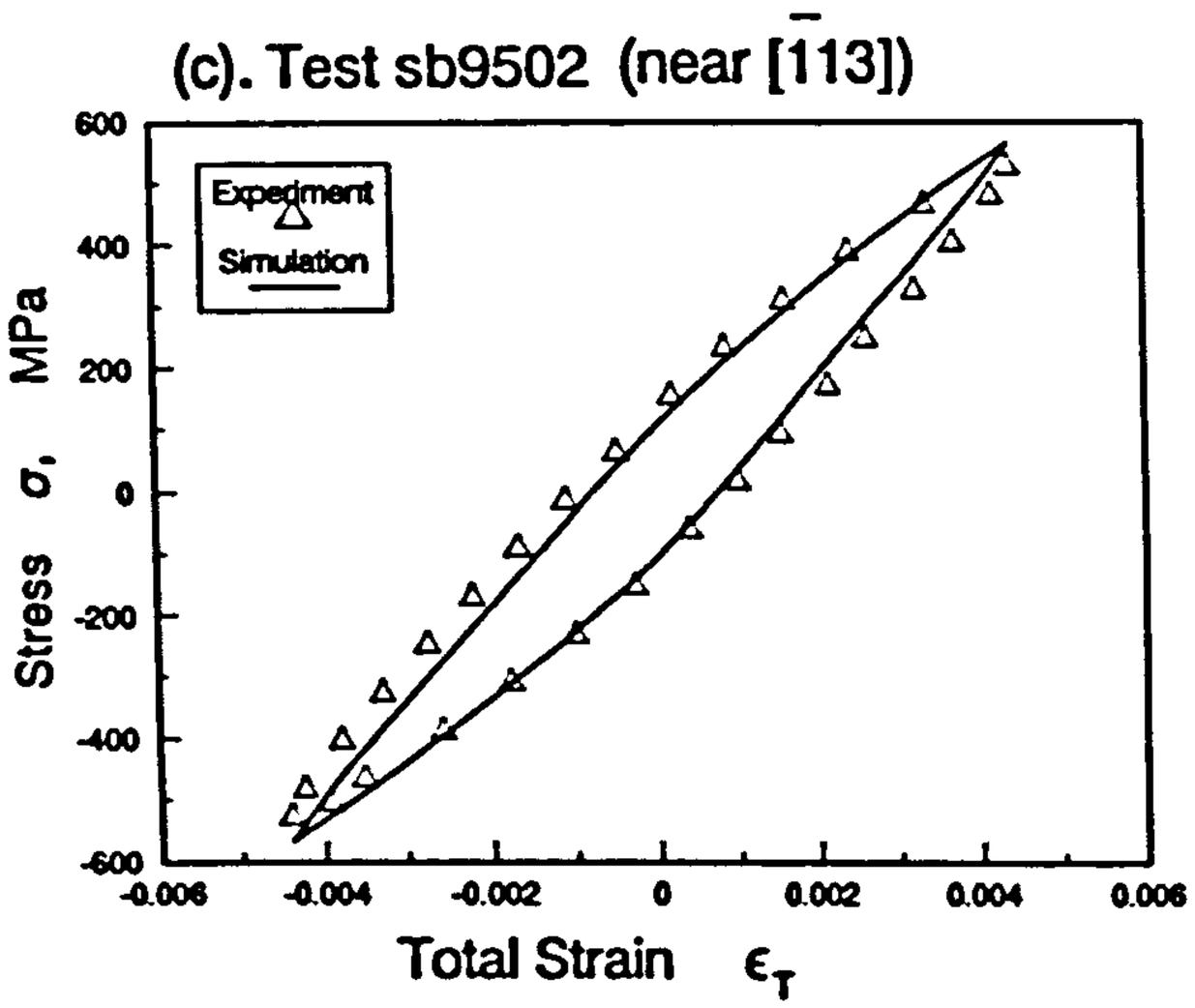

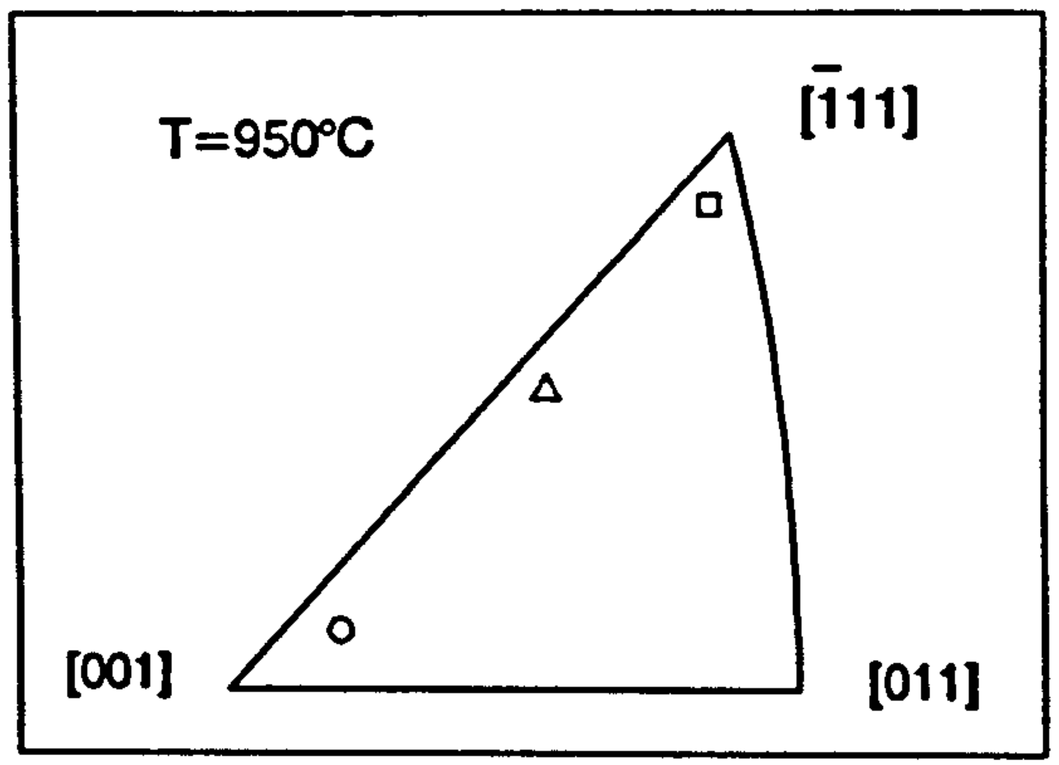

Fig.7.7. Comparison Between Experimental and Simulation Results for Continuous Cycling Tests with Different Orientations

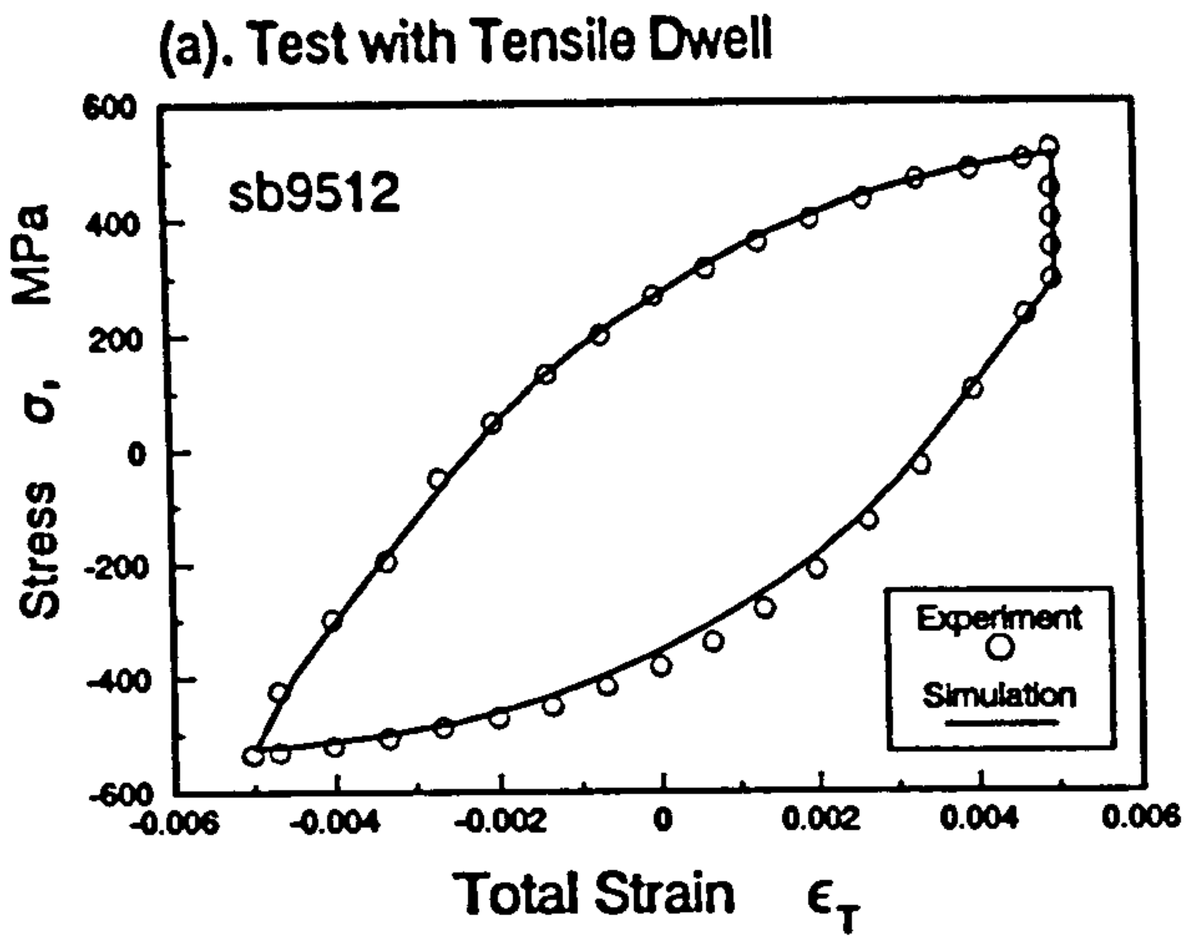

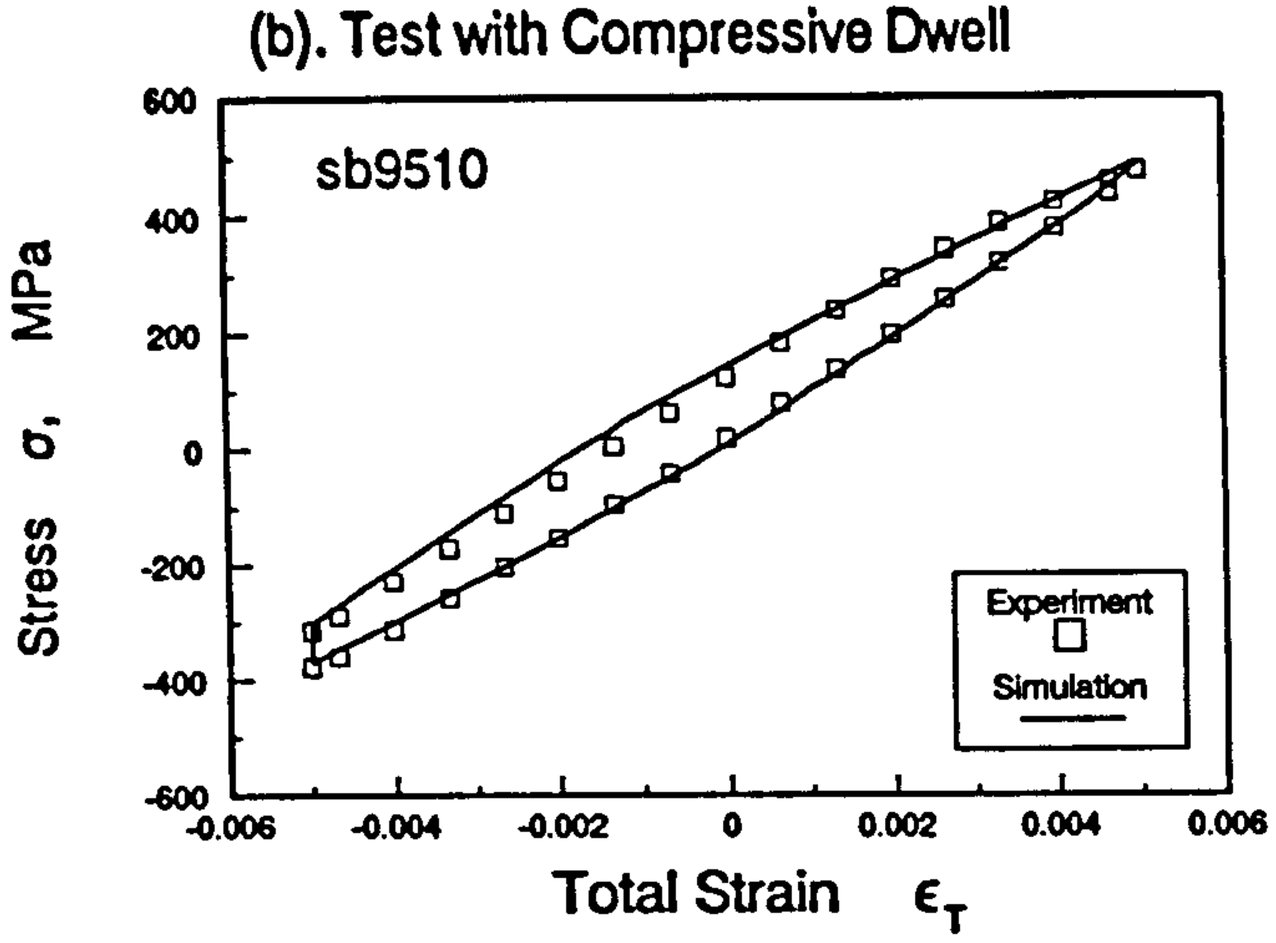

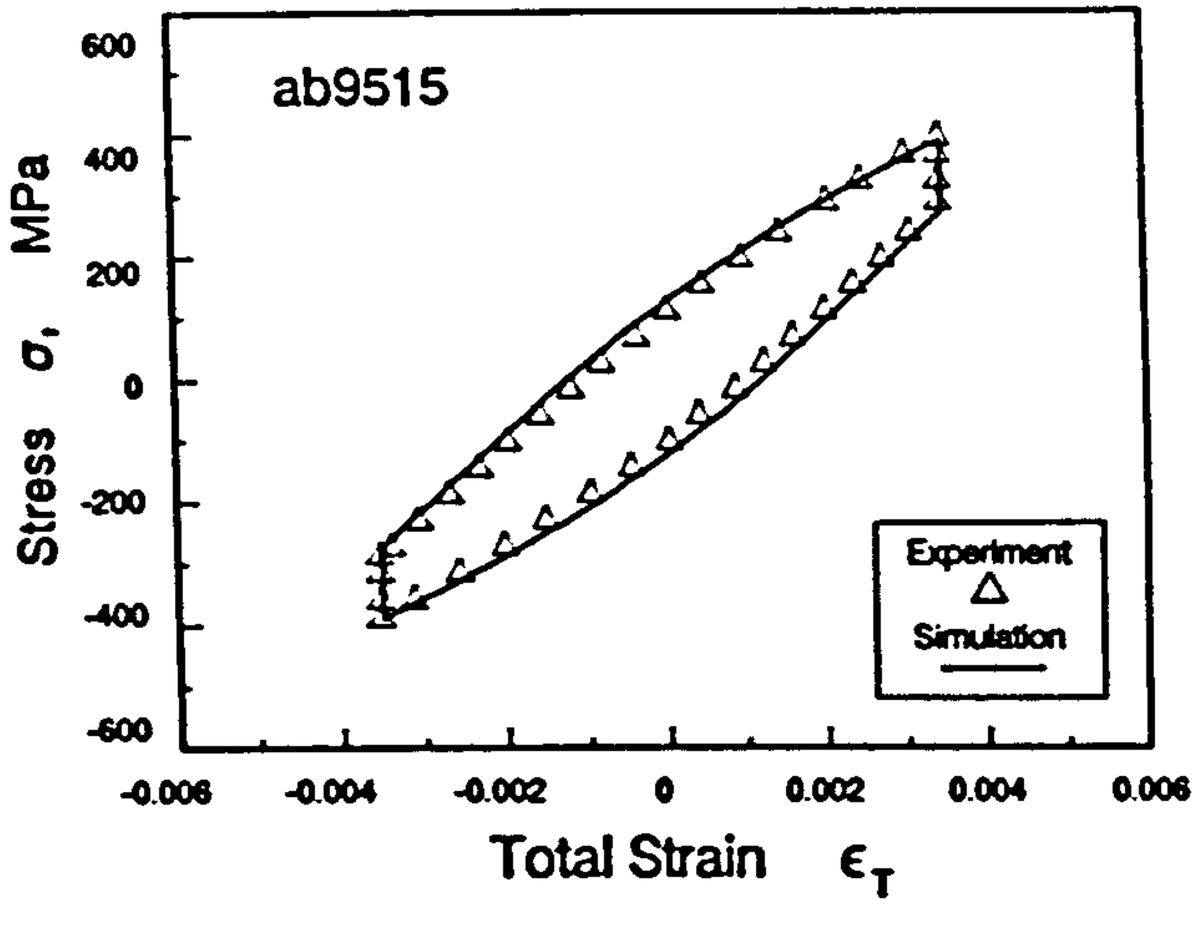

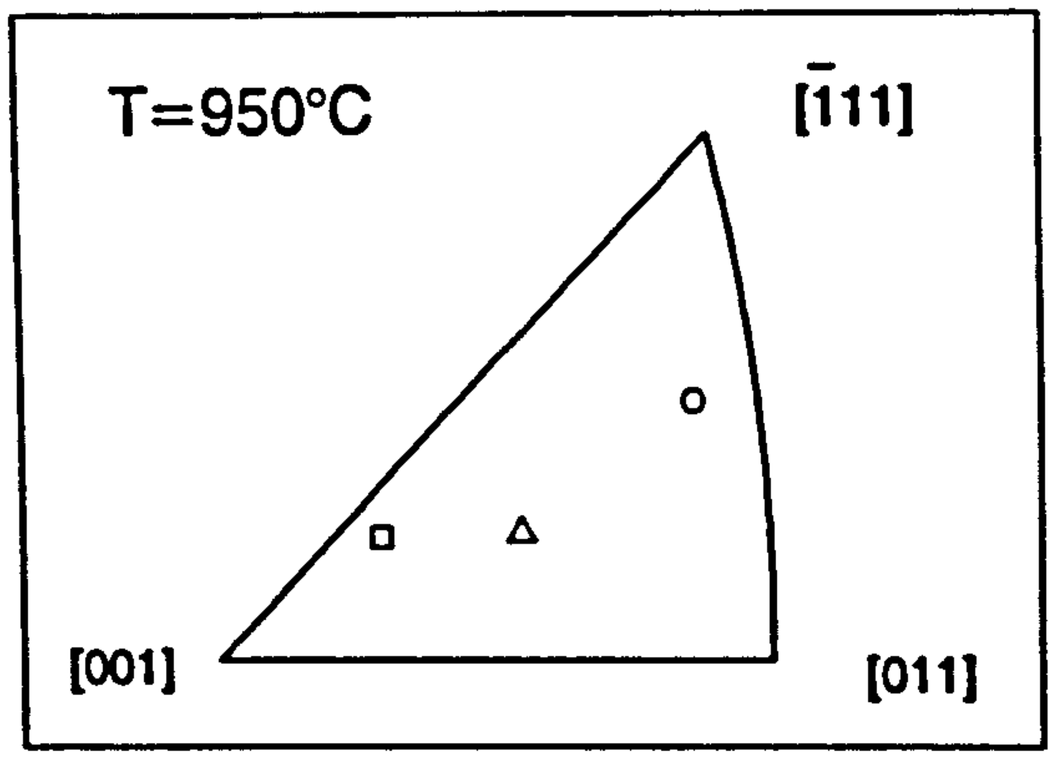

Fig.7.8. Comparison Between Experimental and Simulation Results for Tests with Different Strain Dwells

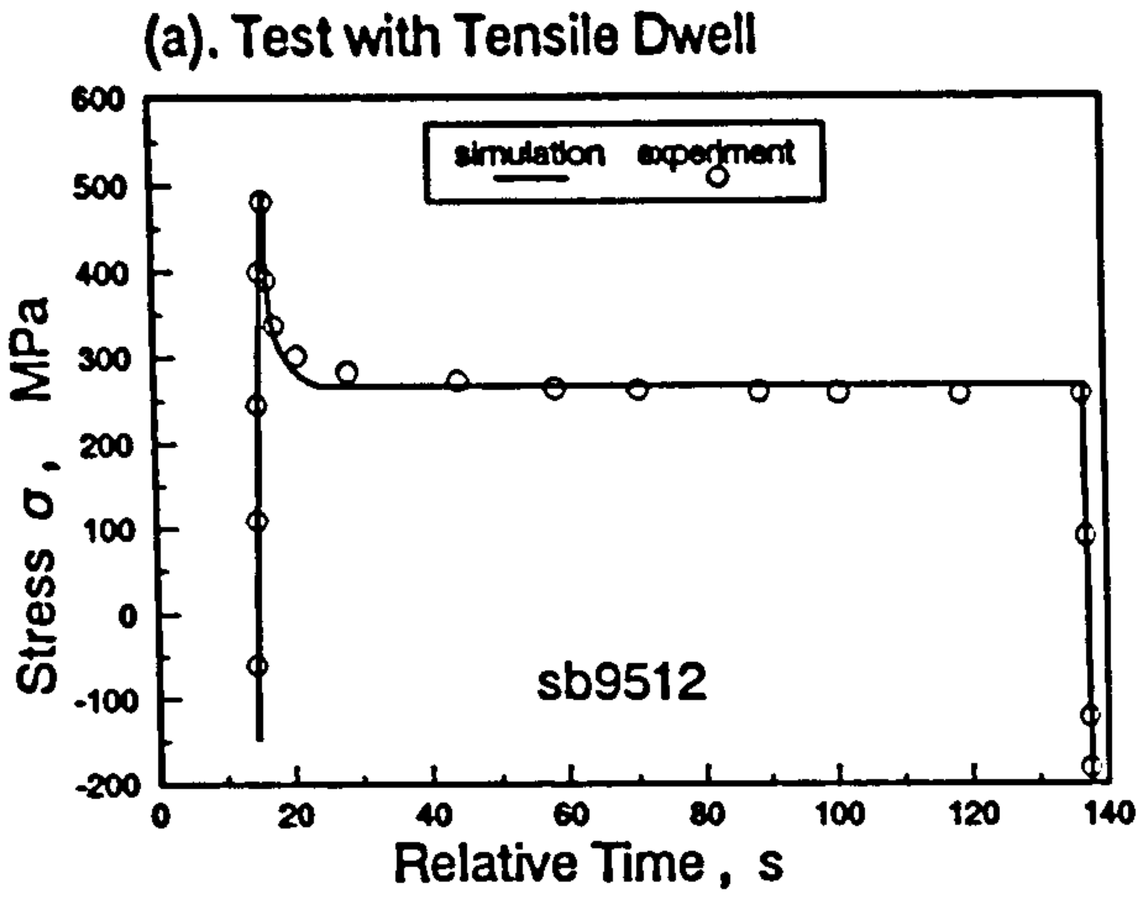

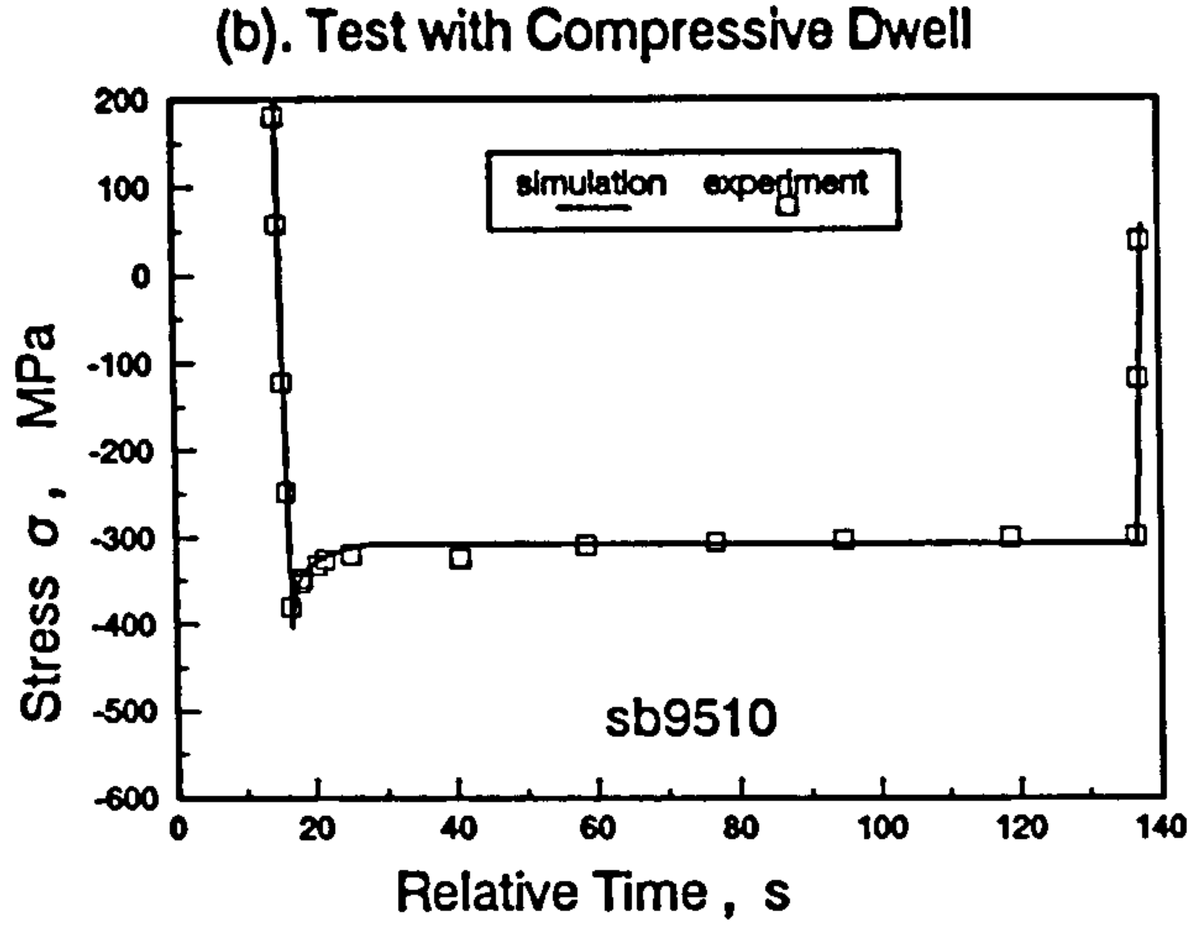

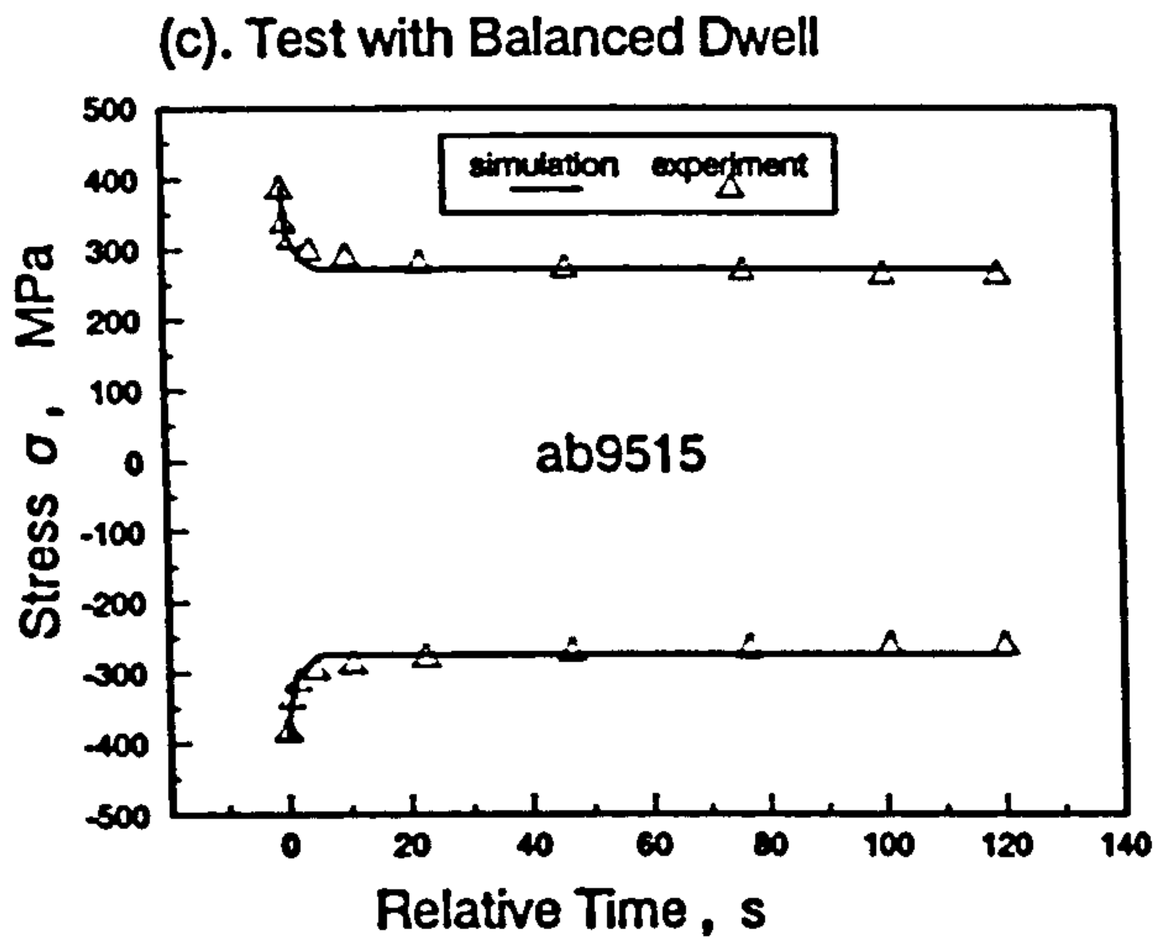

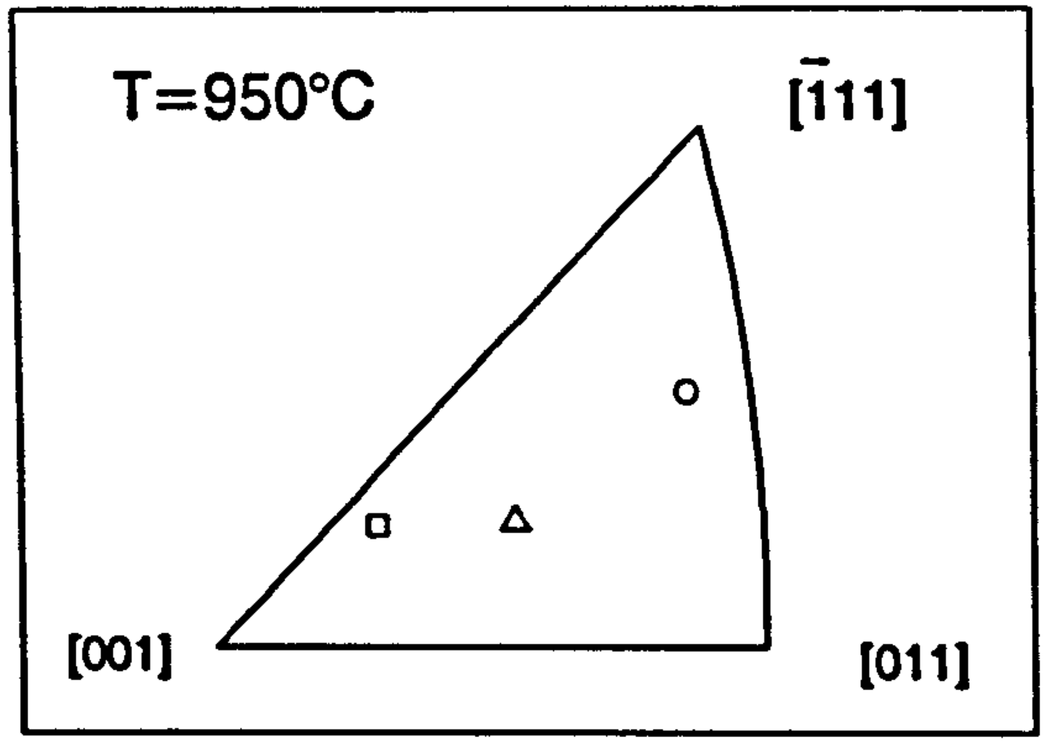

Fig.7.9. Comparison Between Experimental and Simulation Results of Stress Relaxation Response in the Tests with Strain Dwells

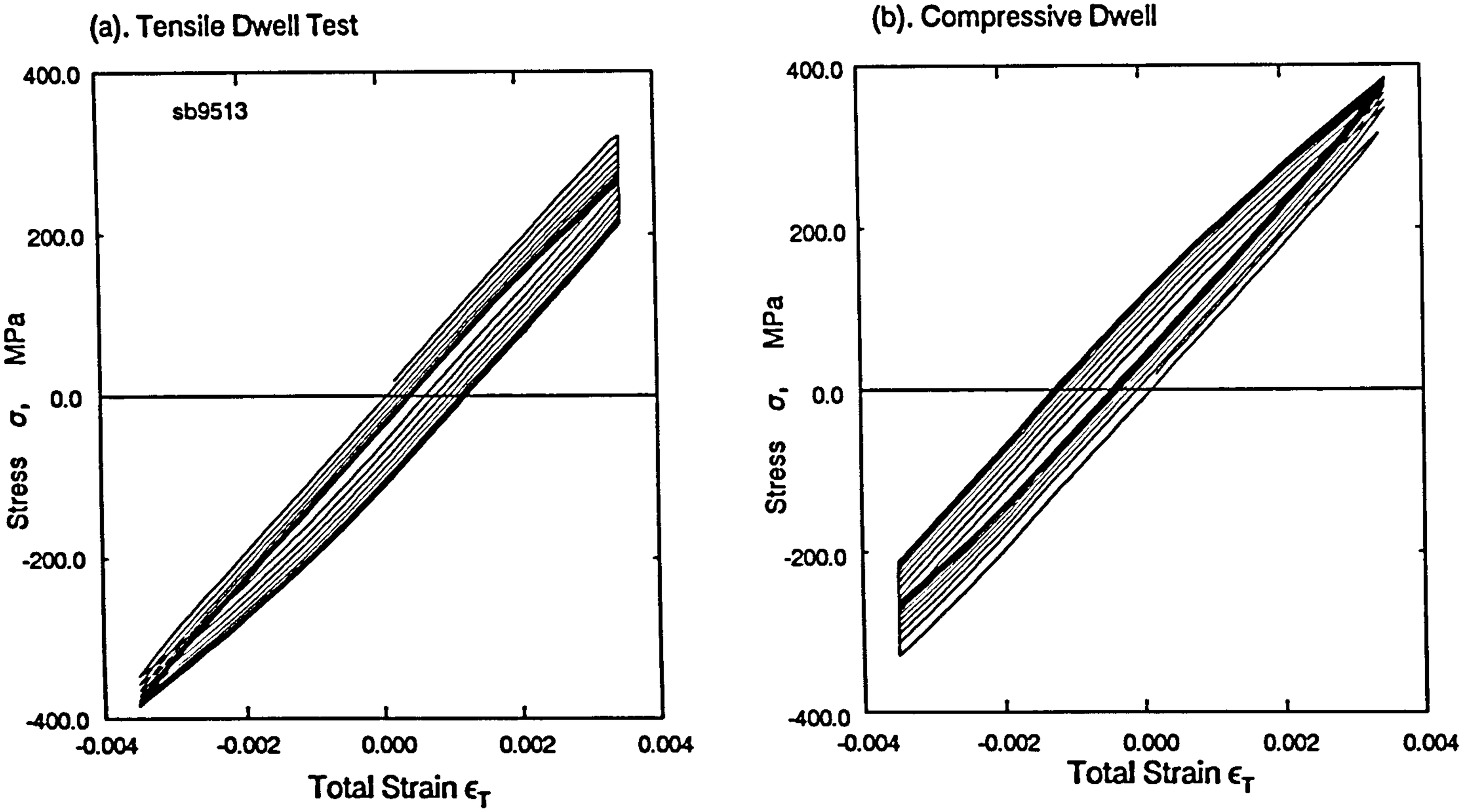

Fig.7.10. Simulation of the Development of Mean Stress in the Tests with Strain Dwells

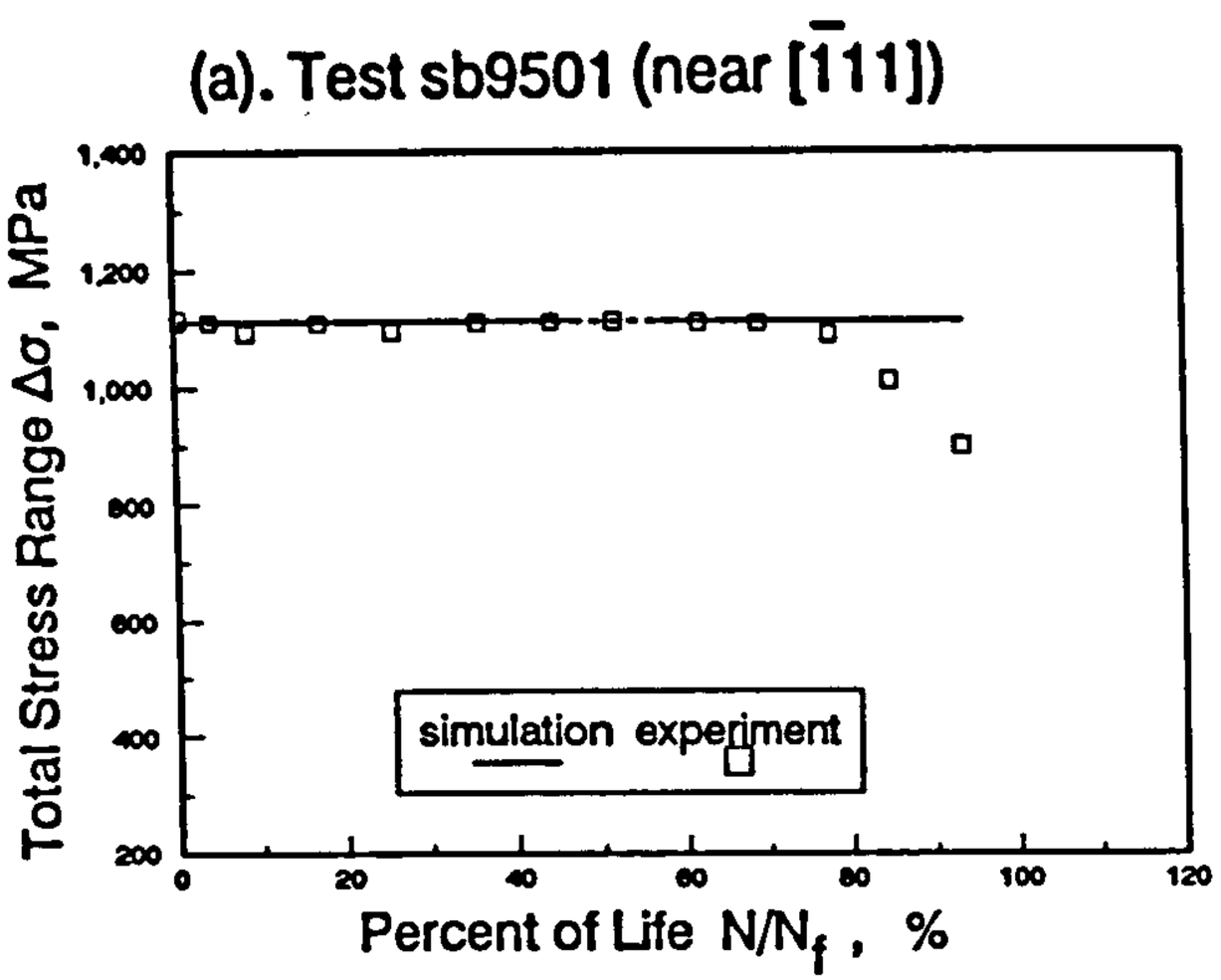

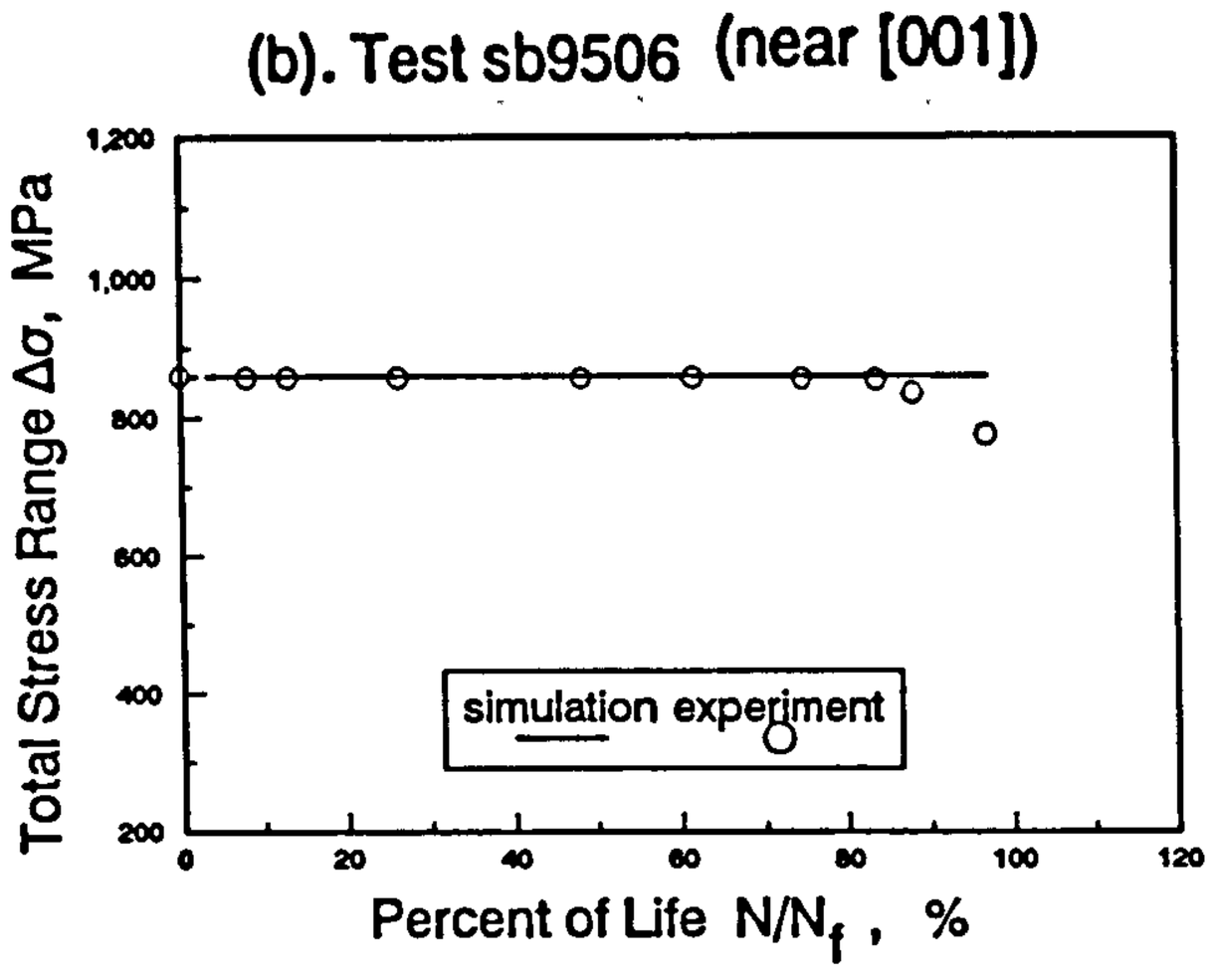

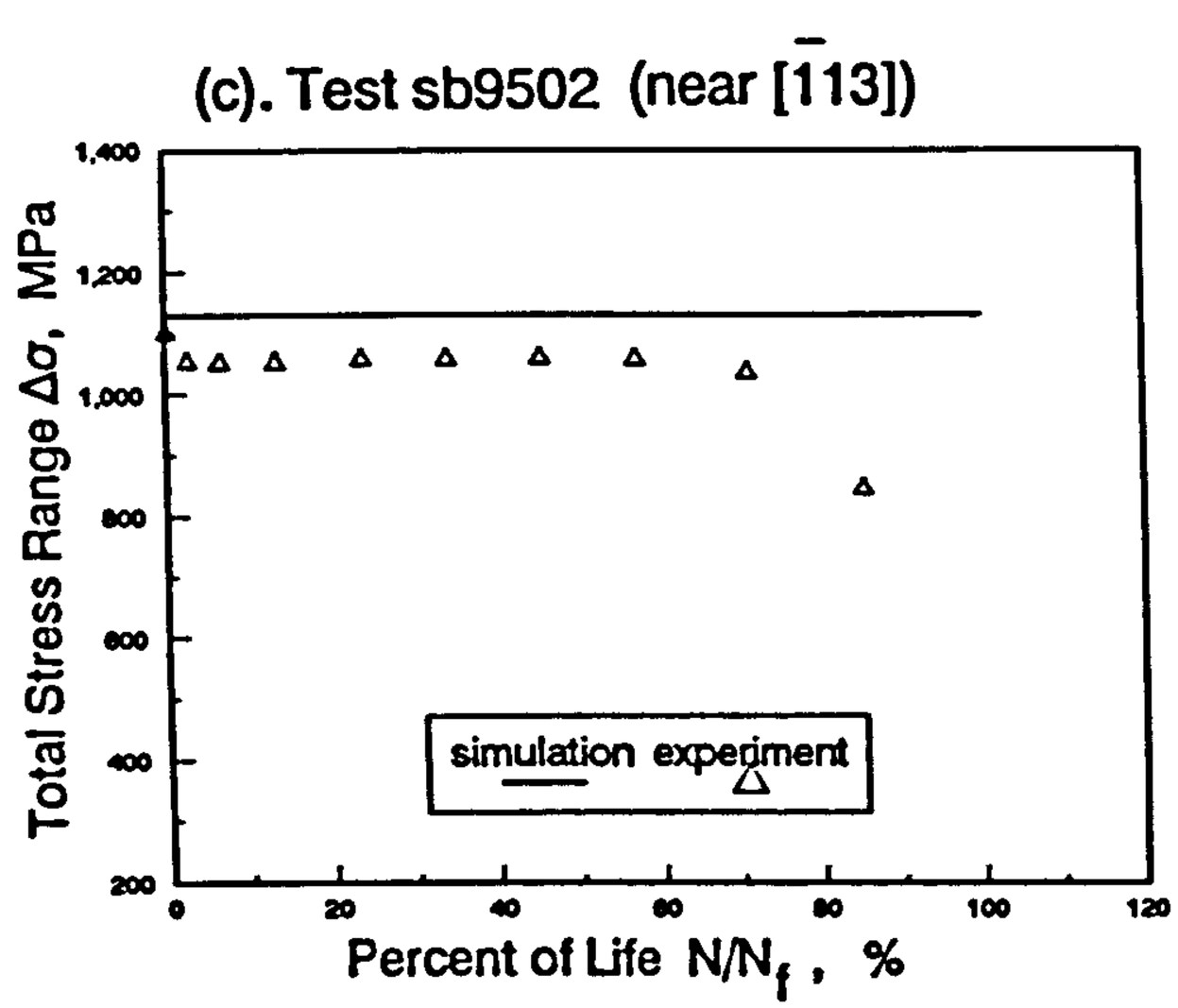

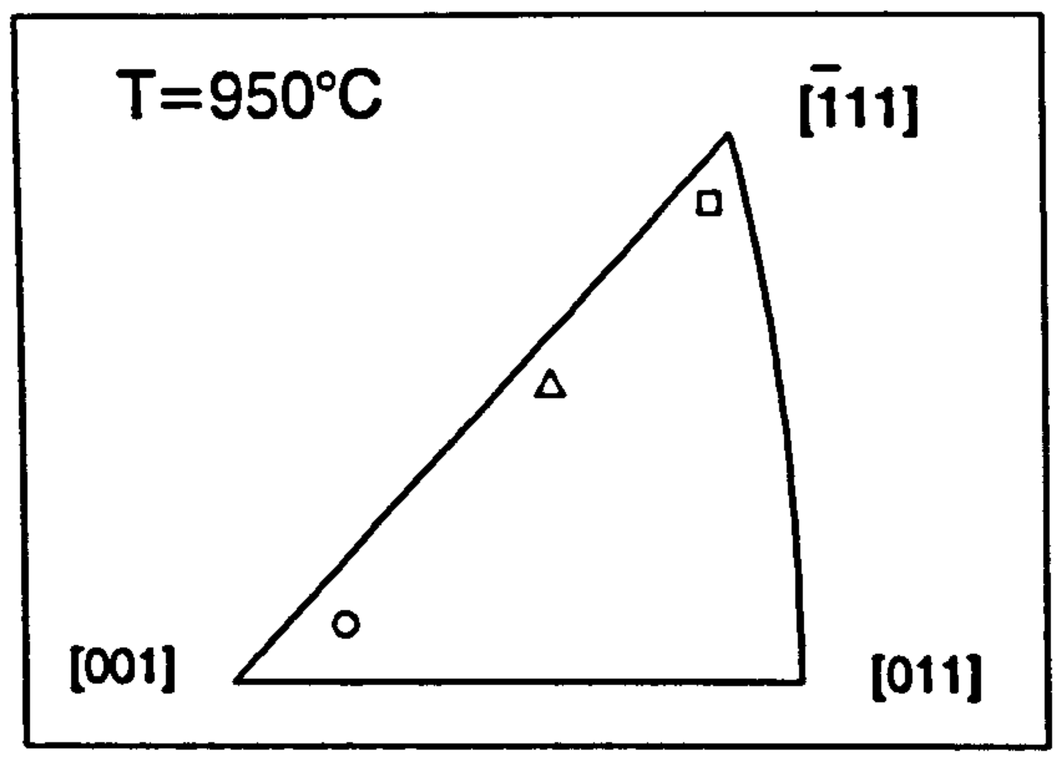

Fig.7.11. Comparison Between Experimental and Simulation Results of the Total Stress Response for Different Continuous Cycling Tests

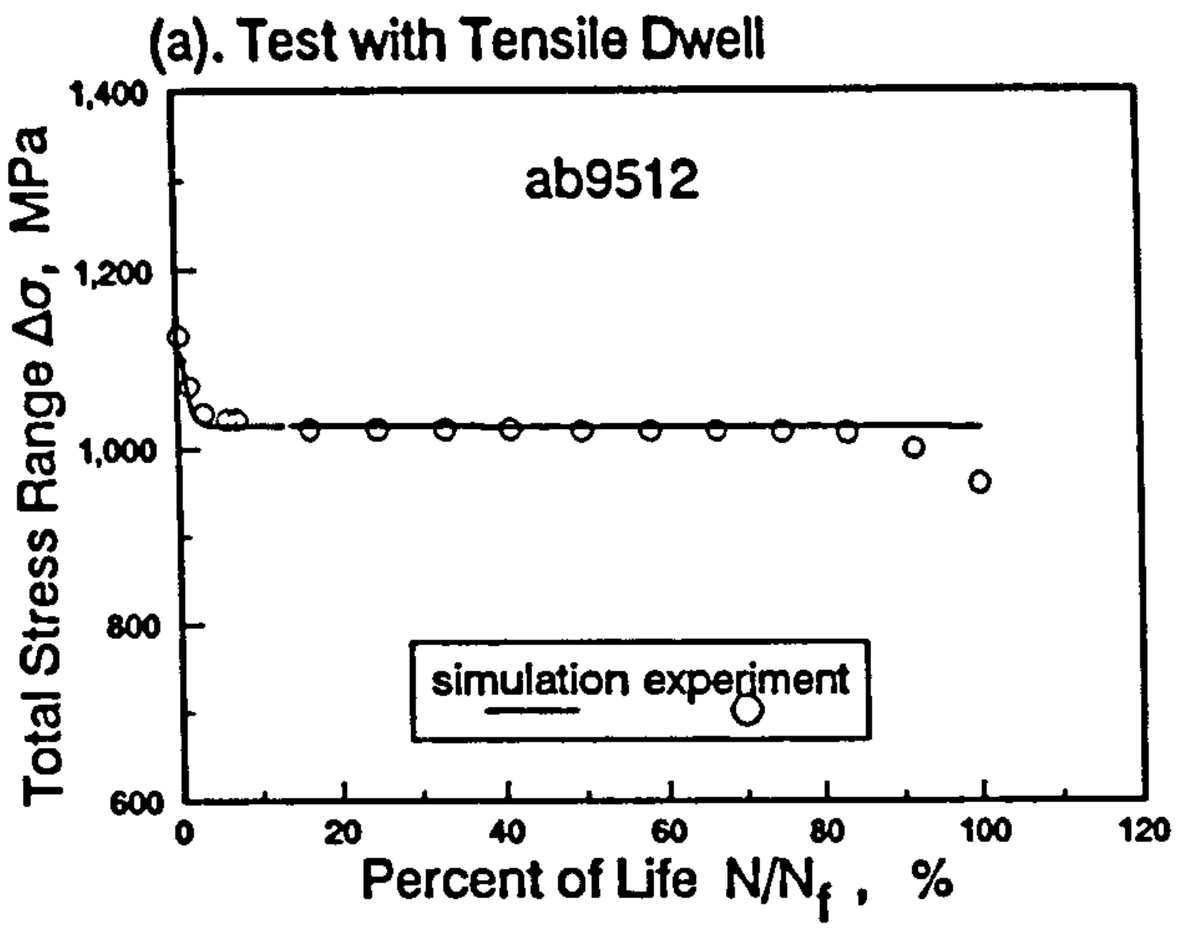

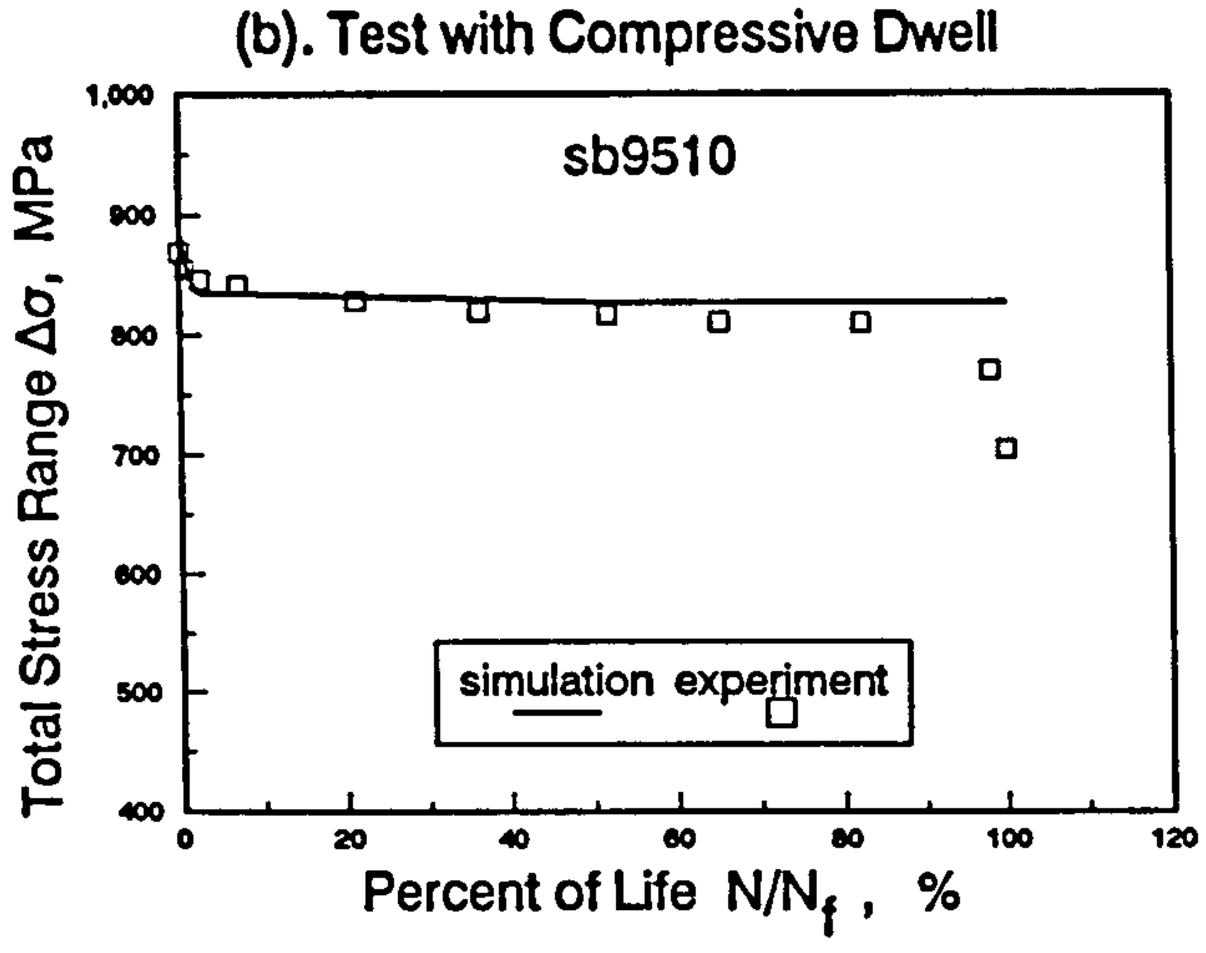

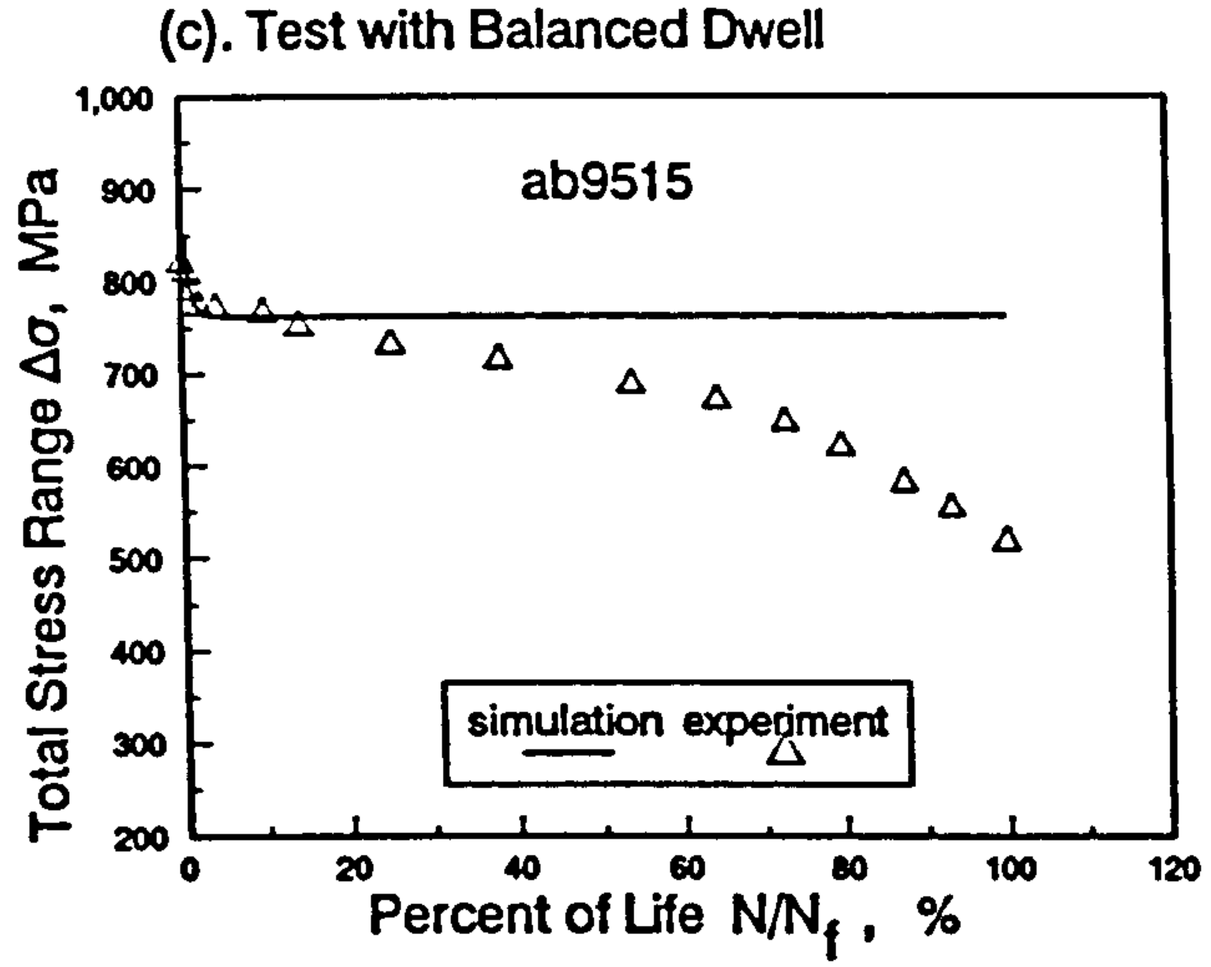

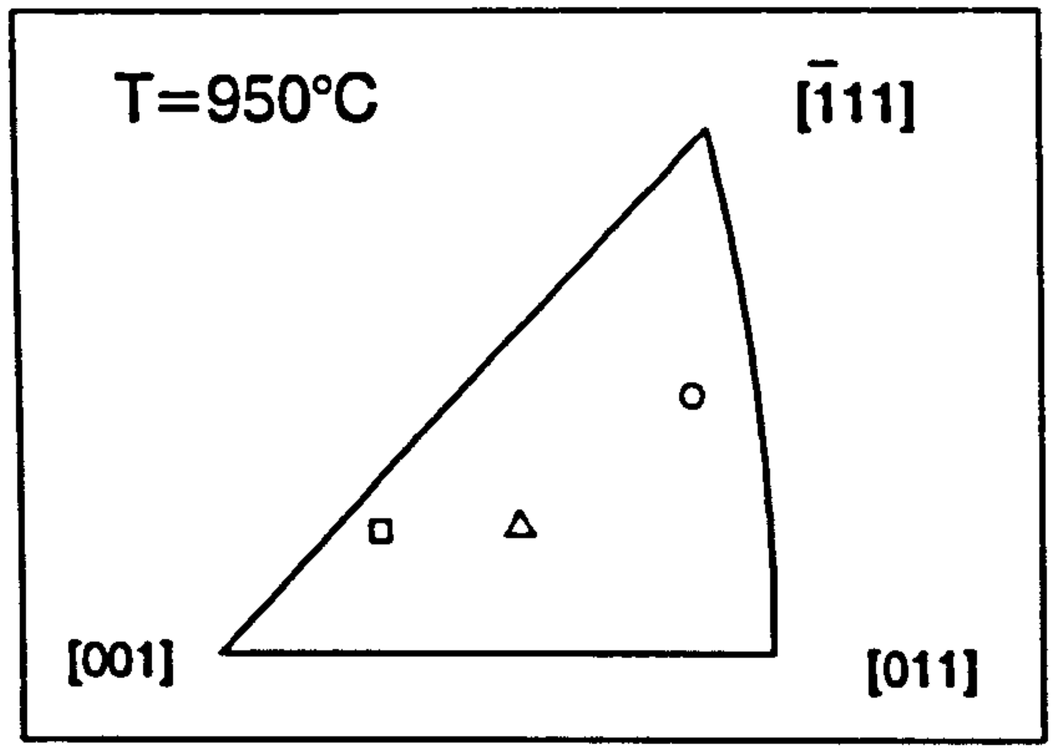

Fig.7.12. Comarison Between Experimental and Simulation Results of the Total Stress Response in the Tests with Strain Dwells

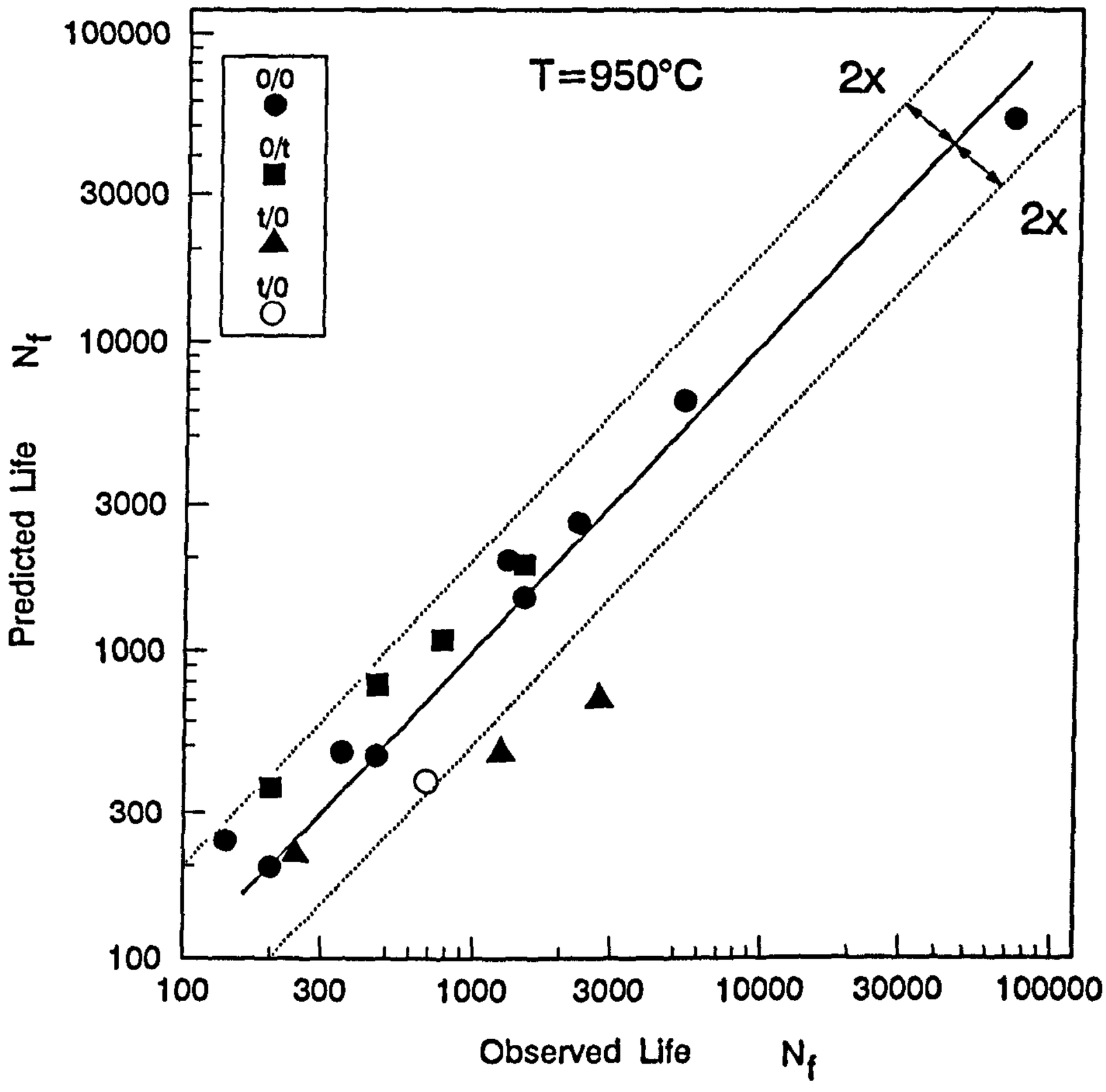

Fig.8.1a. Life Prediction by Coffin-Manson Law at 950°C Using Constants Based on All Tests

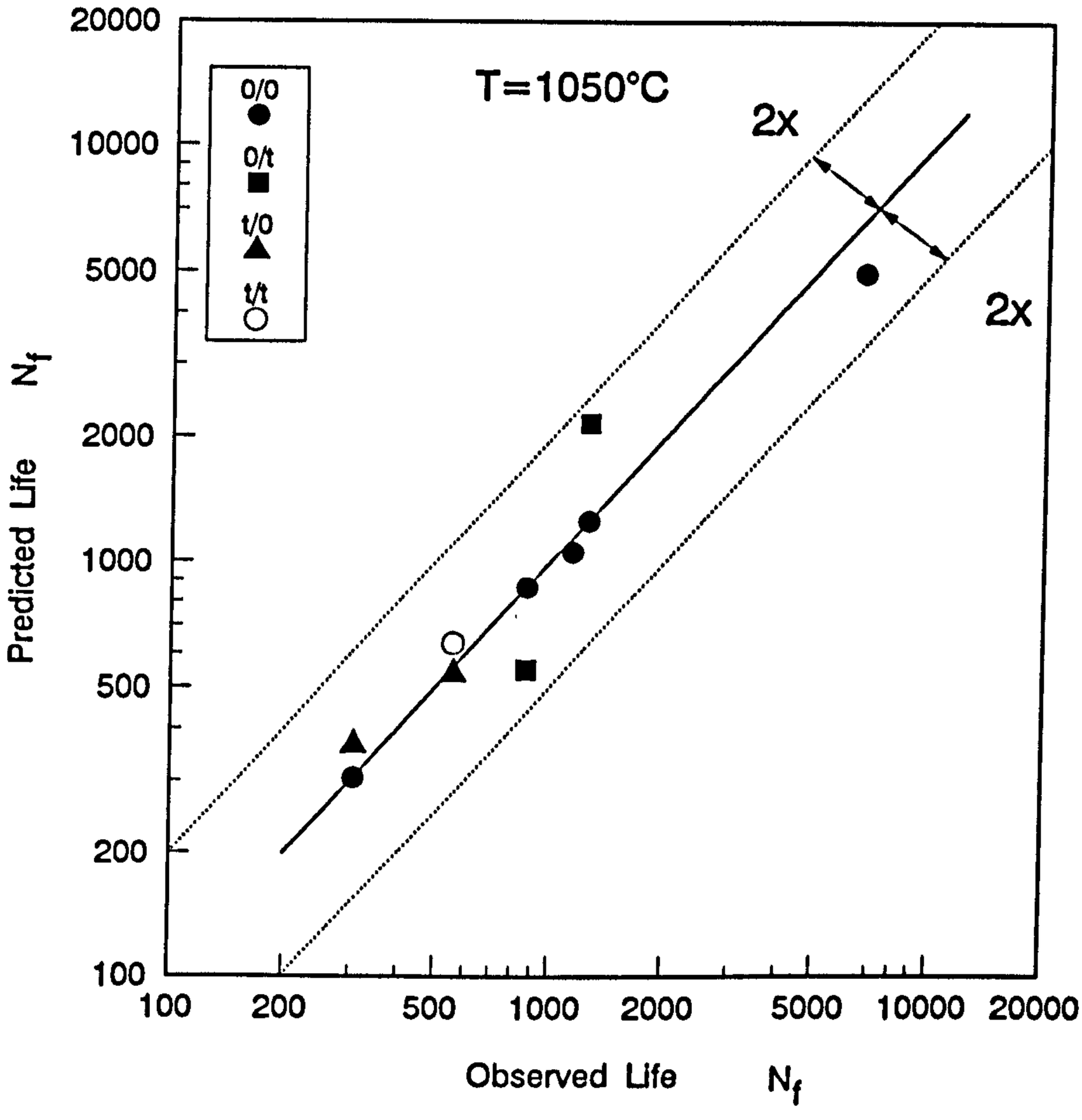

Fig8.1b. Life Prediction by Coffin-Manson Law 1050°C Using Constants Based on All Tests

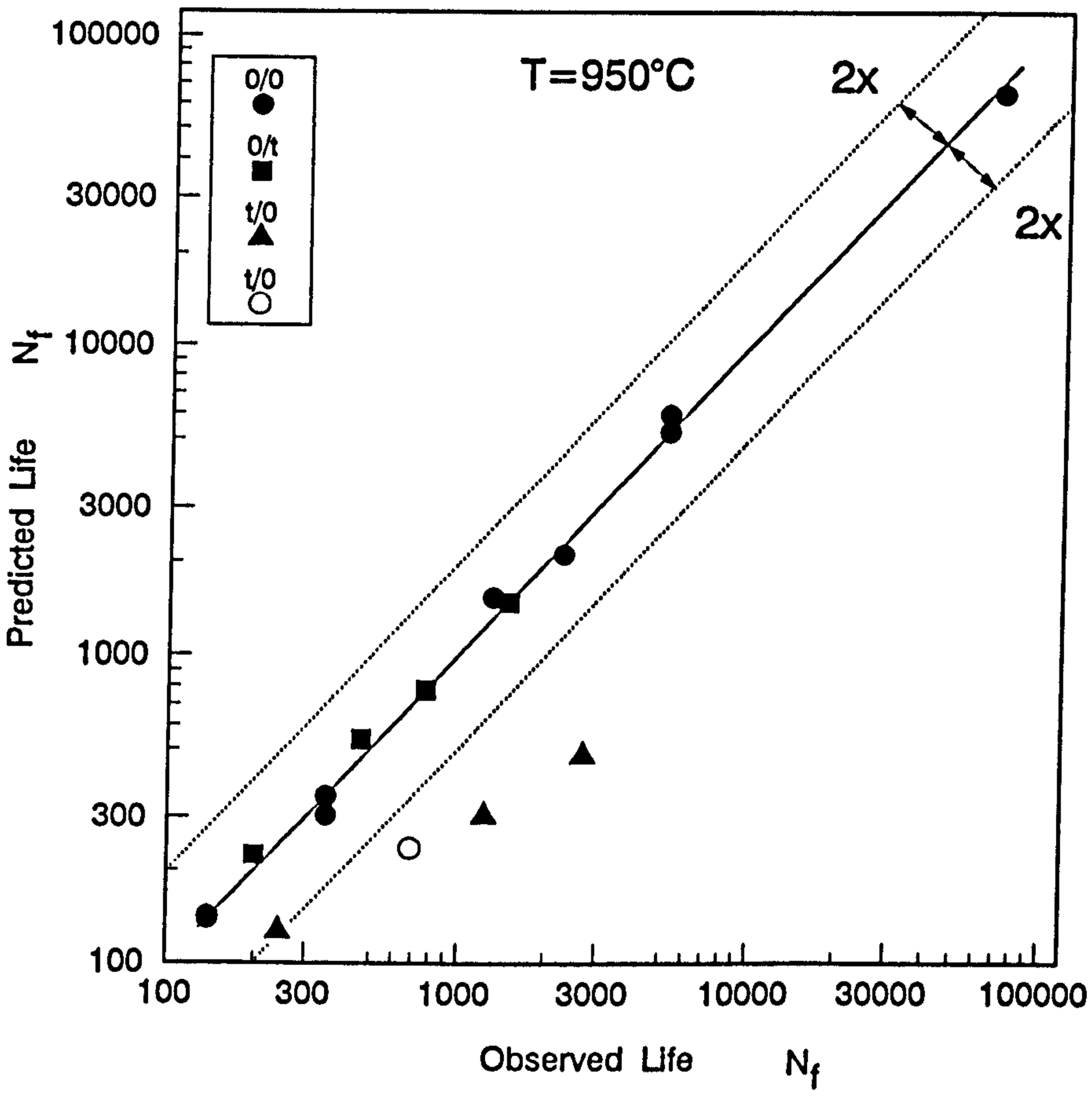

Fig.8.2a. Life Prediction by Coffin-Manson Law at 950°C Using Constants Based on Continuous Tests Alone

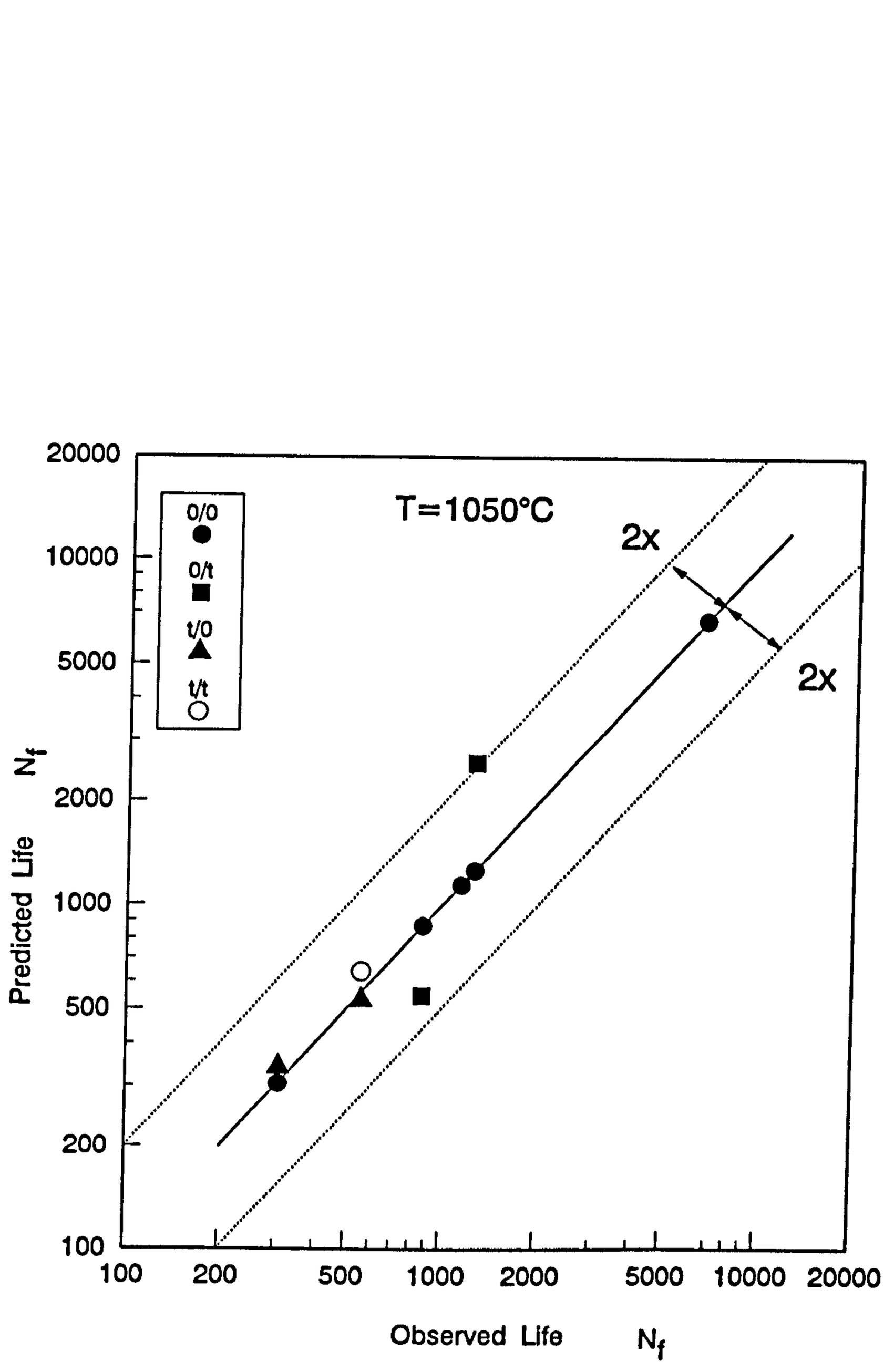

Fig.8.2b. Life Prediction by Coffin-Manson Law at 1050°C Using Constants Based on Continuous Tests Alone

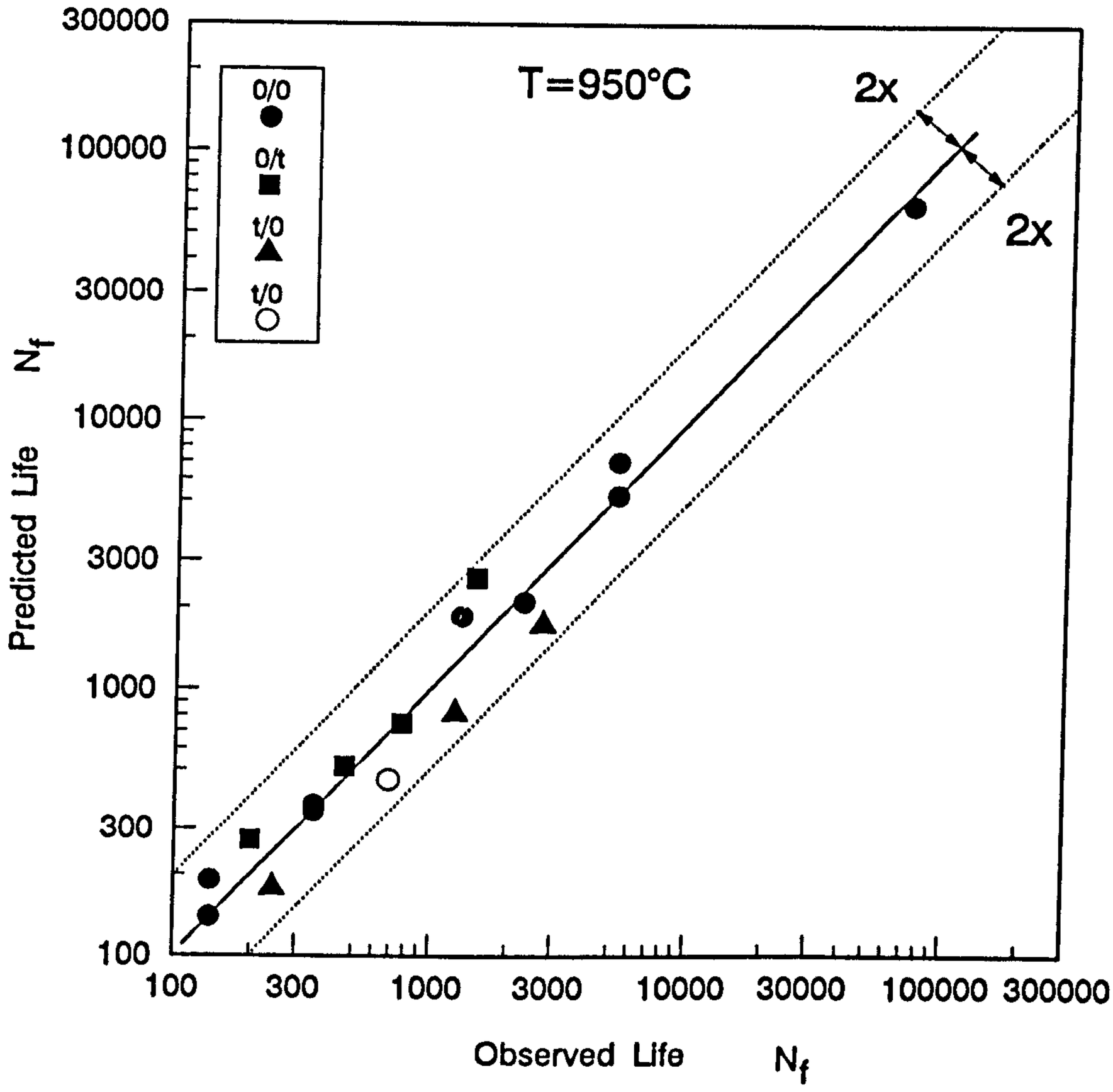

Fig.8.3a. Life Prediction by Damage Function Approach at 950°C Using Constants Based on All Tests

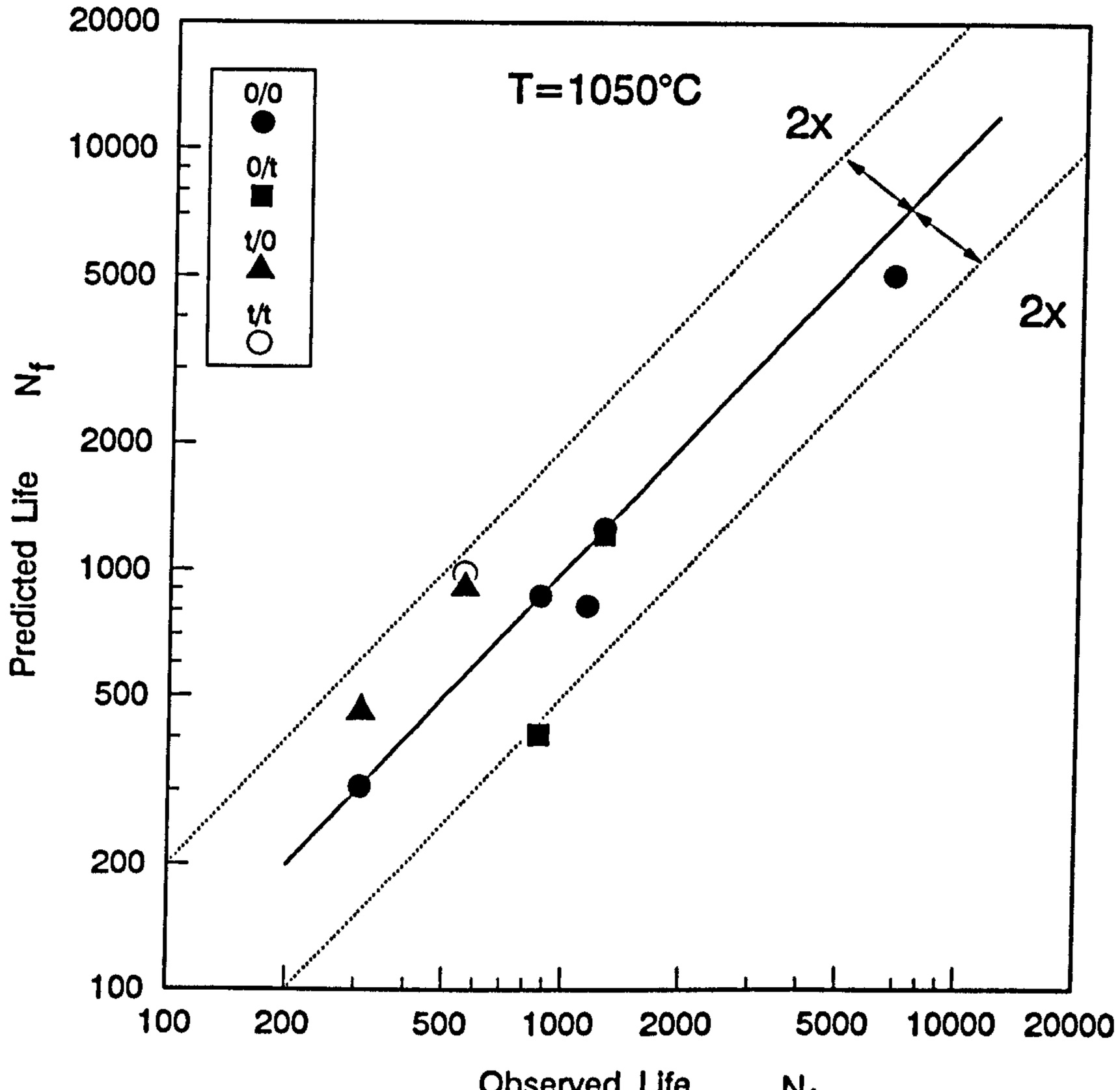

Fig.8.3b. Life Prediction by Damage Function Approach at 1050°C Using Constants Based on All Tests

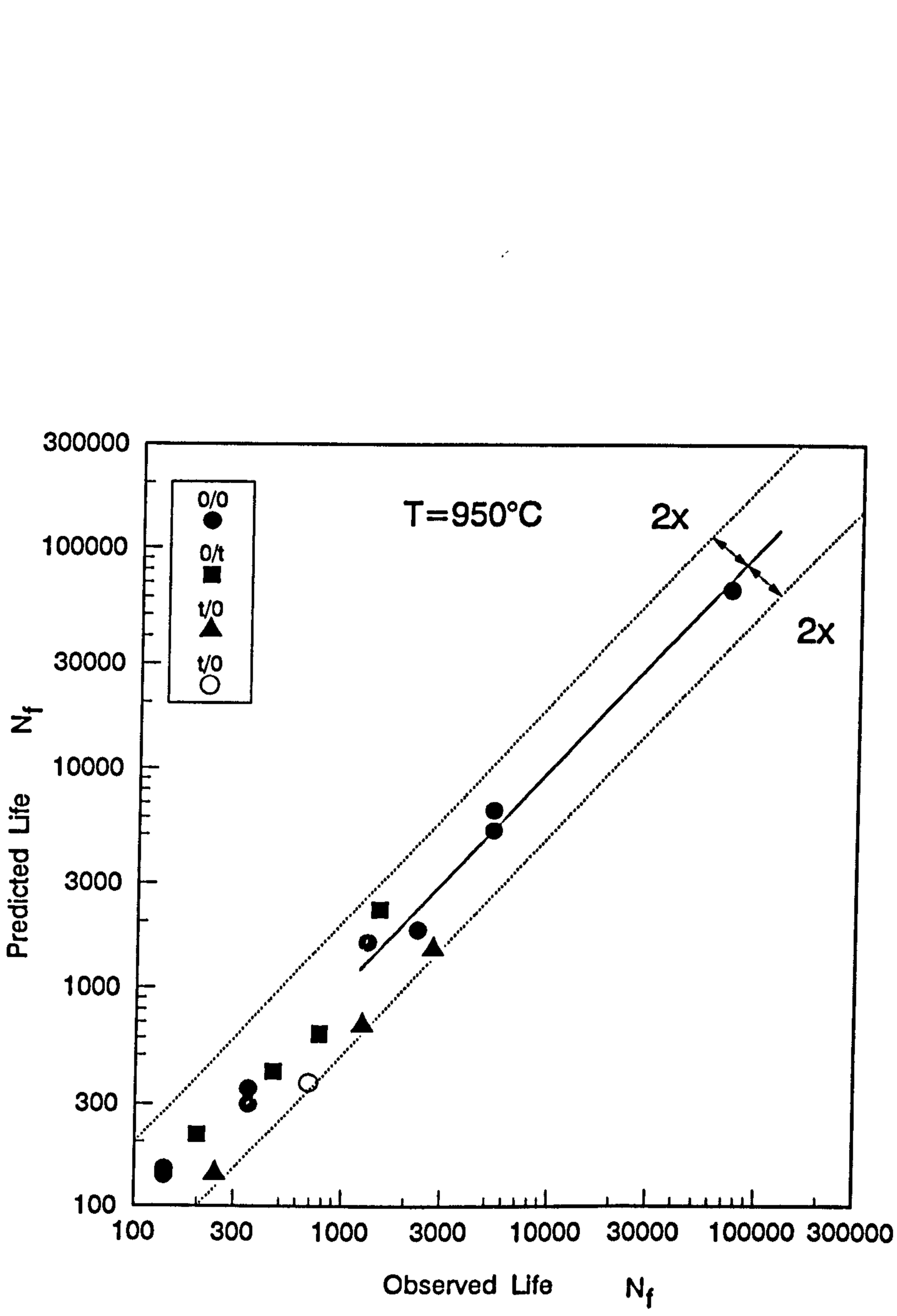

Fig.8.4a. Life Prediction by Damage Function Approach at 950°C Using Constants Based on Continuous Tests Alone

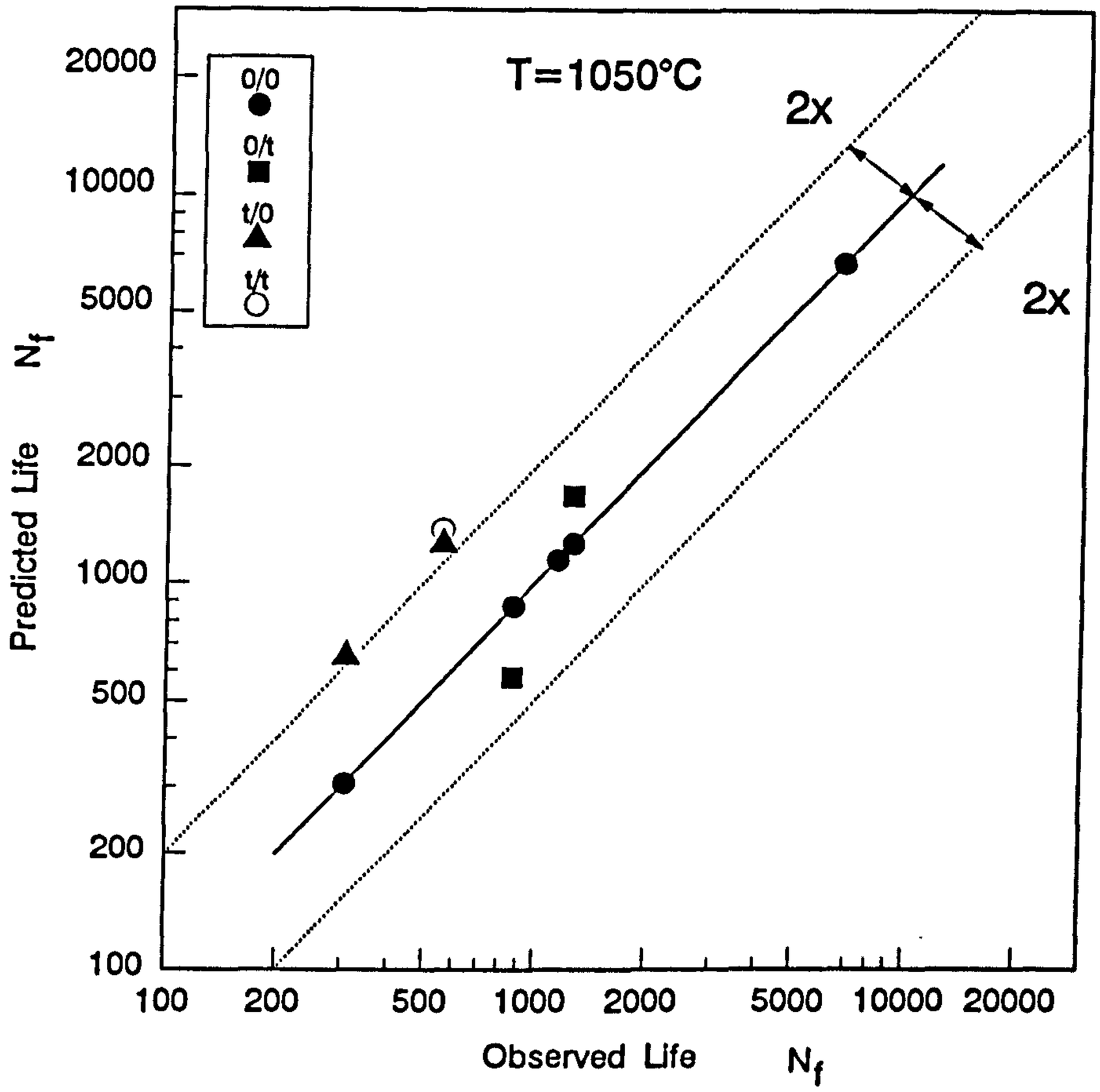

Fig.8.4b. Life Prediction by Damage Function Approach at 1050°C Using Constants Based on Continuous Tests Alone

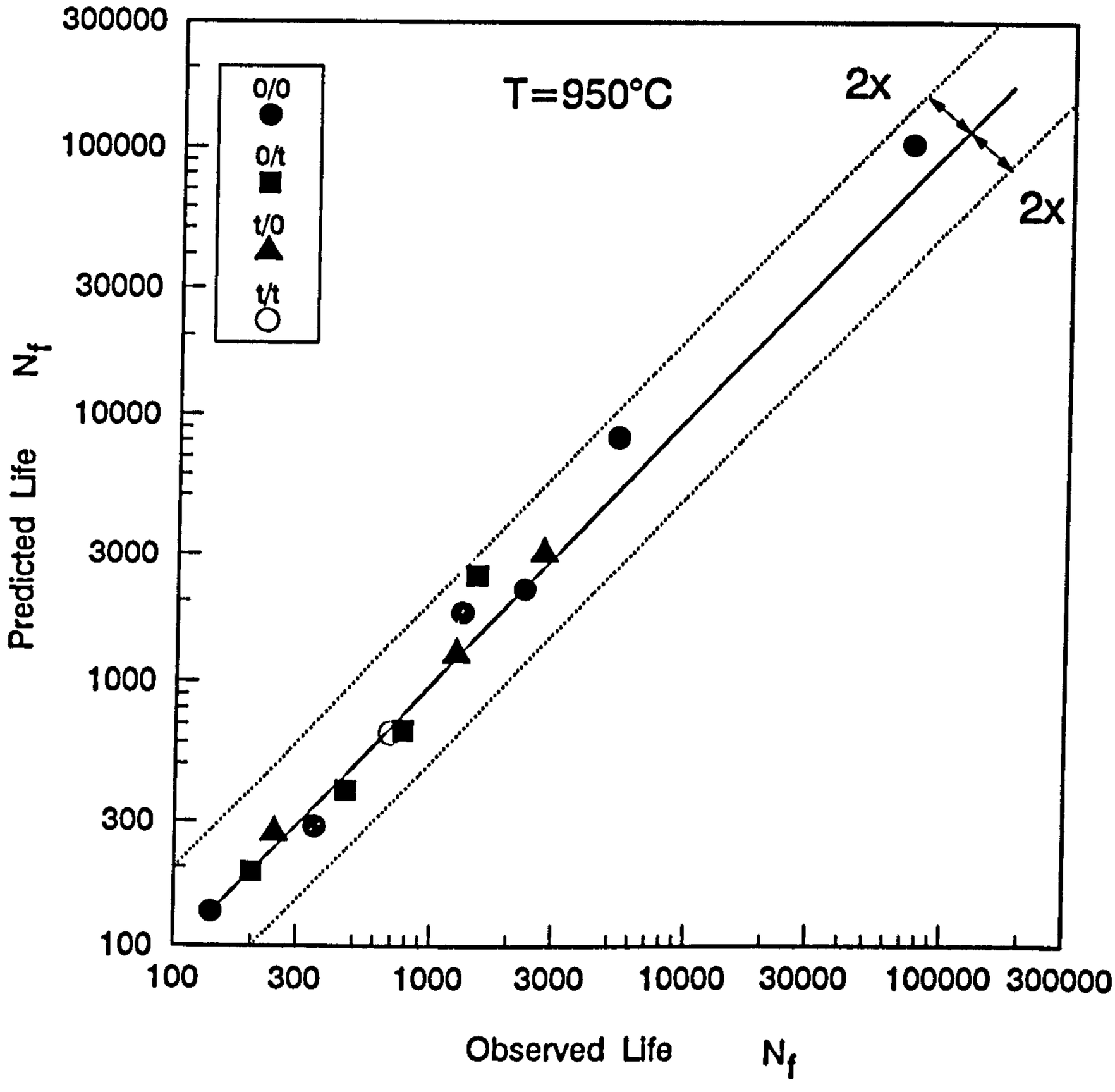

Fig.8.5a. Life Prediction by Frequency Modified Damage Function at 950°C Using Constants Based on All Tests

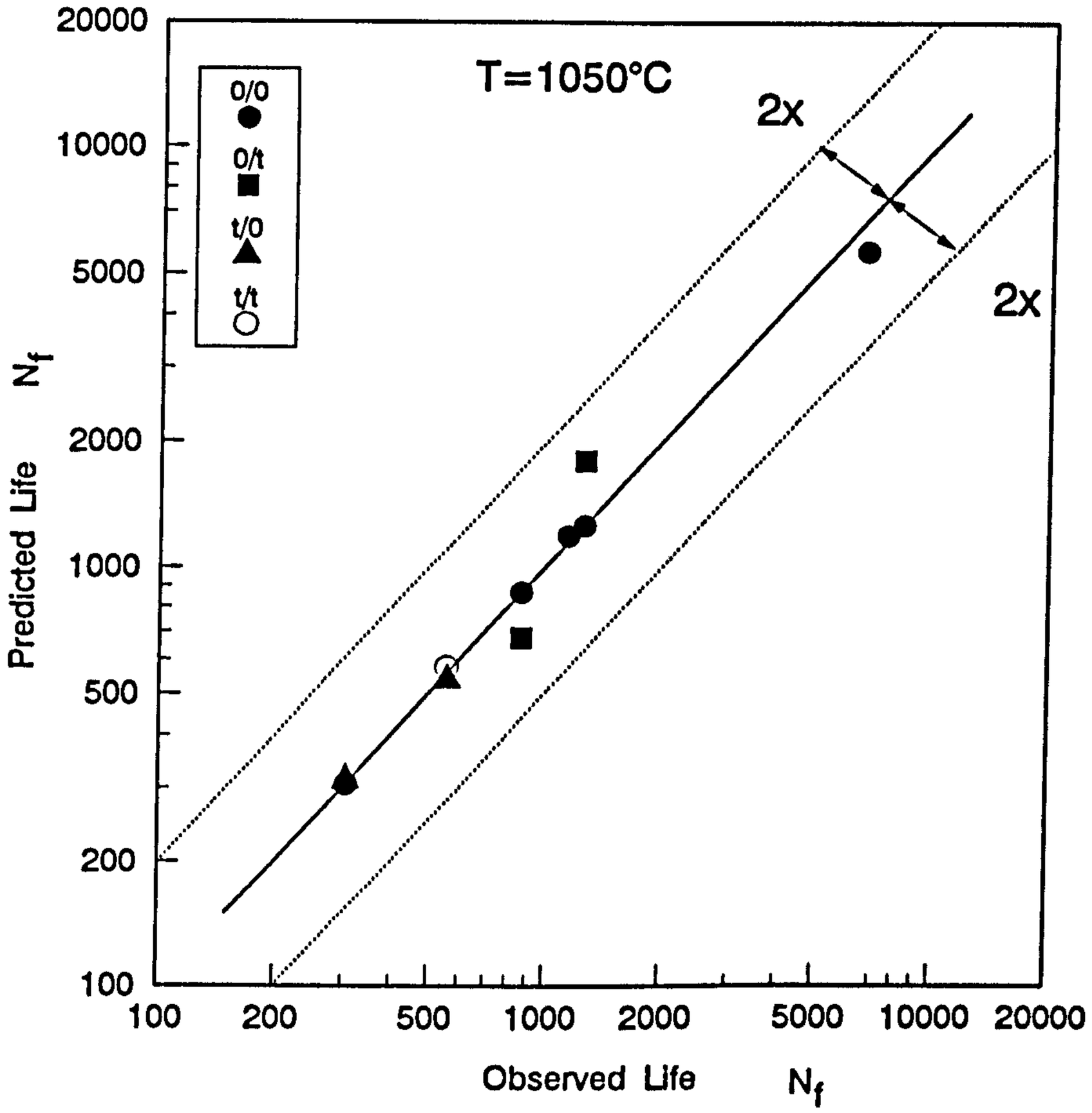

Fig.8.5b. Life Prediction by Frequency Modified Damage Function at 1050°C Using Constants Based on All Tests

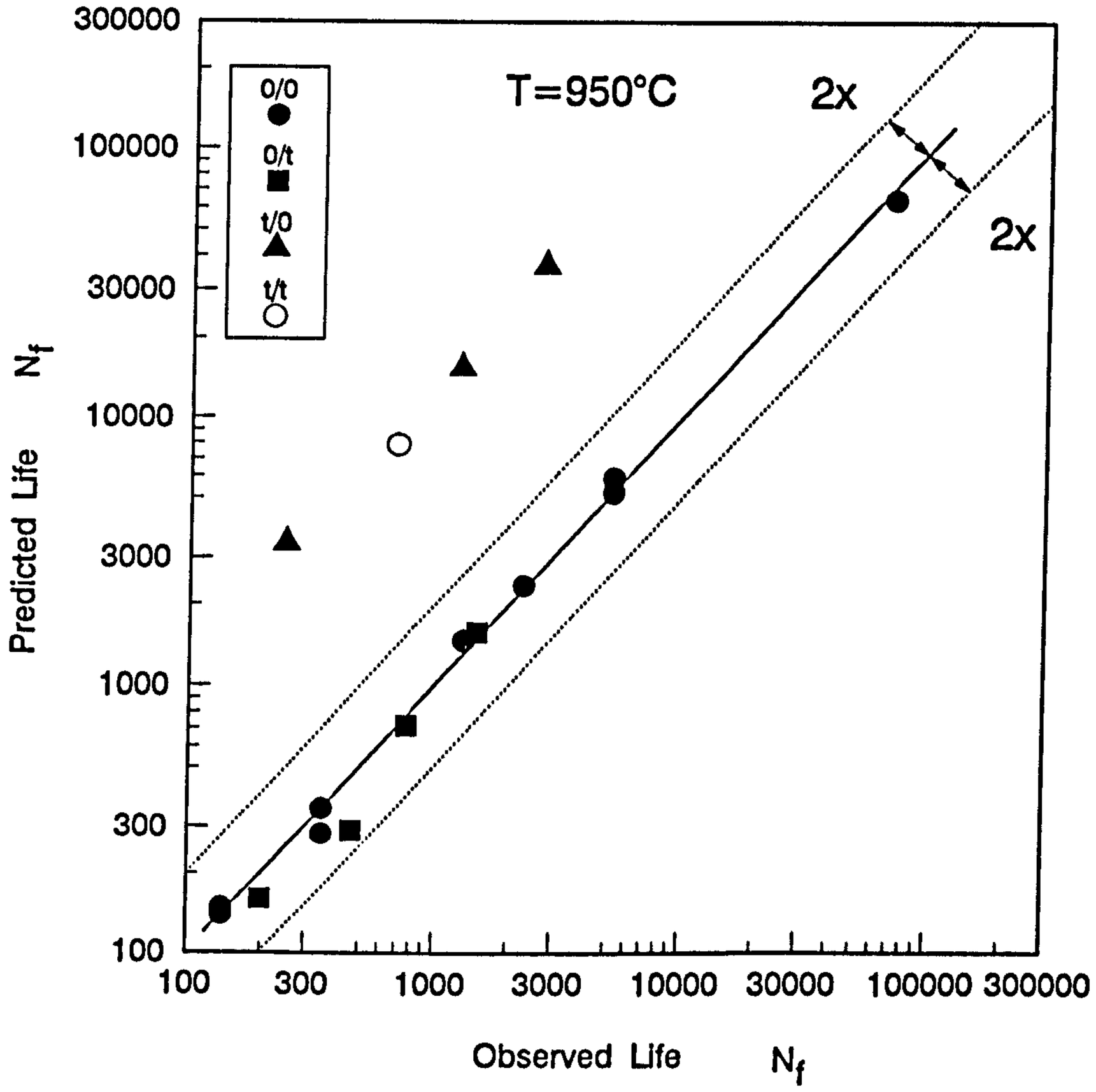

Fig.8.6a. Life Prediction by Frequency Modified Damage Function at 950°C Using Constants Based on Continuous Tests Alone

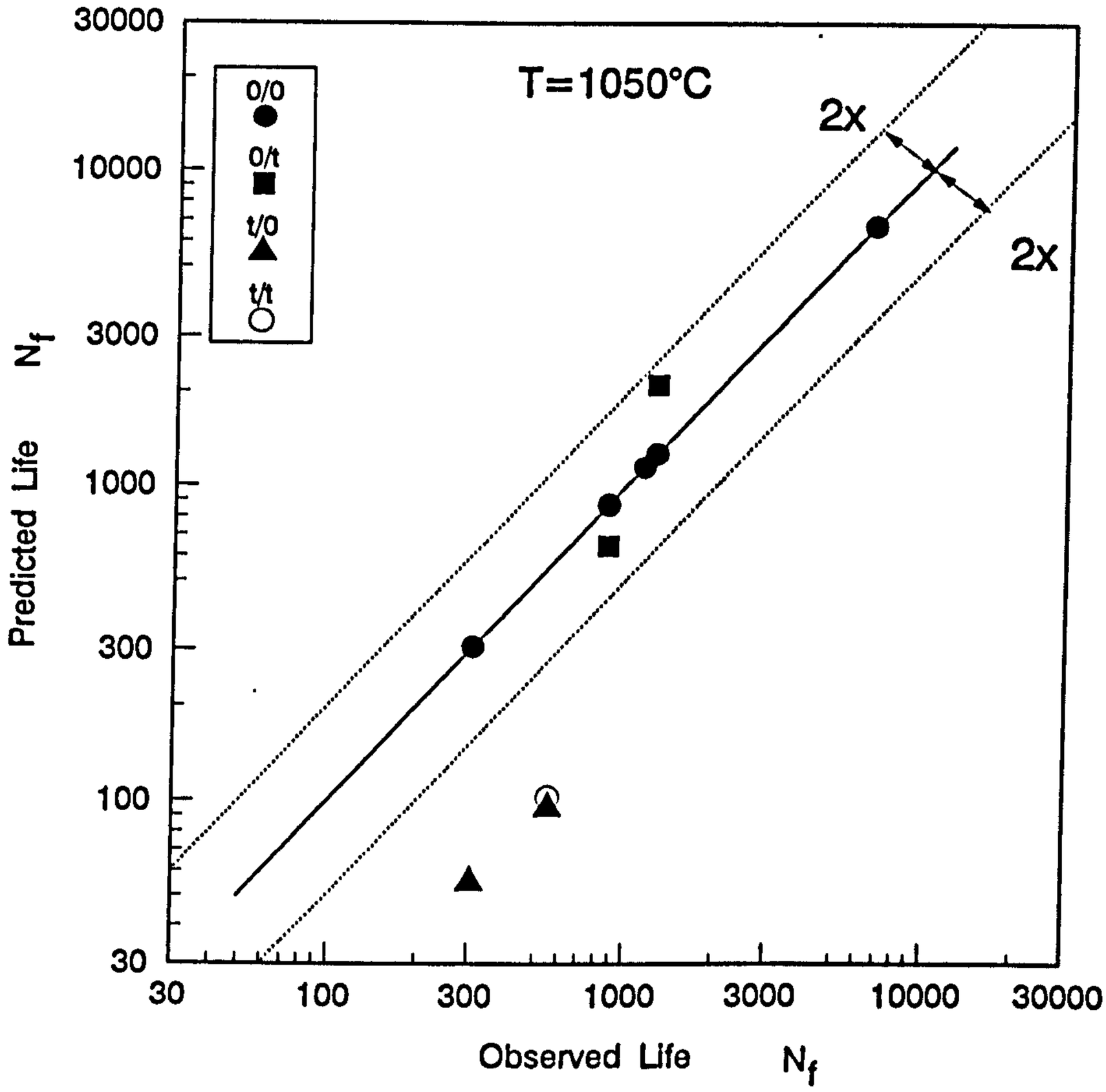

Fig.8.6b. Life Prediction by Frequency Modified Damage Function at 1050°C Using Constants Based on Continuous Tests Alone

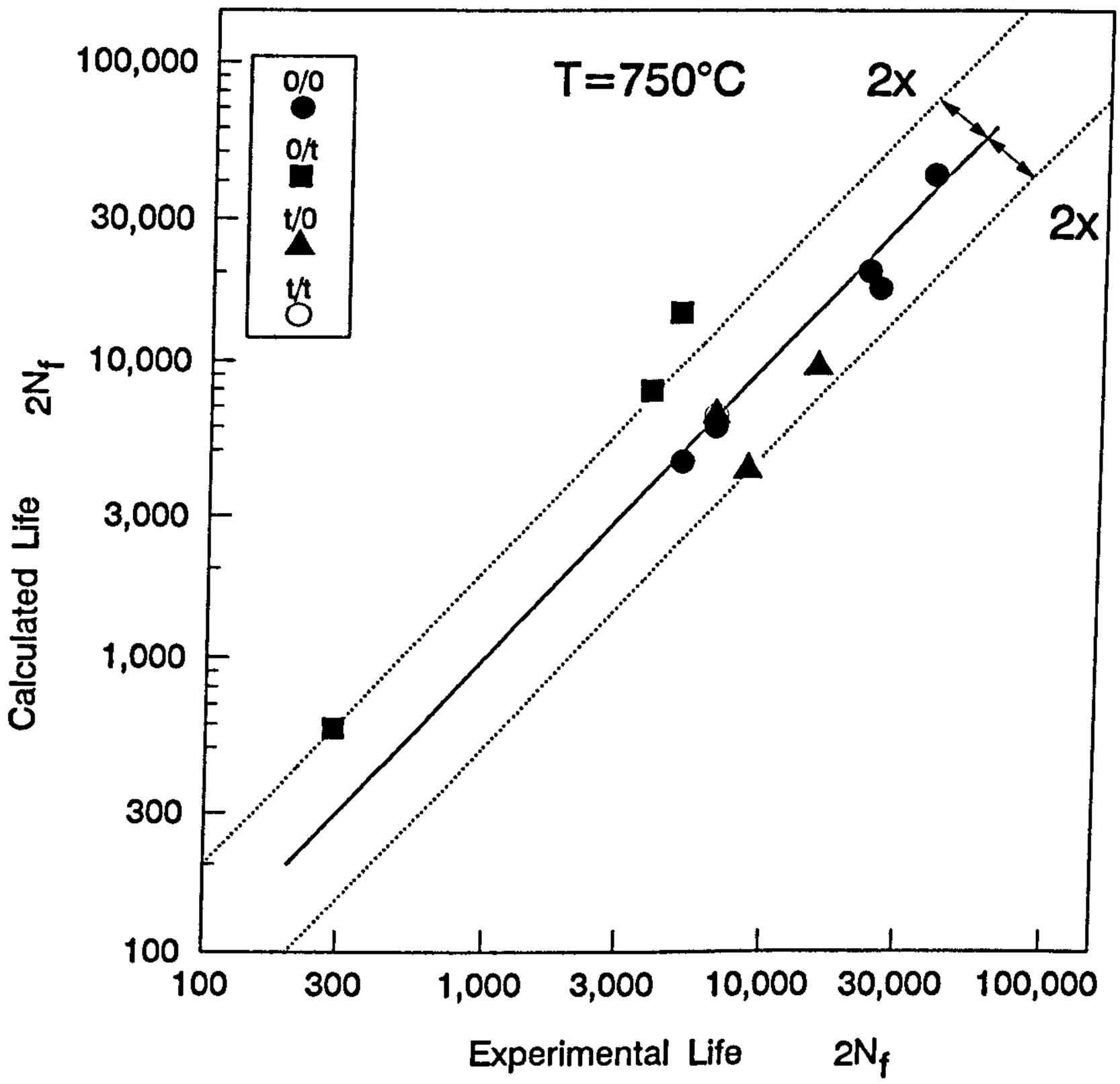

Fig.8.7a. Life Prediction by Morrow's Mean Stress Model (T=750°C)

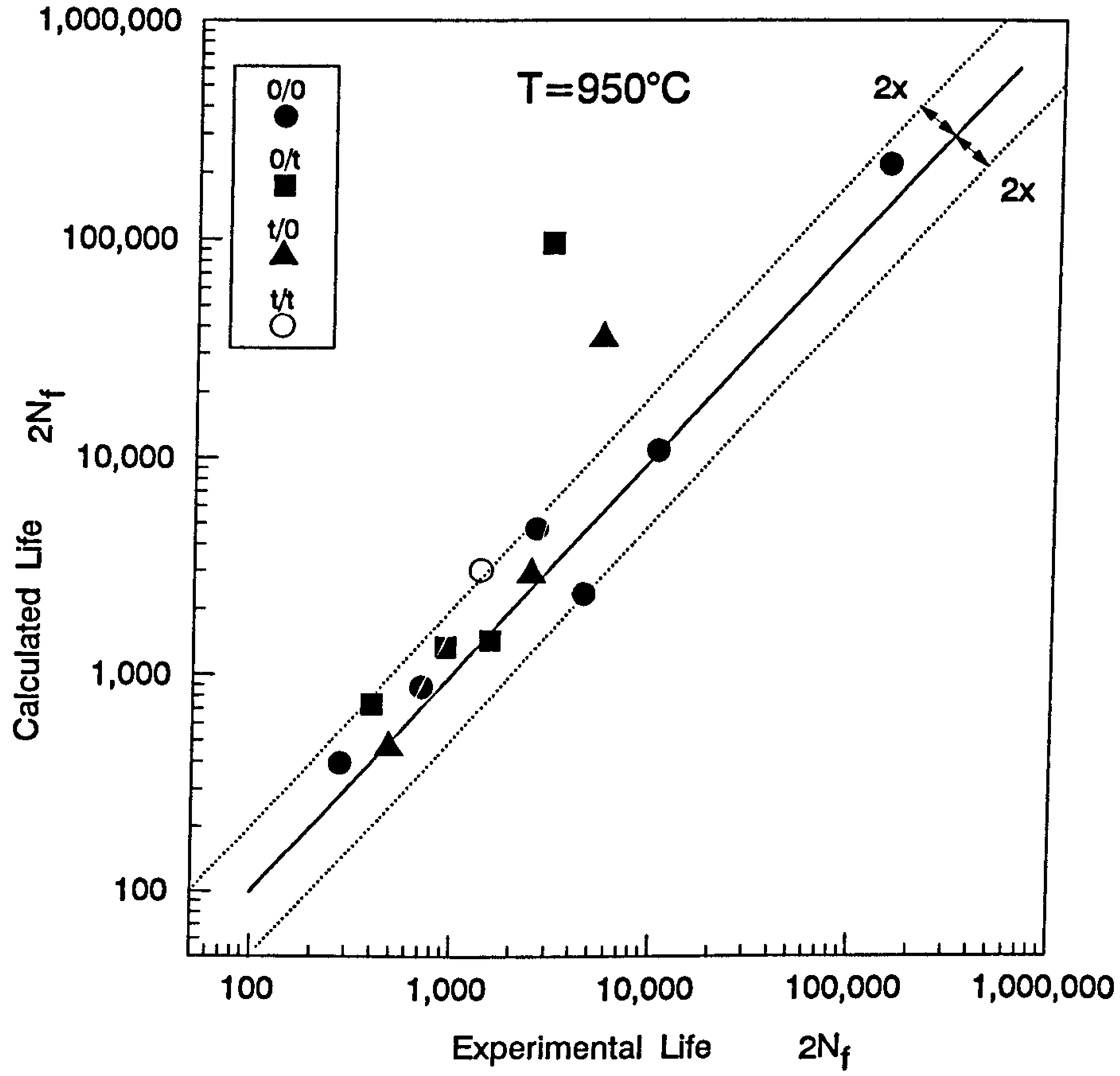

Fig.8.7b. Life Prediction by Morrow's Mean Stress Model (T=950°C)

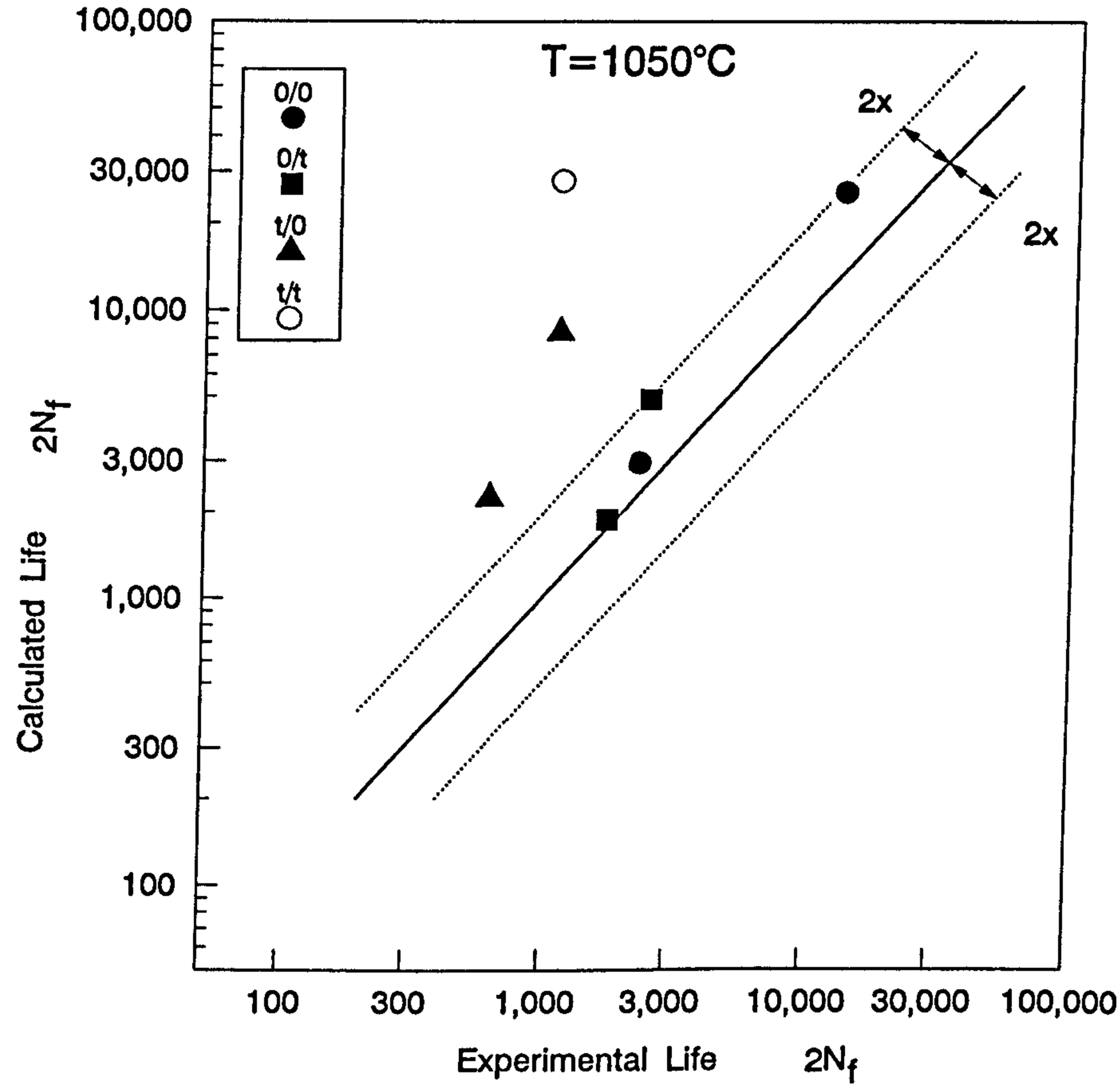

Fig.8.7c. Life Prediction by Morrow's Mean Stress Model (T= 1050°C)

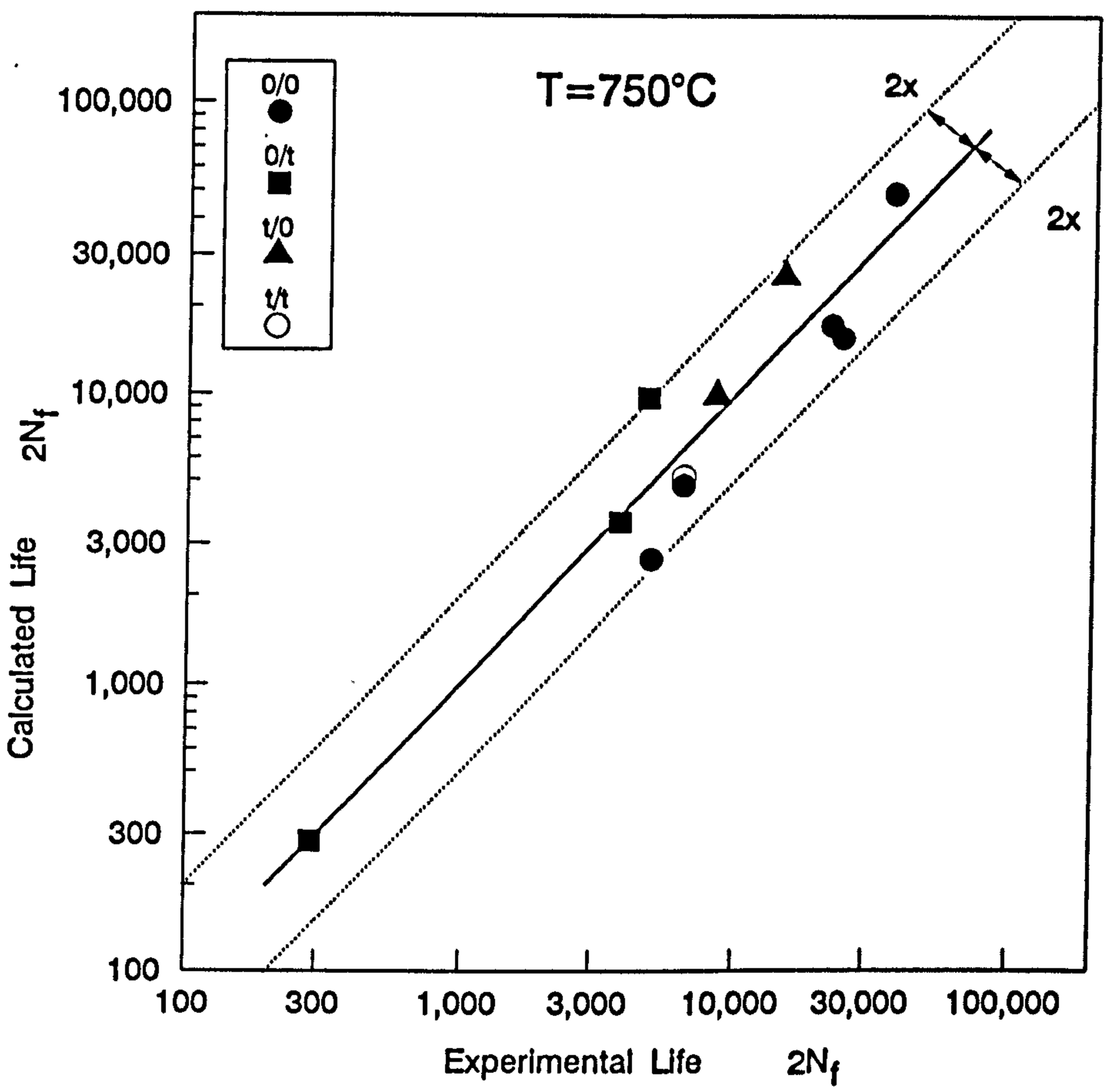

Fig.8.8a. Life Prediction by SWT Mean Stress Model (T=750°C)

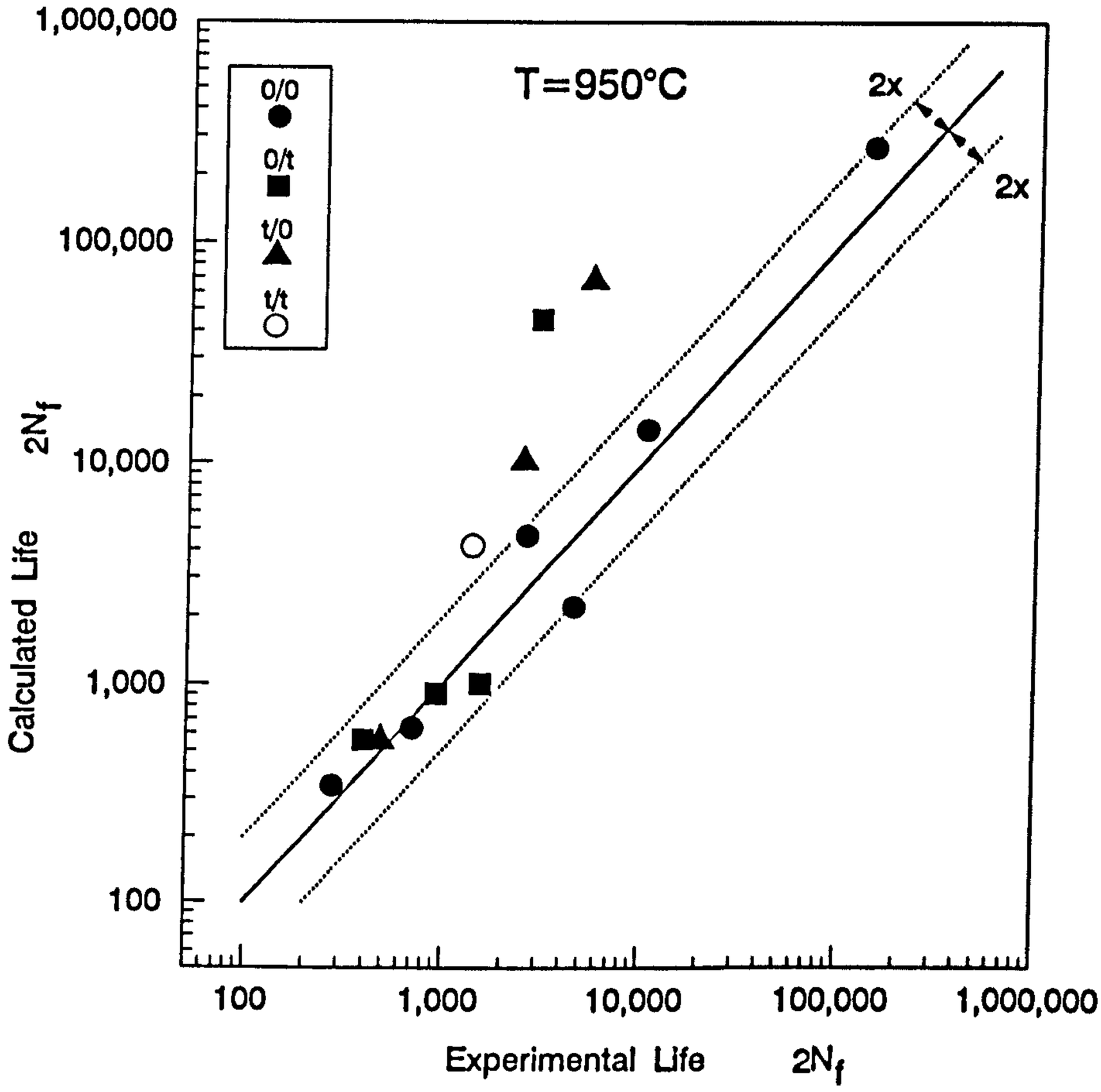

Fig.8.8b. Life Prediction by SWT Mean Stress Model (T=950°C)

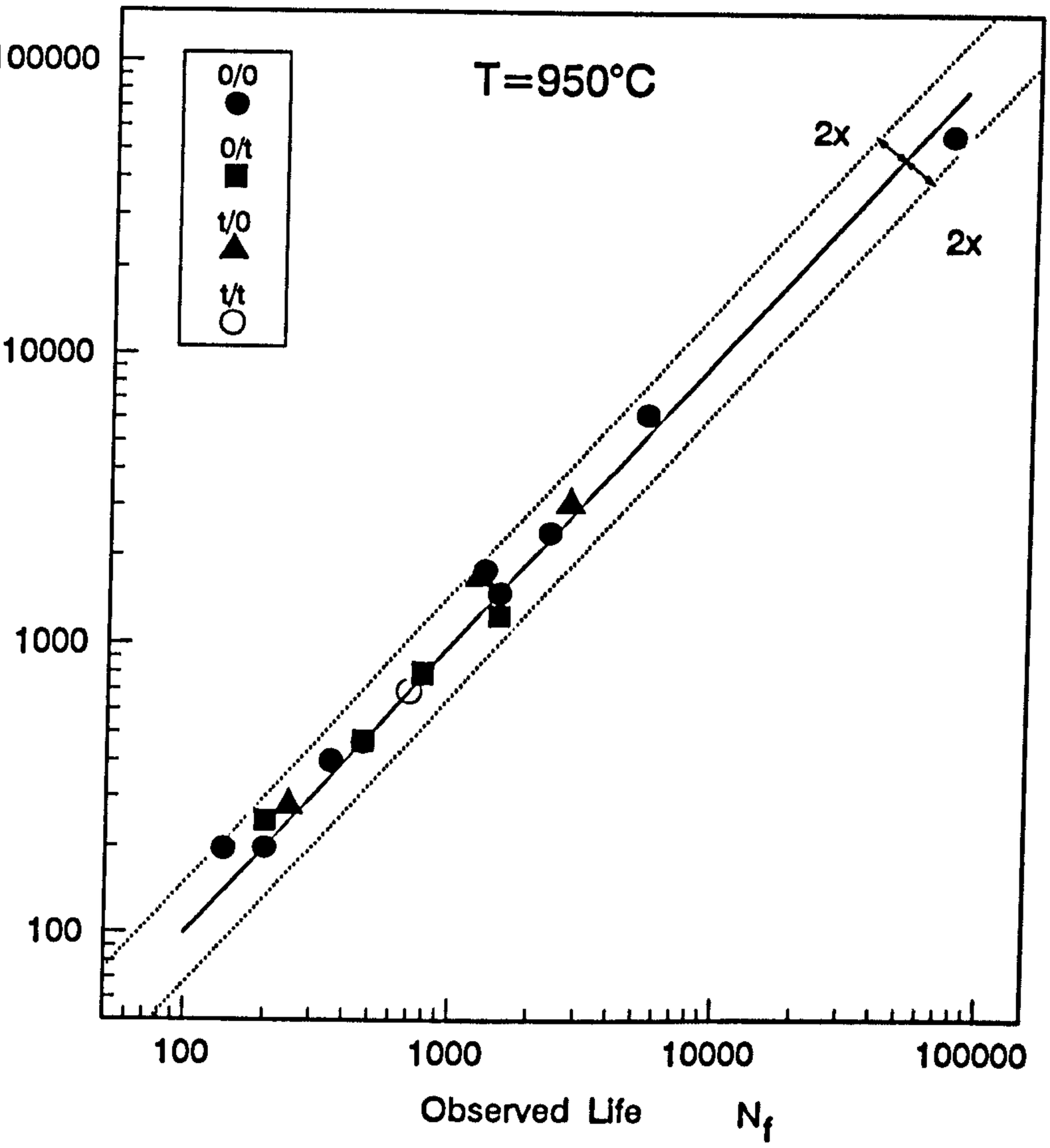

Fig.8.9a. Life Prediction by Modified SRP Method (T=950°C)

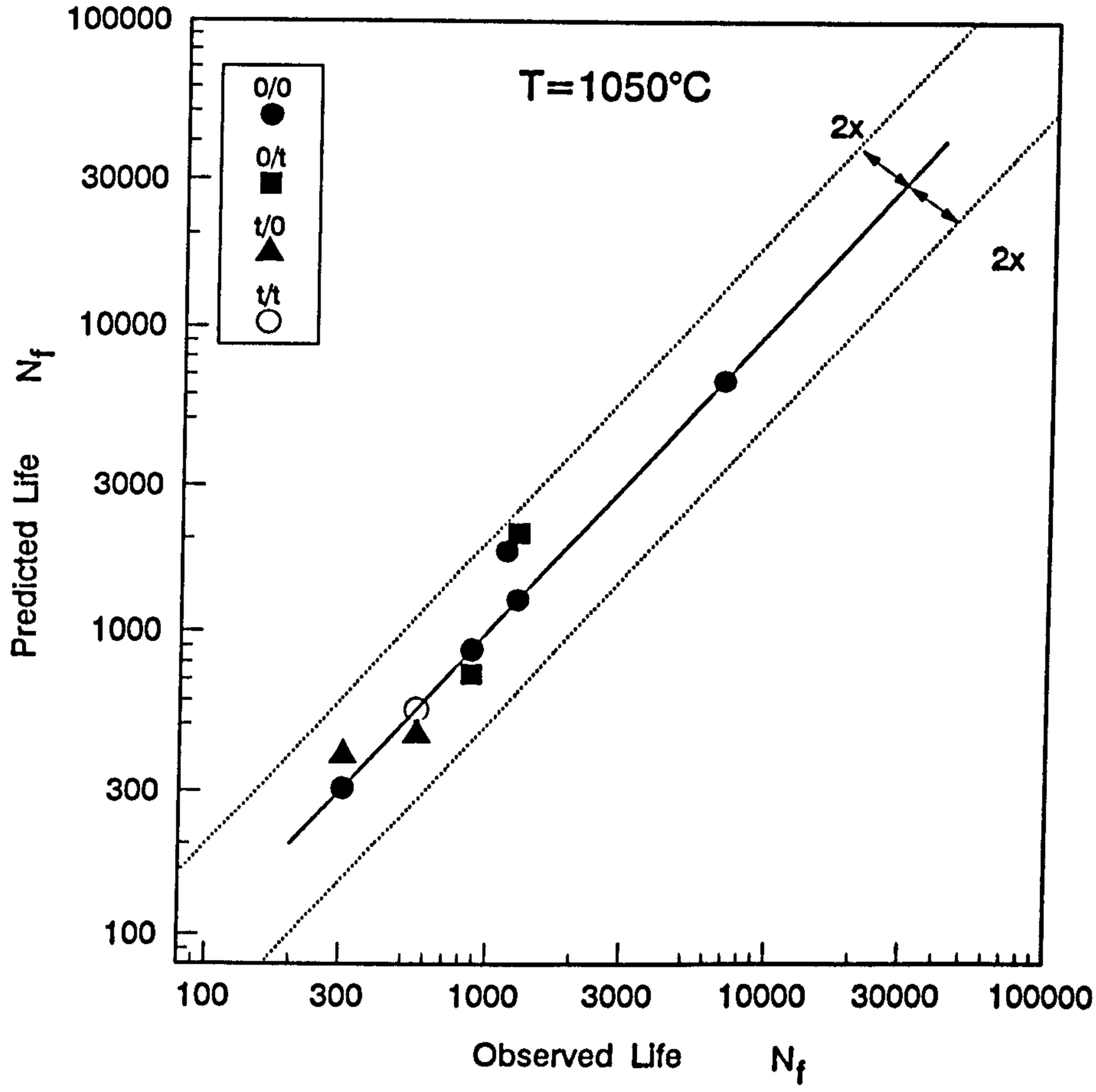

Fig.8.9b. Life Prediction by Modified SRP Method (T=1050°C)

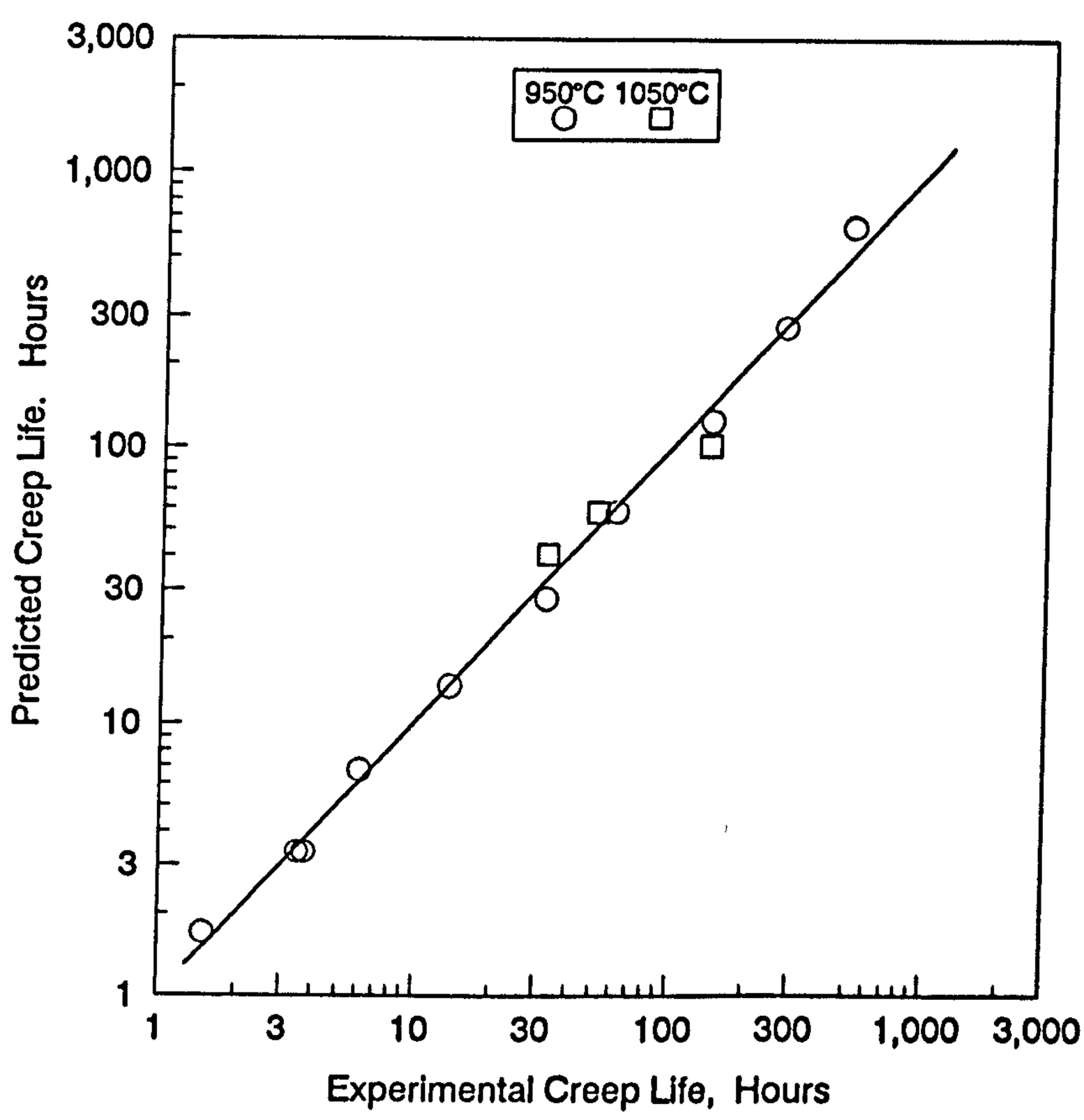

Fig.8.10. Comparison Between Experimenal and Predicted Creep Life by Dorn Type Function

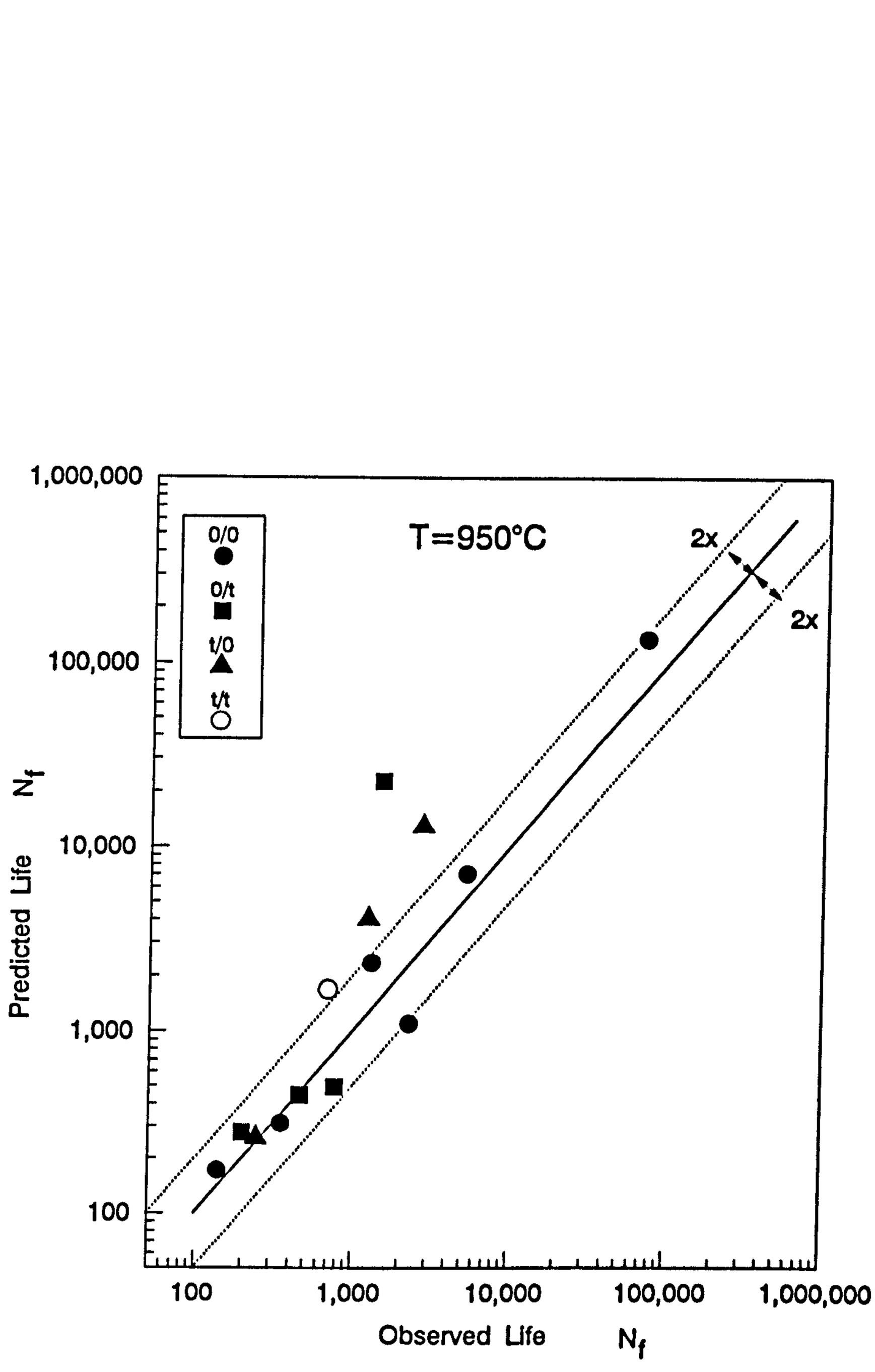

Fig.8.11a. Life Prediction by Modified Linear Damage Summation Rule (T=950°C)

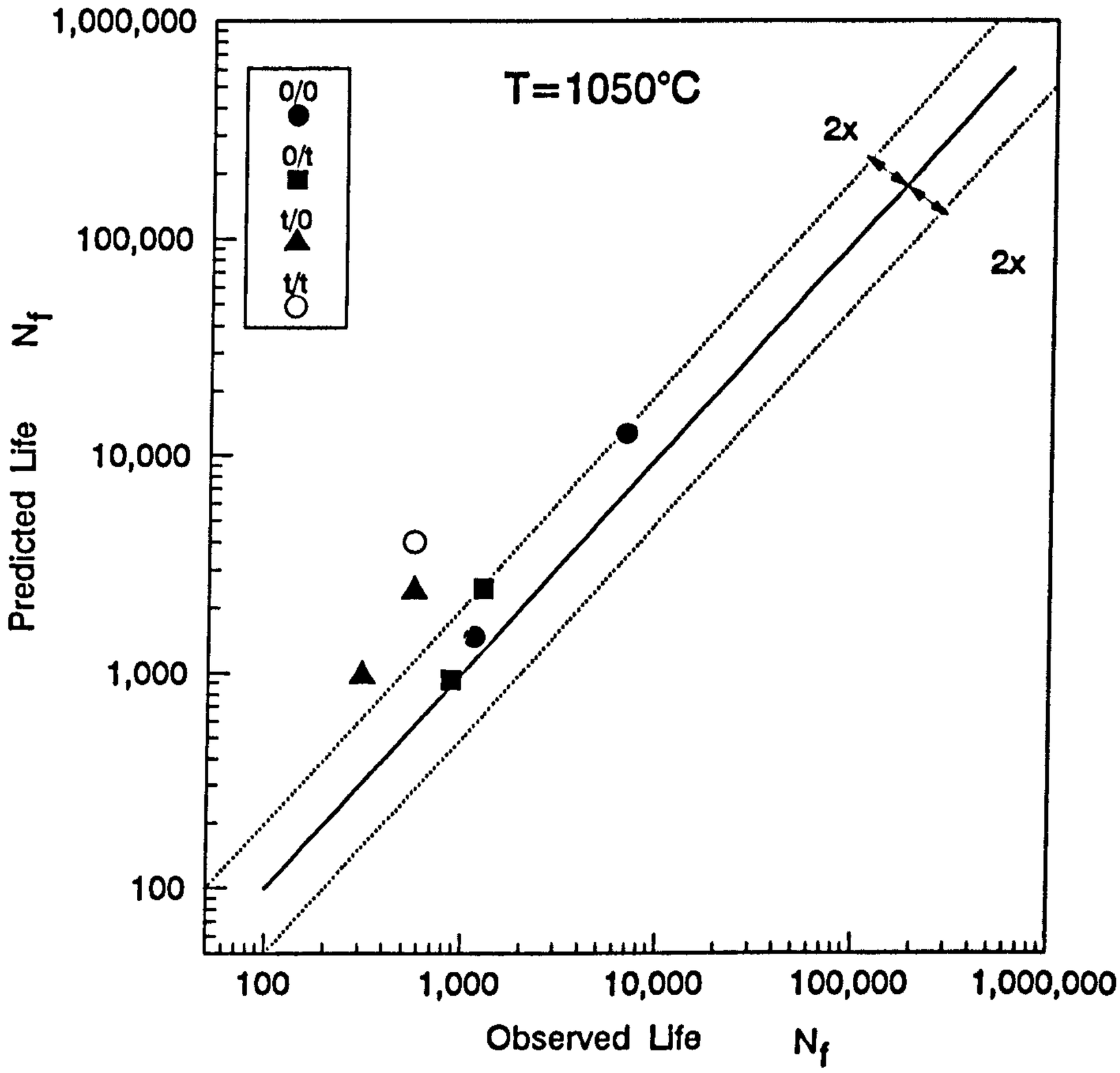

Fig.8.11b. Life Prediction by Modified Linear Damage Summation Rule (T=1050°C)

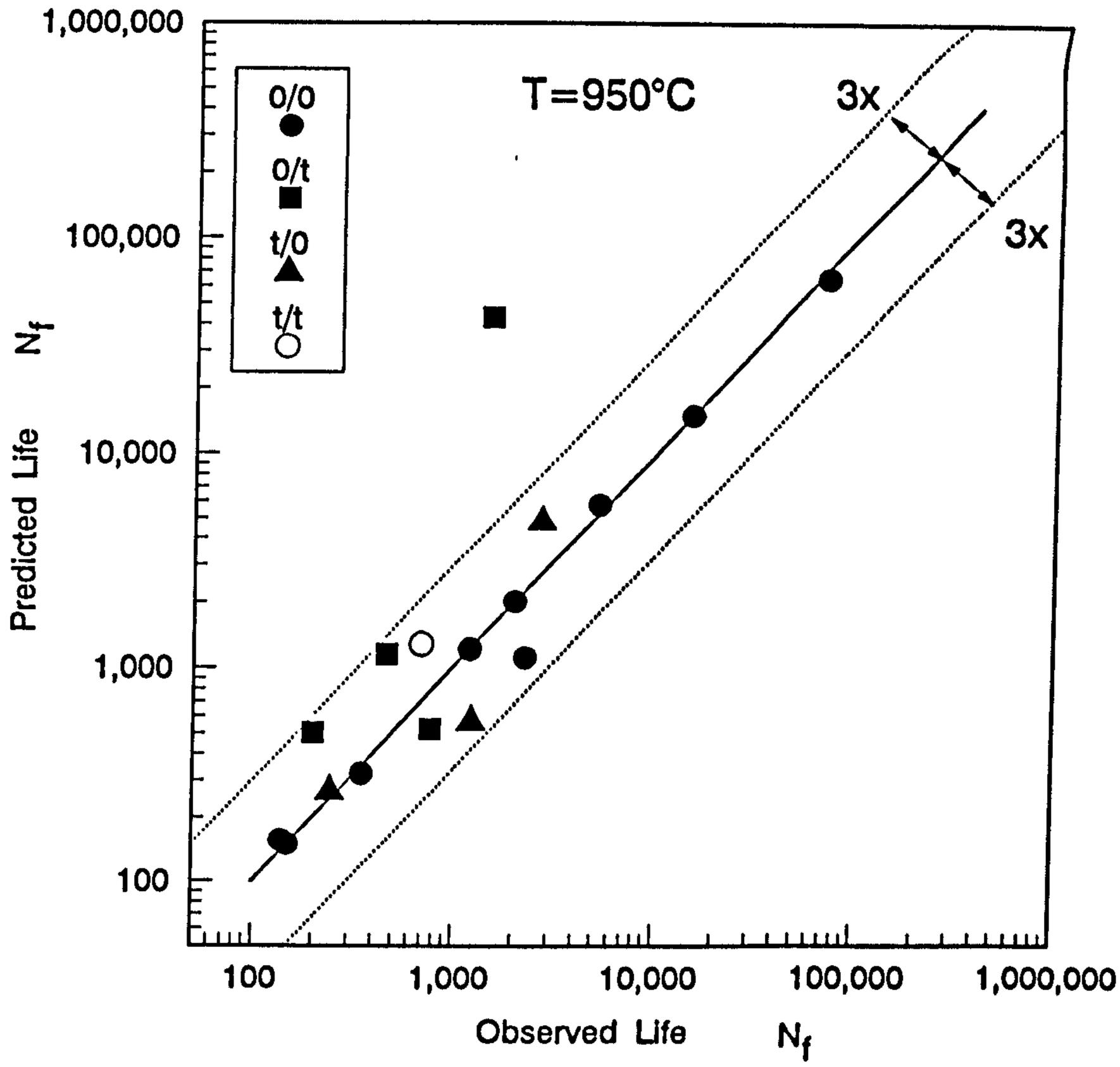

Fig.8.12. Life Prediction by Combined Constitutive Model with Modified Linear Damage Summation Rule

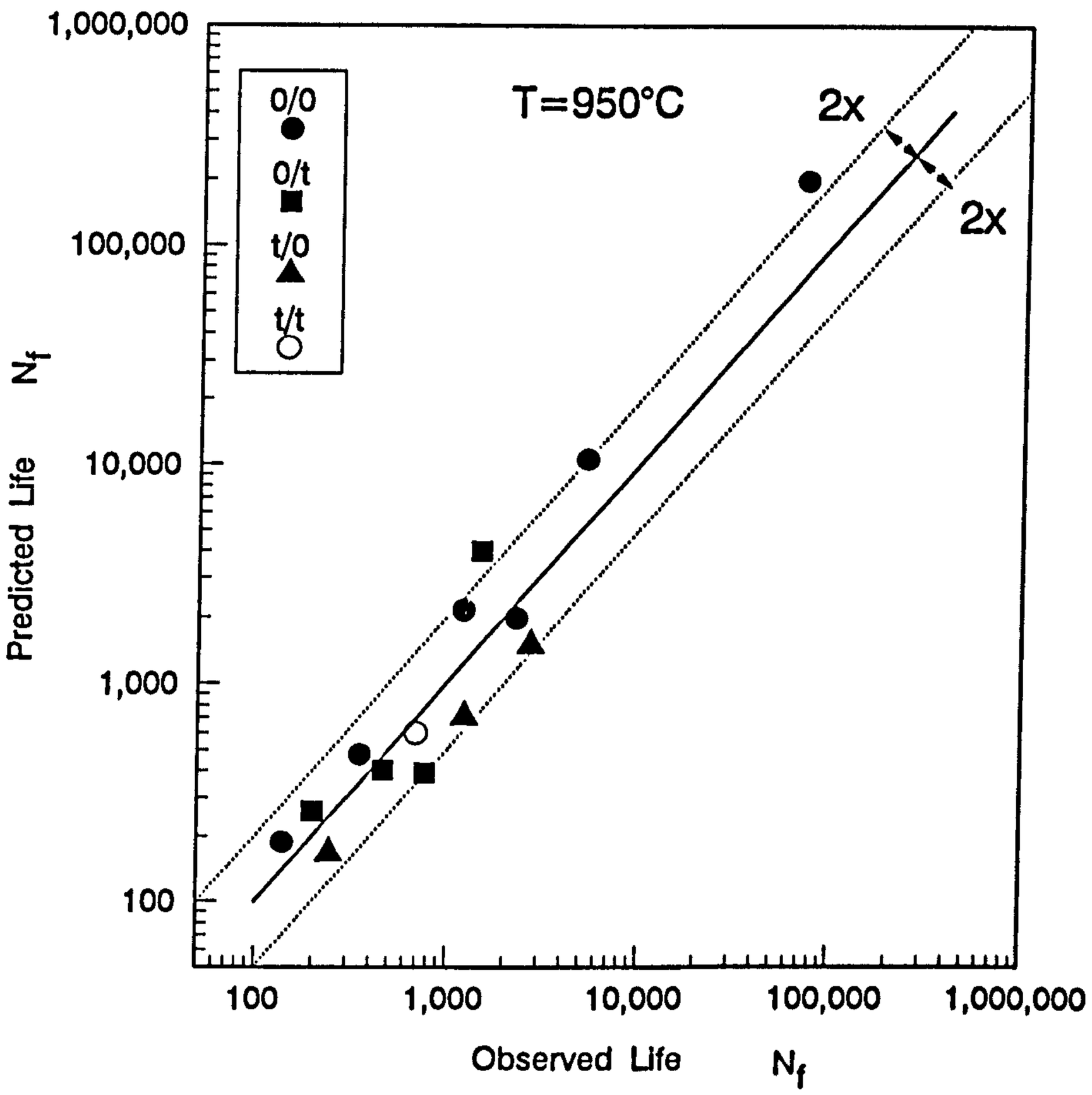

Fig.8.13. Life Prediction by Combined Constitutive Model with Modified SRP Method

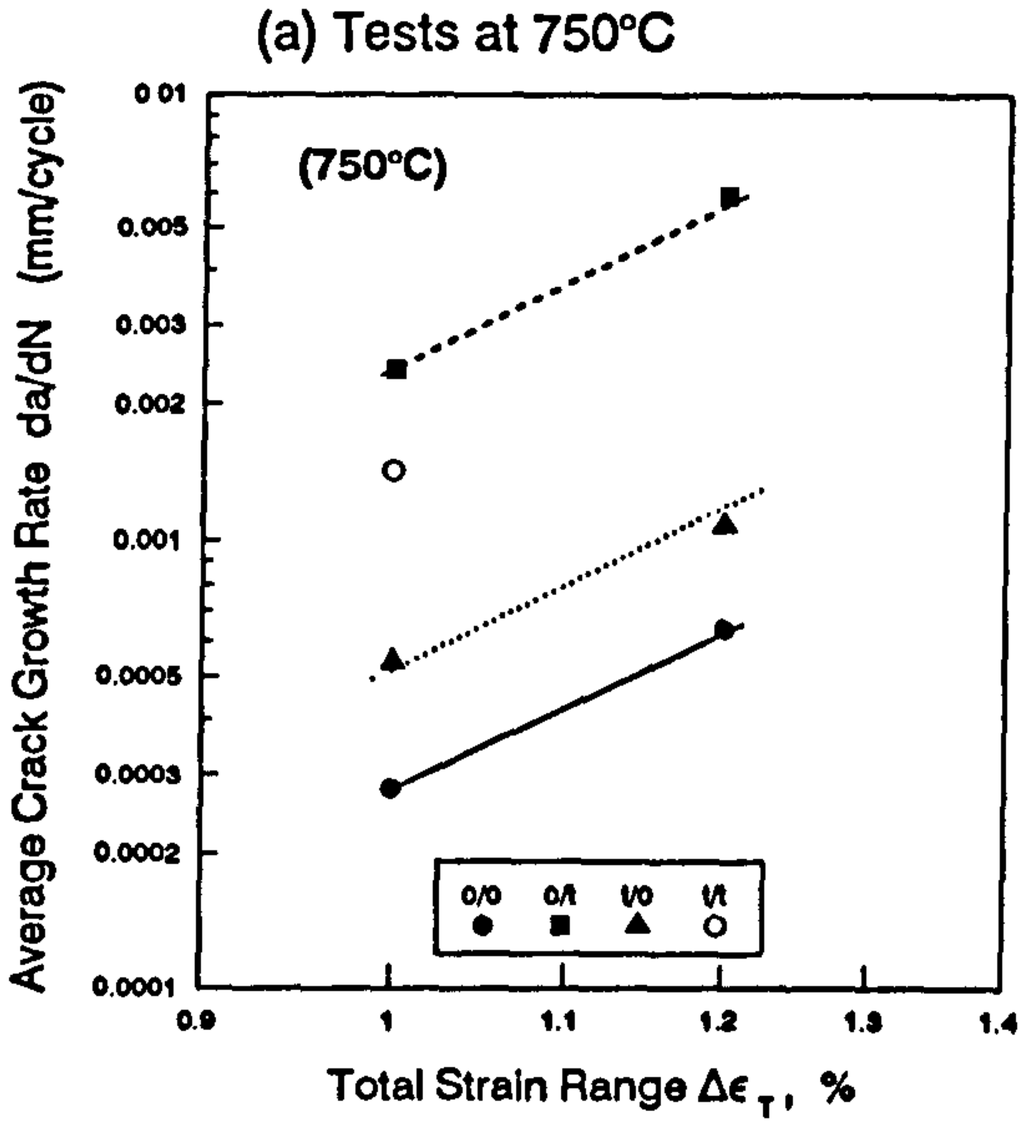

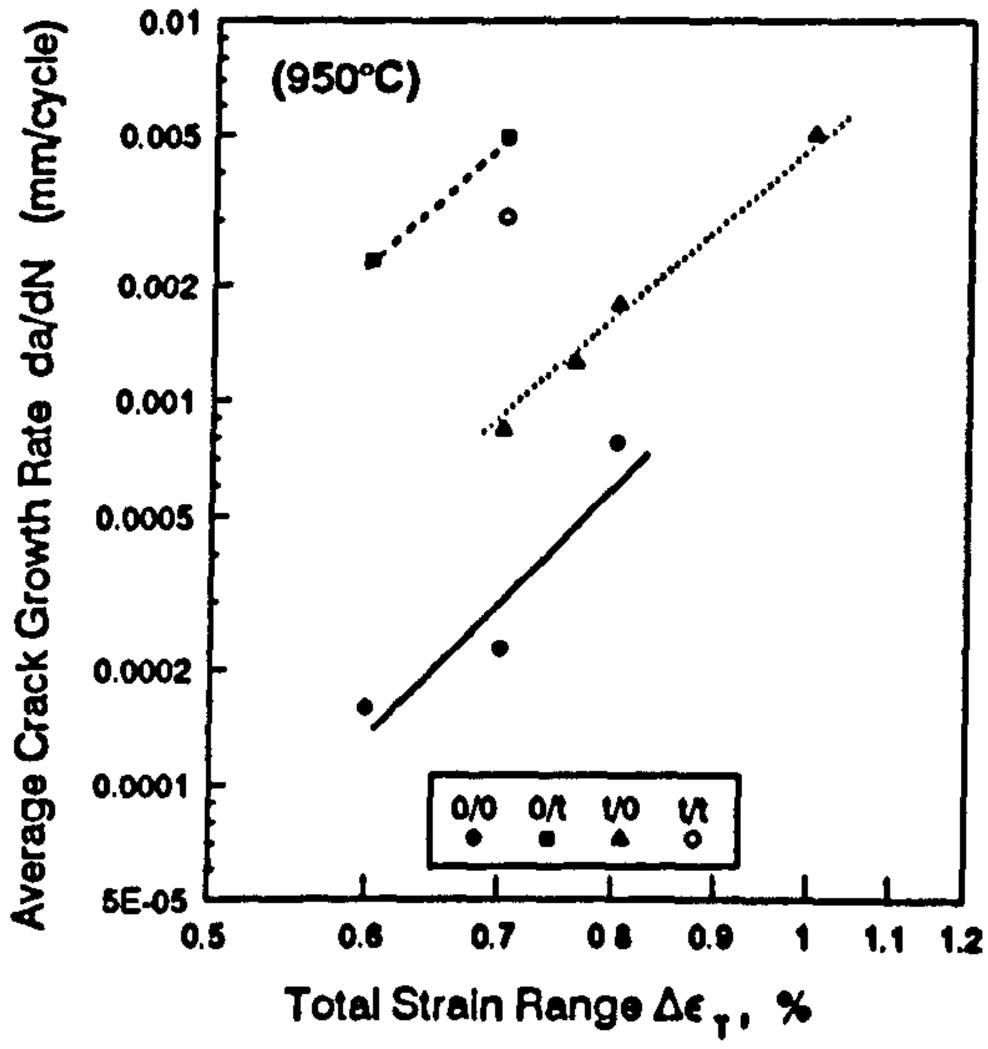

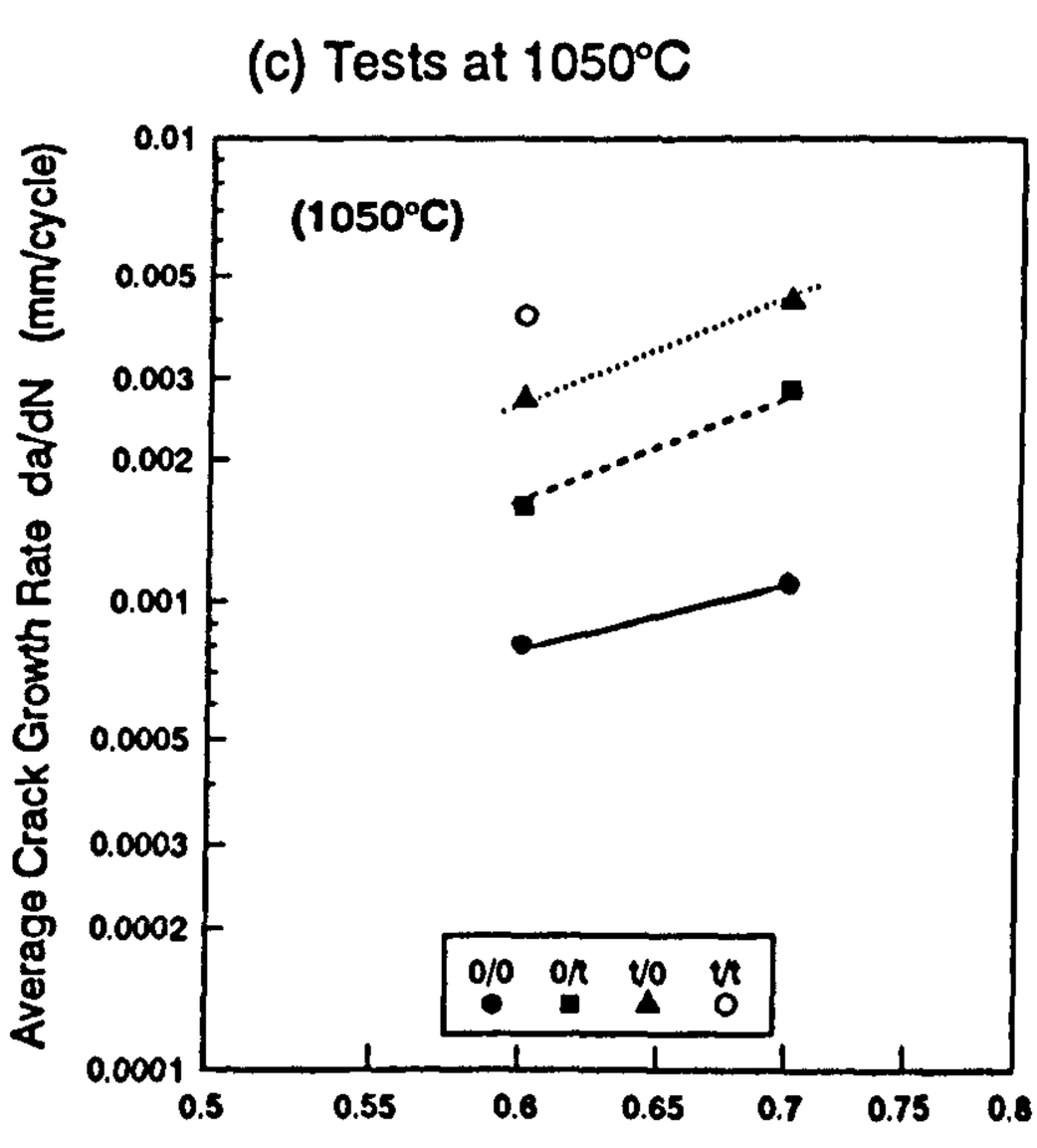

Fig.9.1 Crack Growth Rate as a Function of Total Strain Range

(a) Tests at 750°C
(b) Tests at 950°C
(c) Tests at 1050°C

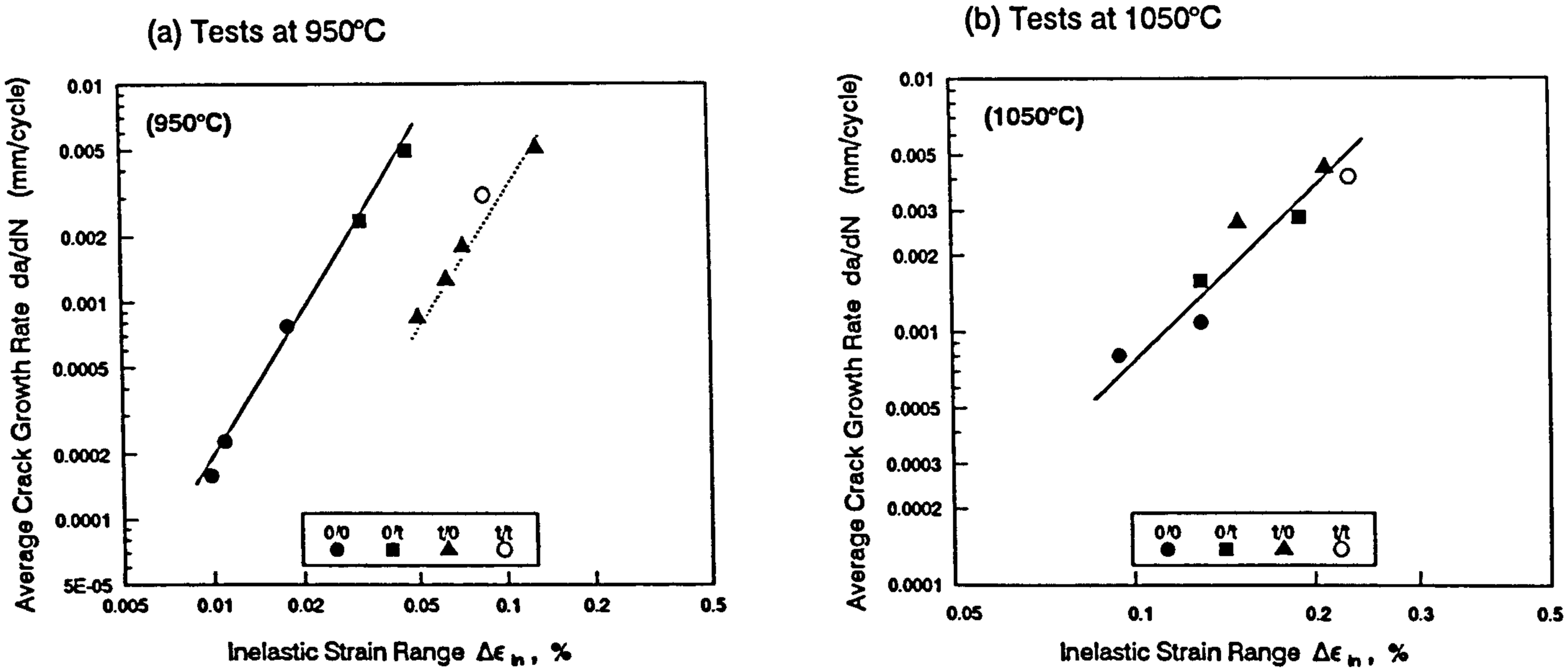

Fig.9.2. Crack Growth Rate as a Function of Inelastic Strain Range
(a) Tests at 950°C
(b) Tests at 1050°C

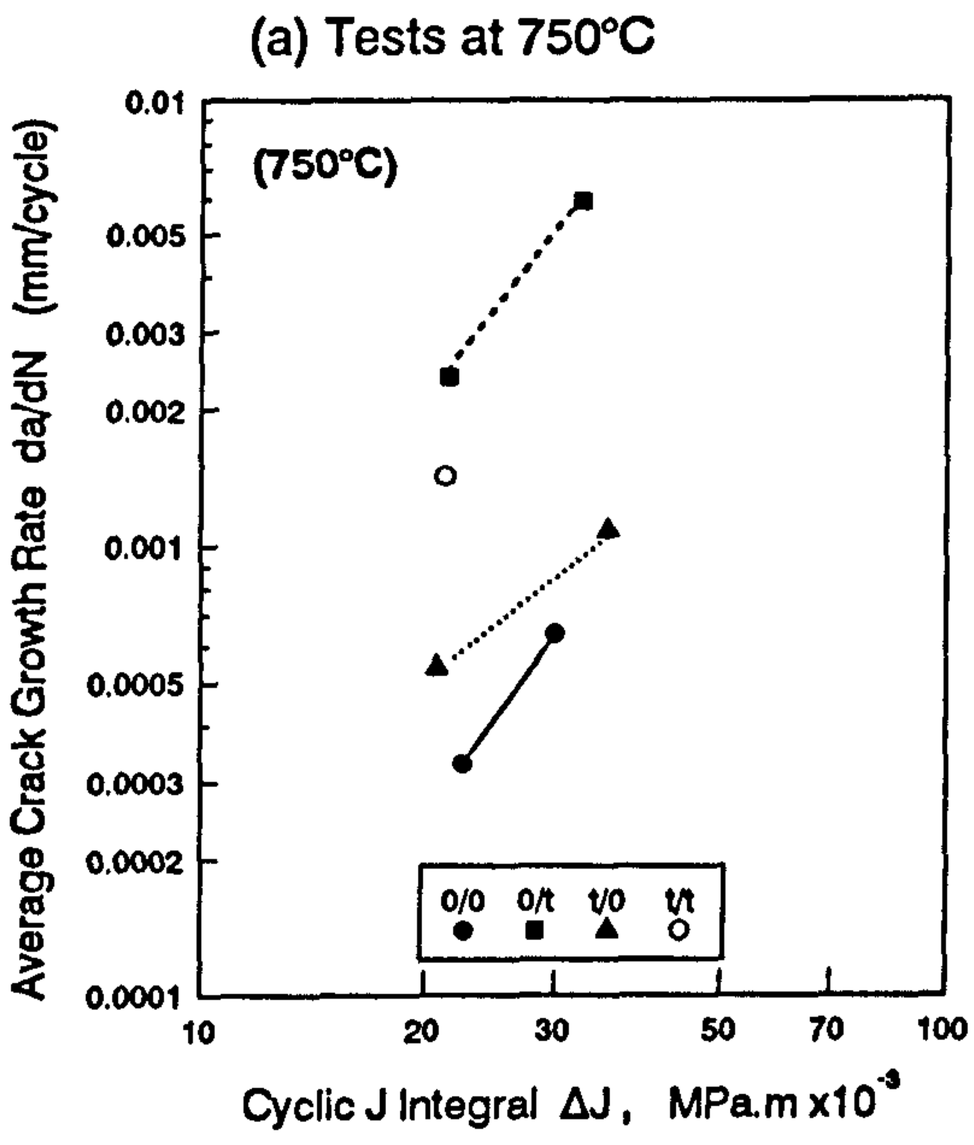

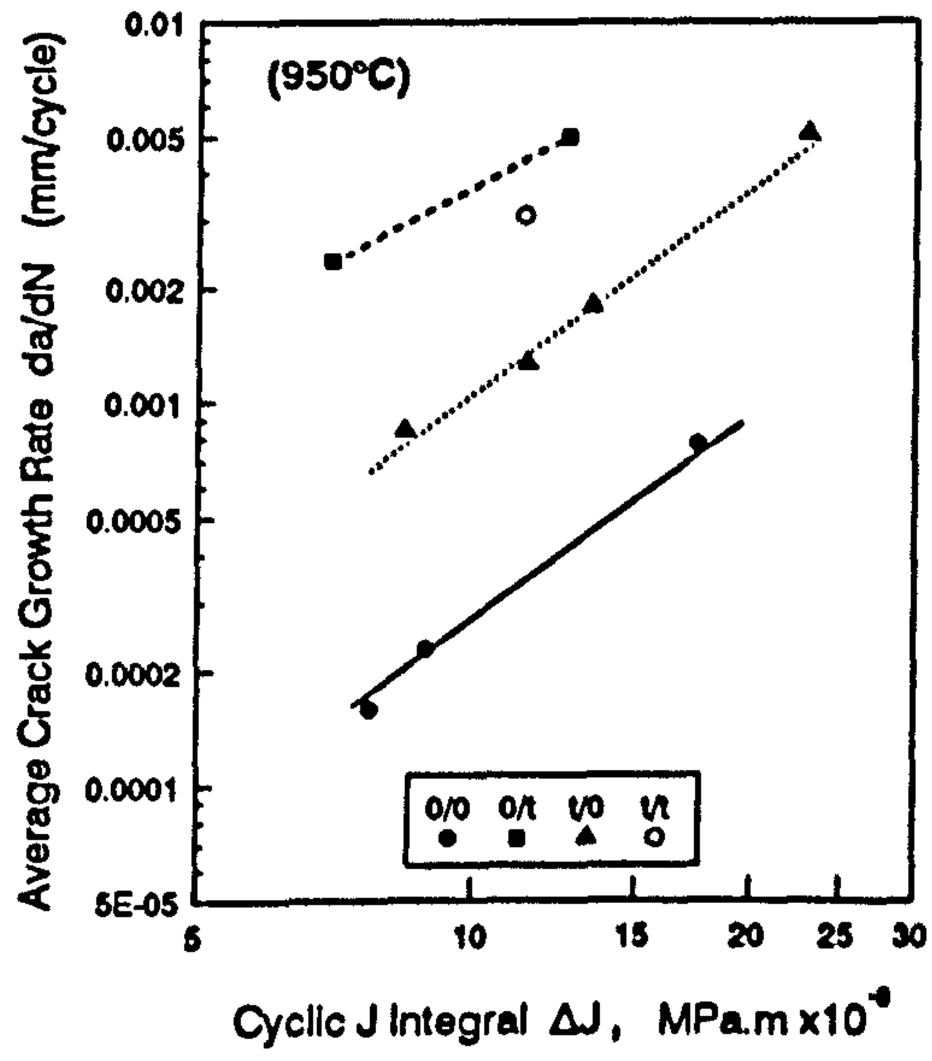

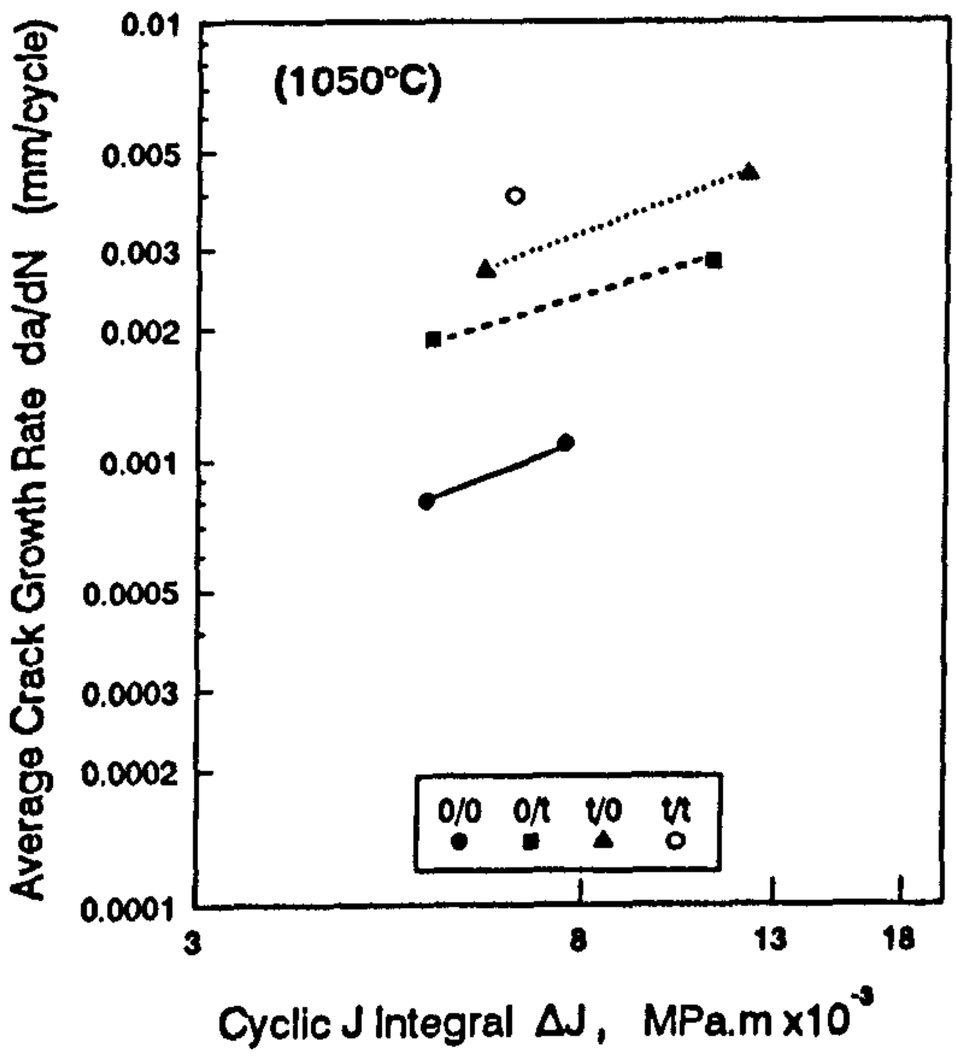

Fig.9.3 Crack Growth Rate as a Function of ΔJ

(a) Tests at 750°C
(b) Tests at 950°C
(c) Tests at 1050°C

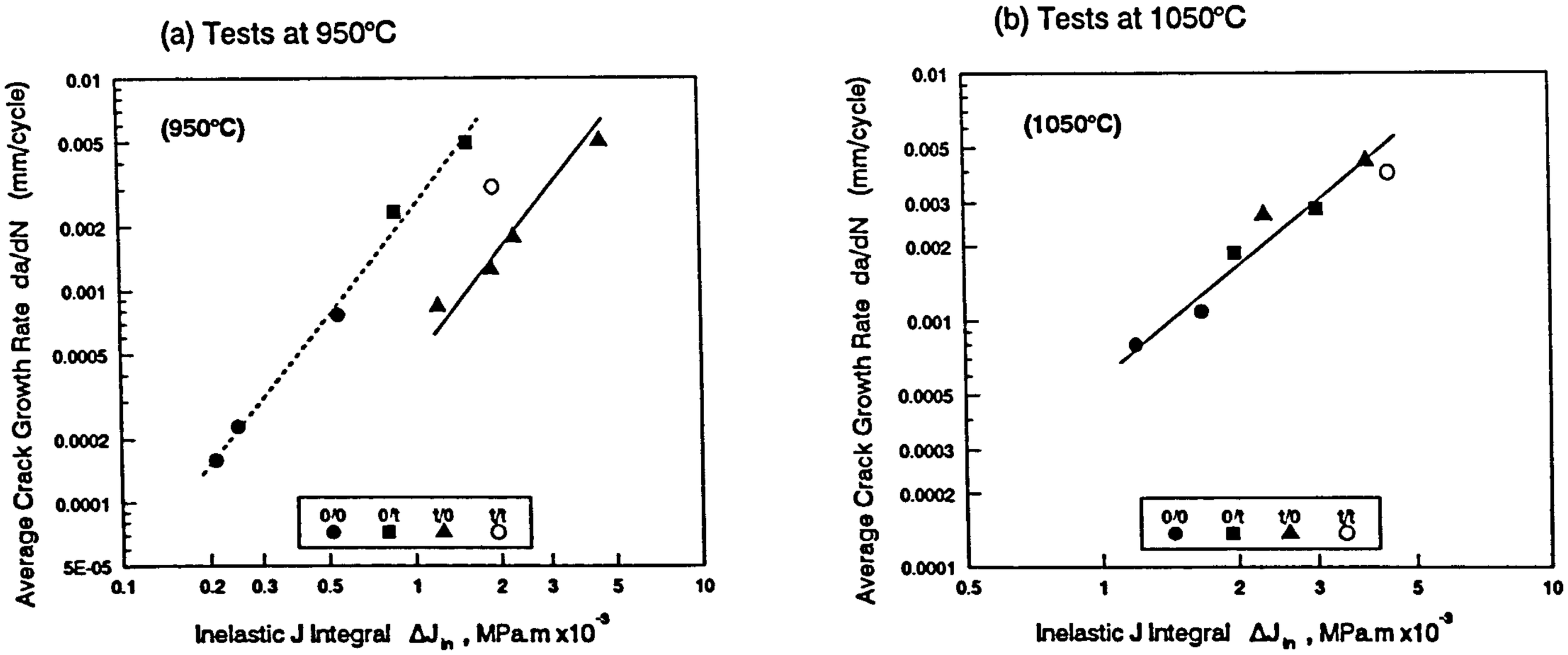

Fig.9.4. Crack Growth Rate as a Function of Inelastic J Integral ΔJ_{In}
(a) Tests at 950°C
(b) Tests at 1050°C

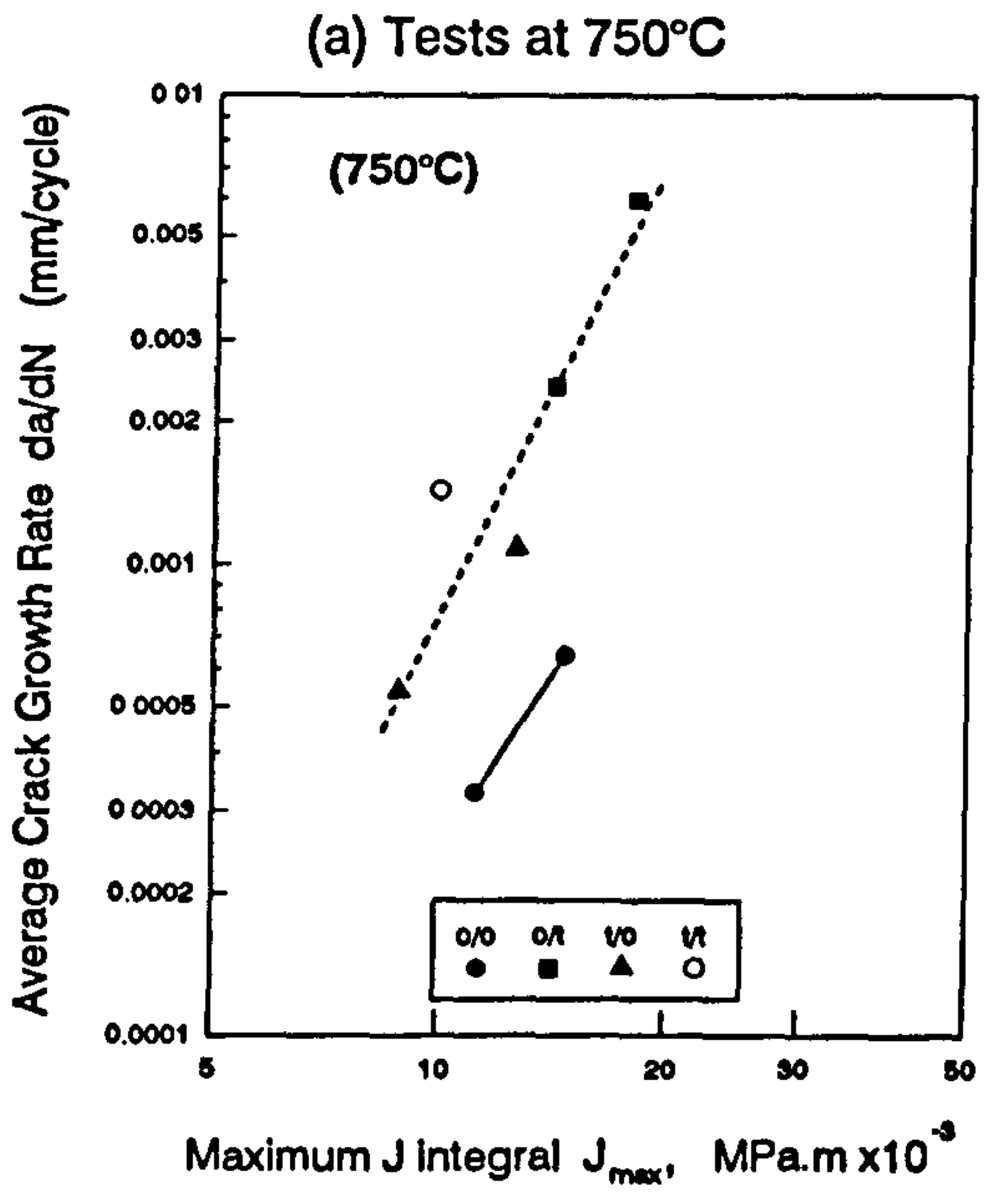

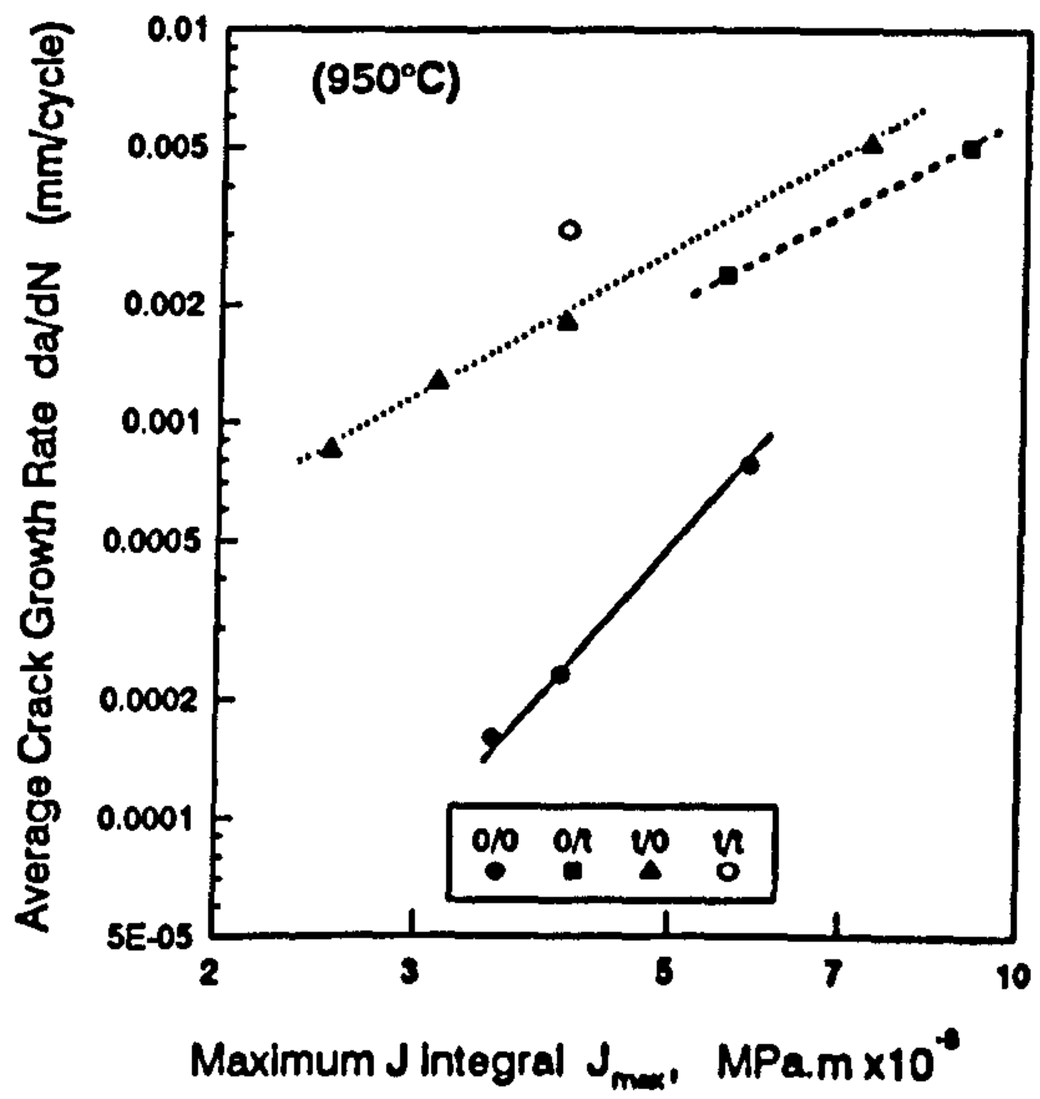

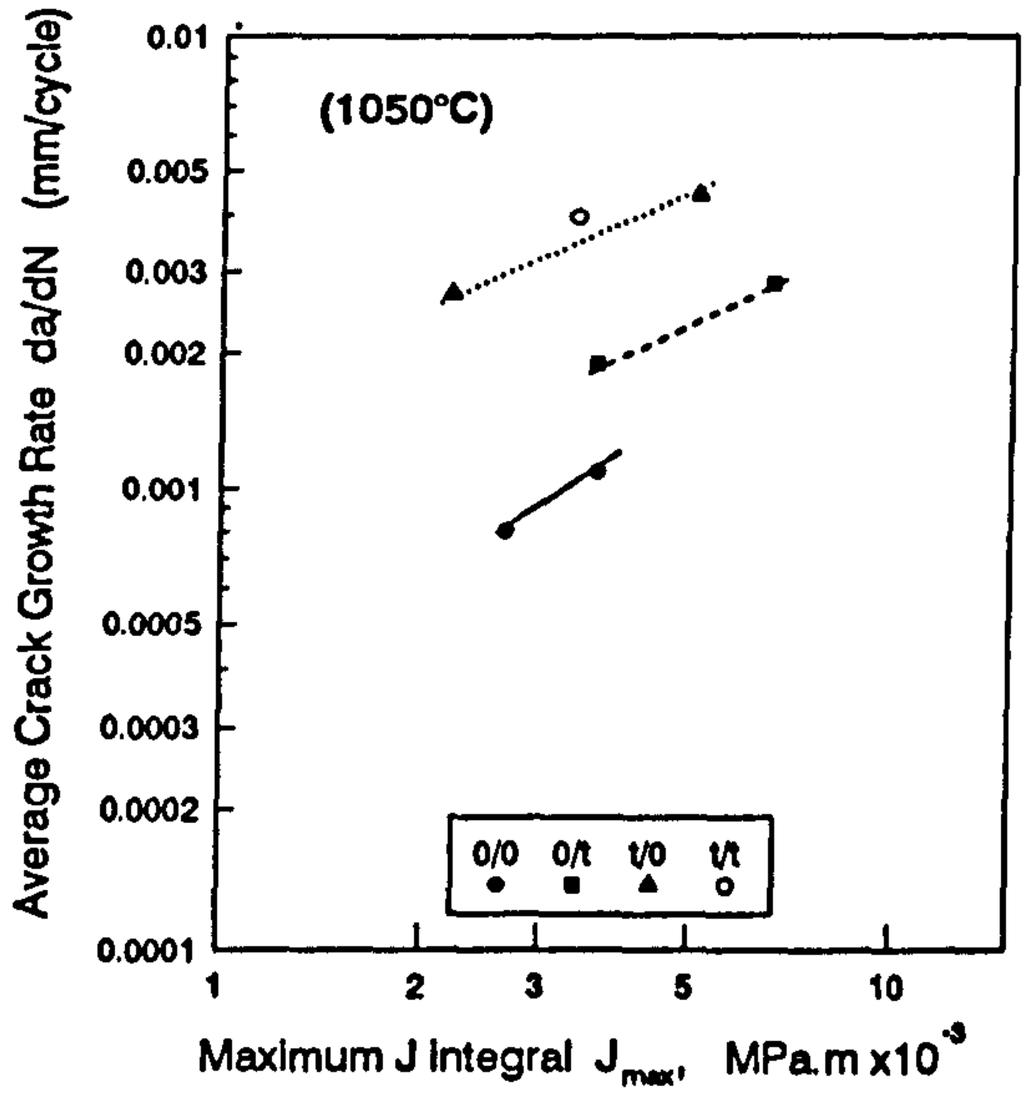

Fig.9.5. Crack Growth Rate as a Function of J_{max}

(a) Tests at 750°C
(b) Tests at 950°C
(c) Tests at 1050°C

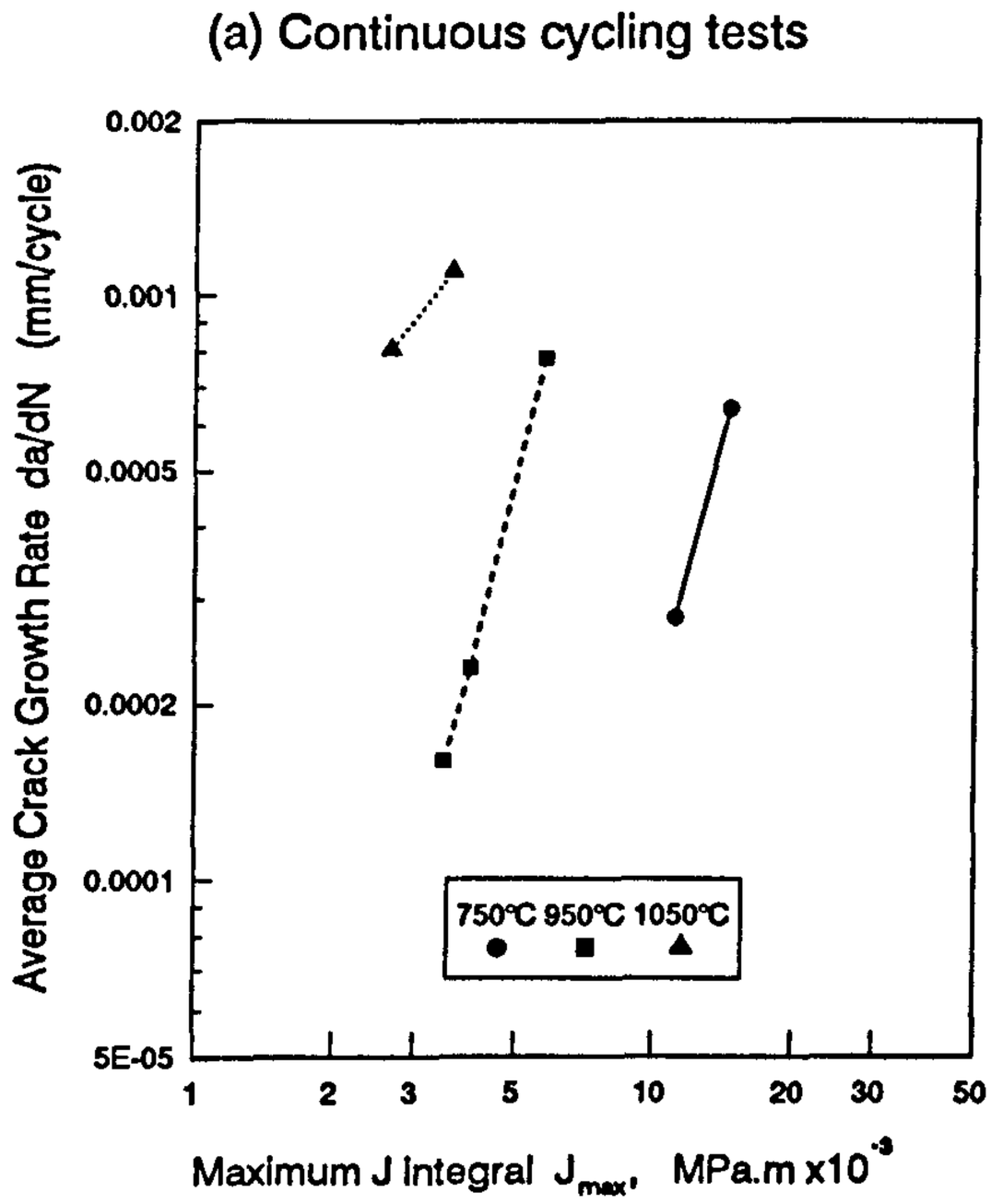

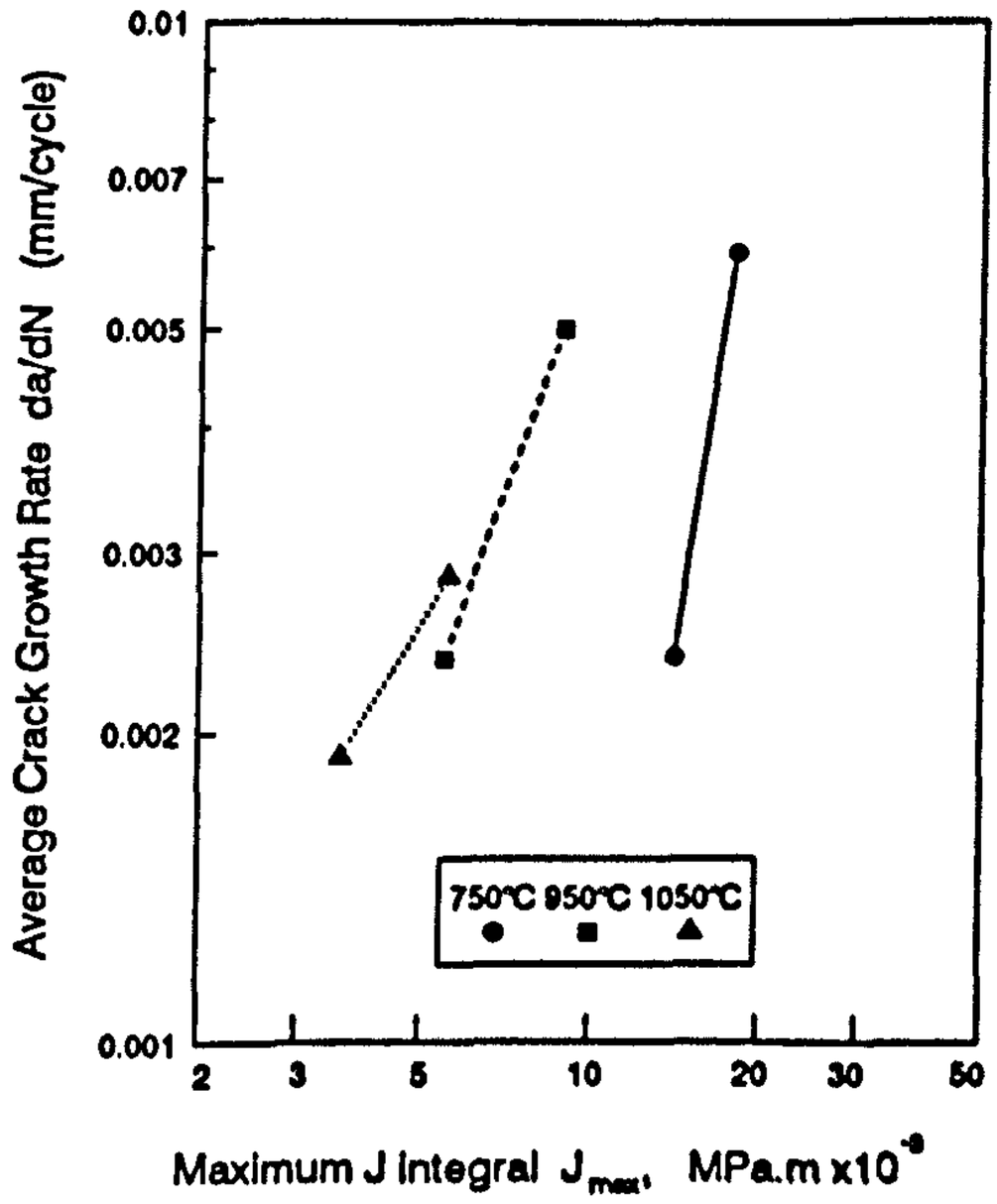

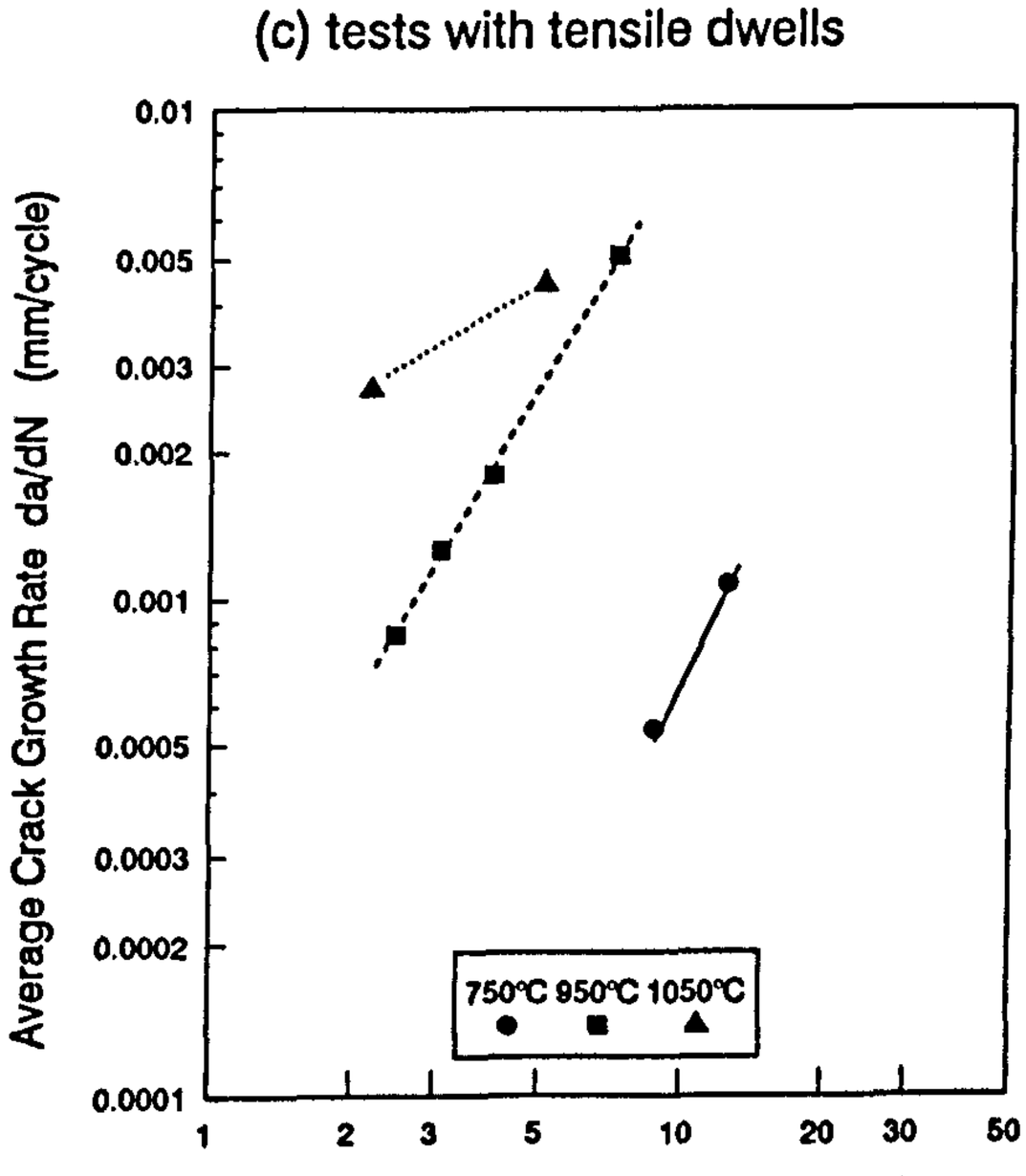

Fig.9.6 Effect of Temperature On Crack Growth Rates

(a) Continuous cycling tests

(b) Tests with compressive dwells

(c) tests with tensile dwells

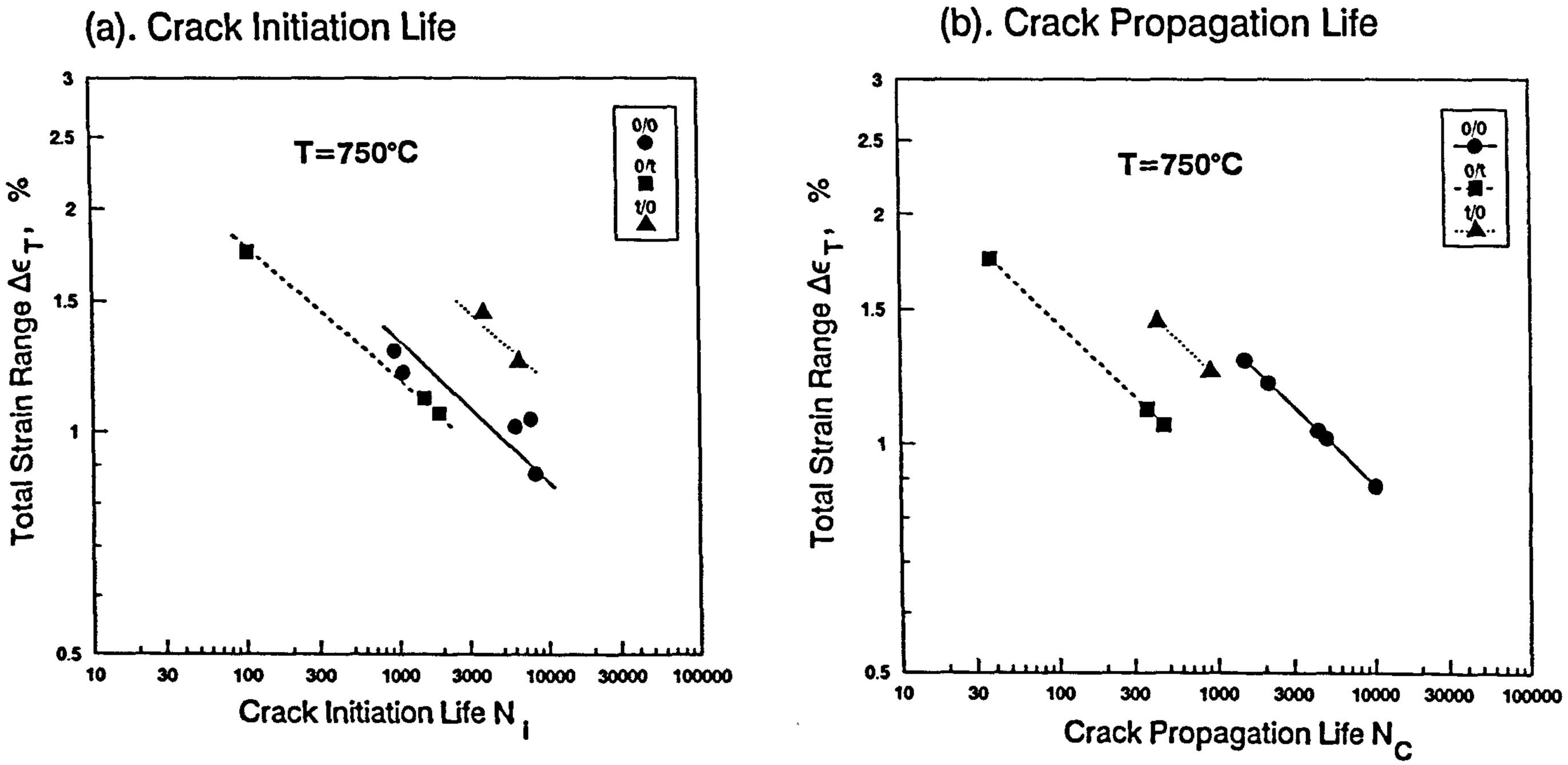

Fig.10.1. Influence of Strain Dwells on Crack Initiation and Propagation for Tests at 750°C

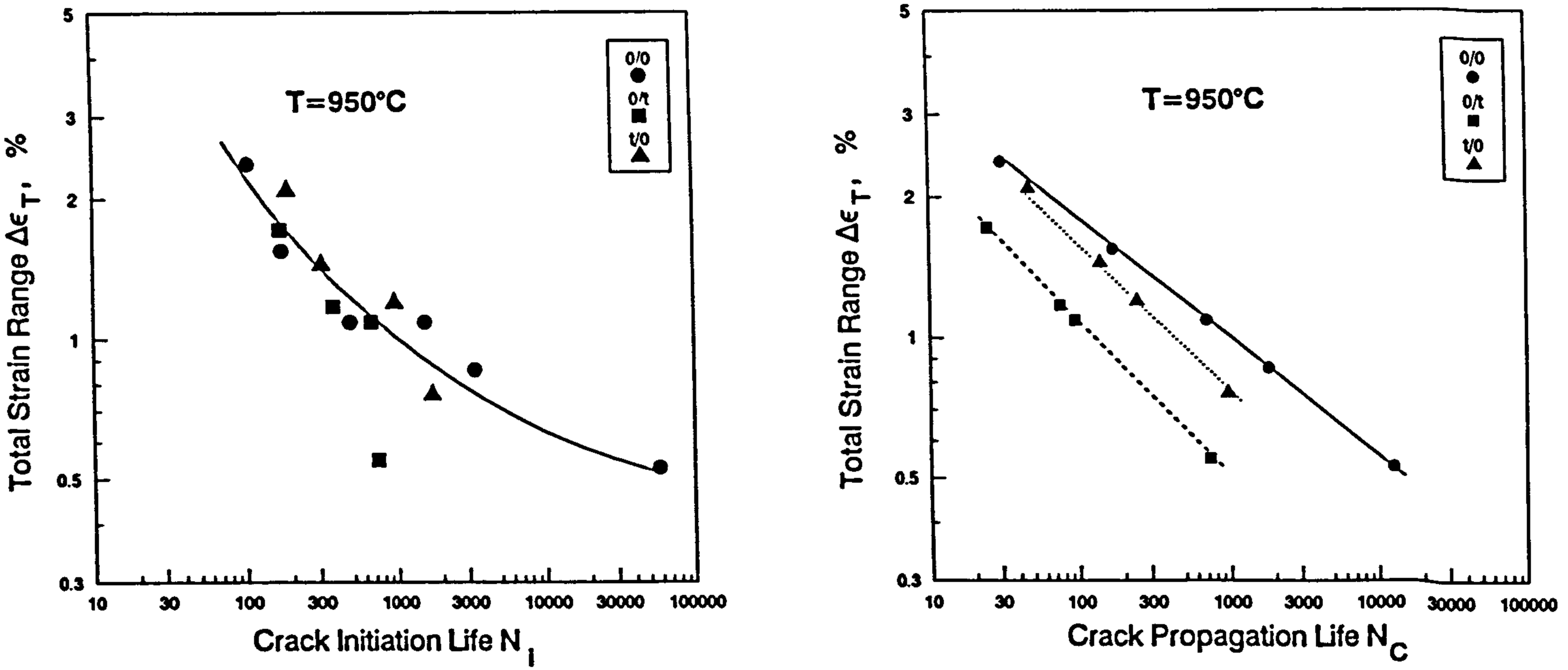

Fig.10.2. Influence of Strain Dwells on Crack Initiation and Propagation for Tests at 950°C

(a). Crack Initiation Life

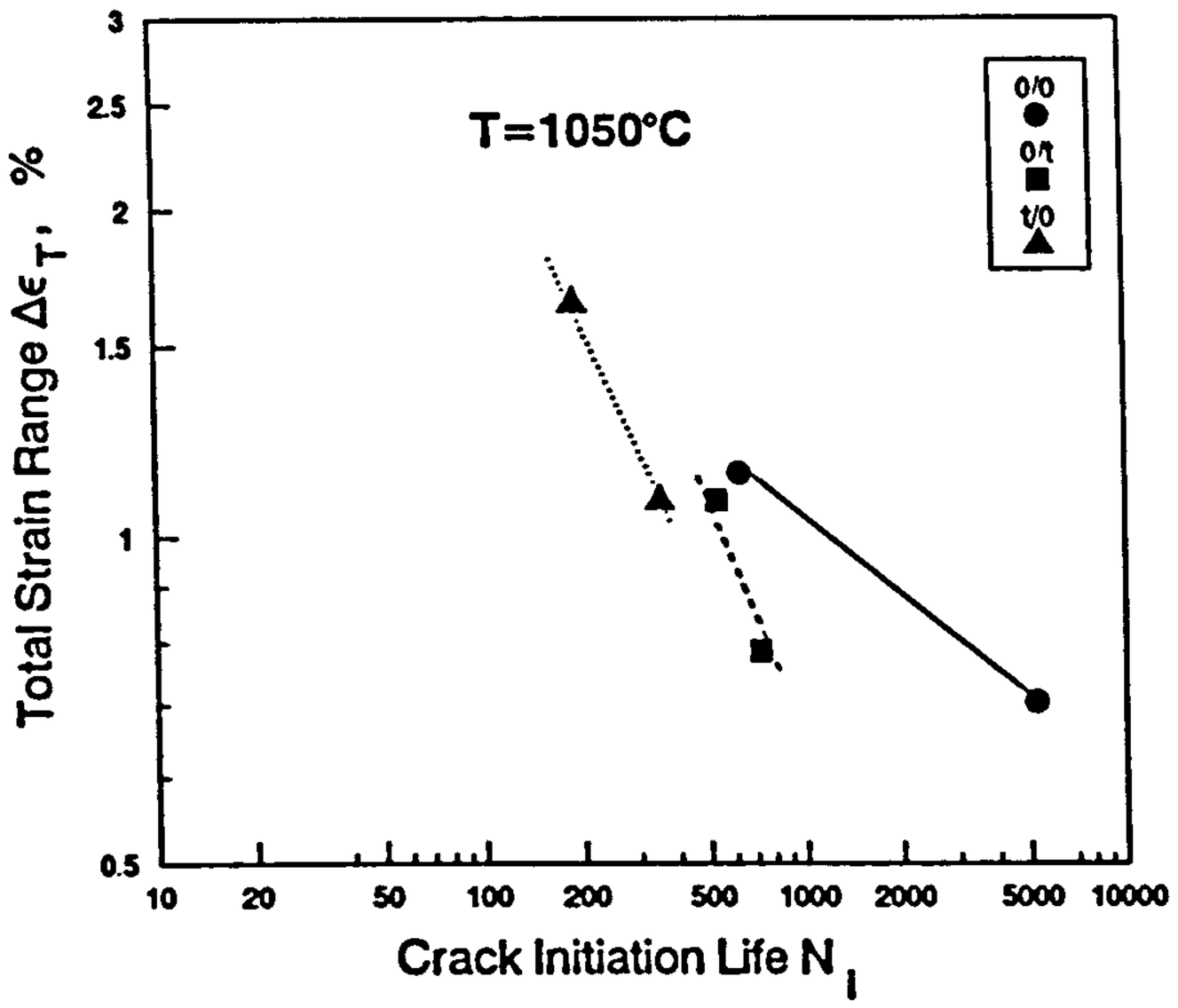

(b). Crack Propagation Life

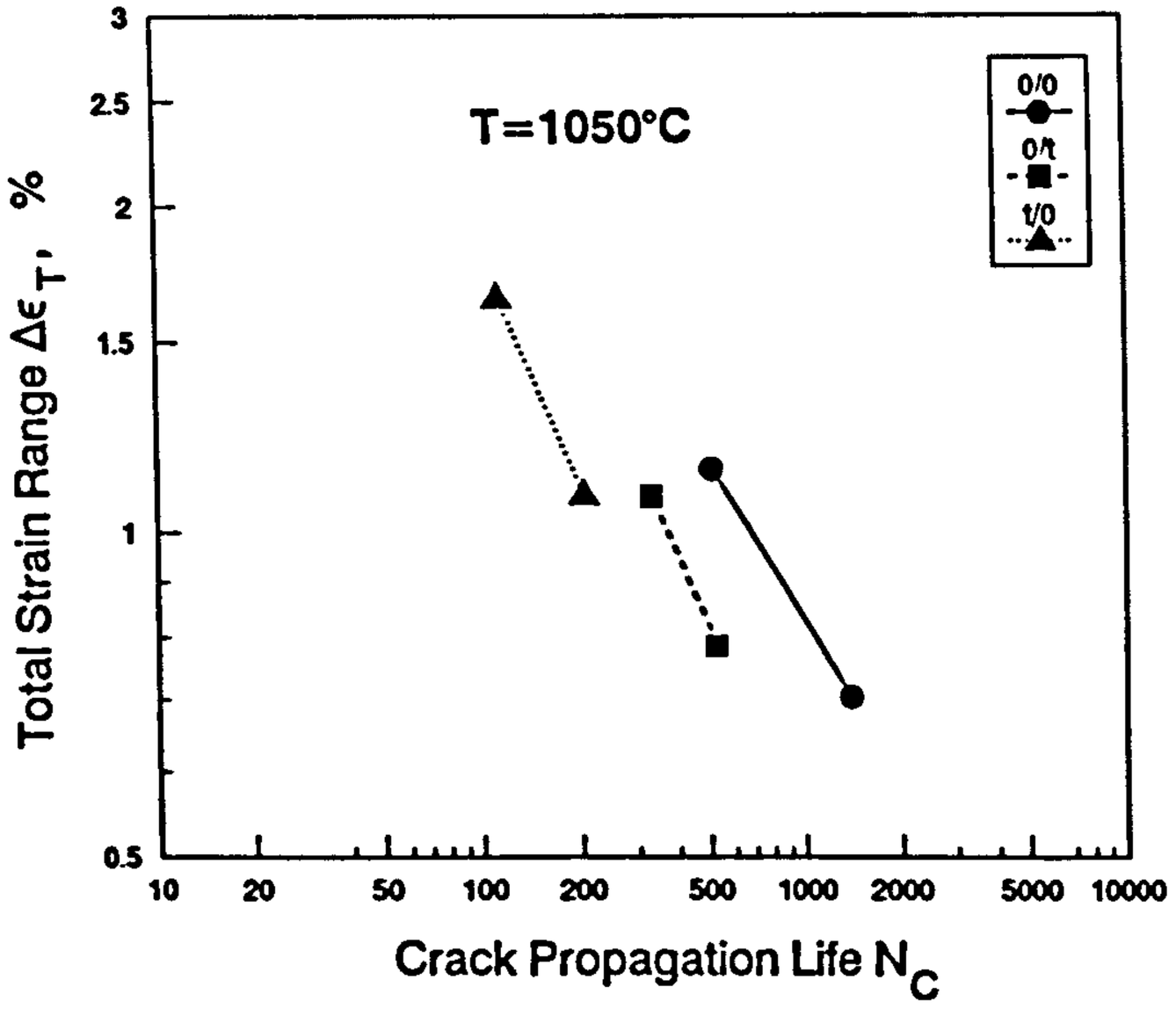

Fig.10.3. Influence of Strain Dwells on Crack Initiation and Propagation for Tests at 1050°C

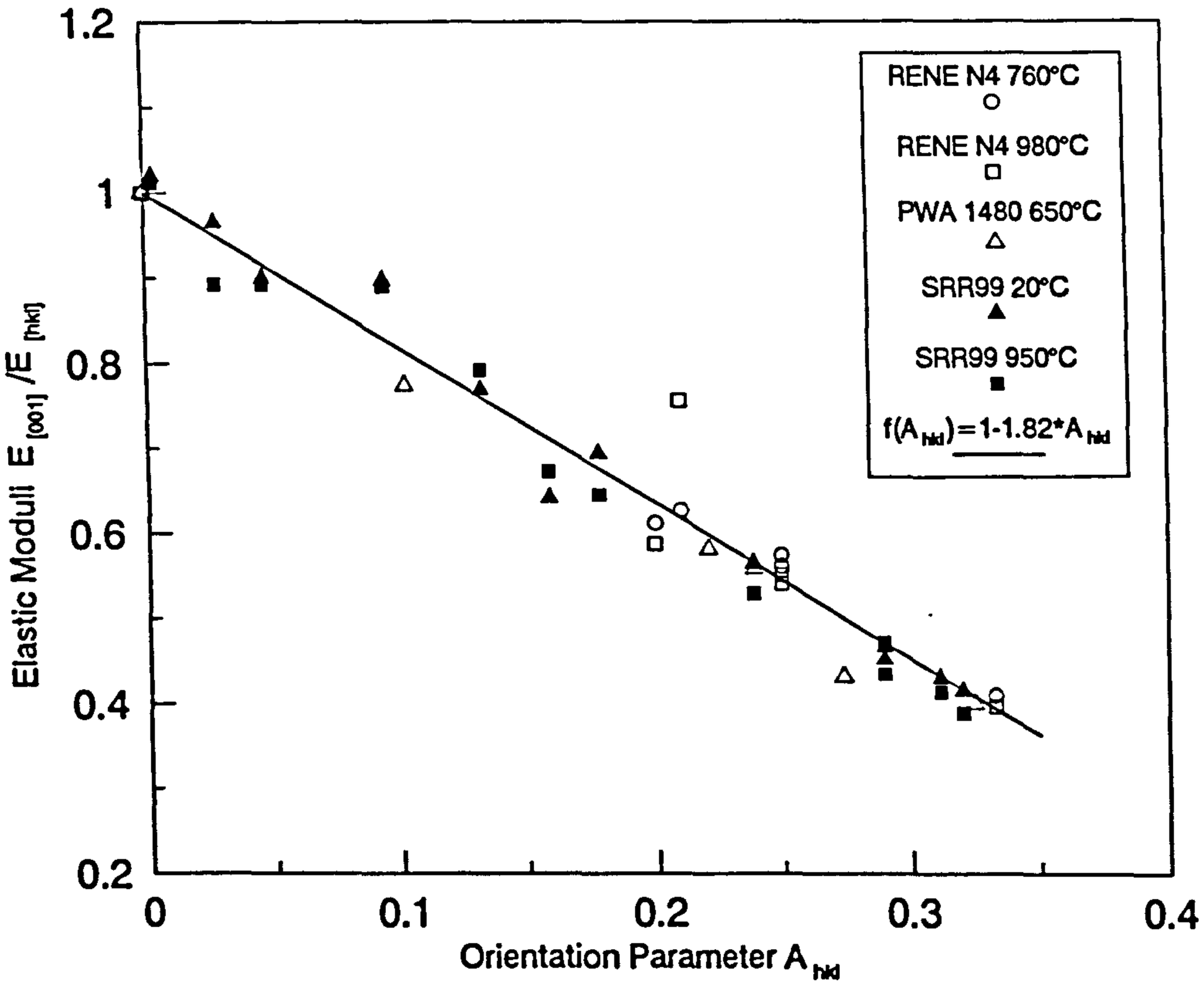

Fig.10.4. Elastic Modulus for Various Single Crystal Nickel Base Superalloys

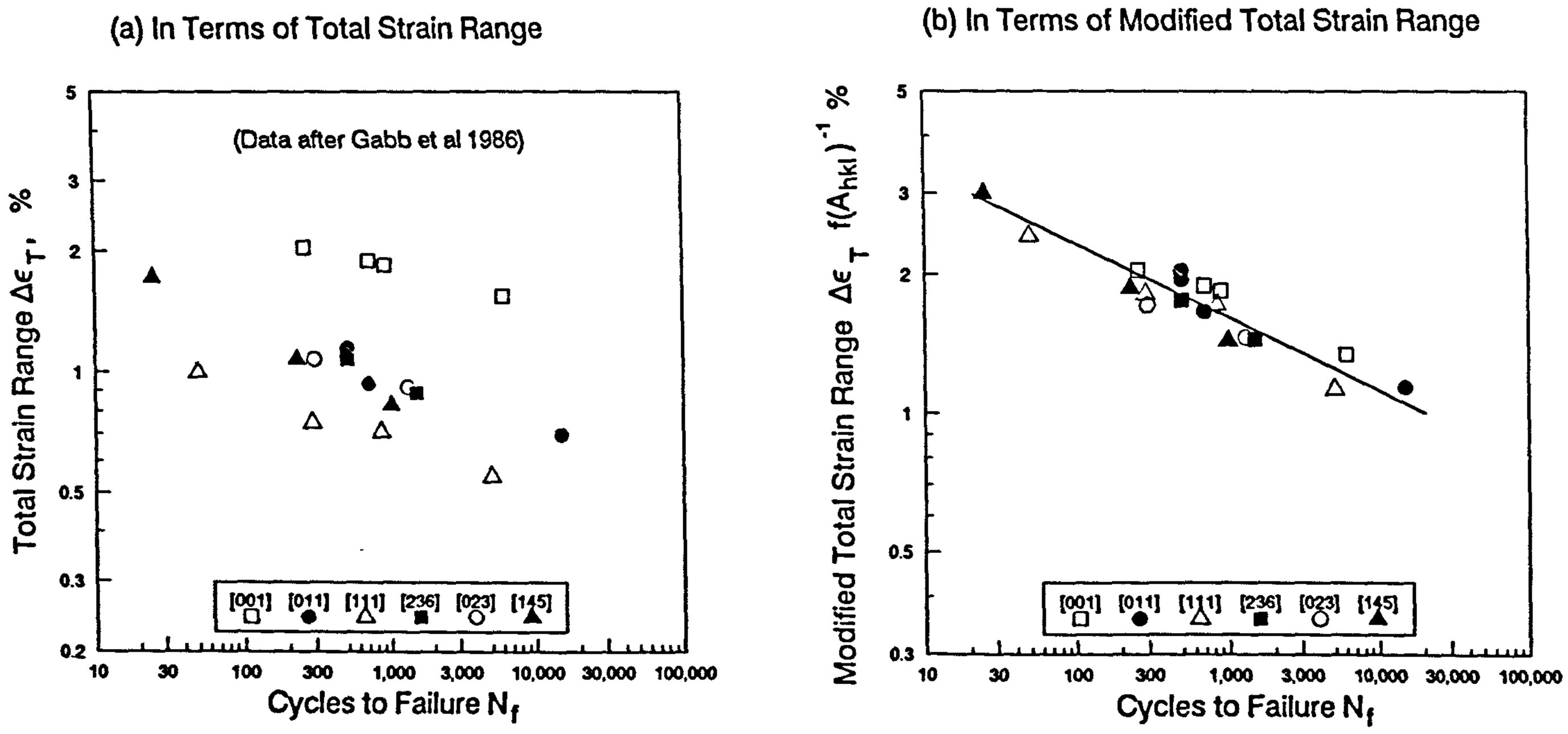

Fig.10.5. Fatigue Life of Single Crystal Rene N4 at 760°C

(a) In Terms of Total Strain Range

(b) In Terms of Modified Total Strain Range

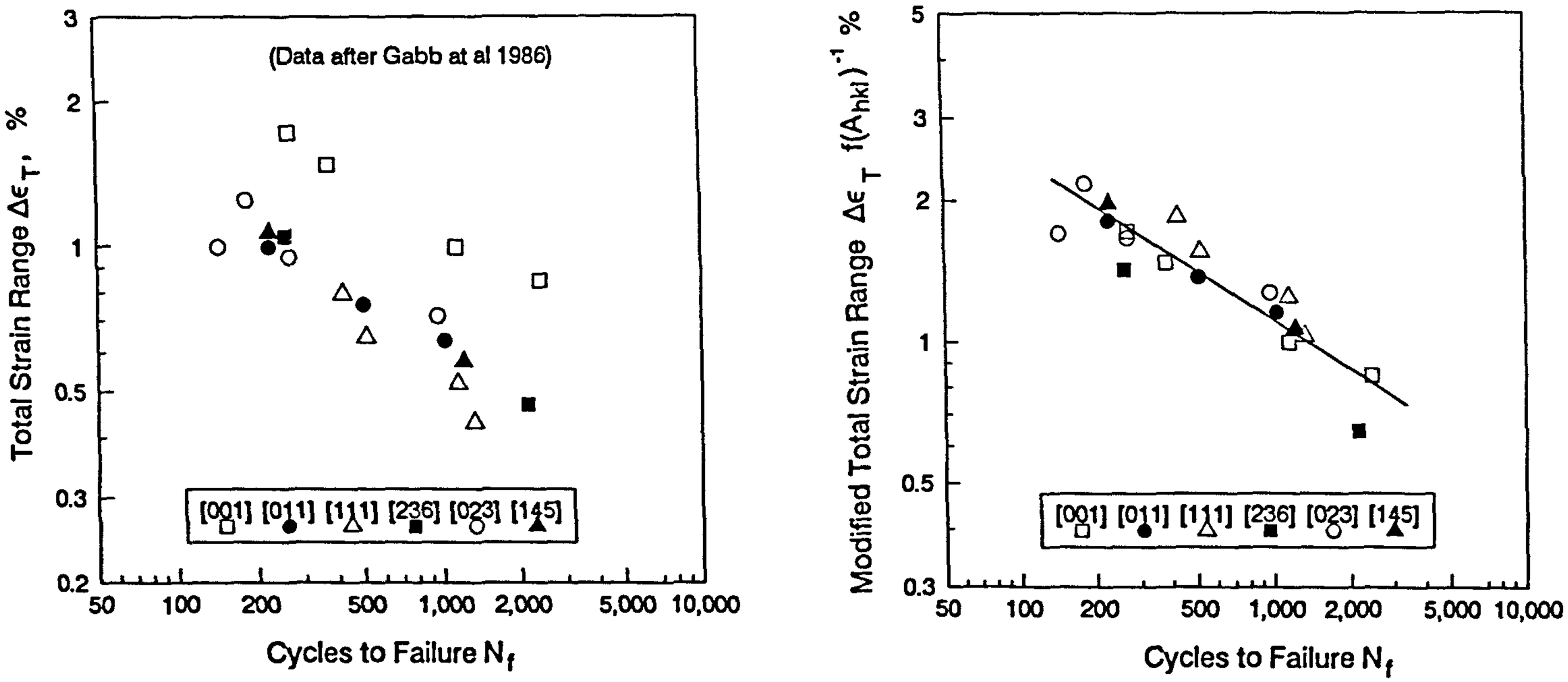

Fig.10.6. Fatigue Life of Single Crystal Rene N4 at 860°C

(a) In Terms of Total Strain Range

(b) In Terms of Modified Total Strain Range

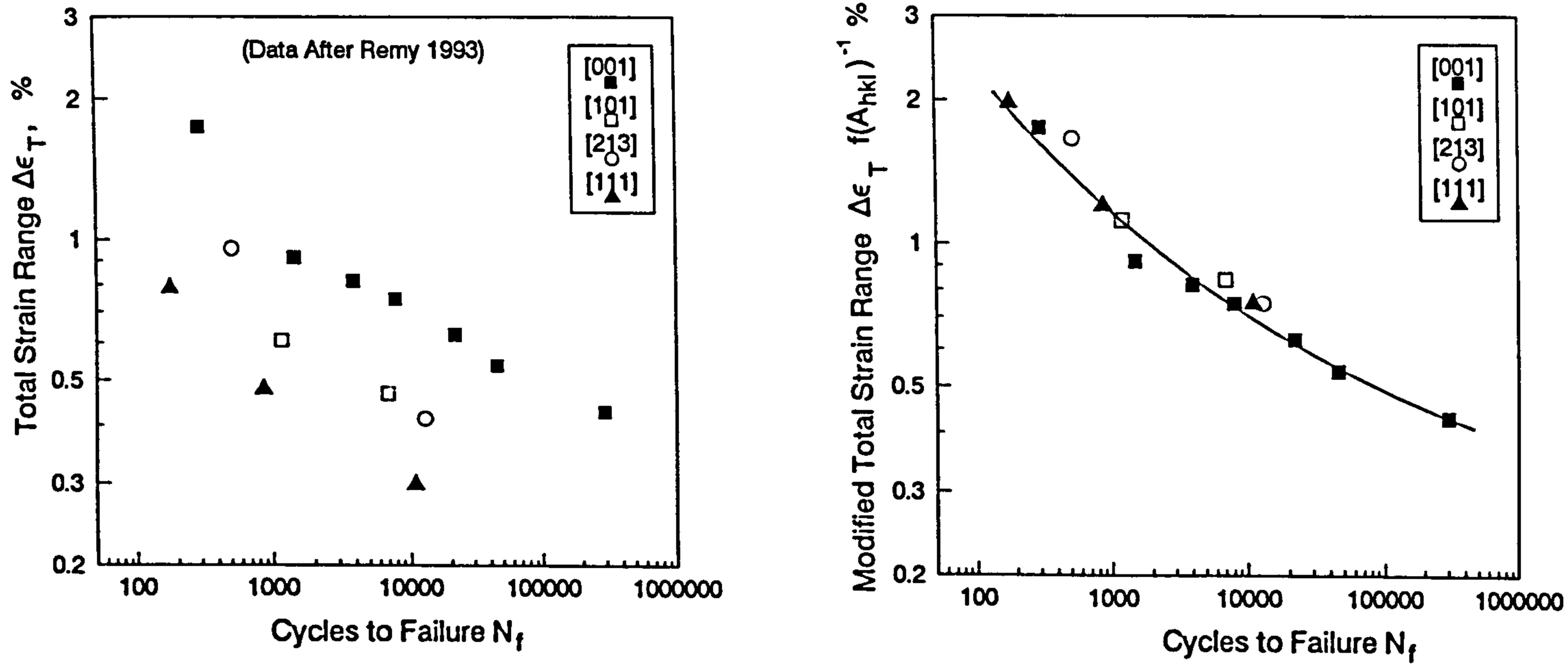

Fig.10.7. Fatigue Life of Single Crystal AM1 at 950°C

(a) In Terms of Total Strain Range

(b) In Terms of Modified Total Strain Range

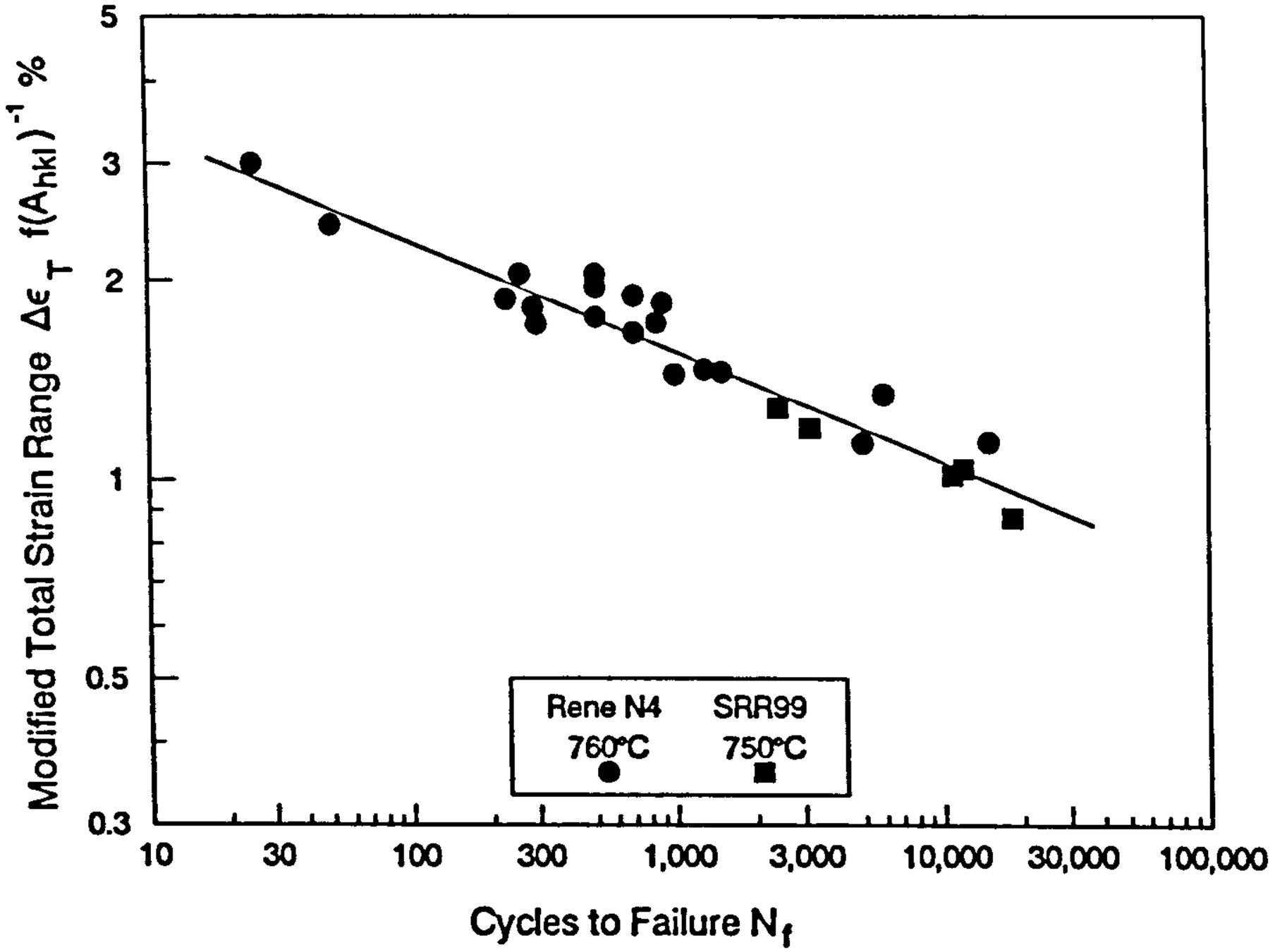

Fig.10.8. Comparison Between the Fatigue Life of Single Crystal SRR 99 and Rene N4

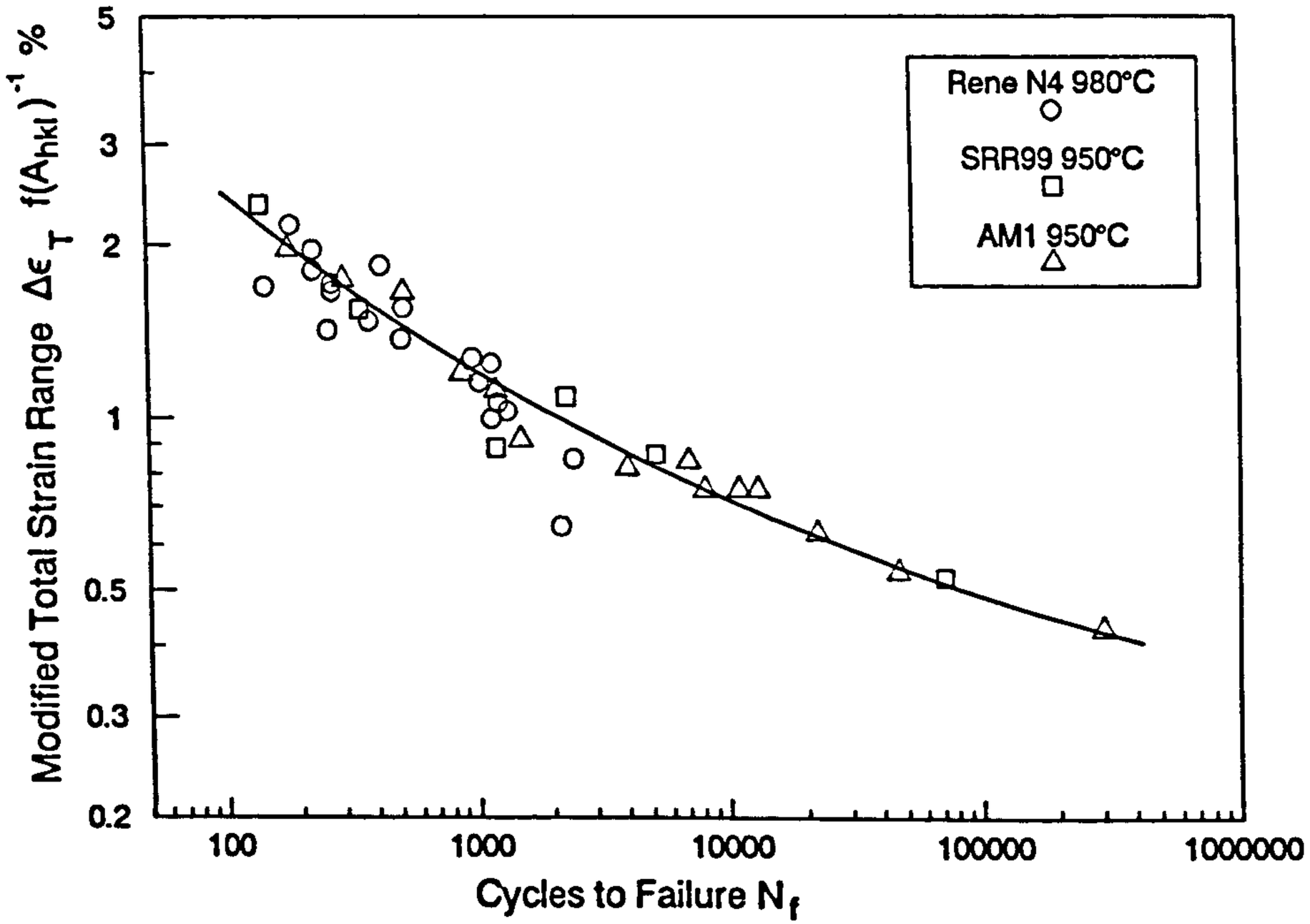

Fig.10.9. Comparison Between the Fatigue Life of Single Crystal SRR99, Rene N4 and AM1

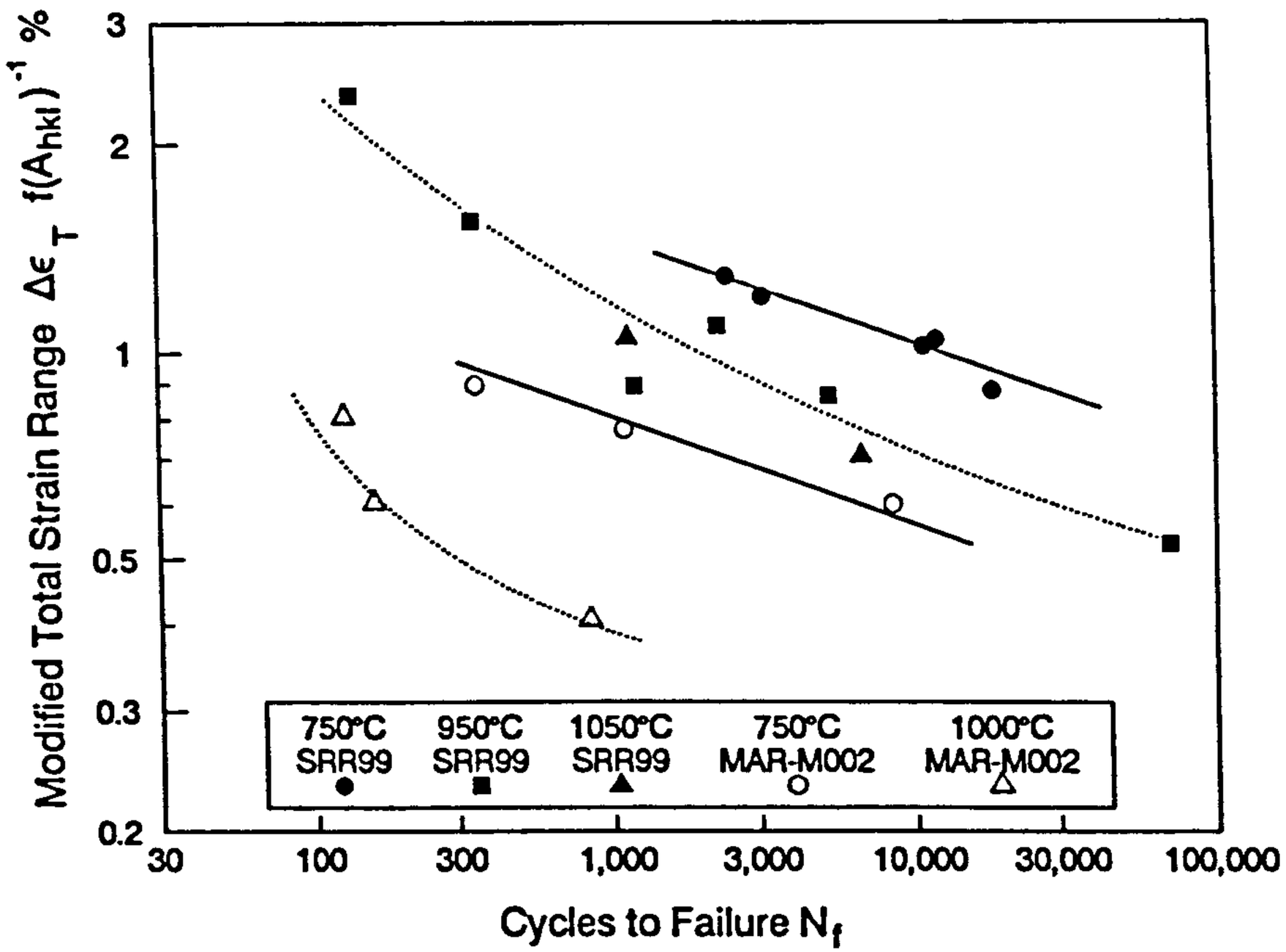

Fig.10.10 Comparison Between the Fatigue Life of Single Crystal SRR99 and Polycrystalline Nickle Base Superalloy MAR-M002

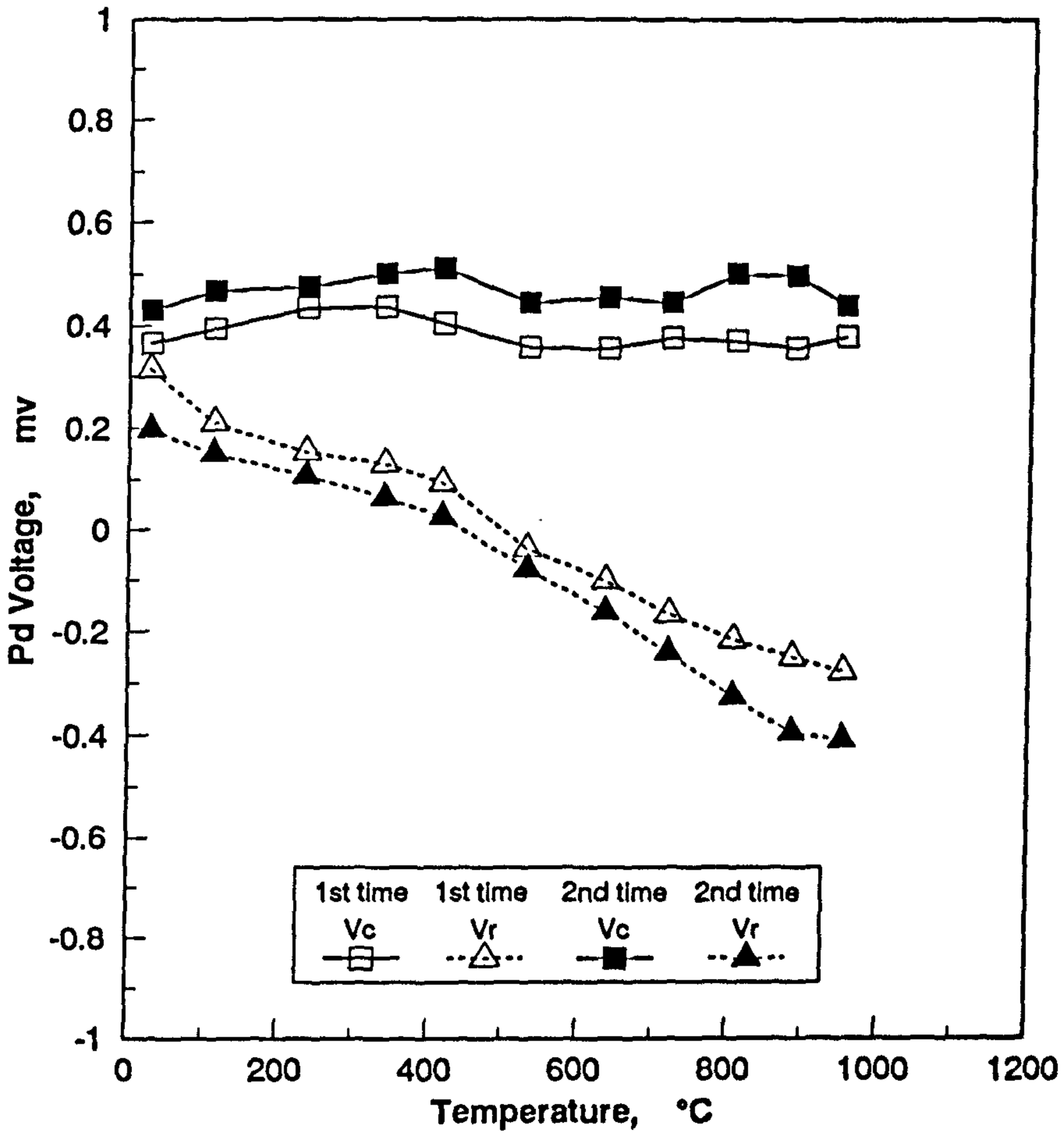

Fig.AII.1. PD Voltage Change with Temperature

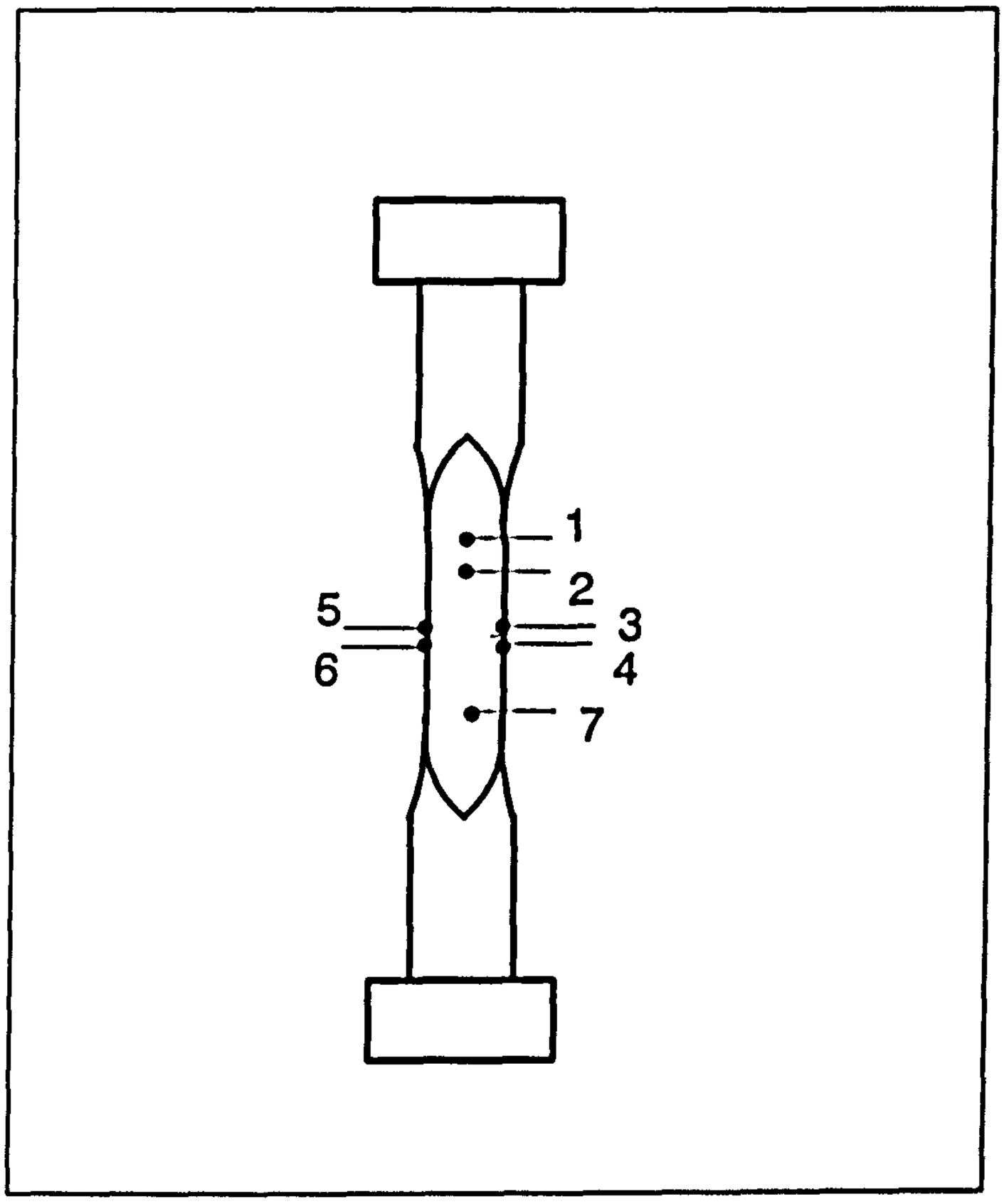

Fig.AII.2. PD Lead Locations for Special Measurement

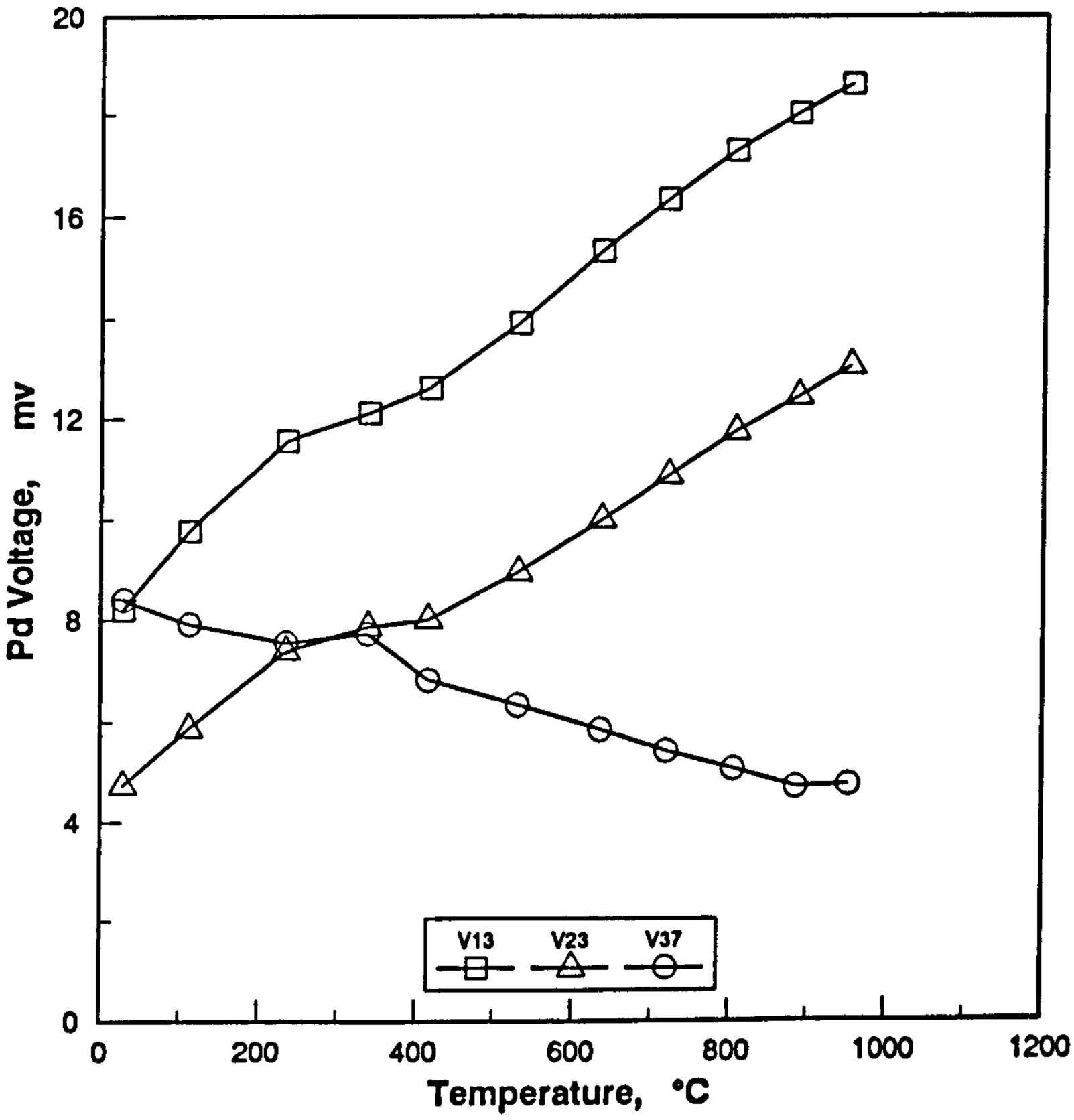

Fig.AII.3. PD Voltage Change with Temperature for Different Lead Locations

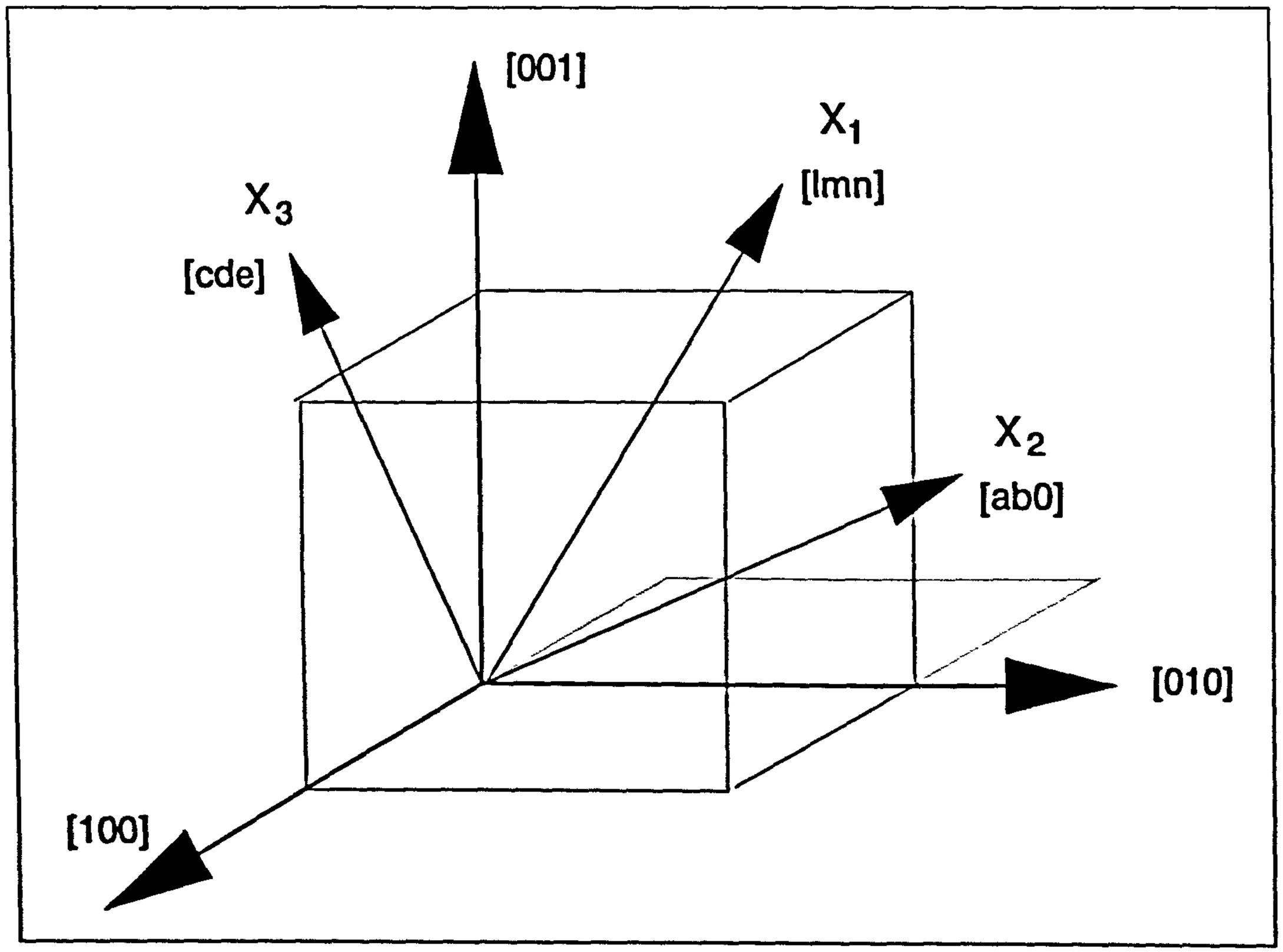

Fig.AV.1. Axis System in the Stress and Strain Transformation

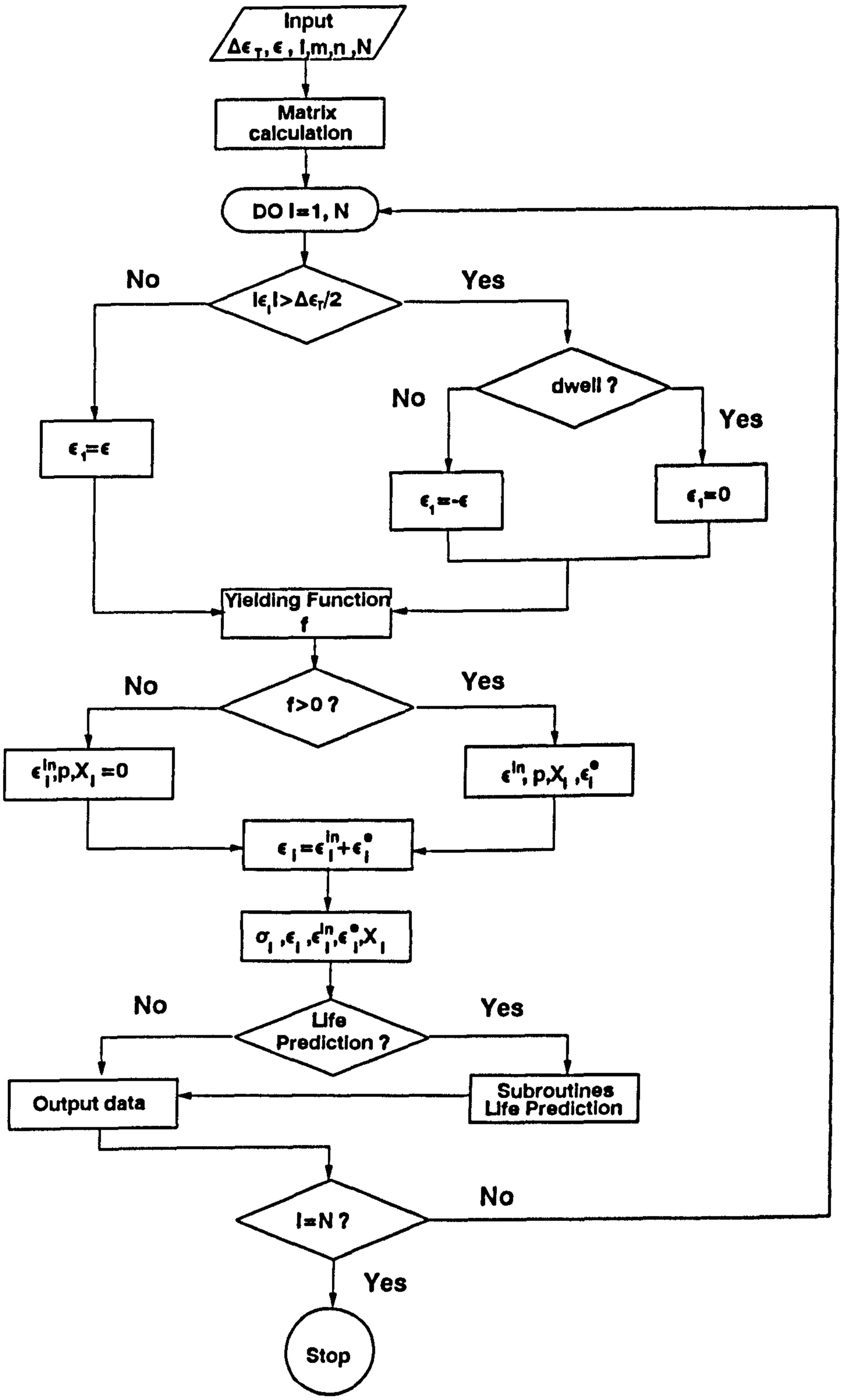

Fig.AVI.1. Flow Chart of FORTRAN Program